The oncolytic adenoviral AdΔΔ mutant sensitizes prostate cancer cells to mitoxantrone by promoting apoptosis and attenuating autophagy.

Carmen Aguirre Hernández

A thesis submitted for the degree of Doctor of Philosophy

December 2016

Centre for Molecular Oncology
Barts Cancer Institute
Barts and The London School of Medicine and Dentistry
Queen Mary University of London
London
United Kingdom

DECLARATION

I, Carmen Aguirre Hernández, confirm that the research presented in this thesis is the result of my own work or that, when it has been carried out in collaboration with others all contributions have been properly acknowledged.

This research has been performed at the Centre for Molecular Oncology, Barts Cancer Institute, Barts and The London School of Medicine and Dentistry, Queen Mary University of London.

I confirm that this thesis has not been previously submitted for the award of a degree by this or any other university.

ACKNOWLEDGEMENTS

First, I would like to express my gratitude to my supervisor Dr. Gunnel Halldén, who welcomed me in her team first as an undergraduate and then as a PhD student. I am very grateful for her endless support and encouragement and for helping me become a researcher. I am also grateful to my second supervisor Dr. Yong-Jie Lu for his useful help, suggestions and guidance.

I would like to thank all past and present members in our group Dr. Hector Maya Pineda, Dr. Katrina Sweeny, Dr. Constantia Pantelidou, Dr. Stella Man and Dr. Elisabete Carapuca for their useful discussions and for teaching me several new techniques. I would also like to mention the undergraduate students that I had the opportunity to supervise and who assisted me during this project: Carolina, Claudia, Yehao and Julia.

I am also grateful to my friends and colleges Pedro, Maria, Cecilia, Teresa, Ana and Maru for their continuous support. I would like to say a special thanks to Pedro, Cecilia and Teresa for useful discussions about the apoptotic studies and to Ana for her help in the Bcl-2 studies.

Finally, I could not finish without thanking my parents and my sister Clara for their unconditional support even in the distance.

ABSTRACT

Prostate cancer (PCa) is the second most common cause of cancer-related deaths in men in the Western world. Advanced PCa is initially managed by anti-androgen therapy however, resistance frequently develops resulting in progressive metastatic disease. The current standard of care for hormone-insensitive PCa includes the cytotoxic drugs docetaxel and mitoxantrone although resistance rapidly develops to all available therapies. We demonstrated that the replication-selective oncolytic adenoviral mutant AdΔΔ enhanced drug-induced cell killing in several preclinical cancer models. AdΔΔ is deleted in the viral E1ACR2 and E1B19K, to prevent pRb-binding and enhance drug-mediated apoptotic cell killing, respectively. In drug-insensitive PCa tumour-xenografts, *in vivo* administration of AdΔΔ greatly enhanced drug-mediated tumour regression. The aim of my thesis project was to investigate the role of apoptosis and pro-survival pathways, including drug-induced autophagy, in AdΔΔ-mediated drug-sensitisation.

I have demonstrated that autophagy was activated in a dose-dependent manner in response to mitoxantrone in the human PCa cell lines PC3, PC3M and 22Rv1. Low doses of mitoxantrone (<EC_{50}-values) caused initiation of autophagy, determined as increased conversion of LC3I to LC3II and increased number of acidic vesicles, indicating autophagosome formation. At higher doses degradation of p62 was also observed, suggesting autophagosome fusion with the lysosome. AdΔΔ attenuated the drug-induced activation of autophagy by restoring basal LC3II/I ratios, and increasing apoptosis, determined as increased PARP-cleavage and mitochondrial depolarization. The autophagy-inducer rapamycin prevented AdΔΔ-mediated sensitization in PC3 cells increasing mitoxantrone EC_{50}-values 3-fold and attenuating apoptosis induction. In contrast, the autophagy-inhibitor chloroquine further sensitized PC3 and 22Rv1 cells to the combination-treatment, decreasing mitoxantrone EC_{50}-values by 40% and increasing apoptotic cell death. Atg7 is a key-factor in the autophagy pathway and siRNA-mediated knockdown prevented increases in LC3II/I ratios. In siAtg7-transfected PC3 cells mitochondrial depolarization was further promoted in combination-treated cells, similar to the results with chloroquine. The cellular Bcl-2-protein has important roles as a mediator of both anti-apoptotic and anti-autophagic functions. In cells transfected with siBcl-2 the LC3II/I ratios increased and AdΔΔ-mediated sensitization to mitoxantrone was prevented, indicating initiation of autophagy. In addition, mitoxantrone-induced degradation of Bcl-2 was attenuated by AdΔΔ infection,

suggesting stabilization of the protein. The mechanisms for the AdΔΔ-mediated increases in cell killing were also demonstrated in 3-dimensional co-culture models of PC3 or 22Rv1 in combination with prostate stromal cells and extracellular matrix proteins using confocal microscopy.

These data demonstrate that AdΔΔ attenuates drug-induced cell survival/rescue and promotes elimination of cancer cells through apoptosis and viral lysis, and that Bcl-2 was essential for the sensitisation.

CONTENTS

LIST OF FIGURES

LIST OF TABLES

LIST OF ABBREVIATIONS

3-MA: 3-Methyladenine

5-FU: 5-fluorouracil

α-SMA: smooth muscle actin

Ad: adenovirus

ADP: adenovirus death protein

ADT: androgen deprivation therapy

AFS: anterior fibromuscular stroma

AMPK: AMP-activated protein kinase

APC: antigen presenting cells

AR: androgen receptor

AR^{fl}: AR full length

AS: active surveillance

ATCC: American Type Tissue Culture Collection

Bcl-2: B-cell lymphoma 2 protein

BSA: bovine serum albumin

CAB: combined androgen blockage

CBP: cAMP-response-element-binding-protein-binding protein

CMA: chaperone-mediated autophagy

CMV: cytomegalovirus

CPE: cytopathic effect

CQ: chloroquine

CR: constant region

CRPC: castrate resistant prostate cancer

CTLA-4: cytotoxic T-lymphocyte-associated protein 4

CZ: central zone

DAPI: 4',6-diamidino-2-phenylindole

DDR: DNA damage response

DHT: dihydrotestosterone

DISC: death-inducing-signalling-complex

DMEM: Dulbecco's Modified Eagle Medium

DMSO: dimethyl sulfoxide

DNA: deoxyribonucleic acid

DPBS: Dulbecco's Phosphate-buffered saline

DRE: digital rectal examination

dsDNA: double stranded DNA

DSG-2: desmoglein-2

EBV: Epstein-Barr virus

EC_{50}: effective concentration at inducing 50% cell death

ECACC: European Collection of Authenticated Cell Cultures

EDTA: ethylenediaminetetraacetic acid

ER: endoplasmic reticulum

ERK1/2: extracellular signal-regulated kinases 1 and 2

FADD: Fas death-domain

FBS: foetal bovine serum

FDA: food and drug administration

FIP200: focal adhesion kinase (FAK) family interacting protein of 200 kD

GFP: green fluorescent protein

GnRH: gonadotropin releasing hormone

GnRH-R: gonadotropin releasing hormone receptor

HAT: histone acetylase transferase

HBV: hepatitis B virus

HCV: hepatitis C virus

hCAR: human coxsackie adenovirus receptor

H/E: hematoxylin and Eosin

HGPIN: high grade prostatic intraepithelial neoplasia

HPV: human papilloma virus

HRP: horseradish peroxidase

HSPG: heparan sulfate proteoglycan (HSPG)

hTERT: human telomerase reverse transcriptase

IFN: interferon

IL: interleukin

JNK: c-Jun N-terminal kinase

KSHV: Kaposi's sarcoma associated herpesvirus

LAMP-2: lysosomal-associated membrane protein 2

LC3B: microtubule-associated proteins light chain 3B

LH: luteinizing hormone

LH-R: luteinizing hormone receptor

LHRH: luteinizing hormone releasing hormone

MBs: microbubbles

MARK: mitogen activated protein kinase

mCRPC: metastatic castrate resistant prostate cancer

MHC: major histocompatibility complex

MOMP: mitochondrial outer membrane permeabilisation

mRNA: messenger RNA

MST: mesenchymal stem cells

mTOR: mechanistic target of rapamycin

MTS: (3-(4,5-dimethylthiazol-2-yl)-5(3-carboxymethoxyphenyl)-2-(4-sulphophenyl)-2H-tetrazolium)

NK: natural killers

NLS: nuclear localization signal

NPs: gold nanoparticles

ns. : non-significant

NSCLC: non-small cell lung cancer

NTP: nucleoside triphosphate

PAGE: polyacrylamide gel electrophoresis

PAP: prostatic acid phosphatase

PARP: poly (ADP-ribose) polymerase

PBMC: peripheral blood mononuclear cell

PBS: phosphate-buffered saline

PCa: prostate cancer

PCR: Polymerase chain reaction

PDAC: pancreatic ductal adenocarcinoma

PE: phosphatidylethanolamide

PEG: polyethylene glycol

pHPMA: poly-[N-(2-hydroxypropyl)methacrylamide]

PI3KC3: class III type phosphoinositide 3-kinase (also called Vps34)

PIN: prostatic epithelial neoplasia

PKAc: protein kinase A catalytic subunit

PMS: phenazine methosulphate

pRB: retinoblastoma protein

PSA: prostate-specific antigen

PZ: peripheral zone

R: rapamycin

RIP: receptor interacting protein

RNA: ribonucleic acid

SA: sialic acid

SDS: sodium dodecyl sulphate

siRNA: short interfering RNA

SR: scavenger receptor

STR: short tandem repeat

TBS: Tris-buffered saline

TE: Tris - EDTA

$TCID_{50}$: Tissue Culture Infectious Dose

TEMED: tetramethylethylenediamine

TK: thymidine kinase

TMRE: tetramethylrhodamine ethyl ester perchlorate

TNF: tumour necrosis factor

TNM: tumour, node and metastasis

Top2: type 2 topoisomerase

Top2cc: Top2 cleavage complex

TRAIL: tumour-necrosis-factor-apoptosis-inducing ligand

Treg: regulatory T-cell

TZ: transition zone

UGE: urogenital sinus epithelium

UGM: urogenital sinus mesenchyme

ULK1: mammalian homolog of yeast Atg1

US: ultrasound

VCAM-1: vascular cell adhesion molecule 1

v/v: volume fraction

w/v: weigh / volume

WW: watchful waiting

UNITS

µM: micromolar

µl: microlitre

bp: base pairs

°C: degree centigrade

g: grams

h: hours

kDa: Kilodalton

mg: milligram

min: minutes

ml: millilitre

mM: milllimolar

ng: nanograms

nM: nanomolar

nm: nanometres

pfu: plaque forming unit

ppc: particles per cell

rpm: Revolutions per minute

s: seconds

V: volts

vp: viral particles

1. INTRODUCTION

1.1 THE PROSTATE

The prostate gland, which is part of the male genitourinary system in mammals (Powers and Marker 2013), is mainly responsible for the production of the components of the seminal fluid, which includes sugars, proteins and ions, and whose mission is the protection of the sperm (Hayward and Cunha 2000, Aslam, Shahid et al. 2013). In the adult male, the prostate gland is surrounding the urethra close to the bladder neck (**Figure *1***) (Timms 2008).

Three structurally different zones can be distinguished within the prostate: the central zone (CZ), the peripheral zone (PZ) and the transition zone (TZ), and include the 25, 70 and 5% of the volume of healthy prostate, respectively (Shen and Abate-Shen 2010). PZ and TZ are derived from the urogenital sinus. The majority of prostate carcinomas (70%) are located in the PZ. In contrast only 25% of carcinomas but all benign prostate hyperplasia are derived from TZ (Lee, Akin-Olugbade et al. 2011). PZ and TZ differ on the composition of their stromal compartment. TZ stroma is compact and predominantly fibromuscular while PZ stroma is looser. CZ is derived from the Wolffian duct and has very low incidence of prostate cancer (**Table *1***) (Lee, Akin-Olugbade et al. 2011).

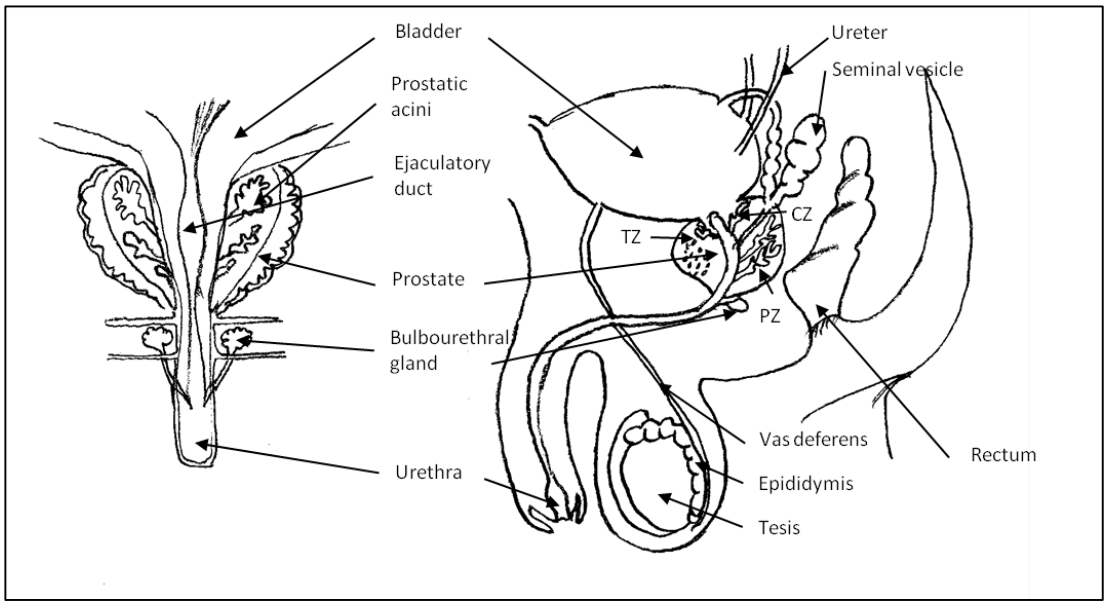

Figure 1. Diagram showing the anatomical position of the adult prostate and associated structures. Central zone (CZ), peripheral zone (PZ), transition zone (TZ), anterior fibromuscular stroma (AFS).

Table 1. Characteristics of the human prostate zones.

	Central Zone (CZ)	Transition Zone (TZ)	Peripheral Zone (PZ)
Volume of healthy prostate (%)	25	5	70
Proposed embryonic origin	Wolffian duct	Urogenital sinus	Urogenital sinus
Epithelium	Complex, large polygonal glands	Simple, small rounded glands	Simple, small rounded glands
Stroma	Compact	Compact	Loose
Origin of prostatic adenocarcinomas (%)	5	25	70
Origin of benign prostatic hyperplasia (%)	---	100	---

Adapted from (Lee, Akin-Olugbade et al. 2011).

The development of the prostate gland starts during embryogenesis. The embryonic urogenital sinus consists of the urogenital sinus mesenchyme (UGM) and the urogenital sinus epithelium (UGE) (Cunha, Hayward et al. 2003). Epithelial-mesenchymal interactions are required for prostatic development and their interactions are reciprocal (Cunha, Ricke et al. 2004). The development of the human prostate gland starts in the 10^{th} week of foetal development and is dependent on androgen stimulation of the androgen receptor (AR) present in the urogenital sinus mesenchyme (Hayward and Cunha 2000). Androgen stimulation promotes epithelial budding, elongation of the duct, cellular proliferation and differentiation of the secretory epithelium (Hayward and Cunha 2000, Cunha, Ricke et al. 2004, Powers and Marker 2013).

During the postnatal period, the epithelium continues its differentiation and starts the synthesis of secretory products (Timms 2008). During puberty, an increase in testosterone levels promotes the growth of the prostate gland (Hayward and Cunha 2000). In the adult prostate, androgens and the AR are needed for the control of the expression of prostate

specific secretory proteins and for keeping the integrity of the gland (Powers and Marker 2013).

The epithelium of the prostate gland forms glandular acini and is composed of basal cells, secretory luminal cells and some neuroendocrine cells, all attached to the basal lamina. Secretory luminal cells are polarised columnar cells that express cytokeratins 8 and 18 and high levels of AR and are responsive to androgens, these cells secrete their products into the luminal space, which would then reach a duct and finally the urethra. Basal cells express p63 and cytokeratins 5 and 14 but low or undetectable levels of AR. Neuroendocrine cells are AR-negative (Shen and Abate-Shen 2010, Barron and Rowley 2012). The prostate epithelium is surrounded by the stroma, which is composed of smooth muscle cells, fibroblast, extracellular matrix, endothelial cells, blood vessels and autonomic nerves (**Figure *2***) (Bonkhoff 2001, Barron and Rowley 2012, Shafi, Cox et al. 2013).

In the healthy adult prostate gland, the AR is expressed in luminal cells and in some basal cells where it controls the production of secreted proteins (**Figure *2***) (Shafi, Cox et al. 2013). The AR can act as a survival factor to regulate the prostate growth in luminal cells but also as an inhibitor of cell proliferation (Shafi, Cox et al. 2013). The AR is activated by binding of androgens such as testosterone or dihydrotestosterone (DHT). DHT results from the conversion of testosterone by 5α-reductase, which is expressed in various tissues, including the prostate (Azzouni, Godoy et al. 2012), and has higher affinity for the receptor (Lindzey, Kumar et al. 1994). Upon binding, AR undergoes conformational changes and dissociates from cytoplasmic chaperones to expose the nuclear localization signal, which enables AR translocation to the nucleus. Nuclear translocation is mediated by α- and β-importins and by dynein-mediated cytoskeletal transport (Wagstaff and Jans 2009, McCrea, Sissung et al. 2016). Once in the nucleus, AR binds to the DNA and recruits different cofactors to regulate the expression of target genes, such as the prostate-specific antigen (PSA) (**Figure *3***) (Koochekpour 2010, Shafi, Cox et al. 2013).

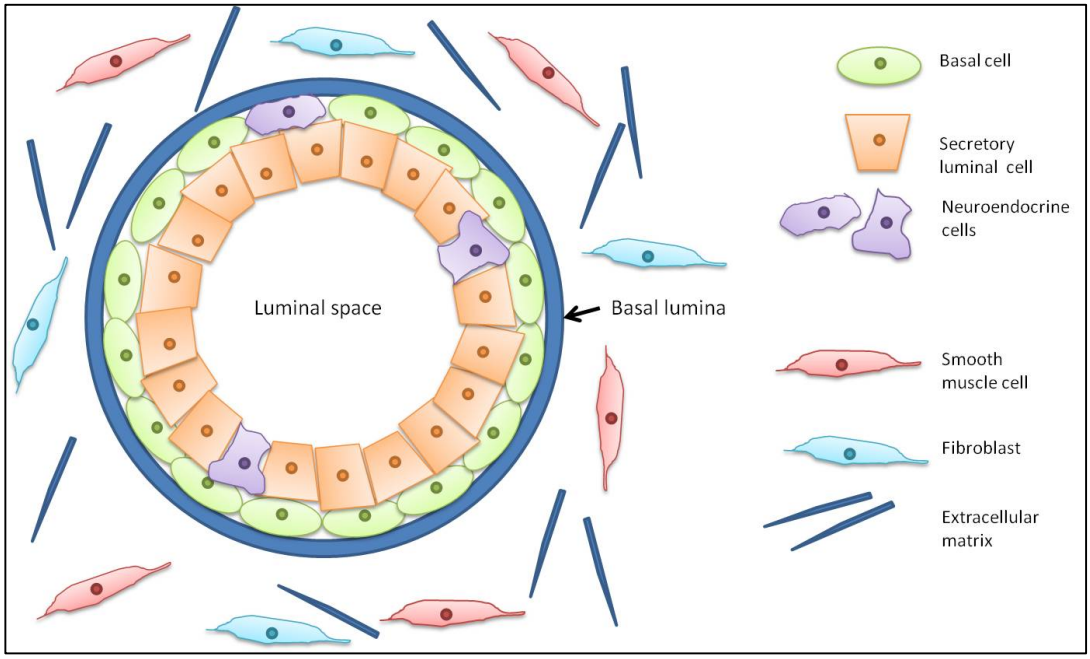

Figure 2. Schematic representation of the prostate basal lamina.

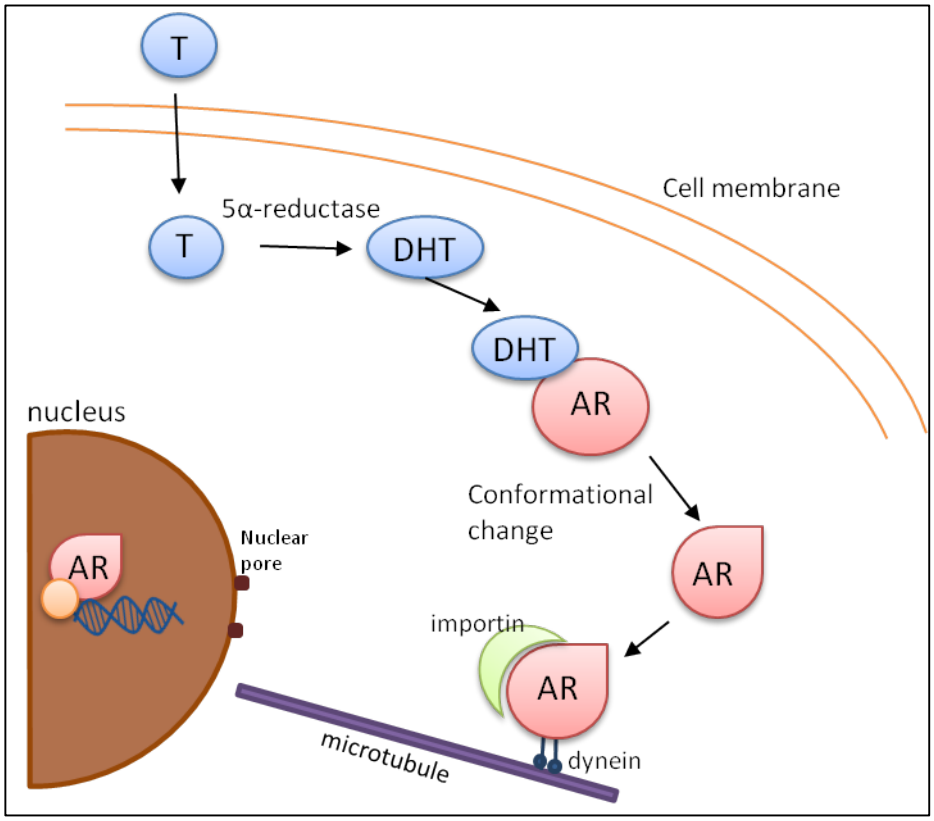

Figure 3. Schematic representation of AR activation. The enzyme 5α-reductase mediates the conversion of testosterone in DHT. DHT binds to AR inducing a conformational change that exposes a AR nuclear localization signal. AR is translocated to the nucleus by α- and β-importins or dyneins. Once in the nucleus, AR, together with additional cofactors activate the transcription of target genes. Androgen receptor (AR), testosterone (T), dihydrotestosterone (DHT).

1.2 PROSTATE CANCER

Prostate cancer (PCa) is the second most common diagnosed cancer in Western men (Jemal, Bray et al. 2011) and the second cause of male cancer-related deaths in the US and third in EU men (Siegel, Ma et al. 2014, Malvezzi, Bertuccio et al. 2015). PCa incidence has increased in Western Countries during the past years (Jemal, Bray et al. 2011). When PCa is detected at an early, localised stage, it can be cured by surgery or radiotherapy or it might not even require treatment, however if PCa progresses, or is diagnosed once it has reached later stages, the patient prognosis worsens (Carles, Castellano et al. 2012). Androgen deprivation therapy (ADT) is applied after failure of localised treatments, ADT promotes remission of the cancer and reduces the PSA levels in 90% of patients (Harris, Mostaghel et al. 2009). Despite its efficacy, after 2-3 years, most cancers become resistant to androgen suppression, this new type of cancer is then known as castrate-resistant prostate cancer (CRPC) (Carles, Castellano et al. 2012, Karantanos, Corn et al. 2013). PCa, including metastatic castration-resistant prostate cancer (mCRPC), frequently metastasises into the bone which is associated with poor prognosis (**Figure *4***) (Karantanos, Corn et al. 2013).

1.2.1 Risk factors of prostate cancer

Age is the predominant risk factor for prostate cancer. PCa incidence greatly increases after reaching 70 years of age in unscreened populations (Cuzick, Thorat et al. 2014). In Europe, only 25% of PCa patients were diagnosed before the age of 65 (Cuzick, Thorat et al. 2014). In the US population, PCa is the first cause of cancer-related deaths in men aged 80 years or older (Jemal, Siegel et al. 2009). Race can also be considered as a risk factor. In the USA, the African-American male population have 2-fold higher incidence of PCa and higher mortality rates when compared to white men of European ancestry while the PCa incidence and mortality is lower in the Hispanic population (Merrill and Sloan 2012). The study of risk factors for PCa in a multi-ethnic cohort from US population resulted in no association between lifestyle and dietary habits with the increased PCa incidence in the US African-American population (Park, Haiman et al. 2015), suggesting that this increased PCa incidence might be related to genetic factors. In Europe, there are also considerable differences, for example, PCa incidence in Sweden is higher than in Spain or Italy (around 2- and 1.5-fold respectively) (Center, Jemal et al. 2012). There is also increased risk of PCa in men who have

a first-degree relative that suffered from the disease, however, only 35% of the familial risk can be associated with known genes (Cuzick, Thorat et al. 2014). The BRCA2 mutation, although rare (one per 300), increases the PCa risk 8.6-fold in men younger than 65 years and is associated with aggressive cancer (Castro, Goh et al. 2013, Goh and Eeles 2014). It has been suggested that PCa development can be related to chronic intraprostatic inflammation as a result of infection although more research is needed to confirm this hypothesis (De Marzo, Platz et al. 2007, Cuzick, Thorat et al. 2014). In addition, smoking can also be considered a risk factor for PCa (Huncharek, Haddock et al. 2010), more specifically, PCa risk may double for current heavy smokers when compared to non-smokers (Zu and Giovannucci 2009). Smoking has also been proposed to play a role in the promotion of metastasis (Zu and Giovannucci 2009). Furthermore, higher PSA levels were detected in individuals with sedentary habits suggesting that physical activity could be associated with a small decrease in PCa risk (Loprinzi and Kohli 2013, Cuzick, Thorat et al. 2014).

1.2.2 Development of prostate cancer

Prostatic intraepithelial neoplasia (PIN) frequently precedes PCa. PIN is characterised by hyperplasia of the luminal epithelium and a reduction in the number of basal cells, but not complete elimination of basal cells, which would later occur in PCa. PIN might develop in high grade prostatic intraepithelial neoplasia (HGPIN) (Shen and Abate-Shen 2010). During HGPIN, the epithelium loses its basal cell differentiation and is associated with stromal invasion (**Figure *4***) (Bonkhoff 2001). Myc overexpression, and chromosomal abnormalities such as the fusion of the androgen-regulated gene TMPRSS2 with ERG, frequently occur during PIN (Baker and Reddy 2013).

Prostatic adenocarcinomas can evolve from multiple genetically different histologic foci and may stay localised and in a latent stage for many years (Shen and Abate-Shen 2010).

The molecular mechanisms that drive PCa initiation, progression, metastasis and appearance of treatment resistance are not completely understood. Fortunately, some recent findings have driven some insights into this topic (**Figure *4***). Reduction, although not complete loss of NKX3.1 expression, located in the 8p21.2 chromosome, frequently appears in PIN and PCa and is associated with PCa initiation (Gelmann 2002, Shen and Abate-Shen 2010). NKX3.1 expression is regulated by inflammation and has been suggested to protect the cell from

DNA damage (Bowen and Gelmann 2010). In addition, NKX3.1 has been reported to regulate epithelial differentiation (Bhatia-Gaur, Donjacour et al. 1999). Myc overexpression, which has been reported in many PIN and in the majority of PCa, has also been associated with PCa initiation (Gurel, Iwata et al. 2008).

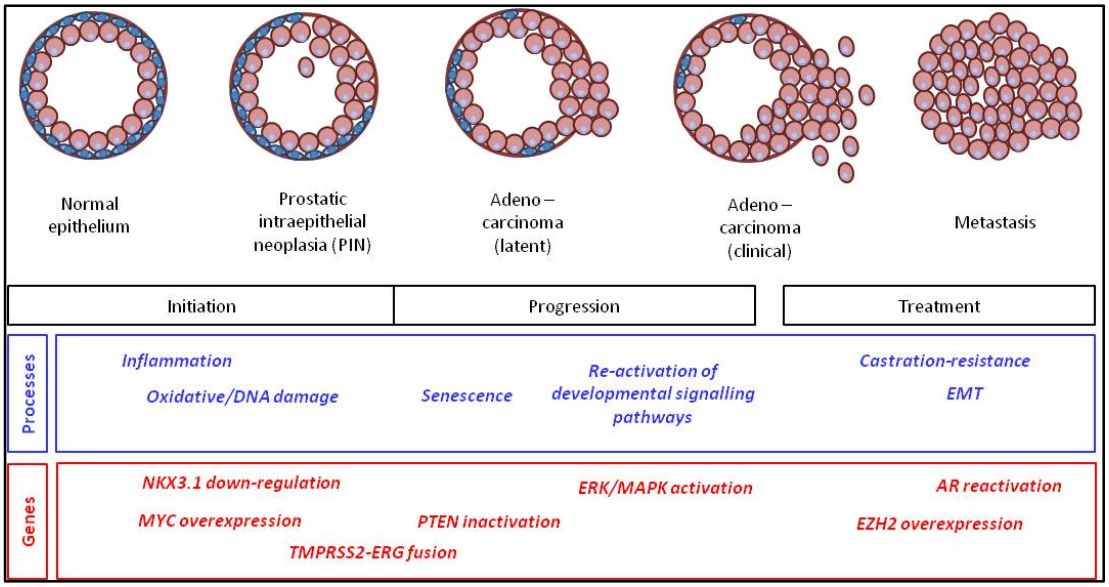

Figure 4. Schematic view of PCa progression. The figure shows the different progression stages of prostate cancer and highlights the genes or molecular pathways, which are proposed to be relevant in each stage. PIN (prostatic epithelial neoplasia), HGPIN (high grade intraepithelial neoplasia), EMT (epithelial to mesenchymal transition), NKX3.1 (transcription factor NK homeobox family 3 locus-1), MYC (myelocytomatosis viral oncogene homologue), TMPRSS2-ERG (trans-membrane protease serine 2-Ets-related-gene), PTEN (phosphatase and tensin homolog), ERK/MAPK (mitogen-activated protein kinase) and EZH2 (enhancer of zeste homolog 2).

Chromosomal rearrangements involving the ETS transcription factor family have been found in around 50% PCa tumours. The translocation of TMPRSS2-ERG is the most frequent of these rearrangements (Tomlins, Rhodes et al. 2005, Baker and Reddy 2013) and has been proposed to promote PCa progression (Shen and Abate-Shen 2010). TMPRSS2 and ERG fusion has been suggested to result from AR-induced chromosomal proximity in the presence of DNA damage (Lin, Yang et al. 2009, Bastus, Boyd et al. 2010).

The PTEN pathway, which would normally inhibit PI3K signalling, is frequently found mutated in prostate cancer (Majumder and Sellers 2005, Powers and Marker 2013). Up-regulation of the PI3K/Akt/mTOR pathway promotes cell proliferation and inhibits apoptosis and is associated with prostate cancer progression (Powers and Marker 2013). PTEN expression levels decrease as the disease progresses. Loss of PTEN, which drives activation of PI3K, has been shown to promote precancerous lesions (King, Xu et al. 2009). PTEN loss and PI3K activation have also been associated with resistance to therapy and poor prognosis (Baker

and Reddy 2013). In addition, the combination of loss of PTEN with other alterations, such as TMPRSS2-ERG translocation, led to progression into more invasive carcinomas (King, Xu et al. 2009).

Elevated levels of phospho-MAPK, which are an indicative of RAS activation, have been found in CRPC patients, especially in metastatic bone lesions (Mulholland, Kobayashi et al. 2012). However, the activation of *Kras* alone in mice did not result in development of PCa (Tomlins, Laxman et al. 2008). In contrast, simultaneous *Kras* activation and PTEN loss in mice resulted in early lethality, invasive carcinoma and development of lung and liver metastasis (Mulholland, Kobayashi et al. 2012). Interestingly, alterations in the PI3K and RAS signalling pathways have been found in around 40% of primary tumours and in up to 90% of metastatic PCa cases (Taylor, Schultz et al. 2010), suggesting that these alterations may play a role in PCa progression.

Deregulated tyrosine kinase signalling, especially through Her2/Neu or SCR tyrosine kinases has been associated with aggressive PCa, progression to metastatic disease and appearance of castrate resistance (Mellinghoff, Vivanco et al. 2004, Fizazi 2007).

Expression of the EZH2 gene, which encodes histone lysine methyltransferase, is frequently found up-regulated in advanced PCa (Saramäki, Tammela et al. 2006) and it has been associated with aggressive disease (Bachmann, Halvorsen et al. 2006). EZH2 has been reported to down-regulate expression of NKX3.1 (Kunderfranco, Mello-Grand et al. 2010) and to target some metastasis-associated genes, promoting down-regulation of E-cadherin (Cao, Yu et al. 2008).

AR signalling plays an important role in the development of the prostate gland and in PCa progression. The AR gene contains 8 exons and encodes for a 100KDa protein. The AR full length (AR^{fl}) protein is the predominant form and contains 4 distinct functional domains: an amino-terminal domain (NTD, encoded by exon 1), a DNA binding domain (DBD, encoded by exons 2 and 3), a hinge region (H, encoded by 5'extreme of exon 4), and a ligand binding domain (LBD, encoded by the remaining exon 4, and exons 5 to 8) (**Figure *5***) (Gelmann 2002). ADT (discussed in section 1.2.4) initially results in cellular apoptosis and tumour regression. AR signalling suppresses proliferation in the normal healthy prostate epithelium. During development of PCa, AR selectively suppresses proliferation of basal cells in the prostate epithelium enhancing proliferation of luminal cells and facilitating metastasis of the tumour (Niu, Altuwaijri et al. 2008). AR signalling can be lost during PCa progression but is often

restored during mCRPC, which can be due to gain of function mutations, constitutively active alternative splicing variants or deregulation due to amplification or overexpression (Knudsen and Penning 2010, Gundem, Van Loo et al. 2015).

Mutations in the AR gene were not detected in early stage PCa patients but were found in 1/5 of patients with more aggressive disease (Marcelli, Ittmann et al. 2000). Point mutations in the ligand-binding domain facilitate AR activation either by bringing the helix 12 closer to the active site, which is formed by helix 3 and 12 of the AR protein (Mak, Hoare et al. 1999), or making the ligand-pocket larger so it can accommodate larger, alternative ligands (Brooke and Bevan 2009, McCrea, Sissung et al. 2016). The H874Y mutation is characteristic of the 22Rv1 cell line (Azad, Volik et al. 2015) and results in the helix 12 being closer to the ligand-binding pocket facilitating AR activation (Duff and McEwan 2005). The T877A mutation, characteristic of the LNCaP cell line (Veldscholte, Berrevoets et al. 1992), results in a larger ligand-binding pocket (Steketee, Timmerman et al. 2002).

Two well-studied AR alternative splicing variants, in addition to AR^{fl}, are the constitutively active AR-V7, which is truncated at the end of exon 3, and AR-V^{v567es}, which lacks exons 5 to 7, has the remaining LBD region in a non-normal translation frame and is not constitutively active but promotes expression of AR^{fl} (**Figure *5***) (Sun, Sprenger et al. 2010, Shafi, Cox et al. 2013). Both AR-V7 and AR-V^{v567es} have been associated with PCa progression and poor survival (Hörnberg, Ylitalo et al. 2011). Both variants have been shown to either homodimerize or heterodimerize with each other or with AR^{fl} (Xu, Zhan et al. 2015). Interestingly, AR-V7 transcription is dependent on AR^{fl} signalling (Watson, Chen et al. 2010). Although both AR^{fl} and AR-V7 target genes that are involved in glycolysis, AR-V7 can differently target genes involved in the Krebs cycle. AR-V7 expression results in increased citrate production and, consequently enhances production of amino acids (Shafi, Putluri et al. 2015). AR-V7 expression has been associated with resistance to enzalutamide or abiraterone treatments, in contrast, patients expressing AR-V7 have retained sensitivity to taxane treatment (Antonarakis, Lu et al. 2015).

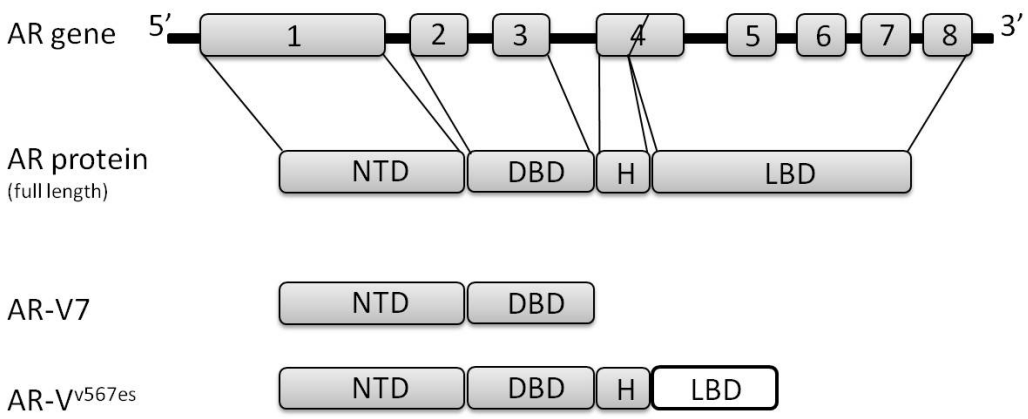

Figure 5. Schematic representation of the AR gene, the AR protein domains and selected AR splicing variants. The AR gene contains 8 exons. The AR full length protein contains 4 functional domains: amino-terminal domain (NTD), a DNA binding domain (DBD), a hinge region (H), and a ligand binding domain (LBD). The AR-V splicing variant is truncated at the end of exon 3 and only contains the NTD and DBD domains. The AR-V^{v567es} splicing variant lacks exons 5 to 7 and has a truncated LDB region with a non-normal translation frame.

1.2.3 Diagnosis of prostate cancer

The prostate specific antigen (PSA) is a glycoprotein secreted by the prostate gland whose expression is regulated by AR (Pezaro, Woo et al. 2014). Under healthy conditions, PSA is released into the prostate lumen but not into the systemic circulation (Catalona, Smith et al. 1991, Shafi, Cox et al. 2013). Damage in the prostate, due to PCa or physical injury, can cause the secretion of PSA into the systemic circulation rather than into the prostate lumen (Catalona, Smith et al. 1991, Shafi, Cox et al. 2013). Detection of PSA in patient's blood can be used for early diagnosis of PCa and for monitoring of cancer regression upon treatment (Pezaro, Woo et al. 2014). The measurement of high PSA levels in blood was first reported to be related to PCa incidence in 1991 (Catalona, Smith et al. 1991) and, combined with digital rectal examination, was proposed for PCa diagnosis. However, over the past two decades, extensive PSA screening has resulted in a large number of unnecessary biopsies, that led to over-diagnosis and over-treatment of low-grade tumours (Pezaro, Woo et al. 2014, Voigt, Zappala et al. 2014). Therefore, discussions addressing whether the PSA test should still be used for diagnosis of early-stage PCa were initiated. With the aim to resolve these doubts, the Prostate World Congress held in Melbourne in August 2013 elaborated a document with 5 consensus statements (Murphy, Ahlering et al. 2014): (1) There is evidence supporting a decrease in prostate cancer-specific mortality in men aged 50-69 that had undergone PSA examination. (2) PCa diagnosis does not necessarily have to be followed by

PCa intervention and low-risk tumours can be monitored by active surveillance. (3) PSA testing should be part of a multivariable approach rather than a single examination. Risk factors (discussed in section 1.2.1) and alternative diagnostic methods and imaging techniques (discussed below in this section) should also be considered. (4) Although it is not currently performed in the majority of cases, PSA screening in men of 40 years of age may help to predict the development of PCa in this group during the next 25 years. (5) Finally, the screening could also be indicated for men over 70 years with general good health (Murphy, Ahlering et al. 2014). The PSA screening, although imperfect, is an important tool for monitoring the effect of treatment of localised disease (Pezaro, Woo et al. 2014). The World Health Organization (WHO) has recomended a PSA cut-off of 3 - 3.1 µg/l in the WHO-calibrated assay as a positive result (**Table *2***) (Stephan, Köpke et al. 2009, Heidenreich, Bastian et al. 2014).

Table 2. Correlation of risk of PCa and PSA levels.

PSA level (ng/ml)	Risk of PCa (%)
0 – 0.5	6.6
0.6 – 1	10.1
1.1 – 2	17.0
2.1 – 3	23.9
3.1 – 4	26.9

Prostate-specific antigen (PSA), prostate cancer (PCa). Adapted from (Heidenreich, Bastian et al. 2014).

Modifications of the current PSA-testing strategies and the development of alternative diagnosis methods are currently being studied. Spacing the interval between PSA tests from 1 year to 2-4 years could diminish the overdiagnosis-associated harm without increasing prostate cancer mortality (Cuzick, Thorat et al. 2014). An improved test is the so called "Kallikrein panel" which measures four markers secreted by the prostate gland (free PSA, total PSA, single-chain intact PSA and human kallikrein 2 (hK2) (Rittenhouse, Finlay et al. 1998)). Increased levels of these markers together with age, serve as parameters in an algorithm that calculates the probability of finding cancer in the patient when performing a biopsy (Voigt, Zappala et al. 2014). This test has shown high specificity at low PSA levels (Cotter, Konety et al. 2016). In addition to the Kallikrein assay, the expression of the non-

coding prostate cancer gene 3 mRNA, often overexpressed in prostate cancer and only produced in prostate tissue (Bussemakers, van Bokhoven et al. 1999), is measured in urine with the PCA3 assay (Cuzick, Thorat et al. 2014). The multiparametric magnetic resonance imaging (MRI) can also be employed for PCa diagnosis and treatment (Barentsz, Richenberg et al. 2012). As a diagnosis method, multiparametric MRI can accurately image the prostate anatomy and determine the specific location of cancer (Salerno, Finelli et al. 2016). Therefore, MRI may help determine whether early-diagnosed PCa requires further treatment or if active surveillance should be recommended.

The grading of PCa is of vital importance for monitoring the disease and selection of the most adequate treatment. A histopathological-based grading system was developed by Prof. D. F. Gleason in the early 1970s (Gleason and Mellinger 1974). The Gleason system designates a number (1-5) to certain architectural patterns and produces a score by adding the first and second most common patterns in an analysed sample. This system was modified and updated in 2005 (Epstein, Allsbrook et al. 2005). With the aim to continue improving this system, further discussion led to the proposal of a new grading system in 2014 (**Table *3***) (Epstein, Egevad et al. 2016).

Table 3. New proposed grading system for PCa.

New grading system	**Gleason Score**	**Histologic definition**	**Probability of recurrence-free progression after radical prostatectomy (%)**
Grade group 1	≤3 + 3 = 6	Only individual discrete well-formed glands	96
Grade group 2	3 + 4 = 7	Predominantly well-formed glands with lesser component of poorly formed/fused/cribriform glands.	88
Grade group 3	4 + 3 =7	Predominantly poorly formed/fused/cribriform glands with lesser component of poorly formed glands	63
Grade group 4	8	Only poorly formed/fused/cribriform glands. Predominantly well-formed glands and a lesser component lacking glands.	48

		Predominantly lacking glands and lesser-component of well-formed glands.	
Grade group 5	9 or 10	Lack of gland formation (or with necrosis) with or without poorly formed/fused/cribriform glands.	26

Adapted from (Matoso and Epstein 2016).

The the tumour, node and metastasis (TNM) staging system, established in 1992 by a joint efford of the American Joint Committee on Cancer and the Union Internationale Contre le Cancer (Beahrs, Henson et al. 1992), is also used for the staging of PCa. The TNM system is based on the clinical and histopathological characteristics of the tumour. This system classifies the disease according to whether it is localised and confined whithin the prostate, affects the lymph nodes or involves the appearance of distant metastasis. The TNM system was updated in 2010 (**Table *4***) (Edge and Compton 2010).

Table 4. American Joint Committe on Cancer TNM classification of prostatic tumours 2010.

Clasification		**Clinical clasification**	**Pathological clasification**
Primary tumour (T)	T0	No evidence of primary tumour	- - -
	T1	Clinically inapparent tumour neither palpable nor visible by imaging	There is no pathological classification
	T2	Tumour confined within the prostate	Organ confined
	T3	Tumour extends through the prostate capsule (may include seminal vesicles)	Extraprostatic extension
	T4	Tumour is fixed or invades adjacent structures other than seminal vesicles such as external sphincter, rectum, bladder, levator muscles, and/or pelvic wall	Invasion of the rectum, levator muscle, and/or pelvic wall
Regional lymph nodes (N)	N0	No regional lymph node with metastases	No positive regional lymph nodes
	N1	Metastases in regional lymph node(s)	Metastases in regional lymph nodes
Distant metastasis (M)	M0	No distant metastasis	No distant metastases
	M1	Distant Metastasis	Distant metastases

Adapted from (Cheng, Montironi et al. 2012).

1.2.4 Current treatment of prostate cancer

More than 50% of PCa diagnosed after PSA testing are classified as low risk early stage tumours and, in most cases, will not result in death. Before undergoing any treatment, low-grade PCa patients may be eligible for active surveillance (AS) or watchful waiting (WW). AS involves monitoring of the disease using PSA tests, digital rectal examination (DRE), imaging and periodic biopsies, WW is a more passive strategy that monitors progression by appearance of symptoms (Ip, Dahabreh et al. 2011, Carter, Clover et al. 2015). Alternatively, patients with early stage tumours can undergo radical prostatectomy or radiation therapy, which can be combined with ADT (Ip, Dahabreh et al. 2011). These treatments are curative in most cases but entail serious side effects such as urinary incontinence or erectile dysfunction (Ip, Dahabreh et al. 2011, Carter, Clover et al. 2015).

1.2.4.1 Hormonal therapy for prostate cancer

Since Huggins and colleagues showed that androgen-ablation therapy resulted in improvement of the clinical condition of mCRPC patients in 1941 (Huggins and Hodges 2002), this therapy has been commonly used with successful results. In 1971, Schally found that overexpression of the hypothalamic luteinizing hormone (LH) releasing hormone (LHRH), also called gonadotropin releasing hormone (GnRH), inhibits the action of LH, which is responsible for the production of testosterone (Schally, Kastin et al. 1971). Androgens bind to the AR present in the hypothalamus and promote the production of GnHR (also called LHRH), which travels to the pituitary gland where it binds to the GnRH receptor (GnRH-R) to induce the production and release of LH. In the testis, LH binds to its receptor (LH-R) inducing testosterone production. Once in the prostate, testosterone is converted into DHT by 5-α reductase, DHT will then bind and activate AR within the prostatic tissue. An increase in testosterone levels negatively regulates the production of LHRH and LH in the hypothalamus and pituitary respectively (**Figure *6***) (Denmeade and Isaacs 2002).

Agonists of the GnRH are currently the standard of care for ADT because of its reversibility, which enables intermittent use (Heidenreich, Bastian et al. 2014). GnRH agonists act by binding to the gonadotropin receptors in the pituitary gland and subsequently promoting LH release. Repeated administration of GnRH agonists promotes downregulation of GnRH-R in the pituitary gland resulting in downregulation of LH expression and finally resulting in castrate levels of testosterone (**Figure *6B***) (Sandow, Von Rechenberg et al. 1978, van Poppel

and Nilsson 2008). Unfortunately, it was recently reported that PCa patients treated with GnRH agonists had higher risk of pulmonary embolism and deep-vein thrombosis (Heidenreich, Bastian et al. 2014). GnRH agonists are frequently combined with AR antagonists, this therapeutic approach is termed combined androgen blockage (CAB) (Pham, Sadowski et al. 2015). Alternatively, the combination of GnRH agonists with radiotherapy resulted in higher 10-years survival when compared to either treatment alone (Widmark, Klepp et al. 2009, Bolla, Van Tienhoven et al. 2010). Similar to radiotherapy, the efficiency of the chemotherapeutic drug docetaxel was also enhanced in combination with the GnRH agonist goserein (Fizazi, Faivre et al. 2015).

GnRH antagonists directly inhibit GnRH receptors in the pituitary gland (**Figure *6B***). In contrast with GnRH agonist, GnRH antagonists do not result in an initial increase in LH and testosterone levels (Klotz, Boccon-Gibod et al. 2008). GnRH antagonist treatment with degarelix resulted in decreased recurrence of PSA elevation (Tombal, Miller et al. 2010) and reduced cardiovascular risk (Albertsen, Klotz et al. 2014).

Upon the discovery of AR in the late 1960s (Anderson and Liao 1968, Bruchovsky and Wilson 1968, Mainwaring 1969), numerous antiandrogens have been developed. Treatment with the steroidal cyproterone was shown to prevent DHT and testosterone binding to AR, however, cyproterone treatment also resulted in loss of libido and impotence, encouraging the research to continue (Wong, Ferraldeschi et al. 2014). In 1989, the non-steroidal anti-androgen flutamide was the first of its class to be approved by the FDA, it acts by competing with DHT for binding to AR (Liao, Howell et al. 1974).

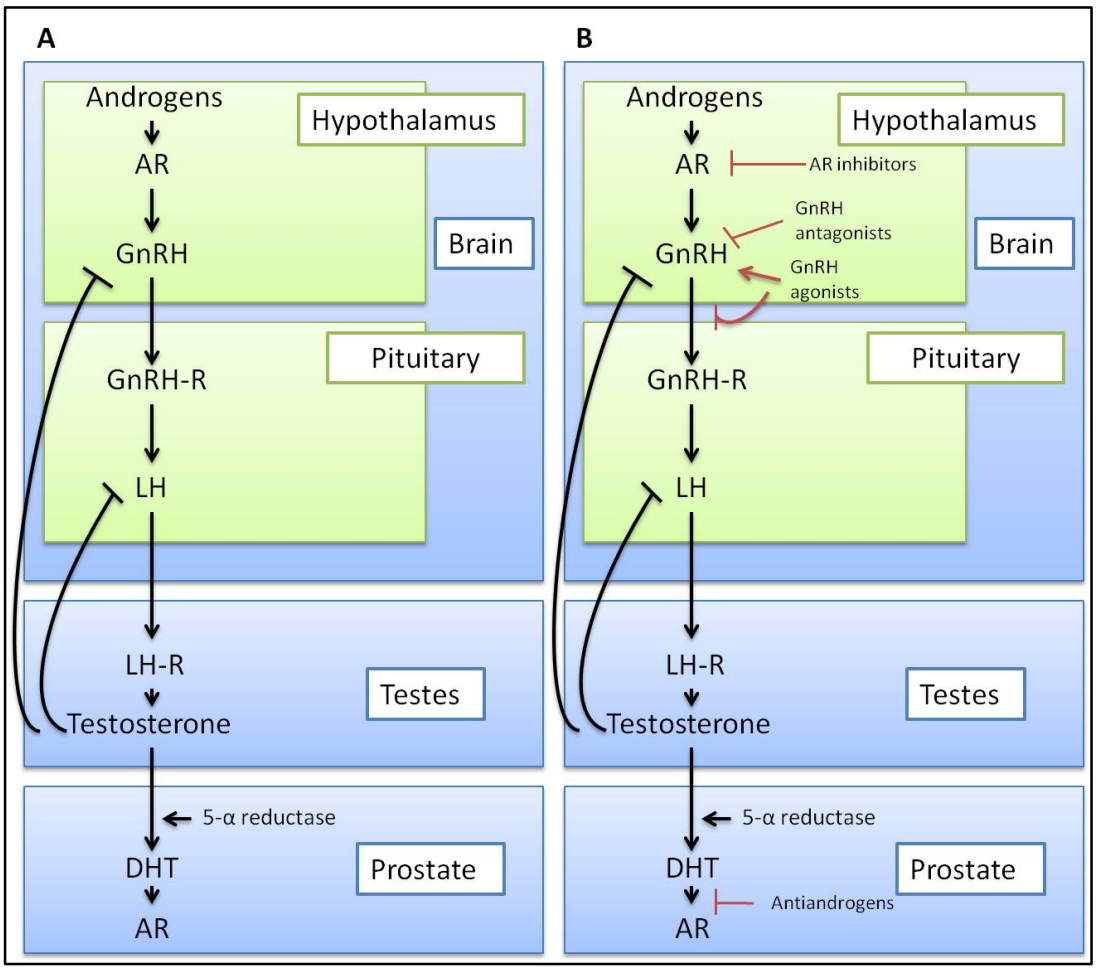

Figure 6. Androgen signalling pathway and ADT. A. Androgen signalling pathway in the regulation of testosterone synthesis and AR activity. **B.** Strategies for ADT (red arrows indicate the mechanism of action of different treatments). LH: luteinizing hormone, GnRH: gonadotropin releasing hormone. GnRH is also called LHRH.

More recently, a new generation of androgen-targeting drugs has emerged. In 2011, Abiraterone was approved by the FDA for treatment of mCRPC in combination with prednisone in patients that have either been treated with docetaxel or have not been treated with any chemotherapy (Danila, Morris et al. 2010, Reid, Attard et al. 2010, Wong, Ferraldeschi et al. 2014). Abiraterone targets the microsomal enzyme CYP17, which is needed for androgen biosynthesis (Wong, Ferraldeschi et al. 2014). The AR antagonist enzalutamide has recently been FDA-approved for treatment of mCRPC after chemotherapy and in chemotherapy naïve mCRPC patients (Beer, Armstrong et al. 2014). Enzalutamide inhibits the action of AR by preventing its nuclear translocation and binding to the DNA (Tran, Ouk et al. 2009).

1.2.4.2 A therapeutic vaccine for prostate cancer

Sipuleucel-T is an autologous therapeutic vaccine, which is directed for treatment of asymptomatic or low-symptomatic CRPC and involves three different concepts. (1) The Granulocyte-Macrophage Colony-Stimulating Factor (GM-CSF) that promotes immune activation. GM-CSF functions as an immune growth and maturation factor that promotes growth and differentiation of antigen presenting cells (APC). (2) The prostatic acid phosphatase (PAP), which is almost exclusively expressed in the prostate, is used to direct the immune response to the prostatic tissue. (3) APC that are extracted from the patient and exposed to a human fusion protein formed by GM-CSF and PAP (Gardner, Elzey et al. 2012, Pieczonka, Telonis et al. 2015). The GM-CSF/PAP fusion protein (PAP C-terminus linked to GM-CSF N-terminus by a Gly-Ser linker) stimulates the patient-extracted APC, which will then present PAP peptides. These stimulated APC, will be injected to the patient where they are expected to promote activation of PAP-specific T-cells. The low-associated risk makes the vaccine suitable to be combined with other CRPC therapies (Gardner, Elzey et al. 2012, Pieczonka, Telonis et al. 2015).

1.2.4.3 Chemotherapy in prostate cancer

Chemotherapy is currently administered to CRPC patients after the failure of other therapies, such as ADT. Chemotherapy treatment in PCa, such as mitoxantrone or docetaxel has been shown to palliate symptoms and reduce pain but has poor effect in improving the survival rate (Carles, Castellano et al. 2012).

Mitoxantrone, combined with low doses of prednisone was the first line of treatment before the introduction of docetaxel (Carles, Castellano et al. 2012). Upon appearance of docetaxel resistance, mitoxantrone is used as a palliative treatment to help improve quality of life and reduce pain (Tannock, de Wit et al. 2004, Carles, Castellano et al. 2012). Mitoxantrone is an anthracenedione agent that acts as a topoisomerase II inhibitor (Pommier, Leo et al. 2010, Wu, Li et al. 2013). Type 2 topoisomerase (Top2) enzymes alter DNA topology by binding to DNA, and producing double strand breaks to promote unwinding during DNA synthesis. As a result, the enzyme forms a covalent bond with the so called Top2 cleavage complex (Top2cc). Finally, DNA is released from the enzyme and the two strands re-joined (Wu, Li et al. 2013). Mitoxantrone maintains the DNA in a cleaved state and prevents the resealing reaction thereby producing DNA double strand breaks (Wu, Li et al. 2013). In addition, mitoxantrone

has been reported to enhance NF-κB transcriptional activity by promoting its binding to DNA, resulting in apoptosis induction (Karl, Pritschow et al. 2009).

Docetaxel and cabazitaxel are currently the first-line chemotherapy treatments for CRPC. Both taxanes act by stabilising microtubules and preventing depolymerisation, resulting in cell cycle arrest and apoptosis (Yue, Liu et al. 2010, Alberti 2013). Taxane treatment affects the mitotic spindle and results in mitotic block, which later results in activation of the apoptotic cascade (Jordan, Wendell et al. 1996).

Docetaxel treatment has been reported to palliate symptoms and decrease PSA levels but its effect on prolonging survival is modest (Dayyani, Gallick et al. 2011). This moderate response to the treatment can be due to defects in cellular apoptosis such Bcl-2 overexpression or PTEN loss, which are commonly found in PCa cell lines, and has been associated with PCa progression in patients (Skjoth and Issinger 2006, Dayyani, Gallick et al. 2011, Powers and Marker 2013). The semisynthetic cabazitaxel is more potent and shows some benefits in patients that had developed resistance to docetaxel (Dayyani, Gallick et al. 2011, Carles, Castellano et al. 2012). Recently, docetaxel has been administered in combination with ADT in non-CRPC patients, improving the efficacy of the treatment (Wong, Ferraldeschi et al. 2014, Fizazi, Faivre et al. 2015).

1.2.5 Treatments for prostate cancer under development

Despite great efforts developing new chemotherapy alternatives, there is no curative treatment for CRPC after docetaxel failure (Carles, Castellano et al. 2012). There is therefore a great need for novel therapies.

Galeterone is an example of a new, under development, therapy for mCRPC. This antiandrogen has a triple mode of action: CYP17 inhibition, AR antagonism and AR degradation and is currently being tested in a Phase III clinical trial against enzalutamine (Bastos and Antonarakis 2016). Safety and efficacy (decreased PSA levels) of galeterone treatment was demonstrated in Phase I and II trials (Bastos and Antonarakis 2016, Montgomery, Eisenberger et al. 2016).

A different example is the immune check point inhibitor Ipilimumab that has been used in clinical trials for various solid cancers, including PCa (Silvestri, Cattarino et al. 2016). Ipilimumab targets the cytotoxic T-lymphocyte-associated protein 4 (CTLA-4) that is expressed in T-cells and down-regulates T-cell activation (Pardoll 2012). Ipilimumab-

mediated targeting of CTLA-4 restores the immune response by depleting regulatory T-cells (Treg). The role of immune check points is to maintain the homeostasis in the immune system, which is commonly achieved by down-regulation of Treg activation. Treg-expressed immunosuppressive cytokines can alter the immune system in cancer patients and check points can be used by tumours to escape from the immune system (Silvestri, Cattarino et al. 2016). Ipilimumab was evaluated in combination with radiotherapy in clinical trials and resulted in an increase in overall survival (Kwilas, Donahue et al. 2012).

Oncolytic adenoviral mutants comprise a promising strategy for treatment of various types of cancers, including PCa. The safety and replication-selectivity has been proven in various clinical trials including patients with PCa (**Table *7*** and **Table *8***). Oncolytic adenoviruses have been engineered to selectively kill cancer cells and its potency has been enhanced following different strategies. In addition, oncolytic viruses have been shown to synergise with chemotherapy drugs (discussed in section 1.4).

1.3 ADENOVIRUS

1.3.1 Classification

Adenovirus (Ad) is a small DNA virus with a linear double stranded DNA of ~36Kb, which is characterised by its non-enveloped icosahedral protein capsid (Russell 2000, San Martin 2012). Due to its broad tropism, adenoviruses are subdivided in 7 species (A - G), which include more than 57 serotypes (**Table 5**) (Russell 2000). Different species can bind to several cellular receptors. The human coxsackie and adenovirus receptor (hCAR) and CD46 are the two main cell surface receptors used by the majority of adenoviral serotypes to attach to the cells, and are expressed in epithelial cells in different tissues in the human body, however some adenoviral serotypes can bind to alternative cellular receptors (Bergelson, Cunningham et al. 1997, Marttila, Persson et al. 2005) (**Table 5**). For example, some species B adenoviruses bind to the desmoglein-2 (DSG-2) receptor (Wang, Li et al. 2011, Arnberg 2012), which is part of the cadherin family, and many species C adenovirus can use, in addition to hCAR, alternative, sometimes unknown receptors, which allow major tropism (Uchino, Curiel et al. 2014).

Infection with adenovirus serotype C in humans usually results in only mild respiratory disease. Infection with Ad4 and Ad14 can, in some cases, develop in acute respiratory disease

(Russell 2009). Ad2 and Ad5, from species C are the most extensively studied for development of oncolytic agents (Leopold and Crystal 2007).

Table 5. Classification of adenoviruses

Species	Serotype/type	Receptor(s)	RGD motif	Tropism
A	12, 18, 31	CAR	Yes	Cryptic (enteric respiratory)
B1	3, 7, 16, 21, 50	CD46, DSG-2, CD80, CD86	Yes	Respiratory, ocular
B2	11, 14, 34, 35	CD46, DSG-2, CD80, CD86	Yes	Renal, respiratory, ocular
C	1, 2, 5, 6	CAR, VCAM-1, HSPG, MHC1-α2, SR	Yes	Respiratory, ocular, lymphoid, hepatic
D	8-10, 13, 15, 17, 19, 20, 22-30, 32, 33, 36-39, 42-49, 51, 53, 54	SA, CD46, CAR	Yes	Ocular, enteric
E	4	CAR	Yes	Respiratory, ocular
F	40, 41	CAR	No	Enteric
G	52	Not determined	Yes	Enteric

Arg-Gly-Asp (RGD), Coxsackie and adenovirus receptor (CAR), Cluster of Differentiation (CD), Desmoglein-2 (DSG-2), heparan sulfate proteoglycan (HSPG), major histocompatibility complex-α2 (MHC1-α2), sialic acid (SA), scavenger receptor (SR), vascular cell adhesion molecule 1 (VCAM-1). Adapted from (Arnberg 2012).

1.3.2 Structure and infection

There are 11 different adenoviral-encoded structural proteins in Ad5 (**Table 6**, **Figure 7**). Structural proteins form part of the encapsidated virus together with several copies of the viral protease, which participates in processing of the capsid precursors prior to assembly (Nemerow, Pache et al. 2009). The viral capsid is composed of the major proteins hexon, penton, fiber and the minor proteins pIX, pIIIa, pVI and pVIII. The pIIIa, pVI and pVIII proteins are cleaved during capsid maturation (Nemerow, Pache et al. 2009). The proteins V, VII and Mu are found associated to the DNA in the viral core. Proteins VII and Mu are also processed

by the viral protease after assembly of virions in the nucleus to modulate the structure of the viral core (Nemerow, Pache et al. 2009).

Adenovirus infection is a two-step process; firstly, the distal C-terminal fiber-knob domain binds onto a cellular receptor, this attachment is followed by a second interaction with cellular integrins, followed by clathrin-mediated internalization. The internalization process is driven by the major capsid proteins. Hexon is the major protein of the capsid, where it acts as the main "building block". The viral capsid contains 240 hexon trimers (Russell 2009, San Martin 2012). A homopentamer termed "penton base" and a homotrimer protein termed "fiber", form a complex that is located at each of the 12 vertex of the icosahedron and is essential for viral internalization (Russell 2009). In order for the virus (Ad5) entry to take place, the C-terminus of the fiber-knob drives the attachment to cell by binding to the cellular receptor CAR (Bergelson, Cunningham et al. 1997, Leopold and Crystal 2007). This interaction causes the fiber to bend, exposing the RGD (Arg-Gly-Asp) loop of the penton base (Wu, Pache et al. 2003), which binds to cellular $\alpha_v\beta3$ and $\alpha_v\beta5$ integrins (***Figure 8***) (Mathias, Wickham et al. 1994, Leopold and Crystal 2007). These interactions trigger downstream PI3K/AKT-mediated activation of Rho family of GTPases and results in virus internalization through clathrin-coated vesicles and endocytosis (Russell 2009). Alternatively, fiber-mediated interaction with the cellular surface has been reported to induce immune inflammatory responses such as activation of extracellular signal-regulated kinases 1 and 2 (ERK1/2), mitogen activated protein kinase (MAPK), c-Jun N-terminal kinase (JNK) and to induce nuclear translocation of NF-kB (Muruve 2004). In adition, the interaction of the RGD (loop of the penton base with integrin $\alpha_v\beta3$ located in the surface of macrophages has been reported to promote interleukin (IL) IL-1α-mediated response (Di Paolo, Miao et al. 2009).

Upon internalization, the acidification of the endosomal pH triggers the disassembly of the protein VI from the virion, which promotes the fragmentation of the membrane and facilitates the virus escape from the endosome (Russell 2009, San Martin 2012). Alternatively to endosomal pH, activation of hCAR and $\alpha_v\beta3$ and $\alpha_v\beta5$ integrins has been shown to directly mediate the exposure of the membrane lytic portion of the protein VI enhancing viral scape from the endosome (Burckhardt, Suomalainen et al. 2011). The reducing conditions within the cytosol have been reported to activate the viral protease, resulting in cleaved of protein

VI, that facilitates the release of the viral genome (Reddy and Nemerow 2014, Kilcher and Mercer 2015).

The partially dissembled virus interacts with cellular dyneins and is translocated though the microtubule network towards the nuclear pore where it completes its disassembly (Leopold and Crystal 2007, San Martin 2012). The viral DNA enters the nucleus where replication of viral DNA and transcription of viral genes takes place (***Figure 8***) (Russell 2009).

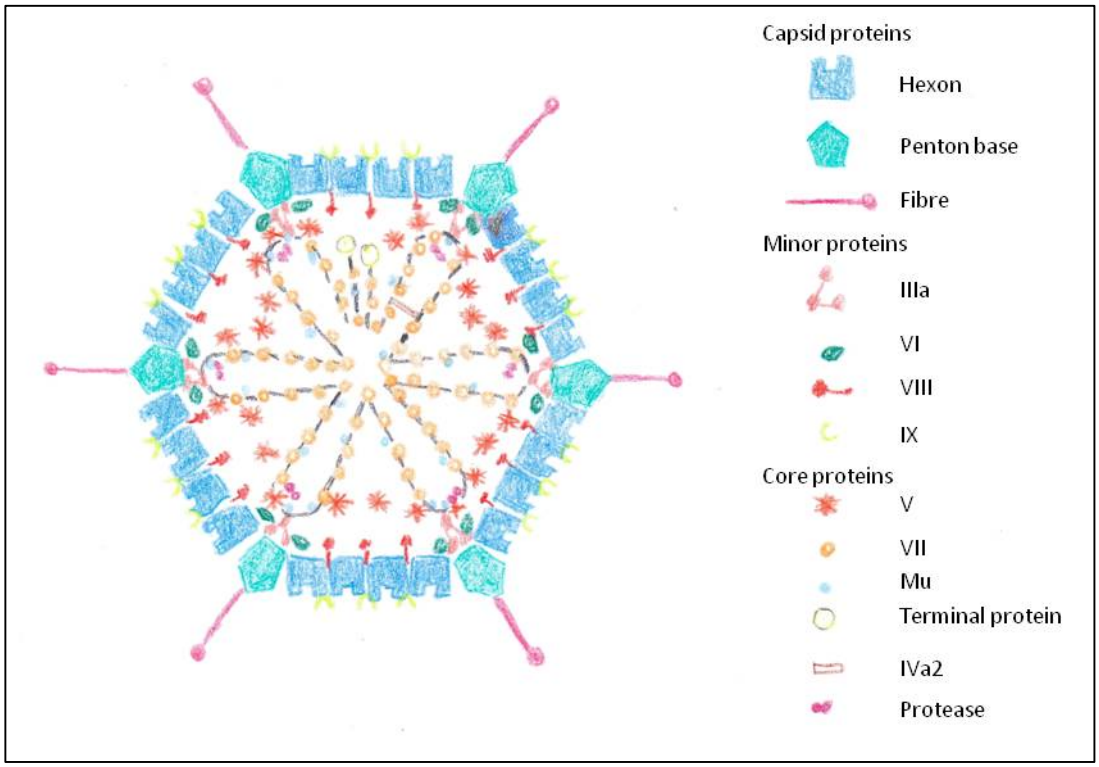

Figure 7. Structure of adenovirus. Schematic representation of adenovirus based on cryo-electron microscopy and crystallography.

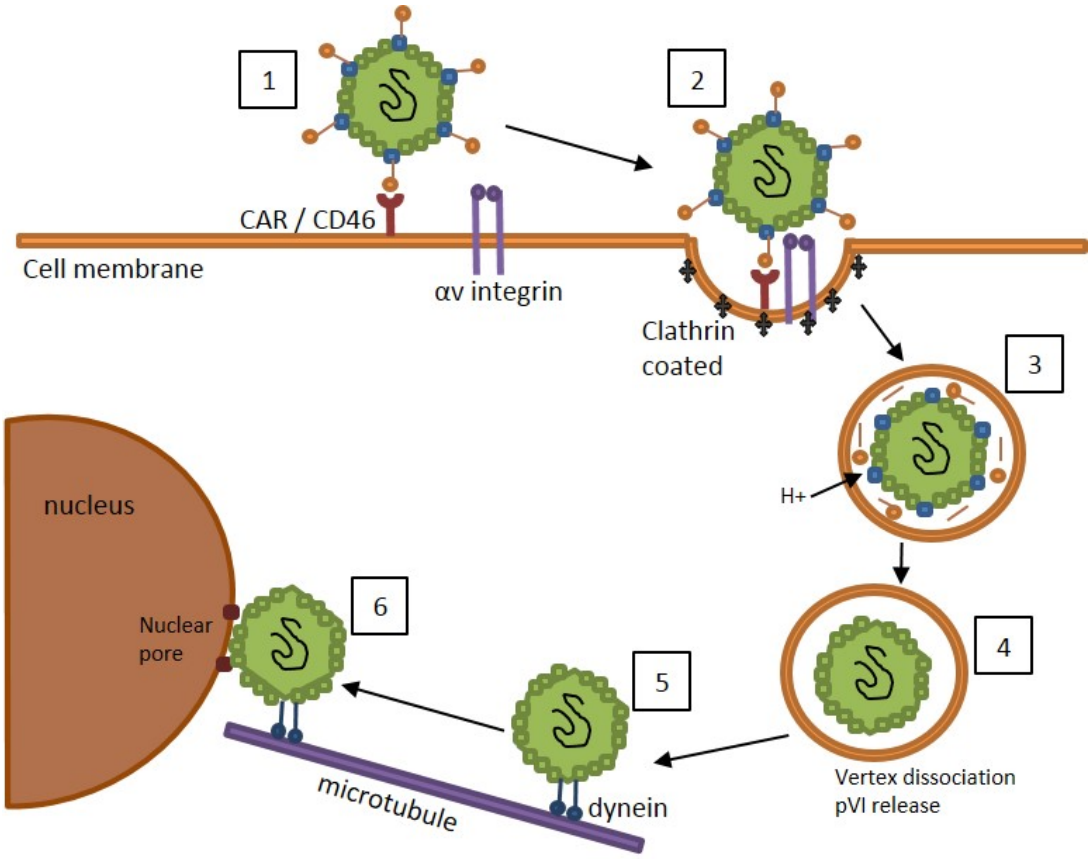

Figure 8. Representation of infection and internalization of adenovirus. (1) Adenovirus attachment to primary cellular receptor (hCAR for Ad5) via hexon protein. (2) Interaction with integrins facilitates clathrin-mediated endocytosis. (3) Start of the dissociation of the virion due to low pH (penton bases, in blue; and fibres, in orange; are the first capsid proteins to be dissociated). (4) Release of polypeptide VI. (5) Dynein-mediated transport of the partially dissembled virion to the nuclear pore. (6) Nuclear import of the viral DNA.

1.3.3 Viral gene transcription

In the viral capsid, DNA is highly condensed and tightly associated with the protein VII, this association in maintained upon infection and until viral transcription takes place (Karen and Hearing 2011). Protein VII-DNA interaction plays a protective role and prevents the activation of the cellular DNA damage response (Karen and Hearing 2011). Once the virion has dissociated and reached the nuclear pore (***Figure 8***), the protein VII – DNA complex is escorted though the nuclear pore by cellular histone H1 (H1), while the remaining components of the capsid stay in the nuclear pore and are finally degraded (Trotman, Mosberger et al. 2001) (Giberson, Davidson et al. 2012). It has been suggested that protein VII must be partially remodelled or removed to allow DNA decondensation and enable the access of the transcription machinery, however some protein must remain to stimulate

transcription. There is still discussion of how this process occurs (Komatsu, Haruki et al. 2011, Giberson, Davidson et al. 2012).

Adenovirus transcription can be temporally divided in two separate events: early transcription takes place before replication of viral DNA while late transcription occurs after viral replication (***Figure 9***) (Russell 2000). The early genes E1A, E1B, E3, and E4 modulate the cell cycle and the cellular DNA damage repair responses to facilitate viral replication. The early genes also alter the cellular immune responses to prevent premature death of the host cell, allowing the virus to replicate and assemble (***Table 6***) (Russell 2000, Berk 2005). Expression of E1A, E1B, E3, and E4 is also required for activation of other viral regions. E2-encoded proteins play a direct role in viral DNA replication (Giberson, Davidson et al. 2012). A major late promoter (MLP) controls the expression of the late L1 to L5 units, which are transcribed in a single transcript that is later processed by alternative splicing (Giberson, Davidson et al. 2012). L1 to L5 units encode for structural proteins. In addition, the IX, IVa2 and the VA RNA I and II are also part of the late transcripts. VA RNA I and II directly play a role in the prevention of the interferon response (Giberson, Davidson et al. 2012). IVa2 plays a role in the activation of the major late promoter (Pardo-Mateos and Young 2004).

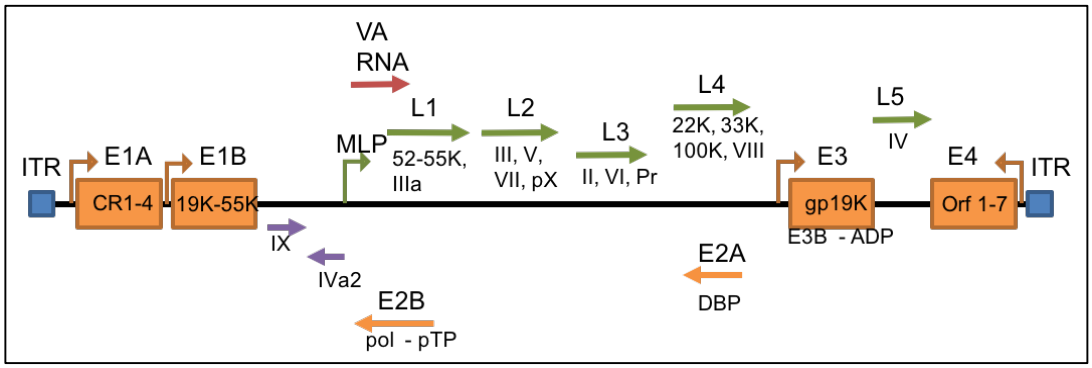

Figure 9. Adenovirus genome. The adenoviral chromosome comprises five early transcription units (E1A, E1B, E2, E3 and E4), showed in orange; two delayed early units (IX and IVa2) in purple, and one late unit under control of the major late promoter (MLP), which encodes for five late mRNA families (L1 to L5), in green. All of them are transcribed by RNA polymerase II. The virus associated (VA) mRNAs, which are transcribed by RNA polymerase III, are shown in red. Arrows show direction of transcription. ITR: Internal terminal repeats.

1.3.4 The role of adenovirus early proteins in modulation of cell cycle

E1A is the first gene to be expressed and is under control of a constitutive promoter (Shenk 2001). The E1A gene contains four conserved regions (CR1, CR2, CR3, and CR4) and encodes

five proteins, which are generated by alternative splicing: 13S, 12S, 11S, 10S and 9S (Stephens and Harlow 1987, Brockmann, Tries et al. 1990, Boulanger and Blair 1991). The smaller 12S protein differs from 13S as 12S lacks the CR3 (***Figure 10B***) (Boulanger and Blair 1991). The large E1A13S protein activates transcription of early viral proteins (Berk 2005). CR1 and CR2 are the E1A regions responsible for inducing the S-phase in the host cell. The cellular transcription factor E2F is normally bound to and repressed by the retinoblastoma protein (pRB) or its family members p130 or p107. Upon pRB phosphorylation in response to growth factors, E2F is released, free E2F activates transcription of several genes promoting cell cycle progression and cell proliferation (Frolov and Dyson 2004). E1ACR2 binds to pRB and releases E2F, therefore inducing S-phase entry (**Figure *10A*** and **Figure *11A***) (Berk 2005).

In addition, E1ACR1 binds to cAMP-response-element-binding-protein-binding protein (CBP) CBP/p300, once recruited CBP/p300 activates transcription of several transcription factors, including p53, NF-κB and c-Myc, through association with histone acetylase transferases (HAT) (**Figure *10A*** and **Figure *11A***) (Berk 2005, Ferreon, Martinez-Yamout et al. 2009, Chang, Hung et al. 2014). Transcriptional activation of E3 and E4 genes is dependent on E1CR3-mediated recruitment of CBP/p300 (Pelka, Ablack et al. 2009). CBP can interact with the anaphase promoting complex/cyclosome APC/C components APC5 and APC7 and promote activation of the APC/C E3 ligase, resulting in controlled sister-chromatid separation and consequent anaphase to metaphase transition. The APC/C tightly controls sister-chromatid separation by promoting the ubiquitination and subsequent degradation of the separase inhibitor, securin (Jia, Kim et al. 2013). Alternatively to its transcriptional activity, E1A-mediated sequestration of p300/CBP has been reported to deregulate APC/C and result in aberrant mitoses, probably by affecting APC/C-mediated regulation of spindle check-points (Turnell and Grand 2012). E1ACR1 has also been shown to interact with both TRRAP and p400 resulting in downstream c-Myc stabilization (**Figure *10A***) (Chinnadurai 2011).

In contrast, the E1A C-terminus negatively regulates oncogenic transformation. E1ACR4 can bind to CtBP and repress its activity (Chinnadurai 2011). More specifically, CtBP can down-regulate expression of the pro-apoptotic PTEN resulting in increased Akt phosphorylation (Chinnadurai 2009). Therefore, E1A-mediated repression of CtBP would prevent PTEN-induced apoptosis. In addition, E1A-CtBP interaction can activate E-cadherin expression by counteracting CtBP transcriptional repression (Arnberg 2012). The E1A C-terminus has also been reported to interact with FOXK1/K2 and DYRK1A/1B resulting in promotion of cell-cycle

exit and epithelial differentiation and inhibition of cell transformation and oncogenesis (**Figure *11B***) (Komorek, Kuppuswamy et al. 2010, Chinnadurai 2011).

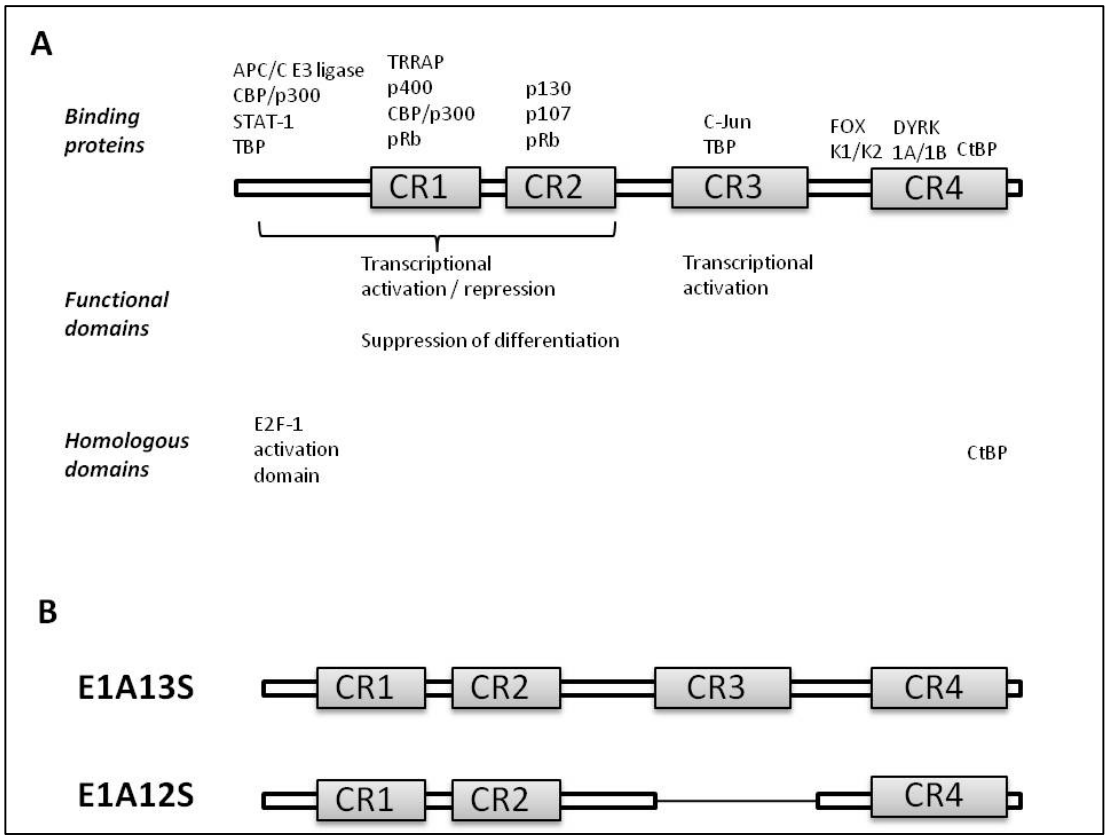

Figure 10. The E1A protein. A. Schematic representation of the E1A protein and some cellular proteins that interact with the E1A proteins. **B.** Differences between the E1A13S and E1A12S proteins.

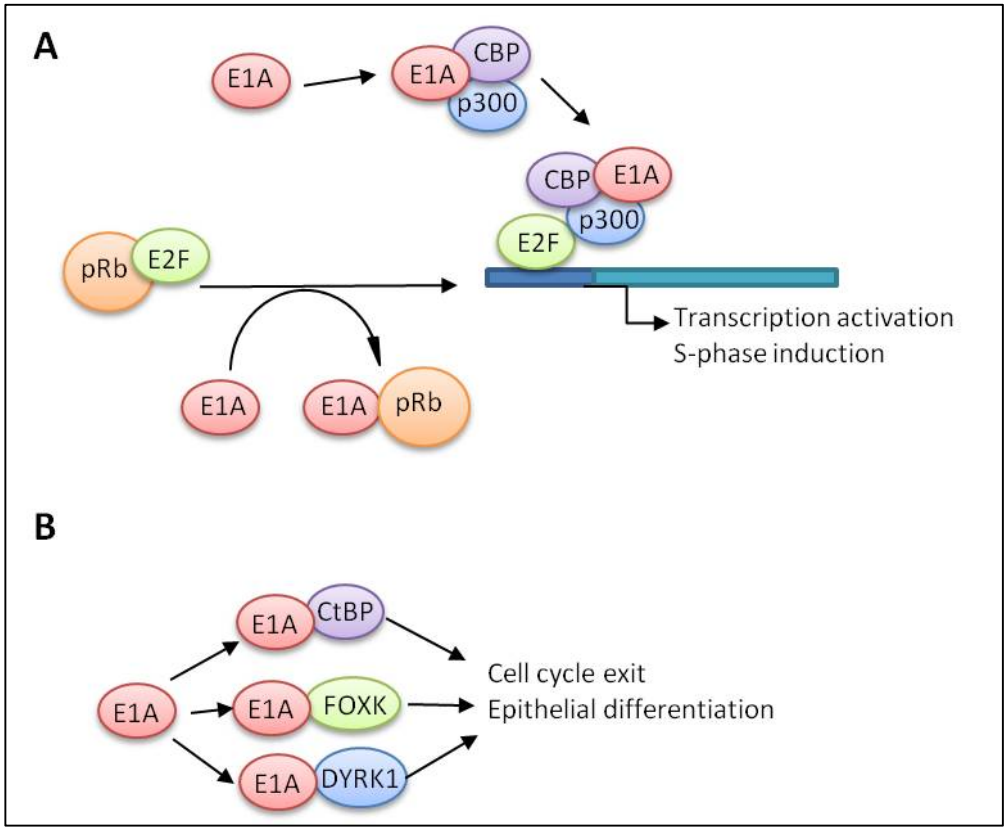

Figure 11. Schematic representation of E1A-mediated regulation of the cell cycle. A. The E1A adenoviral protein promotes S-phase induction by interacting with pRB and p300. **B.** The E1A adenoviral protein promotes cell cycle exit and epithelial differentiation through interaction with CtBP, FOXK1/2 or DYRK1A/1B.

Table 6. Proteins encoded by adenovirus serotype 5

Gene	Protein	Function
E1A	E1A 13S	• Essential for viral replication • Transactivation of viral genes • Binding to multiple cellular factors (See **Figure *10***)
	E1A 12S	• Stabilization of p53 • Binding to multiple cellular factors (See **Figure *10***)
E1B	E1B 19K	• Anti-apoptotic Bcl-2 functional homolog • Possible role in autophagy by binding to Beclin 1 or functions upstream of this pathway
	E1B 55K	• Binding and degradation of p53 • Complex with E4orf6 for mRNA transport to the cytoplasm
E2A	DNA-binding protein	• Chain elongation for DNA replication

E2B	Polymerase	• Viral polymerase: 5'-to-3' polymerase activity and 3'-to-5'-exonuclease activity
	Pre-terminal protein (Pre-TP)	• Binding to 5'-DNA termini • Primer for viral replication
	Terminal protein (TP)	• Core protein. Protects the viral DNA ends by binding to the viral DNA termini
E3	gp19K	• Sequester MHC class I in the endoplasmic reticulum and prevents its expression on the cell surface to prevent recognition by the host immune system (T-cells)
	10.4K/14.5 (RIDα/β)	• Degradation of receptors for Fas-L and TRAIL, preventing apoptosis
	14.7K	• Inhibits TNF-induced apoptosis
	Adenovirus death protein (ADP)	• Promotes cell death to enable virus release (expressed from the mayor late promoter).
E4	E4orf 1	• Promotion of cellular transformation
	E4orf 3	• Inhibits Mre11 → inhibition of MRN complex (DNA-damage response)
	E4orf 4	• Inhibition of E1A activation of E2F
	E4 34K	• Inhibition of cellular non-homologous end joining DNA repair system by degradation of DNA ligase
	E4orf 6/7	• Binding to cellular E2F • Activates E2 promoter • Binding to p53, blocking its transcriptional activity • Inhibition of MRN complex (DNA-damage response) • Inhibits transport of cellular mRNA from the nucleus
IX	Protein IX	• Structural, minor capsid protein. It is located in the outer surface and plays a role in the initiation of the capsid assembly
IVa2	IVa2	• Plays a role in encapsidation by interaction with 52-55K and in the activation of the mayor late promoter
L1	Polypeptide IIIa	• Structural protein. Located under the vertices, inside the virion. Associated with hexon and polypeptide VI. During assembly, it plays a role packaging the viral genome. During uncoating, facilitates the release of the genome
	52/55K	• Required for encapsidation, interacts with IVa2
L2	Penton base (Capsid protein III)	• Structural protein. Located in each of the 12 vertices. Enables virus internalization into the host cell, binds to $\alpha_v\beta3$ and $\alpha_v\beta5$ integrins

	Polypeptide V	• Core protein. It is not clear if either V or Mu promote dissociation of the core proteins from the viral DNA to enable its replication and/or transcription. • Provides a bond between the viral core and the capsid by binding to polypeptide VI or polypeptide VII and the viral DNA
	Polypeptide VII	• Core protein. Tightly binds to DNA. Basic protein. • Mediates viral DNA import into the host nucleus and participates in virus assembly.
	Mu – preMu, (also called protein X or μ)	• Core protein. • The precursor, preMu, can control the shifts to the expression of late viral proteins. • After being cleaved by the viral protease, Mu promotes the packaging of the viral core, which is composed by V, VII and Mu. Cationic protein.
L3	Hexon (Capsid protein II)	• Structural protein. The basic unit that forms the capsid • Binds to factor X
	Polypeptide VI	• Structural protein. Located inside the capsid, associated with polypeptide IIIa and hexon. • Contains an N-terminal amphipathic helix that modifies the curvature of the endosome that contains the virion upon internalization promoting its fragmentation and the escape of the virus from the endosome. Facilitates trafficking to the nucleus.
	Protease	• Core protein. Processes IIIa, VI, VIII, VII and TP
L4	Polypeptide VIII	• Structural protein. Forms a weak bond between the hexon and the rest of the capsid.
	22K	• Plays a role in packaging, regulates the expression of viral proteins by alternative splicing and transition from early to late transcription
	33K	• Plays a role in alternative splicing, regulates gene expression and DNA packaging
	Hexon assembly protein 100K	• Structural protein. Plays a role in the trimerization of hexon protein.
L5	Fiber (Capsid protein IV)	• Structural protein. Located in each of the 12 vertices. Binds to the surface of the host cell receptor CAR

References: (Gallimore and Turnell 2001, Shenk 2001, Horwitz 2004, Hong, Szolajska et al. 2005, Perez-Romero, Gustin et al. 2006, White 2006, Wodrich, Cassany et al. 2006, Baker, Rohleder et al. 2007, Ullman, Reich et al. 2007, Jayaram, Gilson et al. 2008, Russell 2009, Piya, White et al. 2011, San Martin 2012, Wu, Orozco et al. 2012, Wu, Guimet et al. 2013, Bressy and Benihoud 2014, Mangel and San Martín 2014, Biasiotto and Akusjärvi 2015, Klein, Piya et al. 2015).

1.3.5 Viral DNA replication

The replication of the adenoviral genome takes place once the E1A gene products have induced optimal conditions for DNA replication in the host cells, such as S-phase induction, and sufficient E2 gene products have accumulated (Shenk 2001).

The adenoviral DNA carries inverted terminal repeats of about 100bp in each end of the genome. These repeats act as origins of replication, which are identical in both ends (Hoeben and Uil 2013). The viral terminal protein (TP) is covalently attached to each terminal repeat and allows the start of the protein-primed DNA synthesis (Hoeben and Uil 2013). The viral E2-encoded proteins precursor of TP (pTP), viral DNA polymerase and the DNA binding protein (DBP) participate in viral replication together with the cellular transcription factors NFI and Oct-1 (Hoeben and Uil 2013). The pTP protein would be later cleaved by the viral protease to TP prior encapsulation into the virion. The three E2-encoded proteins and the two cellular factors form a pre-initiation complex. DBP, NF1 and Oct-1 promote small changes in the origin structure. In addition, the DBP also binds to ssDNA and protects it from nuclease activity (Kanellopoulos, van der Zandt et al. 1995).

Initiation takes place with the formation of a pTP-trinucleotide intermediate (pTP-CAT) at position 4, pTP-CAT will then jump back 3 positions and get paired with the first 3 nucleotide residues (CAT, at positions 1-3) (King and van der Vliet 1994). pTP-CAT functions as a primer and is later elongated by viral DNA polymerase in the presence of DBP forming a new DNA duplex and displacing the non-template strand (Hoeben and Uil 2013). The newly generated genome copies can be processed and encapsulated in virions or undergo consecutive replication rounds (**Figure *12***).

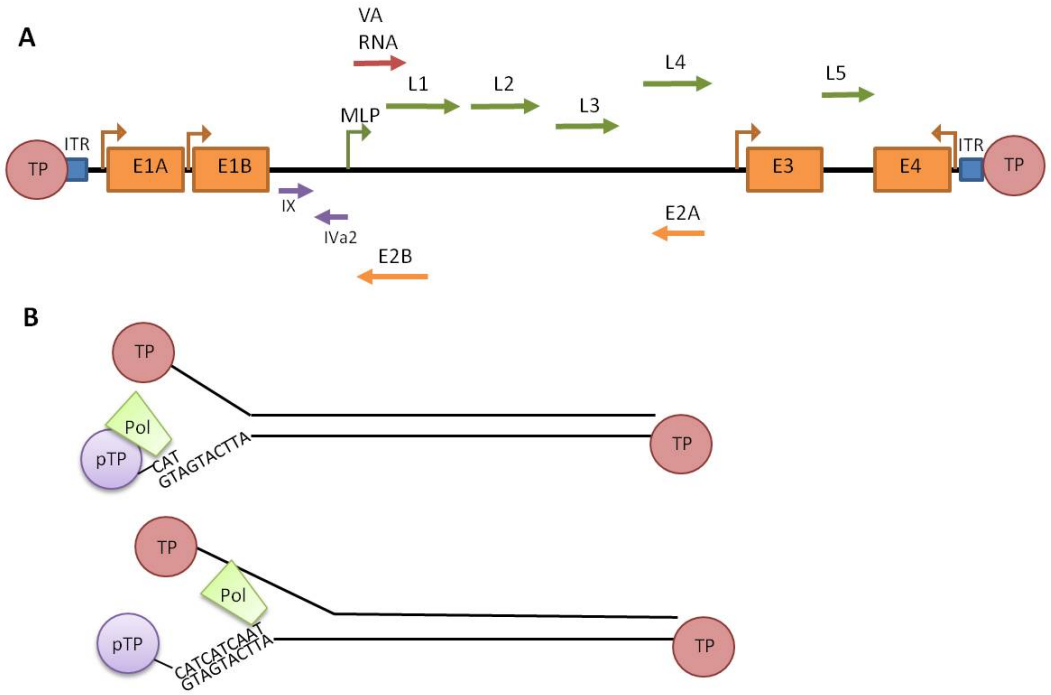

Figure 12. Initiation of adenoviral replication. A. TP protein is bound to each terminal repeat in the adenoviral genome. **B.** Schematic representation of initiation of viral DNA replication. TP remains attached to the DNA end for protection against DNases. pTP acts as a protein primer and forms a trinucleotide intermediate pTP-CAT, which acts as a protein primer and is later elongated. Terminal protein (TP), precursor of terminal protein (pTP), viral polymerase (Pol).

1.3.6 Virion assembly, maturation and lysis

Once the viral genome has been replicated and the viral proteins have been synthesised, new viral particles can be assembled. Two different processes will then take place to complete the production of mature virions, the assembly of the capsid and the encapsulation of the viral DNA.

The mRNA encoding the major capsid proteins hexon, penton and fiber and the four minor capsid proteins IIIa, VI, VIII and X, which are required for capsid assembly, are placed under control of the MLP, encoded by the late transcription units (L1-L5) and are generated by alternative RNA splicing (**Table *6***, **Figure *9***) (Shenk 2001, San Martin 2012). The MLP is active both early and late during infection but its activation is greatly enhanced upon viral replication (Lucas and Ginsberg 1972, Shaw and Ziff 1980). This enhancement in MLP activity takes place by binding of the cellular transcription factor USF/MLTF (Zijderveld, d'Adda di Fagagna et al. 1994). This binding is mediated by the viral IVa2 and L4-22K proteins (Shenk 2001, Backström, Kaufmann et al. 2010). The production of viral proteins is facilitated by

E1B55K and E4orf6. E1B55K can bind to viral mRNA while E4orf6 contains a localization signal that mediates selective export of viral mRNA to the cytoplasm. In addition, E1B55K promotes inhibition of cellular protein synthesis by facilitating export of L4 100K to the cytoplasm. L4 100K prevents the activation of the elF-4F cellular factor, which is responsible of the translation of cellular mRNA (Shenk 2001).

The newly synthesised adenoviral proteins are translocated to the nucleus utilising the nuclear localization signal (NLS) on the viral proteins, where viral particle assembly takes place (Wodrich, Cassany et al. 2006, Mangel and San Martín 2014). The nuclear import of the hexon protein is mediated by protein VI (Wodrich, Cassany et al. 2006). Once in the nucleus, capsid assembly is initiated by the formation of hexon trimers, this interaction is dependent on the L4 100K viral protein, which acts as a scaffold. Hexon assembly is followed by the formation of trimeric fiber structures and the pentameric penton bases (Shenk 2001).

In the encapsidated virus, the viral DNA genome is located in the viral core, inside the icosahedral capsid. This core is composed of the dsDNA genome, the core proteins V, VII and Mu (also called X or μ), the terminal protein (TP) and the adenoviral protease. Packaging of the genomic DNA is mediated by viral proteins IIIa, L1 52/55K, L4 33K, L4 22K and IVa2 (Gustin and Imperiale 1998, Perez-Romero, Gustin et al. 2006, Ma and Hearing 2011, Wu, Orozco et al. 2012, Wu, Guimet et al. 2013).

In the nucleus, a packaging sequence located in the viral dsDNA genome promotes its entry into the capsid. The capsid later undergoes a maturation process that includes cleavage of specific viral proteins (Shenk 2001, Wodrich, Cassany et al. 2006), such as the core proteins VII, Mu, and TP and the capsid proteins IIIa, VI, and VIII, which are synthesised as precursors. These proteins are processed during assembly by the adenoviral protease (Mangel and San Martín 2014). The adenoviral protease is synthesised in an inactive form and is later activated by cleaved pVI (pVIc). How pVI can be cleaved prior activation of the protease is not yet well understood (Baniecki, McGrath et al. 2013). The L1 52/55K protein has been shown to bind to multiple adenoviral proteins such as IIIa and VII, which are processed by the protease (Mangel and San Martín 2014), the ATPase IVa2 (Gustin, Lutz et al. 1996) and to the adenoviral packaging signal (Zhang and Imperiale 2000), but is not found in the mature virion (Hasson, Ornelles et al. 1992). This suggest that L1 52/55K acts as a scaffolding protein (Mangel and San Martín 2014).

Through the studies of differences in structure of a mature (wt) and an immature ts1 (temperature-sensitive) viral particles, better understanding of the maturation process has been reported (Pérez-Berná, Marabini et al. 2009, Silvestry, Lindert et al. 2009) . Polypeptide IIIa and VIII were detected in immature virions in close proximity to the hexon but not in the mature virions indicating that they would later be removed from that position to allow maturation (Pérez-Berná, Marabini et al. 2009). In addition, polypeptide VI was found to interact firmly with hexon in immature virions but this interaction was weakened after protease-mediated VI cleavage in the mature virion. Protein VI cleavage might also allow release of protein VI during infection and internalization. Finally, precursor proteins pVII and pre-Mu were found firmly associated to viral dsDNA, this interaction was loosened in the mature virions (Pérez-Berná, Marabini et al. 2009). It can therefore be concluded that protein cleavage is required for correct maturation of the capsid.

Viral escape from the nucleus is facilitated by changes in the nuclear structure that enable permeabilization of the nuclear membrane. Cellular integrity has been compromised during adenoviral infection by E1B55K-mediated attenuation of cellular protein synthesis. Once in the cytoplasm, damaged cellular integrity facilitates escape of the viral progeny, which takes place through intermediate filaments (Shenk 2001). Adenovirus-mediated cytolysis of infected cells is facilitated by accumulation of the E3-enconded adenovirus death protein (ADP) (Shenk 2001). It has also been suggested that the escape of newly sensitised adenoviral proteins is dependent on active autophagy (Jiang, White et al. 2008).

1.3.7 Modulation of the immune system by adenovirus

Adenovirus can modulate the host immune response by multiple mechanisms. The adenoviral E1A- and E3- encoded proteins attenuate this response while VA RNA I promotes it.

Type 1 interferon (IFN) controls the activation of the anti-viral response in non-infected cells surrounding the site of infection (Zhu, Huang et al. 2007). IFN activation can be promoted by the detection of viral DNA in the cytoplasm by the cytosolic DNA sensor cyclic GMP-AMP (cGAS) (Anghelina, Lam et al. 2016). The E1A adenoviral protein inhibits IFN-mediated response by preventing transcription of its target genes, possibly by competition for p300/CBP binding (Leonard and Sen 1996, Look, Roswit et al. 1998). p300/CBP can bind to STAT1 and activate transcription of IFN (Zhang, Vinkemeier et al. 1996). E1A has been suggested to compete with STAT1 for p300/CBP binding, but also to directly interact with

the STAT1 protein at its N-terminus, resulting in IFN-mediated downregulation (Look, Roswit et al. 1998). Ad12 E1A can also modulate the immune response by preventing NF-κB activation. E1A was reported to prevent protein kinase A catalytic subunit (PKAc) – mediated phosphorylation of NF-κB resulting in decreased transcription and activity of MHC class I (Guan, Jiao et al. 2008). In addition, E4 orf3 has been proposed to inhibit IFN response by promoting promyelocytic leukemia (PML) protein rearrangements and therefore facilitate viral replication in the presence of activated IFN response (Ullman, Reich et al. 2007).

The E3-encoded proteins are not essential for viral replication *in vitro* but play an important role in the modulation of the immune response *in vivo* (Windheim, Hilgendorf et al. 2004, Sester, Ruszics et al. 2013). The E3gp19K viral protein is a transmembrane glycoprotein that is found located in the endoplasmic reticulum (Burgert, Ruzsics et al. 2002) and can attenuate the host immune response by hampering antigen presentation. Expression of E3gp19K blocks the transport of MHC class I to the plasma membrane to prevent activation of cytotoxic T-cells and reduces the levels of cell surface receptors for natural killer cells (Burgert, Maryanski et al. 1987, McSharry, Burgert et al. 2008). E3gp19K has been shown to tightly bind to MHC class I and to prevent the correct processing and presentation of the antigens (Burgert, Maryanski et al. 1987, Cox, Bennink et al. 1991). E3gp19K has also been reported to reduce the recognition of infected cells by natural killer cells (NK). E3gp19K mediates the intracellular sequestration of MHC-I-related chain A and B (MICA/B) molecules in the ER, which are ligands for the major NK receptor NKG2D (McSharry, Burgert et al. 2008). Furthermore, deletion of E3gp19K promotes activation of the host immune response by enhancing tumour antigen presentation (Wold and Gooding 1989, Hermiston, Tripp et al. 1993, Halldén, Hill et al. 2003, Wang, Hallden et al. 2003).

The virus-associated RNAs (VA RNA) are adenoviral non-coding RNAs that accumulate in the cytoplasm of the infected cell to very high levels (10^8 copies/cell) (Mathews and Shenk 1991, Vachon and Conn 2016). VA RNA I is the most abundant and has been reported to modulate the host immune response by multiple mechanisms. Activation of the cellular protein kinase RNA-activated (PKR) protein occurs upon detection of dsRNA within the cytoplasm, which is characteristic of viral infection either by transcription overlapping mRNA from DNA viruses or by detection of dsRNA viruses (Vachon and Conn 2016). VA RNA I inhibits PKR, preventing PKR-mediated shut down of cellular transcription and therefore facilitating transcription of viral genes (Maran and Mathews 1988). VA RNA I has also been associated with promotion

of the IFN response. VA RNA I is partially double stranded and is recognised by retinoic acid-inducible gene I (RIG-I), which leads to IFN induction (Minamitani, Iwakiri et al. 2011).

1.4 ONCOLYTIC ADENOVIRUSES IN CANCER THERAPY

The clinical use of adenovirus serotype 5 (Ad5) for oncolytic therapy has been widely studied in the past two decades. Ad5 is well characterised, can be produced and purified to high titres, is relatively easy to engineer, presents natural tropism for epithelial cells and adenocarcinomas and its pathogenesis is associated with only mild disease (de Vrij, Willemsen et al. 2010, Arnberg 2012). In addition, Ad5 does not integrate into the human genome (Yamamoto and Curiel 2010, Hallden 2013). Ad5 has been engineered to selectively replicate and lyse cancer cells with replication greatly attenuated in healthy cells (Rodriguez, Schuur et al. 1997, Fueyo, Gomez-Manzano et al. 2000, You, Yang et al. 2000, Oberg, Yanover et al. 2010).

1.4.1 Replication-selective adenoviruses

Human adenoviruses species C have natural tropism for epithelial cells in multiple tissues in the body, such as the respiratory, ocular renal and hepatic tissues (Arnberg 2012). When engineering oncolytic adenoviruses, it is necessary to ensure that the mutant is designed to have its infection or replication restricted to cancer cells. Replication-selective oncolytic viruses are engineered so that they would only replicate in target cancer cells but not in normal healthy cells. Replication-selective adenoviruses can be engineered following two different approaches (Bressy and Benihoud 2014).

In the first approach, replication-selectivity in tumour cells is achieved by specific deletions in the adenoviral genome termed complementation deletions, that are required for replication in normal cells but not in cancer cells (such as proteins involved in cell cycle and apoptosis) (Halldén and Portella 2012, Bressy and Benihoud 2014). Replication-selectivity is frequently achieved with specific deletions in the E1-region of the adenovirus genome, which encodes proteins that are responsible for binding to key cellular factors such as p53 or pRB (Bressy and Benihoud 2014). E1B55K-deleted oncolytic adenoviral mutants were the first to be developed and are defective in p53-binding and therefore unable to avoid p53-induced cell cycle arrest in normal cells. E1B55K-deleted mutants were engineered to replicate in cells either defective in p53 or with upstream or downstream mutations such as $p14^{ARF}$ and Bax,

respectively. However, it was later demonstrated that E1B55K-deleted mutants could replicate independently of the p53 status (Goodrum and Ornelles 1998). In addition, decreased replication was also observed in tumours infected with E1B55K-deleted mutants. It was later reported that E1B55K, together with E4orf6, was also required for nuclear export of viral mRNAs, which could explain reduced effectiveness of these mutants (O'Shea, Johnson et al. 2004). The mutant *dl*1520, also known as Onyx-015, and the mutant H101 (both E1B55K- and E3B-deleted) are examples of replication-selective viruses carrying the E1B55K-deletion (You, Yang et al. 2000, Lu, Zheng et al. 2004). Due to the attenuated replication observed in the E1B55K-deleted mutants, a second generation of adenoviral mutants were engineered to be defective in E1A-binding to pRb, by deleting the E1ACR2 domain. The *dl*922-947 (Heise, Hermiston et al. 2000) and AdΔ24 (Fueyo, Gomez-Manzano et al. 2000) are examples. Various E1ACR2-deleted mutants have been reported to result in greater efficacy *in vivo* when compared to E1B55K-deleted mutants (Lockley, Fernandez et al. 2006, Radhakrishnan, Miranda et al. 2010).

In the second approach, tumour-selectivity is achieved by placing the viral genome under control of a tumour-specific promoter (Rodriguez, Schuur et al. 1997, Huang, Savontaus et al. 2003, Hallden 2013, Bressy and Benihoud 2014). The E1A gene is the first to be expressed upon infection (Berk 2005) and has often been placed under control of tissue- of tumour-specific promoters. In the CV787 virus, the E1 genes are placed under control of two prostate-specific response elements, which are regulated by active AR and are upregulated in PCa. In this mutant, the PSA promoter and enhancer controls the expression of the E1A protein while the E1B gene is under control of the promoter/enhancer of the hKLK2 (human glandular kallikrein-2, a human prostate-specific gene) (Rodriguez, Schuur et al. 1997, Yu, Chen et al. 1999, D'Amico, Whittington et al. 2000, Yu, Chen et al. 2001). Transcription of the telomerase gene is upregulated in the majority of cancers (Shay and Wright 2011) and in the Adv-TERTp-E1A mutant, tumour selectivity was achieved by having the expression of E1A controlled by the human telomerase reverse transcriptase (hTERT) promoter (Huang, Savontaus et al. 2003, Nemunaitis, Tong et al. 2010).

1.4.2 Oncolytic-adenoviruses armed with therapeutic transgenes

A different approach for oncolytic viral therapy is the use of viruses as carriers for transgenes of pro-drug converting enzymes. This approach is also called suicide gene therapy. The transgene can replace the E1A or the E3 genes, resulting in a non-replicating or replication-

selective virus, respectively (Doronin and Shayakhmetov 2012, Sweeney and Halldén 2016). An example of this approach is the non-replicating adenoviral vector ADV/RSV-TK, which expresses the thymidine kinase (TK). TK converts the non-toxic ganciclovir or acyclovir into toxic metabolites that can be incorporated in the DNA and result in termination of DNA chain elongation. ADV/RSV-TK has been tested for treatment of prostate cancer in clinical trials (***Table 6***) and resulted in increased apoptosis, activation of local and systemic immune response and antiangiogenic effects (Ayala, Satoh et al. 2006).

1.4.3 Combination of oncolytic adenoviruses with chemotherapy

Although the safety of replication-selective adenoviruses was proven in numerous clinical trials (**Table *7*** and **Table *8***), single agent treatment with oncolytic adenoviruses resulted in only moderate efficacy (Russell 2009, Goldufsky J 2013, Bressy and Benihoud 2014). Interestingly, the treatment efficacy was increased when replication-selective adenoviruses were combined with chemotherapy (Liu and Kirn 2007, Bressy and Benihoud 2014).

1.4.3.1 Mitotic inhibitors

Taxanes, such as paclitaxel or docetaxel prevent microtubule-depolarization, arresting the cell cycle and triggering apoptosis (Jordan and Wilson 2004). The combined treatment of paclitaxel and Onyx-015 resulted in synergistic effects in the treatment of non-small cell lung cancer (NSCLC) *in vitro* in cell lines and primary cultures obtained from lung cancer patients (You, Yang et al. 2000). The combination of docetaxel or paclitaxel with CV787, in which E1A and E1B are placed under control of PSA and hKLK2 promoters, respectively; was reported to synergistically enhance cell death in LNCaP prostate cancer cells (Yu, Chen et al. 2001). CV787-induced synergistic cell killing was suggested to be due to increased viral production and E1A-mediated sensitization to docetaxel.

1.4.3.2 Anti-metabolites

Anti-metabolites can alter nucleotide synthesis by targeting different key enzymes implicated in nucleotide production (Bressy and Benihoud 2014). 5-fluorouracil (5-FU), in combination with Onyx-015, resulted in tumour regression in HCT116 colon xenografts (Heise, Sampson-Johannes et al. 1997). This combined treatment was tested in clinical trials (discussed in section 1.4.4). The combination of OBP-301 (Telomelysin®, E1A and E1B regions under control of hTERT promoter) with gemcitabine resulted in synergistic cell killing both *in*

vitro and *in vivo* in H460, H322, H358 lung cancer cell lines (Liu, Kojima et al. 2009). The synergistic effect was caused by OBP-301-mediated S-phase entry, which was suggested to sensitise infected cells to gemcitabine.

1.4.3.3 Platinum salts

Platinum salts, such as cisplatin, induce the formation of intra- or inter-strand cross-links in the DNA resulting in apoptotic cell death (Bressy and Benihoud 2014). Onyx-015, in combination with cisplatin resulted in increased survival of mice with head and neck H358 xenografts (Heise, Sampson-Johannes et al. 1997). Alternatively, the combination of OBP301 with cisplatin resulted in sensitization of ovarian cancer cells and reduced tumour growth in mice with SKOV3 xenograft tumours (Takakura, Nakamura et al. 2010). In addition, the mutant SG511, an oncolytic virus with Ad5/11 chimeric fibre and E1B55K deletion, for improved infection and replication selectivity respectively; synergistically enhanced cisplatin-induced cell death in HeLa and HT-29 cells by down-regulating Mcl-1 expression and promoting apoptosis (You, Wang et al. 2012).

1.4.3.4 Topoisomerase inhibitors

Treatment with topoisomerase inhibitors induces double strand breaks promoting cell cycle arrest in the G2-phase (Clifford, Beljin et al. 2003). The combination of the AdΔ24 with the topoisomerase I inhibitor irinotecan resulted in enhanced anticancer effect both *in vitro* (in U-85 MG and U-25 MG human glioblastoma cell lines) and *in vivo* (Gomez-Manzano, Alonso et al. 2006). This enhanced cell killing was suggested to be due to AdΔ24-mediated upregulation of topoisomerase I expression and activity and accumulation of cells in S-phase. Enhancement of cell death was also detected in esophageal carcinoma (Ma, Kawamura et al. 2010) and in my group in prostate carcinomas (Radhakrishnan, Miranda et al. 2010) when Onyx-015 was combined with the topoisomerase II inhibitors Vp-16 (etoposide) or mitoxantrone.

We have previously demonstrated that the mutant *dl*922-947 (E1ACR2- and E3B- deleted), synergistically enhanced mitoxantrone- and docetaxel-induced cell death *in vitro* (in PC3, DU145 and LNCaP PCa cells) and *in vivo* in PC3 and DU145 xenografts (Radhakrishnan, Miranda et al. 2010). The combination of *dl*922-947 with mitoxantrone or docetaxel resulted in increased viral uptake and E1A expression. In addition, previous work in my team demonstrated that intratumoural administration of the AdΔΔ oncolytic mutant (E1ACR- and

E1B19K-deleted) caused synergistic cell killing in combination with mitoxantrone or docetaxel in PCa cells and promoted tumour regression in murine PC3 and DU145 xenografts (Oberg, Yanover et al. 2010).

1.4.4 Oncolytic adenoviruses in clinical trials

So far, the clinical use of replication-selective adenoviruses in combination with chemotherapies for cancer treatment has only been approved in China for the replication-selective E1B55K- and E3B-deleted mutant H101 (Lu, Zheng et al. 2004, Garber 2006). Treatment with H101 virus (produced by Shanghai Sunway Biotech) in combination with the chemotherapy agent cisplatin and 5-FU successfully passed a phase III clinical trial for head and neck cancers in China (Xia, Chang et al. 2004, Hughes, Alusi et al. 2015). The combination of H101 with the chemotherapeutic treatment resulted in a response rate of 78.8% of patients, compared to 39.6% for single chemotherapeutic treatment.

However, there are several more recently developed replication-selective adenoviruses that are currently being tested in clinical trials for treatment of different cancers, including prostate cancer, some of them in combination with chemotherapy (**Table *7***).

The Ad5/3-Δ24, which carries a Δ24 deletion in the E1A region and cannot bind to pRB, has been tested in different clinical trials. In the mutant Ad5/3-Δ24 the Ad5 fiber has been modified with the addition of the Ad3 knob and showed enhanced selectivity to DSG-2-expressing ovarian cancer cells, when compared to hCAR-binding Ad5 virus (Kanerva, Mikheeva et al. 2002, Wang, Yumul et al. 2013). Ad3 can bind to DSG-2 and therefore facilitated viral infection (Wang, Li et al. 2011). A phase I clinical trial in recurrent ovarian cancer proved the safety and potential anti-tumour efficacy of Ad5/3-Δ24 (Kim, Dmitriev et al. 2013). Another phase I trial using AdΔ24-RGD, which carries a modified fibre with the RGD polypeptide for targeting of αvβ3- and αvβ5-integrins (Jiang, Gomez-Manzano et al. 2009), for treatment of recurrent malignant gliomas has been completed although the results have not yet been reported (Genesys 2005). More recently, the AdΔ24-RGD mutant was evaluated in a phase I trial for ovarian cancer patients (Kimball, Preuss et al. 2010), that proved its safety but reported low efficacy.

A Telomerase-specific adenovirus (Telomelysin), in which the viral genome is under control of the hTERT promoter, has completed a phase I trial confirming safety and activity in various solid tumours (Nemunaitis, Tong et al. 2010). In addition, Telomelysin is currently being

tested in a Phase I/II clinical trial for hepatocellular carcinoma patients (Oncolys BioPharma 2014).

Table 7. Selected clinical trials with oncolytic adenoviral mutants

Vector	Modifications	Disease	Administration	Results reported
H101 (Lu, Zheng et al. 2004, Hughes, Alusi et al. 2015)	Conditionally-replicating E1B55K and E3B deletions	Head and neck cancer	Daily intratumoral injection during 5 consecutive days in combination with cisplatin and 5-fluorouracil (5FU)	Successfully passed a phase III clinical trial resulting in 78.8% response rate (39.6% for patients treated with chemotherapy only) Approved for use in clinic (China)
AdΔ24-RGD (Kimball, Preuss et al. 2010)	Conditionally-replicating: E1ACR2-deletion (Δ24) Addition of RGD sequences in the fiber-knob	Epithelial ovarian or primary peritoneal adenocarcinomas (21 patients)	Single Intratumoral injection	Phase I study. Overall safety was reported AdΔ24-RGD replication was detected
Ad5/3-Δ24 (Kim, Dmitriev et al. 2013)	Conditionally-replicating: E1ACR2-deletion (Δ24) Addition of Ad3 fiber-knob	Ovarian cancer (10 patients)	Daily intratumoral catheter during 3 consecutive days	Phase I study Overall safety was reported Ad5/3-Δ24 replication was detected
Telomerase-specific Replication Competent Oncolytic Adenovirus (Telomelysin) (Nemunaitis, Tong et al. 2010)	E1A expression under control of the (hTERT) promoter IRES insertion before E1B gene	Various solid tumours (16 patients)	Single intratumoral injection	Phase I study Doses well tolerated. Suggested evidence of antitumour activity

Abbreviations: IRES (internal ribosomal site), hTERT (human telomerase transcriptase gene).

1.4.5 Oncolytic adenoviruses for treatment of prostate cancer

Oncolytic adenoviral mutants have been tested in clinical trials for patients with early stage, localised PCa and locally recurrent PCa after radiotherapy or CRPC (**Table *8*** and **Table *9***). Adenovirus was first used in PCa clinical trials as replication-defective vectors carrying suicide genes. These trials reported low toxicity of the treatment and flu-like only side effects, reviewed in (Schenk, Essand et al. 2010). The mutant Ad5-CD/TKrep (E1B55K-deleted), which carries a fusion gene encoding for the cytosine deaminase (CD) and the herpes simplex virus type-1 thymidine kinase (HSV-1 TK), which confer sensitivity to 5-FC and ganciclovir, respectively is one example of double-suicide therapy (**Table *8***) (Freytag, Rogulski et al. 1998).

More recently, replication-selective adenoviruses were used in clinical trials targeting PCa. Two phase I trials evaluating the CV706 or the CG7870 (previously named CV787), whose genomes are under control of PSA-regulated promoters, have been completed. From trials in locally recurrent radiotherapy-treated PCa and CRPC it was concluded that the viruses were safe and PSA levels decreased (DeWeese, van der Poel et al. 2001, Small, Carducci et al. 2006). A phase I/II clinical trial for CRPC evaluating CV787 in combination with docetaxel and pacitaxel has been completed, although no results have been reported (Yu, Chen et al. 2001, 2005). Freytag and colleges carried out several clinical trials using Ad5-CD/TKrep mutants with reported positive responses and safety (**Table *8***) (Freytag, Khil et al. 2002, Freytag, Stricker et al. 2003, Freytag, Movsas et al. 2007, Freytag, Stricker et al. 2007). In a different study, the Ad-OC-TK vector, in which TK expression is under control of the osteocalcin promoter, was tested in a Phase I/II clinical trial and resulted in reduced pain in CRPC patients with bone metastasis (**Table *8***) (Terao, Shirakawa et al. 2009).

Table 8. Completed clinical trials in prostate cancer patients using adenoviral mutants

Vector	Modifications	Disease stage	Administration	Results reported
Ad5-CD/TKrep + 5-FC + GCV (Freytag, Rogulski et al. 1998)	Conditional replication: E1B55K deletion + suicide therapy (cytosine and thymidine kinase) E3 deletion	Intermediate- to high-risk PCa (15patients) (Freytag, Stricker et al. 2003)	One intraprostatic injection cycle + radiotherapy	Positive interaction as an adjuvant administered prior radiation
		Locally recurrent PCa after radiotherapy (16 patients) (Freytag, Khil et al. 2002), (Freytag, Stricker et al. 2007)	One intraprostatic injection cycle	Decrease in PSA level in 10 patients. 2 years delay on average in the start of ADT
CV706 (DeWeese, van der Poel et al. 2001)	Prostate-specific replication: E1A is under control of PSA promoter. E3B deletion	Locally recurrent PCa after radiotherapy (20 patients)	One intraprostatic injection cycle	< 50% decrease of PSA levels in serum in 5 patients (which lasted for 4 weeks in 4 patients)
CG7870 (Small, Carducci et al. 2006)	Prostate-specific replication: E1A and E1B are under control of hKLK2 and PSA promoter respectively. E3 expression	CRPC (23 patients)	One intravenous injection cycle	No dose-limiting toxicity observed (the dose up to $6x10^{12}$ viral particles). <25-49% decrease of PSA levels in serum in 5 patients
HSV-TK + Ganciclovir **(Ayala, Satoh et al. 2006)**	Non-replicative: E1-E2 deleted. TK expression controlled by the Rous sarcoma virus long terminal repeats promoter	Clinically localysed PCa with high risk of recurrence (23 patients)	One to four intraprostatic injections	Activation of local and systemic immune response, antiangiogenic effect and upregulation of apoptosis

Ad5-yCD/mutKr$_{SR39}$rep-ADP + 5-FC + GCV (Freytag, Movsas et al. 2007)	Conditional replication: E1B55K deletion + suicide therapy (cytosine and thymidine kinase) E3 deletion	Intermediate- to high-risk PCa (9 patients)	One or two intraprostatic injection cycle + radiotherapy	Overall decrease in tumour-positive post-treatment biopsies
Ad-OC-TK + Valacyclovir **(Terao, Shirakawa et al. 2009)**	Non-replicative: E1A gene replaced by herpes simplex virus thymidine kinase gene under control of osteocalcin promoter	CRPC with or without bone metastasis (6 patients)	One injection. Directly injected in the localysed tumour or bone metastases.	Reduced pain, correlated with decreased PSA

Abbreviations: 5-FC (5-fluorocytosine), AFP (adenovirus death protein), ATP (androgen deprivation therapy), CD (cytosine deaminase), GCV (ganciclovir), TK (thymidine kinase), herpes simplex virus type-1 thymidine kinase (HSV-1 TK).

1.4.5.1 Oncolytic immunotherapy in PCa

A novel promising strategy comprises the stimulation of the host immune response with the aim to direct the response to target and eliminate cancer cells. Oncolytic viral mutants can be designed to express cytokines that redirect the host immune system to infected cancer cells. Numerous mutants have been constructed to express GM-CSF, or interleukins IL-12, IL-24, CD40L and FLT3L (**Table *9***) (Mukhopadhaya, Mendecki et al. 2007, Pesonen, Diaconu et al. 2012, Kim, Lee et al. 2013, Yang, Xue et al. 2014, Freytag, Zhang et al. 2015, Sarkar, Quinn et al. 2015). As an example, Freytag and colleges developed the Ad5-yCD/mutTKSR39rep-hIL12 that expresses TK, together with IL-12 (Freytag, Zhang et al. 2015). IL-12 is a proinflammatory cytokine that activates innate and adaptive immune responses by promoting antigen presentation (Leonard, Sherman et al. 1997).

Table 9. Oncolytic mutants currently being tested in clinical trials for prostate cancer.

Vector	Modifications	Disease stage (number of patients)	Administration
Ad5-yCD/ mutTK(SR39)rep-hNIS (Phase I) **(Barton, Stricker et al. 2011)**	Replication-selective: E1B55K deleted. Fusion gene of E1 and CD and TK. hNIS replaces E3 region. All inserts under control of human cytomegalovirus promoter.	Clinically localised PCa. (6 patients)	One intraprostatic injection at multiple sites + intravenous administration of $Na_{99}mTcO_4$
Ad5-yCD/ mutTK(SR39) rep-hIL12 (Phase I) **(Freytag, Zhang et al. 2015, Stricker 2015)** **NCT02555397**	Replication-selective: E1B55K deleted. HSV-1 TK_{SR39} fusion gene (yCD/mutTK$_{SR39}$) in the E1 region and a single-chain murine IL-12 gene in the E3 region	Clinically localised PCa with high risk of recurrence (Recruiting, 15 patients estimated)	Single intraprostatic injection + radiotherapy
CTL104/GM-CSF (AdNRGM) (Phase I) **(Searle, Mautner et al. 2015)** **UKCRN study ID: 13599**	NTR activates the prodrug CB1954; GM-CSF activates antitumor immune responses	Not published	Locally relapsed PCA; intraprostatic injection + intravenous administration of CB1954

Adapted from (Sweeney and Halldén 2016). Abbreviations: hNIS (human sodium iodide symporter), 5-FC (5-fluorocytosine), CD (cytosine deaminase), TK (thymidine kinase), GM-CSF (Granulocyte-macrophage colony-stimulating factor).

1.4.6 Administration of oncolytic adenoviruses

Efficient delivery of oncolytic viruses to target cancer cells is essential to achieve treatment efficacy. Administration of oncolytic viruses can be performed following two different strategies: intratumoural administration or systemic vascular delivery (de Vrij, Willemsen et al. 2010). The intratumoral delivery is the most commonly used administration method for oncolytic adenoviral mutants in PCa treatment. Adenoviral infection is dependent on the expression of the adenoviral receptor. hCAR is usually expressed in low levels in many cancer cells, including PCa, hampering viral infection (de Vrij, Willemsen et al. 2010, Sweeney and Halldén 2016). In addition, the stromal compartment and the extracellular matrix forms a physical barrier that hampers viral transduction into cancer cells and the spread of viral

vectors (Kuppen, van der Eb et al. 2001). Destruction of the matrix with collagenase or metalloproteinases has been reported to enhance distribution of oncolytic herpes-viruses (McKee, Grandi et al. 2006). Some clinical trials for oncolytic adenoviruses in PCa have used multiple injections to improve viral transduction but did not report any significant difference in treatment efficacy, when compared to single administration (Ayala, Satoh et al. 2006, Freytag, Movsas et al. 2007).

Systemic administration would enable virus to reach metastatic lesions, however this is currently less feasible with adenovirus based mutants. In addition to the difficulties to overcome the stromal barrier surrounding the blood vessels, oncolytic adenoviral vectors may accumulate in non-target tissues that express hCAR and integrins, such as the respiratory, ocular renal and hepatic tissues, and be cleared from blood circulation (Arnberg 2012). Ad5 has high hepatic tropism and intravascular injection is rapidly transduced into the liver (Huard, Lochmüller et al. 1995). Adenoviral vectors are rapidly sequestered and destroyed by Kupffer cells in the liver (Tao, Gao et al. 2001). This interaction has been proposed to be mediated by binding of the hexon hypervariable regions (HVRs) to scavenger receptors and promotes anti-viral immune response (Xu, Tian et al. 2008, Khare, Reddy et al. 2012). Kupffer cells-mediated sequestration and destruction of adenoviruses result in cell necrosis and has been proposed to activate innate and adaptive immune responses (Liu and Muruve 2003). In addition, adenoviruses have high affinity for binding to hepatocytes, which has been shown to be dependent of the viral hexon binding to coagulation factor X (Waddington, McVey et al. 2008). Factor X binding to Ad5 brings the virus to heparan sulfate proteoglycans located in the surphase of hepatocytes, therefore promoting viral transduction (Lopez-Gordo, Denby et al. 2014). This binding is especially strong in Ad5 and Ad2 serotypes, which are the most commonly used vectors, but lower in other serotypes such as Ad3, Ad26 or Ad48 (Waddington, Parker et al. 2007, Short, Rivera et al. 2010). As an example, the substitution of Ad3 hexon onto an Ad5 vector resulted in reduced binding to factor X and decreased liver sequestration (Short, Rivera et al. 2010). Interestingly, it has been reported that factor X can be used by adenovirus as a receptor to infect hCAR-negative adrenal glands (Tran, Ouisse et al. 2013). Pre-existing humoral immunity against adenovirus is common in humans. Consequently, neutralising immunoglobulins can hamper the systemic administration of viral vectors (Abbink, Lemckert et al. 2007, de Vrij, Willemsen et al. 2010). The complement protein C1q binds to IgM-neutralised adenoviral particlesresulting in activation of the classical component pathway via C3 cleavage (Cichon, Boeckh-Herwig et al. 2001). It has also been reported that C3 can bind to adenovirus in the

absence of antibody recognition, resulting in activation of the alternative complement pathway (Jiang, Wang et al. 2004). The adenoviral fiber knob can bind to the complemement component C4-binding protein resulting in enhanced vhepatocyte transduction (Shayakhmetov, Gaggar et al. 2005). The interaction of factor X with the adenoviral particle results in liver sequestration and increased toxicity but protects the viral particle from neutralization of IgM antibodies or recognition by the complement system, these interactions should be considered in the desing of new adenoviral vectors (Lopez-Gordo, Denby et al. 2014). Finally, adenovirus shows high affinity for binding to human erythrocytes expressing hCAR and complement receptor 1 (CR-1) (Carlisle, Di et al. 2009). Recently, Rojas and colleges reported that erythrocyte-binding to adenovirus did not reduce viral transduction in long term in nude mice A549 xenografts, suggesting that the hampered systemic delivery of adenoviral vectors was mainly due to liver sequestration or neutralizing antibodies (Rojas, Moreno et al. 2016).

1.4.7 Strategies for enhanced infection and prolonged blood circulation of adenovirus.

1.4.7.1 Modification of the adenoviral capsid

The adenoviral capsid has been modified to enhance targeted transfection of the vector and prevent liver accumulation and immunogenic neutralization. The most frequent alterations include modification of the fiber-knob or incorporation of fiber domains from different adenoviral serotypes that do not depend on hCAR binding. As an example, the hCAR binding sequence in the Ad5 fiber has been replaced with the CD46 binding sequence of Ad35 (Takagi-Kimura, Yamano et al. 2013). CD46 is highly expressed in mesothelioma cells and consequently, the modified virus resulted in increased infectivity in MSTO-211H and NCI-H2052 mesothelioma cell lines (Takagi-Kimura, Yamano et al. 2013). CD46 is a member of the complement regulatory proteins family (Merle, Noe et al. 2015). Infection of peripheral blood mononuclear cells (PBMC) with the fiber-pseudotyped Ad5 vectors Ad5.F16, Ad5.F35 and Ad5 Ad5.F37 (fibers from Ad16, Ad35 and Ad37, respectively), which tarjet the CD46 receptor, resulted in enhanced infection and increased IFN-α expression, when compared to Ad5wt (Iacobelli-Martinez and Nemerow 2007). In this study, Ad-binding to CD46 also resulted in stimulation of the Toll-like receptor 9 (TLR9) and consequent promotion of NF-kB activation in HeLa cells. Importantly, CD46 is expressed in several tissues within the human body, including hematopoietic cells, skeletal muscle and hepatocytes (Segerman, Mei et al.

2000, Iacobelli-Martinez and Nemerow 2007, Atlas 2017). This broad distribution of CD46 expression could possibly result in off target infection resulting in decreased treatment efficacy. Another example of fiber-modified adenovirus is the oncolytic Ad5-Δ24-RGD (Fueyo, Alemany et al. 2003). The RGD-4C peptide motif can directly interact with $\alpha_v\beta3$- and $\alpha_v\beta5$-integrins. Consequently, the insertion of RGD into the fiber resulted in 6-fold increase in infection in D54 MG, U-251 MG, U-87 MG, T98G, U-138 MG glioma cells and increased survival of mice carring U-87 MG xenografts (Fueyo, Alemany et al. 2003). The safety and anti-tumour efficacy (reduced tumour growth) of Ad5-Δ24-RGD virus was demonstrated in a Phase I clinical trial for patients with recurrent ovarian cancer (Kimball, Preuss et al. 2010).

Alternatively to fiber modifications, additional epitopes in the adenoviral capsid can be modified to improve viral tropism. The hypervariable regions (HVRs) in the Ad5 hexon have been exchanged with Ad48 HVRs that have lower seroprevalence. The resulting Ad5HVR48 vector was able to evade pre-existing anti-Ad5 antibodies (Teigler, Penaloza-MacMaster et al. 2014). However, Ad5HVR48 infection unexpectetly promoted in a strong proinflamatory response *in vivo* resulting in higher toxicity (Coughlan, Bradshaw et al. 2012). Interestingly, Ad5HVR48 does not bind to factor X (Waddington, McVey et al. 2008) and therefore showed reduced liver transduction (Coughlan, Bradshaw et al. 2012). In addition, capsid protein IX has been modified to express the tumour necrosis factor ligand (TRAIL). TRAIL receptor is highly expressed in cancer cells and, therefore, this modification resulted in improved targeting, reduced liver tropism and increased apoptosis in mice models (Wang, Yu et al. 2016).

1.4.7.2 Alternative strategies for enhanced infection and prolonged blood circulation of adenovirus.

As discussed in section 1.4.6, systemic administration of oncolytic adenoviral vectors results in low transduction efficacy due to rapid clearance from the bloodstream. As an alternative strategy to capsid modification, viral particles can be coated with synthetic polymers to avoid host defence responses and reduce liver accumulation (Kreppel and Kochanek 2008, Kang and Yun 2010). The coating of viral particles can be performed by chemical modification of the adenoviral capsid, by electrostatic interactions of cationic polymers with the negatively-charged capsid, or finally, by using cells as carriers.

The chemical modification of adenovirus with hydrophilic polymers such as PEG resulted in attenuation of innate immune response (Mok, Palmer et al. 2005), longer clearing times in

blood (Alemany, Suzuki et al. 2000) and prevented anti-Ad antibody neutralization (Fisher, Stallwood et al. 2001). Unfortunately, this conjugation frequently prevented viral attachment to hCAR and therefore resulted in reduced infection as the PEG concentration increased (Mok, Palmer et al. 2005, Kim, Kim et al. 2012). Using a different strategy, Fisher et *al.* demonstrated that the covalent coating of adenoviral particles with the hydrophilic polymer poly-[N-(2-hydroxypropyl)methacrylamide] (pHPMA) could avoid neutralization (Fisher, Stallwood et al. 2001). In this study, pHRMA was functionalised with targeting molecules such as the vascular endothelialgrowth factor, which facilitated ligand-mediated but hCAR-independent viral internalization into the cells. More recently, pHRMA was further functionalised with quaternary ammonium groups (N^+R_4) with the aim to counteract the negatively-charged adenoviral capsid (Subr, Kostka et al. 2009). Ad5 particles coated with pHRMA-N^+R_4 showed reduced binding to factor X and erythrocytes.

The adenoviral capsid is negatively charged due to the abundance of acidic amino acids that can be found in the hexon protein, such as a sequence of 16 consecutives glutamic acid molecules (Karlin and Brendel 1988). The coating of the adenovirus can also be achieved by physical electrostatic interactions. The coating of the adenoviral particles with positively-charged polymers such as poly(L-lysine), poly(ethylenimine) or chitosan resulted in increased infection and transgene expression (Kim, Kim et al. 2012). Recently, poly(ethylene glycol)-b-poly{N-[N-(2-aminoethyl)-2-aminoethyl]-l-glutamate (PNLG)-conjugated adenoviral particles resulted in increased transduction efficacy, when compared to naked virus (Choi, Kim et al. 2015). In this study, viral transduction increased with the addition of the amino group but decreased as the length of the PEG molecule increased. The work of Vetter and colleges is another example (Vetter, Virdi et al. 2013). In this study, adenoviral particles were coated with cationic polyamidoamine (PAMAM) dendrimers. PAMAM-coated adenovirus resulted in increased infection in both low hCAR-expressing U87MG and high hCAR-expressing HuH7 cells. In a different study, Zeng and colleagues (Zeng, Han et al. 2012) demonstrated that coating adenovirus with 2-aminoethanethiol to amino-$(EO)_n$/$(AGE)_m$-CYS (APC), a cationic PEG derivate, protected the virus from neutralising anti-adenovirus antibodies *in vitro* in hCAR-positive A549 cells and hCAR-negative B16 and SKOV3 cells. Unfortunately, the majority of currently available cationic polymers result in cellular toxicity or aggregation of erythrocytes (Kim, Kim et al. 2012).

An additional alternative approach to enhance viral transduction into the tumour is the use of mesenchymal stem cells (MSC), which have natural cancer tropism, for delivery of the

adenoviral mutants (Sherman, Shaker et al. 2016). The intravenous administration of MSC preloaded with oncolytic adenoviruses resulted in specific delivery of viral vectors to lung and breast tumours in mice and increased survival. In the same study, naked adenoviruses accumulated in the liver (Hakkarainen, Särkioja et al. 2007). This approach was tested in patients with refractory neuroblastoma and resulted in excellence tolerance in all patients (n=4) and complete remission in one patient (García-Castro, Alemany et al. 2010, Pesonen, Kangasniemi et al. 2011). Macrophagues have also been used to enhance viral transduction to otherwise difficult to access prostatic tumours (Muthana, Giannoudis et al. 2011). In this study, hypoxia-regulated E1A/B-expressing macrophagues were transfected with PSA-AdV5-GFP (a PSA-regulated-adenovirus), whose replication was selective to prostate cancer cells. Once the macrophages reached hypoxic areas of prostatic tumours, E1A/B expression was activated, thereby allowing viral replication. Newly sinthetised viral particles spread and infect surrounding areas of the tumour.

An additional strategy to increase adenoviral uptake and avoid its rapid clearance from the blood is the packaging of viral particles into microbubbles (MBs). MBs are ultrasound (US) contrast agents used in the clinic to increase cell membrane permeability upon exposure to US and enhance molecular extravasation (Sorace, Warram et al. 2012). MB-packaging of adenovirus has been reported to promote localised delivery of the vectors (Howard, Forsberg et al. 2006, Warram, Sorace et al. 2012). Additional studies using US directed MBs-Ad therapy in *in vivo* in LnCap xenografts resulted in a 95% enhancement of viral transduction in the target tissue (Sorace, Warram et al. 2013).

1.4.7.3 The use of nanoparticles to coat oncolytic adenoviruses

Nanoparticles can be defined as distinct particles whose size is between 1 to 50nm. Gold nanoparticles are usually coated with an organic layer to protect them from aggregation. In addition, this organic coating dictates the surface structure and functionalities of the gold particle (Zhou, Ralston et al. 2009). The most common and simplest method for nanoparticle synthesis is the sodium citrate-mediate aqueous reduction of gold (Lee and Meisel 1982).

Different studies have assessed the toxicity and biodistribution of gold nanoparticles. Toxicity of gold nanoparticles of 13.5nm *in vivo* was assessed by Zhang and colleagues (Zhang, Wu et al. 2010). In this study, no obvious effect, demonstrated by no weight changes, could be detected in mice after the administration of low concentrations of nanoparticles. In contrast, a trend towards higher toxicity was detected after the administration of higher

concentrations (550-2200μg/kg), determined by decreased body weight, blood cells and haematocrit. The degree of toxicity was also dependent on the administration route. Tail vein injection resulted in the lowest toxicity while oral or intraperitoneal administration resulted higher toxicity.

Distribution of gold nanoparticles *in vivo* has been shown to be size-dependent. Small nanoparticles of 5-15nm were more extensively distributed than larger particles of 50-100nm, although, in both cases the majority of nanoparticles were found in the liver and spleen (Sonavane, Tomoda et al. 2008) (De Jong, Hagens et al. 2008). Interestingly, 20nm gold nanoparticles but not larger 100nm nanoparticles were able to cross the blood-retinal barrier (Kim, Kim et al. 2009). Biodistribution of gold nanoparticles has also been reported to be functionalization-dependent. Galactose-containing PEG conjugation enhanced accumulation of gold nanoparticles in liver hepatocytes (Khlebtsov and Dykman 2011). In addition, TNF-modified nanoparticles selectively targeted solid tumours (Khlebtsov and Dykman 2011).

Functionalization of gold nanoparticles can be performed by physical adsorption of native ligands, by chemical attachment via thiolated groups or by the use of biofunctional linkers such as PEG with COOH and SH groups (Khlebtsov and Dykman 2011).

The surface modification of gold nanoparticles with the hydrophilic polymer PEG is expected to prolong the blood circulation time. PEG-modified nanoparticles prevented binding to other molecules by steric effects and are stable in biological environments (Liu, Shipton et al. 2007, Sanz, Conde et al. 2012). In addition, thiolated PEG-modified nanoparticles facilitated further functionalization with dsRNA and short oligonucleotides (Sanz, Conde et al. 2012). Functionalization of the gold nanoparticles with c-myc targeting siRNA was reported to efficiently knock-down c-myc protein *in vitro* in HeLa cells and *in vivo* in the invertebrate Hydra and in mouse (Conde, Ambrosone et al. 2012). c-myc siRNA was added to nanoparticles via either ionic or covalent interactions. In the ionic method, negatively charged siRNA would attach to quaternary ammonium groups (R_4N^+) that had been previously bound to PEG-COO^- spacers. In the covalent method, PEG-coated nanoparticles were functionalized with thiolated siRNA via thiol bonds.

Although the coating of adenoviral mutants with gold nanoparticles has not been widely studied, some reports have been published. A complex formed of an adenoviral vector and gold/iron magnetic nanoparticles has been reported to easily penetrate the plasma

membrane in the presence of a magnetic force and independently of cellular receptors (Kamei, Mukai et al. 2009). In addition, the coating of adenoviral vectors with gold nanoparticles has been studied for their use in hyperthermic tumour cell ablation. In this study, an adenoviral vector encoding for luciferase under control of CMV promoter (AdCMVLuc) was covalently bound to the gold-nanoparticles demonstrating retained infectivity even in the presence of this covalent binding (Everts, Saini et al. 2006).

1.5 APOPTOSIS

Apoptosis is the most extensively studied form of programmed cell death. Its fine modulation is essential for preserving cell homeostasis and preventing tumourigenesis, as apoptosis evasion is found in most types of cancers (Hanahan and Weinberg 2000, Zielinski, Eigl et al. 2013, Fulda 2015). Several signalling pathways can modulate apoptosis, here I briefly describe some steps in the process that are necessary to understand the several interactions of various adenoviral proteins in apoptosis modulation.

Apoptosis can be triggered through two different pathways, the extrinsic and the intrinsic (Zielinski, Eigl et al. 2013). The extrinsic pathway is activated upon binding of death factors to their receptors, including the tumour-necrosis-factor-apoptosis-inducing ligand (TRAIL) receptor and the tumour necrosis factor (TNF) receptor (Ashkenazi 2008). This binding stabilises the Fas death-domain (FADD) (Scott, Stec et al. 2009), that recruits caspase 8, promotes the formation of the death-inducing-signalling-complex (DISC) and finally results in caspase 8 activation (Fulda 2015). Active caspase 8 can continue the extrinsic pathway by directly cleaving caspase 3, or indirectly by promoting the apoptotic intrinsic mitochondrial pathway by cleavage of Bid (**Figure *13***) (Zielinski, Eigl et al. 2013, Fulda 2015).

The intrinsic apoptotic pathway can be triggered by intracellular signals such as DNA damage, hypoxia or the absence of growth factors (Lorenzo, Arnoldussen et al. 2007). The apoptotic intrinsic mitochondrial pathway is initiated when the pro-apoptotic Bcl-2 family member BID is cleaved by caspase 8. The resulting tBID (truncated BID) is translocated to the mitochondrial membrane where it interacts with the pro-apoptotic Bcl-2 family member BAX (Shore and Nguyen 2008, Wang and Tjandra 2013). As a result of this interaction, active BAX is inserted into the mitochondrial membrane where it homo-oligomerizes or forms the BAK-BAX complex recruiting the inactive anti-apoptotic Bcl-2 member BAK (Shore and Nguyen 2008). Both interactions promote mitochondrial outer membrane depolarisation (MOMP)

leading to cytochrome-C release (White 2006, Lovell, Billen et al. 2008), which binds to Apaf-1, promoting the formation of the apoptosome and induction of caspase 9 mediated apoptosis (Favaloro, Allocati et al. 2012). The formation of the mitochondrial pore can be prevented by anti-apoptotic Bcl-2 family members, such as Bcl-2 and Bcl-xL. Bcl-xL can compete with BAK for binding to the BH3 domain of tBID, the resulting binding is stable and therefore this interaction prevents BAK activation. Bcl-2 or Bcl-xL can also directly bind to active BAX preventing its oligomerization. As a result, the Bcl-xL protein can hamper BAX induced mitochondrial membrane permeabilization in two different ways (**Figure *13***) (Shore and Nguyen 2008).

The p53 protein is a well-known tumour suppressor that coordinates the cellular response to different cellular stress factors and protects against proliferation of DNA damaged cells (Moll and Petrenko 2003, Kruse and Gu 2009). p53 plays a key role modulating the cell response to multiple types of stress that can result in cell cycle arrest, apoptosis, senescence, DNA repair or autophagy (Kruse and Gu 2009). The p53 protein is unstable with a short half-life. Under normal conditions the E3 ligase MDM2 binds to p53 thereby inhibiting its transcriptional activator role and promoting its degradation (Haupt, Berger et al. 2003, Moll and Petrenko 2003). The activation of p53 is promoted by inhibition of its degradation, p53 can then accumulate in the nucleus and induce transcription of multiple genes, including the proapoptotic PUMA protein, which contains a BH3 domain and can bind to and inhibit antiapoptotic Bcl-2 family members (Lorenzo, Arnoldussen et al. 2007). Independent of its transcription activity, cytoplasmic p53 can promote apoptosis binding to antiapoptotic Bcl-2 proteins (Bcl-2 and Bcl-x_L) and disrupting its interaction with the proapototic BAX and BAK (**Figure *13***) (Hanahan and Weinberg 2000, Chipuk and Green 2006, Lorenzo, Arnoldussen et al. 2007).

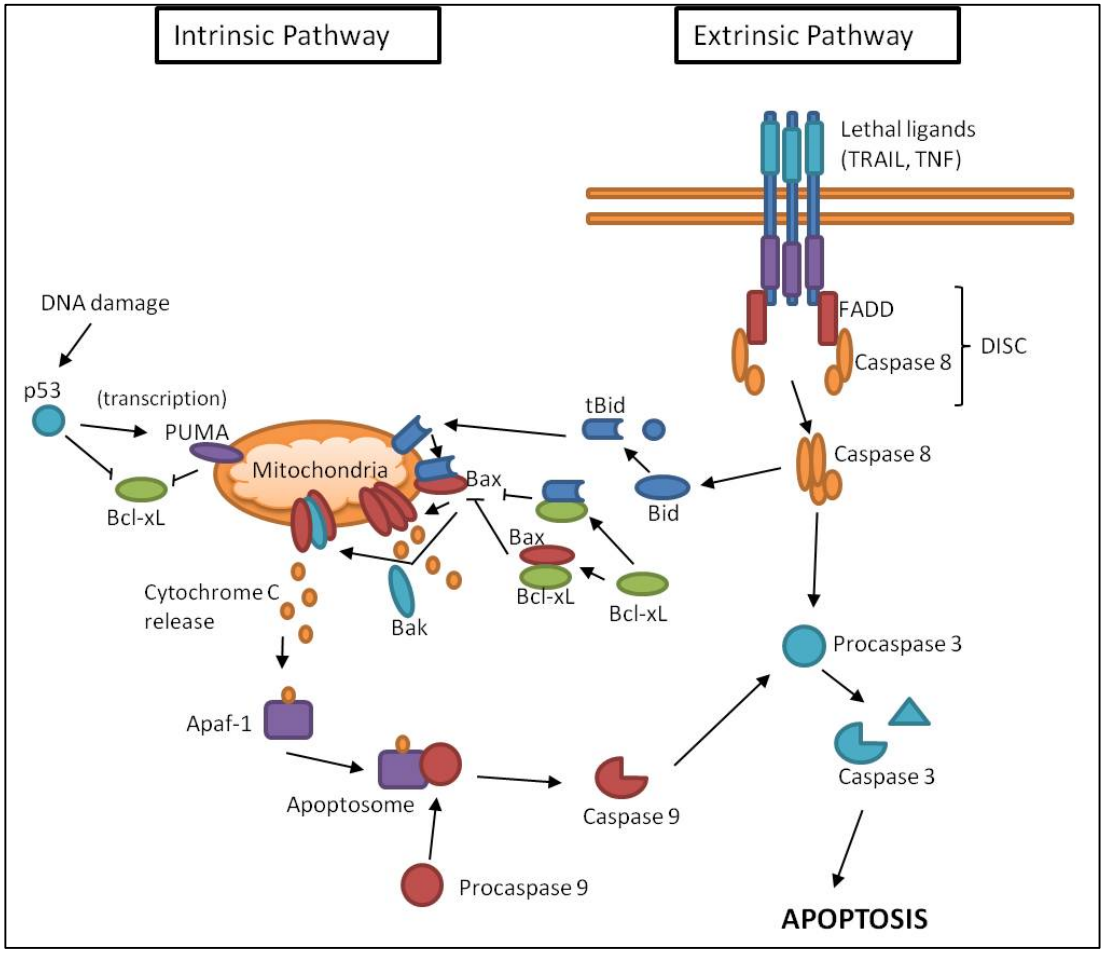

Figure 13. Schematic representation of the apoptotic pathway. See text for explanation.

1.5.1 Apoptosis and prostate cancer

The aim of most cancer therapies, including chemotherapy, radiation or hormone deprivation, is to eliminate cancer cells that typically involve the initiation of apoptotic signalling in response to cytotoxic stress (Lorenzo, Arnoldussen et al. 2007, Zielinski, Eigl et al. 2013). This strategy can be hampered when the cancer presents mutations in the apoptotic pathway or over-expression of pro-survival proteins (Zielinski, Eigl et al. 2013). The anti-apoptotic proteins Bcl-2 and Bcl-xL have been found to be over-expressed in various cancers, including prostate cancer (Lorenzo, Arnoldussen et al. 2007). Over-expression of Bcl-2, Bcl-xL, Bcl-w and Mcl-1 has been reported to promote resistance to chemotherapy in CRPC (Krajewska, Krajewski et al. 1996, Yoshino, Shiina et al. 2006). In addition, Bcl-xL expression is higher in mCPRP when compared to primary tumours or normal prostate tissue, suggesting that increased Bcl-xL expression may contribute to PCa progression to metastatic disease

and/or CRPC (Sun, Tang et al. 2008). Down-regulation of antiapoptotic Bcl-2 proteins resulted in renewed sensitisation to docetaxel treatment (Zielinski, Eigl et al. 2013). Survivin is an anti-apoptotic protein that can inhibit apoptosis by blocking the caspase cascade, over-expression of survivin has been found in primary prostate tumours with increasing expression levels when the cancer progressed (Lorenzo, Arnoldussen et al. 2007). High survivin expression was detected in AR-independent DU145 and PC3 prostate cancer cells but not in AR-sensitive LNCaP cells (Zhang, Latham et al. 2005). The tumour suppressor p53 protein is frequently found mutated in cancer, including CRPC. p53 expression decreases as prostate cancer progresses, indicating that its absence may contribute to tumour progression (Lorenzo, Arnoldussen et al. 2007). In addition, high levels of the p53 inhibitor MDM2 are common in most cancers, including prostate cancer, and are associated with poor prognosis (Leite, Franco et al. 2001, Lorenzo, Arnoldussen et al. 2007).

1.5.2 The role of adenovirus early proteins in modulation of apoptosis

The adenoviral early proteins can play different roles in apoptosis modulation. The E1A-encoded proteins promote apoptosis by multiple mechanisms while the E1B-, E3- and E4-encoded proteins prevent apoptosis to enable the viral life cycle to take place.

The E1A protein can induce apoptosis through both p53 stabilization and through p53-independent pathways (Putzer, Stiewe et al. 2000). As a response to E1A-induced cell cycle progression and DNA damage, E1A promotes apoptosis by p53 stabilization (White 2006). E1ACR2 is responsible for pRB binding and E2F release, free E2F1 promotes expression of p14, which subsequently blocks MDM2-induced p53-degradation thereby promoting apoptosis (Putzer, Stiewe et al. 2000). In addition, E1A expression has been reported to suppress p21 and MDM2 expression leading to p53 stabilization enhancing p53-induced DNA-damage response (Chattopadhyay, Ghosh et al. 2001, Yamasaki, Tazawa et al. 2012). E1A-mediated stabilization of p53 can also be achieved by facilitating p53 binding to MDM4, which inhibits p53 nuclear export (**Figure *14***) (Li, Day et al. 2004).

E1A has been reported to induce apoptosis in p53-deficient cells (Putzer, Stiewe et al. 2000). E1A also sensitises cells to TNFα-induction of apoptosis by promoting TNFα activation of procaspase 8. This sensitisation was reported to be dependent on E1A-binding to both pRB and p300 (Perez and White 2003). E1A-mediated E2F release has also been shown to promote apoptosis by inhibition of nuclear factor NF-κB (Deng, Kloosterbooer et al. 2002). Active NF-κB can positively regulate expression of the c-FLIP, which functions as a caspase 8

inhibitor (Kreuz, Siegmund et al. 2001). E1A has been reported to down-regulate c-FLIP expression by directly inhibiting its transcription or promoting its degradation, therefore sensitising cells to TNF-α-induced apoptosis (Perez and White 2003). E1A has also been reported to suppress miR-520 expression. miR-520 down-regulation enhances PP2A/C expression, which inhibits NF-κB, finally resulting in reduced tumour invasiveness (Su, Chen et al. 2010). In addition, E1A has been reported to completely suppress myeloid cell leukemia 1 (Mcl-1), an anti-apoptotic Bcl-2 family member (Cuconati, Mukherjee et al. 2003). In uninfected cells, Mcl-1 forms a complex with the pro-apoptotic BAK protein. In the absence of Mcl-1, BAK can complex with BAX promoting mitochondrial depolarization and apoptosis (**Figure *14***) (Cuconati, Mukherjee et al. 2003).

E1A expression plays a role in inhibition of tumour invasiveness and metastasis. As an example, E1A can inhibit expression of type IV collagenase and prevent tumour invasiveness (Yu and Hung 1998). E1A enhances expression of E-cadherin, which is frequently found down regulated in many cancers, including PCa, resulting in reduced invasion (Frisch 1994, Rubin, Mucci et al. 2001). Expression of HER2/neu enhances angiogenesis and has been associated with increased metastasis in cancer patients (Chang, Hung et al. 2014). E1A-CR2 interaction with pRB has been shown to repress HER2/neu promoter and inhibit metastasis potential in B104-1-1 neuroblastoma cells (Chen and Hung 1997). Interestingly, E1A has also been reported to inactivate HER2/neu, Akt and IKK signalling resulting in inhibition of angiogenesis (Lee, Tai et al. 2003, Chang, Hung et al. 2014).

The E1B gene encodes two proteins, E1B55K and E1B19K. The E1B proteins prevent E1A-induced apoptosis and therefore facilitate viral replication (White 2006). The E1B55K protein binds to p53 and counteracts E1A-induced p53 stabilization and consequently apoptosis induction (Berk 2005). E1B55K-binding to p53 also induces G1/S transition (Bressy and Benihoud 2014). The E1B19K protein blocks p53-independent apoptosis (Berk 2005). E1B19K is a homolog of the anti-apoptotic Bcl-2 protein; following tBID activation of the pro-apoptotic Bcl-2 family member BAX, E1B19K recognises and binds a BH3 motif of BAX preventing the formation of the BAX-BAK complex and therefore prevents the permeabilization of the mitochondrial membrane and subsequent apoptosis (**Figure *14***) (White 2006).

The E3-encoded proteins RIDα and RIDβ (formerly E3 10.4K and 14.5K, respectively) promote internalization of TNF and therefore prevent TRAIL-mediated apoptosis induction (Krajcsi, Dimitrov et al. 1996, Lichtenstein, Doronin et al. 2004). E3 6.7K is required for RID-mediated

internalization and degradation of TRAIL receptor 2 (Benedict, Norris et al. 2001, Lichtenstein, Doronin et al. 2004). In addition, as previously described on section 1.3.7, E3gp19K prevents MHC1 presentation protecting the infected cell from being killed by cytotoxic (**Figure *14***) T cells (Lichtenstein, Toth et al. 2004).

The dsDNA adenoviral genome can be sensed in the nucleus as double strand breaks and therefore activate the cellular DNA damage response (DDR) (Turnell and Grand 2012, Turner, Wilkinson et al. 2014). The sensor protein complex Mre11/Rad50/Nbs1 (MRN) can detect DNA damage and activate the cellular response (Williams, Lees-Miller et al. 2010). The adenoviral proteins E1B55K, E4orf3 and E4orf6 can interact in different steps in this cellular response. E1B55K and E4orf6 form a complex that promotes Mre11 degradation. E4orf3 can promote sequestration of components of the MRN complex (Araujo, Stracker et al. 2005, Stracker, Lee et al. 2005). In addition to E1B55K-mediated inhibition of p53 transcription, the E1B55K-E4orf6 complex promotes p53 degradation (Hart, Ornelles et al. 2007). Moreover, E4orf3 attenuates p53 activity by inhibitory methylation of p53-target promoters (Soria, Estermann et al. 2010). The poly(ADP-ribose) polymerase-1 (PARP-1) is activated as a response of DNA damage. PARP-1 activation can be followed by apoptosis inducing factor (AIF) translocation to the nucleus. AIF nuclear localization promotes PARP-1 –mediated DNA fragmentation and caspase-independent cell death. Either E1B55K or E4orf3 have been reported to prevent AIF translocation and nuclear fragmentation (Turner, Wilkinson et al. 2014).

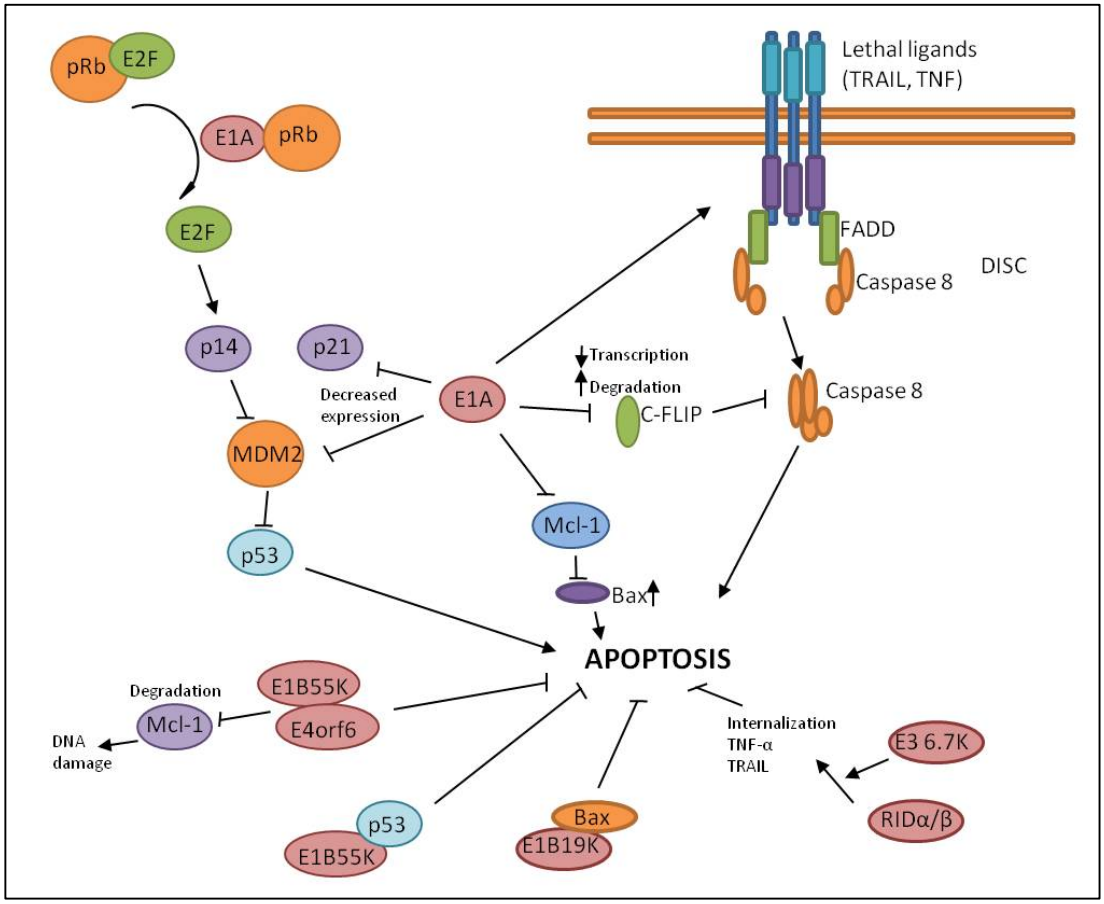

Figure 14. Schematic representation of the interactions of the adenoviral proteins in the apoptotic pathway. E1A protein promotes apoptosis while E1B, E3 and E4 proteins protect the host cell from cell death. See text for more detailed explanation. Viral proteins are shown in red.

1.6 AUTOPHAGY

Autophagy is an auto-catabolic process that involves the sequestration of cytoplasmic components inside a double membrane vesicle for degradation to provide the cell with energy and new building blocks (Chen and Karantza 2011, Lozy and Karantza 2012). The autophagy process can be considered as a cell survival mechanism as it acts by maintaining cell homeostasis by degradation of misfolded, or no longer used, proteins and non-functional organelles. Autophagy promotes cell survival under stress conditions such as hypoxia, nutrient deprivation or cytotoxic stress (Glick, Barth et al. 2010, Chen and Karantza 2011). However, autophagy is also considered a non-apoptotic programmed form of cell death under conditions of irreparable cell damage (Chen and Karantza 2011).

The autophagy process can be classified in three different types. Macroautophagy requires the incorporation of the components to be degraded in double-membrane vesicles termed autophagosomes that later fuse with lysosomes to form the autophagolysosome. In contrast, during microautophagy, lysosomes directly sequester cytosolic components and process them to their degradation. In both mechanisms, the incorporation can be both selective or non-selective (Glick, Barth et al. 2010). Chaperone-mediated autophagy (CMA) is the third type of autophagy. In CMA, the lysosome specifically recognises chaperone-bound proteins via its membrane receptor lysosomal-associated membrane protein 2 (LAMP-2) and proceeds to degrade the contents (Saftig, Beertsen et al. 2008, Glick, Barth et al. 2010).

The process of macroautophagy, hereafter termed autophagy, is most extensively studied due to its role in disease and cancer and can be divided in 5 stages (**Figure *15***). (1) The process starts with the isolation of the double membrane vesicle, which is termed phagosome, (2) followed by the formation of the Atg5 and Atg12 complex and its interaction with Atg16 in the membrane. Formation of the Atg5-Atg12-Atg16 complex promotes curvature of the phagosome membrane and recruits the microtubule associated protein 1 light chain 3 (LC3B) (Glick, Barth et al. 2010). (3) The process continues with the binding of LC3BII to both sides of the membrane, promoting the elongation of the phagosome. LC3B is found in most cells although its expression is increased in cells undergoing autophagy. Upon the induction of the process, LC3B is cleaved by Atg4 resulting in LC3BI, which is now conjugated to phosphatidylethanolamide (PE) generating LC3BII in a reaction mediated by Atg7 (Glick, Barth et al. 2010, Hoare, Young et al. 2011). (4) Upon LC3BII binding, the developing membrane may sequester the degradation targets in a selective or random way, LC3BII has been proposed to play a role in this selection (Glick, Barth et al. 2010). In addition, p62/SQSMT1 (p62) is responsible for the selection of ubiquitinilated protein aggregates, also, p62 contains a domain for binding to LC3B (Lippai and Low 2014). (5) Finally, the already formed autophagosome fuses with the lysosome to form the autophagolysosome and promote degradation of its contents (Glick, Barth et al. 2010). The LAMP-2 protein is required at this stage to facilitate the fusion between autophagosome and lysosome (Saftig, Beertsen et al. 2008).

Multiple signalling pathways can contribute to autophagy modulation. The mechanistic target of rapamycin (mTOR) is a serine/threonine kinase and is considered a master regulator of autophagy (Yang and Klionsky 2010). In the presence of nutrients or growth factors, the PI3K/AKT/mTOR signalling pathway remains active, which allows promotion of cell

proliferation and inhibits autophagy (Chen and Karantza 2011). mTOR status can also be modulated by AMP-activated protein kinase (AMPK); during starvation or hypoxia conditions, AMPK is activated by LKB1, active AMPK inhibits mTOR therefore promoting autophagy (Chen and Karantza 2011). Inhibition of mTOR allows the formation of the ULK complex, which is necessary for autophagy initiation (Lamb, Yoshimori et al. 2013).

The ULK1 (mammalian homolog of yeast Atg1) protein forms a complex with mammalian (m)Atg13, FIP200 (focal adhesion kinase (FAK) family interacting protein of 200 kD) and Atg101. In nutrient rich conditions, mTOR interacts with the ULK1 complex (ULK1-Atg13-FIP200-Atg101) inhibiting its activity. During starvation, mTOR dissociates enabling ULK1 complex to recruit Atg proteins and promote autophagosome formation (Mizushima 2010). The nucleation of the autophagosome membrane takes place in proximity to the endoplasmic reticulum (ER) and the mitochondria (Gallagher, Williamson et al. 2016).

In addition, Beclin 1 plays a key role in autophagy modulation. Beclin 1 interacts with the class III type phosphoinositide 3-kinase (PI3KC3)/Vps34 and forms the Beclin 1-Vps34-Vps35 complex, that promotes the initiation of the phagosome formation and positively regulates autophagy (Kang, Zeh et al. 2011, Marquez and Xu 2012). The activation of the Beclin 1-Vps34-Vps35 complex is downstream dependent of ULK1 complex activation. ULK phosphorylates and activates Beclin 1, this activation is dependent on Atg14L binding to ULK (Gallagher, Williamson et al. 2016). Assembly of the Beclin 1 complex takes place in proximity to ER and mitochondria. Subsequent binding to Atg14L results in accumulation of PI3-P and finally promotes downstream Atg5-Atg12-mediated LC3BI lipidation (**Figure *15***) (Gallagher, Williamson et al. 2016).

The formation of the Atg12-Atg5 complex and its subsequent binding to Atg16 to form the Atg12-Atg5-Atg16 complex, is required for lipidation of LC3BI into LC3BII and LC3BII-binding to the autophagosome membrane (Nakatogawa 2013). Atg7 is an E1 type enzyme and is required for both the activation of Atg5 by conjugation to Atg12 and lipidation of LC3BI (Nakatogawa 2013, Otomo, Metlagel et al. 2013). Atg16 interacts with Atg5 and recruits it to the forming autophagosome membrane. Alternatively, Atg12 interacts with Atg3, therefore, Atg12-Atg5 conjugation recruits Atg3 to the forming membrane (Otomo, Metlagel et al. 2013). Both Atg7 and Atg3 are required for LC3B activation and lipidation (Tanida, Yamasaki et al. 2012). Conversion of LC3BI to LCB3II followed by binding to the autophagosome membrane is essential for autophagy initiation (**Figure *15***) (Ravikumar, Sarkar et al. 2010).

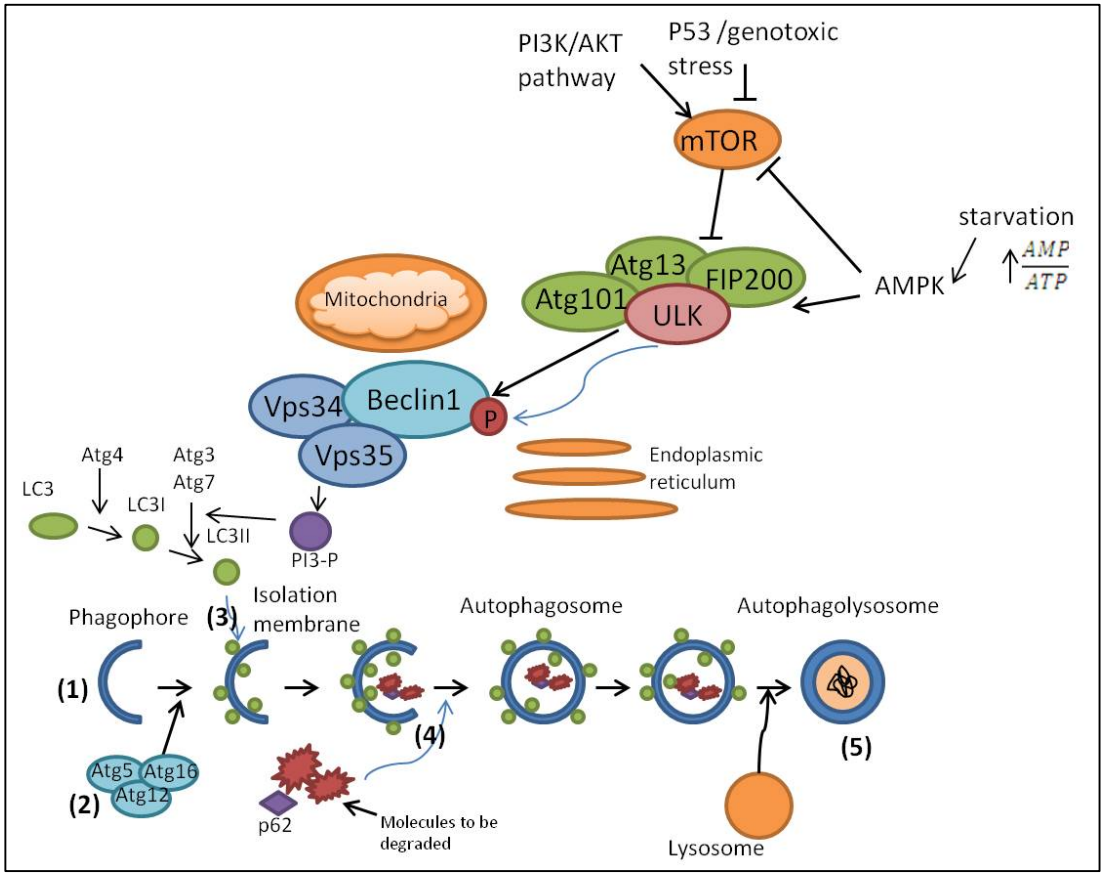

Figure 15. Schematic representation of the autophagy pathway and its upstream regulation. The autophagy process can be divided in 5 stages. (1) The process starts with the isolation of the double membrane vesicle, which is termed phagophore, (2) followed by the formation of the Atg5 and Atg12 complex and its interaction with Atg16 in the membrane. (3) LC3B is cleaved, lipidated and bound to the phagophore membrane. (4) Sequestration of molecules to be degraded. Both LC3B and p62 have been suggested to play a role in the selection of the autophagosome components. (5) Autophagosome fusion with lysosome and degradation of the components.

1.6.1 The role of autophagy in Prostate Cancer

Autophagy plays a dual role in cancer. Under stress and nutrient deficiency conditions, activation of the autophagy mechanism can promote cell survival and delay apoptosis in cancer, however some autophagy-related genes are commonly found mutated suggesting that autophagy deficiency can also lead to tumourigenesis (Ziparo, Petrungaro et al. 2013).

The role of autophagy in cell death or promotion of cell survival in cancer is still controversial and it might be dependent on the cancer stage (Chen and Karantza 2011, Ziparo, Petrungaro et al. 2013). It has been proposed that at early cancer stages, inhibition of autophagy allows accumulation of free radicals and therefore promotes tumourigenesis (Ziparo, Petrungaro et al. 2013). The loss of Beclin 1 in many prostate cancers supports this statement. In contrast,

under stress conditions such nutrient deficiency or hypoxia, autophagy can act as a cell survival mechanism providing cancer cells with new energy sources during later stages (Ziparo, Petrungaro et al. 2013).

Beclin 1 has been considered a tumour suppressor gene after being found monoallelicaly lost in breast, prostate and ovarian cancers (Kondo, Kanzawa et al. 2005, Chen and Karantza 2011, Ziparo, Petrungaro et al. 2013). Beclin 1 is a BH3 domain only protein and can interact with the antiapoptotic members of the Bcl-2 family (Marquez and Xu 2012), the implications of this interaction will be further described below (section 1.7).

The PI3K/AKT signalling pathway plays an important role in cell proliferation, autophagy induction and apoptosis inhibition (Toker and Yoeli-Lerner 2006, Yoeli-Lerner and Toker 2006, Chen and Karantza 2011). Activation of AKT by phosphorylation requires its association with the plasma membrane, once active, it is released and can act on multiple substrates. Active AKT has been reported to speed prostate tumour growth and promote PCa progression (Graff, Konicek et al. 2000). PTEN is the main negative regulator of AKT activation (Song, Salmena et al. 2012), and loss of PTEN is a frequent event in human PCa progression as it allows AKT activation (Majumder and Sellers 2005). PTEN expression levels can be correlated to the prostate cancer stage; complete loss of PTEN commonly takes place when prostate cancer reaches more advanced stages (Majumder and Sellers 2005). The mammalian target of rapamycin (mTOR) is a downstream target of AKT, lack of AKT inhibition due to PTEN loss positively modulates mTOR activity inhibiting autophagy and increasing cell growth (Majumder and Sellers 2005, Lorenzo, Arnoldussen et al. 2007).

It has been suggested that cancer cells induce autophagy as a response to chemotherapy treatment in an attempt to restore cellular homeostasis. This response contributes to the development of drug resistance. Chemotherapy-induced autophagy can also promote cell death by either driving the cell towards apoptosis or resulting in autophagic cell death (Sui, Chen et al. 2013).

In prostate cancer, ADT with the antiandrogen bicalutamide caused hypoxia and therefore up-regulated autophagy in LNCaP xenografts by inhibiting the key regulator mTOR (Ming, Byrne et al. 2013, Ziparo, Petrungaro et al. 2013). ADT-promoted nutrient deficiency contributed to the activation of the AMPK, which inhibits mTOR and induces autophagy (Meijer and Codogno 2007, Ziparo, Petrungaro et al. 2013, Farrow, Yang et al. 2014). Taxane-based chemotherapy has also been reported to induce autophagy (Farrow, Yang et al. 2014).

Taken together, androgen withdrawal and chemotherapy treatments promote autophagy, as a consequence, autophagy inhibition can be proposed as a therapeutic strategy for insensitive PCa. Moreover, autophagy upregulation has been correlated to poor response to radiotherapy in PCa patients (Koukourakis, Kalamida et al. 2015). Indeed, blocking of autophagy with the pharmacological inhibitor chloroquine resulted in increased apoptosis in LNCaP cells (Ziparo, Petrungaro et al. 2013) and autophagy inhibition by siRNA targeting Beclin1 or Atg7 sensitised this cell line to ADT (Li, Jiang et al. 2008). A number of clinical trials are currently using autophagy inhibitors, such as chloroquine or 3-MA, in combination with chemotherapy for prostate cancer treatment (Chen and Karantza 2011, Ziparo, Petrungaro et al. 2013, Farrow, Yang et al. 2014).

However, the role of autophagy in cancer progression remains controversial. Autophagy upregulation has been observed in apoptosis-defective cell lines as a result of chemotherapy treatment and has been associated with increased cell death. Autophagy induction with mTOR inhibitors has been tested in preclinical cancer models in combination with chemotherapy (Sui, Chen et al. 2013). As an example, the combination of the mTOR inhibitor RAD001 with the chemotherapeutic alkylating agent temozolomide enhanced cell killing by promoting autophagy-associated cell death in U-87 glioma cells (Josset, Burckel et al. 2013).

1.6.2 The role of adenovirus in autophagy

The role of adenovirus in autophagy modulation has been investigated by several teams (Piya, White et al. 2011, Rodriguez-Rocha, Gomez-Gutierrez et al. 2011, Tazawa, Kagawa et al. 2013, Klein, Piya et al. 2015). Infection with wild type or replication-selective (hTERT-Ad) mutants has been reported to induce autophagy-associated cell death in malignant glioma cells (Ito, Aoki et al. 2006, Marquez and Xu 2012). Infection of malignant brain tumour cells with oncolytic adenoviruses containing tumour-specific promoters (hTERT promoter) to facilitate viral replication or engineered fiber-knobs to facilitate infection resulted in enhancement of autophagic cell death (Tazawa, Kagawa et al. 2013). These observations suggested that enhancement of infection and replication drives the autophagy process from its cytoprotective function to promote cell death. Some viruses, including adenovirus, require AKT activation in infected cancer cells to stimulate synthesis of viral proteins (Shertz and Cardenas 2011, Klein, Piya et al. 2015).

Adenovirus E1A, E1B and E4 early proteins can interact with the autophagic process (Tazawa, Kagawa et al. 2013). Infection of lung carcinoma A549 cells with Adwt resulted in autophagy induction, which was reduced when infected with an E1B-deleted adenovirus and barely detectable when infected with an E1A- and E1B- deleted virus (Rodriguez-Rocha, Gomez-Gutierrez et al. 2011). These findings implicated that E1A- and E1B-encoded proteins may play roles in autophagy induction or viral replication. The E1B19K protein has been proposed to disrupt the inhibitory Beclin 1-Bcl-2 complex, therefore allowing the assembly of the Beclin 1-Vps34-Vps35 complex and inducing autophagy in A549 and U87 MG cells (***Figure 11*** and ***Figure 12***) (Piya, White et al. 2011). In the same study, an E1B19K-deleted mutant was not able to induce autophagy (Piya, White et al. 2011). In contrast, E4-orf4 was reported to activate mTOR and inhibit autophagy-induction in U2OS cells (O'Shea, Klupsch et al. 2005).

Adenovirus-induced autophagy did not affect the starvation-induced AMPK/mTOR pathway in various cell types (such as UG87MG, U251MG, A549 and MEF) (Klein, Piya et al. 2015). In contrast, adenovirus has been reported to mediate phosphorylation of JNK1 and JNK2, therefore promoting Bcl-2 phosphorylation and its dissociation from the Beclin 1-Bcl-2 complex, resulting in autophagy induction (Klein, Piya et al. 2015). Interestingly, the same team recently reported that active autophagy is required for MHC II-mediated presentation of adenoviral antigens in infected cells. Consequently, autophagy inhibition prevented detection of viral-encoded antigens in MEF and A549 cells (**Figure *16***) (Klein, Jiang et al. 2016).

Interestingly, E1A-mediated activation of E2F1 through pRB-binding can also modulate miRNA levels in infected cells (Tazawa, Kagawa et al. 2013). E2F1 expression resulted in upregulation of miR-7 levels and consequently suppression of the epidermal growth factor receptor (EGFR) in H1299 and A549 cells (Tazawa, Yano et al. 2012). EGFR is upstream of the PI3K-Akt-mTOR signalling pathway, therefore its suppression may inhibit mTOR and promote autophagy (Wu, Tan et al. 2009). E2F1 can also up-regulate the expression of miR-93 and miR-106, which causes down-regulation of p21 promoting autophagic and apoptotic cell death in H358 and H460 cell lines (Yamasaki, Tazawa et al. 2012, Tazawa, Kagawa et al. 2013). Adenovirus infection also up-regulates expression of miR-15 and miR-16 which down-regulate the antiapoptotic Bcl-2 family member Mcl-1 promoting an enhancement of chemotherapy induced apoptotic cell death (**Figure *16***) (Tazawa, Kagawa et al. 2013).

In addition, adenovirus can disrupt the autophagic process during its endosome-mediated entry into the cells. The adenoviral protein RID-α counteracts adenovirus-induced autophagy and enables the virus to escape from the endosome prior to fusion with the lysosome

(Cianciola and Carlin 2009). The viral polypeptide VI can also interact with the endosome membrane facilitating the virus escape from the endosome (**Figure *16***) (Wiethoff, Wodrich et al. 2005, San Martin 2012).

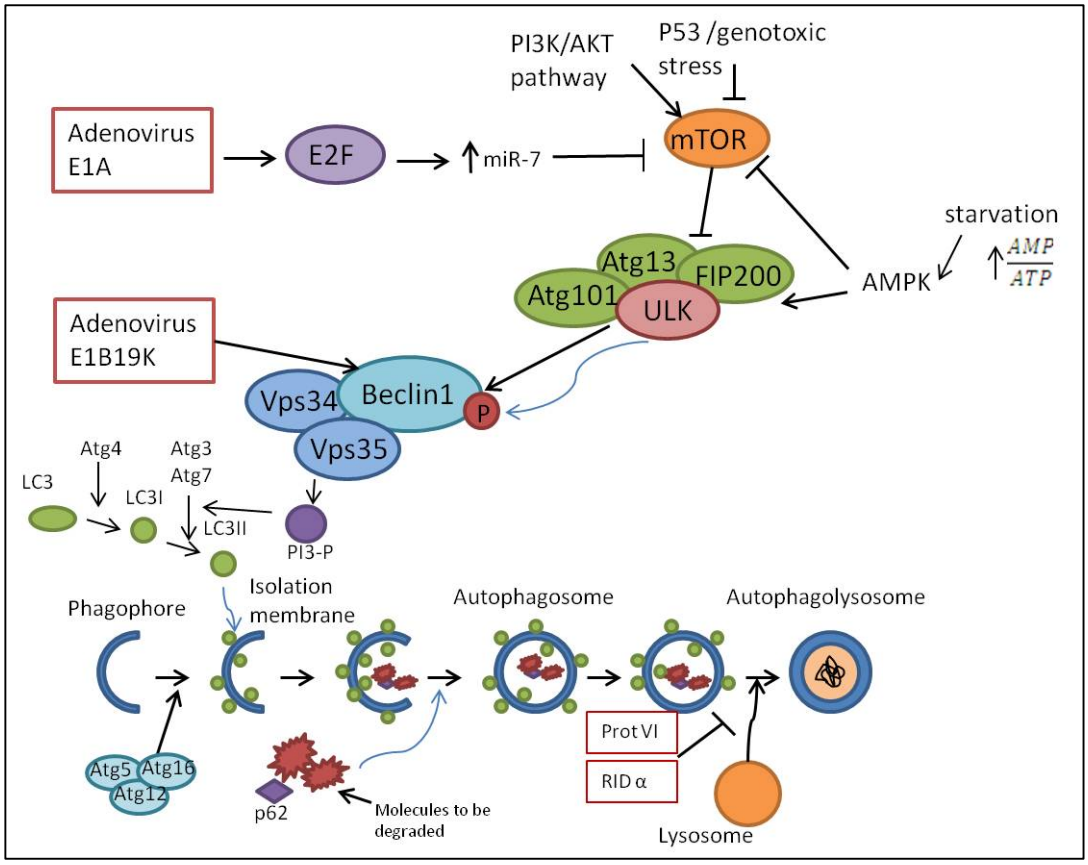

Figure 16. Schematic representation of the role of adenovirus in autophagy. The figure shows how E1B19K, E1A and other adenoviral proteins such as the polypeptide VI and RIDα can interact in this process. See text for more detailed explanation. Adenoviral proteins are marked in red squares.

1.7 THE CROSSTALK BETWEEN AUTOPHAGY AND APOPTOSIS

Autophagy can be considered both a cell survival and death mechanism (Chen and Karantza 2011). However, autophagy-related cell death has never been reported in mammalian cells under healthy physiological conditions, in addition, the pro-survival role of autophagy can be achieved by inhibiting apoptosis (Gordy and He 2012). It has been established that autophagy inhibition promotes apoptosis while suppression of apoptosis causes autophagy (Marquez and Xu 2012).

The interaction of Beclin 1 with the antiapoptotic Bcl-2 or Bcl-xL proteins is one of the potential points for crosstalk between the apoptotic and autophagic pathways (Marquez and Xu 2012). The formation of the Beclin 1-Bcl-2 complex prevents the formation of the Beclin 1-Vps34-Vps35 complex and impedes autophagy initiation (Gordy and He 2012). During nutrient deficiency conditions, c-Jun N-terminal kinase (JNK) phosphorylates Bcl-2 disrupting its interaction with Beclin 1 and allowing autophagy induction (Wei, Pattingre et al. 2008). Cellular localization determines the outcome of this process as Bcl-2 can only be phosphorylated by JNK when located close to the endoplasmic reticulum (Marquez and Xu 2012). However, in conditions of extreme starvation, in which the cell is no longer viable, JNK1 hyperphosphorylates Bcl-2 causing its dissociation from Bax and promoting caspase-dependent apoptotic cell death (**Figure *17***) (Li, Gao et al. 2016). The Beclin-1-Bcl-2 complex can also be disrupted by DARP-mediated Beclin-1 phosphorylation (Zalckvar, Berissi et al. 2009). Proapoptotic BH3-only proteins BAD and BAX can bind to Bcl-2 or Bcl-xL proteins and disrupt its complex with Beclin 1 (Gordy and He 2012). Interestingly, over-expression of Bax prevents autophagy by degrading Beclin 1 (**Figure *17***) (Luo and Rubinsztein 2010).

Bcl-2 can play an inhibitory role in the regulation of both apoptotic and autophagic pathways. This dual role suggests it possibility as a therapeutic target (Marquez and Xu 2012).

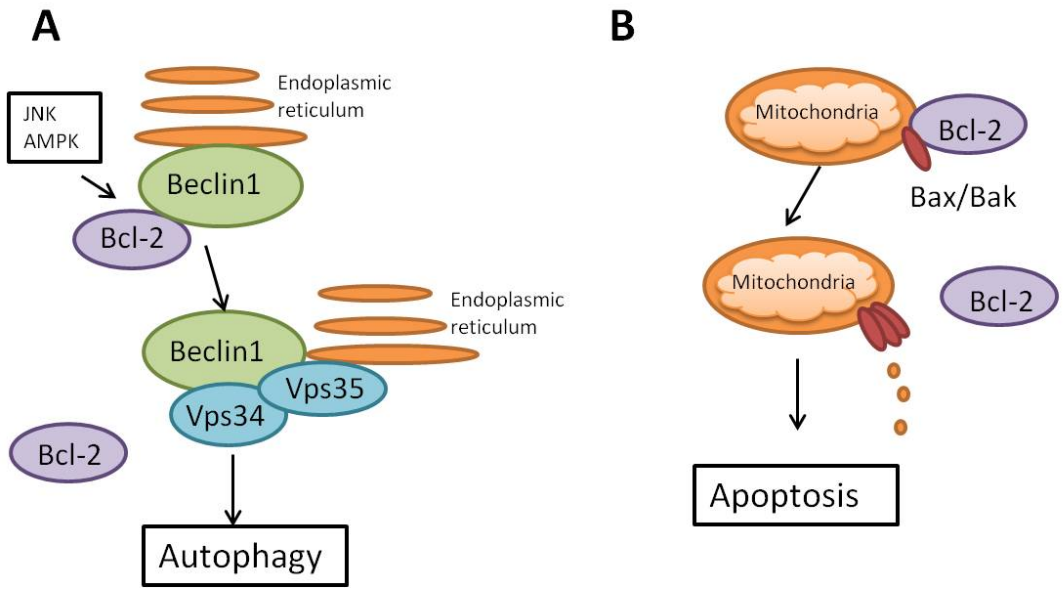

Figure 17. Schematic representation of the role of Bcl-2 in autophagy and apoptosis modulation. Bcl-2 can bind to multiple BH-3 only proteins such as Beclin 1, BAD and BAX. **A.** Bcl-2 binding to Beclin 1 results in its sequestration and inhibition of autophagy. **B.** Bcl-2 binding to the proapoptotic BAK and BAX prevents mitochondrial depolarization and subsequent apoptosis.

In addition to the Beclin 1-Bcl-2 interaction, the autophagic and apoptotic pathways meet at additional points. Upon autophagy initiation, Atg5 is activated by cleavage of its N-terminus, this proteolytic product has been shown to translocate to the mitochondrial membrane and disrupt the Bcl-xL-BAX complex, resulting in cytochrome-c release and subsequent apoptosis (Yousefi, Perozzo et al. 2006, Marquez and Xu 2012). Atg5 N-terminus binding to Bcl-xL could prevent the antiapoptotic Bcl-xL binding to BAX, and therefore promote BAX-induced mitochondrial depolarisation and apoptosis. Similar to this mechanism, Beclin 1 has been shown to undergo caspase cleavage during apoptosis, cleaved Beclin 1 is no longer able to initiate autophagy, so this cleavage results in autophagy inhibition (Gordy and He 2012). Cleaved Beclin 1 C-terminus can translocate to the mitochondria membrane and promote cytochrome-c release (**Figure *18***) (Wirawan, Vande Walle et al. 2010).

In addition to its pro-apoptotic role, p53 can down regulate LC3B expression at a post-transcriptional level in conditions of nutrient deprivation (Li, Gao et al. 2016). Interestingly, the antiapoptotic protein FLIP has been reported to bind to Atg3 and prevent LC3BI lipidation into LC3BII, therefore preventing autophagy initiation (Li, Gao et al. 2016).

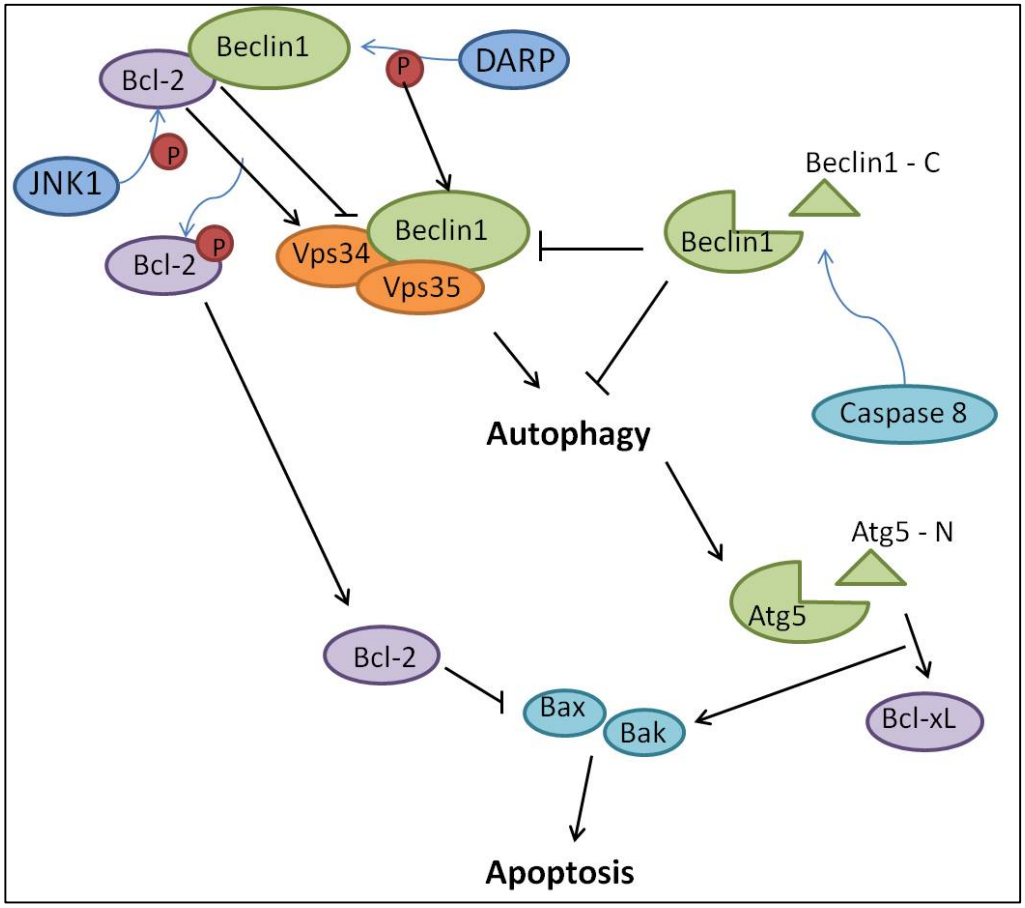

Figure 18. Schematic representation of the crosstalk between autophagy and apoptosis. The Bcl-2 protein plays an inhibitory role in both autophagy and apoptosis by binding Beclin 1 or Bax and Bak, respectively. The Atg5 cleaved N-terminus promotes apoptosis by preventing Bcl-xL inhibitory binding to Bak. Cleaved Beclin 1 is not able to induced apoptosis while Beclin 1 C-terminus can promote Cytochrome-C release.

1.8 NECROSIS

Necrosis is a cell death mechanism characterised by distint morphological changues such as increased cell volumen, disruption of the plasma membrane, and swelling of organelles, particularly of mitocondria (Golstein and Kroemer 2007, Kroemer, Galluzzi et al. 2009). Unlike apoptosis, necrotic cell death is associated with local inflamation and induction of innate immune response (Festjens, Vanden Berghe et al. 2006). Although in some cases necrosis can occur in an accidental unprogramed way, it can also be the result of a programmed signal transduction pathway. The term necroptosis reffers to an specific programmed necrotic cell death that is induced by signalling though TNFα, TRAIL and FasL

(Wu, Liu et al. 2012) and regulated by the thirosine kinase receptor interacting protein 1 and 3 (RIP1 and RIP3) (Festjens, Vanden Berghe et al. 2007). Upon activation of the TNF receptor, RIP decides the fate of teh cell activating either apoptosis or necroptosis. Apoptosis inhibition as well as RIP3 phosphorilation has been suggested to promote necroptosis (Cho, Challa et al. 2009, Wu, Liu et al. 2012). Active autophagy has been suggested to promote necroptosis by either increasing the amount of reactive oxigen species (ROS) released from the mitocondria (Yu, Wan et al. 2006) and by overactivating PARP (Yu, Wan et al. 2006).

1.9 THREE DIMENSIONAL CULTURES

1.9.1 Introduction to 3-dimensional cultures

Two-dimensional monolayer culture of cancer immortalised cell lines has been widely used for the study and development of new drug treatments for cancer therapeutics and has produced valuable data in cancer biology (Sharma, Haber et al. 2010). However, findings from 2-dimensional cultures are often different from similar studies *in vivo* and in the clinic. Some reasons for these differences are, for example, changes in interactions between cells, changes in cell morphology and the lack of extracellular matrix (ECM) (Birgersdotter, Sandberg et al. 2005, Imparato, Urciuolo et al. 2015).

The application of 3-dimensional culture models has been developed to better mimic the *in vivo* behaviour of native tumours, filling the gap between 2-dimensional and animal models by allowing the study of complex disease processes *ex vivo* and providing a more reliable platform for preclinical drug screening (Imparato, Urciuolo et al. 2015).

Various three-dimensional culture models have been developed in order to overcome the limitations of 2-dimensional monolayer cultures. Human tumour spheroids are frequently used. Spheroids form cellular aggregates when single cells are cultured in non-adherent conditions. This classical technique, developed in the early 70s (Sutherland, McCredie et al. 1971), better replicates solid tumours in many aspects, including cell morphology, gene expression, growth kinetics and in the responses to chemotherapy (Lin and Chang 2008). Spheroids are commonly used for the study of drug diffusion into the tumour however, as penetration of large drug molecules in tumours is often hampered by the collagen present in the ECM (Eikenes, Tufto et al. 2010), the lack of a matrix in spheroids represents one of the limitations of this technique.

The culture of cells in 3-dimensional cultures has evolved with the use of matrices or gels to create scaffolds that mimic the ECM. Matrigel, collagen and hyaluronic acid (HA) are widely used to recreate this matrix (Weaver, Petersen et al. 1997, Gurski, Jha et al. 2009, Fallica, Maffei et al. 2012). Matrigel is formed by several compounds including ECM molecules such as collagen type IV, laminin, cytokines and growth factors. This material aids in the formation of cellular architectures that are seen *in vivo* and also promotes cell migration and differentiation. Unfortunately, the variable composition of matrigel might be a problem in drug screening (Kleinman and Martin 2005).

Cells cultured in collagen gels aggregate in 3-dimensional structures similar to spheroids. In addition to cell-cell attachment, cells grown in these structures form cell-matrix attachments, better mimicking tissues *in situ* (Bates, Edwards et al. 2000). Cells grown in collagen resulted in increased resistance to chemotherapy when compared to the same cell line cultured in monolayer (Bates, Edwards et al. 2000). In addition, despite intrinsic variability (due to chemical crosslinking, pH and temperature), properties of collagen gels are more reproducible than the properties of Matrigel (Imparato, Urciuolo et al. 2015).

In addition to natural matrices, synthetic biomaterials such as PEG-based hydrogel models (Ehrbar, Rizzi et al. 2007) or polylactic acid (PLA) particles (Horning, Sahoo et al. 2008), have also been used for 3-dimensional cultures with the aim of better mimicking *in vivo* tumours.

In summary, cells cultured in matrices or gels better resemble tumour morphology than 2-dimensional cultures, however, they tend to form aggregates similar to spheroids rather than diffusing into the matrix and, therefore, show similar limitations as spheroids.

Use of the 3-dimensional models discussed above has provided significant knowledge about drug diffusion and cellular responses in regard to culture conditions. However, those models rely on the culture of a single cell type, or monoculture. Tumours consist of multiple cell types, and therefore, improved 3-dimensional culture models, that could better resemble tumour complexity, would help advance cancer research.

The 3-dimensional co-cultures were first developed to study skin pathology. Bell et al (Bell, Ivarsson et al. 1979) showed that keratinocytes seeded on top of a collagen layer, which had been coated with dermal fibroblasts, were able to differentiate in normal epidermis. This model was successfully used for the treatment of extensive burn injuries. Since then, skin cultures have been used for the study of the role of cell-cell and cell-matrix interactions in

skin development and differentiation (Stark, Willhauck et al. 2004, Boehnke, Mirancea et al. 2007).

The stromal compartment has been shown to hamper the penetration of therapeutic agents into the tumours and therefore contribute to treatment resistance (Davies Cde, Berk et al. 2002). The co-culture of stromal and tumour cells could better replicate human tumours. The co-culture of epithelial and stromal cancer cells on a Matrigel-coated transwell allowed the study of the effect of epithelial-stromal interactions in tumour progression, invasion and drug response (Froeling, Mirza et al. 2009, Froeling, Marshall et al. 2010, Coleman, Watt et al. 2014).

1.9.2 3-dimensional cultures in Prostate Cancer

Several models of 3-dimensional cultures have been used for the study of different aspects of PCa (Fang, Sittadjody et al. 2013, Ellem, De-Juan-Pardo et al. 2014).

Spheroids are the most popular 3-dimensional culture models in PCa research. Prostate cells are grown in spheroids by providing them with an anchorage-independent microenvironment, either by growing them on purified ECM gels or employing the hanging drop technique (Ellem, De-Juan-Pardo et al. 2014).

The prostate tissue is composed of luminal epithelia from which most prostate carcinomas originate, basal and endocrine cells, all of them surrounded by stromal tissue (***Figure 2***). The prostate stroma is composed of extracellular matrix, smooth muscle, nerves, fibroblast and myofibroblasts, endothelial and inflammatory cells. The interaction between all these components can determine prostate cancer initiation, progression, invasion and also the response to treatment (Ellem, De-Juan-Pardo et al. 2014). In fact, prostate cancer associated fibroblast (CAF) have been shown to promote tumorigenesis of benign epithelia (Ao, Franco et al. 2007). The co-culture of stromal and epithelial PCa can provide significant new information about the role of stroma in PCa progression and development (Ellem, De-Juan-Pardo et al. 2014). In addition, the study of epithelial – stroma interaction may help to advance the understanding of development of drug resistance.

Fang et at (Fang, Sittadjody et al. 2013) developed a 3-dimensional model where the PCa cells C4-2 were co-cultured with the normal prostate stromal cells WPMY-1 in alginate hydrogel microspheres. In this study, direct interaction of the two cell types was not allowed by growing them in separate sub-layers, allowing the study of paracrine interactions. This

work demonstrated that PCa co-cultures can be used for the study of cell-cell paracrine interactions by measuring E-cadherin secretion.

The co-culture of both stromal and epithelial PCa cells in polymeric scaffolds would allow the study of cell-cell interactions and provide significant information about different stages of PCa progression, angiogenesis and metastasis.

1.9.3 The use of 3-dimensional cultures for testing of oncolytic adenoviruses

The use of 3-dimensional co-cultures for the pre-clinical testing of oncolytic adenoviruses has not been widely studied. 3-dimensional monocultures such as spheroids has been used as models for testing the efficacy of oncolytic adenoviruses and to better study viral infection and replication in a platform that would resemble *in vivo* tumours (Lam, Hemminki et al. 2007). The authors found that viral infection and replication was 4-fold greater in monolayers than in 3-dimensional ovarian primary cancer cells spheroids one week after infection. However, replication levels were equal 2 weeks after infection, suggesting that, although encountering initial resistance due to the decreased surface/volume ratio, the virus had successfully replicated and penetrated several cell layers in the 3-dimensional spheroid culture. Virus propagation was indirectly detected by expression of viral-encoded luciferase. Adenovirus has also been shown to effectively deliver transgenes into 3-dimensional organoids (Wang, Zhang et al. 2014). In this study, organoids were derived from mice intestinal crypts and grown in a matrigel matrix. The addition of a GFP-expressing adenovirus into the organoid-containing Matrigel resulted in very poor infection rates. However, infection rates were improved by pre-incubating the virus with organoids prior seeding into the matrix.

1.9.4 3-dimensional model for PCa used in this study

Prof. Hemant Kocher and Prof. John Marshall at our Institute, have established a 3-dimensional model for pancreatic ductal adenocarcinoma (PDAC) that allows the study of the interactions between cancer and stromal cells. The pancreatic stromal cells are embedded in a collagen/matrigel matrix and the epithelial cancer cells can either be embedded in the gel together with the stromal cells to study epithelial-stromal interactions or be seeded on top of the gels to study invasion. The cultures can be raised on top of a grid and fed from underneath to create a nutrient gradient to promote invasion (Froeling, Mirza et al. 2009, Froeling, Marshall et al. 2010, Coleman, Watt et al. 2014). Mini-3-dimensional

cultures were later generated by polymerising the collagen/matrigel matrix inside a transwell® insert. Cancer and stromal cells were seeded on top of the gel and fed from underneath to promote invasion into the gel (Coleman, Watt et al. 2014).

With the aim of generating a 3-dimensional co-culture model that would enable the investigation of viral infection, spread and prevention of tumour cell invasion, the pancreatic 3-dimensional culture model described above was adapted to prostate cancer cell lines and prostate stromal cells. This work was in collaboration with Dr Stella Man (our team) who had previously established additional 3-dimensional PDAC-stromal cell and prostate cancer-stromal cell models. In my study, I used the prostate cancer epithelial PC3 and 22Rv1 cells and the normal prostate stromal PrSC cells (**Figure *19***).

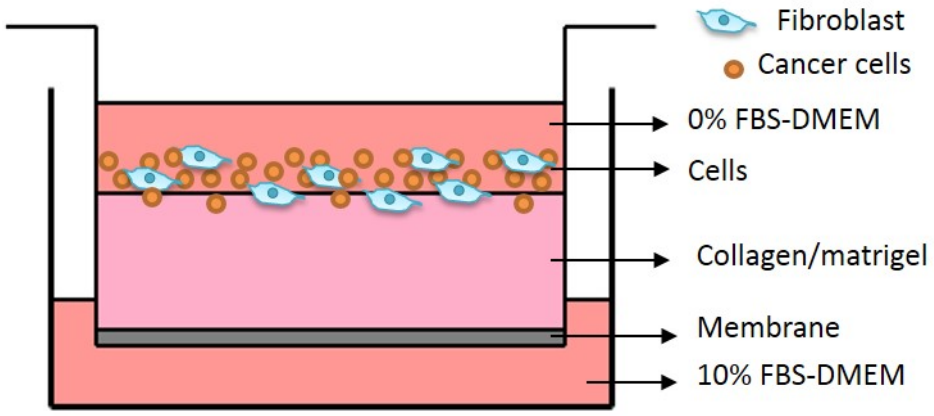

Figure 19. The 3-dimensional culture model used in this project. Transwells® were placed in 24-wells plates. The collagen/matrigel was placed on top of collagen-coated transwells® as described in the methods section. Cancer and stromal cells were seeded together on top of the gel. Cells were fed from underneath the gel with 10% FBS-DMEM to create a FBS gradient and promote invasion into the gel. 0% FBS-DMEM was added on top of the cells to prevent them from drying.

1.10 SUMMARY OF ONCOLYTIC ADENOVIRUSES FOR TREATMENT OF PROSTATE CANCER

In summary, I have discussed how in PCa, once resistance to ADT has developed, the disease remains incurable and chemotherapy treatment may only palliate the symptoms and, in the best scenario prolong survival for a few months. The recent development of novel antiandrogens (discussed in sections 1.2.4 and 1.2.5) is expected to improve the outcome of the treatment, however further research is still needed for treatment of castrate-resistant prostate cancer patients.

Cancer treatment with oncolytic adenoviruses has reported great advances in the past two decades. The safety of oncolytic adenoviruses has been widely proven in several clinical trials treating different types of cancers, including PCa, while moderate efficacy was also reported (**Table *7*** and **Table *8***). Several preclinical studies have shown how oncolytic adenoviruses synergise with several chemotherapeutic drugs and enhance cancer cell death, including PCa *in vitro* and *in vivo* models (discussed in section 1.4.3). However, further mechanistic studies are still needed to completely understand this enhanced cell killing.

Clinical trials for PCa, in which oncolytic adenoviruses have been either administered alone or combined with radiotherapy, have confirmed the safety of the mutants. Efficacy was confirmed with overall decreases in PSA levels (**Table *8***). Novel oncolytic mutants for the treatment of PCa have been generated with a special interest in the stimulation of the host immune response (**Table *9***) and are currently being tested in clinical trials.

The administration of oncolytic adenoviruses is usually restricted to intratumoural injections due to the rapid clearance of adenoviral vectors from the bloodstream. Several promising strategies, including the modification of the viral capsid, or the coating of viral vectors with polymers or nanoparticles, are being developed to enhance infectivity and specificity of the vectors (discussed in section 1.4.7).

1.11 RESEARCH RATIONALE

1.11.1 Background of the project

Previous work in our group includes the development of the potent and replication-selective oncolytic adenoviral mutant AdΔΔ (E1ACR2- and E1B19K-deleted). The deletion of E1ACR2 prevents the E1A protein from interacting with pRB and E2F remains bound. Therefore, S-phase is not induced by the mutant, which prevents viral replication in normal cells and consequently, only cancer cells with deregulated cell cycle support AdΔΔ replication (Oberg, Yanover et al. 2010, Cherubini, Kallin et al. 2011). The absence of the E1B19K protein prevents binding to the proapoptotic Bcl-2 family members BAK and BAX and therefore promotes apoptosis, which is induced by E1A expression and or cytotoxic agents (Putzer, Stiewe et al. 2000, White 2006). In prostate cancer cell lines, the combined treatment of AdΔΔ with the cytotoxic drugs mitoxantrone or docetaxel resulted in synergistic cell killing

and promoted tumour regression in murine xenograft models of prostate cancer (Oberg, Yanover et al. 2010). Further work showed that the sole expression of the E1A12S protein in the absence of viral replication was sufficient to enhance mitoxantrone- and docetaxel-induced cell death in prostate cancer cell lines (Miranda, Maya Pineda et al. 2012). Additional findings in our team demonstrated that deletion of the E1B19K protein only, generating the replicating AdΔE1B19K mutant, enhanced gemcitabine-induced apoptotic cell death in models of pancreatic cancer (Leitner, Sweeney et al. 2009, Pantelidou, Cherubini et al. 2016). Furthermore, our team found that in combination with gemcitabine, only mutants with the E1B19K gene deleted caused enhanced apoptotic cell killing (Pantelidou, Cherubini et al. 2016). The increased apoptosis was the result of increased E1A expression in E1B19K mutants (AdΔΔ and AdΔ19K). Additional, but yet unpublished work, demonstrated that the expression profiles of miRNAs were different in PC3 prostate cancer cells infected with a non-replicating E1A12S-expressing mutant, mitoxantrone-treated and in cells treated with the combination under synergistic conditions. For example, miRNAs that are typically down-regulated in human prostate cancer had increased expression in response to virus and mitoxantrone including members of the miR-15/16 family (Maya Pineda 2013, Tazawa, Kagawa et al. 2013). The miR-15/16 family regulates cell cycle, apoptosis and survival pathways. Other identified miRNAs were down-regulated in response to the combination treatment e.g. miR-99 that targets mTOR and consequently would promote autophagy in prostate cancer. Taken together, these findings led us to investigate the role of apoptosis and autophagy in combination-treated prostate cancer models and if AdΔΔ and/or E1A expression alone could inhibit autophagy and thereby promote apoptosis.

1.11.2 Aims and objectives of the project

The current project was a continuation of previous work in my team that demonstrated that AdΔΔ can synergistically interact with the cytotoxic drugs mitoxantrone and docetaxel to enhance cell killing in PCa models (Oberg, Yanover et al. 2010). The overall goal of this project was to determine the role of AdΔΔ, in combination with the cytotoxic drug mitoxantrone, in the enhanced cell death focusing on apoptosis and autophagy regulation in the 22Rv1, PC3 and PC3M PCa cells.

We hypothesised that AdΔΔ-mediated enhancement of mitoxantrone-induced apoptotic cell killing was caused by AdΔΔ-mediated attenuation of drug-induced autophagy. We anticipated that identification of key cellular factors responsible for the increased cell killing would enable future developments of improved therapeutics for late stage prostate cancer patients, either small molecule drugs or improved oncolytic viruses.

1.11.2.1 Objectives:

A major objective was to elucidate the cellular mechanism by which AdΔΔ modulates apoptosis and autophagy in mitoxantrone-treated PCa cells. Another objective was to explore whether autophagy-inhibition in AdΔΔ-infected cells could reverse chemotherapy-resistance and enhance drug-induced cell killing in PCa as previously proposed using pharmacological autophagy-inhibitors (Chen and Karantza 2011, Ziparo, Petrungaro et al. 2013, Farrow, Yang et al. 2014).

1.11.2.2 Aims:

- To determine whether AdΔΔ attenuates mitoxantrone-induced autophagy in PCa cells
- To investigate whether AdΔΔ-mediated autophagy-inhibition increases sensitivity to mitoxantrone by enhancing apoptotic cell killing in PCa cells that are highly insensitive to drug-induced killing (models of resistance)
- To dissect the cellular mechanism of AdΔΔ-mediated attenuation of autophagy
- To validate the findings from cells grown on plastic in more physiologically relevant models such as 3-dimensional co-cultures of PCa and stromal cells
- To improve on adenoviral uptake in PCa cells that are poorly infectible and therefore insensitive to viral cell killing

2 MATERIALS AND METHODS

2.1 REAGENTS

Mitoxantrone (Onkotrone®) hydrochloride for injection (20mg/ml; 4.5mM) was purchased from Baxter (Norfolk, UK), and kept at 4°C. Staurosporine (Sigma-Aldrich, MI, USA) was reconstituted in DMSO to 1mM and stored at -20°C. Rapamycin (Calbiochem, La Jolla, CA, USA) was dissolved in DMSO to 100µM and stored at -20°C. Chloroquine (Sigma-Aldrich) was dissolved in H_2O to 100mM and kept in aliquots at -20°C. Tetramethylrhodamine ethyl ester perchlorate (TMRE), purchased from Invitrogen (Paisley, UK), was dissolved in DMSO to 1mg/ml and kept at -20°C. The CellTiter 96® AQeous Non-Radioactive Cell Proliferation Assay, composed of MTS reagent (3-(4,5-dimethylthiazol-2-yl)-5(3-carboxymethoxyphenyl)-2-(4-sulphophenyl)-2H-tetrazolium) (CellTiter 96® AQueous MTS Reagent Powder) and phenazine methosulphate (PMS), was purchased from Promega (Southampton, UK). 1g of MTS was dissolved in 500ml of DPBS, MTS and PMS were both stored at -20°C. Penicillin and streptomycin (Penicillin 10000 units/ml, Streptomycin 10mg/ml), and Trypsin-EDTA solutions were purchased from Sigma-Aldrich and stored at 4°C. Bovine serum albumin (BSA) was purchased from Sigma-Aldrich and used for the preparation of different buffers, or purchased from New England Biolab and used for the preparation of a standard curve for protein quantification. Formalin solution was purchased from Sigma-Aldrich and used for fixing. DNase and RNase free H_2O was purchased from Sigma-Aldrich.

2.2 CELL LINES AND CULTURE CONDITIONS

The human prostate carcinoma cell lines 22Rv1 (ATCC, USA), and PC3 (ECACC, UK) were used in this study. The 22Rv1 cells were previously derived from a xenograft, of the androgen-dependent CWR22 xenograft and serially passaged in mice after castration-induced regression and relapse of the parental CWR22 (Sramkoski, Pretlow et al. 1999). The CWR22 xenograft was generated from a primary prostatic human carcinoma (Nagabhushan, Miller et al. 1996). PC3 cells were previously isolated from a grade IV vertebral metastatic prostate tumour (Kaighn, Narayan et al. 1979) and are a model for bone metastasis. A subline of PC3 cells, the PC3M cells (a kind gift from Dr. Prabhkar Rajan, Centre for Molecular Oncology, BCI) were previously isolated from metastases in mice injected with PC3 cells, and have more aggressive growth characteristics than the parental PC3 cell line (Stephenson, Dinney et al.

1992). Normal human prostate stromal cells PrSC (Lonza, NH, USA) were used in the 3-dimensional co-culture studies. **Table 10** highlights some genetic characteristic of PC3 and 22Rv1 cell lines.

The human embryonic kidney cell line HEK293 and the sub-line JH293 (CRUK Cell Services, London, UK) were used for replication studies and viral production.

Cells were cultured in Dulbecco's Modified Eagle Medium (DMEM) supplemented with 10% foetal bovine serum (FBS; Gibco, Life technologies, CA, USA) and 1% penicillin and streptomycin (Penicillin 10000 units/ml, Streptomycin 10mg/ml) at 37°C and 5% CO_2. Infections with different viruses were performed in 1ml 0% FBS-DMEM for 2-3h in 6-well plates or in 100µl 2% FBS-DMEM when cultured in 96-well plates. All cell lines were obtained from departmental stocks ($N_{2(l)}$ storage) that had previously been authenticated by short tandem repeat (STR) profiling (LGC Standards, Middlesex, UK) in 2010 and 2015. The PC3M cells had previously been authenticated by Dr Rajan.

Table 10. Genetic status of 22Rv1 and PC3 PCa cell lines.

	22Rv1 Prostate xenograft	PC3 Bone metastasis	Significance
p53	+	-	Tumour suppressor, modulation of cell proliferation and apoptosis
AR	+ Two AR forms; wt and truncated AR-V7 (splice variant, lacks the C-terminal domain, receptor constitutively active) Androgen independent	- (no mRNA or protein expressed) Androgen independent	AR wt; sensitive to androgen deprivation treatment AR mutant; constituvely active and insensitive to androgen deprivation treatment
PSA	(mRNA only)	-	AR-regulated gene: detection of PSA in

		(no mRNA or protein expressed)	patient's blood is used for early diagnosis of PCa
pRB (retinoblastoma protein)	+	+	Regulation of S-phase induction
Bcl-2	+	+	Over expressed in PCa → Inhibition apoptosis
PTEN	+	-	PTEN positive cells more easily enter apoptosis
CAR (coxsackie adenovirus receptor)	High	Low	CAR facilitates Ad infection (attachment receptor)
Integrin $\alpha_v\beta_3$	Low	Low	$\alpha_v\beta_3$ facilitates Ad infection (internalization receptor)
Integrin $\alpha_v\beta_5$	Low	Low	$\alpha_v\beta_5$ facilitates Ad infection (internalization receptor)

+ protein is expressed, - protein is not expressed. References: (Pandha, Stockwin et al. 2003, Skjoth and Issinger 2006, Olsson, Feber et al. 2007, Adam, Ekblad et al. 2012, Thangavel, Boopathi et al. 2014, Cunningham and You 2015, Lu, Lonergan et al. 2015).

PC3M cells show similar characteristics to PC3, from which they were derived. PC3M cells do not express AR or PSA (Sobel and Sadar 2005).

2.3 ADENOVIRUSES

The species C wild type adenovirus type 5 Ad5tg (also referred to as Ad5wt) was previously generated from pTG3602 (Oberg, Yanover et al. 2010). The replication-selective AdΔΔ mutant (AdE1ACR2- and AdE1B19K- deleted), the non-replicating AdE1A12S (Ad12S) (CMV-E1A12S replacing E1 region and E3 genes deleted) and AdGFP (CMV-GFP replacing E1 region and E3 genes deleted) mutants were produced and characterized as previously described (***Figure 20***) (Miranda 2009, Oberg, Yanover et al. 2010). During my thesis work I produced one batch each of Ad5wt and AdΔΔ. Ad12S, AdGFP and another batch of AdΔΔ were produced by previous members of the group (**Table *11***).

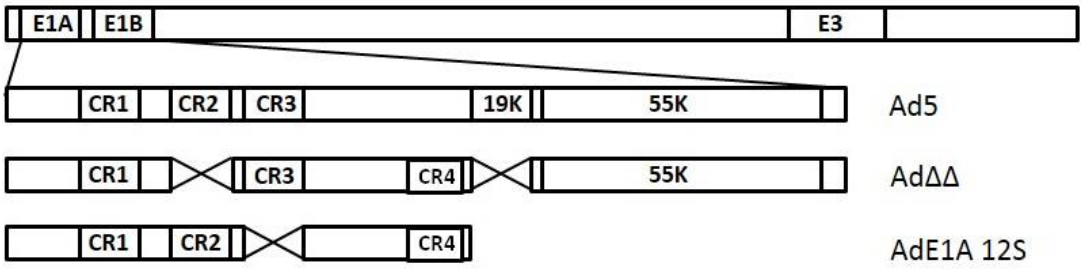

Figure 20. Schematic representation of adenoviruses used in this study. The AdΔΔ mutant is deleted in the E1ACR2 and in E1B19K for replication selectivity and apoptosis promotion, respectively. The AdE1A12S (Ad12S) mutant contains the E1A12S protein (deleted in E1ACR3) under control of a CMV promoter. Ad5wt and AdΔΔ have intact E3 genes while E3 is deleted in the AdE1A12S mutant.

Table 11. Virus batches used in this study.

Virus	Batch	vp/ml	pfu/ml	vp/pfu ratios
Ad5wt	270314	4.12xE10	4xE10	1.0
AdΔΔ	260109	2.4xE11	1.56xE10	15.4
AdΔΔ	050314	2.82xE11	1.22xE11	2.3
Ad12S	160912	2.91xE11	4.91E+08	592.7
AdGFP	100811	2.78E+11	2.03E+08	1369.5

2.3.1 Viral production

Primary viral expansions were generated by infecting a T175 flask of HEK293 cells at 80% confluency with 30µl of purified stock of the desired virus. The flask was monitored daily and medium and cells were collected upon appearance of cytopathic effects (CPE), usually 48-72 h post-infection, and stored at -80°C. HEK293 were seeded in 16 T175 flasks in 10% FBS-DMEM and grown to 80% confluency. The medium was then replaced with 2% FBS-DMEM and flasks were infected with 250µl/flask from the primary expansion. Cells and medium were collected upon appearance of CPE and when cell detachment was observed (usually 72h post-infection).

Collected cells and medium were centrifuged at 2000rpm for 10min at 4°C, the resulting supernatant was discarded and the pellets were washed in cold PBS and centrifuged at 1000rpm for 10min at 4°C. PBS was discarded and the cell pellets resuspended in 12ml of cold 10mM Tris-HCl (pH 8.0). The tubes were stored at -80°C or directly freeze-thawed three

times in liquid N_2/37°C, to release viral particles from the cells, and centrifuged at 6000rpm, for 10min at room temperature. The resulting supernatants were added on top of a previously prepared caesium chloride (CsCl) gradient, 3.5" ultracentrifuge tubes (Beckman Coulter, High Wycombe, UK) and centrifuged at 25000rpm for 2h at 15°C in a Beckman SW28 swing-out rotor in an Optima LE-80K ultracentrifuge. The CsCl gradient was prepared with 10ml 1.25g/ml CsCl under-layered with 7.6ml 1.4g/ml CsCl solution. After centrifugation, three bands were visible in the tube. The top band corresponded to the remaining cell debris and the middle band to empty viral particles, and both bands were discarded. The band of interest, containing encapsulated viral particles, was located at the bottom. This band was extracted using a 19G needle. The extracted virus was added on top of 2" ultracentrifuge tubes containing a CsCl solution (2.5ml 1.35g/ml) and centrifuged overnight at 40000rpm for 15h at 15°C in a Beckman SW55Ti swing-out rotor. The purified virus was collected using a 19G needle and the resulting volume diluted 2-3 fold (up to a maximum of 12ml) with TSG buffer (96mM NaCl, 0.5mM Na_2-HPO_4, 2.8mM KCl, 0.3mM $MgCl_2$, 0.5mM $CaCl_2$ and 30% (v/v) glycerol adjusted to pH7.5). The suspension was dialysed for 24h at 4°C using a 3-12ml Slide-a-Lyser (Pierce Biotechnology, IL, USA) against a buffer containing 10mM Tris-HCl (pH7.5), 1mM $MgCl_2$, 150mM NaCl and 10% (v/v) glycerol. The purified and dialysed virus was extracted from the dialysis chamber, aliquoted and stored at -80°C.

2.3.2 Viral characterization

2.3.2.1 Determination of viral particle counts

Viral DNA content was measured to determine the particle counts of the purified virus with a Quanti-iT PicoGreen dsDNA assay kit (Invitrogen) using a Tecan Infinite F200 plate reader (Tecan, Mannedorf, Switzerland) and Magellan software version 6.3 (Tecan). Viral stocks were diluted 1:2 in Tris-EDTA buffer (TE; 10mM Tris-HCl (pH8), 1mM EDTA) containing 0.5% SDS and heat-inactivated at 56°C for 10min. The virus was diluted (neat virus, 1:2, 1:6, 1:10) in TE buffer and 100µl were assayed in triplicates in a 96-well plate. An already characterised Ad5wt was used as a control. Lambda-phage DNA (provided in the kit) was serially diluted (1/5 dilutions) in TE buffer and used to generate a standard curve, starting at 500ng/ml. 100µl of Pico Green reagent (1/200 diluted) was added to each well. Absorbance was measured at 535nm after excitation at 485nm. The DNA concentrations of the standard curve (lambda-phage DNA-dilutions) were plotted versus fluorescence. Viral particle counts

(vp/ml) were calculated by linear regression analysis taking the dilution of the samples into account, and assuming that 1 µg DNA = $2.7x10^{10}$vp.

2.3.2.2 Determination of the number of infectious particles by the Tissue Culture Infectious Dose ($TCID_{50}$) assay

JH293 cells (10,000 cells/well) were seeded in 96-well plates in a total volume of 200µl/well of 10% FBS-DMEM. The following day, 20µl of dilutions of the purified virus ($1/10^5$ – $1/10^7$ dilutions) were prepared in 0% FBS-DMEM and added to the top row of the previously seeded cells.

Serial dilutions of the added sample were performed in the seeded plates serially transferring 20µl of one row to the row bellow. The last row was left uninfected as controls. Plates were incubated for 7 to 10 days and scored for signs of CPE, determined as an area of infection within the monolayer surrounded by uninfected cells. The assay was performed in duplicates or triplicate plates. The titre of each sample was calculated using a validated Excel spread-sheet based on the following equations and expressed as plaque forming units per ml (pfu/ml) (O'Reilly 1994).

$TCID_{50} = 10^{L - d(s - 0.5)}$

$TCID_{50}$ /ml = $TCID_{50}$ x v

L = lowest dilution with CPE

d = log difference between dilution steps

s = Σ proportion of CPE+ wells in each row

v = infection volume = 0.02ml

pfu/ml = Log $TCID_{50}$ x µ

Where $\mu = -\ln p = 0.69$

According to the Poisson distribution:

µ is the mean concentration of infectious particles at a given dose

p is the proportion of cultures remaining uninfected = 0.5

2.3.2.3 Validation of deletions and identity of the produced virus by PCR

To characterise the newly produced viruses, expected deletions in the mutants were verified by PCR. Eight primer sets specific for Ad5 and one set specific for E1A12S were used (**Table**

12 and **Table *13***). Viral DNA was extracted using a QIAmp DNA Blood Mini Kit (Qiagen, Manchester, UK) according to the manufacturer's instructions. DNA was eluted in 200µl Buffer AE (suplied in the kit). 20µl of proteinase K (Qiagen) were added to the purified DNA to avoid protein contamination. Purity and concentration of DNA samples were assessed using the NanoDropTM1000 Spectrophotometer (Thermo Fisher Scientific). DNA and RNA concentrations are determined at 260nm following the formulas bellow (Gallagher 2001):

Beer-Lambert equation:

$$A = \varepsilon bc$$

Where A = absorbance, ε = molar absortion coefficient, b = path length and c = concentration. Given that ε and b are constant, absorbance is proportional to the concentration. When using a 1 cm path length, ε= 20.

$$DNA\left(\mu g/_{ml}\right) = (OD_{260})\ x\ (dilution\ factor) x\ (50\ \frac{\mu g\ DNA/_{ml}}{1\ OD_{260}\ unit})$$

$$RNA\left(\mu g/_{ml}\right) = (OD_{260})\ x\ (dilution\ factor) x\ (40\ \frac{\mu g\ DNA/_{ml}}{1\ OD_{260}\ unit})$$

The PCR reaction was prepared in a PCR tube containing 50ng of purified viral DNA, 2.5µl of each forward and reverse primers (**Table *12***), 1µl 50x dNTPS (10mM each), 3µl 10x PCR buffer and 1µl Taq polymerase made up to a final volume of 30µl with DNase and RNase free H_2O. DNA was amplified by 35 cycles (94°C 40s, 62°C 60s, 72°C 90s) in a Gene Amp PCR system 9700 (Applied Biosystems; Thermo Scientific). Amplified products were analysed together with a Quick-Load® 100 bp DNA Ladder (New England Biolabs) on a 1.5% agarose gel in the presence of Ethidium Bromide (EtBr). Characterization of new viral batches was performed by other members in my group.

Table 12. PCR primers used to confirm virus deletion status.

Primer set	Direction	Sequence (5' to 3')
1	5' forward	CCCGGTGAGA TTCCTCAAGAGGCCAC
	3' reverse	CCGGACCCAAGGCTCTCTGCTCTCCGGCTGCTCGGGC
2	5' forward	GTAATGTTGGCGGTGCAGGAAGGGATTG
	3' reverse	GGGTCCCCCGTATTCCTCCGGTGATAATGAC

3	5’ forward	GTGTTCGCTTTGCTATATGAGGACCTGTGGC
	3’ reverse	CCTCGATACATTCCACAGCCTGGCGACGCCCACC
4	5’ forward	CCTGTGATTGCGTGTGTGG
	3’ reverse	GACAACAGTAGCAGGCGATTC
5	5’ forward	GCATCTGTGGAGAGCGGTTGTGAGACAC
	3’ reverse	GCGCCAGCAGATCAAGCTCATTAGCGC
6	5’ forward	GCTTAATGACCAGACACCGTCCTGAGTG
	3’ reverse	GCACCAAGTGA TCGGGCCTCAGCTCC
7	5’ forward	CACCCTCACGCTCATCTGCAGCCTCATCACTGTGG
	3’ reverse	CTTCAGACGGTCTTGCGCGCTTCA TCTGC
8	5’ forward	CGCTGGGGTCGCCACCCAAGATGATTAGG
	3’ reverse	GAGTAGGGTACAGACCAAAGCGAGCACTG
E1A12S	5’ forward	GCGCGCACCATGAGACATATTATCTGCC
	3’ reverse	CTCGAGTTATGGCCTGGGGCGTTTAC

Table 13. Regions of the Ad5 genome targeted by PCR primer sets and expected size of DNA fragments.

Primer set	5’ binding site	3’ binding site	Target sequence	Expected PCR product size for Ad5 (bp)
1	476	853	E1A start	377
2	767	1029	E1A-CR2	262
3	1069	1453	E1A end	384
4	1554	2086	E1B-19K	532
5	2073	2440	E1B-55K	367
6	2383	3434	E1B-55K	1051
7	29915	31038	E3B	1123
8	28715	29135	E3-gp19K	420
E1A12S	476	1453	E1A	800

2.4 CELL VIABILITY ASSAYS

2.4.1 MTS cell proliferation assay

The PC3, PC3M, PrSC (10,000 cells/well) and 22Rv1 (20,000 cells/well) cells were seeded 24h before treatment and/or infection with 10% FBS-DMEM in 96-well plates in a total volume of 100µl/well. Cells were treated as described below.

Cell viability was measured using the CellTiter 96® AQeous Non-Radioactive Cell Proliferation Assay (MTS; Promega) according to the manufacturer's instructions 3 to 5 days after treatment (as indicated) using untreated cells (fixed doses) and/or cells treated with viruses alone or with the combination of viruses and rapamycin or chloroquine (sensitisation assay) as controls. The tetrazolium compound MTS, in the presence of PMS, is converted by metabolically active cells into a soluble formazan dye, whose absorbance can be detected at 490nm. The amount of absorbance is directly proportional to the number of viable cells and was used to measure cell viability (Dunigan, Waters et al. 1995).

$$\%\ cell\ death = 100 - \left(\frac{Abs_{sample} - Abs_{medium}}{Abs_{untreated} - Abs_{medium}}\right)$$

2.4.1.1 Determination of EC_{50}–values

Cells were seeded as described in section 2.4.1. On the day of treatment, medium was decanted and replaced with 90 µl of 2% FBS-DMEM. To determine the effective dose that killed 50% of cells (EC_{50}-value), dose-response curves for Ad5wt, AdΔΔ and Ad12S and mitoxantrone were generated treating the cells with 10 µl of serial dilutions of viruses and mitoxantrone. Serial dilutions of virus were performed in 0% FBS-DMEM starting at 100,000 particles per cell (ppc) and mitoxantrone starting at 200µM (for PC3 cells) or 40µM (for 22Rv1, PC3M and PrSC cells).

2.4.1.2 Fixed doses of virus in combination with mitoxantrone

Cells were seeded as described in section 2.4.1. On the day of treatment, medium was decanted and replaced with 80 µl of 2% FBS-DMEM. Dilutions of the treatments were prepared in 0% FBS-DMEM and 10-fold more concentrated since final dilution was 1/10 in the well. 10 µl of the indicated doses of Ad5wt, AdΔΔ, and Ad12S and/or mitoxantrone were

added to the cells and incubated at a final volume of 100 µl. In wells treated with a single agent, an additional 10 µl of 0% FBS-DMEM was added to make up to the 100 µl final volume.

Theoretical-additive cell killing effects of mitoxantrone and virus were calculated by adding the cell death caused by each single agent treatment alone. The combined treatment of mitoxantrone and virus resulted in more than additive cell killing effect when the cell death as a result of the combined treatment was significantly higher than the theoretical additive.

2.4.1.3 Sensitisation: Dose-response to mitoxantrone in the presence of fixed doses of drugs and/or virus

Cells were seeded as described in section 2.4.1. On the day of treatment, medium was decanted and replaced with 70 µl of 2% FBS-DMEM. Dose-response curves to mitoxantrone were generated treating the cells with 10 µl of serial dilutions of the drug. Serial dilutions of mitoxantrone were performed in 0% FBS-DMEM starting at 200µM for PC3 cells or 40µM for 22Rv1 cells. 10 µl of the indicated doses of Ad5wt, AdΔΔ and Ad12S at fixed doses and/or chloroquine or rapamycin were added to mitoxantrone-treated cells in a final volume of 100 µl. Dilutions of the treatments were prepared in 0% FBS-DMEM and 10-fold more concentrated since final dilution was 1/10 in the well. In wells treated with mitoxantrone only, or together with a single agent, 20 µl or 10 µl of 0% FBS-DMEM was added to make up to the 100 µl final volume.

2.4.2 Trypan Blue exclusion assay

The PC3 (200,000 cells/well) and 22Rv1 (400,000 cells/well) cells were seeded 24h before treatment and/or infection in 2 ml in 10% FBS-DMEM in 6-well plates. Cells were infected with indicated fixed doses of Ad5wt, AdΔΔ or Ad12S in 0% FBS-DMEM, and/or treated with the indicated fixed doses of mitoxantrone in 10% FBS-DMEM at 2-3h after infection. Cells were trypsinised 3 days after treatment and the percentages and numbers of live cells (cell/ml) were determined by adding Trypan Blue solution (Sigma-Aldrich). The Trypan blue dye is able to internalise in dead cells with damaged cell membranes while it does not stain live cells with intact membranes (Strober 2001). Cells were mixed with Trypan blue dye (1:1) and detected using a BioRad TC20 automated counter. The amount of cell death is expressed as 100% - % of live (unstained) cells.

$$\%\ cell\ death = 100\% - (\%\ of\ live\ cells)$$

2.5 DETERMINING CHANGES IN PROTEIN EXPRESSION

2.5.1 Protein extraction, quantification and sample preparation

The PC3, PC3M (200,000 cells/well) and 22Rv1 (400,000 cells/well) cells were seeded in 2 ml in 10% FBS-DMEM in 6-well plates 24h before treatment. Cells were infected with indicated fixed doses of Ad5wt, AdΔΔ or Ad12S in 0% FBS-DMEM, and/or treated with the indicated fixed doses of mitoxantrone in 10% FBS-DMEM at 2-3h after infection and collected 48h later (unless otherwise indicated) by trypsinization, pelleted and washed in PBS. Cells were lysed in RIPA buffer (50mM Tris-HCl, 150mM NaCl, 1mM EDTA, 1% (v/v) NP40 and 0.1% (w/v) SDS) supplemented with PhosphoSTOP phosphatase inhibitor and protease inhibitor cocktail (Roche Diagnostics, Switzerland). Lysis was allowed at 4°C for 30min and samples were stored at -80°C. Before use, the protein extracts were centrifuged at 10,000rpm for 15min at 4°C, and the cell pellets were discarded.

Protein extracts were quantified using the Bradford assay (Bio-Rad). 5µl of 1/5 diluted protein extracts were added to 195 µl of 1x Bradford dye reagent in duplicates. Serial dilutions of BSA (starting concentration 1mg/ml) were used to construct a standard curve. Absorbance was detected using the 560nm filter of the Victor3TM-1420 multilabel plate reader (PerkinElmer, MA, USA). 5x Laemmli buffer (2% SDS, 250mM Tris-HCl pH7.5, 5mM EDTA, 50% glycerol and bromophenol blue (0.25% w/v)) was added to the protein extracts, with β-mercaptoethanol (2% v/v) added immediately before use. Samples were heated at 95°C for 5 - 10 min and stored at -20°C.

2.5.2 SDS-PAGE and immunoblotting

Equal amounts (15 – 20µg) of protein lysates were loaded and separated on denaturing SDS-PAGE. 4% Polyacrylamide/bis-acrylamide stacking gels were prepared using ProtoGel 30% (w/v) acrylamide/methylene bisacrylamide solution (37.5:1 ratio), 4x ProtoGel Stacking Buffer, TEMED (all from National Diagnostics, GA, USA) and 10% w/v ammonium persulfate (APS). 10-12% Polyacrylamide/bis-acrylamide resolving gels were prepared using ProtoGel 30%, 4x ProtoGel Resolving buffer, TEMED and 10% APS. A PageRuler Prestained protein ladder (10-180KDa) (Fermentas; Thermo Scientific) was included on every gel as a reference for protein size. Protein separation was performed by running the gels at 120V for 75min in

a Bio-Rad system (Bio-Rad) in the presence of running buffer containing 25mM Tris-HCl pH7.4, 250mM glycine and 0.1% SDS. After separation, proteins were transferred to polyvinylidene fluoride membranes (PVDF; Immobilon, Millipore) by wet protein transfer using the Mini Trans-Blot® electrophoretic transfer cell system (Bio-Rad) at 200mA for 100min. Membranes were blocked in 0.1% Tween-20/ 5% milk (Marvel Morrison's) diluted in Tris-buffered saline (TBS) for 1h at room temperature, washed in 0.1% Tween-20/TBS and incubated overnight at 4°C with the respective primary antibodies at dilutions listed in **Table 14**. Antibodies were diluted in 0.1% Tween-20/TBS 5% BSA. Membranes were washed in 0.1% Tween-20/TBS 5 times (5 min each) prior to and after incubation with a secondary antibody diluted in 0.1% Tween-20/TBS 5% milk. Signals were detected by horseradish peroxidase-conjugated (HRP) secondary (Dako) antibodies and chemiluminiscence reagent (Western Lightning Plus-ECL, PerkinElmer Inc.) followed by autoradiography (Fuji Medical X-Ray film, Fuji Film) or digital capture (Chemidoc, GE Healthcare). Densitometric analysis was performed using Image J software. The densitometry value of each band was related to the corresponding loading control to calculate ratios.

Table 14. Antibodies used for immunoblotting

MW of target protein (KDa)	Antibody	Species	Dilution	Type	Supplier	Catalogue number
15 – 18	LC3B	Rabbit	1/3000	Primary	Abcam	Ab51520
26	BCL-2	Mouse	1/1000	Primary	Dako	M0887
32 (cleaved 12 – 17)	Total Caspase 3	Rabbit	1/1000	Primary	Cell signalling biotechnology, Inc.	#9662
42	actin	Goat	1/2000 – 1/5000	Primary	Santa Cruz Biotechnology, Inc.	sc-1615
35 – 45	Ad E1A	Mouse	1/2000	Primary	Gene Tex	GTX23165
52	Beclin 1	Rabbit	1/1000	Primary	Abcam	ab62557
55	Atg5 (Atg5-Atg12)	Rabbit	1/2000	Primary	Cell signalling biotechnology, Inc.	#2630
62	p62	Mouse / Rabbit	1/1000	Primary	Santa Cruz Biotechnology, Inc./ Abcam	sc-28359 / ab109012

70	Ku-70	Goat	1/5000	Primary	Santa Cruz Biotechnology, Inc.	sc-1486
77	Atg7	Rabbit	1/2000	Primary	Merk Millipore	MABN1124
108	Ad hexon (capsid proteins)	Goat	1/1000	Primary	Abcam	ab36851
116 - 89	PARP	Rabbit	1/1000	Primary	Santa Cruz Biotechnology, Inc.	sc-9542 / sc-9541
130	Vinculin	Mouse	1/5000	Primary	Abcam	ab18058
---	Anti-rabbit-HRP	Goat	1/2000	Secondary	Dako	P0448
---	Anti-goat-HRP	Rabbit	1/2000	Secondary	Dako	P0449
---	Anti-mouse-HRP	Rabbit	1/2000	Secondary	Dako	P0447

2.6 FLOW CYTOMETRY

2.6.1 Assesment of mitochondrial membrane depolarization by TMRE staining determined by flow cytometry

The PC3, PC3M (100,000 cells/well) and 22Rv1 (400,000cells/well) cells were seeded in 10% FBS-DMEM in 6-well plates 24h before treatment and/or infection. Cells were infected with fixed doses of AdΔΔ at 20ppc for PC3M and 22Rv1, and at 500ppc for PC3; Ad5wt at 20ppc for PC3M in 0% FBS-DMEM, and/or treated with fixed doses of mitoxantrone at 10 and 25nM for 22Rv1, 450nM and 900nM for PC3 and PC3M, rapamycin (50nM) and/or chloroquine (10μM) in 10% FBS-DMEM 2-3h after infection. Cells and medium were collected at 24, 48, 72, 96, and 120h after treatment by trypsinization. Overnight treatment with staurosporine at 1μM (Sigma-Aldrich) was included as a positive control for apoptosis. Cells were washed in PBS, and resuspended in 500 μl of PBS containing 40μl of 1μg/μl TMRE solution (Sigma-Aldrich). Cells were stained for 30 min at 37°C in the dark. After incubation, cells were washed in PBS and resuspended in 500μl of 4',6-diamidino-2-phenylindole (DAPI; Sigma-Aldrich) and diluted in PBS to the final concentration of 1μg/ml.

Cells were detected in a BD LSRFortessa™ (Becton Dickinson, Oxford, UK) gated with lasers YG 585/15 nm versus V 450/50 nm and analysed using BD FACSDiva™ software (Becton

Dickinson). 10,000 cells were analysed per sample. Cells were gated to exclude the debris and gated as in ***Figure 21***.

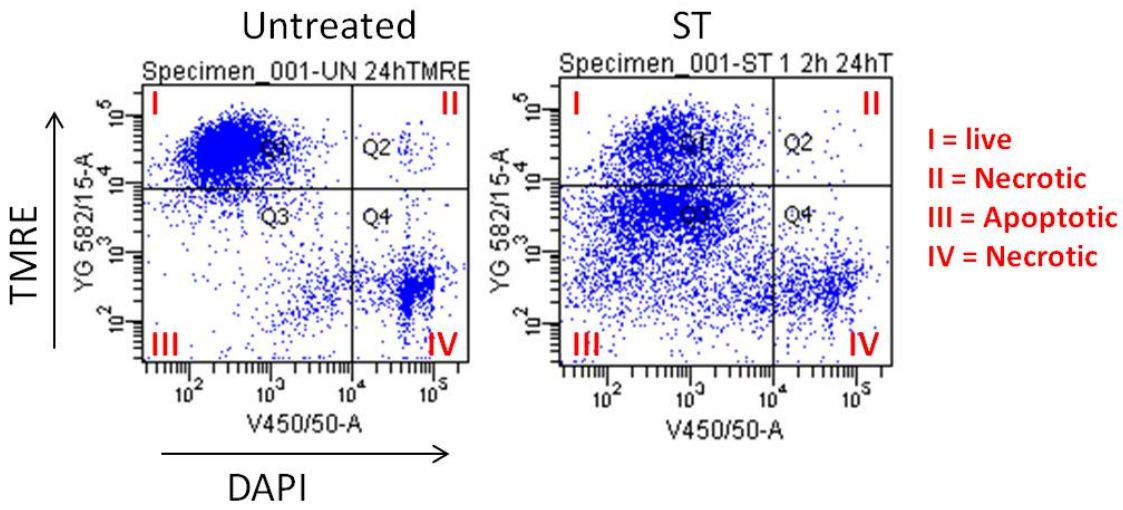

Figure 21. Example of assessment of mitochondrial membrane depolarization by TMRE staining. In this example, 22Rv1 cells treated with the apoptotic inducer staurosporine (ST) underwent depolarization of the mitochondrial membrane, which can be measured as an increase in the number of cells in quadrant III and is a positive indication for apoptosis.

2.6.2 Infectivity determined by flow cytometry

PC3, PrSC (200,000 cells/well) and 22Rv1 (400,000cells/well) cells were seeded in 10% FBS-DMEM in 2ml in 6-well plates 24h before treatment and/or infection. 22Rv1 and PC3 cells were treated with mitoxantrone at 25nM and 900nM for 22Rv1 and PC3, respectively, and 50nM rapamycin or chloroquine at 5µM (22Rv1) or 10µM (PC3). The cells were infected with AdGFP at 10-1000ppc in 0% FBS-DMEM. 2-3h after treatment, the medium was replaced with 10% FBS-DMEM with or without drugs. PrSC cells were infected with AdGFP at 100-1000ppc in 0% FBS-DMEM. 2-3h after treatment, the medium was replaced with 10% FBS-DMEM. Cells were collected 48h after treatment by trypsinization, washed with PBS and detected on a FACS Calibur cytometer (Becton Dickinson Immunocytometry Systems) and/or a BD LSRFortessa™ cytometer (Becton Dickinson, Oxford, UK) and analysed by the BD FACSDiva™ software (Becton Dickinson). 10,000 cells were analysed per sample. Cells were gated to exclude the debris and analysed as in ***Figure 22***.

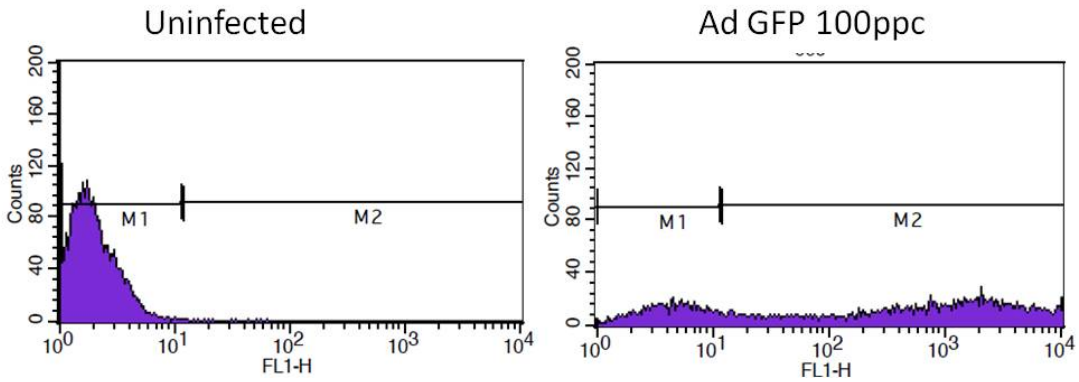

Figure 22. Example of measurement of the percentage of infected 22Rv1 cells by FACS CALIBUR. M1 was adjusted to comprise close to 100% of uninfected cells. M2 comprises GFP positive infected cells.

2.6.3 Assesment of apoptosis by Annexin V staining determined by flow cytometry

The PC3 (75,000 cells/well) cells were seeded in 1ml in 12-well plates 24h before treatment. Cells were infected with AdΔΔ at 500ppc in 0% FBS-DMEM, and/or treated with mitoxantrone at 450 and 900nM, in 10% FBS-DMEM 2-3h after infection. Cells were collected by trypsinisation, washed with PBS, and resuspended in Annexin-binding buffer (10 mM HEPES-KOH, 140 mM NaCl, and 2.5 mM $CaCl_2$, pH 7.4). Cells were incubated with 5 µl of Alexa Fluor® 488 Annexin V (Invitrogen, CA, USA) and DAPI (final concentration 1µg/ml) in a total volume of 100 µl for 15min in the dark. After the incubation period, 400 µl of Annexin-binding buffer were added to each sample. Samples were kept on ice and analysed immediately by flow cytometry. Samples were detected in a BD LSRFortessa™ (Becton Dickinson, Oxford, UK) gated with lasers 585/30nm versus 450/50nm and analysed using BD FACSDiva™ software (Becton Dickinson). 10,000 cells were analysed per sample. Cells were gated to exclude the debris and gated as in ***Figure 23***.

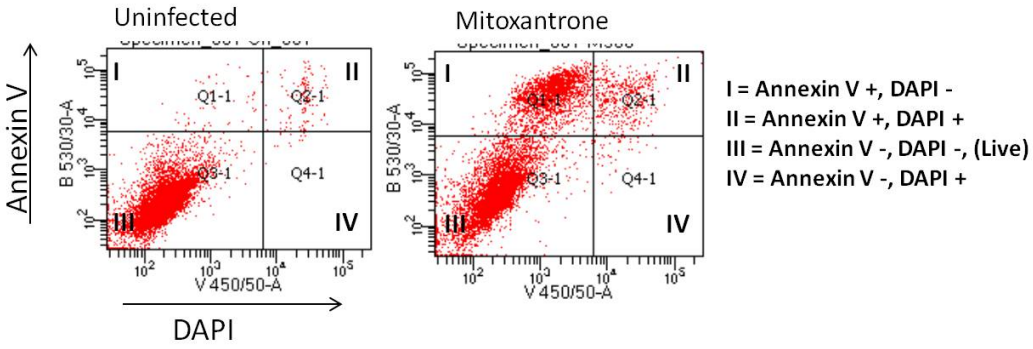

Figure 23. Example of assessment of apoptosis by Annexin V staining. In this example, PC3 cells treated with the pro-apoptotic drug mitoxantrone underwent translocation of phosphatidylserine

from the inner to the outer surface of the cellular membrane, where it binds to Annexin V. Annexin V positive cells were detected in quadrant I and II, and were considered positive for apoptosis.

2.6.4 Staining for surface receptors determined by flow cytometry

The PrSC (200,000 cells/well) cells were seeded 24h prior to collection. 22Rv1 (400,000 cells/well) cells were seeded 24h before treatment. All cell lines were seeded in 2ml 10% FBS-DMEM in 6 well plates. 22Rv1 cells were treated with mitoxantrone (25nM) or left untreated as a control, and collected 48h after treatment by trypsinisation. Once collected, all cell lines were washed twice in 2ml 0.1% BSA in DMEM and incubated with 100µl of the indicated antibody (**Table *15***), diluted 1/100 in 0.1% BSA in DMEM at 4°C in the dark for 30min-1h. After incubation cells were washed twice in 2ml 0.1% BSA in DMEM and incubated with a secondary anti-mouse Alexa Fluor® 488 antibody (Life technologies) diluted 1/250 in 0.1% BSA in DMEM, at 4°C in the dark for 30min-1h. Cells were washed twice with 2ml 0.1% BSA in DMEM and detected on a FACS Calibur cytometer (Becton Dickinson Immunocytometry Systems, UK) and/or a BD LSRFortessa™ cytometer (Becton Dickinson, Oxford, UK) and analysed by the BD FACSDiva™ software (Becton Dickinson). 10,000 cells were analysed per sample. Cells were gated to exclude the debris and analysed as in ***Figure 24***.

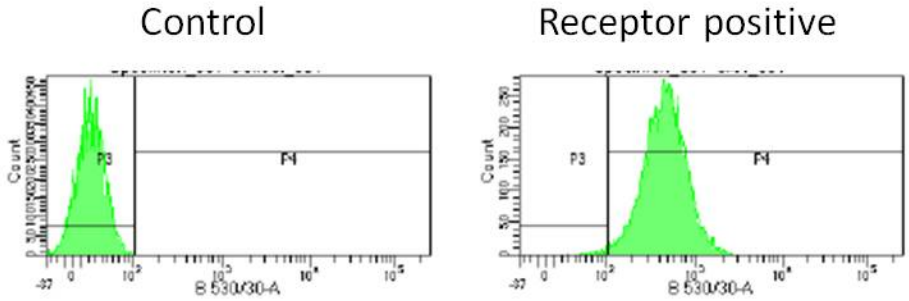

Figure 24. Example of assessment of expression of surface receptors by antibody staining and detection by flow cytometry. In this example, PC3M cells were assessed for expression of CAR (right) using the corresponding antibody. The shift of the peak signal was detected as positive for expression of the receptor. P3 was adjusted to comprise close to 100% of cell in the negative control, P4 comprises cells that are positive for the receptor.

Table 15. Antibodies used in flow cytometry

Antibody	Species	Dilution	Type	Supplier	Catalogue number
Anti-Integrin $\alpha_v\beta3$	Mouse	1/100	Primary	Merk Millipore	MAB1976Z

Anti-Integrin $\alpha_v\beta5$	Mouse	1/100	Primary	Merk Millipore	MAB1961Z
Anti-CAR	Mouse	1/100	Primary	ATCC (VA, USA)	CRL-2379

2.6.5 Autophagy determined by Lysotracker flow cytometry

The PC3 (75,000 cells/well) cells and the 22Rv1 (150,000 cells/well) were seeded in 1ml in 12-well plates 24h before treatment. Cells were infected with AdΔΔ at 500ppc and 20ppc for PC3 and 22Rv1, respectively in 0% FBS-DMEM, and/or treated with mitoxantrone at 450 for PC3 cells or at 10 and 25nM for 22Rv1 cells in 10% FBS-DMEM 2-3h after infection. At 72h or 120h after treatment for 22Rv1 and PC3 cells, respectively, medium was removed from cells and replaced with 50nM Lysotracker® green (Invitrogen) diluted in 10% FBS-DMEM, incubation was allowed for 1h at 37°C in the dark. After incubation, cells were trypsinised and washed twice with PBS. Samples were kept on ice and analysed immediately by flow cytometry. Samples were detected in a BD LSRFortessa™ (Becton Dickinson, Oxford, UK) with laser 530nm and analysed by the BD FACSDiva™ software (Becton Dickinson). 10,000 cells were analysed per sample. Cells were gated to exclude the debris and gated as in ***Figure 25***.

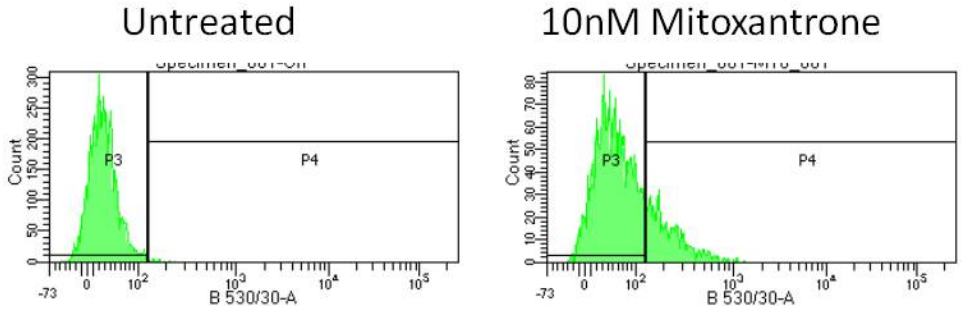

Figure 25. Example of autophagy assessment by Lysotracker®. In this example, 22Rv1 cells were assessed by Lysotracker staining. The shift of the peak signal was detected as positive for acidic vesicles. P3 was adjusted to comprise close to 100% of untreated cells, P4 comprises cells that are positive for acidic vesicles.

2.7 Replication assay (Tissue culture Infective Dose, $TCID_{50}$)

2.7.1 Infection, collection and virus extraction

The PC3, PrSC (200,000 cells/well) and 22Rv1 (400,000cells/well) cells were seeded in 2ml 10% FBS-DMEM in 6-well plates 24h before treatment and/or infection. Cells were infected with Ad5wt and AdΔΔ at 200ppc for PC3 and 100ppc for 22Rv1 and PrSC cells, in 0% FBS-

DMEM for 2-3h. Medium was replaced by 10% FBS-DMEM with or without 50nM rapamycin, 10µM chloroquine and/or mitoxantrone at 900nM and 25nM for PC3 and 22Rv1, respectively; or 10% FBS-DMEM (PrSC cells). Medium and cells were collected after 24, 48 and 72h by detaching cells from plates by scraping and samples were stored at -80°C. Samples were processed and assayed as described in section 2.3.2.2. Samples were diluted 1/100 – 1/1000 before adding them to the first row of 96-well plates previously seeded with 10000 JH293 cells.

2.8 ISOLATION OF MRNA AND QUANTIFICATION CDNA AND GENOMIC DNA (QPCR)

2.8.1 Viral genome amplification (sample preparation)

The PC3 (200,000 cells/well) and 22Rv1 (400,000cells/well) cells were seeded in 10% FBS-DMEM in 6-well plates 24h before treatment and/or infection. Cells were infected with Ad5wt and AdΔΔ at 3000ppc for PC3 and 25ppc for 22Rv1 in 0% FBS-DMEM for 2-3h when medium was replaced by 10% FBS-DMEM with or without 50nM rapamycin, 10µM chloroquine and/or mitoxantrone at 900nM for PC3 and 25nM for 22Rv1. Cells were collected at 2, 48 and 72h after treatment by trypsinisation, pelleted and stored at -80°C until all time points were collected. Total DNA, including viral DNA, was purified using the QIAamp DNA Blood Mini Kit (QIAGEN, Netherlands) according to the manufacturer's instructions (described on section 2.3.2.3). DNA was eluted in 200µl Buffer AE. Purity and concentration of DNA samples were assessed using the NanoDropTM1000 Spectrophotometer (Thermo Fisher Scientific) as described above (section 2.3.2.3).

Purity of the sample was determined calculating A260/A280 and A260/A230 ratios (ratio A260/A280=1.8-2.0 and ratio A260/A230=2.0-2.2). Purified DNA was diluted to 15ng/µl. Amplification of the viral E2A gene was performed by quantitative PCR (qPCR) analysis. The cellular GAPDH gene was used as an internal control. Primer sequences are listed on ***Table 17***.

2.8.2 mRNA sample preparation for analysis by reverse transcriptase quantitative PCR (RT-qPCR)

The PC3 (200,000 cells/well) cells were seeded 24h before treatment and/or infection, in 10% FBS-DMEM in 6-well plates. Cells were infected with 500ppc of Ad5wt or AdΔΔ in 0% FBS-DMEM for 2-3h when medium was replaced by 10% FBS-DMEM with or without 450nM mitoxantrone. Cells were collected 12 and 48h later and RNA was immediately extracted using the RNeasy Mini Kit (QIAGEN, Netherlands) according to the manufacturer's instructions. Purity and concentration were measured as described above (section 2.3.2.3). Purified RNA was stored at -80°C. The purified RNA was diluted so that all samples had the same amount (~0.7μg) and was transcribed into coding DNA (cDNA) using a High-Capacity RNA-to-cDNA™ Kit (Applied Biosystems), which contains the MuLV reverse transcriptase enzyme, RNase inhibitor, dNTPs, random octamers, and oligo dT-16.

2.8.3 Quantitative PCR (qPCR)

Two or three qPCR reactions were set-up per sample in a total volume of 20μl as detailed in **Table *16***. qPCR was performed in MicroAmp® optical 96-well reaction plates covered with MicroAmp® optical adhesive film (Applied Biosystems), using an Applied Biosystems 7500 Instrument. Default amplification cycle conditions were used (**Figure *26***). Melting (dissociation) curves for each primer set were generated for primer quality control.

Table 16. Volumes for qPCR

Volume (μl)	Reagent
0.6	Forward primer (listed in ***Table 17***)
0.6	Reverse primer (listed in ***Table 17***)
10	Power SYBR Green MasterMix
2	DNA template
6.8	DNase free/ RNase free water

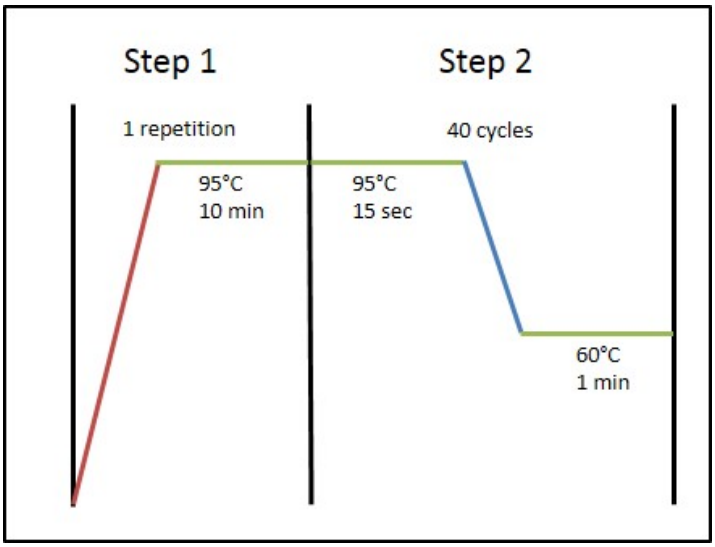

Figure 26. Thermal cycling conditions used in this study. Amplification of samples can be divided in two steps. Step 1 activates the enzyme and denatures the DNA template by heating the samples at 95°C for 10 min. Step 2 amplifies the samples by heating them for 15 sec at 95°C for DNA strands separation, followed by 1 min at 60°C for DNA ligation and amplification. Step 2 is repeated for 40 cycles.

Quantification of amplification results was performed following the $\Delta\Delta C_t$ method:

ΔC_t1 = C_t (sample A gene of interest) – C_t (sample A control gene)

ΔC_t2 = C_t (control sample gene of interest) – C_t (control sample control gene)

$\Delta\Delta C_t = \Delta C_t1 - \Delta C_t2$

Fold change expression = $\mathbf{2}^{\boldsymbol{\Delta\Delta C_t}}$

Threshold cycle (C_t): the cycle number at which the fluorescence signal crosses the threshold (Livak and Schmittgen 2001).

For the viral genome amplification assay, results for E2A were normalised to GAPDH and the fold difference was calculated by normalising again against the average of the E2A/GAPDH ratios of the 2h samples in each assay. For the Bcl-2 mRNA analysis, results for Bcl-2 were normalised to GAPDH and then the fold difference was calculated by normalising again against the average of the Bcl-2/GAPDH ratios of the 12h samples in each assay.

Table 17. Primers used in qPCR assays

Gene	Forward / reverse	Sequence 5' → 3'
E2A	Forward	GGATACAGCGCCTGCATAAAAG
E2A	Reverse	CCAATCAGTTTTCCGGCAAGT
Bcl-2	Forward	GCCCTGTGGATGACTGAGTA
Bcl-2	Reverse	GCCAGGAGAAATCAAACAGAGG
GAPDH	Forward	TGGGCTACACTGAGCACCAG
GAPDH	Reverse	GGGTGTCGCTGTTGAAGTCA

2.9 siRNA EXPERIMENTS

2.9.1 Transfection

Short interfering RNA (siRNA) was used to silence the expression of Atg5, Atg7 and Bcl-2 proteins. To ensure maximum silencing, commercially available pools containing four siRNA sequences targeting the mRNA of interest were used (***Table 18***). A non-targeting siRNA pool was used as a negative control. The siRNA buffer (5X) (Dharmacon, GE) was diluted to 1X in DNase and RNase free water to re-suspend the siRNA pools to a final concentration of 20µM. Dharmafect 2 (Dharmacon, GE) was used as a transfection reagent.

The PC3 cells (100,000 – 200,000 cells/well) were seeded in 2ml in antibiotic free 10% FBS-DMEM in 6-well plates. The cells were transfected 24h after seeding with 50 or 100nM of the corresponding siRNA pool (**Table 18**) following the manufacturers' instructions (Dharmacon).

Tube A and B (***Table 19***) were incubated at room temperature for 5 min, and then mixed together and incubated for 20 min to allow interaction of siRNA with the transfection reagent. 400 µl of transfection mix per well were added to the cells and transfection was allowed overnight at 37°C and 5% CO_2, medium was then replaced with 10% FBS-DMEM.

Table 18. siRNAs used in this thesis

Target	Company / product	Catalogue number
BCL-2	Dharmacon / ON-TARGET plus SMARTpool	L-003307-00
ATG5	Dharmacon / ON-TARGET plus SMARTpool	L-004374-00
ATG7	Dharmacon / ON-TARGET plus SMARTpool	L-020112-00
Non-Targeting	Dharmacon / siGENOME Control Pool #2	D-001206-14-05

Table 19. Transfection reagents

	Reagent	Volumes (per well)
Tube A	Dharmafect 2	6 µl
	0% FBS-DMEM	194 µl
Tube B	siRNA	5 µl (50nM in well)
	siRNA Buffer (1x)	95 µl
	0% FBS-DMEM	100 µl

2.9.2 Cell viability assay of siRNA transfected cells

For cell viability MTS assays, cells were trypsinised 24h after transfection and reseeded in 96-well plates (5,000 cells/well). Cells were treated 24h after seeding with 1/5 serial dilutions of mitoxantrone starting at 40µM, and/or a fixed dose of 500ppc Ad$\Delta\Delta$. Cell viability was measured by MTS assays 5 days after treatment (***Figure 27***) as described above (section 2.4.1).

2.9.3 Detection of protein expression by immunoblotting of siRNA transfected cells

When checking the knock-down efficiency in cells analysed by the MTS assay, cells were trypsinised 24h after transfection and reseeded in 6 well plates (100,000 cells/well). Cells were then treated 24h after seeding as indicated and collected for immunoblotting in parallel with the MTS assay.

In independent assays, cells were seeded in 6-well plates (100,000 cells/well), transfected the following day as described above, and treated with mitoxantrone at 450nM and/or AdΔΔ at 500ppc four days after transfection. Cells were collected 48h after treatment (6 days after transfection) (**Figure *27***).

Samples were purified, quantified, electrophoresed, blotted and incubated as described above (section 2.5).

2.9.4 Detection of apoptosis by TMRE staining in siRNA transfected cells

Cells were seeded in 6-well plates (100,000 cells/well), transfected the following day as described above, and treated with indicated doses of mitoxantrone at 100nM and/or AdΔΔ at 500ppc 24h after transfection. Cells were collected 5 days after treatment (6 days after transfection) (**Figure *27***) and stained and analysed as described above (section 2.6.1).

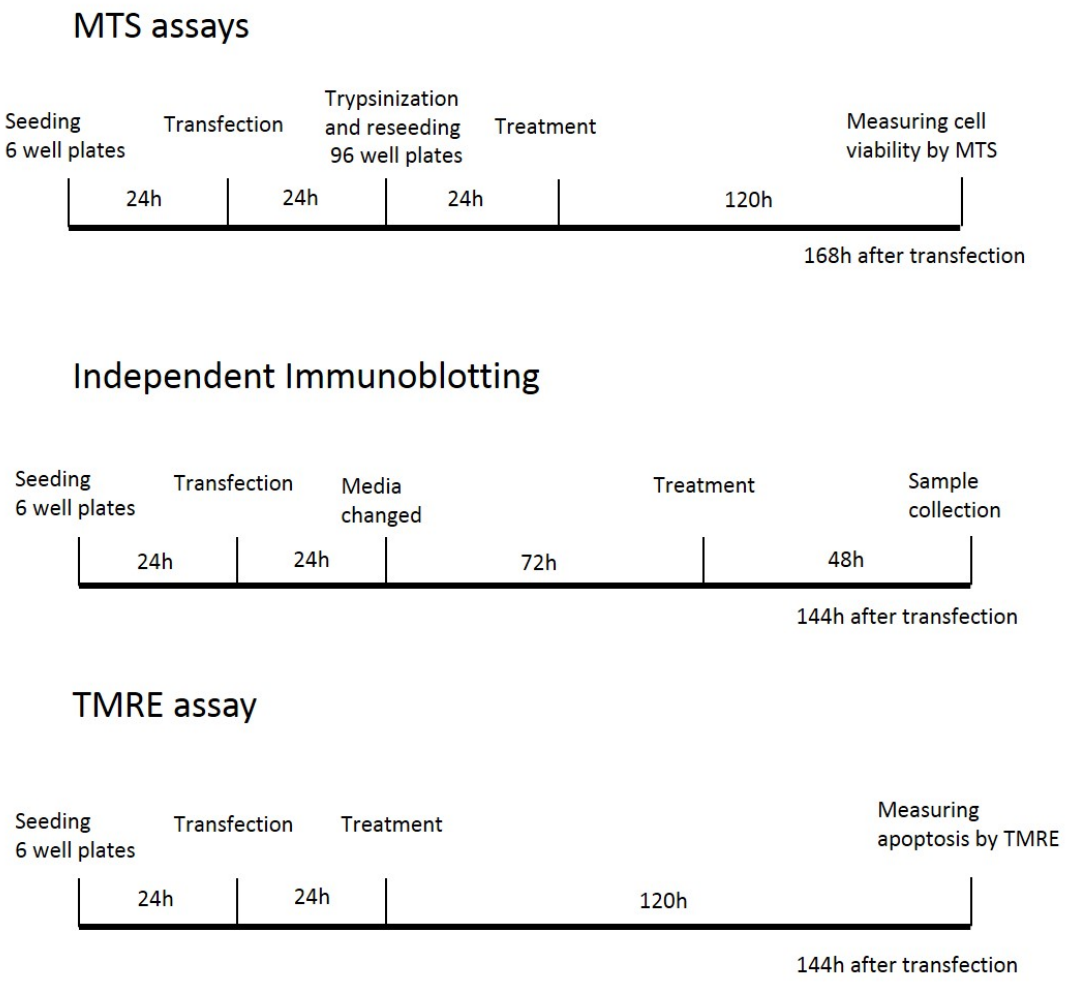

Figure 27. Schematic time-line for siRNA studies.

2.10 3-DIMENSIONAL (3D) CO-CULTURES

2.10.1 Gel casting and cell seeding

Transwells® (Corning Incorporated Catalog N. 07-200-82, NY, USA) were placed in 24-well plates and coated with 300µl of collagen type I (1/100 diluted in PBS) for 1h at 37°C, and excess discarded. The collagen/matrigel was prepared as in ***Table 20***, 120 µl of gel mix was added to each transwell and allowed to solidify for 2h at 37°C. When preparing the gel mix, collagen and matrigel and the mix were kept on ice to prevent them from solidifying. Once gels were set, 200 µl containing 100,000 cells in 10% FBS-DMEM were added to the top of the gel. When culturing epithelial cancer cells and stromal fibroblast cells together, cells were mixed in a ratio 2:1 (stromal:epithelial) and total number of cells was 100,000. The day of seeding, 600 µl of 10% FBS-DMEM was added underneath the transwell. 24h after seeding, medium covering the cells was replaced with 200 µl of 0% FBS-DMEM while medium underneath the transwell was replaced with 350 µl of fresh 10% FBS-DMEM to create an FBS gradient and promote cell invasion into the gel. When untreated, medium was replaced every 3 days.

Table 20. Components of collagen/matrigel matrix

Reagent	Volume (for 8 gels)
Collagen type I (Collagen type I, rat tail, Corning, MA, USA)	525 µl
Matrigel (Matrigel Matrix, Basement matrix. Corning, MA, USA)	175 µl
10x medium	100 µl
10% FBS-DMEM	100 µl
FBS (filtered)	100 µl
NaOH (1M)	45 µl

2.10.2 Treatment of the 3-dimensional cultures

On the day of treatment all medium was removed and replaced with either fresh medium (0% FBS-DMEM on top of the cells, 10% FBS-DMEM underneath the transwells) or the treatments described below. 3-dimensional cultures were infected with 200µl containing

AdΔΔ (100-200 ppc for PrSC-22Rv1 and 1000ppc for PrSC-PC3) at indicated times. The total number of cells (both epithelial and stromal cells) was taken into account when calculating the viral dose. Infection medium was prepared in 0% FBS-DMEM and added only on top of the cells. Mitoxantrone treatment (10nM for PrSC-22Rv1 and 450nM for PrSC-PC3) was added both on top of the cells and underneath the transwell (200µl of treatment in 0% FBS-DMEM on top and 350µl of treatment in 10% FBS-DMEM underneath the transwell). When cultures were treated with virus and drug on the same day, infections were performed in the morning and 6-8h later, mitoxantrone was added as described above without removing the infection medium.

2.10.3 Fixing and processing of the 3-dimensional cultures

At the indicated time points, all medium was removed and transwells were placed in clean 24 well plates. The cells and transwells were fixed in formalin (200 µl) on top of the cells and 500 µl at the bottom for a minimum of 1 day or until all time points were collected. The gel-cultures were excised from the transwells, placed in 70% ethanol for >24h and embedded in paraffin for sectioning.

Paraffin embedding was performed by incubating the samples in 95% ethanol for 1h and washing them four times in clean absolute ethanol for 90 min. Samples were then washed twice in clean xylene for 1h. Finally, samples were immersed in paraffin wax for 1h at 58 °C, this step was performed twice. After parafin embedding, samples were cut in 4µm sections using a Leica RM2255 rotary microtome.

Hematoxylin and Eosin staining was perfomed using an automatic Leica ST5010 autostainer and coverslipper. In brief, nuclei were stained with hematoxylin, washed for 1-2 seconds in 0.3% acid alcohol followed by 1-2 min incubation in eosin.

Paraffin embedding, sectioning (4µm) and Hematoxylin and Eosin (H/E) staining was performed by Barts Cancer Institute Pathology service.

2.10.4 Immunofluorescence staining of cells grown in the 3-dimensional cultures

Paraffin sections were dewaxed and rehydrated as detailed in ***Table 21***. Sections were boiled in citrate buffer (tri-sodium citrate 0.01M, pH 6) for 8-10 min, washed in PBS, blocked in PBS ABC buffer (2% BSA + 10% FBS in PBS) for 1h at room temperature and incubated with primary antibodies (***Table 22***) diluted in PBS ABC buffer (1h at room temperature or overnight

at 4°C). After incubation, sections were washed in 0.05% Tween-20/PBS for 5 min x 3 times prior to and post incubation with a secondary antibody. Sections were incubated with Alexa Fluor® secondary antibodies (***Table 22***) (diluted in PBS) for 1h at room temperature. After a final PBS wash, sections were covered in DAPI (1:1000 diluted in H_2O, Sigma Aldrich) for 2 min and washed in PBS for 5 min x 2 times. A drop of mounting medium (FluorSave® Reagent, Calbiochem) and a coverslip was added to each section for microscope analysis. Preparations were allowed to dry at room temperature in the dark and stored at -20°C.

Table 21. Dewaxing protocol

Solution	**Time**
Xylene	2 x 5min (every new wash with fresh xylene)
100% EtOH	5 min, then 2min with new EtOH
90% EtOH	2 min
70% EtOH	2 min
50% EtOH	2 min
dH_2O	5 min

Table 22. Antibodies used for microscopy

Antibody	Species	Dilution	Type	Supplier	Catalogue number
Ad E1A	Mouse	1/500	Primary	Gene Tex	GTX23165
LC3B	Rabbit	1/500	Primary	Abcam	Ab51520
α-SMA (smooth muscle actin)	Mouse	1/300	Primary	Dako	M085
Alexa Fluor M488	Goat	1/500	Secondary	Life technologies	A11001
Alexa Fluor M568	Goat	1/500	Secondary	Life technologies	A11004
Alexa Fluor R594	Chicken	1/500	Secondary	Life technologies	A21442

2.11 MICROSCOPY

2.11.1 Light field microscopy

Hematoxylin and Eosin stained slides were imaged with an AxioCam HRc camera incorporated in a brightfield Axiophot microscope by using AxioVision software. 3 to 8 sections were imaged per condition and one to two images were taken per each section to capture the whole section, using the 10x objective.

2.11.2 Confocal microscopy

The sections were stained with fluorescently-labelled antibodies (**Table *22***) as described above (section 2.10.4) and imaged using the oil objectives (40x, 100x) of the confocal laser-scanning microscope Zeiss LSM710. 1 to 4 sections were imaged per condition and 2 to 4 pictures were taken per each section. 405nm, 488nm and 543nm lasers were used to detect blue (DAPI), green (M488) and red (M568 and R594) staining, respectively.

2.11.3 Quantification of microscopy images

The number of cells per confocal image was quantified manually using the cell counter plugin from ImageJ software. The total number of DAPI positive cells seen in each image and cells positive for the indicated staining were quantified. The same magnification was used for quantification of all conditions in the same assay so equal areas could be analysed. Quantified H/E images were taken with the 10x objective while quantified confocal images were taken with the 40x objective.

2.12 GOLD NANOPARTICLE (NP) EXPERIMENTS

In collaboration with Prof Pilar Martinez (Universidad Francisco de Vitoria (UFV), Madrid, Spain) we obtained gold nanoparticles (NP). The NPs had previously been synthesised by Dr. Jesus Martinez de la Fuente (Instituto de Nanociencia de Aragon (INA), Zaragoza, Spain) and consist of a gold core that is functionalised with polyethylene glycol-containing ammonium groups (PEG-NR_4^+) to generate positively charged particles. The collaborators Prof Martinez and Dr de la Fuente had previously validated, characterised and quantified the NPs. The NPs were stored in dark glass bottles, to avoid non-specific binding to plastic, at 4°C in the dark.

2.12.1 Cell viability assays in the presence of NPs

The PC3 (10,000 cells/well) and 22Rv1 (20,000 cells/well) cells were seeded 24h before infection in 100 µl 10% FBS-DMEM in 96-well plates.

For the sensitization assays, to determine EC_{50}-values, dose-response curves to AdΔΔ were generated. AdΔΔ was serially diluted in 0% FBS-DMEM starting at 100,000 ppc. In cells treated with AdΔΔ only, medium was decanted and replaced with 90 µl of 2% FBS-DMEM, then 10 µl of serial dilutions were added to the cells. For cells treated with AdΔΔ and NPs, 10 µl of the respective viral dilution was pre-incubated in 90 µl of 2% FBS-DMEM containing 0.01pmoles of NPs for 20 min at room temperature in the dark. After the incubation, the total volume of 100 µl was added to cells, in which medium had been previous decanted. All samples were prepared in triplicates.

For the fixed dose assays, PC3 cells were treated with AdΔΔ at 500ppc, mitoxantrone at 450nM or the combination of virus and drug, alone or in the presence of a fixed dose or NPs (0.01pmol per well). Treatments were prepared in triplicates in separate plates in a final volume of 100 µl 2% FBS-DMEM, in the presence or absence of 0.01pmol of NPs and pre-incubated for 20 min at room temperature in the dark. After the incubation, the total volume of 100 µl was added to the cells, in which medium had been previous decanted.

Cell viability was measured after 3 or 4 days, for 22Rv1 and PC3 cells, respectively, by the MTS assay as described in section 2.4.1.

2.12.2 Infectivity assays in the presence of NPs

The PC3 (200,000 cells/well) and 22Rv1 (400,000 cells/well) cells were seeded 24h before infection in 2ml 10% FBS-DMEM in 6-well plates.

Cells were infected with the non-replicating AdGFP at the indicated doses (10-500ppc), in the presence or absence of 0.5pmoles of NPs. AdGFP and NPs were pre-incubated for 20 min at room temperature in dark as described in section 2.12.1. Cells were infected in 1ml 0% FBS-DMEM, for 2-3 h and medium was replaced with 10% FBS-DMEM. Cells were collected 48h after infection by trypsinization and washed in PBS. The percentages of GFP-positive cells were determined by flow cytometry as described in section 2.6.2.

2.12.3 Replication assays ($TCID_{50}$) in the presence of NPs

The PC3 (200,000 cells/well) and 22Rv1 (400,000 cells/well) cells were seeded 24h before infection in 2ml 10% FBS-DMEM in 6-well plates. Cells were infected with AdΔΔ at 100ppc, in the presence or absence of 0.5pmoles of NPs. AdΔΔ and NPs were pre-incubated for 20 min at room temperature in dark as described in section 2.12.1. Cells were infected in 1ml 0% FBS-DMEM, infection was allowed to proceed for 2-3 h and medium was replaced with 10% FBS-DMEM. Cells and medium were collected at indicated time points (48 – 72h). Samples were processed and assayed as described in section 2.3.2.2. Samples were diluted 1/100 – 1/1000 before addition.

2.13 STATISTICAL ANALYSIS

The parametric t-test and one-way Anova tests were performed to assess wheter observed differences were statistically significant. The un-paired t-test was performed to compare two pairs of means and determine the p-value. The one-way Anova test was used to compare the means of three or more unmatched groups. A Bonferroni post-test was perfomed after the one-way Anova test to compare every mean pair by pair and determinine the p-value. When comparing EC_{50}-values from 3 independent experiments (n=3), normality of the distribution was assumed to allow the use of parametric tests. All statistical tests were performed using GraphPad Prism 5 software.

3 RESULTS

3.1 MITOXANTRONE-INDUCED CELL KILLING IS ENHANCED IN COMBINATION WITH ADΔΔ BY PROMOTION OF APOPTOSIS AND ATTENUATION OF AUTOPHAGY IN 22RV1, PC3, AND PC3M CELLS.

3.1.1 22Rv1, PC3 and PC3M cells show different sensitivity to adenovirus infection and mitoxantrone treatment.

To assess the potency and cytotoxicity of the adenoviral mutants in three different human prostate cancer cell lines, cell viability assays were performed. PC3 cells (p53-, AR- and PTEN-) are a model for bone metastasis and are highly insensitive to cytototoxic drug treatment and infection (Oberg, Yanover et al. 2010, Liu, Zhu et al. 2013). The PC3M cell line is a PC3 sub-line, which has more aggressive growth characteristics (Sobel and Sadar 2005). 22Rv1 cells (p53+, AR+ and PTEN+) are more sensitive to both chemotherapy treatment and adenoviral infection (Oberg, Yanover et al. 2010, Chappell, Lehmann et al. 2012). Dose-response curves to three viruses Ad5wt, AdΔΔ and Ad12S were generated and cell viability measured to determine the effective concentration required to kill 50% of cells (EC_{50}). Cell viability was measured by MTS assays as an indirect measurement of cell death, as previously demonstrated in my team (Oberg, Yanover et al. 2010, Miranda, Maya Pineda et al. 2012). To verify cell death rather than growth arrest I later performed Trypan Blue exclusion assays that clearly identify dead cells (section 3.1.3). Ad5wt is wild type virus serotype 5 and was used as control for virus infection. AdE1A12S is a non-replicating Ad5-mutant expressing only the E1A12S protein and was used as a control for E1A expression only (Miranda, Maya Pineda et al. 2012). AdΔΔ is an oncolytic Ad5-mutant that replicates only in cancer cells with deregulated cell cycle control by deletion of the E1ACR2-domain preventing pRb-binding in normal cells (Oberg, Yanover et al. 2010). AdΔΔ is also deleted in the anti-apoptotic E1B19K gene to promote apoptosis in the presence of apoptosis-inducing drugs. Infection with AdΔΔ effectively killed all tested prostate cancer cell lines including 22Rv1, PC3 and PC3M (**Table *23***, **Figure *28A***). PC3 cells were the most insensitive to adenovirus-induced cytoxicity resulting in significantly higher EC_{50}-values for Ad5wt and AdΔΔ ($p<0.001$ and $p<0.05$) than in 22Rv1 cells. The differences were 21-fold for Ad5wt in PC3 cells compared to 22Rv1 cells (4596 ± 630ppc vs. 221.4 ± 77.7ppc) and 6-fold for AdΔΔ in PC3 cells compared to 22Rv1 cells (1049 ± 91ppc vs. 155.7 ± 10.6ppc). Due to the high resistance to viral infection, longer time points were used in the cell killing studies for PC3 cells. AdΔΔ had significantly higher cell killing

efficacy than Ad5wt demonstrated by 4-fold lower EC_{50}-values in PC3 cells ($p<0.01$) (**Table *23***). The increased cell killing-efficacy of the AdΔΔ virus, when compared to Ad5wt, can be explained by the deletion in the E1B19K gene, which facilitates E1A-induced apoptotic cell death. It was previously established that mutants with the E1ACR2 region deleted were more potent than Ad5wt in certain cell types, including PC3 cells (Oberg, Yanover et al. 2010). Surprisingly, the PC3M cells were more sensitive to AdΔΔ-induced cell killing than the parental PC3 cells resulting in the lowest EC_{50}-value (44.8 ± 6.6ppc) of all tested cell lines (statistics could not be performed due to insufficient number of repeats) (**Table *23***). The cytotoxicity of the non-replicating Ad12S virus was assessed in 22Rv1 and PC3 cells. In 22Rv1 cells, infection with Ad12S resulted in lower cell killing efficacy, demonstrated by a higher EC_{50}-value of 846.0 ± 104.5ppc; 4-fold and 5-fold higher than Ad5wt and AdΔΔ, respectively in these cells. The poor cell killing by Ad12S can be explained by its inability to replicate and consequently, to lyse cells. Due to this low cell killing efficacy, it was not possible to generate EC_{50}-values for Ad12S in PC3 cells (EC_{50} > 30,000ppc) (**Table *23***, **Figure *28A and* Figure *29***). The observed differences in viral cell killing efficacy between cell lines might be explained by differences in the expression levels of hCAR in each cell lines. Differences will be studied bellow (section 3.2.4).

The cell killing-efficacy of the cytotoxic drug mitoxantrone was also assessed in the three prostate cancer cell lines 22Rv1, PC3 and PC3M. 22Rv1 cells were the most sensitive to the drug with an EC_{50}-value of 321.5 ± 30.7nM, which was approximately 7-fold and 11-fold lower than the values in PC3 and PC3M, respectively; the differences were significant for PC3 cells ($p<0.001$ for PC3). In contrast with its high sensitivity to AdΔΔ-induced cell killing, the PC3M cell line was the most resistant cell line to mitoxantrone with the EC_{50} = 3566 ± 546nM. PC3 also showed high resistance to the drug with EC_{50}-value = 2276.6 ± 419.8nM (**Table *23***, **Figure *28B and* Figure *29***).

Table 23. EC_{50}-values (±SD) generated for 22Rv1, PC3 and PC3M cells.

	22Rv1	PC3	PC3M
Ad5wt (ppc)	221.4 ± 77.7	4596 ± 630	Not generated
AdΔΔ (ppc)*	155.7 ± 10.6	1049 ± 91	44.8 ± 6.6
Ad12S (ppc)	846.0 ± 104.5	> 30000	Not generated
Mitoxantrone (nM)	321.5 ± 30.7	2276.6 ± 419.8	3566 ± 546

**AdΔΔ batch 050314. All data are averages ± SD, n=3, except for mitoxantrone data in PC3M, n=2. Cell viability was measured 3 days after treatment (5 days for PC3 cells) by MTS assay. PC3M data was generated by Ms Julia San Millan, a visiting student in our team.*

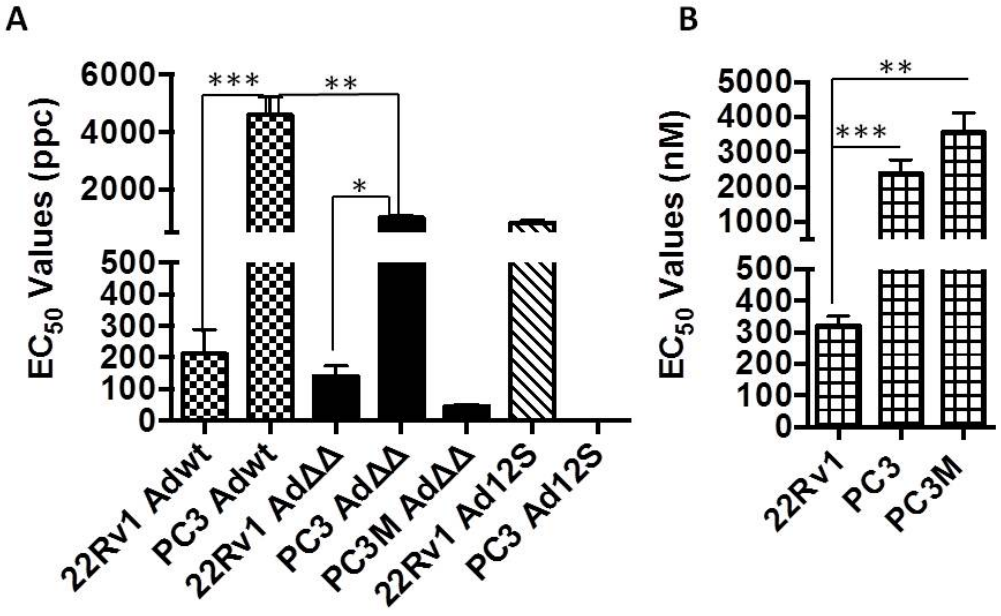

Figure 28. 22Rv1, PC3 and PC3M cells show different sensitivity to adenovirus infection and mitoxantrone treatment. A. EC_{50}-values generated for Adwt, AdΔΔ, and Ad12S in 22Rv1, PC3, and PC3M cells. ¥ indicates that the Ad12S virus was not potent enough to generate dose response curves in PC3 cells. **B.** EC_{50}-values generated for Mitoxantrone in 22Rv1, PC3 and PC3M cells**. A and B.** Cells were treated with increasing doses of virus (starting concentration 100,000 ppc) or mitoxantrone (starting concentration 40µM, 200µM for PC3 cells) to generate dose-response curves and EC_{50}-values. Cell viability was measured 3 days after treatment (5 days for PC3 cells) by MTS assay, averages ±SD, n=3 (n=2 for mitoxantrone in PC3M). One-way Anova with Bonferroni post-test. *p<0.05, **p<0.01, ***p<0.001. The PC3M data was generated by Ms Julia San Millan, a visiting student in our team.

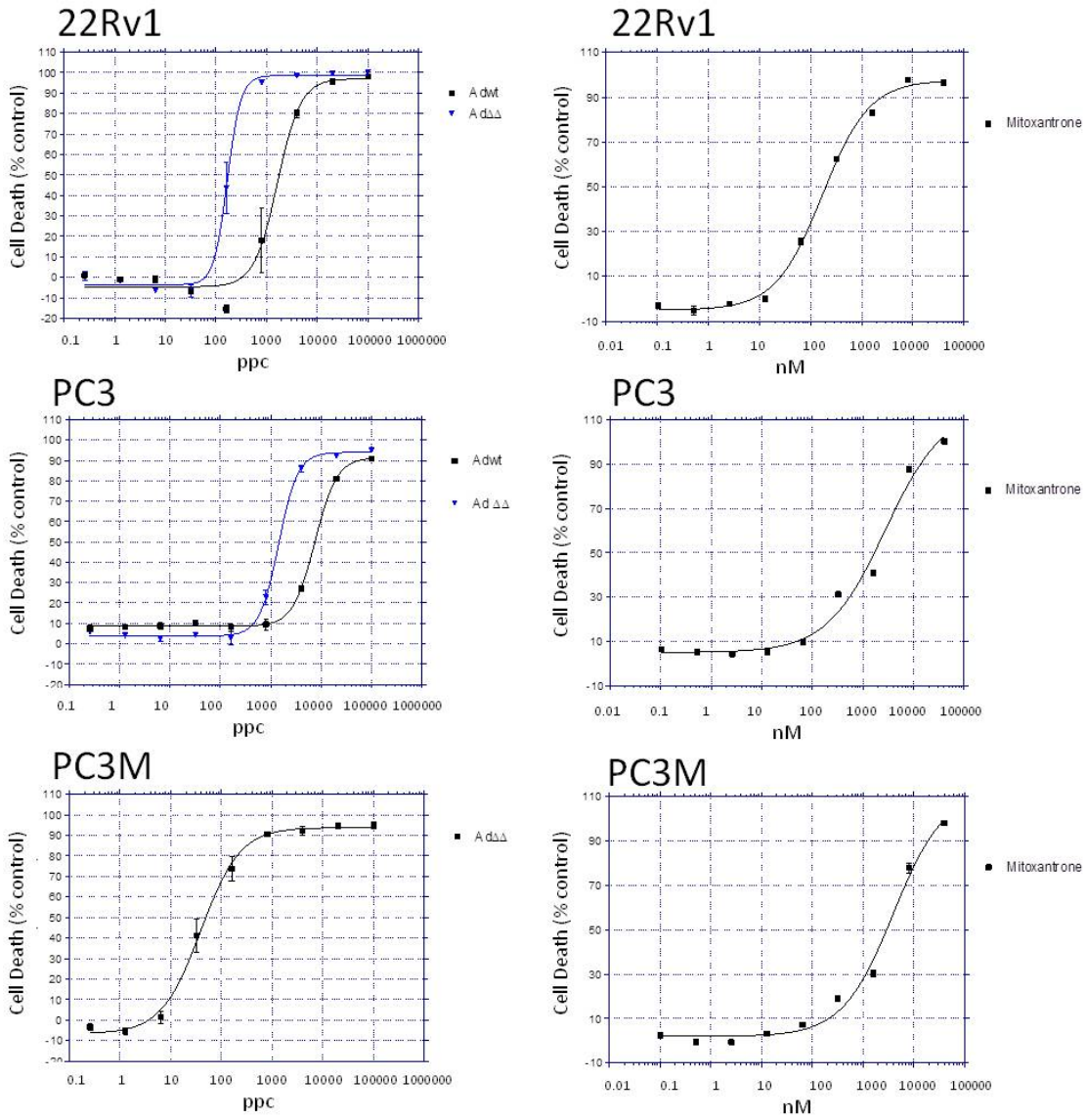

Figure 29. Representative dose-response curves that generated the data in Figure 28. 22Rv1, PC3 and PC3M were treated with increasing doses to Adwt or AdΔΔ (starting concentration 100,000 ppc) or mitoxantrone (starting concentration 40µM, 200µM for PC3 cells) to generate dose response curves and calculate EC_{50}-values. Cell viability was measured 3 days after treatment (5 days for PC3 cells) by MTS assay. The PC3M data was generated by Ms Julia San Millan, a visiting student in our team.

3.1.2 Mitoxantrone-induced cell killing is enhanced by the adenoviral mutants AdΔΔ and Ad12S in 22Rv1 and PC3 prostate cancer cells.

The replication-selective AdΔΔ and the non-replicating Ad12S mutants have been previously reported to synergise with mitoxantrone in 22Rv1, PC3, LNCaP and DU145 prostate cancer cell lines (Oberg, Yanover et al. 2010, Miranda, Maya Pineda et al. 2012). To establish

conditions for enhanced cell killing in this study, sub-optimal doses of Ad5wt, AdΔΔ, and Ad12S that caused 10-20% of cell death were selected from the dose-response data (**Table *23***, **Figure *28***) and added to cells treated with increasing doses of mitoxantrone (**Figure *30***, **Figure *31***). In PC3 cells, the selected doses of AdΔΔ and Ad12S, at 1000ppc and 5000ppc, respectively, sensitised the cells to mitoxantrone-induced cell death (**Figure *30 A and B and* Figure *32***). Infection with AdΔΔ and Ad12S decreased the EC_{50}-values for mitoxantrone 12-fold and 15-fold to 316.45 ± 2.15nM and 413.45 ± 9.45nM, respectively, compared to 2276.5 ± 419.8 for mitoxantrone alone. The decrease in EC_{50}-values was significant ($p<0.01$) for AdΔΔ and Ad12S, when compared to mitoxantrone alone. In contrast, infection with Ad5wt at 1000ppc did not result in sensitization to mitoxantrone in PC3 cells. A small and unsignificant increase was noted in mitoxantrone EC_{50}-values in Ad5wt-infected PC3 cells. In 22Rv1 cells, AdΔΔ and Ad12S, but not Ad5wt, decreased mitoxantrone EC_{50}-values at selected doses that killed 10-40% of cells alone; 25ppc for Ad5wt and AdΔΔ, and 100ppc for Ad12S (**Figure *31 A and B and* Figure *32***). At these doses, infection with AdΔΔ and Ad12S decreased mitoxantrone EC_{50}-values 2-fold and 2.3-fold to 179.5 ± 94.0nM and 157.6 ± 91.0nM, respectively, when compared to 365.7 ± 63.6nM for mitoxantrone alone. Sensitization to mitoxantrone was significant ($p<0.05$) in 22Rv1 cells when infected with Ad12S, compared to mitoxantrone alone. Cell killing as a response to the selected viral doses alone is shown (***Figure 30C, Figure 31C***). These assays were performed using an older batch of AdΔΔ (batch 260109), which had a higher vp/pfu ratio (15.3vp/pfu), compared to the newer batch (050314; 2.3vp/pfu). The same batch of Ad5wt was used in all assays (270314; 1.03vp/pfu). Ad5wt had lower vp/pfu ratio and therefore higher number of infective particles per ml than AdΔΔ (batch 260109). As a consequence, in cells treated with equal doses (ppc) of Ad5wt and AdΔΔ, the Ad5wt appeared to be more potent than AdΔΔ (***Figure 30C and Figure 31C***). Due to its inability to replicate, higher doses of Ad12S at 5000ppc for PC3 and 100ppc for 22Rv1, respectively had to be used.

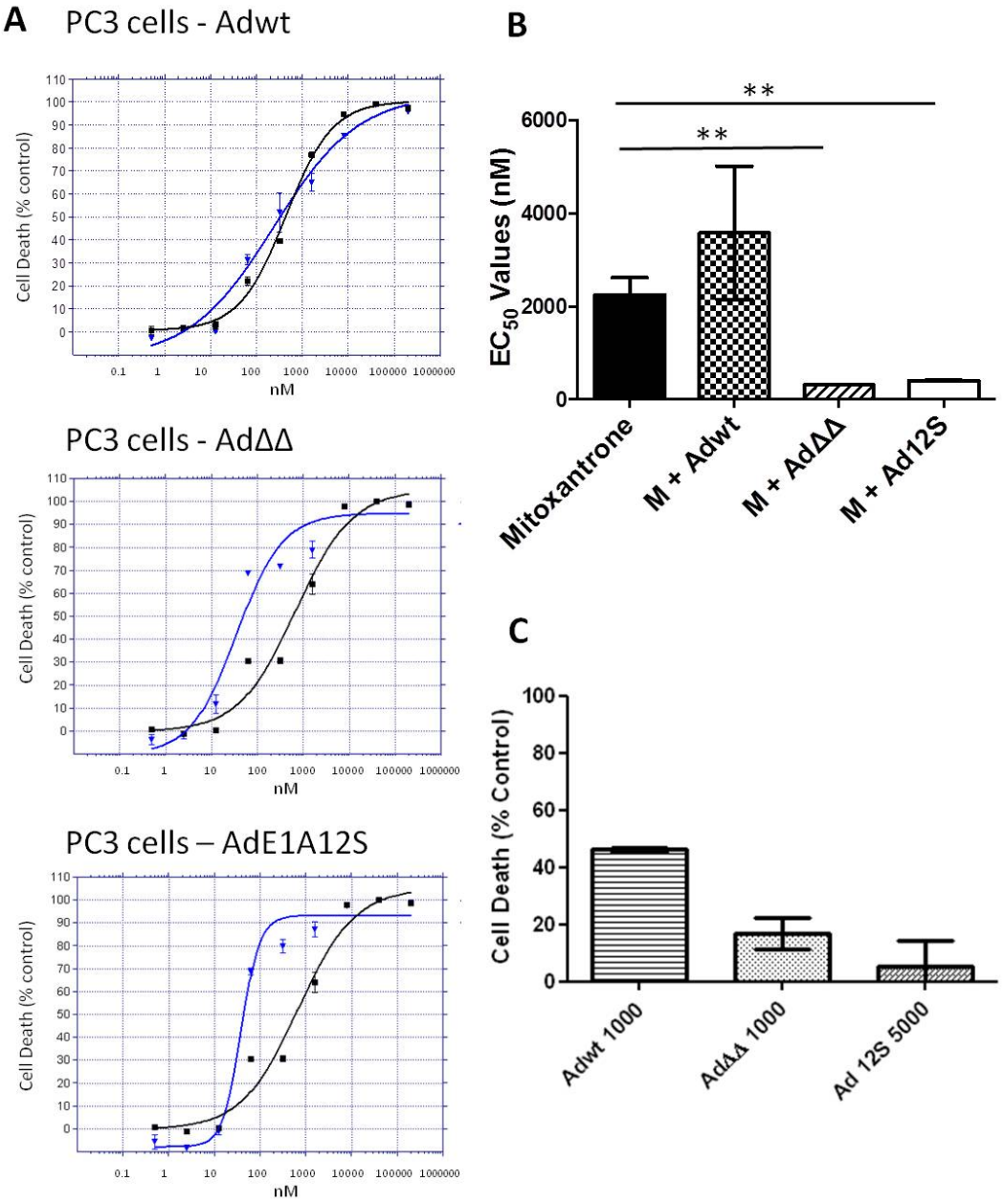

Figure 30. Mitoxantrone-induced cell killing is significantly increased in combination with the adenoviral mutants AdΔΔ and Ad12S in PC3 cells. Dose-response curves to mitoxantrone combined with a fixed dose of virus that killed 10 – 40% of cells alone; Adwt or AdΔΔ at 1000ppc or AdE1A12S at 5000ppc. **A.** Representative dose-response curves for mitoxantrone alone (black) or in combination with a fixed dose of the indicated adenovirus (blue). **B.** EC_{50}-values of mitoxantrone and the combination of mitoxantrone and the indicated virus. Unpaired t-test, averages ±SD, n = 3, **p<0.01. **C.** Cell death caused by selected adenovirus doses; Adwt or AdΔΔ at 1000ppc or AdE1A12S at 5000ppc. Cell viability was measured by MTS assay 5 days after treatment. This assay was perfomed with AdΔΔ batch 260109.

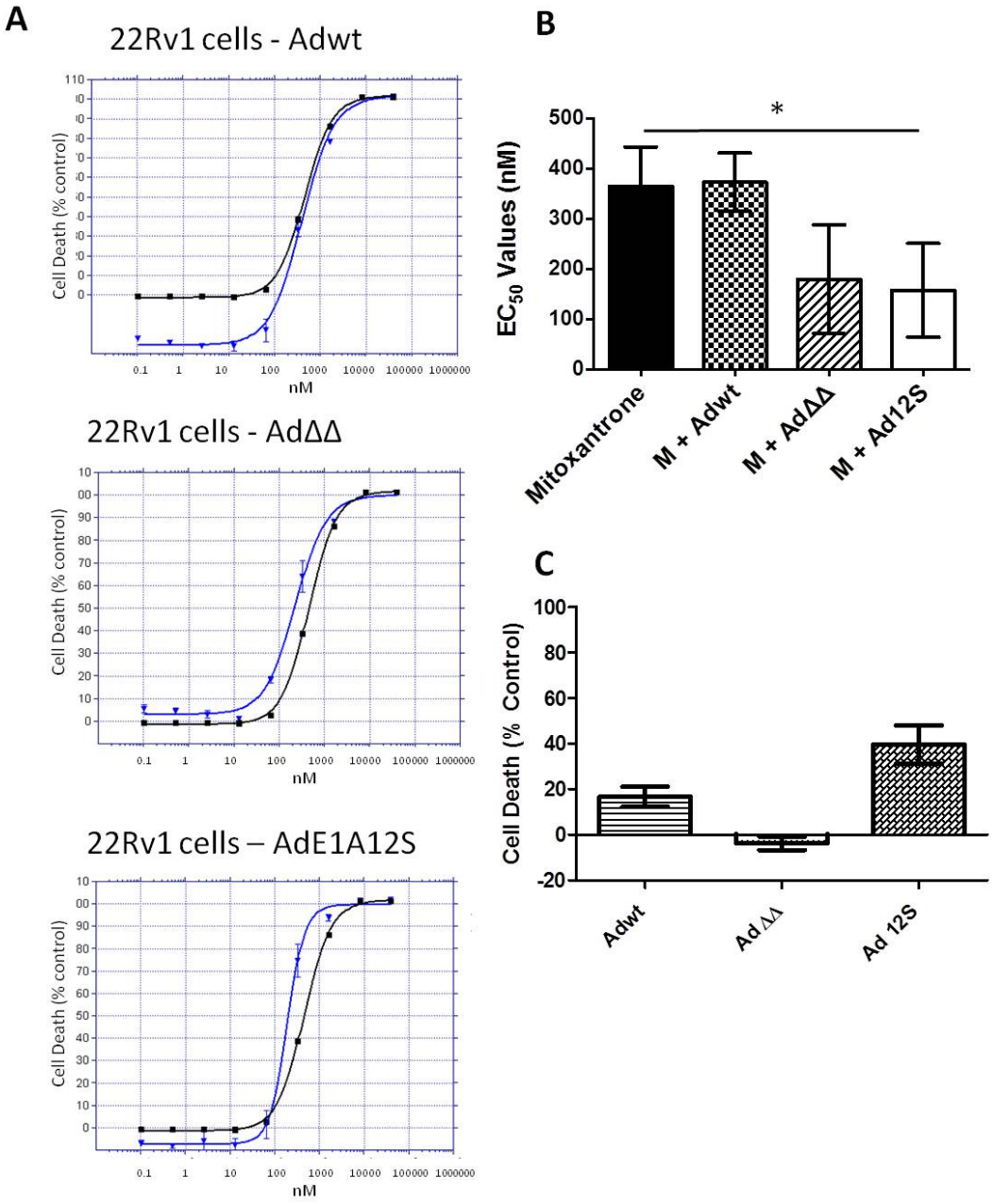

Figure 31. Mitoxantrone-induced cell killing is significantly increased only in combination with Ad12S in 22Rv1 cells. Dose-response curves to mitoxantrone combined with a fixed dose of virus that killed 10 – 40% of cells alone; Adwt or AdΔΔ at 25ppc or AdE1A12S at 100ppc. **A.** Representative dose-response curves for mitoxantrone alone (black) or in combination with a fixed dose of indicated adenovirus (blue). **B.** EC_{50}-values of mitoxantrone and the combination of mitoxantrone and the indicated virus. Unpaired t-test, averages ±SD, n = 3, *p<0.05. **C.** Cell death caused by selected adenovirus doses; Adwt or AdΔΔ at 25ppc or AdE1A12S at 100ppc. Cell viability was measured by MTS assay 3 days after treatment. This assay was perfomed with AdΔΔ batch 260109.

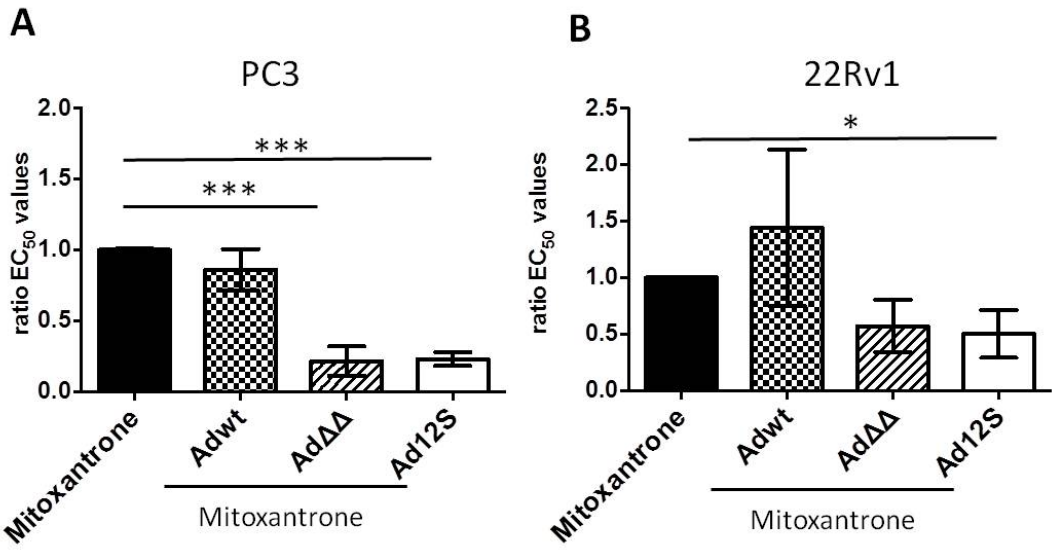

Figure 32. AdΔΔ and Ad12S sensitise PC3 and 22Rv1 cells to mitoxantrone. EC_{50}-values were calculated for each experiment. The sensitisation ratios were calculated as (EC_{50}-value Ad+Mitoxantrone/EC_{50}-values mitoxantrone only), and averages ± SD are shown. Unpaired t-test, *p<0.05, ***p<0.001, n=3. EC_{50}-ratios were calculated from data in **Figure 30** and **Figure 31**.

3.1.3 The combination of sub-optimal doses of AdΔΔ and mitoxantrone causes more than additive cell killing in PC3 and PC3M cells.

To enable further investigation of the enhanced cell killing and to determine appropriate doses to be used in future mechanistic studies, combinations of fixed doses of viruses and mitoxantrone were examined. Cell viability was measured by MTS assay as an indirect measurement of cell death. Doses of viruses that caused 10-20% cell killing alone at 500, 20 and 15ppc for Ad5wt and AdΔΔ in PC3, PC3M and 22Rv1, respectively, and at 5000 and 50ppc for Ad12S in PC3 and 22Rv1 were used. The viral doses were combined with fixed doses of mitoxantrone that caused 5-40% cell death in PC3 cells (225, 450 and 900nM), 20-30% in PC3M cells (450 and 900nM) and 10-60% in 22Rv1 cells (3, 10 and 25nM) (**Figure *33***, **Figure *34***, **Figure *35***). In PC3 cells, the combined treatment of AdΔΔ at 500ppc with all tested doses of mitoxantrone (225, 450, 900nM) resulted in more than additive cell death that was significantly higher compared to mitoxantrone alone ($p<0.05$ for 225nM and $p<0.001$ for 450 and 900nM). This enhancement of mitoxantrone-induced cell killing was emulated with the Ad12S virus when combined with all tested doses of mitoxantrone and was significantly higher ($p<0.001$) compared to mitoxantrone alone at all doses of the drug (**Figure *33A***). As expected the Ad5wt virus did not significantly enhance mitoxantrone-induced cell killing in PC3 cells. To verify that the decreased cell viability induced by AdΔΔ was caused by cell death

rather than growth arrest, the cell exclusion dye Trypan blue was used to directly detect dead cells. Similar results to those in the MTS assay were obtained in PC3 cells using the Trypan blue dye (**Figure *33B***). The combined treatment of AdΔΔ or Ad12S with all tested doses of mitoxantrone (225, 450 and 900nM) resulted in a trend towards more than additive cell killing, statistical analysis could not be performed due to insufficient number of repeats (n=2) (**Figure *33B*).** Analysis of cell viability in PC3M cells resulted in similar results to those observed in PC3 cells (**Figure *34***). In these cells, the combined treatment of AdΔΔ at 20ppc with all tested doses of mitoxantrone (450, 900nM) resulted in enhancement of mitoxantrone-induced cell death determined by the MTS viability assay. Statistical analysis could not be performed due to the limited number of repeats (n=2) (**Figure *34***). In 22Rv1 cells, a trend towards more than additive cell killing was observed when AdΔΔ or Ad12S at 15 and 50ppc, respectively, were combined with low doses of mitoxantrone at 3, 10 and 25nM, using the Trypan blue dye (**Figure *35***). Interestingly, the combined-treatment of Ad5wt at 15ppc and mitoxantrone appeared to inhibit cell killing when compared to the expected theoretical additive effect in 22Rv1 cells (**Figure *35***). Due to the high sensitivity of 22Rv1 cells to virus and mitoxantrone, MTS data generated for this cell line under these conditions could not be reliably reproduced.

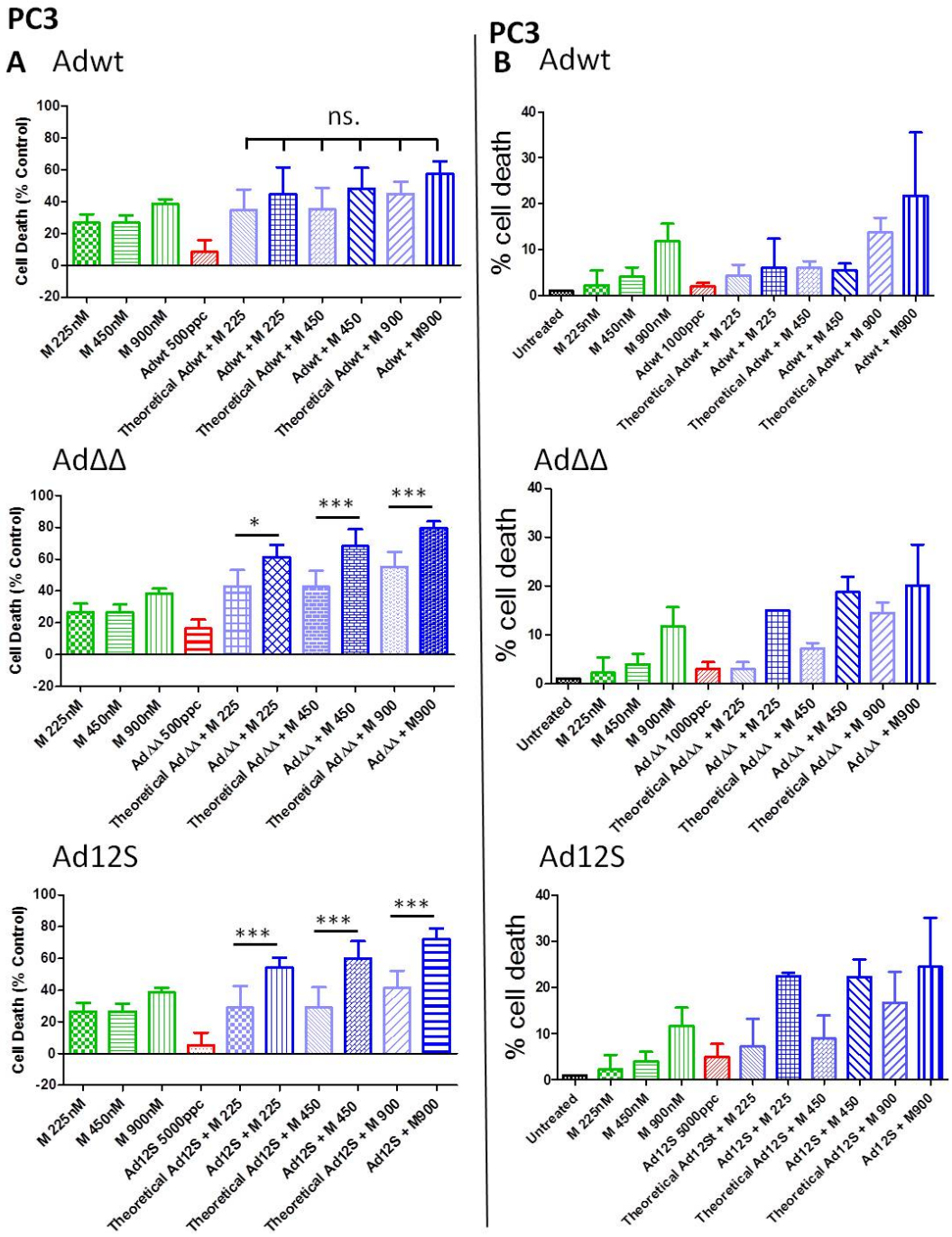

Figure 33. The combined treatment of AdΔΔ or Ad12S with low doses of mitoxantrone (M) causes more than additive cell killing in PC3 cells, but not in combination with Adwt. PC3 cells were treated with the indicated doses of Adwt or AdΔΔ at 500ppc or Ad12S at 5000ppc and/or indicated doses of mitoxantrone at 225, 450 or 900 nM. Cell death caused by viruses alone is shown in red. Cell death that resulted from the combined treatment is shown in dark blue and pale blue shows the theoretical values that were calculated from the sum of the cell death caused by the single agent treatments alone. The combined treatment caused more than additive effects when the dark blue bar was higher than the pale one. **A.** Cell viability was measured by the MTS assay 120h after treatment, averages ±SD, n=4, One-way Anova with Bonferroni post-test. *p<0.05, ***p<0.001 **B.** Cell killing was measured by Trypan blue 72h after treatment, averages ±SD, n=2. This assay was perfomed with AdΔΔ batch 050314.

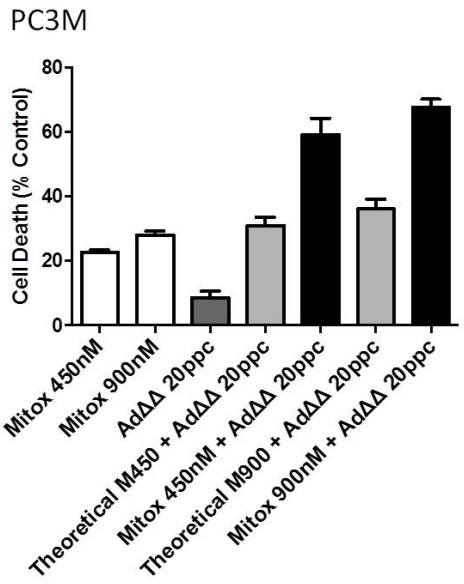

Figure 34. The combined treatment of AdΔΔ with low doses of mitoxantrone (Mitox) causes more than additive cell killing in PC3M cells. PC3M cells were treated with mitoxantrone at 450 and 900nM and/or AdΔΔ at 20ppc. Cell viability was measured by the MTS assay 3 days after treatment, averages ±SD, n=2. Data produced in collaboration with Ms Julia San Millan. This assay was performed with AdΔΔ batch 050314.

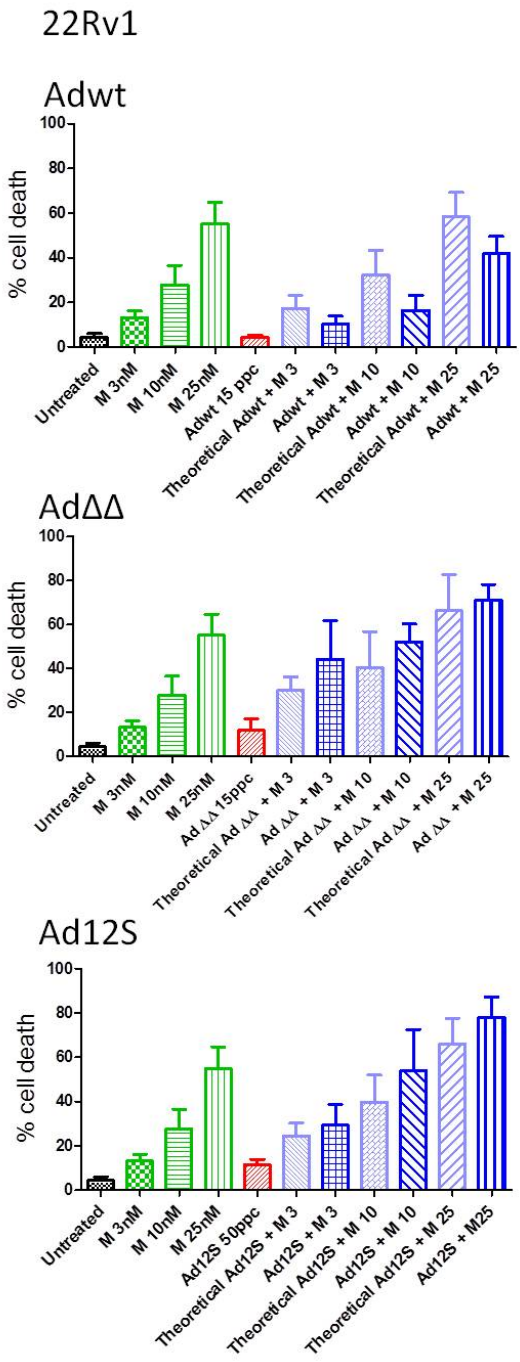

Figure 35. The combined treatment of low doses of AdΔΔ or Ad12S with low doses of mitoxantrone (M) causes a trend towards more than additive cell killing in 22Rv1 cells, but not in combination with Adwt. 22Rv1 cells were treated with indicated doses of Adwt or AdΔΔ at 15ppc or Ad12S at 50ppc and/or the indicated doses of mitoxantrone at 3, 10 or 25 nM. Cell death caused by viruses alone is shown in red. Cell death that resulted from the combined treatments is shown in dark blue and pale blue shows the theoretical values that were calculated from the sum of the cell death caused by the single treatments alone. The combined treatments caused more than additive effects when the dark blue bar was higher than the pale one. Cell death was measured by Trypan blue exclusion assay 72h after treatment, averages ±SD, n=2. This assay was perfomed with AdΔΔ batch 050314.

3.1.4 Summary of the studies of AdΔΔ-mediated enhancement of mitoxantrone cell killing in 22Rv1, PC3 and PC3M prostate cancer cells.

So far I have shown that AdΔΔ enhanced mitoxantrone-induced cell killing in PC3, 22Rv1 and PC3M prostate cancer cells. 22Rv1 and PC3M cells were significantly more sensitive to AdΔΔ-induced cytotoxicity than PC3 cells. PC3 and PC3M cells were more resistant to mitoxantrone-treatment showed by high EC_{50}-values while 22Rv1 cells were more sensitive (**Table *23*** and **Figure *28***). In agreement with previous findings in my group, infection with AdΔΔ and Ad12S sensitised PC3 and 22Rv1 cells to mitoxantrone. It is interesting to note that in the highly insensitive PC3 cells, AdΔΔ- and Ad12S-mediated sensitization to mitoxantrone was more potent than in the more sensitive 22Rv1 cells, as shown with 12-fold and 15-fold decreases in mitoxantrone EC_{50}-values in PC3 cells infected with AdΔΔ and Ad12S, respectively, compared to 2-fold and 2.3-fold decreases in 22Rv1 cells (**Figure *30*** and **Figure *32***). PC3 cells were highly insensitive to single agent treatment with both virus and drug compared to 22Rv1 cells, and required treatment with higher doses (**Table *23***). Decreased EC_{50}-values to mitoxantrone was also seen in 22Rv1 cells treated with AdΔΔ or Ad12S, sensitization to the drug was significant only for Ad12S infection (**Figure *31*** and **Figure *32***). In addition, combining fixed sub-optimal doses of each virus with fixed sub-optimal doses of mitoxantrone caused significantly more than theoretical additive increases in cell killing in PC3 and PC3M cells (***Figure 33***). It can be concluded that the combined treatment of AdΔΔ or Ad12S with mitoxantrone enhanced cell killing and increased the efficacy of the drug. These findings indicate that the addition of AdΔΔ may enable the use of lower doses of drugs *in vivo* (or in patients) to avoid unwanted toxicity.

Two different assays were performed to measure viral and drug-induced cytotoxicity. The MTS assay is a cell viability assay that detects cellular metabolic capacity as an indirect measurement of cell death. The Trypan blue assay detects cells with damaged membranes as a direct measurement of cell death. In PC3 cells, similar results were obtained with both assays. These findings confirmed that the lack of metabolic activity detected in the MTS assay is due to cell death and not to growth arrest and has been shown previously in other PCa cell lines (Oberg, Yanover et al. 2010).

3.1.5 The E1B19K-deleted mutants AdΔΔ and Ad12S counteract mitoxantrone-induced autophagy initiation in PC3, 22Rv1 and PC3M cells.

It has previously been reported that both androgen withdrawal (Ming, Byrne et al. 2013, Ziparo, Petrungaro et al. 2013) and chemotherapy treatment (Farrow, Yang et al. 2014) promote autophagy in *in vitro* and *in vivo* in various cancer models. Treatment with the antiandrogen bicalutamide caused hypoxia and therefore autophagy induction in LNCaP xenografts by inhibiting the key regulator mTOR (Ming, Byrne et al. 2013). In addition, treatment with paclitaxel and taxol induced autophagy in NIH/3T3 mouse fibroblast and MDA-MB-231 breast cancer cells, respectively (Eum and Lee 2011, Notte, Leclere et al. 2011).

The induction of autophagy in response to the drug-treatments was suggested to act as a cell survival mechanism. Previous studies in my group suggested that AdΔΔ infection or E1A-expression alone, could partially decrease mitoxantrone-induced LC3I to II conversion in PC3 and 22Rv1 cells (Maya Pineda 2013). Therefore, we hypothesised that the enhanced cell killing in response to AdΔΔ may involve inhibition of autophagy and could be developed as a therapeutic strategy for chemotherapy-resistant PCa.

In order to elucidate the effects of AdΔΔ on drug-mediated autophagy and whether its inhibition contributed to the synergistic cell killing in combination with mitoxantrone, the role of early and late phases of autophagy was explored. Induction and completion of autophagy was determined by increased LC3BI conversion to LC3BII and degradation of p62, respectively (Klionsky, Abeliovich et al. 2008). The conversion of LC3BI into LC3BII, and therefore an increased LC3BII/I ratio, is required for the initiation of autophagy and can be used as a marker for autophagy activation by immunoblotting. Degradation of p62 can also be detected by immunoblotting and is considered a marker for autophagy completion. Cells were treated with Ad5wt, AdΔΔ or Ad12S and mitoxantrone at doses determined in the previous section 3.1.3 that, when combined, resulted in more than additive cell killing in PC3 and PC3M cells and additive cell killing in 22Rv1 cells (**Figure *33***, **Figure *34*** and **Figure *35***).

In PC3 cells treated with Ad5wt and AdΔΔ at 500ppc or Ad12S at 5000ppc, infection alone did not induce autophagy, seen as no changes in LC3BII/I ratios and p62 levels compared to uninfected cells (***Figure 36A and B***). Infection with Ad12S even resulted in a trend towards reduction of basal autophagy levels detected as a lower LC3BII/I ratio by approximately 50%. As expected, autophagy initiation was induced in PC3 cells in response to mitoxantrone treatment at 225, 450 and 900nM. This induction was seen as 1.5 – 2-fold increases in

LC3BII/I ratios compared to untreated cells and was dose-dependent. Interestingly, expression of p62 increased 3 – 4-fold in PC3 cells treated with the low doses of mitoxantrone at 225 and 450nM. In contrast, p62 expression did not change in PC3 cells treated with 900nM mitoxantrone when compared to untreated cells (***Figure 36A and C***). In PC3 cells treated with low doses of mitoxantrone at 225 and 450nM, infection with AdΔΔ and Ad12S resulted in a strong trend towards counteraction of mitoxantrone-induced conversion of LC3BI into LC3BII. However, when treated with 900nM mitoxantrone, co-infection with AdΔΔ or Ad12S did not modify the increased LC3BII/I ratios, suggesting that at the highest dose of 900nM the mitoxantrone-mediated induction of autophagy was too potent for the virus to counteract. Importantly, no further increases in LC3II/I ratios were observed in the combination treated cells (***Figure 36A and B)***. The combined treatment of AdΔΔ or Ad12S with mitoxantrone resulted in decreased expression of p62 compared to mitoxantrone alone (***Figure 36A and C***). More specifically, the combination of AdΔΔ with 450 and 900nM mitoxantrone resulted in an approximately 50% decrease in p62 levels when compared to mitoxantrone-only treated cells. The combination of Ad12S and 450nM mitoxantrone resulted in a 4-fold decrease in p62 expression when compared to mitoxantrone only and was even lower than basal levels. The p62 expression was barely detectable in cells treated with Ad12S in combination with 900nM mitoxantrone (***Figure 36A and C***). The combined treatment of Ad5wt and all tested doses of mitoxantrone (225, 450 and 900nM) caused no changes in p62 expression or LC3BII/I ratios when compared to mitoxantrone-only treated cells (***Figure 36***). Unfortunately, monitoring of p62 expression proved problematic as experimental replicas were quite variable and p62 expression was often difficult to detect, possibly because of antibody instability. In contrast, LC3II/I expression was highly reproducible. These data indicated that only high doses of mitoxantrone resulted in decreased p62 levels and completion of autophagy. It is possible that higher doses or longer treatment times are necessary for completion of autophagy in PC3 cells, even in the presence of potent autophagy-induction seen as high ratios of LC3II/I. In combination-treated cells, AdΔΔ and Ad12S inhibited the mitoxantrone-induced initiation of autophagy and prevented the accumulation of p62, reflected in the lower levels of the protein in infected cells compared to mitoxantrone-treatment only.

To further investigate the effects on autophagy by AdΔΔ-infection in mitoxantrone-treated PC3 cells, the formation of acidic vesicles, as a positive marker of autophagy, was measured by staining with the Lysotracker dye (**Figure *37***). The Lysotracker-mediated detection of acidic vesicles is an indication of the fusion of autophagosomes and lysosomes and therefore, an

increase in the signal can indicate autophagy completition. Alternatively, increased Lysotracker staining may also indicate an overall increase in the number of lysosomes. Stained cells were detected by flow cytometry. Treatment with the autophagy-inducer rapamycin was used as a positive control. Rapamycin-treatment increased the number of acidic vesicles, when compared to untreated cells (**Figure *37***). In agreement with the increased mitoxantrone-dependent LC3BII/I ratios (***Figure 36A and B***), PC3 cells treated with 450nM mitoxantrone increased the number of cells with positive vesicles to 11.5 ± 3.4 %. The combined treatment of mitoxantrone and AdΔΔ at 500ppc reduced the number of positive cells to 5.0 ± 0.6 %. The difference between mitoxantrone and the combined treatment was significant ($p<0.01$). Infection with AdΔΔ alone even reduced the levels of acidic vesicles when compared to untreated cells suggesting a decrease in basal autophagy (**Figure *37***). These data support the findings from the AdΔΔ-mediated attenuation of mitoxantrone-induced LC3II/I ratios and indicated that the decrease in autophagy-inititation was reflected in decreased fusion of autophagosomes with lysosomes.

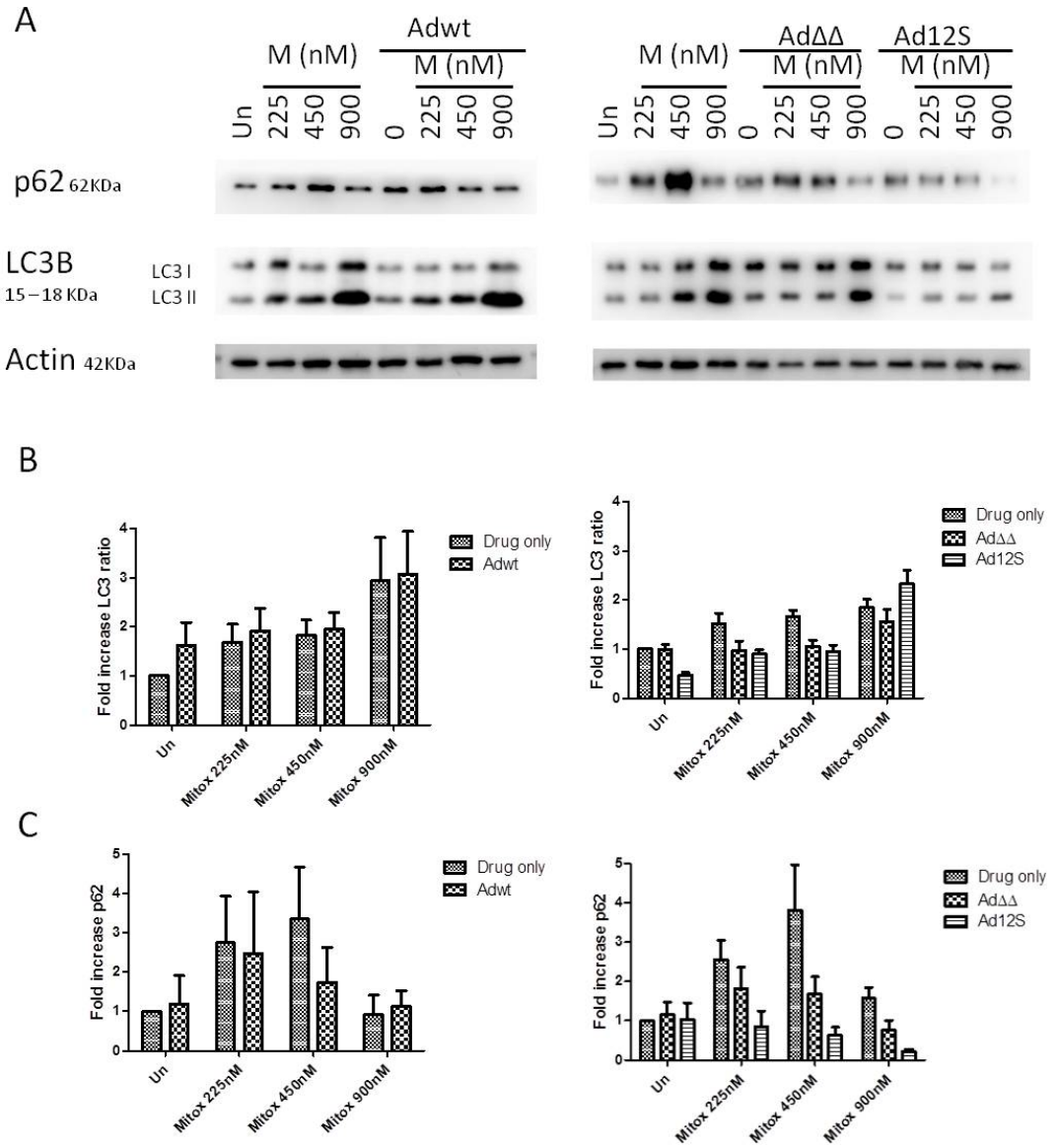

Figure 36. Mitoxantrone promotes autophagy initiation that is counteracted by AdΔΔ or Ad12S adenoviral mutants in PC3 cells. **A.** Immunoblotting for p62 and LC3BII/I proteins in PC3 cells treated with mitoxantrone at 225, 450, 900nM and/or Adwt or AdΔΔ at 500ppc and Ad12S at 5000ppc. Representative images of 3 to 6 immunoblots. **B.** Densitometry quantification of LC3BII/I expression. LC3BII/I ratio is expressed as LC3II (lower band) divided by LC3I (higher band), averages ±SD, n=6. **C.** Densitometry quantification of p62 expression, averages ±SD, n=3. All densitometry values were normalised to the loading control before calculating ratios. **B and C.** One-way Anova with Bonferroni post-test was performed but resulted in no significant differences. This assay was performed with AdΔΔ batch 050314.

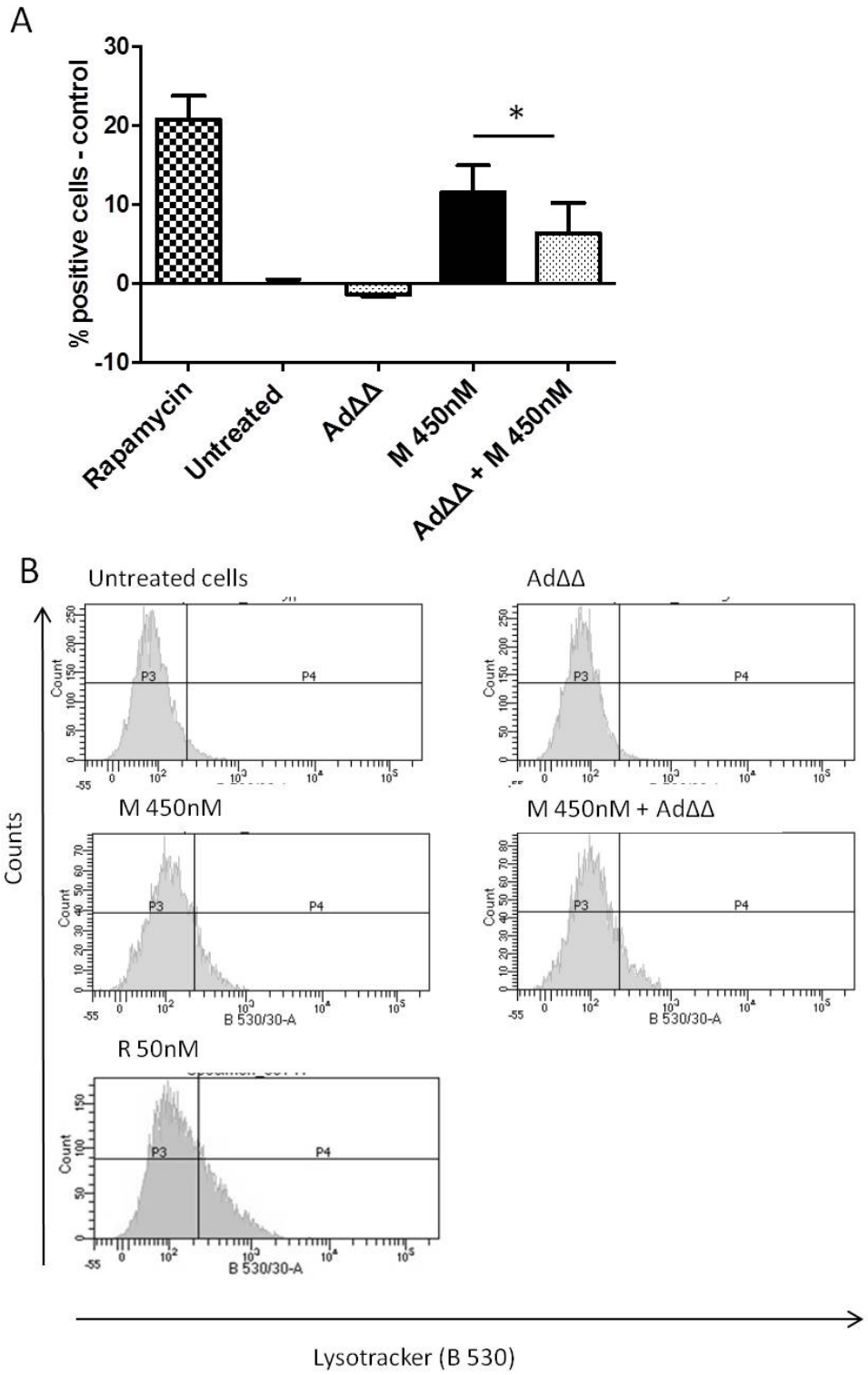

Figure 37. Mitoxantrone increases the number of cellular acidic vesicles that are reduced in combination with AdΔΔ in PC3. A. PC3 cells were treated with mitoxantrone (M) at 450nM, AdΔΔ at 500ppc or the combination of both treatments and collected 120h post-treatment. Rapamycin (R) at 50nM was used as a positive control. Cells were stained with the Lysotracker dye and analysed by flow cytometry, averages ±SD, n=4. The number of positive cells – control is shown. Lysotracker signal was detected on the laser B 530/30. Unpaired t-test, **p<0.01. **B.** Representative flow cytometry data. This assay was performed with AdΔΔ batch 050314.

In 22Rv1 cells, similar to PC3 cells, infection with Ad5wt or AdΔΔ at 20ppc, or Ad12S at 100ppc did not induce autophagy, shown as no changes in LC3BII/I ratios and p62 expression (**Figure 38**). Autophagy was induced in 22Rv1 cells in response to mitoxantrone treatment at 3, 10 and 25nM, seen as a 2 – 3-fold increase in LC3BII/I ratios that were dose-dependent and an approximately 50% decrease in p62 expression when compared to untreated cells. This increase in LC3BII/I ratios and degradation of p62 indicated initiation and completion of the autophagic pathway, respectively (***Figure 38***). In agreement with PC3 data, infection with AdΔΔ and Ad12S resulted in a non-significant counteraction of mitoxantrone-induced increases in LC3BII/I ratios in 22Rv1 cells treated with low doses of mitoxantrone at 3 and 10nM. In cells treated with the higher dose of 25nM mitoxantrone, co-infection with AdΔΔ decreased mitoxantrone-induced increases in LC3BII/I ratios from 3-fold to 2. (***Figure 38A and B***). These data suggest that at the highest dose of 25nM mitoxantrone, drug-mediated induction of autophagy was too potent for the virus to counteract in agreement with the findings in PC3 cells treated with the highest dose of mitoxantrone. The combined treatment of AdΔΔ and Ad12S with all tested doses of mitoxantrone (3, 10 and 25nM) did not affect p62 expression levels when compared to mitoxantrone-only treated cells (***Figure 38A and C***). In contrast, the combined treatment of Ad5wt with all tested doses of mitoxantrone did not change LC3BII/I ratios when compared to mitoxantrone-only treated cells (***Figure 38A and B***). However, p62 expression increased approximately 2-fold when compared to mitoxantrone-only treated cells (***Figure 38A and C***). These data indicate that, in combination-treated cells, AdΔΔ and Ad12S, but not Ad5wt inhibited the mitoxantrone-induced initiation of autophagy at low doses of the drug but did not affect p62 expression.

Changes in acidic vesicle formation were also monitored in 22Rv1 cells. Cells treated with 10 and 25nM mitoxantrone showed 18.8 ± 4.4% and 10.4 ± 4.2 % increases in the number of positive cells, respectively (***Figure 39***). The combination of 10nM mitoxantrone with AdΔΔ at 20ppc reduced the number of cells that were positive for acidic vesicles by 50%, when compared to 10nM mitoxantrone only. This reduction in acidic vesicles was significant ($p<0.01$). Single treatment with AdΔΔ only slightly increased the number of positive cells to 3.7 ± 1.9 % (***Figure 39***). In agreement with PC3 findings, these data indicated that AdΔΔ-mediated attenuation of mitoxantrone-induced autophagy could also be detected in 22Rv1 cells at later stages in the autophagic pathway.

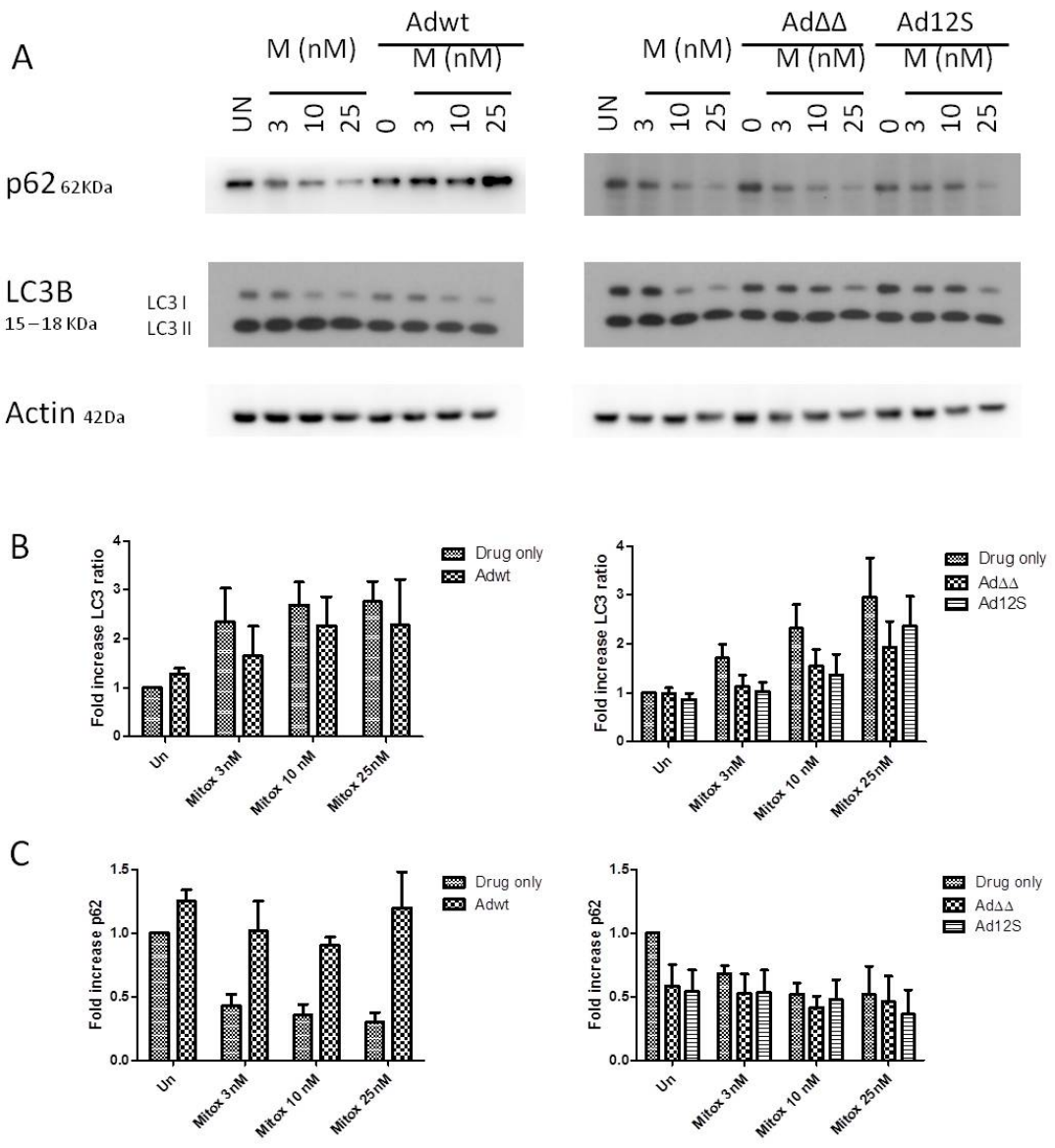

Figure 38. Mitoxantrone induces autophagy that is counteracted by AdΔΔ or Ad12S mutants in 22Rv1 cells. A. Immunoblotting for p62 and LC3BII/I proteins in 22Rv1 cells treated with mitoxantrone at 3, 10, 25nM and/or infected with Adwt or AdΔΔ at 20ppc and Ad12S at 100ppc. Representative images, from 4 experiments. **B.** Densitometry quantification of LC3BII/I expression. LC3BII/I ratios are expressed as LC3II (lower band) divided by LC3I (higher band), averages ±SD, n=4. **C.** Densitometry quantification of p62 expression, averages ±SD, n=4. All densitometry values were normalised to the loading control before calculating ratios. **B and C.** One-way Anova with Bonferroni post-test was performed but resulted in no significant differences. This assay was performed with AdΔΔ batch 050314.

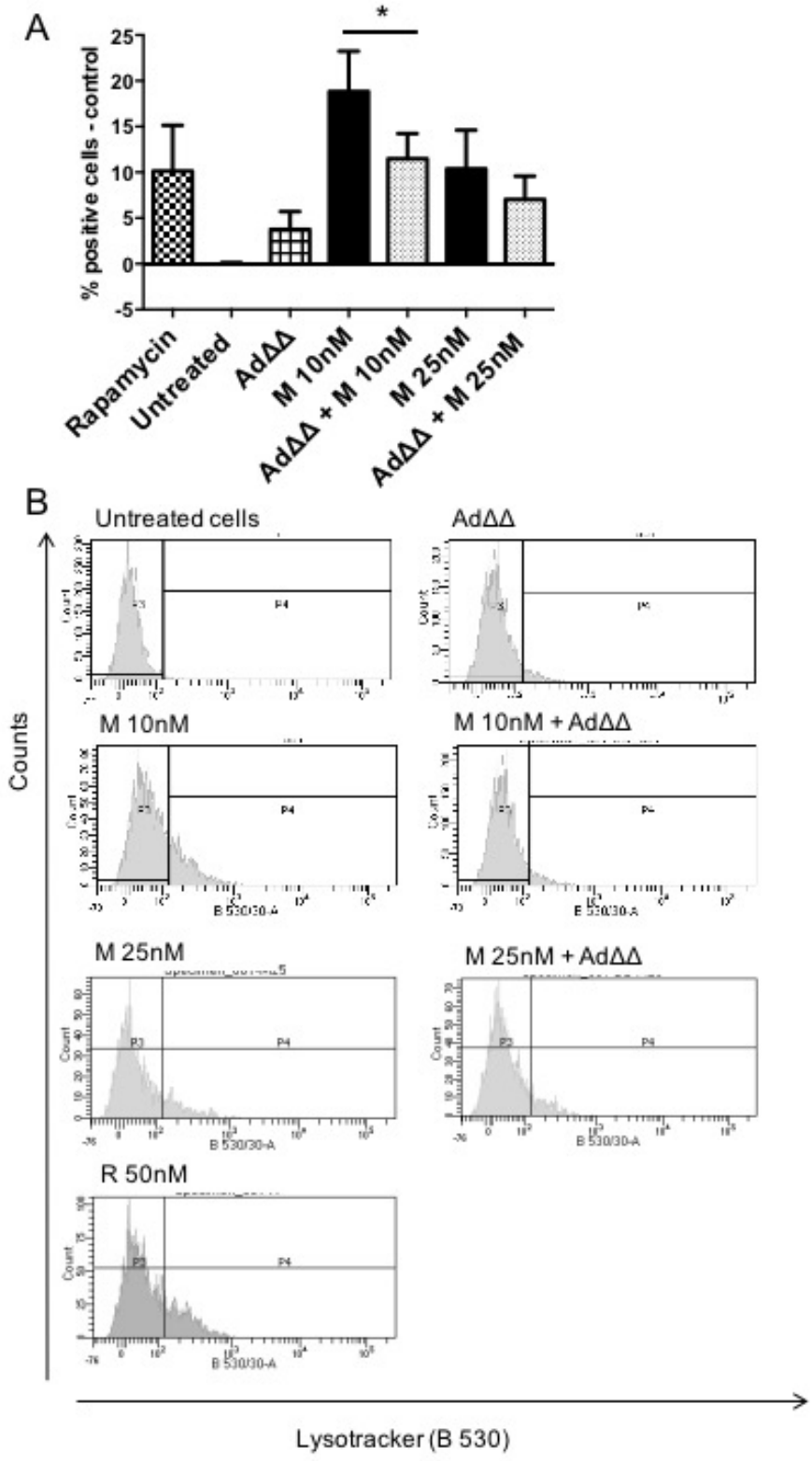

Figure 39. Mitoxantrone increases the number of cellular acidic vesicles that are reduced in combination with AdΔΔ in 22Rv1 cells. A. 22Rv1 cells were treated with mitoxantrone (M) at 10 and 25nM or AdΔΔ at 20ppc or the combination of both treatments and collected 72h later. Rapamycin (R) at 50nM was used as a positive control. Cells were stained with Lysotracker dye and analysed by flow cytometry, averages ±SD, n=3. The number of positive cells – control is shown. One-way Anova with Bonferroni post-test, *p<0.05. **B.** Representative flow cytometry results from A. This assay was performed with AdΔΔ batch 050314.

To determine if autophagy was modulated also in PC3M cells in response to the combination treatments, similar studies were performed in these cells. Infection with Ad5wt or AdΔΔ at 20ppc did not change LC3BII/I ratios when compared to untreated cells. However, infection with AdΔΔ or Ad5wt promoted p62 degradation resulting in 60% and 80% decreases compared to basal levels, respectively (**Figure *40A, B and C***). Both doses of mitoxantrone (450 and 900nM) caused 3.5-fold increases in LC3BII/I ratios when compared to untreated cells. The combined treatments of AdΔΔ or Ad5wt with 450 or 900nM mitoxantrone resulted in a trend towards reduction of mitoxantrone-dependent increases in LC3BII/I ratios by 2-fold (**Figure *40A and C***). No significant changes in p62 expression levels in response to the combined treatment of AdΔΔ or Ad5wt with 450 or 900nM mitoxantrone in PC3M cells compared to mitoxantrone-only treated cells were observed. The combined treatment of AdΔΔ or Ad5wt with 450nM mitoxantrone resulted in small decreases in p62 expression of around 20% and 40%, respectively. In contrast, the combined treatments of AdΔΔ or Ad5wt with the higher dose of 900nM mitoxantrone, resulted in small increases in p62 expression levels compared to mitoxantrone-only treated cells (**Figure *40A and B***). These data indicate that, in combination-treated cells, both Ad5wt and AdΔΔ attenuated the mitoxantrone-induced initiation of autophagy at low doses of the drug, however, no clear effect of p62 expression was oberved.

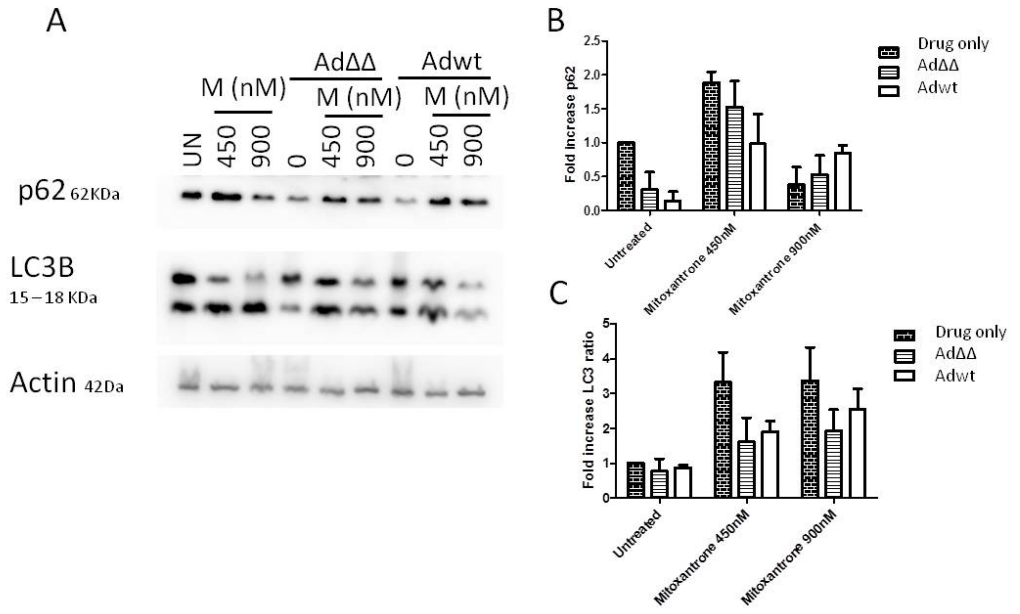

Figure 40. Mitoxantrone induces autophagy that is counteracted by Adwt or AdΔΔ in PC3M cells. A. Expression of LC3BII/I and p62 by immunoblotting. PC3M cells were treated with mitoxantrone (450 and 900nM) and/or Adwt or AdΔΔ at 20ppc and collected 2 days after treatment, n=2. **B.** Densitometry quantification of LC3BII/I were expressed as LC3II (lower band) divided by LC3I (higher band), averages ±SD, n=2. **C.** Densitometry quantification of p62 expression, averages ±SD, n=2. All densitometry values were normalised to the loading control before calculating ratios. Data generated in collaboration with Ms Julia San Millan. This assay was performed with AdΔΔ batch 050314.

These data demonstrate that AdΔΔ attenuated mitoxantrone-induced increases of LC3BII/I ratios in all tested PCa cell lines, PC3, 22Rv1 and PC3M at the lower drug-doses. In contrast, Ad5wt did not have any effect on LC3BII/I ratios in PC3 and 22Rv1 cells. Infection with the non-replicating E1A-expressing Ad12S virus resulted in similar effects as seen for AdΔΔ infection, which suggested that the attenuation was mainly due to the expression of the E1A protein, as this is only protein expressed by Ad12S. In contrast to the LC3BII/I results, infection with AdΔΔ or Ad12S did not prevent p62 degradation and under some conditions, promoted p62-degradation. However, these data might also indicate that infection with AdΔΔ or Ad12S only affected initial steps in the autophagy pathway. The findings were confirmed by determining the number of cells that were positive for acidic vesicles. Treatment with mitoxantrone alone resulted in increased number of positive vesicles that decreased in combination with AdΔΔ-infection in both PC3 and 22Rv1 cells. AdΔΔ-mediated attenuation of mitoxantrone-dependent initiation of autophagy indicated that infection with AdΔΔ might block this pathway, at least in the presence of low doses of mitoxantrone and cell killing was enhanced by activation of other cellular mechanisms.

3.1.6 AdΔΔ and Ad12S enhance mitoxantrone-induced apoptotic cell death in PC3, 22Rv1 and PC3M cells.

The E1A-encoded viral proteins are well stablished to promote apoptosis by multiple mechanisms while the E1B-, E3- and E4-encoded proteins prevent premature apoptosis to enable completion of the viral life-cycle (see section 1.5.2). Previous findings in my team demonstrated that the replicating AdΔE1B19K mutant (E1B19K-deleted), enhanced gemcitabine-induced apoptotic cell death in models of pancreatic cancer (Leitner, Sweeney et al. 2009, Pantelidou, Cherubini et al. 2016). The increased apoptosis was the result of increased E1A expression in E1B19K mutants (AdΔΔ and AdΔ19K).

In order to investigate whether the AdΔΔ-mediated attenuation of mitoxantrone-induced autophagy was paralleled by increased apoptosis, changes in apoptosis markers were investigated in the PC3, 22Rv1 and PC3M cells. Cells were treated with Ad5wt, AdΔΔ and Ad12S and mitoxantrone at doses determined in sections 3.1.3 and 3.1.5 that, when combined, resulted in more than additive cell killing in PC3 and PC3M cells and additive cell killing in 22Rv1 cells (**Figure *33***, **Figure *34*** and **Figure *35***).

PC3 cells were treated with Ad5wt, AdΔΔ at 500ppc or Ad12S at 5000ppc alone or in combination with 225, 450 or 900nM mitoxantrone and cleavage of PARP and pro-caspase 3 were assessed by immunoblotting (**Figure *41***). Treatment with low doses of mitoxantrone at 225 and 450nM resulted in non-significant increased PARP cleavage (***Figure 41A and B***; indicated with black arrow). Mitoxantrone treatment increased the ratio of cleaved PARP/pro-PARP by 1.5 – 2-fold. Treatment with the highest tested dose of mitoxantrone at 900nM also showed non-significant increased cleavage of PARP; the cleaved PARP/proPARP ratio was increased by 3-fold, when compared to untreated cells. Infection with Ad5wt, AdΔΔ and Ad12S resulted in promotion of PARP cleavage in PC3 cells increasing PARP ratios 6-fold, 5-fold and 4 fold compared to basal levels, respectively (***Figure 41A and B***). The combined treatment of AdΔΔ with 225 and 450nM mitoxantrone induced 5-fold increases in PARP ratios, when compared to untreated cells. This increase was similar to AdΔΔ-only infected cells. The combined treatment of Ad12S and all tested doses of mitoxantrone (225, 450 and 900nM) resulted in a strong trend towards increased PARP cleavage when compared to single agent treatments. The combination of Ad12S and 900nM mitoxantrone resulted in a 6-fold increase in the PARP ratio when compared to untreated cells. The combined treatment of Ad5wt with all tested doses of mitoxantrone (225, 450, 900nM) resulted in 4-fold increases in PARP ratios, when compared to untreated cells. These results were

surprising since infection with Ad5wt alone induced a 6-fold increase in the PARP ratio, implying that the combination-treatments with Ad5wt caused less apoptotic death than virus alone but more than mitoxantrone alone (***Figure 41A and B***). No changes in pro-caspase 3 were detected in PC3 cells (data not shown). Other members of the team had previously observed that pro-caspase 3 cleavage could not be induced by the typical apoptosis-inducing agents (e.g. staurosporin, cisplatin; unpublished data).

Apoptosis was also investigated by assessing depolarization of the mitochondrial membrane in PC3 cells by flow cytometry of cells stained with tetramethylrhodamine ethyl ester (TMRE) 48 – 120h after treatment. Cells treated with 900nM of mitoxantrone promoted depolarization of the mitochondrial membrane in 14.1 ± 0.7% of cells at 72h, this percentage gradually increased over time up to 34.5 ± 3.1% at 120h. Treatment with 450nM mitoxantrone slightly promoted apoptosis in 12.5 ± 2.7% of cells only 120h after treatment (***Figure 41C***). Single agent treatment with AdΔΔ at 500ppc did not induce apoptosis in PC3 cells at any time-point (48 – 120h). In order to investigate the effects of the combined treatments of AdΔΔ and mitoxantrone on the mitochondrial depolarization, PC3 cells were treated with AdΔΔ in combination with 450 and 900nM mitoxantrone. The combined treatment of AdΔΔ and 450nM mitoxantrone promoted mitochondrial membrane depolarization in 21.3 ± 2.0% of cells, this percentage was higher when compared with mitoxantrone-only treated cells. The combination of AdΔΔ with 900nM mitoxantrone resulted in a trend towards enhanced mitoxantrone-induced apoptosis at 72h although it was similar to mitoxantrone only treatment at later time-points (***Figure 41C***).

To further examine the roles of mitochondrial depolarization and PARP cleavage in PC3 cells and strengthen the evidence for enhanced apoptosis in response to the combined treatment of AdΔΔ and mitoxantrone, changes in Annexin V staining were determined by FACS. Annexin V positive cells indicate that phosphatidylserine has translocated from the inner to the outer surface of the cellular membrane, which enables binding of Annexin V thus indicating apoptotic cell death. Mitoxantrone treatment with 450 and 900nM increased Annexin V positive cells in a dose-dependent manner reaching 7.6 ± 0.5% and 27.2 ± 8.2 % for 450 and 900nM mitoxantrone, respectively (***Figure 41D***). The combined treatment of AdΔΔ and 450nM mitoxantrone resulted in 23.0 ± 4.6% of Annexin V positive cells, enhancing apoptosis when compared to mitoxantrone only (***Figure 41D***). Similar to the TMRE data, AdΔΔ did not further promote apoptosis in PC3 cells treated with 900nM mitoxantrone.

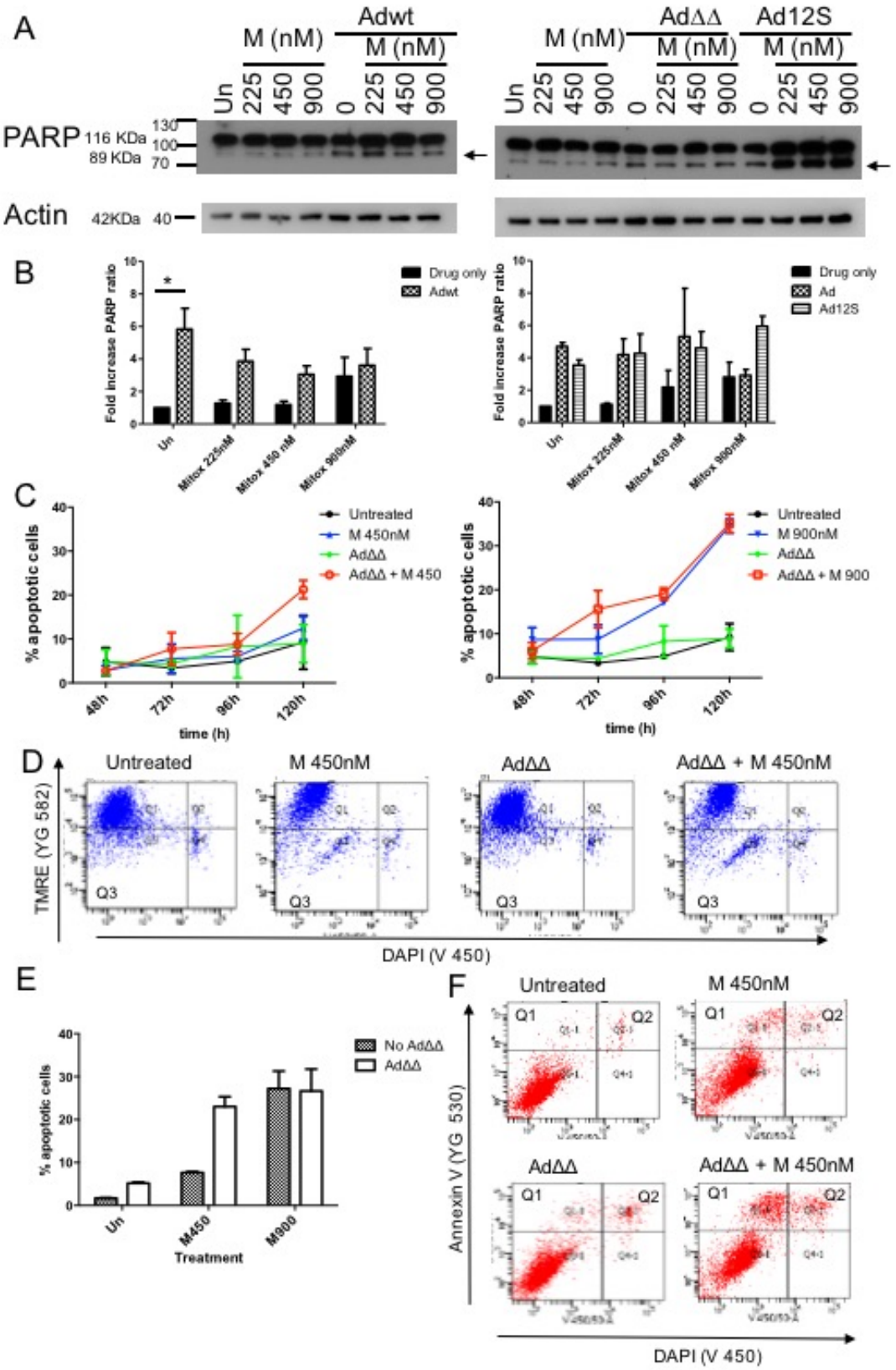

Figure 41. AdΔΔ increases mitoxantrone–induced apoptotic cell killing in PC3 cells. A. Expression of PARP detected by immunoblotting (cleaved PARP is indicated with black arrow)**.** PC3 cells were treated with Adwt or AdΔΔ at 500ppc or Ad12S at 5000ppc and/or indicated doses of mitoxantrone at 225, 450 or 900 nM and collected 48h after treatment. One representative immunoblot of 3**. B.**

Densitometry values of cleaved PARP (lower band) divided by proPARP (higher band). All densitometry values were normalised to the loading control. One-way Annova with Bonferroni post-test, *p<0.05, averages ±SD, n=3**. C.** PC3 cells were treated with AdΔΔ at 500ppc and/or indicated doses of mitoxantrone at 450 or 900 nM and collected at indicated time points. Mitochondrial depolarization was measured as an indication of apoptosis by loss of TMRE staining (Q3), n=2. TMRE and DAPI staining were detected with the lasers YG 582/15 and V 450/50, respectively. **D.** Representative images from FACS analysis in C, samples collected 120h after treatment. **E.** PC3 cells were treated with AdΔΔ at 500ppc and/or indicated doses of mitoxantrone at 450 or 900 nM and collected at 120h. Appearance of Annexin V staining was measured as an indication of apoptosis (Q1 + Q2), averages ±SD, n=2. Annexin V and DAPI staining were detected with the lasers YG 530/30 and V 450/50, respectively. **F.** Representative images from FACS analysis in E. This assay was performed with AdΔΔ batch 050314.

Similar studies were performed in 22Rv1 cells, treated with increasing doses of mitoxantrone. Non-significant increased PARP-cleavage was seen with 3, 10 and 25nM of drug (indicated with black arrow) in a dose-dependent manner by 2-3-fold compared to untreated cells (**Figure *42A and B***). In addition, treatment with 3, 10 and 25nM mitoxantrone resulted in a dose-dependent decrease in pro-caspase 3 indicating increased apoptosis (**Figure *42A***). Single treatment with AdΔΔ and Ad12S promoted 5-fold increases in cleaved PARP/proPARP ratios. The combined treatment of either AdΔΔ or Ad12S with all tested doses of mitoxantrone (3, 10 and 25nM) resulted in a strong trend towards increased cleaved PARP/proPARP ratios, compared to single agent treatment with mitoxantrone. The combined treatment of AdΔΔ with all tested doses of mitoxantrone (3, 10 and 25nM) further increased the cleaved PARP/proPARP ratios by 7-, 9- and 13-fold, respectively. Similar to AdΔΔ, the combined treatment of Ad12S with all doses of mitoxantrone (3, 10 and 25nM) further increased PARP-cleavage by 9-, 11- and 20-fold compared to untreated cells. Ad12S in combination with mitoxantrone at 3, 10 and 25nM, resulted in potent apoptosis-induction. Infection with Ad5wt did not increase PARP ratios in 22Rv1 cells. On the contrary, Ad5wt infection decreased basal cleaved-PARP levels. The combination of all tested doses of mitoxantrone (3, 10 and 25nM) with Ad5wt, AdΔΔ or Ad12S did not change the levels of pro-caspase, which remained similar to those in mitoxantrone-treated cells (**Figure *42A and B***).

Depolarization of the mitochondrial membrane was also measured over time in 22Rv1 cells (***Figure 42C***). Mitoxantrone-treatment promoted mitochondrial membrane depolarization in 22Rv1 cells similar to the observations in PC3 cells. However, responses were different in terms of doses and timings, the 22Rv1 cells were more sensitive to mitoxantrone-induced mitochondrial depolarization. Treatment with 25nM mitoxantrone promoted mitochondrial depolarization in 35.4 ± 14.5% of cells as early as 24h after treatment in 22Rv1 cells (***Figure 42C***) and reached 49.4 ± 13.5% after 48h, and was maintained at a similar level up to 72h

after treatment. Treatment with 10nM mitoxantrone promoted mitochondrial depolarization in 21.0 ± 6.5% of cells 24h after treatment. And reached 28.7 ± 10.5% after 48h, and was maintained at a similar level up to 72h after treatment (***Figure 42C***). Infection with AdΔΔ at 20ppc induced mitochondrial depolarization in 17.9 ± 3.2% of cells 72h after treatment. The combined treatment of AdΔΔ and 10nM mitoxantrone resulted in a trend towards increased mitochondrial depolarization in 38.9 ± 12.9% and 38.0 ± 3.9% of cells after 48 and 72h, respectively, compared to mitoxantrone only. The combined treatment of 25nM mitoxantrone and AdΔΔ did not further increase mitochondrial depolarization compared to mitoxantrone-only treated cells (***Figure 42C***). It was not possible to perform the Annexin V assay in 22Rv1 cells due to buffer incompatibility, which had previously been observed by other members in the team.

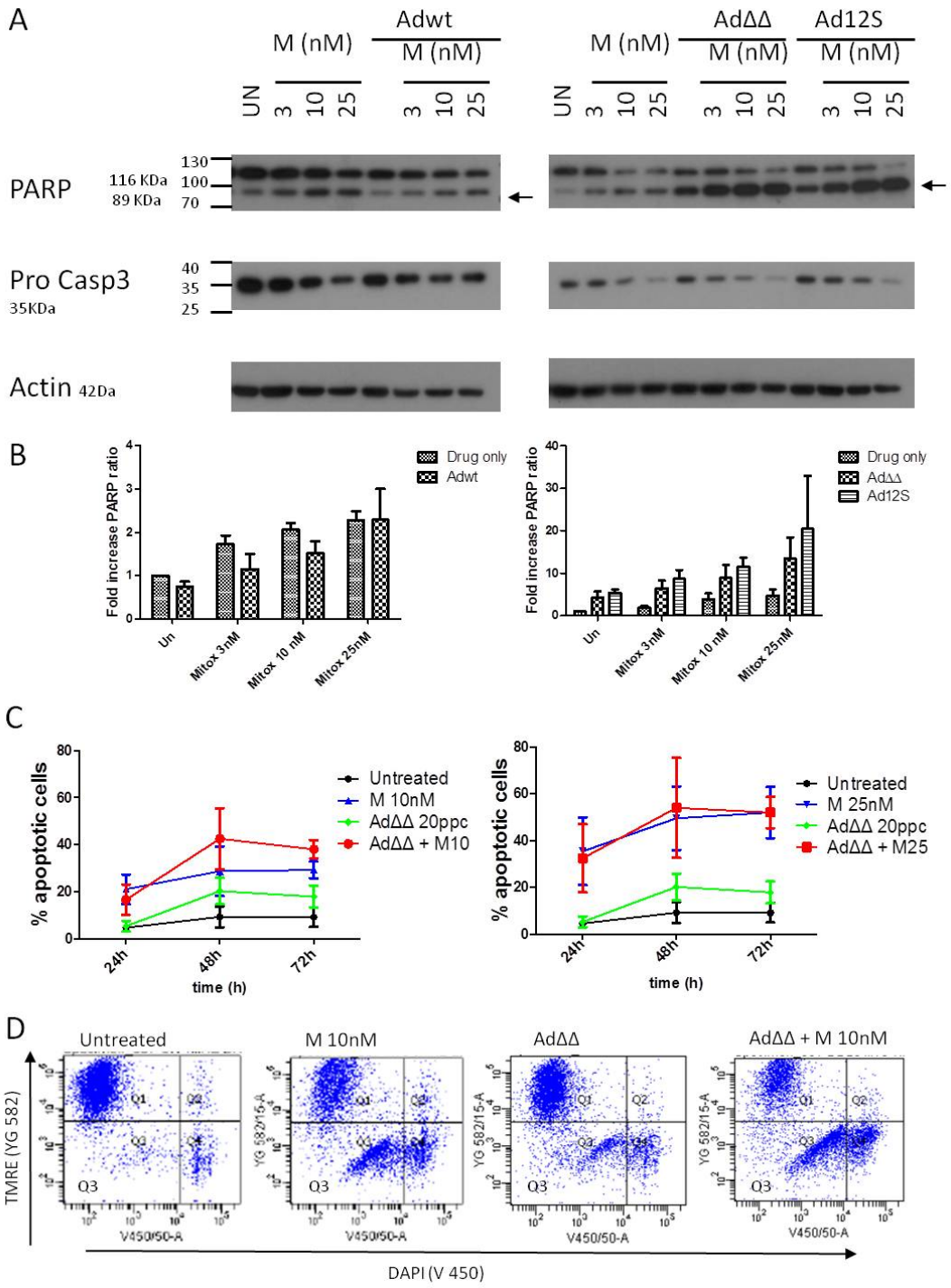

Figure 42. AdΔΔ increases mitoxantrone–induced apoptotic cell killing in 22Rv1 cells to a greater extent than Adwt. A. Expression of PARP and pro-caspase 3 by immunoblotting (cleaved PARP is indicated with black arrow). 22Rv1 cells were treated with Adwt or AdΔΔ at 15ppc or Ad12S at 50ppc and/or indicated doses of mitoxantrone at 3, 10 or 25 nM and collected 48h after treatment. One representative immunoblot of 3. **B.** Densitometry values of cleaved PARP (lower band) divided by proPARP (higher band). All densitometry values were normalised to the loading control before calculating ratios. One-way Annova with Bonferroni post-test was performed but resulted in no significant differences, averages ±SD, n=3. **C.** 22Rv1 cells were treated with AdΔΔ at 20ppc and/or indicated doses of mitoxantrone at 10 or 25 nM and collected at indicated time points, averages ±SD, n=2. Mitochondrial depolarization was measured as an indication of apoptosis by loss of TMRE staining (Q3). TMRE and DAPI staining were detected with the lasers YG 582/15 and V 450/50,

respectively. **D.** Representative images from FACS analysis in C, samples collected 72h after treatment. This assay was performed with AdΔΔ batch 050314.

The enhancement of apoptosis-related markers was also assessed in PC3M cells using the TMRE staining and FACS analysis. Treatment with 450 and 900nM of mitoxantrone resulted in increased mitochondrial depolarization, however these increases were not dose-dependent. Treatment with 450nM mitoxantrone resulted in the highest increase with 48.7 ± 3.5% of cells undergoing depolarization of the mitochondrial membranes. Treatment with 900nM mitoxantrone only, resulted in 41.4 ± 4.1% of apoptotic cells (**Figure *43***). Mitochondrial depolarization appeared earlier in PC3M cells than in PC3 cells; 72h after treatment versus 120h in PC3 cells with a maximum of 34.5% of cells (**Figure *41D and* Figure *43***). At 120h after treatment all PC3M cells were dead and data could not be generated at this time-point. Treatment with Ad5wt or AdΔΔ at 20ppc induced mitochondrial depolarization in 15.8 ± 9.5% and 25.7 ± 17.5% of cells, respectively (**Figure *43A***). The combined treatment of AdΔΔ with 450 and 900nM mitoxantrone increased the mitochondrial depolarization over that of mitoxantrone alone. This increase was significant ($p<0.001$ and $p<0.0001$ for 450 and 900nM, respectively). The percentage of cells undergoing mitochondrial depolarization was increased to 65.8 ± 5.4% and 61.5 ± 5.6% for AdΔΔ in combination with 450 and 900nM, respectively. In contrast, the effect of the combinations of Ad5wt with both tested doses of mitoxantrone (450 and 900nM) did not differ from that observed in mitoxantrone-only treated cells (**Figure *43***).

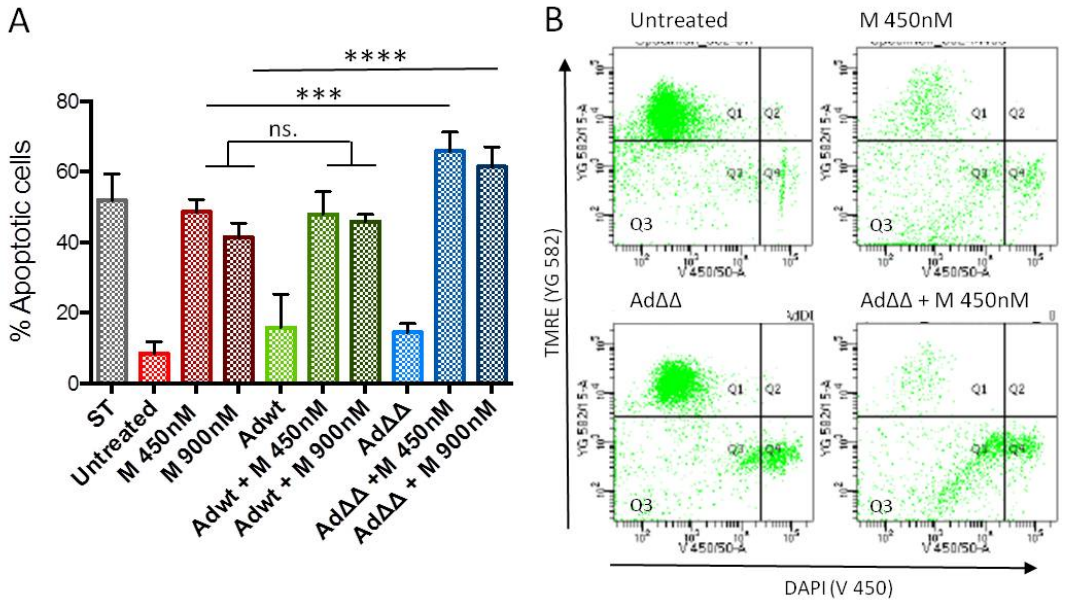

Figure 43. The combined treatment of AdΔΔ and mitoxantrone enhances drug-induced mitochondrial depolarization in PC3M cells. A. PC3M cells were treated with mitoxantrone (M) at 450 and 900nM and/or Adwt or AdΔΔ at 20ppc and collected 3 days after treatment. Staurosporine (ST) 1µM was added as a positive control. Mitochondrial depolarization was measured as an indication of apoptosis by loss of TMRE staining (Q3). TMRE and DAPI staining were detected with the lasers YG 582/15 and V 450/50, respectively. One-way Anova with Bonferroni post-test ***p<0.001, ****p<0.0001, averages ±SD, n=3. **B.** Representative selected images from FACS analysis in A. Data produced in collaboration with Ms Julia San Millan. This assay was performed with AdΔΔ batch 050314.

These findings demonstrated that mitoxantrone-treatment resulted in depolarization of the mitochondrial membrane in PC3, PC3M and 22Rv1 cells while all viruses had minimal effects. Co-infection with AdΔΔ further increased the mitochondrial depolarization in all tested cell lines. In PC3 cells, mitoxantrone-treatment promoted Annexin V staining, this staining was increased by co-treatment with AdΔΔ. Finally, both AdΔΔ and Ad12S enhanced mitoxantrone-induced PARP-cleavage in PC3 and 22Rv1 cells, suggesting that this enhancement was due to the expression of the E1A adenoviral protein. The TMRE, Annexin V and PARP data confirmed that mitoxantrone-treatments induced apoptosis, which was further increased by co-infection with AdΔΔ. It can also be concluded that AdΔΔ-mediated enhancement of mitoxantrone-induced cell killing, demonstrated by additive or more than additive cell killing as a result of the combination-treatment (section 3.1.2 and 3.1.3), was due to promotion of apoptosis.

3.1.7 Ad-mediated attenuation of mitoxantrone-induced autophagy is directly related to Ad-mediated enhancement of apoptosis.

Aiming to establish a possible relationship of the attenuation of mitoxantrone-induced autophagy-initiation and the enhancement in mitoxantrone-induced apoptosis in PC3, 22Rv1 and PC3M cells, the data were further processed. LC3BII/I ratios were directly compared with the apoptotic markers for PARP cleavage, mitochondrial depolarization and Annexin V staining (***Figure 44***).

In mitoxantrone-treated PC3 cells treated with 450 and 900nM, the drug induced increases in LC3II/I ratios (***Figure 44A***; open red bars). AdΔΔ infection, in combination with both doses of the drug, attenuated mitoxantrone-induced increase in LC3II/I ratios (filled red bars) (***Figure 44A***). A similar effect was also seen with the Lysotracker staining (**Figure *37***). Mitoxantrone treatment at 450 and 900nM promoted apoptotic cell death in PC3 cells showed by TMRE and Annexin V assays (***Figure 44A***; open blue bars). Apoptosis was further promoted when PC3 cells were treated with 450nM mitoxantrone in combination with AdΔΔ (filled blue bar), although not when the mitoxantrone dose was increased to 900nM, suggesting that cells might have reached the maximum level of apoptosis induction at this time-point (***Figure 44A***). Similar results were seen in 22Rv1 and PC3M cells. In 22Rv1 cells, mitoxantrone treatment at 10 and 25nM increased LC3II/I ratios (***Figure 44B***; open red bars). This induction was attenuated by co-infection with AdΔΔ (***Figure 44B;*** filled red bars). In 22Rv1 cells mitoxantrone also promoted apoptosis, determined by TMRE and increased PARP cleavage (open blue bars). Apoptosis induction was further promoted when AdΔΔ was combined with mitoxantrone (filled blue bars) at 10nM for TMRE assay and 10 and 25nM for PARP cleavage. Similar to PC3 cells, the higher tested dose of mitoxantrone (25nM) reached a maximum in the TMRE assay and could not be further increased by AdΔΔ (***Figure 44B***). These results were also reproducible in PC3M cells, in which mitoxantrone induced an increase in LC3II/I ratios (***Figure 44C***; open red bar), that was attenuated by AdΔΔ when combined with all tested doses of mitoxantrone (450, 900nM; filled red bars). Also in agreement with other cell lines, 450 and 900nM mitoxantrone treatment induced apoptosis in PC3M cells (open blue bars), this induction was further increased when both doses of mitoxantrone were combined with AdΔΔ (***Figure 44C***).

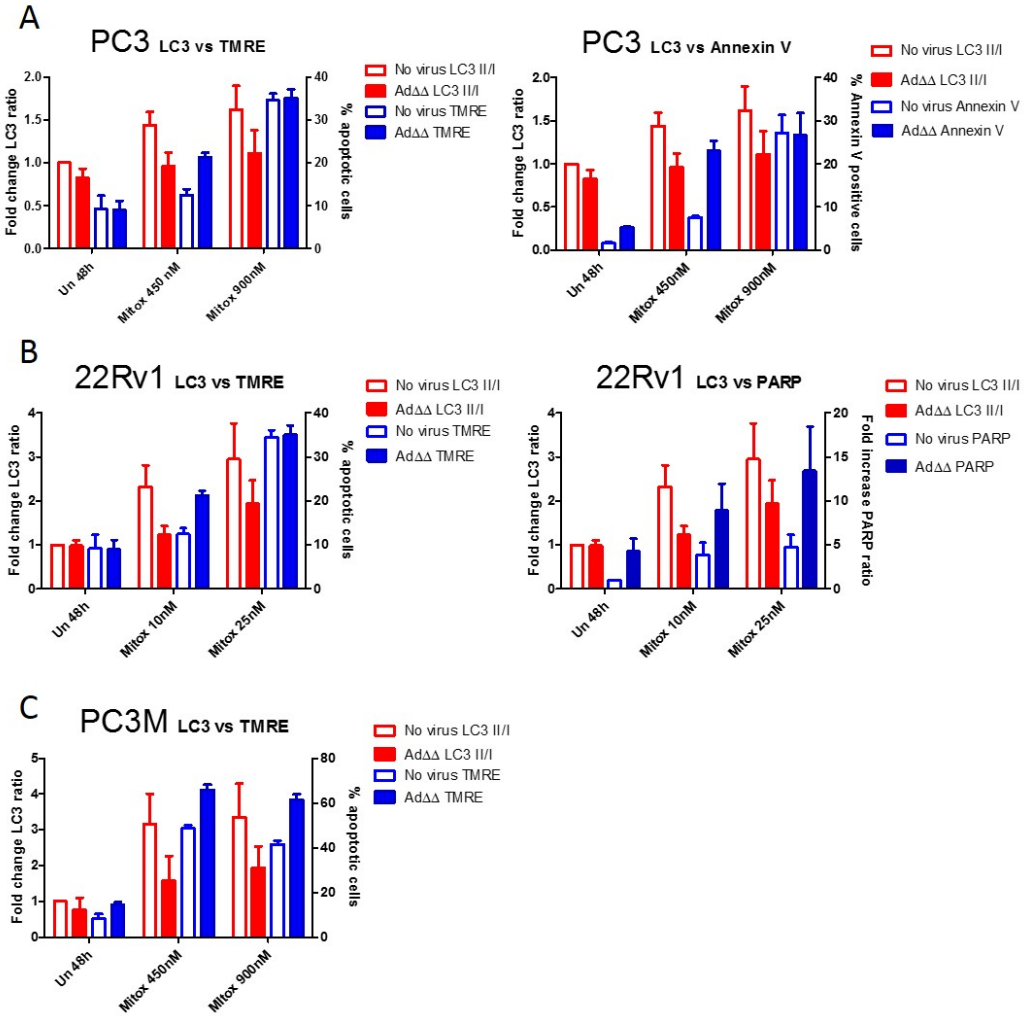

Figure 44. AdΔΔ-mediated attenuation of autophagy is related to increases in apoptosis in PC3, PC3M and 22Rv1 cells. A-C. Autophagy initiation was measured by LC3II/I ratios in 22Rv1, PC3 and PC3M cells 48h after treatment. **A.** Apoptosis was measured in PC3 cells by loss of TMRE staining and gain on Annexin V signal 120h after treatment. **B.** Apoptosis was measured in 22Rv1 cells by loss of TMRE staining and increase of PARP cleavage 48h after treatment**. C.** Apoptosis was measured in PC3M cells by loss of TMRE staining 72h after treatment. Data generated from ***Figure 36, Figure 38, Figure 40, Figure 41, Figure 42, and Figure 43.***

3.1.8 Summary of the studies on AdΔΔ-dependent effects on mitoxantrone-mediated autophagy and apoptosis.

The findings presented in this section (3.1) demonstrate that the cellular responses to mitoxantrone and virus differ in the human prostate cancer cell lines PC3, 22Rv1, and PC3M. Infection with AdΔΔ enhanced mitoxantrone-induced cell killing in all tested prostate cancer cell lines but to different degrees. Low doses (<EC_{40}) of AdΔΔ that enhanced mitoxantrone-induced cell killing resulted in attenuation of mitoxantrone-induced initiation of autophagy

and promoted mitoxantrone-induced apoptosis. AdΔΔ-mediated attenuation of mitoxantrone-induced autophagy could be detected at early stages in the autophagic pathway by attenuation of LC3BII conversion and at later stages by Lysotracker staining. However, prevention of autophagy completion by measuring p62 expression could not be confirmed. Autophagy attenuation and apoptosis-promotion was also demonstrated with the Ad12S mutant in combination with mitoxantrone in PC3 and 22Rv1 cells, suggesting that the expression of the small E1A12S adenoviral protein was essential for the sensitisation.

We hypothesised that attenuation of autophagy and promotion of apoptosis could be the mechanisms by which AdΔΔ enhanced mitoxantrone-induced cell killing. The work in the following sections aimed to further investigate this hypothesis.

3.2 INHIBITION OF AUTOPHAGY ENHANCES MITOXANTRONE-INDUCED CELL KILLING BY PROMOTING APOPTOSIS IN PC3 AND 22RV1 CELLS, BOTH IN THE PRESENCE AND ABSENCE OF ADENOVIRUS.

3.2.1 The autophagy-inhibitor chloroquine increases AdΔΔ and Ad12S-mediated sensitization to mitoxantrone in PC3 and 22Rv1 cells while the autophagy-inducer rapamycin prevents Ad-mediated sensitization in PC3 cells.

In order to further investigate the effect of autophagy-modulation in AdΔΔ-mediated enhancement of mitoxantrone-induced cell death, the autophagy-inducer rapamycin and the late-stage autophagy-inhibitor chloroquine were added to PC3 and 22Rv1 cells treated with Ad5wt, AdΔΔ, Ad12S and mitoxantrone, followed by assessment of cell viability. Rapamycin is an established mTOR-inhibitor and promotes the formation of the ULK complex, which is necessary for autophagy initiation and therefore triggers the autophagy pathway (Lamb, Yoshimori et al. 2013). Chloroquine is a late stage autophagy-inhibitor that blocks the fusion between the autophagosome and lysosome by increasing the lysosomal pH (Chikte, Panchal et al. 2014).

In PC3 and 22Rv1 cells, rapamycin at 25, 50 and 100nM and chloroquine at 5 and 10µM were verified to induce and block autophagy, respectively, by immunoblotting of LC3B and p62 over time at 24, 48 and 72h. Chloroquine increased LC3BII conversion and promoted p62 accumulation while rapamycin-treatment increased LC3BII conversion and promoted p62 degradation in PC3 and 22Rv1 cells (***Figure 45A and B***). In clinical trials, both rapamycin and chloroquine are given daily at doses of 2 – 6mg and 600mg, respectively, in combination with other anticancer therapies (Rangwala, Chang et al. 2014, Buijsen, van den Bogaard et al. 2015).

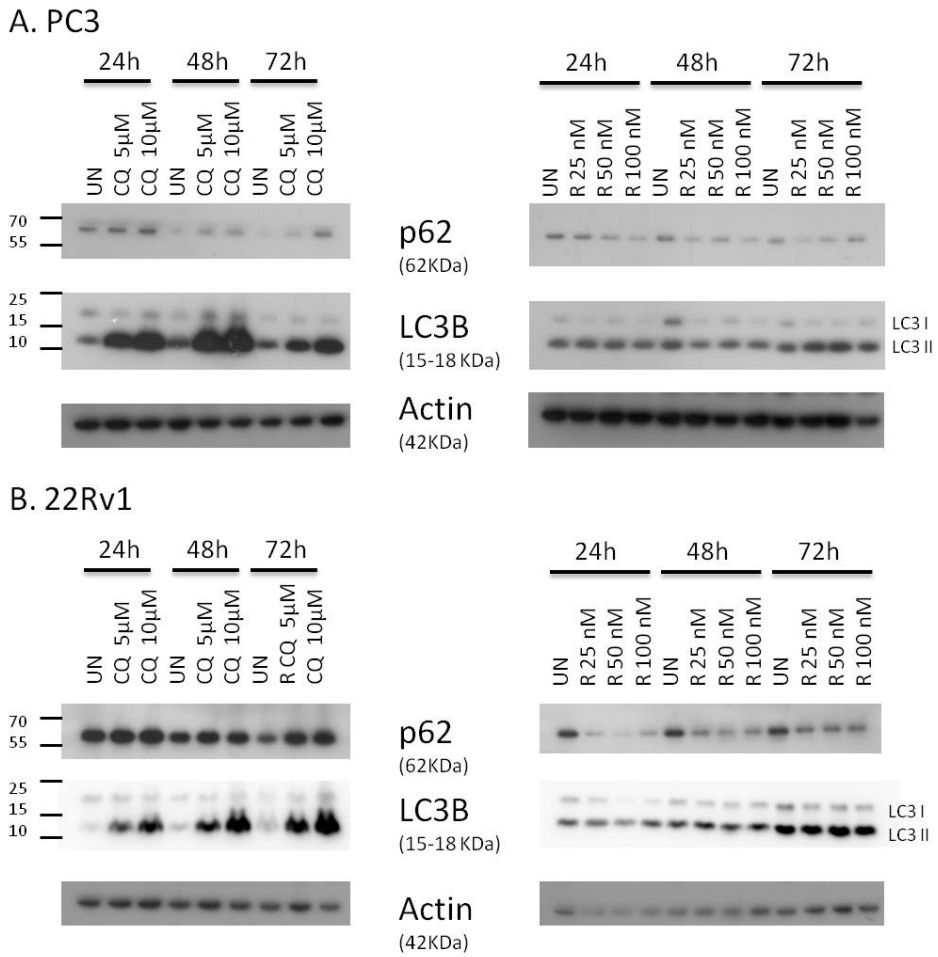

Figure 45. Rapamycin promotes and chloroquine blocks autophagy in PC3 and 22Rv1 cells. A. Expression of p62 and LC3BII/I in representative immunoblots (n=2) of PC3 cells treated with chloroquine (CQ) or rapamycin (R) at indicated doses and collected at indicated time points (24 – 72h). **B.** Expression of p62 and LC3BII/I in representative immunoblots (n=2) of 22Rv1 cells treated with chloroquine (CQ) or rapamycin (R) at indicated doses and collected at indicated time points (24 – 72h).

Selected doses of chloroquine at 10µM or rapamycin at 50nM that had been verified to block and induce autophagy (***Figure 45A***), respectively, were added to PC3 cells treated with increasing doses of mitoxantrone, alone or in combination with previously selected doses of Ad5wt or AdΔΔ at 500ppc, or Ad12S at 5000ppc. These doses of AdΔΔ and Ad12S had previously been shown to sensitise cells to mitoxantrone (section 3.1.2). The addition of chloroquine to mitoxantrone-treated cells sensitised cells to mitoxantrone-induced cell death and resulted in an approximate 70% decrease in EC_{50}-value (**Figure *46A,* Figure *47,* Table *24***). In contrast, treatment with rapamycin resulted in a clear de-sensitization and increased the EC_{50}-value to mitoxantrone 2-fold, this increase was significant ($p<0.05$) (**Figure *46A,* Figure *47,* Table *24***). The combined treatment of chloroquine with Ad5wt, AdΔΔ or Ad12S, maintained and even increased sensitization to mitoxantrone, decreasing the EC_{50}-values by 82%, 85% and 89% for Ad5wt, AdΔΔ or Ad12S, respectively, when compared to

mitoxantrone. Although there was a trend towards increased sensitization to mitoxantrone as a result of the combined treatment of chloroquine and virus, compared to viruses alone, this increase was not significant. Furthermore, the combined treatment of rapamycin with Ad5wt, AdΔΔ or Ad12S, clearly prevented the sensitization and resulted in higher EC_{50}-values. The increases in EC_{50}-values as a result of addition of rapamycin were significant ($p<0.001$ for Ad5wt and AdΔΔ; $p<0.01$ for Ad12S) when compared to cells treated with mitoxantrone and the corresponding virus and when compared to mitoxantrone-only treated cells ($p<0.001$ for Ad5wt and AdΔΔ) (**Figure *46A,* Figure *47,* Table *24***).

Changes in sensitization to mitoxantrone as a result of autophagy modulation were also assayed in 22Rv1 cells. Selected doses of chloroquine at 10µM or rapamycin at 25nM that had been verified to block and induce autophagy (***Figure 45B***), respectively, were added to 22Rv1 cells treated with increasing doses of mitoxantrone, alone or in combination with Ad5wt or AdΔΔ at 20ppc or Ad12S at 50ppc. These doses of AdΔΔ and Ad12S had previously been shown to sensitise cells to mitoxantrone (section 3.1.2). In agreement with the findings in PC3 cells, the addition of chloroquine to mitoxantrone-treated cells sensitised 22Rv1 cells to mitoxantrone-induced cell death and resulted in a decreased EC_{50}-value by 40% when compared to mitoxantrone alone (**Figure *46B,* Figure *48,* Table *24***). This decrease was significant ($p<0.05$). Surprisingly, rapamycin treatment did not cause any changes in mitoxantrone EC_{50}-values in this cell line. The combined treatment of chloroquine with AdΔΔ or Ad12S, maintained and even slightly increased sensitization to mitoxantrone by decreasing mitoxantrone EC_{50}-values 25% and 75% for AdΔΔ or Ad12S, respectively. The combined treatment of chloroquine and Ad12S resulted in a significant ($p<0.001$) decrease in EC_{50}-value when compared to mitoxantrone. Co-treatment of chloroquine and the Ad5wt virus did not affect mitoxantrone EC_{50}-values. The combined treatment of rapamycin with Ad5wt, AdΔΔ or Ad12S, did not result in significant changes in 22Rv1 cells. The combined treatment of rapamycin and AdΔΔ slightly increased mitoxantrone EC_{50}-values when compared to cells treated with AdΔΔ and mitoxantrone only, although this increase was not significant (**Figure *46B,* Figure *48,* Table *24***).

These results demonstrated that inhibition of late-stage autophagy with chloroquine sensitised PC3 and 22Rv1 cells to mitoxantrone and maintained and even further increased AdΔΔ- and Ad12S-mediated sensitization to the drug. In contrast, autophagy-induction with rapamycin resulted in potent de-sensitization to mitoxantrone in PC3 cells only, and even reverted AdΔΔ- and Ad12S-mediated sensitization to the drug. The previous data (section

3.1.5) showed that mitoxantrone-treatment promoted autophagy-initiation in PC3, 22Rv1 and PC3M cells. In combination with the findings from the studies with chloroquine and rapamycin (in this section) it may be suggested that inhibition of the later stages in the autophagy process is a potential approach to enhance mitoxantrone-induced cell death.

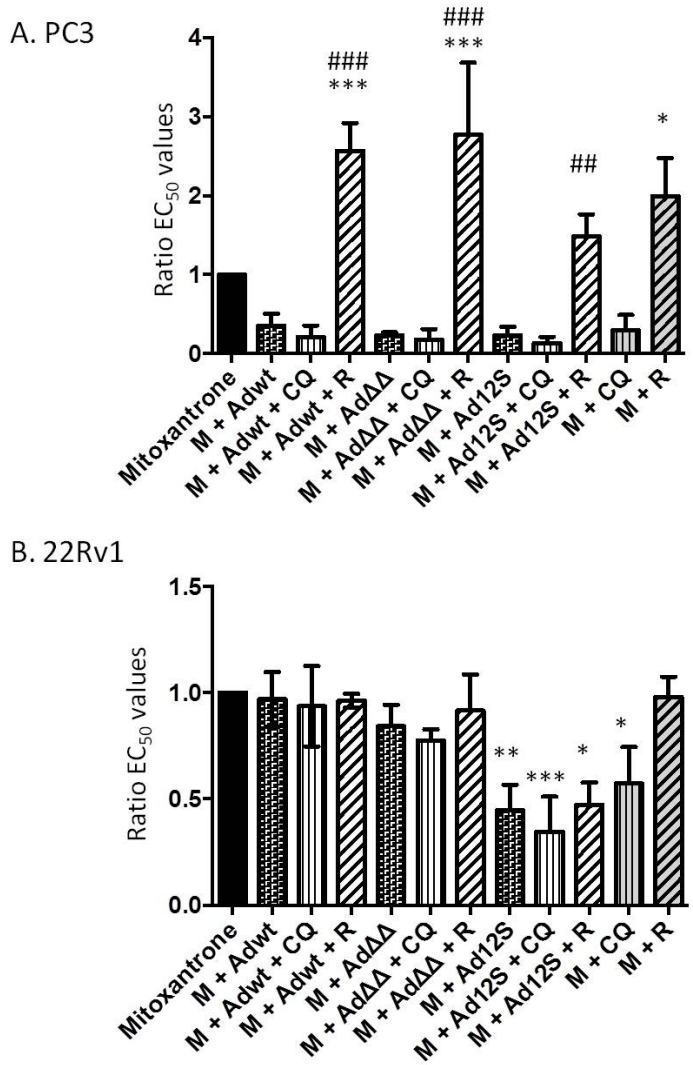

Figure 46. Sensitization to mitoxantrone with AdΔΔ and Ad12S in PC3 and 22Rv1 cells is increased by the autophagy-inhibitor chloroquine while the autophagy-inducer rapamycin prevents Ad-mediated sensitization in PC3 cells. Fixed doses of Adwt, AdΔΔ and Ad12S that killed 10-30% of cells alone and/or chloroquine (CQ) or rapamycin (R) were added to mitoxantrone-treated cells. **A.** EC_{50}-values were generated with dose-response curves of mitoxantrone in combination with fixed doses of chloroquine at 10μM, rapamycin at 50nM, Adwt and AdΔΔ at 500ppc or Ad12S at 5000ppc, or the combined treatment of chloroquine or rapamycin and one of the viruses. Cell viability was measured by MTS assay 5 days after treatment. **B.** EC_{50}-values generated with dose-response curves to mitoxantrone in combination with fixed doses of chloroquine at 10μM, rapamycin at 25nM, Ad5wt and AdΔΔ at 20ppc or Ad12S at 50ppc, or the combined treatment of chloroquine or rapamycin and one of the viruses. **A. and B.** EC_{50} ratios were generated by dividing (EC_{50}-values Ad -and/or R, CQ-+Mitoxantrone)/(EC_{50}-value mitoxantrone only). Averages ± SD, n=3. One-way Anova with Bonferroni post-test. *p<0.05, **p<0.01, ***p<0.001 (* indicates comparison to mitoxantrone control and # indicates comparison to M + virus). This assay was performed with AdΔΔ batch 050314.

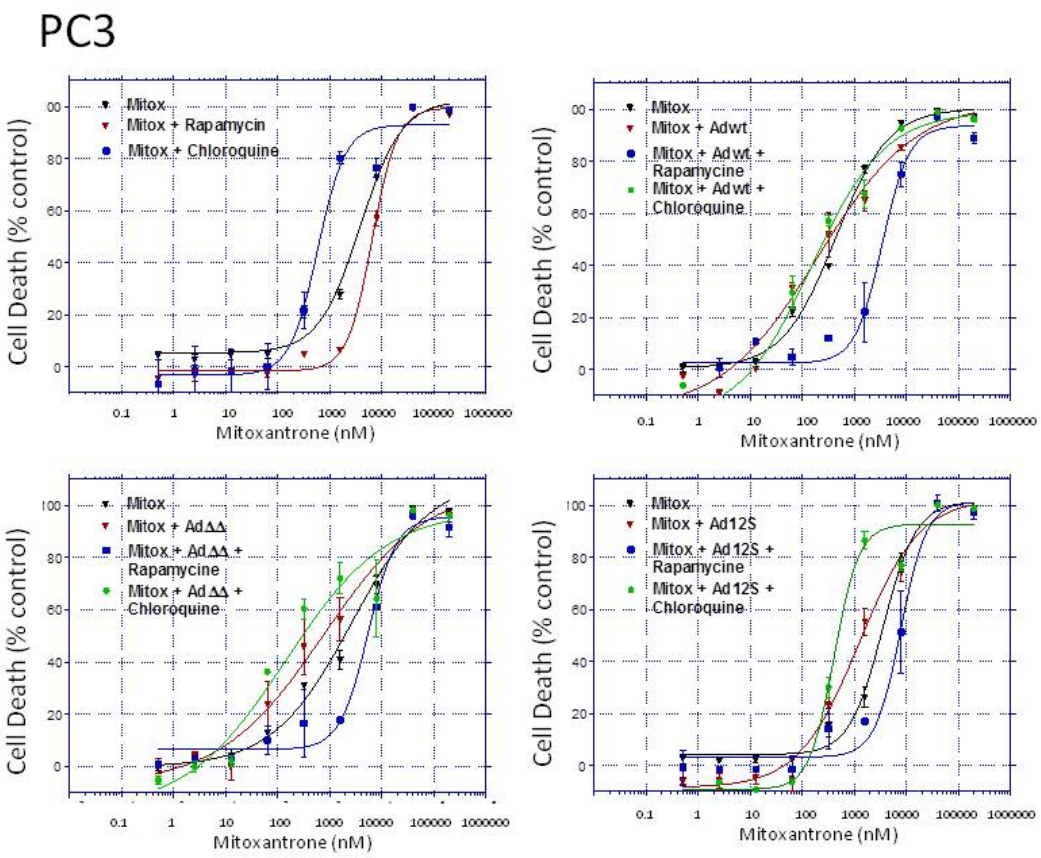

Figure 47. Representative dose-response curves from the data in Figure 46 for PC3 cells. Dose-response curves of mitoxantrone (Mitox) in combination with fixed doses of chloroquine at 10µM, rapamycin at 50nM, Ad5wt and AdΔΔ at 500ppc or Ad12S at 5000ppc, or the combined treatment of chloroquine or rapamycin and one of the viruses. Cell viability was measured by MTS assay 5 days after treatment.

22Rv1

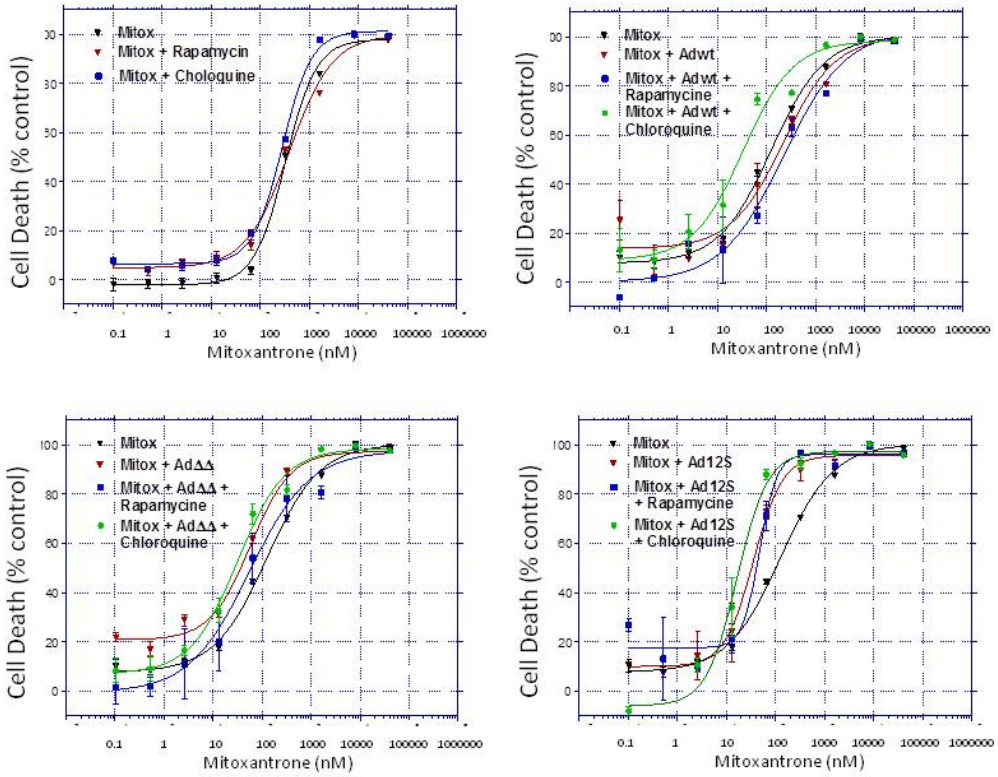

Figure 48. Representative dose-response curves from the data in Figure 19 for 22Rv1 cells. Dose-response curves of mitoxantrone (Mitox) in combination with fixed doses of chloroquine at 10µM, rapamycin at 25nM, Adwt and AdΔΔ at 20ppc or Ad12S at 50ppc, or the combined treatment of chloroquine or rapamycin and one of the viruses. Cell viability was measured by MTS assay 3 days after treatment.

Table 24. Mitoxantrone EC_{50}-values (±SD) generated in PC3 and 22Rv1 cells.

EC_{50}-values (nM)	**PC3**	**22Rv1**
Mitoxantrone	2375.7 ± 1333.6	306.9 ± 70.5
Mitoxantrone + Rapamycin	4648.0 ± 2289.3	305.2 ± 99.2
Mitoxantrone + Chloroquine	564.9 ± 21.6	180.5 ± 75.9
Mitoxantrone + Ad5wt	956.0 ± 899.1	300.5 ± 99.5
Mitoxantrone + Ad5wt + Rapamycin	5815 ± 2614.0	297.6 ± 79.6
Mitoxantrone + Ad5wt + Chloroquine	426.6 ± 206.6	281.8 ± 43.4
Mitoxantrone + AdΔΔ	560.6 ± 295.2	246.9 ± 65.3
Mitoxantrone + AdΔΔ + Rapamycin	6026.3 ± 2704.3	258.9 ± 15.5
Mitoxantrone + AdΔΔ + Chloroquine	346.5 ± 139.5	224.1 ± 38.4

Mitoxantrone + Ad12S	627.7 ± 490.1	136.9 ± 74.8
Mitoxantrone + Ad12S + Rapamycin	3963.7 ± 2345.3	143.56 ± 74.2
Mitoxantrone + Ad12S + Chloroquine	280.0 ± 93.7	109.4 ± 80.3

AdΔΔ batch 050314. All data are averages ± SD, n=3.

3.2.2 Chloroquine further promotes apoptosis while rapamycin decreases apoptotic death in 22Rv1 and PC3 cells treated with AdΔΔ and mitoxantrone.

The results presented in sections 3.1.5 and 3.1.6 demonstrated that AdΔΔ enhanced cell killing by attenuating mitoxantrone-induced autophagy and promoting apoptosis in 22Rv1 and PC3 cells. To further investigate the role of autophagy-inhibition in the enhancement of cell killing, apoptosis was determined in cells treated with AdΔΔ and mitoxantrone in the presence of the autophagy-inhibitor chloroquine or the -inducer rapamycin. Mitochondrial depolarization was assessed in PC3 cells 120h after treatment, since the previous studies proved maximum apoptosis-induction at this time point (**Figure *41***). Treatment with the apoptosis-inducer staurosporine at 1µM for 15h was used as a positive control. The combined treatment of AdΔΔ at 750ppc and 450nM mitoxantrone resulted in increased number of cells undergoing mitochondrial depolarization compared to single agent treatments (24.0 ± 9.5% for combined treatment and 18.3 ± 10.2% for mitoxantrone alone) (**Figure *49***). As previously shown (section 3.1.6), the higher dose of 900nM mitoxantrone greatly induced mitochondrial depolarization in 39.7 ± 17.7% of cells. However, this induction could not be further enhanced in combination with AdΔΔ. The addition of rapamycin to PC3 cells treated with 450 and 900nM mitoxantrone alone or in combination with AdΔΔ, inhibited mitoxantrone-induced mitochondrial depolarization. The addition of rapamycin to cells treated with 450nM reduced mitochondrial depolarization from 18.3 ± 10.2% to 8.4 ± 3.6% and in cells infected with AdΔΔ and treated with mitoxantrone and rapamycin depolarization was slightly higher 17.3 ± 8.9% of cells but reduced compared to virus and drug alone. Rapamycin-mediated decreases in mitochondrial depolarization in cells treated with the combined treatment or with 450nM mitoxantrone alone were noted but were not significant. Similarly, the addition of rapamycin to cells treated with 900nM reduced depolarization to 19.8 ± 7.9%. The addition of rapamycin to cells treated with the combination of AdΔΔ and 900nM mitoxantrone reduced mitochondrial depolarization to 16.9 ± 7.3%. This decrease was significant ($p<0.01$) in cells treated with rapamycin and 900nM mitoxantrone (**Figure *49***). On the contrary, the addition of chloroquine enhanced

mitoxantrone-induced mitochondrial depolarization, alone and in combination with AdΔΔ, increasing the percentage of cells undergoing mitochondrial depolarization to 38.5 ± 6.7% and 46.2 ± 5.5% for 450nM mitoxantrone alone and in combination with AdΔΔ, respectively. This increase was significant ($p<0.01$) in both conditions. Chloroquine did not further promote mitoxantrone-induced mitochondrial depolarization in combination with 900nM mitoxantrone (**Figure *49***).

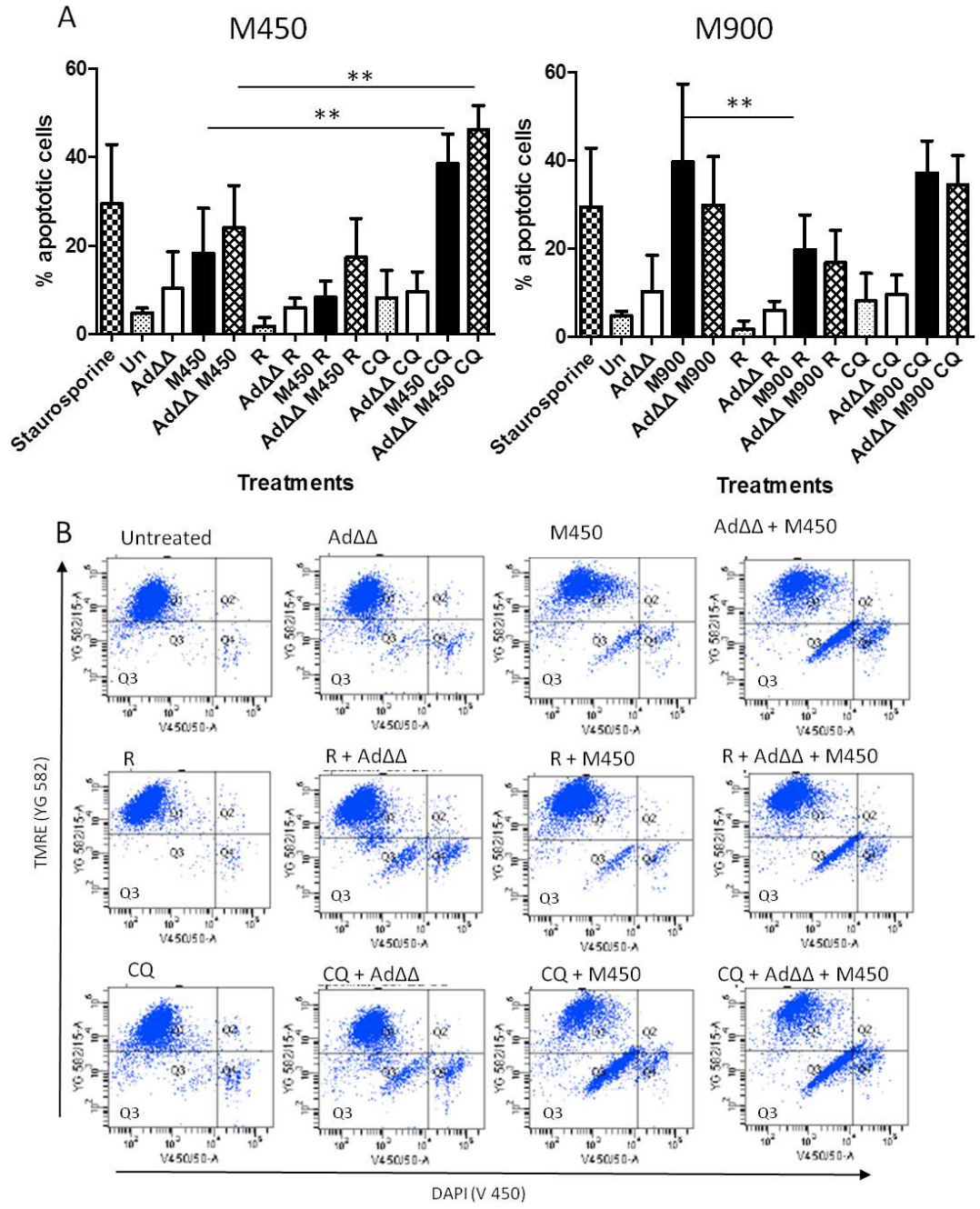

Figure 49. Chloroquine further promotes apoptosis in cells treated with the combined treatment of mitoxantrone and AdΔΔ while rapamycin decreases apoptosis in PC3 cells. A. PC3 cells were treated with AdΔΔ at 750ppc and/or indicated doses of mitoxantrone at 450 or 900 nM and/or rapamycin at

50nM, chloroquine at 10µM and collected at 120h. Mitochondrial depolarization was measured as an indication of apoptosis by loss of TMRE staining (Q3). TMRE and DAPI staining were detected with the lasers YG 582/15 and V 450/50, respectively. Averages ± SD, n=4. One-way Anova with Bonferroni post-test. *p<0.05 **p<0.01, ***p<0.001, ****p<0.0001. **B**. Representative FACS images. This assay was performed with AdΔΔ batch 050314.

Depolarization of the mitochondrial membrane was also determined in 22Rv1 cells treated with AdΔΔ and mitoxantrone in the presence of the autophagy inhibitor chloroquine or the inducer rapamycin. Depolarization of the mitochondrial membrane was measured in 22Rv1 cells 72h after treatment. Treatment with 10 and 25nM mitoxantrone induced mitochondrial depolarization in a dose dependent manner, reaching 27.2 ± 4.8% and 52.5 ± 5.5% of cells, respectively (**Figure *50***). As previously shown (**Figure *42***), the combined treatment of 10nM mitoxantrone and AdΔΔ at 20ppc enhanced mitoxantrone-induced mitochondrial depolarization resulting in 41.5 ± 12.5% of cells. The addition of rapamycin did not significantly affect apoptosis in 22Rv1 cells. These data are in agreement with the lack of effect on the EC_{50}-values of mitoxantrone in response to rapamycin-treatment, shown in the MTS data (section 3.2.1; **Table *24***). In contrast, chloroquine treatment further promoted mitochondrial depolarization in 22Rv1 cells treated with 10 and 25nM mitoxantrone alone or in combination with AdΔΔ. Chloroquine treatment increased the percentages of cells undergoing mitochondrial depolarization from 27.2 ± 4.8% and 41.5 ± 12.5% to 79.8 ± 8.6% and 66.3 ± 11.7% for 10nM mitoxantrone alone and in combination with AdΔΔ, respectively. These increases were significant ($p<0.0001$ and $p<0.05$) for 10nM mitoxantrone alone and in combination with AdΔΔ. Chloroquine treatment resulted in a non-significant increase in depolarization in cells treated with 25nM mitoxantrone, alone or in combination with AdΔΔ. Similar to the findings in PC3 cells, AdΔΔ did not further promote mitochondrial depolarization in cells treated with both mitoxantrone and chloroquine (**Figure *50***).

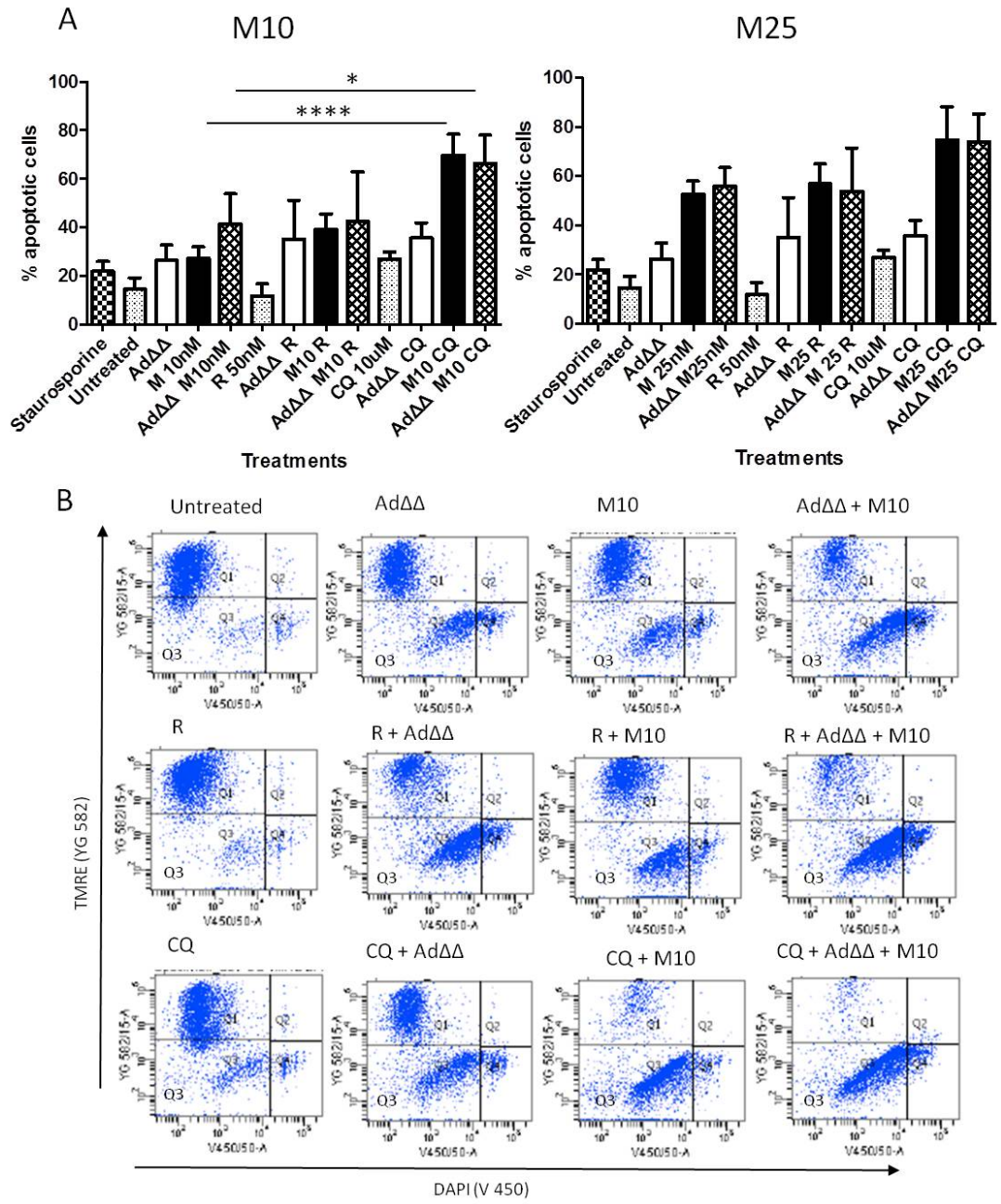

Figure 50. Chloroquine further promotes apoptosis in 22Rv1 cells treated with the combined treatment of mitoxantrone and AdΔΔ. A. 22Rv1 cells were treated with AdΔΔ at 20ppc and/or indicated doses of mitoxantrone at 10 or 25 nM and/or rapamycin at 50nM, chloroquine at 10uM and collected at 72h. Mitochondrial depolarization was measured as an indication of apoptosis by loss of TMRE staining (Q3). TMRE and DAPI staining were detected with the lasers YG 582/15 and V 450/50, respectively. Averages ± SD, n=3. One-way Anova with Bonferroni post-test, *p<0.05, ****p<0.0001. **B.** Representative FACS images. This assay was performed with AdΔΔ batch 050314.

These data demonstrated that chloroquine-treatment promoted mitoxantrone-induced apoptosis in the presence and absence of AdΔΔ, in both PC3 and 22Rv1 cells. However, AdΔΔ did not further increase apoptosis in cells treated simultaneously with mitoxantrone and

chloroquine. In contrast, rapamycin treatment resulted in decreased apoptosis in PC3 cells both in the presence and absence of AdΔΔ, but had no significant effect in 22Rv1 cells. These findings were in agreement with the cell viability data that showed that chloroquine sensitised PC3 and 22Rv1 cells to mitoxantrone and maintained or further increased AdΔΔ- and Ad12S-mediated sensitization to the drug (section 3.2.1; **Table *24***). Taken together, these results confirmed that pharmacological inhibition of late-stage autophagy enhanced AdΔΔ-mediated sensitization to mitoxantrone by attenuating autophagy and by promoting apoptotic cell death.

3.2.3 Chloroquine treatment causes blockage of autophagy that is attenuated by AdΔΔ in 22Rv1 but not in PC3 cells.

The results presented in section 3.2.2 demonstrated that the autophagy inhibitor chloroquine enhanced mitoxantrone-induced depolarization of the mitochondrial membrane, alone and in combination with AdΔΔ in PC3 and 22Rv1 cells. In contrast, rapamycin only decreased depolarization of the mitochondrial membrane in PC3 cells. To determine whether rapamycin and chloroquine had the expected effects on the autophagy markers LC3B and p62 also under these conditions I investigated the expression patterns in both cell lines (***Figure 51***, ***Figure 52*** and ***Figure 53***).

PC3 cells were treated with Ad5wt or AdΔΔ at 500ppc, or Ad12S at 5000ppc in combination with 450nM of mitoxantrone, in the presence of rapamycin at 50nM or chloroquine at 10μM. Rapamycin treatment induced initiation of autophagy shown by a 2-fold increase in LC3BII/I ratio but did not affect p62 expression in this study (***Figure 51***). The combined treatment of rapamycin with mitoxantrone resulted in a 3.5-fold increase in LC3BII/I ratio and accumulation of p62. In cells infected with Ad5wt or AdΔΔ and treated with mitoxantrone and rapamycin, LC3BII/I ratios were maintained and even slightly increased compared to cells treated with mitoxantrone and rapamycin only. These results suggested that AdΔΔ could not prevent rapamycin induction of autophagy, neither in cells treated with rapamycin alone or in combination with mitoxantrone (***Figure 51***). Infection with Ad12S, in combination with mitoxantrone and rapamycin reduced the LC3BII/II ratio and p62 levels compared to non-infected cells. These results suggested that the Ad12S mutant but not AdΔΔ, attenuated rapamycin-induced autophagy both alone and in combination with mitoxantrone (***Figure 51***). Statistical analysis could not be performed due to the limited number of repeats (n=2).

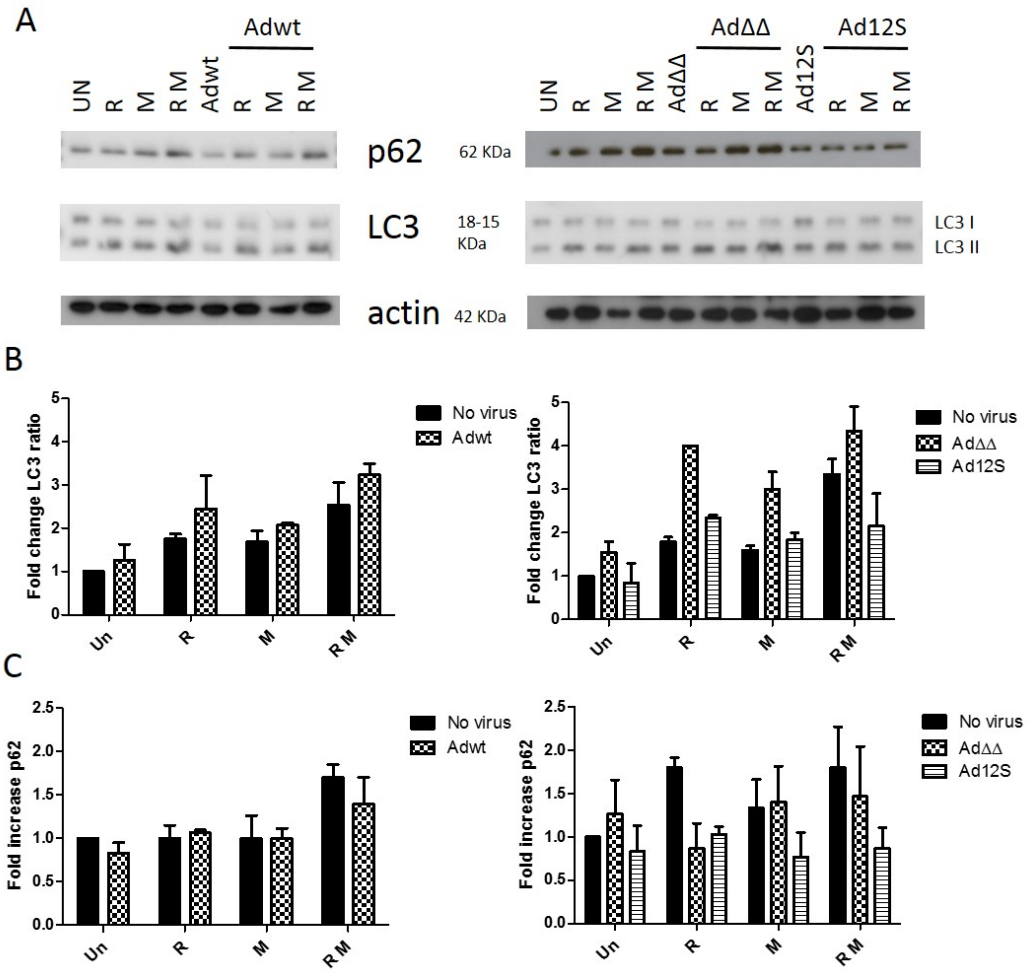

Figure 51. The combined treatment of mitoxantrone and rapamycin promotes LC3I to LC3II conversion, which is not counteracted by adenovirus. A. PC3 cells were infected with Adwt or AdΔΔ at 500ppc or Ad12S at 5000ppc and/or treated with mitoxantrone at 450 nM and/or rapamycin at 50nM and collected at 48h. Representative immunoblots, n=2. **B.** Densitometry quantification of LC3BII/I expression. LC3BII/I ratios are expressed as LC3II (lower band) divided by LC3I (higher band). **C.** Densitometry quantification of p62 expression. All densitometry values were normalised to the loading control before calculating ratios. **B and C.** Averages ± SD. Statistical analysis could not be performed due to the limited number of repeats (n=2). This assay was performed with AdΔΔ batch 050314.

Chloroquine treatment resulted in autophagy blockage in PC3 cells, demonstrated by a 4-fold increase in LC3BII/I ratio and accumulation of p62 (***Figure 52***). The combined treatment of chloroquine and mitoxantrone resulted in a small non-sifnificant decrease in LC3BII/I ratios, which may suggest that mitoxantrone released chloroquine-induced blockage. Infection with AdΔΔ or Ad12S in PC3 cells treated with chloroquine and mitoxantrone resulted in 3-fold increase in LC3BII/I ratios compared to untreated control, but reduced LC3BII/I ratios when compared to the combined treatment of chloroquine and mitoxantrone (***Figure 52***). Ad5wt did not have any additional effects in combination with mitoxantrone and chloroquine (***Figure 52***). The increases in LC3BII levels as a result of chloroquine-treatment

did not allow accurate quantification of the results. Furthermore, statistical analysis could not be performed due to the limited number of repeats (n=2).

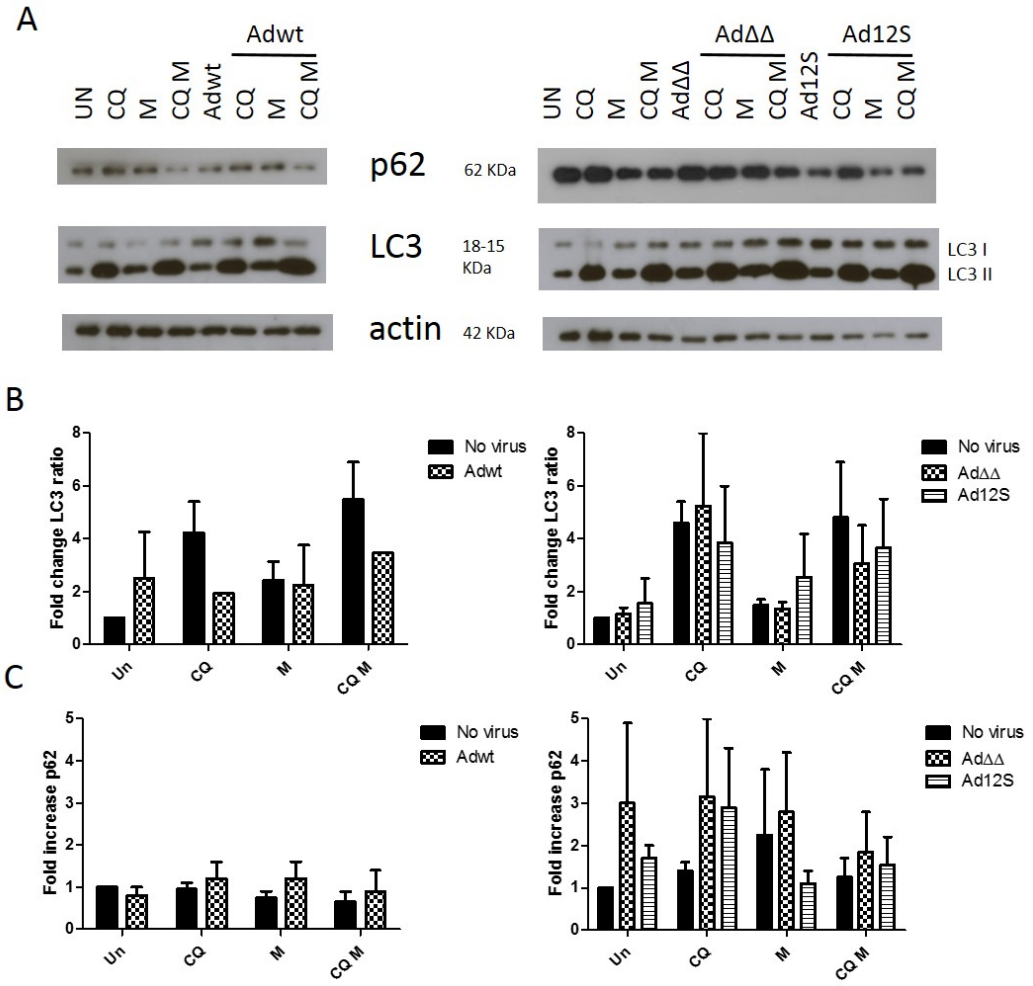

Figure 52. Chloroquine treatment results in autophagy blockage in PC3 cells. **A.** PC3 cells were infected with Ad5wt or AdΔΔ at 500ppc or Ad12S at 5000ppc and/or treated with mitoxantrone at 450nM and/or Chloroquine at 10uM and collected at 48h. Representative immunoblots, n=2. **B.** Densitometry quantification of LC3BII/I expression. LC3BII/I ratios are expressed as LC3II (lower band) divided by LC3I (higher band). **C.** Densitometry quantification of p62 expression. All densitometry values were normalised to the loading control before calculating ratios. **B and C.** Averages ± SD. Statistical analysis could not be performed due to the limited number of repeats (n=2). This assay was performed with AdΔΔ batch 050314.

In 22Rv1 cells, rapamycin treatment at 50nM clearly induced autophagy, demonstrated by a 2-fold increase in LC3BII/I ratio and degradation of p62 (***Figure 53***). This induction was maintained when rapamycin was combined with mitoxantrone at 10nM. Infection with Ad5wt and AdΔΔ at 20ppc, counteracted rapamycin-induced LC3BII/I conversion and restored basal LC3II/I levels. However, the combination of either Ad5wt or AdΔΔ with rapamycin did not attenuate rapamycin-induced p62 degradation. Infection with Ad5wt and AdΔΔ did not reverse the LC3BII conversion in cells treated with the combination of

rapamycin and mitoxantrone (***Figure 53***). Single agent treatment with chloroquine at 10µM blocked late-stage autophagy demonstrated by accumulation of LC3BII shown by 2-fold increases in LC3BII/I ratios but no degradation of p62. The combined treatment of chloroquine and mitoxantrone resulted in a small non-significant decrease LC3BII/I ratio and degradation of p62 when compared to chloroquine alone. These results suggested that mitoxantrone attenuated chloroquine-induced blockage. Infection with Ad5wt and AdΔΔ, in cells treated with chloroquine only, also attenuated the effect of chloroquine. However, infection with Ad5wt or AdΔΔ, in combination with chloroquine and mitoxantrone did not result in effects on the chloroquine-induced blockage (***Figure 53***). Statistical analysis could not be performed due to the limited number of repeats (n=2).

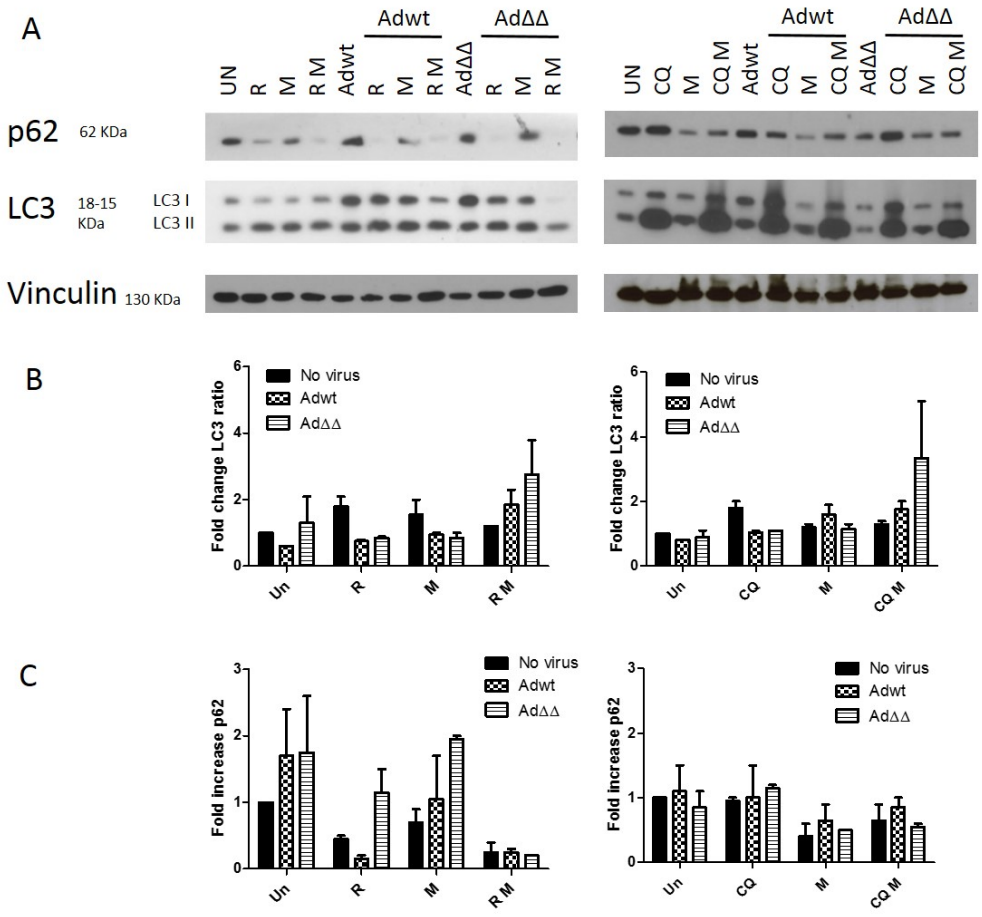

Figure 53. Adenovirus attenuates mitoxantrone- or rapamycin-induced LC3II conversion. Adenovirus slightly attenuates chloroquine-induced autophagy blockage in the absence of mitoxantrone. A. 22Rv1 cells were infected with Ad5wt or AdΔΔ at 20ppc and/or treated with mitoxantrone at 10nM and/or rapamycin at 50nM, chloroquine at 10µM and collected at 48h. Representative immunoblots, n=2. **B.** Densitometry quantification of LC3BII/I expression. LC3 ratio is expressed as LC3II (lower band) divided by LC3I (higher band). **C.** Densitometry quantification of p62 expression. All densitometry values were normalised to the loading control before calculating ratios. **B and C.** Averages ± SD. Statistical analysis could not be performed due to the limited number of repeats (n=2). This assay was performed with AdΔΔ batch 050314.

The aim of these studies was to assess the effects of an autophagy inhibitor and an autophagy inducer in 22Rv1 and PC3 cells infected with Ad5wt, AdΔΔ or Ad12S in the presence of mitoxantrone. However, the increases in LC3BII levels as a result of chloroquine-treatment did not allow accurate quantification of the results. Furthermore, the experiments were too time-consuming to repeat more than 3 times which would be required to generate higher quality immunoblots. Data shown in this section (3.2.3) suggested that rapamycin induced autophagy-initiation in PC3 cells and induced complete autophagy in 22Rv1 cells, both alone and in combination with mitoxantrone. Rapamycin-induced increases in LC3BII/I ratios were slightly attenuated by infection with Ad5wt and AdΔΔ in 22Rv1 cells only, while rapamycin-induced p62 degradation was not affected. Treatment with chloroquine resulted in considerable increases in LC3BII/I ratios in PC3 and 22Rv1 cells, which were slightly attenuated by Ad5wt and AdΔΔ in 22Rv1 cells. The addition of mitoxantrone to chloroquine-treated cells slightly attenuated the chloroquine-induced increased LC3BII/I ratios in PC3 and 22Rv1 cells and decreased p62 accumulation in 22Rv1 cells. It can be concluded, as expected, that rapamycin and chloroquine caused autophagy induction and blockage, respectively. However, these data did not provide reliable information of the effect of chemical modulation of autophagy in cells treated with the combination of mitoxantrone and AdΔΔ.

3.2.4 Mitoxantrone with or without the addition of rapamycin or chloroquine enhances adenoviral infection in PC3 and 22Rv1 cells.

In order to determine whether the effect of mitoxantrone on the adenoviral life-cycle contributed to the enhanced cell killing, viral infection, replication and gene expression were assessed in PC3 and 22Rv1 cells.

Viral infection was assessed using the non-replicating GFP-expressing virus AdGFP, an Ad5 mutant with identical capsid to Ad5wt, AdΔΔ and Ad12S. Intensity of the GFP signal was measured by flow cytometry (***Figure 54***). The amount of GFP detected depends on the uptake of virus and expression of early genes but not on replication. The effect of mitoxantrone-treatment on AdGFP-infection was assessed in PC3 and 22Rv1 cells. Cells were pre-treated with mitoxantrone 24h prior to infection; doses of AdGFP (10 ppc and 1000ppc for 22Rv1 and PC3 cells, respectively) were selected to infect 20 to 30 % of cells. In PC3 cells, treatment with 900nM mitoxantrone increased infection 1.7-fold, this increase was significant

(p<0.001) (***Figure 54C***). Mitoxantrone-dependent enhancement of infection was maintained in the presence of rapamycin or chloroquine and was significant (p<0.001) when compared to infection with AdGFP alone (***Figure 54C***). PC3 cells were also infected with AdGFP at 100 and 1000ppc alone or in combination with 50nM rapamycin or 10μM chloroquine (***Figure 54A***). Infection with the two doses of AdGFP resulted in a dose-dependent increase in positive cells to 2.7 ± 0.3% and 22.3 ± 6.8%, for 100ppc and 1000ppc, respectively (***Figure 54A***). Co-treatment with rapamycin did not affect infection at any of the tested doses of virus. The combination of AdGFP at 1000ppc and chloroquine increased viral infection to 26.2 ± 3.5% of cells. This increase was significant (p<0.05) (***Figure 54A***). This chloroquine-dependent increase in viral infection could possibly be explained by chloroquine-mediated promotion of virus escape from the endosome.

Similar results were seen in 22Rv1 cells treated with 25nM mitoxantrone, which increased infection 1.5-fold and was significant (p<0.001) (***Figure 54D***). The mitoxantrone-dependent enhancement of infection was maintained in the presence of rapamycin or chloroquine in 22Rv1 cells and was significant (p<0.001) when compared to infection with AdGFP alone (***Figure 54D***). In 22Rv1 cells, infection with AdGFP at 10 and 100ppc caused dose-dependent GFP-expression of 26.2 ± 6.3% and 78.9 ± 5.7%, respectively (***Figure 54B***). Neither treatment with 50nM rapamycin or 10μM chloroquine significantly affected uptake in 22Rv1 cells (***Figure 54B***). Single agent treatment with rapamycin significantly (p<0.01) enhanced infection in 22Rv1 cells when pre-treated (***Figure 54D***), although no increases were observed with the combinations without pre-treatment (***Figure 54B***).

Previous work in my group demonstrated that treatment with the chemotherapeutic drugs mitoxantrone and docetaxel increased AdGFP uptake and increased expression of $\alpha_v\beta3$- and $\alpha_v\beta5$-integrins in PC3, DU145 and LNCaP prostate cancer cells (Radhakrishnan, Miranda et al. 2010). Expression of hCAR, $\alpha_v\beta3$- and $\alpha_v\beta5$-integrins was very low in PC3 cells and was only detected in 2.9 ± 0.2%, 4.8 ± 0.1% and 6.5 ± 0.2% of cells, respectively (Adam, Ekblad et al. 2012) and did not increase in the presence of mitoxantrone (Radhakrishnan, Miranda et al. 2010). In order to assess if this also was the case in 22Rv1 cells, the cells were treated with 25nM mitoxantrone and expression of $\alpha_v\beta3$- and $\alpha_v\beta5$-integrins and hCAR was measured by flow cytometry. Higher expression levels of $\alpha_v\beta5$ and hCAR were detected while $\alpha_v\beta3$ was present at very low levels (***Figure 54E***). Expression of $\alpha_v\beta3$- and $\alpha_v\beta5$-integrins, and hCAR was detected in 4.2 ± 3.2%, 15.6 ± 5.5% and 13.8 ± 0.7% of cells, respectively. Expression of $\alpha_v\beta5$-integrin and hCAR was increased to 27.7 ± 1.0% and 28.1 ± 1.7% of cells, respectively, in

mitoxantrone-treated cells, when compared to non-treated cells. Statistics could not be performed due to insufficient number of repeats. 22Rv1 cells showed low levels of $\alpha_v\beta3$-integrin, which was not increased after mitoxantrone treatment (***Figure 54E***).

In summary, these data demonstrate that 22Rv1 cells are more sensitive to adenoviral infection than PC3 cells, as expected because of the lower EC_{50}-values. The higher infectivity is probably due to increased expression of $\alpha_v\beta5$-integrin and hCAR expression, compared to PC3 cells. In addition, mitoxantrone pre-treatment enhanced adenoviral infection, likely as a result of mitoxantrone-mediated increases in the expression of the cellular $\alpha_v\beta5$-integrin and hCAR in 22Rv1 cells.

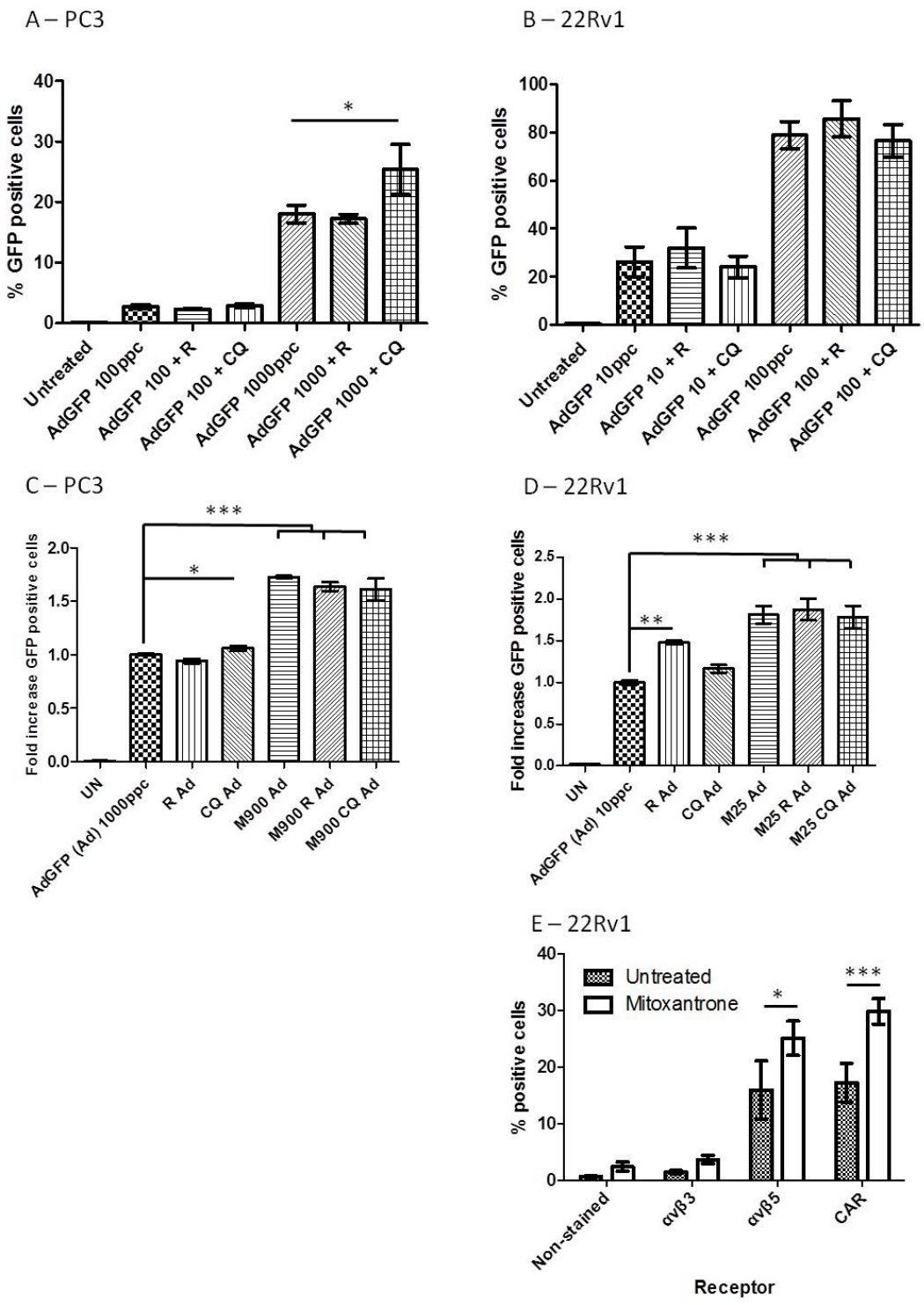

Figure 54. Mitoxantrone promotes adenoviral infection in 22Rv1 and PC3 cells. A. PC3 cells were treated with chloroquine at 10μM, or rapamycin at 50nM and simultaneously infected with AdGFP at indicated doses. Averages ± SD, n=3, unpaired T-test *p<0.05. **B.** 22Rv1 cells were treated with chloroquine at 10μM or rapamycin at 50nM and simultaneously infected with AdGFP at indicated doses. Averages ± SD, n=2. **C.** PC3 cells were treated with mitoxantrone at 900nM and/or chloroquine at 10μM, or rapamycin at 50nM for 24h; the treatment was then replaced with AdGFP infection at 1000ppc. Averages ± SD, n=3. One-way Annova with Bonferroni post-test, *p<0.05, **p<0.01, ***p<0.001. **D.** 22Rv1 cells were treated with mitoxantrone at 25nM and/or chloroquine at 10μM, or rapamycin at 50nM for 24h; the treatment was then replaced with AdGFP infection at 10ppc. Averages

± SD, n=3, One-way Annova with Bonferroni post-test, *p<0.05, **p<0.01, ***p<0.001. **A-D.** Samples were analysed 48 h after infection, GFP signal was measured as an indication of infection by flow cytometry. **E.** 22Rv1 cells were treated with mitoxantrone at 25nM. Expression of cell surface receptors was measured by flow cytometry, n=2.

3.2.5 Mitoxantrone with or without the addition of rapamycin or chloroquine decreases adenoviral replication in PC3 and 22Rv1 cells.

To continue investigating the effects of mitoxantrone-treatment in combination with chloroquine or rapamycin on the viral life cycle, viral genome amplification, viral replication, and expression of viral proteins were assessed in PC3 and 22Rv1 cells. PC3 cells were infected with Ad5wt or AdΔΔ at 200ppc in the presence of 50nM rapamycin or 10µM chloroquine and collected 48 and 72h after treatment and replication was measured by $TCID_{50}$ assays. The standard viral dose for $TCID_{50}$ assays (100ppc) was doubled in these experiments due to the previously observed low infectivity in PC3 cells (**Figure *54***). Ad5wt and AdΔΔ replicated to similar levels in PC3 cells. Ad5wt-replication was $4.9x10^6$ ± $4.6x10^6$ pfu/ml and $7.8x10^6$ ± $4.3x10^6$ pfu/ml at 48 and 72h post infection, respectively, while AdΔΔ-replication was $4.8x10^6$ ± $1.0x10^6$ pfu/ml and $6.01x10^6$ ± $2.7x10^6$ pfu/ml (***Figure 55A***). The combination or either Ad5wt or AdΔΔ with rapamycin resulted in a non-significant enhancement of viral replication, replication increased 1.7-fold and 2.1-fold for Ad5wt and 2.7-fold and 2.9-fold for AdΔΔ at 48 and 72h, respectively. In contrast, the combination of either Ad5wt or AdΔΔ with chloroquine attenuated viral replication by approximately 75% for Ad5wt at 48 and 72h; and by 40% and 70% for AdΔΔ at 48 and 72h, respectively (***Figure 55A***). It could be suggested that chloroquine treatment might interfere in correct viral processing. Replication was later assessed in the presence of 900nM mitoxantrone at 72h since treatment for this period of time had previously shown the highest viral replication. Mitoxantrone attenuated replication by 88% and 97% for Ad5wt and AdΔΔ, respectively, these decreases were significant ($p<0.05$) for AdΔΔ (***Figure 55B***). Mitoxantrone-mediated attenuation of viral replication was maintained in the presence of rapamycin and chloroquine. The combined treatment of mitoxantrone and 50nM rapamycin also attenuated viral replication when compared to treatment with rapamycin alone by 98% and 99.8% for Ad5wt and AdΔΔ alone, respectively. Likewise, the combined treatments with mitoxantrone and 10µM chloroquine attenuated viral replication when compared to chloroquine alone 99.8% and 99.5% for Ad5wt and AdΔΔ, respectively (***Figure 55B***).

Because of the inconclusive results from the replication assays regarding the effects of chloroquine on viral replication (decreased replication ***Figure 55A***; no change ***Figure 55B)***, changes in viral genome amplification were examined (qPCR ***Figure 55C***). Amplification of AdΔΔ at 3000ppc was time-dependent in PC3 cells. Mitoxantrone treatment at 900nM attenuated viral amplification, which was decreased by 96% and 87% for 48 and 78h, respectively. These mitoxantrone-mediated decreases in viral genome copies were also observed in 50nM rapamycin treated cells. The combined treatment of rapamycin and mitoxantrone resulted in a 94% and 85% decreases in genome amplification at 48h and 72h, respectively, when compared to rapamycin alone. In AdΔΔ-infected cells amplification was barely detectable in PC3 cells treated with mitoxantrone in combination with chloroquine (***Figure 55C***). AdΔΔ dose was increased in this assay a different bacth was used (batch 050314), which had a higher vp/pfu ratio (15.3vp/pfu), compared to the newer batch (050314; 2.3vp/pfu).

Finally, expression of the early and late viral genes, E1A and hexon, were assessed in PC3 cells treated with 900nM mitoxantrone in combination with 50nM rapamycin or 10µM chloroquine. Expression of E1A and hexon was detected in PC3 cells infected with Ad5wt or AdΔΔ at 500ppc and was not affected by rapamycin or chloroquine. Treatment with mitoxantrone attenuated E1A expression in Ad5wt-infected cells, which was maintained when cells were treated with the combination of mitoxantrone and rapamycin (***Figure 55D***). E1A expression was barely detectable in the presence of the combined treatment of mitoxantrone and chloroquine in Ad5wt-infected cells. Expression of hexon was hardly detectable in Ad5wt-infected PC3 cells when treated with mitoxantrone, alone or in combination with either rapamycin or chloroquine, confirming that mitoxantrone treatment interferes with viral replication (***Figure 55D***). Mitoxantrone treatment did not strongly affect E1A expression in AdΔΔ-infected cells. On the other hand, the combination of AdΔΔ and mitoxantrone decreased hexon expression, indicating attenuation of viral replication. Similar effects were seen when mitoxantrone was combined with rapamycin. Similar to Ad5wt-treated cells, the combination of mitoxantrone with chloroquine in AdΔΔ-infected cells potently attenuated E1A expression and decreased hexon expression to barely detectable levels (***Figure 55D***).

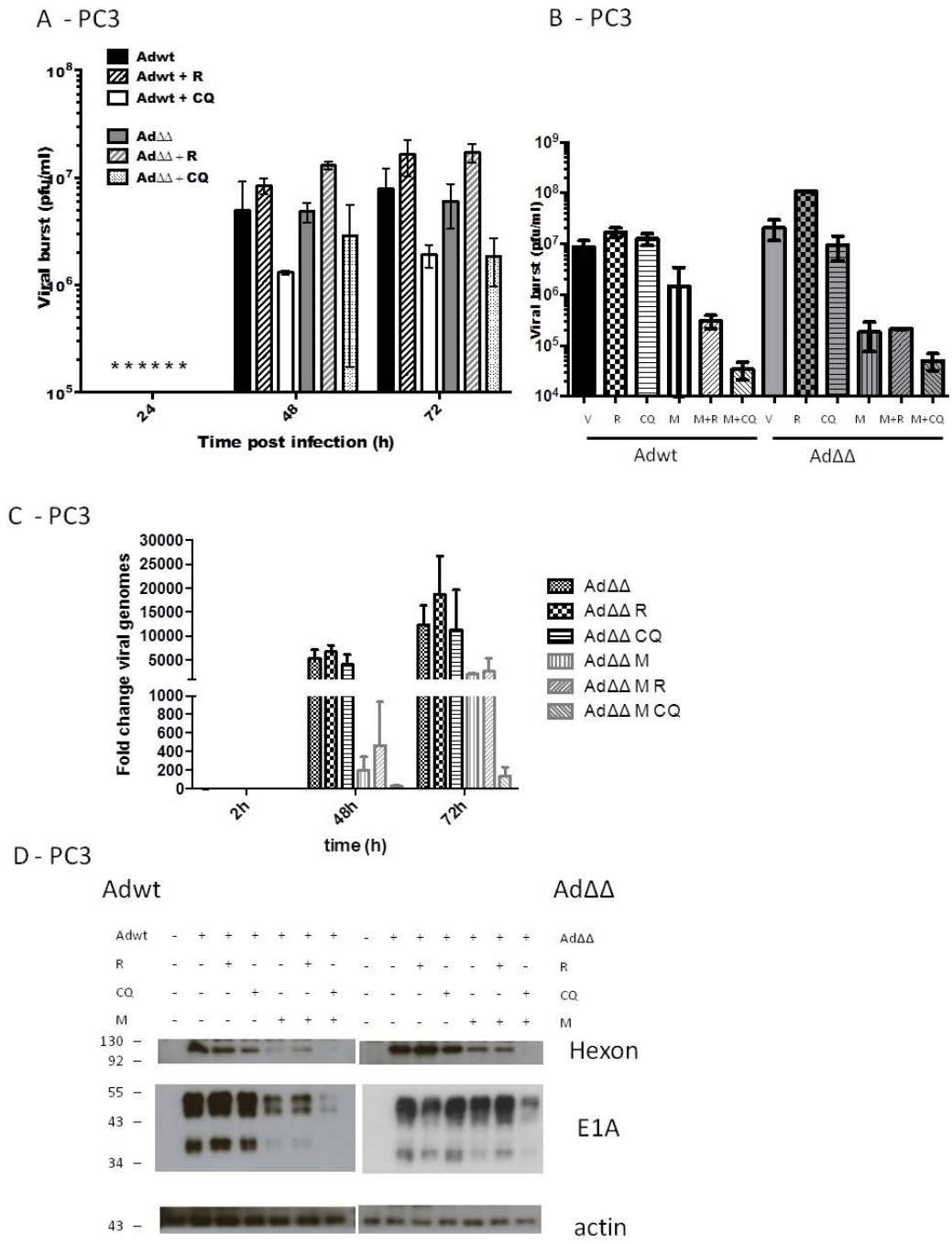

Figure 55. Mitoxantrone impairs viral replication and protein expression in PC3 cells. A. PC3 cells were infected with Ad5wt or AdΔΔ at 200ppc and treated with rapamycin (R) at 50nM or chloroquine (CQ) at 10µM, and collected at indicated time points. Averages ± SD, n=2. *indicates that viral concentration was below the detection limit, which was 5xE5 pfu/ml in this assay. **B.** PC3 cells were infected with Ad5wt or AdΔΔ at 200ppc and treated with mitoxantrone (M) at 900nM, rapamycin (R) at 50nM or chloroquine (CQ) at 10µM and collected at 72h. Averages ± SD, n=3. **A and B.** Viral burst was measured by a $TCID_{50}$ assay. **C.** PC3 cells were infected with AdΔΔ at 3000ppc and treated with mitoxantrone (M) at 900nM, rapamycin (R) at 50nM or chloroquine (CQ) at 10µM and collected at indicated time points. Total DNA was purified and the E2A adenoviral gene was amplified by qPCR for quantification of viral genomes. Fold changes in amplification of viral genomes were calculated by normalising to E2A amplification values 2h after treatment, n=2. **D.** PC3 cells were infected with Ad5wt or AdΔΔ at 500ppc and/or treated with mitoxantrone at 450 nM and/or Rapamycin at 50nM,

Chloroquine at 10μM and collected at 48h. Representative immunoblots n=2. A, B and C were performed with AdΔΔ batch 260109, D was performed with AdΔΔ batch 050314.

Viral replication, quantification of viral genomes and expression of viral proteins was also assessed 22Rv1 cells. Cells were infected with Ad5wt or AdΔΔ at 100ppc in the presence of 50nM rapamycin or 10μM chloroquine and collected 48 and 72h after treatment. Viral replication was determined by the $TCID_{50}$ assay. In contrast to PC3 cells, Ad5wt replicated more effectively than AdΔΔ in 22Rv1 cells, resulting in 5.1-fold and 3.5-fold increases at 48 and 72h compared to AdΔΔ. Ad5wt concentration was $2.0x10^7 \pm 9.6x10^5$ pfu/ml and $3.3x10^7 \pm 1.1x10^7$ pfu/ml at 48 and 72h, while AdΔΔ-replication was $3.9x10^6 \pm 1.3x10^6$ pfu/ml and $9.6x10^6 \pm 1.8x10^6$ pfu/ml at 48 and 72h, respectively (***Figure 56A***). There were no significant effects of either rapamycin or chloroquine treatments on viral replication. Replication was also assessed in the presence of 25nM mitoxantrone at 72h after treatment since this time point resulted in slightly higher viral replication in 22Rv1 cells (***Figure 56B***). In Ad5wt-infected cells, rapamycin or chloroquine, had no significant effect on replication neither alone or in combination with 25nM mitoxantrone. Nevertheless, the combined treatment of mitoxantrone and chloroquine resulted in a non-significant attenuation of Ad5wt replication, which was decreased by 86%, when compared to Ad5wt alone, and by 70% when compared with Ad5wt and chloroquine only (***Figure 56B***). A similar trend was observed in 22Rv1 cells treated with AdΔΔ, neither rapamycin nor chloroquine affected AdΔΔ-replication. A trend towards attenuation of AdΔΔ-replication was observed in cells treated with mitoxantrone alone or in combination with either rapamycin or chloroquine. AdΔΔ-replication was decreased by 70%, 67% and 91% in cells treated with mitoxantrone alone, or in combination with rapamycin or chloroquine, respectively (***Figure 56B***).

To verify the replication data viral genome amplification was also quantified in 22Rv1 cells. Cells were infected with AdΔΔ at 25ppc and treated with either 50nM rapamycin or 10μM chloroquine, alone or in combination with 25nM mitoxantrone. No clear effects on AdΔΔ genome amplification were observed with any treatment. A trend towards increased amplification was observed in the presence of rapamycin for 48h but was not maintained after 72h. A trend towards increased viral amplification after treatment with mitoxantrone, alone and in combination with rapamycin was detected at 72h but not at the earlier 48h time point. An overall time-dependent increase of viral genome copies was detected (***Figure 56C***).

Finally, expression of the early E1A and the late hexon adenoviral genes were assessed in 22Rv1 cells treated with 10nM mitoxantrone in combination with 50nM rapamycin or 10µM chloroquine. 22Rv1 cells were infected with Ad5wt or AdΔΔ at 20ppc. Surprisingly, E1A expression was increased in the presence of mitoxantrone, either as a single agent or in combination with rapamycin or chloroquine in cells infected with Ad5wt (***Figure 56D***). Hexon expression was not affected by any of the treatments in Ad5wt-infected cells (***Figure 56D***). Single agent treatment with AdΔΔ resulted in decreased hexon expression when compared to Ad5wt indicating lower levels of replication for AdΔΔ (***Figure 56D***). In agreement with the hexon data, decreased AdΔΔ-replication compared to Ad5wt was observed in the $TCID_{50}$ replication-assays (***Figure 56A and B)***. Surprisingly, expression of both E1A and hexon was increased in AdΔΔ-infected cells treated with the combination of mitoxantrone and rapamycin or mitoxantrone and chloroquine (***Figure 56D***). Increased E1A and hexon expression might indicate increased viral replication, but did not agree with the mitoxantrone-dependent decrease in AdΔΔ-replication observed in the $TCID_{50}$ assays**.**

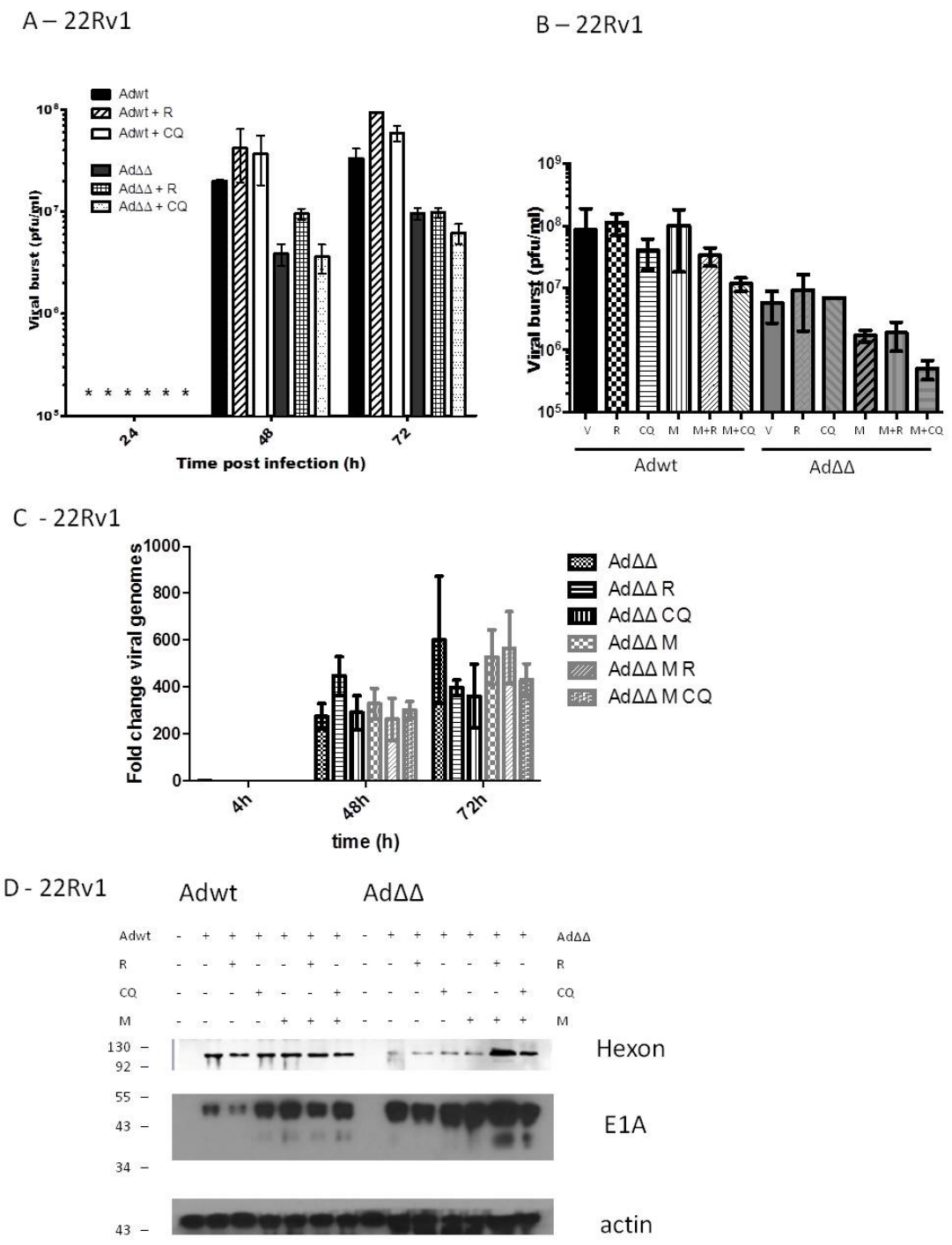

Figure 56. Neither mitoxantrone, rapamycin nor chloroquine significantly affects viral replication in 22Rv1 cells. A. 22Rv1 cells were infected with Ad5wt or AdΔΔ at 100ppc and treated with rapamycin (R) at 50nM or chloroquine (CQ) at 10µM, and collected at indicated time points. Averages ± SD, n=2. *indicates that viral concentration was below the detection limit, which was 5xE5 pfu/ml in this assay. **B.** 22Rv1 cells were infected with Ad5wt or AdΔΔ at 100ppc and treated with mitoxantrone (M) at 25nM, rapamycin (R) at 50nM or chloroquine (CQ) at 10µM and collected at 72h. Averages ± SD, n=2. **A and B.** Viral burst was measured by a $TCID_{50}$ assay. **C.** 22Rv1 cells were infected with AdΔΔ at 25ppc and treated with mitoxantrone (M) at 25nM, rapamycin (R) at 50nM or chloroquine (CQ) at 10µM and collected at indicated time points. Total DNA was purified and the E2A adenoviral gene was amplified by qPCR for quantification of viral genomes. Fold changes in amplification of viral genomes were calculated by normalising to E2A amplification values 2h after treatment, n≥2. **D.** 22Rv1 cells were

infected with Ad5wt or AdΔΔ (20ppc) and/or treated with mitoxantrone at 10 nM) and/or rapamycin at 50nM, chloroquine at 10μM and collected at 48h. Representative immunoblots, n=2. This assay was perfomed with AdΔΔ batch 260109.

3.2.6 Summary of studies of chemical modulation of autophagy with rapamycin or chloroquine

These findings demonstrated that late-stage autophagy inhibition with chloroquine sensitised both PC3 and 22Rv1 cells to mitoxantrone-induced cell death. Chloroquine also sensitised the cells to mitoxantrone in the presence of Ad5wt, AdΔΔ and Ad12S in PC3 and AdΔΔ and Ad12S in 22Rv1 cells. Autophagy-induction with rapamycin-treatment desensitised PC3 cells to mitoxantrone and reversed Ad5wt-, AdΔΔ- and Ad12S-mediated sensitization. Chloroquine-treatment induced depolarization of the mitochondrial membrane in PC3 and 22Rv1 cells treated with mitoxantrone alone or in combination with AdΔΔ. In contrast, rapamycin-treatment attenuated depolarization of the mitochondrial membrane in PC3 cells treated with mitoxantrone alone or in combination with AdΔΔ.

PC3 cells were more resistant to adenoviral infection as could be expected from the significantly higher EC_{50}-values compared to 22Rv1 cells (section 3.1.1). It is likely that the poor infectivity was due to the low levels of expression of the $\alpha_v\beta5$-integrin and hCAR in PC3 cells (4.8 ± 0.1% and 6.5 ± 0.2% of cells) (Adam, Ekblad et al. 2012), compared to the higher levels in 22Rv1 cells (15.6 ± 5.5% and 13.8 ± 0.7% of cells, for $\alpha_v\beta5$-integrin and hCAR, respectively; **Figure *54***). Pre-treatment for 24h with mitoxantrone stimulated viral uptake both in PC3 and 22Rv1 cells, and was likely a result of mitoxantrone-mediated increases in the expression of the cellular hCAR and/or $\alpha_v\beta3$- and/or $\alpha_v\beta5$-integrins, receptors that are required for viral binding and internalization. Addition of rapamycin or chloroquine to the mitoxantrone-treated cells, did not further affect infection. Ad5wt and AdΔΔ replicated to similar levels in PC3 cells. In contrast, AdΔΔ replication was lower in 22Rv1 cells compared to replication of Ad5wt. Treatment with rapamycin enhanced replication of both Ad5wt and AdΔΔ in PC3 cells while mitoxantrone-treatment attenuated viral replication; decreases that were observed in both the $TCID_{50}$ and qPCR genome amplification assays. Expression of the late-viral protein hexon was also attenuated in the presence of mitoxantrone in PC3 cells infected with either Ad5wt or AdΔΔ. It can therefore be concluded that mitoxantrone-treatment attenuated viral replication in PC3 cells. Expression of the early E1A protein was attenuated by mitoxantrone-treatment in Ad5wt-infected PC3 cells. In 22Rv1 cells, a trend towards decreased replication in cells treated with mitoxantrone was noted. However, no

significant decreases in viral genome amplification or gene expression were detected in cells treated with either single agents or the combinations.

Surprisingly, the combined treatment conditions with AdΔΔ, mitoxantrone and chloroquine, that caused increased apoptotic cell death (sections 3.2.1 and 3.2.2), resulted in strongly attenuated viral replication in PC3 cells and a similar trend in the 22Rv1 cells. These findings indicated that the observed increases in cell death were not due to increased viral replication but rather viral E1A expression that was not significantly altered by any treatment. Nevertheless, these findings suggested that E1A-induced cytotoxicity was effective even at relatively low expression levels.

In summary, the data in this section indicated that autophagy-inhibition promoted apoptotic cell death. These data support the proposed hypothesis that attenuation of autophagy and promotion of apoptosis are mechanisms involved in the enhancement of cell killing in response to AdΔΔ and mitoxantrone. The work in the following sections was aimed at further investigating the effects on these pathways by siRNA knock-down of key autophagy factors.

3.3 AUTOPHAGY INHIBITION BY ATG7 KNOCK-DOWN ENHANCES MITOXANTRONE-INDUCED APOPTOSIS.

3.3.1 Atg5 and Atg7 are efficiently knocked-down in PC3 cells.

The findings so far demonstrated that AdΔΔ enhanced mitoxantrone-induced apoptotic cell killing and attenuated mitoxantrone-dependent autophagy-initiation in PC3, 22Rv1 and PC3M cells. Moreover, inhibition of drug-induced autophagy with chloroquine significantly increased mitoxantrone-dependent apoptotic death to levels higher than those induced by AdΔΔ in combination with mitoxantrone. A trend towards further induction of apoptosis in cells treated with mitoxantrone and chloroquine was also observed in the presence of AdΔΔ in both PC3 and 22Rv1 cells. In order to investigate if the pro-apoptotic effect of late stage autophagy-inhibition by chloroquine also occurred when early stage autophagy-inititation was prevented, Atg5 and Atg7 were targeted for knock-down. Both Atg5 and Atg7 are essential for inititation of autophagy and are key factors in the formation of the autophagosome membrane formation (Tanida, Yamasaki et al. 2012, Nakatogawa 2013). To explore whether inhibition of autophagy-initiation would further sensitise the cells to mitoxantrone, Atg5 and Atg7 were knocked-down in PC3 cells using the respective siRNA pools (**Table *18***). The PC3 cell line was selected since these cells showed the highest AdΔΔ-mediated sensitization to mitoxantrone and the most potent response to chloroquine and rapamycin treatments in cell viability and apoptotic assays (**Figure *46***, **Figure *49*** and **Figure *50***).

In order to assess the knock-down efficiency, PC3 cells were transfected with a non-targeting siRNA (siNT) pool and siRNA pools targeting Atg5 (siAtg5) or Atg7 (siAtg7). Dharmafect transfection reagent was added to PC3 cells to facilitate siRNA transfection, including the non-transfected cells. Transfection efficiency for siAtg5 was monitored over time at 24 – 144h. Transfection with siAtg5 at 50 and 100nM resulted in potent knock-down of the protein 72 and 144h after transfection (**Figure *57***) when compared to the siNT and non-transfected controls. The specificity of the siRNAs was confirmed as transfection with siNT resulted in no changes in the expression of Atg5 or the loading control. The Atg5 protein was detected as a complex with Atg12 as expected. Free Atg5 could not be detected at any of the tested conditions (data not shown). siAtg5 transfection resulted in a trend towards decreased levels of LC3BII at 72 and 144h, indicating attenuation of basal levels of autophagy initiation (**Figure *57***). These findings indicated that 50nM siAtg5 were sufficient to efficiently knock-down Atg5 and attenuate LC3BII/I conversion.

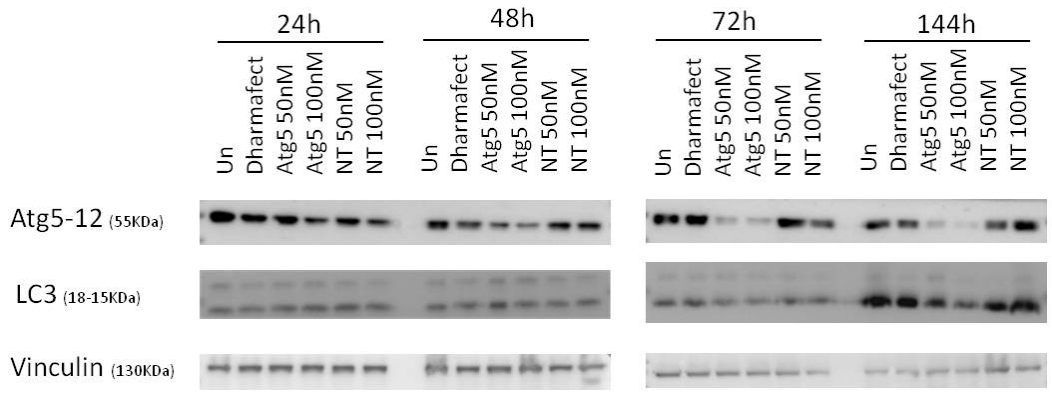

Figure 57. Atg5 is knocked-down from 72 to 144h after transfection. PC3 cells were transfected with pools of non-targeting (NT) siRNA or Atg5 (Atg5) siRNA, or the transfection reagent alone (Dharmafect) and collected at indicated time points (24, 48, 72 and 144h). Immunoblotting for Atg5 and LC3BII/I. n=1.

Transfection efficiency for siAtg7 was also monitored over time at 24 – 144h. Based on findings with Atg5 (**Figure *57***) that demonstrated 50nM siAtg5 to be sufficient for efficient knock-down, transfection was performed with siNT and siAtg7 at 50nM only. Transfection with siAtg7 resulted in potent knock-down of the protein 48 to 144h after transfection, compared to siNT and non-transfected controls (**Figure *58***). A decrease in Atg7 expression was also detected at the 24h time-point. In this preliminary study, transfection with siAtg7 did not appear to prevent LC3BII/I conversion however, in later experiments, prevention of LC3BII/I conversion was confirmed (**Figure *60***).

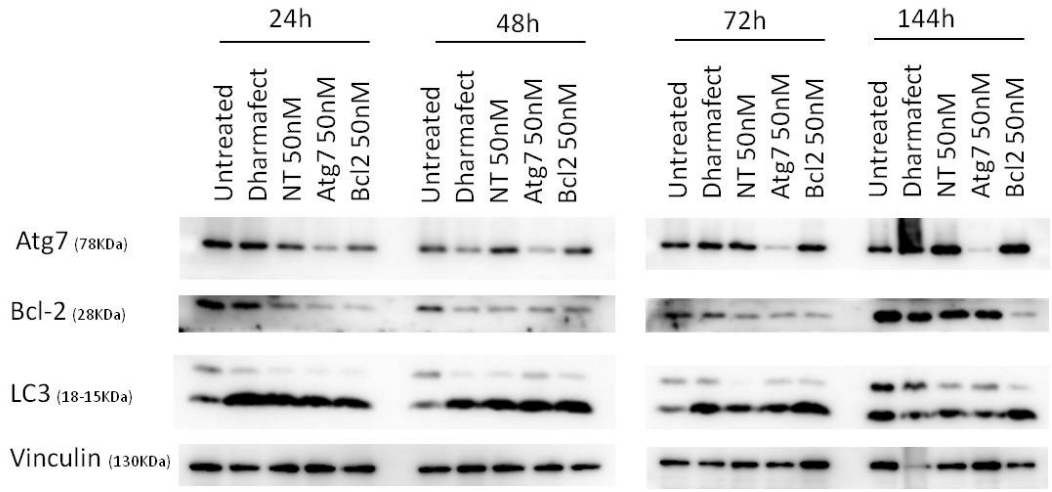

Figure 58. Atg7 is knocked-down from 24h to 144h after transfection and Bcl-2 is knocked-down after 144h in PC3 cells. PC3 cells were transfected with a non-targeting (NT) siRNA and Atg7 (Atg7) siRNA or Bcl-2 (Bcl-2) siRNA or the transfection reagent alone (Dharmafect) and collected at the indicated times after transfection (24, 48, 72 and 144h). Immunoblotting for Atg7, Bcl-2 and LC3BII/I, n=1.

3.3.2 Atg5 or Atg7 knock-down prevent LC3BI to II conversion even in the presence of mitoxantrone and Atg7 knock-down promotes mitoxantrone-induced apoptosis.

In order to assess the effect of siAtg5 and siAtg7 knock-down on mitoxantrone-dependent cell killing, siAtg5 and siAtg7 transfected PC3 cells were treated with mitoxantrone at 450nM or AdΔΔ at 500ppc or the combination of both agents 96h post-transfection as explained in (**Figure *27***). First, autophagy modulation was assessed by immunoblotting of the early and late markers LC3B and p62, respectively.

Transfection of PC3 cells with siAtg5 or siAtg7 efficiently knocked-down expression of Atg5 and Atg7 and resulted in undetectable protein levels (**Figure *59A*** and **Figure *60A***) 144h after transfection. Transfection with siAtg5 resulted in autophagy inhibition, demonstrated by a 50% decrease in LC3BI to LC3BII conversion compared to siNT treated cells with LC3BII expressed lower than basal levels, and no degadation of p62 (***Figure 59A-C***). In addition, a trend towards p62 accumulation was noted when compared to siNT-transfected cells with a 1.5 – 2-fold increase in p62 levels (***Figure 59C***). However, those effects were not statistically significant. Interestingly, treatment with 450nM mitoxantrone did not counteract siAtg5-mediated autophagy-inhibition and did not induce LC3BI to LC3BII conversion (***Figure 59B-C***). Similarly, siAtg7 transfection resulted in prevention of autophagy initiation, demonstrated by greatly decreased LC3BI to LC3BII conversion and no degration of p62, both in untreated and mitoxantrone-treated (450nM) PC3 cells (**Figure *60***). More specifically, siAtg7 transfection caused an approximately 50% decrease in LC3BII/I ratios, when compared to siNT cells and an accumulation of LC3BI. Treatment with 450nM mitoxantrone did not induce LC3BI to LC3BII conversion in siAtg7 cells. Similarly to Atg5 data, those effects were not statistically significant.

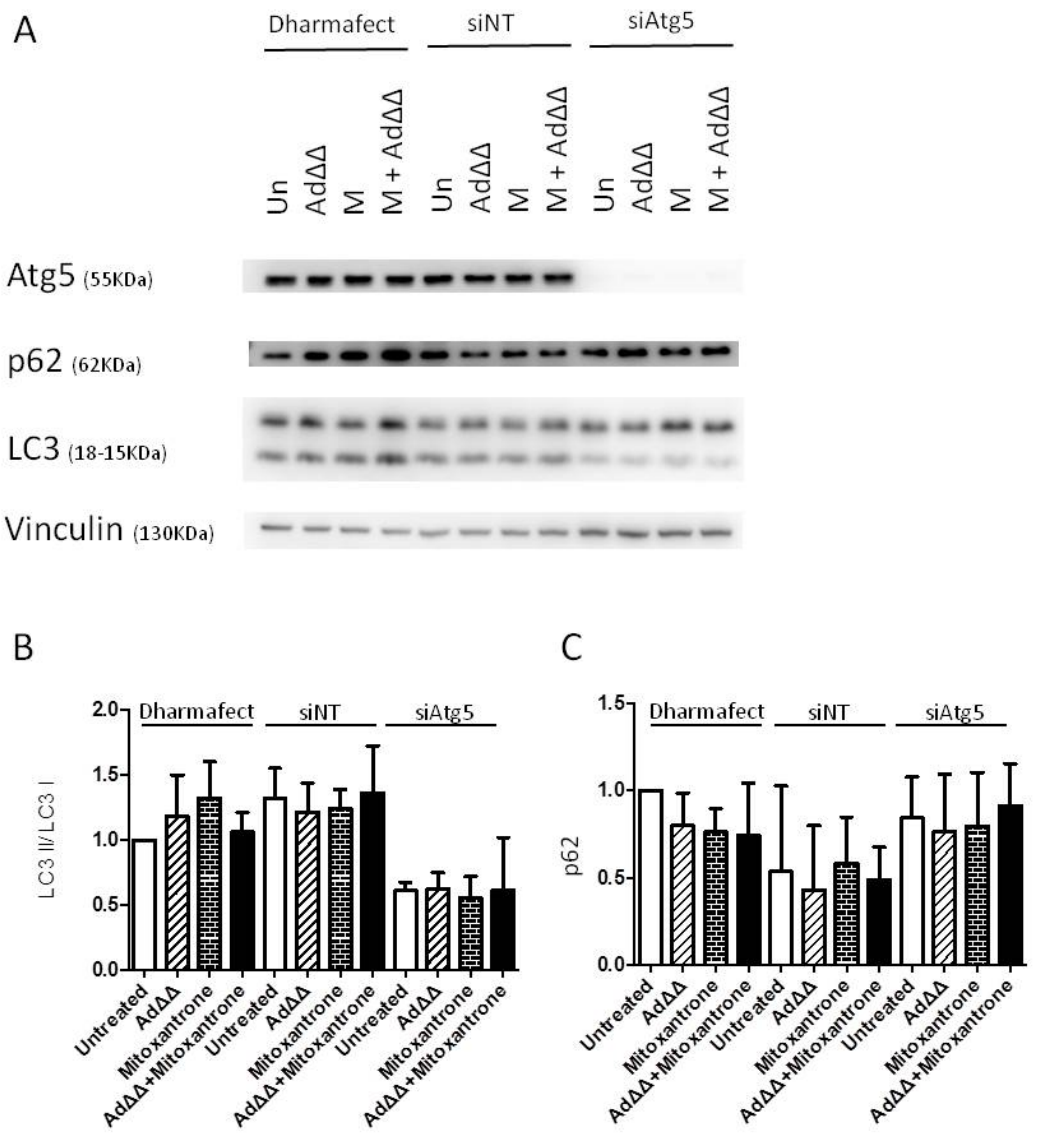

Figure 59. Atg5 knock-down prevents LC3BII conversion even in the presence of mitoxantrone. A. Fixed doses of AdΔΔ at 500ppc and/or mitoxantrone at 450nM were added to PC3 cells 4 days after transfection. Cells were transfected with a non-targeting siRNA (siNT), Atg5 siRNA (siAtg5) or the transfection reagent alone (Dharmafect). Samples were collected 48h after treatment. Representative immunoblots, n=3. **B.** Densitometry quantification of LC3B expression from A. LC3B ratio is expressed as LC3BII (lower band) divided by LC3BI (higher band). Each band normalised to the loading control. Averages ± SD, n=3. **C.** Densitometry quantification of p62 expression from A. p62 was divided by loading control. Averages ± SD, n=3. **B and C**. One-way Anova with Bonferroni post-test was performed but resulted in no significant differences. This assay was performed with AdΔΔ batch 050314.

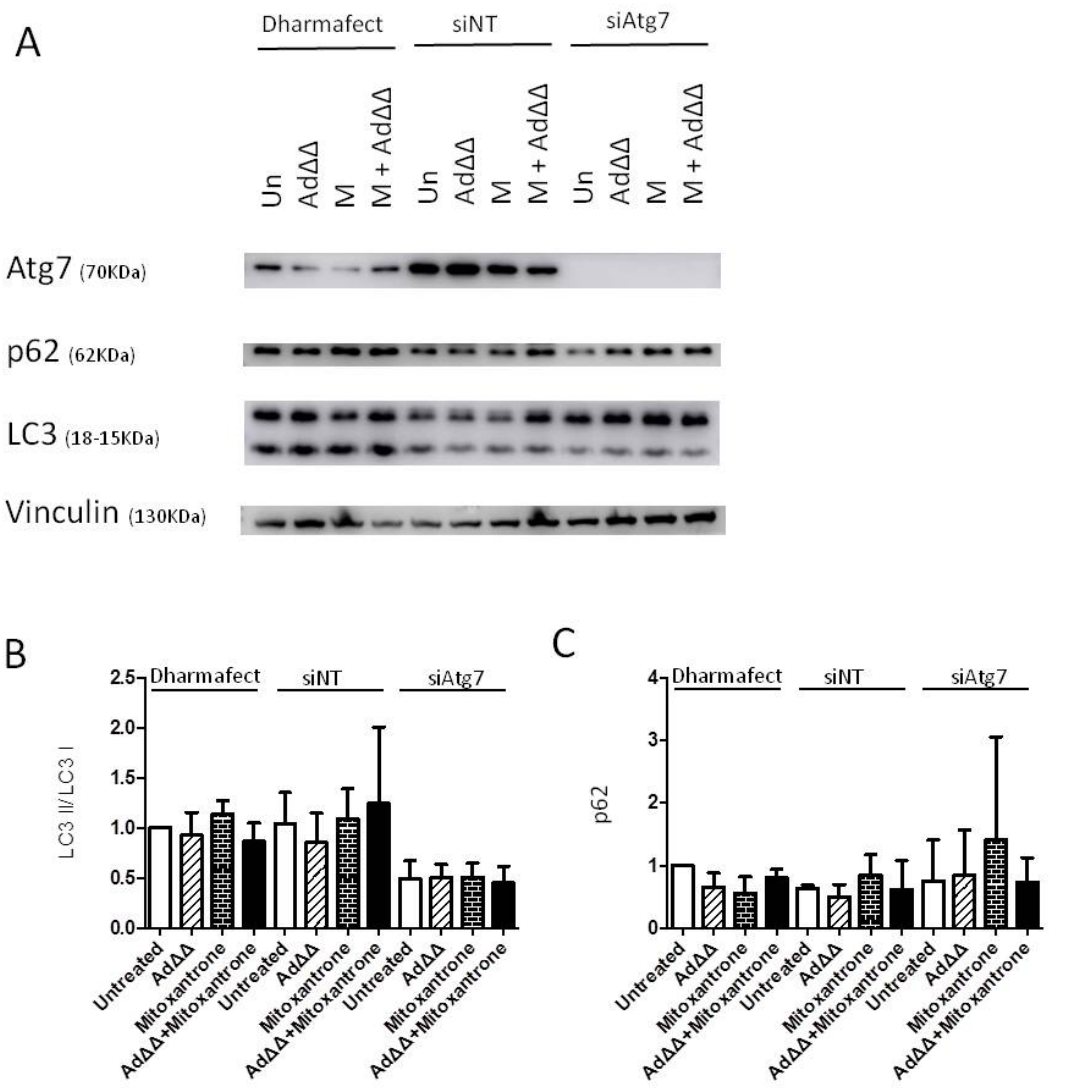

Figure 60. Atg7 knock-down prevents LC3BI to II conversion even in the presence of mitoxantrone. A. Fixed doses of AdΔΔ at 500ppc and/or mitoxantrone at 450nM were added to PC3 cells 4 days after transfection. Cells were transfected with a non-targeting siRNA (siNT), Atg7 siRNA (siAtg7) or the transfection reagent alone (Dharmafect). Samples were collected 48h after treatment. Representative immunoblots, n=3. **B.** Densitometry quantification of LC3 expression from A. LC3B ratios are expressed as LC3BII (lower band) divided by LC3BI (higher band). Each band was normalised to the loading control. Averages ± SD, n=3. **C.** Densitometry quantification of p62 expression from A. p62 was divided by loading control. Averages ± SD, n=3. **B and C**. One-way Anova with Bonferroni post-test was performed but resulted in no significant differences. This assay was performed with AdΔΔ batch 050314.

In order to confirm whether inhibition of autophagy correlated with apoptosis induction, as previously observed with chloroquine-dependent autophagy inhibition (**Figure *49***), PC3 cells were transfected with the siAtg7 or siNT pools followed by assessment of mitochondrial depolarization by TMRE staining. The transfected cells were treated with 100nM mitoxantrone or AdΔΔ at 500ppc or the combination of both agents as described in section

2.9 (**Figure *27***). A slightly lower dose of mitoxantrone was selected compared to previous experiments, due to an observed overall increase in sensitivity to mitoxantrone in transfected cells, which will be discussed below (section 3.3.3).

I previously showed that AdΔΔ-infection enhanced mitoxantrone-induced mitochondrial depolarization in non-transfected cells (section 3.1.6). In agreement with these findings, mitoxantrone-treatment induced mitochondrial depolarization in siNT-transfected cells, which was enhanced in the presence of AdΔΔ (**Figure *61***). Transfection with siAtg7 further promoted mitochondrial depolarization in cells treated with this low dose of 100nM mitoxantrone (**Figure *61***). from 51.3 ± 4.5% in siNT cells to 63.1 ± 3.3% in siAtg7 cells ($p<0.001$). Depolarization of the mitochondrial membrane was also increased in siAtg7 cells treated with the combination of mitoxantrone and AdΔΔ compared to combination-treated siNT cells (**Figure *61***), from 57.2 ± 5.1% in siNT cells to 70.9 ± 3.5% in siAtg7 cells ($p<0.0001$). A non-significant higher levels of mitochondrial depolarization was noted in both siNT and siAtg7 transfected cells treated with mitoxantrone and AdΔΔ compared to mitoxantrone alone. Mitochondrial depolarization levels were not significantly affected by siAtg7 transfection in untreated or AdΔΔ-infected cells compared to siNT cells.

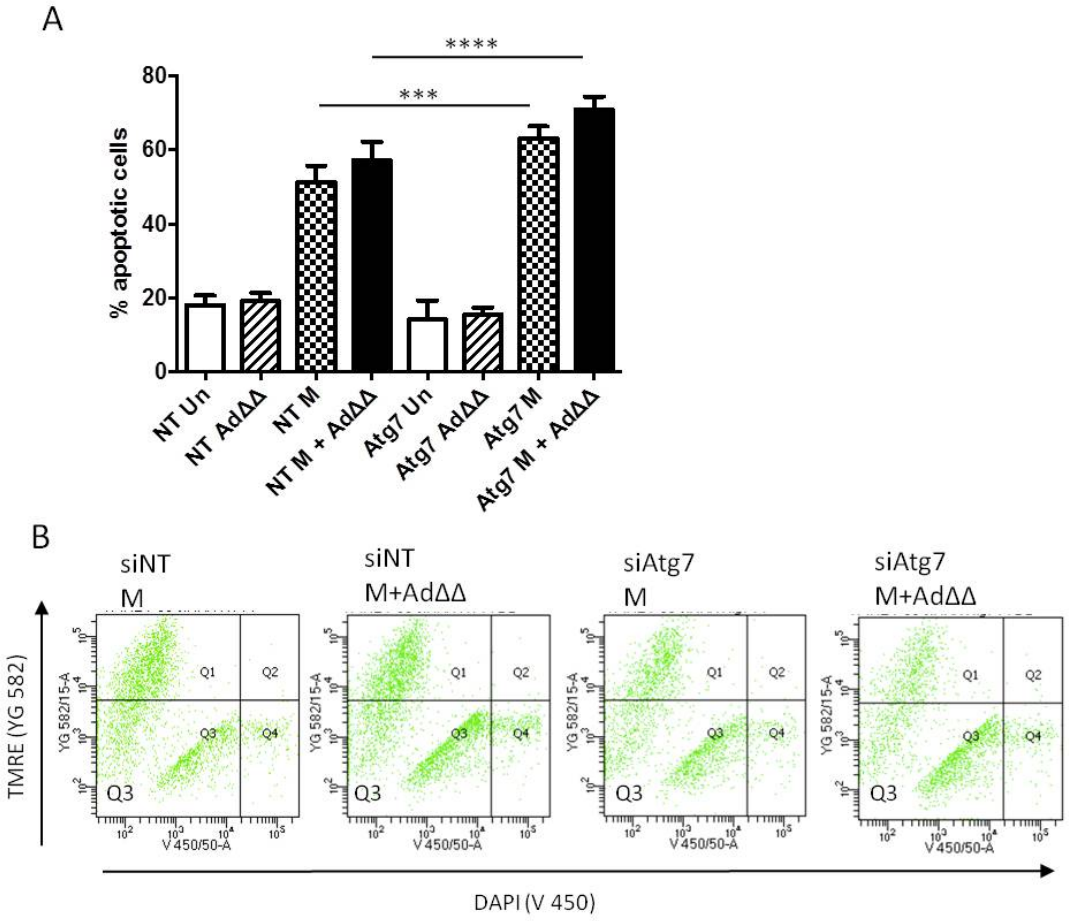

Figure 61. Atg7 knock-down promotes depolarization of the mitochondrial membrane in PC3 cells. A. Fixed doses of AdΔΔ at 500ppc and/or mitoxantrone at 100nM were added to PC3 cells 24h after transfection. Cells were transfected with pools of non-targeting siRNA (NT) or Atg7 siRNA. Samples were collected 5 days after treatment. Mitochondrial depolarization was measured as an indication of apoptosis by loss of TMRE staining (Q3). TMRE and DAPI staining were detected with lasers YG 585/15 and V 450/50, respectively. Averages ± SD, n=3. One-way Anova with Bonferroni post-test. ***p<0.001, ****p<0.0001. **B.** Representative FACS images from A.

In summary, Atg5 and Atg7 were effectively knocked-down using pools of the corresponding siRNAs. Autophagy-inhibition in siAtg5 and siAtg7 transfected cells was demonstrated by greatly decreased LC3BII conversion and no p62 degradation. Interestingly, autophagy-inhibition was associated with increased mitochondrial depolarization in siAtg7 cells treated with mitoxantrone alone and in combination with AdΔΔ, indicating increased apoptosis. These data indicated that autophagy inhibition promoted apoptosis in mitoxantrone-treated cells. These findings agreed with chloroquine-mediated promotion of mitoxantrone-induced apoptosis (section 3.2.2) and therefore confirmed the hypothesis that inhibition of mitoxantrone-dependent autophagy-initiation promoted apoptosis. Apoptosis modulation was not assessed in siAtg5 transfected cells.

3.3.3 Atg5 or Atg7 knock-down does not affect AdΔΔ-mediated sensitization to mitoxantrone.

I demonstrated (section 3.3.2) that siAtg7-mediated autophagy-inhibition promoted mitoxantrone-induced apoptosis. In order to assess whether the increased apoptosis was paralleled by increased sensitisation to AdΔΔ in mitoxantrone-treated cells, cell viability assays were performed. A fixed dose of AdΔΔ at 500ppc, that sensitised PC3 cells to mitoxantrone (**Figure *32***), was added in combination with increasing doses of mitoxantrone to cells that had been transfected with siAtg5, siAtg7 or siNT.

Infection with AdΔΔ at 500ppc resulted in potent sensitization to mitoxantrone in siAtg7-, siNT and non-transfected cells, demonstrated by decreased EC_{50}-values for mitoxantrone (**Figure *62A and B,* Figure *64,* Table *25***). Co-infection with AdΔΔ reduced mitoxantrone EC_{50}-values by 73%, 77% and 78% for non-transfected cells and cells transfected with siNT or siAtg7, respectively. Data were processed to generate sensitization ratios (**Figure *62B***). The differences in EC_{50}-ratios for mitoxantrone alone or in combination with AdΔΔ were significant for all tested conditions ($p<0.01$ for non-transfected and siAtg7 cells, and $p<0.0001$ for siNT cells) (**Figure *62B***). The EC_{50}-values to mitoxantrone as a single agent were 116.1 ± 51.6 nM, 101.2 ± 18.3 nM and 248.3 ± 101.4 nM for non-transfected cells, siNT cells or siAtg7 cells, respectively. Importantly, these EC_{50}-values for mitoxantrone were lower compared to previous studies in PC3 cells grown under regular conditions (without transfection reagent) where the EC_{50}-value was 2276.5 ± 419.8 nM (***Table 23***). This fact suggested that cells became more sensitive to chemotherapy-treatment in the presence of the transfection reagent (**Figure *62A,* Table *25***). Interestingly, a trend was noted towards increased EC_{50}-value to mitoxantrone in siAtg7 cells treated with mitoxantrone only, when compared to the siNT or the non-transfected controls (**Figure *62A,* Table *25***).

From mitoxantrone dose-response data, I selected a dose of mitoxantrone (at 60nM) that resulted in 20 – 40% cell death. Results from the cell death assays were reanalysed and normalised to untreated non-transfected cells (Dharmafect control) (**Figure *62C***). Transfection with either siNT or siAtg7 resulted in an overall increase in cell death when compared to non-transfected control cells (**Figure *62C***). There were no significant differences between siNT or siAtg7 cells at any of the selected treatments (mitoxantrone at 60nM and

AdΔΔ at 500ppc or the combination of both). Effective Atg7 knock-down was confirmed in all the replicas, one representative immunoblot is shown (**Figure *62D***).

Surprisingly, despite promoting apoptosis, siAtg7 tranfection did not appear to cause detectable decreases in cell viability under these experimental conditions.

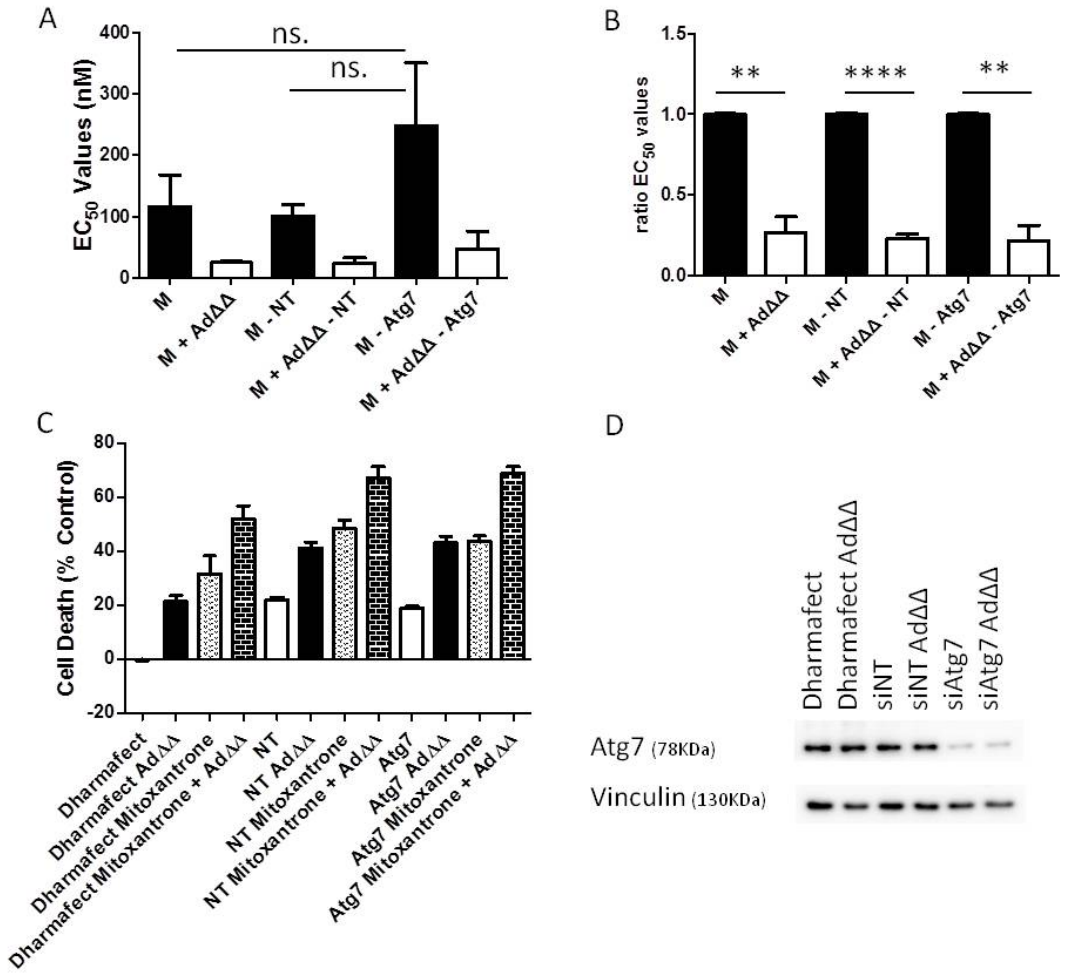

Figure 62. Inhibition of autophagy with Atg7 siRNA does not affect AdΔΔ-mediated sensitization to mitoxantrone. A. A fixed dose of AdΔΔ at 500ppc that killed 10-30% of cells was added to mitoxantrone-treated cells. EC_{50}-values generated with dose-response curves of mitoxantrone in combination with fixed doses of AdΔΔ at 500ppc. PC3 cells were previously transfected with a non-targeting (NT) siRNA, Atg7 siRNA or the transfection reagent alone. Averages ± SD, n=3. One-way Anova with Bonferroni post-test. **B.** Ratio of EC_{50}-values in A expressed as EC_{50} combined treatment / EC_{50} mitoxantrone. Averages ± SD, n=3. Unpaired t-test, **p<0.01 ****p<0.0001. **C.** Selected fixed doses from the dose-response data of mitoxantrone at 60nM, AdΔΔ at 500ppc and the combination of both in PC3 cell previously transfected with a non-targeting (NT) siRNA, Atg7 siRNA or the transfection reagent alone. Averages ± SD, n=3. **A-C.** Cell viability was measured by MTS assay 5 days after treatment. **D.** Representative immunoblot for Atg7, n=3. PC3 cells were infected AdΔΔ at 500ppc. PC3 cells were previously transfected with a non-targeting (NT) siRNA, Atg7 siRNA or the transfection reagent alone (Dharmafect). These assays were performed with AdΔΔ batch 050314.

Because of non-detectable decreases in cell viability of siAtg7-mediated autophagy inhibition (shown in **Figure *62***), sensitization experiments were repeated in siAtg5-tranfected PC3 cells (**Figure *63***) to further investigate the role of inhibition of autophagy-initiation on drug-dependent cell death.

Infection with AdΔΔ resulted in potent sensitization to mitoxantrone in all cells; non-transfected cells and cells transfected with siNT or siAtg5 (***Figure 63A and B,*** **Figure *64,* Table *25***). The data were processed to generate sensitization ratios (***Figure 63B***), demonstrating that the differences in EC_{50}-ratios for mitoxantrone alone and in combination with AdΔΔ were significant for all tested conditions ($p<0.0001$ for non-transfected cells and siNT cells, and $p<0.001$ for siAtg5 cells) (***Figure 63B***). Fixed doses were selected from the dose-response data and reanalysed. Both siNT or siAtg5 treated cells caused overall increases in cell death compared to the non-transfected control (***Figure 63C***) but, no significant differences between siNT or siAtg5 cells at any of the selected treatments, mitoxantrone at 60nM and AdΔΔ at 500ppc or the combination of mitoxantrone and AdΔΔ, were observed. Effective Atg5 knock-down was confirmed in all the replicas, one representative immunoblot is shown (***Figure 63D***).

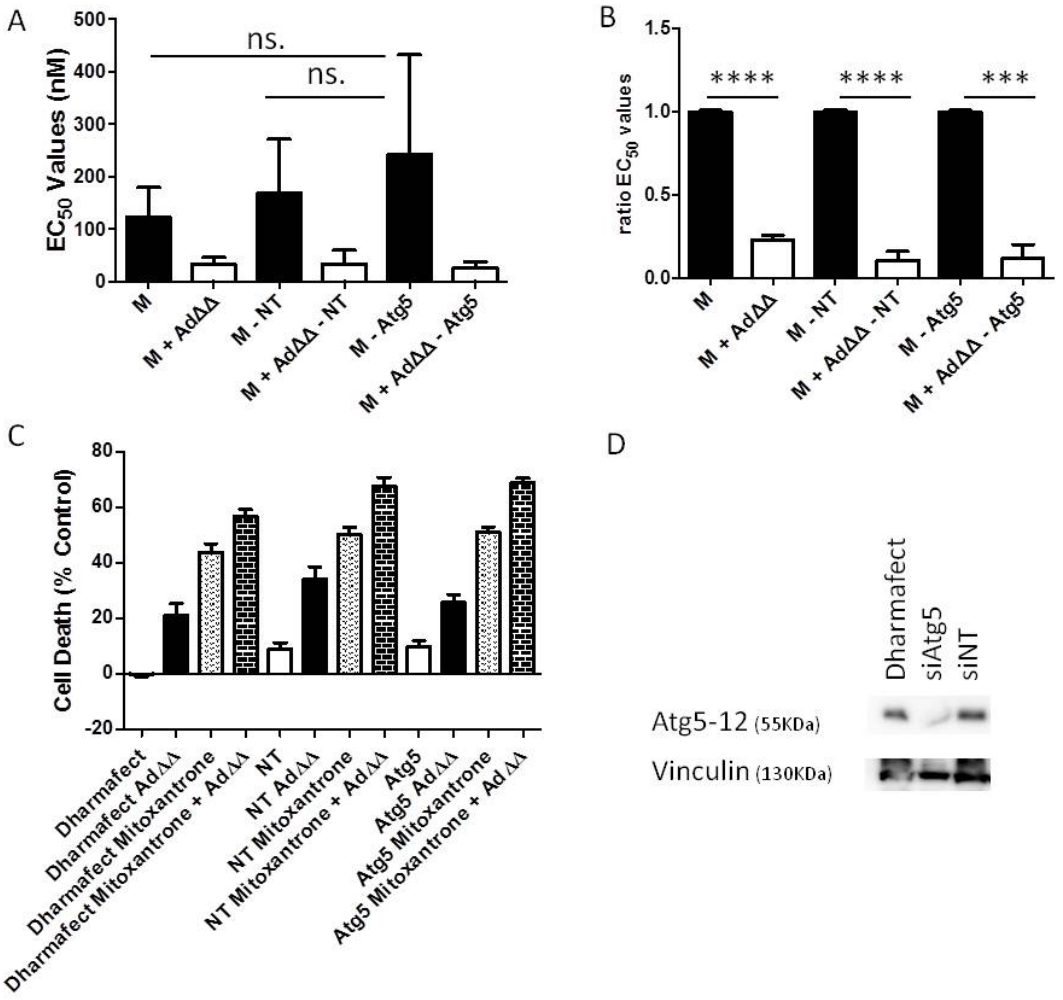

Figure 63. Inhibition of autophagy with Atg5 siRNA does not affect AdΔΔ-mediated sensitization to mitoxantrone. A. A fixed dose of AdΔΔ at 500ppc that killed 10-30% of cells was added to mitoxantrone-treated cells. EC_{50}-values were generated with dose-response curves to mitoxantrone in combination with fixed doses of AdΔΔ at 500ppc. PC3 cells were previously transfected with a non-targeting (NT) siRNA, Atg5 siRNA or the transfection reagent alone. Averages ± SD, n=4. One-way Anova with Bonferroni post-test. **B.** Ratio of EC_{50}-values in A expressed as (EC_{50} combined treatment) / (EC_{50} mitoxantrone). Averages ± SD, n=4, Unpaired t-test, ***p<0.001 ****p<0.0001. **C.** Selected fixed doses from the dose-response data of mitoxantrone at 60nM, AdΔΔ at 500ppc and the combination of both in PC3 cells previously transfected with a non-targeting siRNA, Atg5 siRNA or the transfection reagent alone. Averages ± SD, n=4. **A-C.** Cell viability was measured by MTS assay 5 days after treatment **D.** Representative immunoblot for Atg5, n=3. PC3 cells were transfected with a non-targeting (NT) siRNA, Atg5 siRNA or the transfection reagent alone (Dharmafect). This assay was performed with AdΔΔ batch 050314.

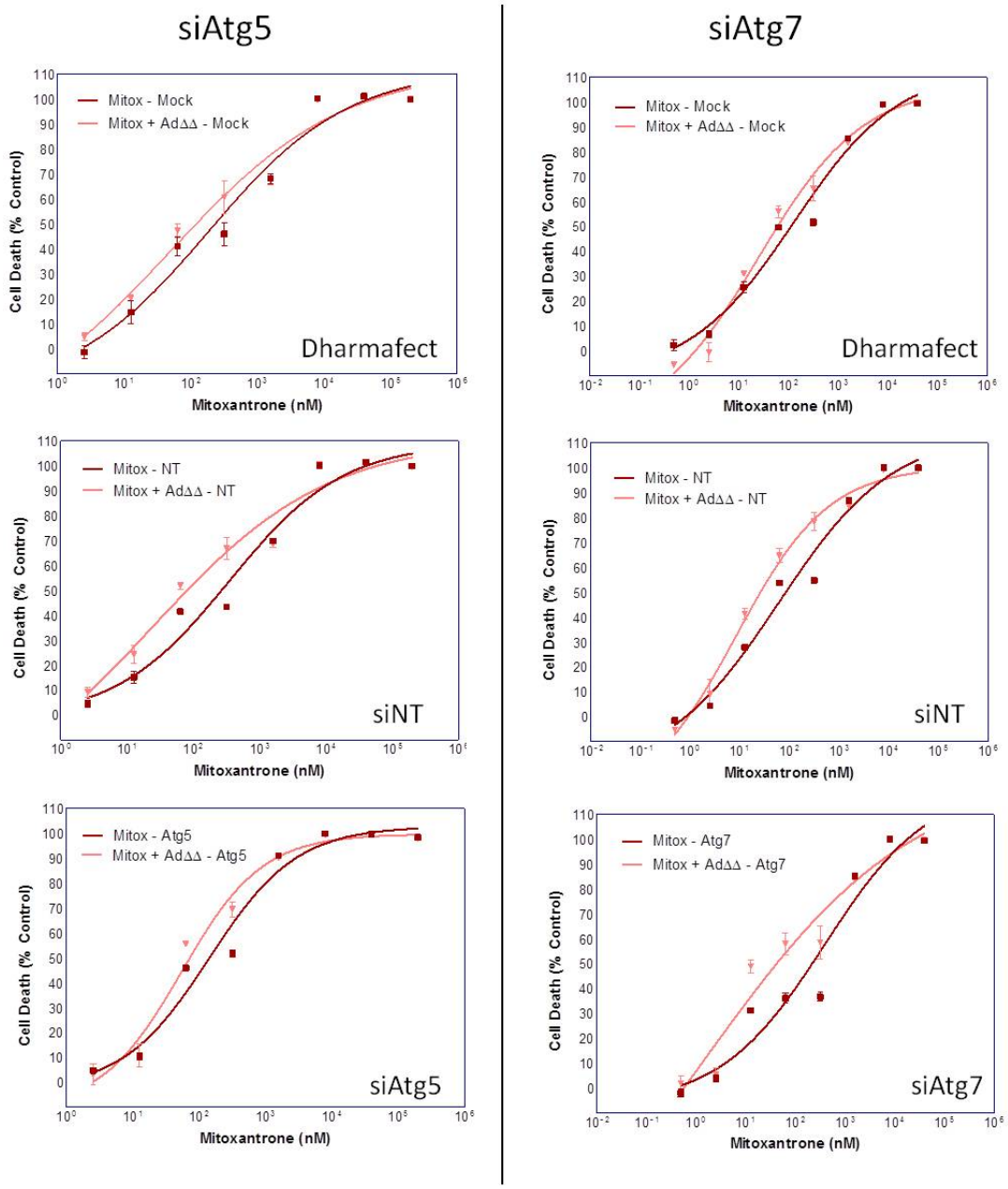

Figure 64. Representative dose-response curves from siAtg5 and siAtg7 studies. The figure illustrates one representative experiment, for each siRNA, from the data presented in Figure 62 and Figure 63. Dose-response curves to mitoxantrone in combination with fixed doses of AdΔΔ at 500ppc. PC3 cells transfected with a non-targeting (NT) siRNA, Atg5 siRNA (siAtg5) and Atg7 siRNA (siAtg7) or the transfection reagent alone.

Table 25. EC_{50}-values (±SD) generated for mitoxantrone in siAtg5 and siAtg7 transfected PC3 cells.

	siAtg5 experiments Mitoxantrone (nM)	siAtg7 experiments Mitoxantrone (nM)
Non-transfected*	2276.5 ± 419.8	2276.5 ± 419.8
Non-transfected + AdΔΔ*	316.5 ± 2.1	316.5 ± 2.1

Dharmafect	122.8 ± 56.3	116.1 ± 51.6
Dharmafect + AdΔΔ	32.7 ± 12.6	25.1 ± 2.1
siNT	168.1 ± 103.4	101.2 ± 18.3
siNT + AdΔΔ	33.3 ± 26.0	24.3 ± 8.5
Target siRNA (Atg5 or Atg7)	242.5 ± 189.9	248.3 ± 101.4
Target siRNA (Atg5 or Atg7) + AdΔΔ	25.7 ± 11.9	47.7 ± 28.0

Data generated with AdΔΔ batch 050314. *These cells were not transfected nor treated with the Dharmafect transfection reagent, data taken from ***Figure 30***.

In summary, knock-down of Atg5 or Atg7 did not increase AdΔΔ-mediated sensitization to mitoxantrone. Early stage autophagy-inhibition with siAtg5 or siAtg7 did not significantly sensitise cells to either mitoxantrone-treatment or AdΔΔ-infection. However, a trend towards increased EC_{50}-values to mitoxantrone was noted in siAtg5 or siAtg7 transfected cells. Inhibition of autophagy-initiation with siAtg5 or siAtg7 did not affect cell killing and contrasted with the findings using the late stage autophagy-inhibitor chloroquine, which further enhanced both cell killing and apoptosis under similar conditions.

3.3.4 Atg7 and Atg5 knock-down does not significantly affect viral gene expression or replication in PC3 cells.

In order to investigate whether the different responses to siAtg5 and siAtg7 versus chloroquine were caused by attenuation of the viral life cycle, changes in viral gene expression were determined by immunoblotting for E1A and hexon.

Protein knock-down was verified in PC3 cells transfected with siAtg5 or siAtg7 and cells were infected with AdΔΔ at 500ppc alone or in combination of 450nM mitoxantrone (**Figure *59*** and **Figure *60***), the same samples were used to assay expression of the viral proteins. Expression of the early viral E1A gene was not affected by siAtg5 or siAtg7 when compared to siNT or non-transfected control cells (**Figure *65***). Treatment with mitoxantrone did not result in any changes in E1A expression in cells transfected with siAt5 or siAtg7 compared to the siNT transfected cells or non-transfected cells. Hexon expression was monitored as an indication of viral late gene expression and replication. In agreement with the E1A data, no changes in hexon expression were observed in siAtg5 or Atg7 cells compared to the siNT or non-transfected control cells. Mitoxantrone treatment did not affect hexon expression in cells transfected with siAtg5 or siAtg7 or siNT or non-transfected cells.

Therefore, it was concluded that knock-down of Atg5 or Atg7 did not affect E1A and hexon expression and that viral replication was not affected. However, a viral replication assay such as the $TCID_{50}$ should be performed to confirm this observation. These findings indicated that AdΔΔ was functional under the different transfection conditions and the observed results were not caused by an impairment in the viral life-cycle.

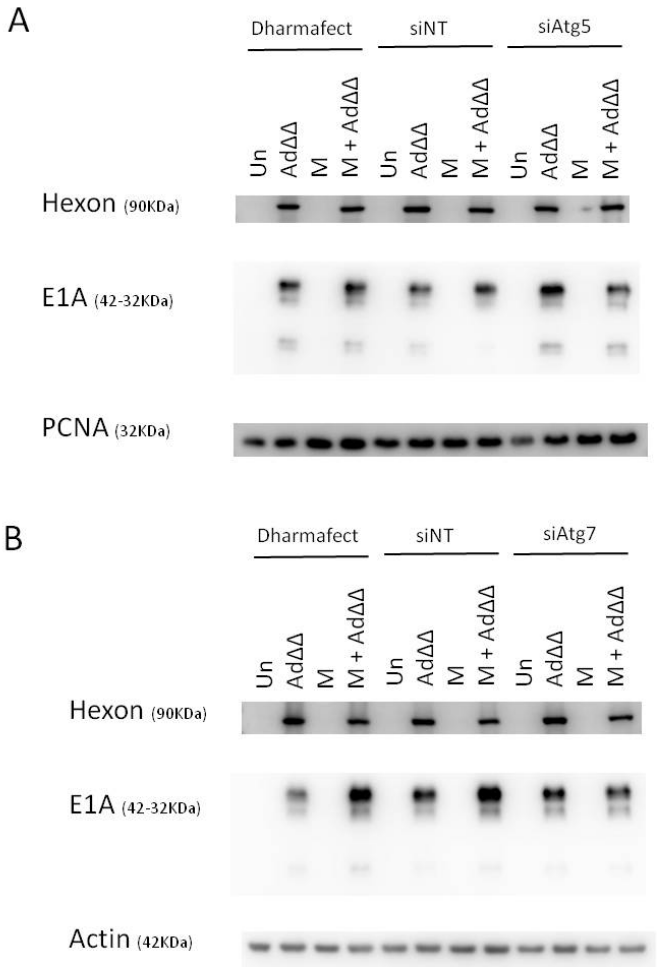

Figure 65. Knock-down of Atg7 and Atg5 does not significantly affect viral gene expression or replication in PC3 cells. A. Fixed doses of AdΔΔ at 500ppc and/or mitoxantrone at 450nM were added to PC3 cells 4 days after transfection. Cells were previously transfected with a non-targeting siRNA (siNT), Atg5 siRNA (siAtg5) or the transfection reagent alone (Dharmafect). Samples were collected 48h after treatment. Representative immunoblots, n=3. **B.** Fixed doses of AdΔΔ at 500ppc and/or mitoxantrone at 450nM were added to PC3 cells 4 days after transfection. Cells were previously transfected with a non-targeting siRNA (siNT), Atg7 siRNA (siAtg7) or the transfection reagent alone (Dharmafect). Samples were collected 48h after treatment. Representative immunoblots, n=3. Data generated with AdΔΔ batch 050314.

3.3.5 Summary and conclusions from the studies with Atg5 and Atg7 knock-down in PC3 cells.

These findings indicated that knock-down of Atg5 or Atg7 prevented autophagy-initiation, demonstrated by decreased LC3I to LC3II conversion. Autophagy-inhibition as a result of Atg7 knock-down enhanced mitoxantrone-induced apoptosis both in cells treated with drug alone and in AdΔΔ co-infected cells. The enhancement of apoptosis was in agreement with the data from chloroquine-treatment that enhanced apoptotic death in cells treated with mitoxantrone and a trend towards increased apoptosis in combination-treated cells. Taken together, these findings demonstrated that autophagy-inhibition promoted mitoxantrone-induced apoptosis. However, the data suggested that siAtg5 or siAtg7 transfection did not further sensitise PC3 cells to AdΔΔ-mediated enhancement of cell death in combination with mitoxantrone. Importantly, inhibition of early stage autophagy-initiation in response to mitoxantrone did not increase cell killing in contrast to late stage inhibition with chloroquine.

3.4 BCL-2 KNOCK-DOWN PREVENTS ADΔΔ-MEDIATED SENSITIZATION TO MITOXANTRONE AND PROMOTES AUTOPHAGY IN PC3 CELLS.

It has been established that the Bcl-2 protein plays a main role in the crosstalk between apoptosis and autophagy regulation (Marquez and Xu 2012). While Bcl-2 is an important anti-apoptotic protein that binds to Bax and Bak and prevents mitochondrial depolarization (Shore and Nguyen 2008), Bcl-2 is also an anti-autophagic protein through binding to Beclin1. The formation of the Beclin 1-Bcl-2 complex prevents the formation of the Beclin 1-Vps34-Vps35 complex, which promotes autophagy-initiation (Pattingre, Tassa et al. 2005, Gordy and He 2012). In wild type Ad5, the anti-apoptotic viral E1B19K protein functions as a Bcl-2 homologue to prevent premature apoptosis. E1B19K has also been reported to displace Bcl-2 from the Beclin 1 complex and induce autophagy (Piya, White et al. 2011). In order to determine whether AdΔΔ (deleted in E1B19K) was dependent on a functional Bcl2-Beclin1 complex to attenuate drug-induced autophagy, PC3 cells were transfected with an siRNA pool targeting Bcl-2 (***Table 18***).

3.4.1 Bcl-2 is efficiently knocked-down in PC3 cells.

In order to assess the knock-down efficiency, PC3 cells were transfected with non-targeting siRNA (siNT) or Bcl-2 (siBcl-2) siRNA pools (***Table 18***). Dharmafect transfection reagent was added to PC3 cells to facilitate siRNA transfection, including the non-transfected cells. Based on findings with siAtg5 and siAtg7 (**Figure *57*** and **Figure *58***) that demonstrated that 50nM siRNA were sufficient for efficient knock-down, transfection was performed with siNT and siBcl-2 at 50nM. Transfection efficiency for siBcl-2 was monitored over time at 24 – 144h. Knock-down of the Bcl-2 protein was only detected 144h after transfection (**Figure *58***). Bcl-2 knock-down could not be confirmed at earlier time-points (24 – 72h) due to generally low expression levels in all tested conditions (siNT, siBcl-2 and non-transfected cells). siBcl-2 transfection resulted in increased LC3BII/I ratio 72 to 144h after transfection, indicating induction of autophagy-initiation (**Figure *58***).

3.4.2 Bcl-2 knock-down promotes autophagy in PC3 cells but does not affect apoptosis modulation.

In order to confirm Bcl-2 knock-down and potential effects on autophagy, siBcl-2 PC3 cells were treated with mitoxantrone at 450nM, AdΔΔ at 500ppc or the combination of both

treatments 96h post-transfection (as explained in **Figure *27***), followed by assessment of expression of Bcl-2 and the autophagy markers LC3B and p62.

Transfection of PC3 cells with siRNA to Bcl-2 efficiently knocked-down the protein that was undetectable by immunoblotting 6 days after transfection (***Figure 66A***). Bcl-2 knock-down resulted in a trend towards increased levels of autophagy-initiation, demonstrated by an 1.5 – 2-fold increase in LC3II/I ratios compared to siNT cells (***Figure 66A and B***). Increased LC3II/I ratios were maintained in siBcl-2 cells treated with AdΔΔ or mitoxantrone or the combination of both agents. These results indicated that AdΔΔ infection did not prevent autophagy-initiation in siBcl-2 cells. A trend towards degradation of p62 was observed in siBcl-2 cells treated with AdΔΔ or mitoxantrone but not in untreated cells (***Figure 66A and C***).

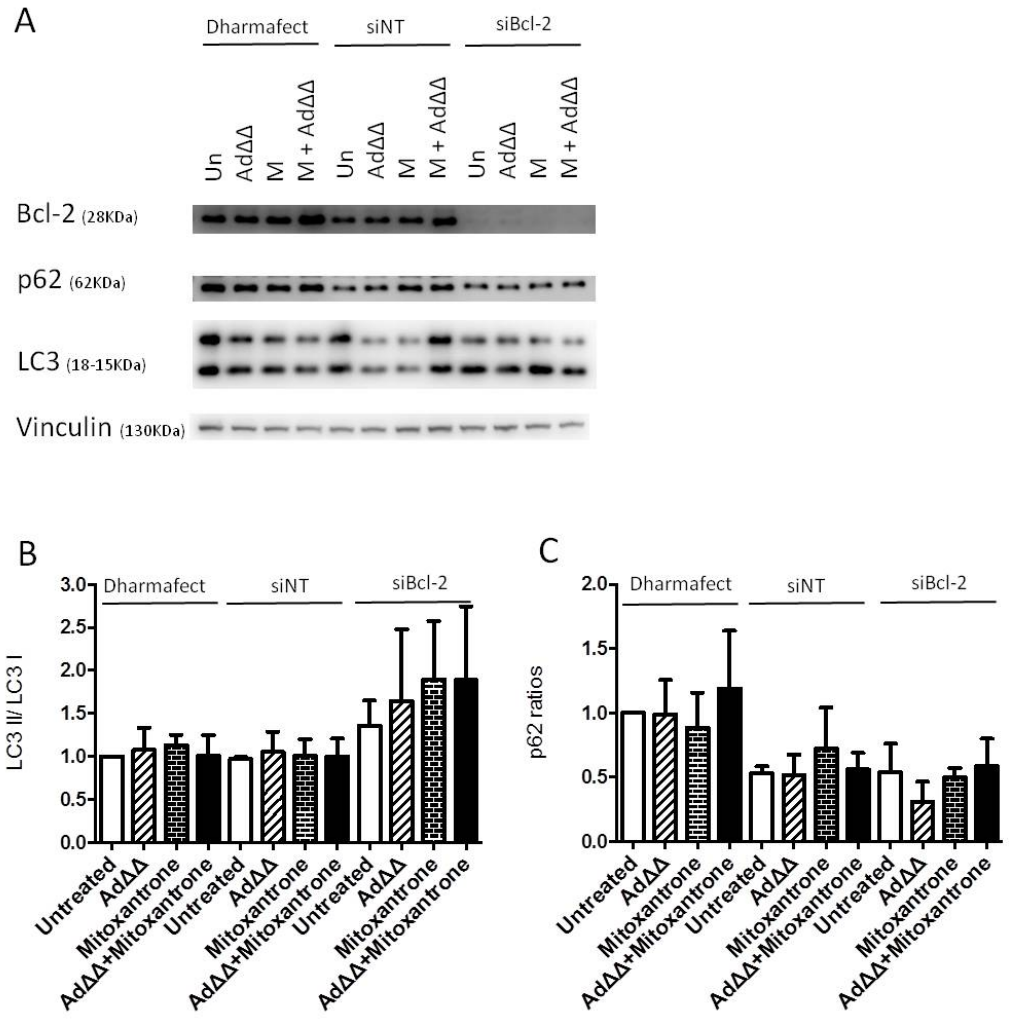

Figure 66. Bcl-2 knock-down promotes autophagy-initiation in PC3 cells. A. Fixed doses of AdΔΔ at 500ppc and/or mitoxantrone at 450nM were added to PC3 cells 4 days after transfection. Cells were transfected with non-targeting siRNA (siNT), Bcl-2 siRNA (siBcl-2) or the transfection reagent alone (Dharmafect). Samples were collected 48h after treatment. Representative immunoblots, n=3. **B.** Densitometry quantification of LC3B expression from A. LC3 ratio is expressed as LC3BII (lower band)

divided by LC3BI (higher band). Averages ± SD, n=3**. C.** Densitometry quantification of p62 expression from A. p62 ratio is expressed as p62 divided by loading control. Averages ± SD, n=3**. B and C**. One-way Annova with Bonferroni post-test was performed but resulted in no significant differences. Data generated with AdΔΔ batch 050314.

To investigate whether siBcl-2-induced autophagy-initiation was related to changes in apoptosis, depolarization of the mitochondrial membrane was assessed in siBcl-2 cells.

PC3 cells were treated with 100nM mitoxantrone, AdΔΔ at 500ppc or with the combination of both agents (**Figure *67***). Mitoxantrone-treatment increased mitochondrial depolarization in siNT and siBcl-2 cells. Infection with AdΔΔ resulted in a trend towards increased mitochondrial depolarization in mitoxantrone-treated siNT and siBcl-2 cells, when compared to mitoxantrone-only treated cells. No significant differences were observed in apoptosis induction in cells transfected with siBcl-2 and siNT cells at any of the tested treatments (mitoxantrone, AdΔΔ or the combined treatment) (**Figure *67***). Although a trend towards increased apoptosis with AdΔΔ in siBcl-2 cells was noted.

In conclusion, siBcl-2-mediated autophagy-induction did not correlate with changes in apoptosis.

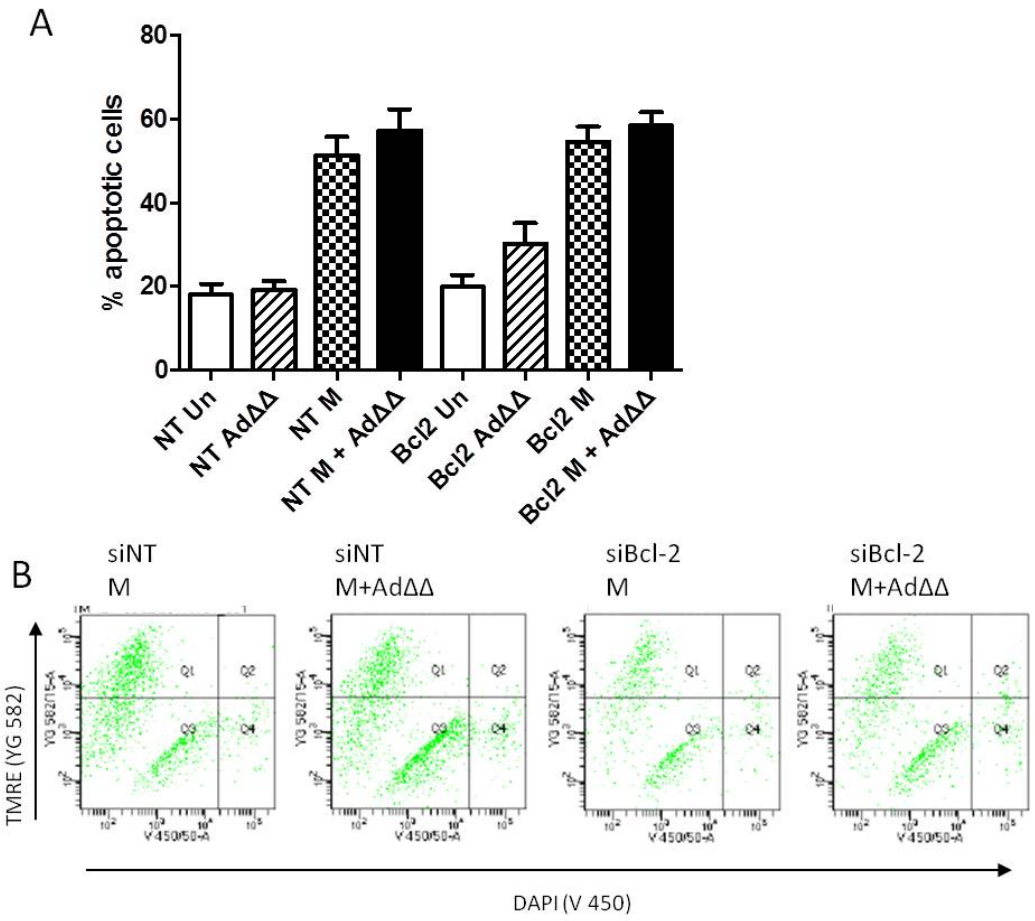

Figure 67. Bcl-2 Knock-down does not affect apoptosis modulation in PC3 cells. A. Fixed doses of AdΔΔ at 500ppc and/or mitoxantrone at 100nM were added to PC3 cells 24h after transfection. Cells were transfected with a non-targeting siRNA (NT) or Bcl-2 siRNA. Samples were collected 5 days after treatment. Mitochondrial depolarization was measured as an indication of apoptosis by loss of TMRE staining. TMRE and DAPI staining was detected with laser YG 582/15 and V 450/50, respectively. Averages ± SD, n=3. One-way Anova with Bonferroni post-test, no signicant differences between siNT and siBcl-2 cells. **B.** Representative FACS images from A. Data generated with AdΔΔ batch 050314.

3.4.3 Bcl-2 is required for AdΔΔ-mediated sensitization to mitoxantrone in PC3 cells.

In order to assess the effects of Bcl-2 knock-down on AdΔΔ-mediated sensitization to mitoxantrone, a fixed dose of AdΔΔ at 500ppc was added in combination with increasing doses of mitoxantrone to cells that had previously been transfected with a siNT or siBcl-2. Infection with AdΔΔ resulted in potent sensitization to mitoxantrone in siNT and non-transfected controls but did not sensitize the siBcl-2 transfected cells to mitoxantrone (***Figure 68A and B,*** **Figure 69,** **Table *26***). Co-infection with AdΔΔ reduced mitoxantrone EC_{50}-values by 72% and 74% for non-transfected cells and siNT transfected cells, respectively, but no change was observed in siBcl-2 transfected cells. Data were processed to generate sensitization

ratios (**Figure *68B***). The differences in EC_{50}-ratios for mitoxantrone alone or in combination with AdΔΔ were significant for non-transfected and siNT cells ($p<0.0001$). Unpaired t-test demonstrated that the addition of AdΔΔ to increasing doses of mitoxantrone did not decrease mitoxantrone EC_{50}-ratio in siBcl-2 transfected cells (***Figure 68B***). Similary to siAtg5 and siAtg7 cell viability studies, EC_{50}-values to mitoxantrone in non-transfected cells and siNT transfected cells were lower compared to the previously generated data (in non-transfection studies) EC_{50}-value = 2276.5 ± 419.8 nM (***Table 23***). More specifically, EC_{50}-values were 103.8 ± 39.4 nM, 121.2 ± 46.2 nM and 820.6 ± 674.2 nM for non-transfected cells, siNT transfected cells or siBcl-2 transfected cells, respectively. Interestingly, in siBcl-2 transfected cells treated with mitoxantrone as a single agent, the EC_{50}-value to mitoxantrone was greatly increased, compared to siNT or non-transfected controls. The increase in EC_{50}-value in siBcl-2 transfected cells was significant ($p<0.05$) when compared to siNT and non-transfected cells (***Figure 68A***). The increased EC_{50}-value might indicate that siBcl-2 tranfected cells were more resistant the drug, compared to siNT or non-transfected controls

The cell viability was reanalysed and normalised to untreated non-transfected cells at 60nM mitoxantrone alone, AdΔΔ at 500ppc or the combination of both treatments (***Figure 68C***). Transfection with siBcl-2 resulted in an overall increase in cell death when compared to siNT cells (***Figure 68C***). This increase was highly significant ($p<0.0001$) in non-treated siBcl-2 transfected cells when compared to siNT transfected cells. AdΔΔ infection at 500ppc or 60nM mitoxantrone treatment resulted in increased cell death in siBcl-2 cells compared to siNT transfected cells. This increase was significant ($p<0.05$) compared to both AdΔΔ infection and mitoxantrone treatment. Interestingly, the combined treatment of AdΔΔ and mitoxantrone resulted in a significant ($p<0.01$) increase in cell death in siNT transfected cells but did not significantly increase cell death in siBcl-2 transfected cells, when compared to mitoxantrone-only treated cells (***Figure 68C***). Effective Bcl-2 knock-down was confirmed in all the replicas, one representative immunoblot is shown (***Figure 68D***).

In summary, AdΔΔ-mediated sensitization to mitoxantrone was prevented in siBcl-2 transfected PC3 cells. These data indicated that expression of Bcl-2 was required for sensitization. In agreement with the role of Bcl-2 as a major anti-apoptotic factor, Bcl-2 knock-down alone resulted in increased cell death when compared to siNT transfected cells. In addition, the combined treatment of mitoxantrone with AdΔΔ significantly enhanced cell killing in siNT transfected but not in siBcl-2 transfected cells, suggesting that Bcl-2 expression was required for AdΔΔ-mediated enhancement of mitoxantrone-induced cell death. The

EC_{50}-value for mitoxantrone increased in siBcl-2 transfected cells, when compared to non-transfected cells and siNT transfected cells, indicating that siBcl-2 transfection desensitised PC3 cells to mitoxantrone.

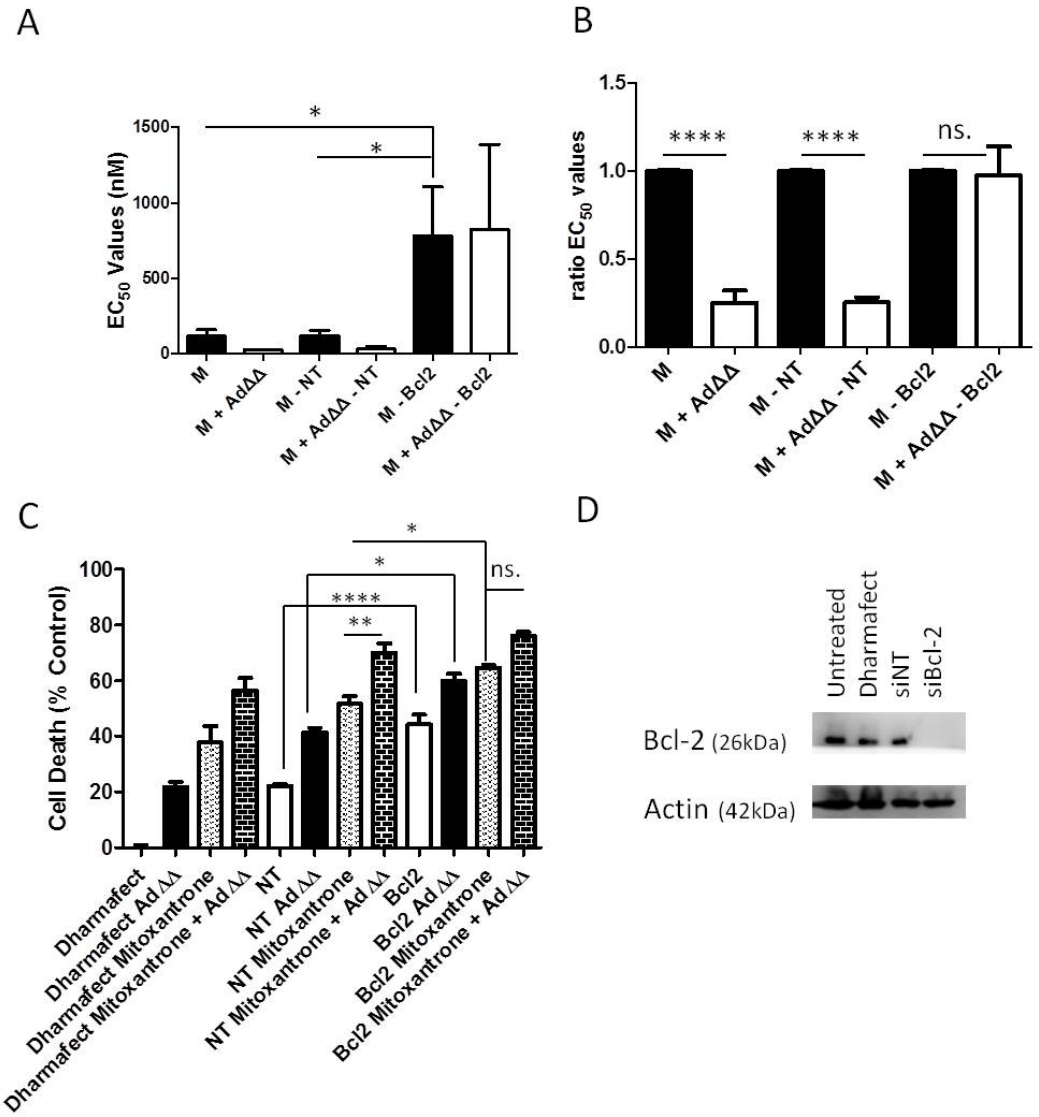

Figure 68. Bcl-2 expression is required for AdΔΔ-mediated sensitization to mitoxantrone in PC3 cells. **A.** A fixed dose of AdΔΔ that killed 10-30% of cells at 500ppc was added to mitoxantrone-treated cells. EC_{50}-values generated with dose-response curves to mitoxantrone in combination with a fixed dose of AdΔΔ at 500ppc. PC3 cells were previously transfected with a non-targeting siRNA (NT), Bcl-2 siRNA or the transfection reagent alone. Averages ± SEM, n=4. One-way Anova with Bonferroni post-test, *p<0.05. **B.** Ratio of EC_{50}-values in A, expressed as EC_{50} for mitoxantrone in the combined treatment / EC_{50} for mitoxantrone alone. Averages ± SEM, n=4. Unpaired t-test, ****p<0.0001. **C.** Selected fixed doses of mitoxantrone at 60nM, AdΔΔ at 500ppc and the combination of both in PC3 cells previously transfected with a non-targeting siRNA (NT), Bcl-2 siRNA or the transfection reagent alone (Dharmafect). Averages ± SEM, n=4**.** One-way Anova with Bonferroni post-test, *p<0.05, **p<0.01, **** p<0.0001. **A, B and C.** Cell viability was measured by MTS assay 5 days after treatment. **D.** Representative immunoblot for Bcl-2, n=3. PC3 cells were transfected with a non-targeting (NT) siRNA, Bcl-2 siRNA or the transfection reagent alone (Dharmafect). Data generated with AdΔΔ batch 050314.

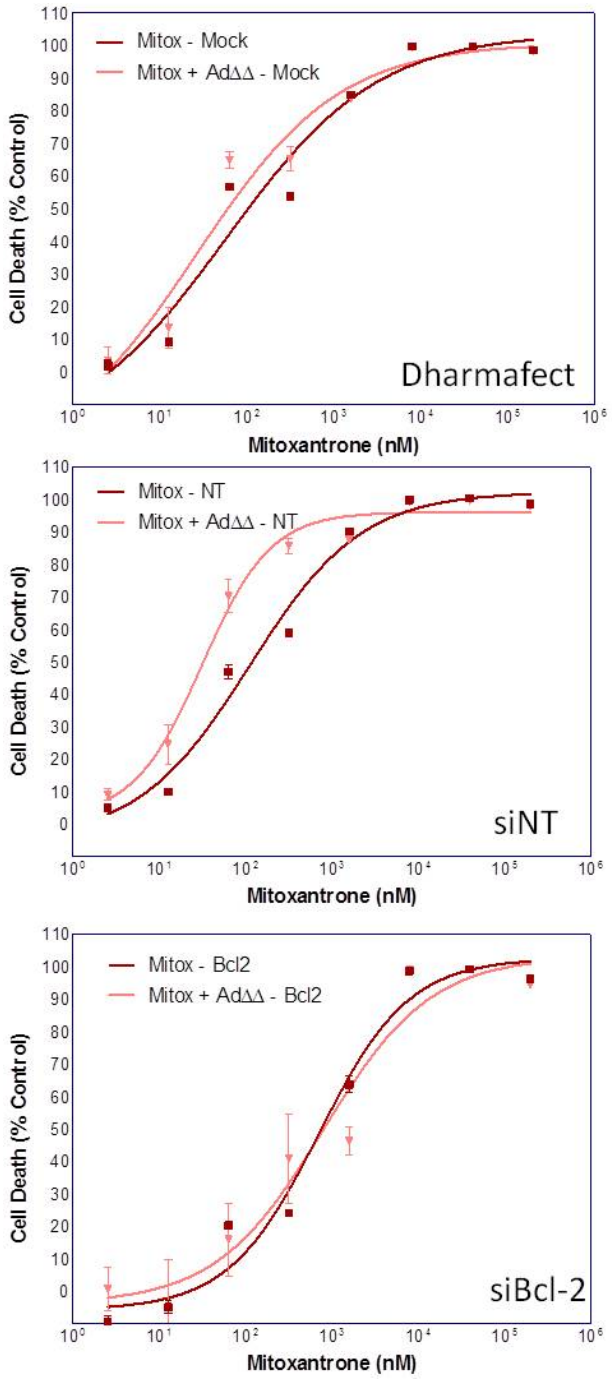

Figure 69. Representative dose-response curves from studies with siBcl2 transfected PC3 cells. The figure represents results from one experiment that generated the data in Figure 68. Dose-response curves to mitoxantrone in combination with fixed doses of AdΔΔ at 500ppc. PC3 cells transfected with a non-targeting (NT) siRNA, Bcl-2 siRNA (siBcl-2) or the transfection reagent alone.

Table 26. EC_{50}-values (±SD) generated for mitoxantrone in siBcl-2 transfected PC3 cells.

	Mitoxantrone (nM)
Dharmafect	103.8 ± 39.4
Dharmafect + AdΔΔ	25.1 ± 2.1
siNT	121.2 ± 46.2
siNT + AdΔΔ	34.0 ± 20.2
Target siRNA (Bcl-2)	820.6 ± 386.8
Target siRNA (Bcl-2) + AdΔΔ	882.4 ± 674.2

n=4

3.4.4 Bcl-2 knock-down might decrease expression levels of adenoviral proteins in mitoxantrone-treated PC3 cells.

In order to assess whether the knock-down of Bcl-2 interfered with the viral life cycle, adenoviral early and late gene expression was analysed by immunoblotting of E1A and hexon viral proteins in siBcl-2 PC3 cells.

The expression levels of E1A and hexon proteins were not affected in siBcl-2 transfected cells infected with AdΔΔ alone, compared to the siNT transfected cells or the non-transfected cells (**Figure *70***). However, mitoxantrone treatment in combination with AdΔΔ, resulted in a trend towards decreased expression of both E1A and hexon proteins when compared to the siNT transfected or the non-transfected cells. These data suggested that expression of early adenoviral proteins and AdΔΔ replication were slightly attenuated by mitoxantrone in siBcl-2 transfected PC3 cells. However, different replicas showed some variability in E1A and hexon expression levels in siBcl-2 transfected cells (n=3). Therefore, additional replicas would be needed to confirm the effect of mitoxantrone treatment in the expression of viral proteins in siBcl-2 tranfected cells.

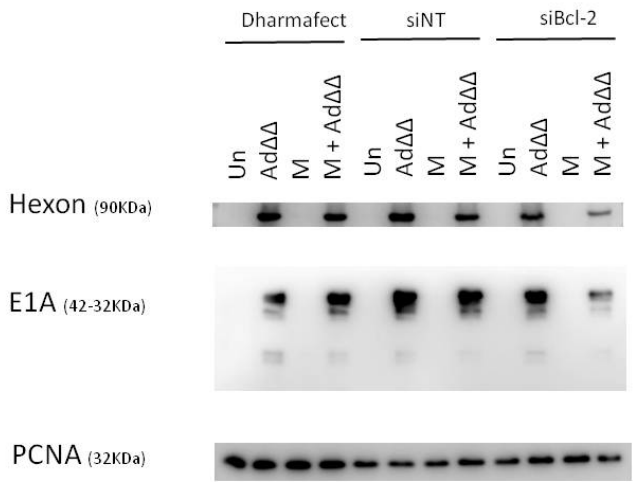

Figure 70. Bcl-2 knock-down interferes with the expression of viral early and late proteins in mitoxantrone-treated PC3 cells. Fixed doses of AdΔΔ at 500ppc and/or mitoxantrone at 450nM were added to PC3 cells 4 days after transfection. Cells were previously transfected with a non-targeting siRNA (siNT), Bcl-2 siRNA (siBcl-2) or the transfection reagent alone (Dharmafect). Samples were collected 48h after treatment. One out of 3 immunoblots for hexon and E1A proteins, n=3. Data generated with AdΔΔ batch 050314.

3.4.5 Mitoxantrone-treatment decreases Bcl-2 expression while AdΔΔ-infection attenuates the decrease.

I showed that the expression of the Bcl-2 protein was required for AdΔΔ-mediated sensitization to mitoxantrone (section 3.4.3). In order to investigate whether the combined treatment of mitoxantrone and AdΔΔ modulated Bcl-2 expression, PC3 cells were treated with Ad5wt, AdΔΔ or Ad12S in combination with selected doses of mitoxantrone, followed by assessment of changes in Bcl-2 mRNA and protein levels.

PC3 cells were treated with Ad5wt or AdΔΔ at 500ppc, 450nM mitoxantrone or the combination of virus and drug. Bcl-2 mRNA levels were detected by RT-qPCR (***Figure 71A***). Infection with Ad5wt or AdΔΔ did not significantly change Bcl-2 mRNA levels at the tested time-points (12 and 48h after treatment). Mitoxantrone-treatment at 450nM resulted in a non-significant increase in Bcl-2 mRNA levels both alone and in combination with Ad5wt or AdΔΔ at 12 and 48h post-treatment. Mitoxantrone-treatment decreased Bcl-2 mRNA levels to 0.3-fold at 12h post-treatment when compared to untreated cells. This decrease was maintained in the presence of Ad5wt and AdΔΔ.

Changes in Bcl-2 protein levels were assessed by immunoblotting. PC3 cells were treated with Ad5wt or AdΔΔ at 500ppc or Ad12S at 5000ppc, mitoxantrone at 225, 450 and 900nM,

or the combined treatment of virus and mitoxantrone. Treatment with increasing doses of mitoxantrone (225, 450 and 900nM) resulted in a dose-dependent decrease in Bcl-2 expression (***Figure 71B***). Single infection with Ad5wt, AdΔΔ or Ad12S slightly increased Bcl-2 expression levels when compared to the untreated control. Interestingly, the combined treatment of AdΔΔ or Ad12S with mitoxantrone resulted in a trend towards increased Bcl-2 expression when compared to mitoxantrone-only treated cells. More specifically, the combination of AdΔΔ with 225nM mitoxantrone resulted in increased Bcl-2 expression when compared to mitoxantrone only. The combination of Ad12S with all tested doses of mitoxantrone (225, 450 and 900nM) resulted in potent increases in Bcl-2 expression, when compared to mitoxantrone-only treated cells (***Figure 71B***). Infection with Ad5wt in mitoxantrone-treated cells did not result in any changes in Bcl-2 protein expression when compared to mitoxantrone-only treated cells.

In summary, mitoxantrone treatment decreased expression of Bcl-2 both at the mRNA and protein levels. Mitoxantrone-induced decreases in Bcl-2 protein levels were attenuated by AdΔΔ-infection and, more potently, by Ad12S-infection. Given that AdΔΔ-infection did not affect Bcl-2 mRNA levels but resulted in increased Bcl-2 protein expression, it can be concluded that AdΔΔ stabilized Bcl-2 protein and prevented its degradation. This decrease in drug-induced Bcl-2 protein degradation was likely caused by potent E1A expression as observed for cell infected with the non-replicating Ad12S mutant.

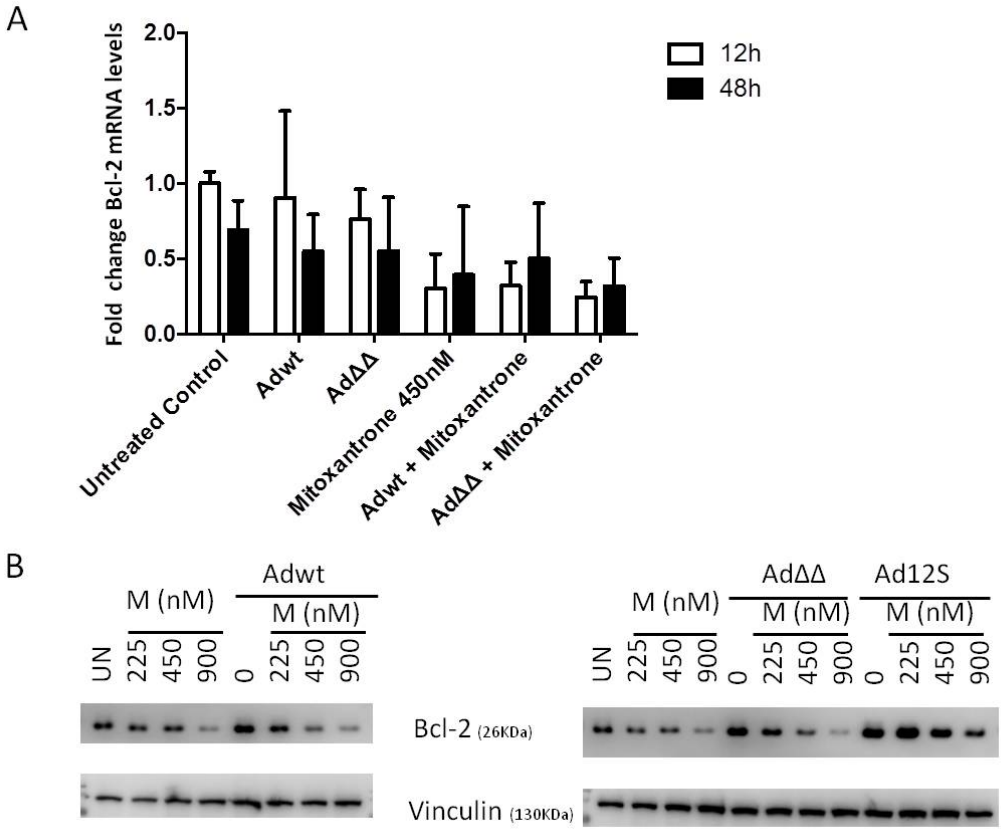

Figure 71. Mitoxantrone decreases Bcl-2 mRNA and protein expression in PC3 cells. **A.** PC3 cells were treated with a fixed dose of Adwt or AdΔΔ at 500ppc and/or mitoxantrone at 450nM and collected at indicated time points. Expression of Bcl-2 mRNA was measured by real-time qPCR. Averages ± SEM, n=3. **B.** PC3 cells were treated with fixed doses of Adwt, AdΔΔ at 500ppc or Ad12S at 5000ppc and/or mitoxantrone at 225, 450 and 900nM. Bcl-2 expression was assessed by immunoblotting. Representative immunoblots, n=2. Data generated with AdΔΔ batch 050314.

3.4.6 Summary and conclusions on the role of Bcl-2 in modulation of AdΔΔ-mediated sensitization to mitoxantrone.

To conclude, the findings demonstrated that the expression of Bcl-2 was required for AdΔΔ-mediated sensitization to mitoxantrone in PC3 cells. In agreement with the role of Bcl-2 as a major anti-apoptotic factor, knock-down alone caused more cell death compared to siNT transfected cells. In addition, siBcl-2 promoted autophagy initiation, demonstrated by increased LCB3II/I ratio, which was not counteracted by AdΔΔ infection. Furthermore, knock-down of Bcl-2 resulted in a trend towards attenuated expression of viral proteins in the presence of mitoxantrone. The decreased expression of viral proteins may contribute to the absence of AdΔΔ-mediated sensitization to mitoxantrone in siBcl-2 cells. In addition, mitoxantrone-treatment resulted in decreased expression of Bcl-2 at mRNA and protein

levels in non-transfected cells. Decreased Bcl-2 expresion was attenuated at the protein level by AdΔΔ infection or expression of the E1A protein alone, suggesting E1A-mediated stabilization of Bcl-2.

3.5 EXPLORING VIRAL EFFICACY AND AUTOPHAGY IN CULTURE MODELS MIMICKING THE TUMOUR MICROENVIRONMENT: 3-DIMENSIONAL CO-CULTURES OF STROMAL AND EPITHELIAL CELLS.

In order to investigate whether the increased cell killing and decreased activation of autophagy also occurred in PCa models that more accurately resembled the tumour microenvironment *in situ*, 3-dimensional cultures were developed. The epithelial prostate carcinoma PC3 or 22Rv1 cells were grown together with the normal human prostate stromal cells (PrSC) under various conditions in a matrix consisting of collagen type-I and matrigel.

3.5.1 Characterization of prostate stromal cells (PrSC)

The PrSC cells were characterised by assessing sensitivity to viral infection, drug-mediated cell killing, permissibility to replication and expression of cell surface receptors. Sensitivity to AdΔΔ- and mitoxantrone-induced cell death was determined in standard 2-dimensional cultures. PrSC cells were highly resistant to both virus and drug with EC_{50}-values of 3350 ± 719.4ppc and 1975.5 ± 34.69nM for AdΔΔ and mitoxantrone, respectively (**Figure *72***). EC_{50}-values in PrSC were similar to treatment-resistant PC3 cells (EC_{50}-values: 1048.9 ± 91.1ppc and 2276.6 ± 419.8nM for AdΔΔ and mitoxantrone, respectively; **Figure *28***, **Table *23***) but higher than treatment-sensitive 22Rv1 cells (EC_{50}-values: 155.7 ± 10.6ppc and 321.5 ± 30.7nM for AdΔΔ and mitoxantrone, respectively; **Figure *28***, **Table *23***).

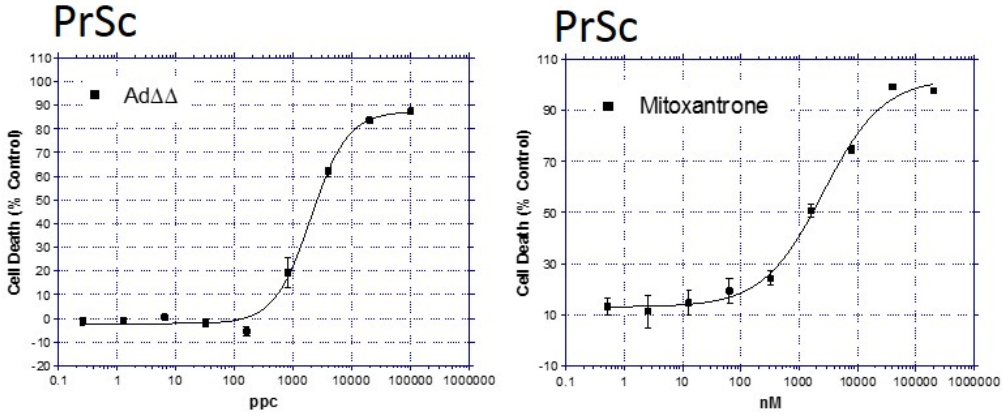

Figure 72. Representative dose-response curves in PrSC cells. PrSC cells were treated with increasing doses of AdΔΔ or mitoxantrone to generate dose-response curves and calculate EC_{50}-values. Cell viability was measured 3 days after treatment by MTS assay. Data were generated by Ms Julia San Millan, a visiting student in our team, using AdΔΔ batch 050314.

To determine the degree of infectivity PrSC cells were infected with the non-replicating AdGFP mutant followed by assessment of GFP expression by flow cytometry as a measure of transduction rates. Infection with AdGFP at 100 and 1000ppc resulted in a dose-dependent increase in viral transduction in 4.4 ± 0.9 and 30.9 ± 8.1 % of cells, respectively (***Figure 73A and B***). Infection levels in PrSC were similar to those in the highly insensitive PC3 cells, in which 100 and 1000ppc resulted in infection of 2.7 ± 0.3 and 22.3 ± 6.8 % of cells (**Figure *54***). The PrSC cells were highly insensitive to infection compared to 22Rv1 cells, in which 10ppc infected 26.2 ± 6.3 % of cells. These results demonstrated that the levels of infection were low and likely caused the higher EC_{50}-value in these cells, as could be expected for fibroblast cells that are not a natural target for adenovirus.

In order to further explore the causes of the poor infection levels, expression of the viral cell surface receptors was assessed; hCAR and integrins $\alpha_v\beta3$ and $\alpha_v\beta5$ that facilitate adenoviral attachment and internalization, respectively. PrSC cells expressed integrins $\alpha_v\beta3$ and $\alpha_v\beta5$ in 31.8 ± 30.3 and 31.7 ± 16.7 % of cells, respectively (***Figure 73C and D***). Interestingly, integrin $\alpha_v\beta3$ and $\alpha_v\beta5$ expression in PrSC cells was higher than that in 22Rv1 cells (4.2 ± 3.2% and 15.6 ± 5.5%; ***Figure 54***) and in PC3 cells, which were previously reported to express $\alpha_v\beta3$-integrin and $\alpha_v\beta5$-integrin at 4.8 ± 0.1% and 6.5 ± 0.2% of cells, respectively (Adam, Ekblad et al. 2012). Expression of hCAR was barely detectable in PrSC cells (***Figure 73C and D***). hCAR expression was similar in PC3 cells with only 2.9 ± 0.2% of cells positive for CAR, but much lower than in 22Rv1 cells, in which hCAR was expressed in 13.8 ± 0.7% of cells (***Figure 54***).

To determine whether the PrSC cells were permissive to viral replication, cells were infected with Ad5wt or AdΔΔ at 100ppc and replication was determined 24-72h post-infection with the $TCID_{50}$ assay (***Figure 73E***). As expected, Ad5wt replicated to approximately 100-fold higher levels than AdΔΔ and replication was time dependent. At 24, 48 and 72h post-infection Ad5wt replication was $1.6x10^8 \pm 2.4x10^7$, $2.8x10^9 \pm 2.5x10^9$ and $5.3x10^{10} \pm 2.3x10^{10}$ pfu/ml, respectively, while AdΔΔ was $1.3x10^6 \pm 3.8x10^5$, $3.7x10^7 \pm 2.6x10^7$ and $4.5x10^8 \pm 5.1x10^8$ pfu/ml, respectively (***Figure 73E***).

In conclusion, PrSC cells were moderately resistant to adenoviral infection, which may be explained by low expression levels of hCAR. The expression of $\alpha_v\beta3$- and $\alpha_v\beta5$-integrins appeared not to sufficiently facilitate infection in the absence of hCAR in PrSC cells similar to the findings in PC3 cells. In addition, AdΔΔ replicated poorly in PrSC compared to Ad5wt confirming the AdΔΔ-selectivity for cancer cells, as previously demonstrated (Oberg, Yanover et al. 2010). Therefore, in agreement with other observations that adenovirus poorly

replicates in non-epithelial normal cells (Wold and Horwitz 2007, Arnberg 2012) high EC_{50}-values for AdΔΔ in PrSC cells could be explained by the observed low infection and replication levels in these cells.

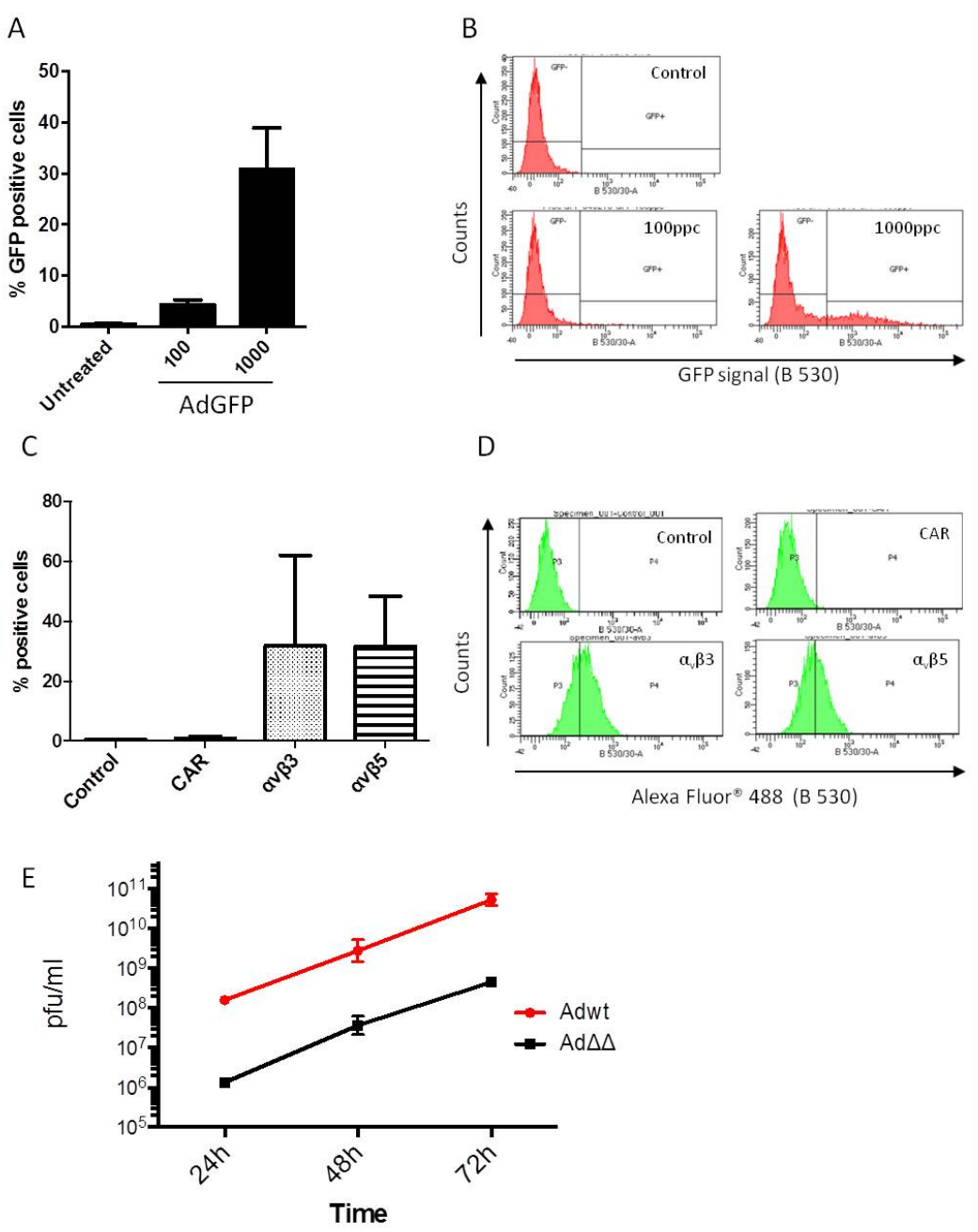

Figure 73. PrSC are insensitive to adenovirus infection due to low expression levels of Ad-receptors. **A.** PrSC cells were infected with AdGFP at 100 and 1000ppc. GFP expression was measured by flow cytometry 48h after infection, n=2. The GFP signal was detected with laser B 530/30. **B.** Representative FACS images from A. **C.** Expression of indicated cell surface receptors in PrSC cells measured by flow cytometry**,** n=2. Alexa Fluor 488-labelled antibody signal was detected with laser B 530/30. **D.** Representative FACS images from C. **E.** PrSC were were infected with Adwt or AdΔΔ at 100ppc and collected at indicated time points after infection (24, 48 and 72h), n=2. Viral bursts were measured by a $TCID_{50}$ assays. **A-E.** Data produced in collaboration with Ms Julia San Millan. Data generated with AdΔΔ batch 050314.

3.5.2 PrSC cells stimulate 22Rv1 and PC3 cells to grow and invade into the 3-dimensional cultures.

The PrSC cells were mixed with either PC3 or 22Rv1 cells at a ratio of 2:1 (stromal/epithelial cells) and seeded on top of a collagen/matrigel matrix, in transwells®. The bottom chamber contained 10% FBS-DMEM and the top of the gel with cells was immersed in 0% FBS-DMEM to promote cell invasion. Cell growth and invasion into the gel in 22Rv1 or PC3 cultures cells was observed in preliminary studies (**Figure *74***). 22Rv1 cells seeded alone on top of the collagen/matrigel matrix were viable and grew to form 5 – 8 cell layers but did not invade into the gel (***Figure 74A***). In contrast, the co-cultures of PrSC and 22Rv1 cells resulted in increased growth and thickness of the cell layer and invasion into the gel (indicated by double-head arrows) (***Figure 74B***). PC3 cells seeded alone on collagen/matrigel matrix did not appear to proliferate and formed only a viable monolayer on top of the gel (***Figure 74C***). Similar to 22Rv1, the co-cultures of PC3 and PrSC cells greatly promoted cell growth and increased the thickness of the cell layer (***Figure 74D***). Cell invasion into the gel was also seen in the PrSC-PC3 co-cultures (single-head arrow) but was much less compared to the PrSC-22Rv1 co-cultures.

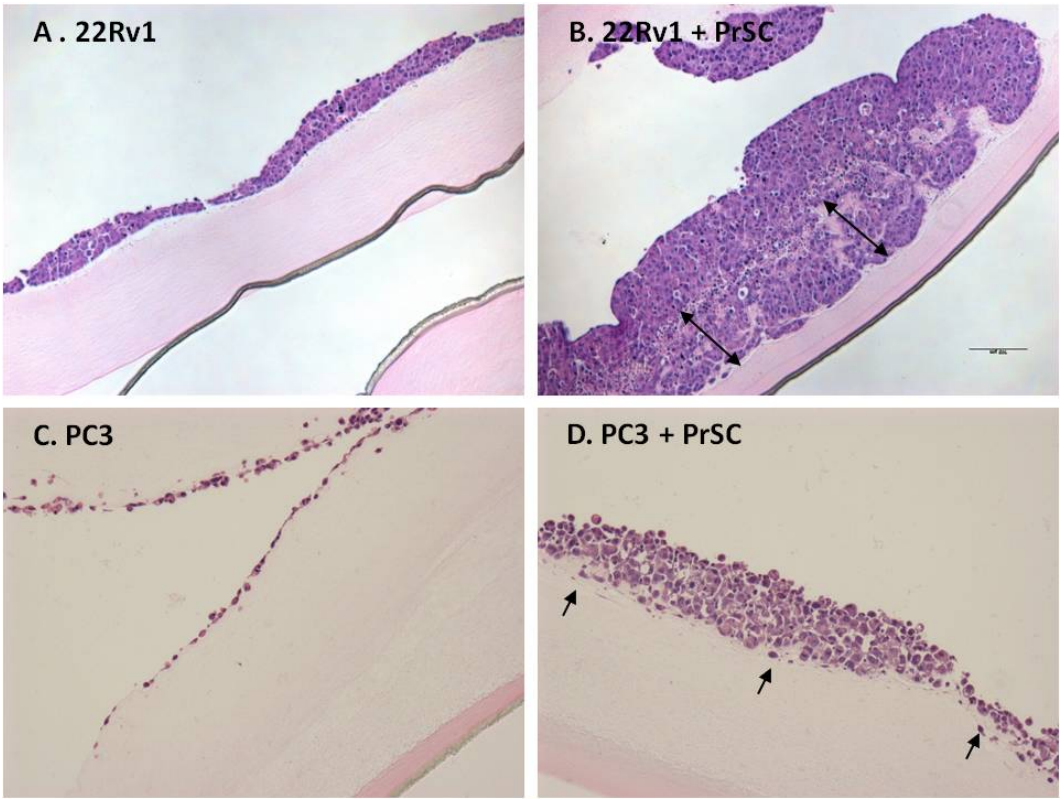

Figure 74. The presence of stromal cells (PrSC) promotes epithelial cancer cell growth in 3-dimensional cultures. A. 22Rv1 cells were seeded on top of a collagen/matrigel and fixed 10 days after seeding. **B.** 22Rv1 and PrSC cells were previously mixed and seeded on top of a collagen/matrigel

at a ratio of 2:1 (stromal/epithelial cells) and fixed 10 days after seeding. Double-head arrows show invasion into the gel. **C.** PC3 cells were seeded on top of a collagen/matrigel and fixed 8 days after seeding. **D.** PC3 and PrSC cells were previously mixed and seeded on top of a collagen/matrigel at a ratio of 2:1 (stromal/epithelial cells) and fixed 8 days after seeding. Single-head arrows indicate single cell invasion. **A-D.** Samples were fixed in formalin, embedded in paraffin, sectioned (4µm) and stained for Hematoxylin and Eosin (H/E).

3.5.3 The combination of AdΔΔ and mitoxantrone efficiently prevents growth and invasion of 22Rv1 and PC3 cells in the 3-dimensional co-cultures.

To determine the efficacy of AdΔΔ-mediated enhancement of mitoxantrone-induced cell death, the 3-dimensional PrSC-PC3 and PrSC-22Rv1 co-cultures were treated with the combination of virus and drug. Because of the multiple cell layers, viral doses were increased around 10-fold and 2-fold for 22Rv1 and PC3 cells, respectively, compared to the 2-dimensional cultures and both virus and drug were added 2-3 times over the indicated time-periods.

In a preliminary study, 3-dimensional PrSC-PC3 co-cultures were treated with AdΔΔ at 1000ppc, mitoxantrone at 450nM or the combination of both treatments on day 3 and 5 and analysed 8 days after seeding (***Figure 75***). The co-cultures of PrSC-PC3 cells started to grow and invade into the gel as early as 3 days after seeding (***Figure 75B***) and continued growing and invading for a total of 8 days, when they were terminated and fixed (***Figure 75C;*** invasion is indicated with black arrows). In contrast, PC3 cells without PrSC, formed only a monolayer on top of the gel even after 8 days (***Figure 75A***). Mitoxantrone-treatment at 450nM was added both on top a bellow the cells and resulted in a thinner cell layer with fewer invading cells compared to non-treated cells (***Figure 75D and G***). Infection with AdΔΔ at 1000ppc, added on top of the cells only, also caused higher levels of cell death compared to untreated control cells, seen as a thinner cell layer (***Figure 75E and G***). However, AdΔΔ did not appear to decrease PrSC-mediated invasion of PC3 into the matrix. The combined treatment of AdΔΔ and mitoxantrone resulted in decreased thickness of the cell layer when compared to untreated control cells (***Figure 75F and G***). In addition, cells on the top of the cell layer detached, suggesting that they were dying as a result of the treatment. Surprisingly, the combined treatment appeared to have a thicker cell layer compared to the corresponding single agent treatments. However, these observations were from one experiment and would need to be repeated and quantified to conclude any differences between treatments.

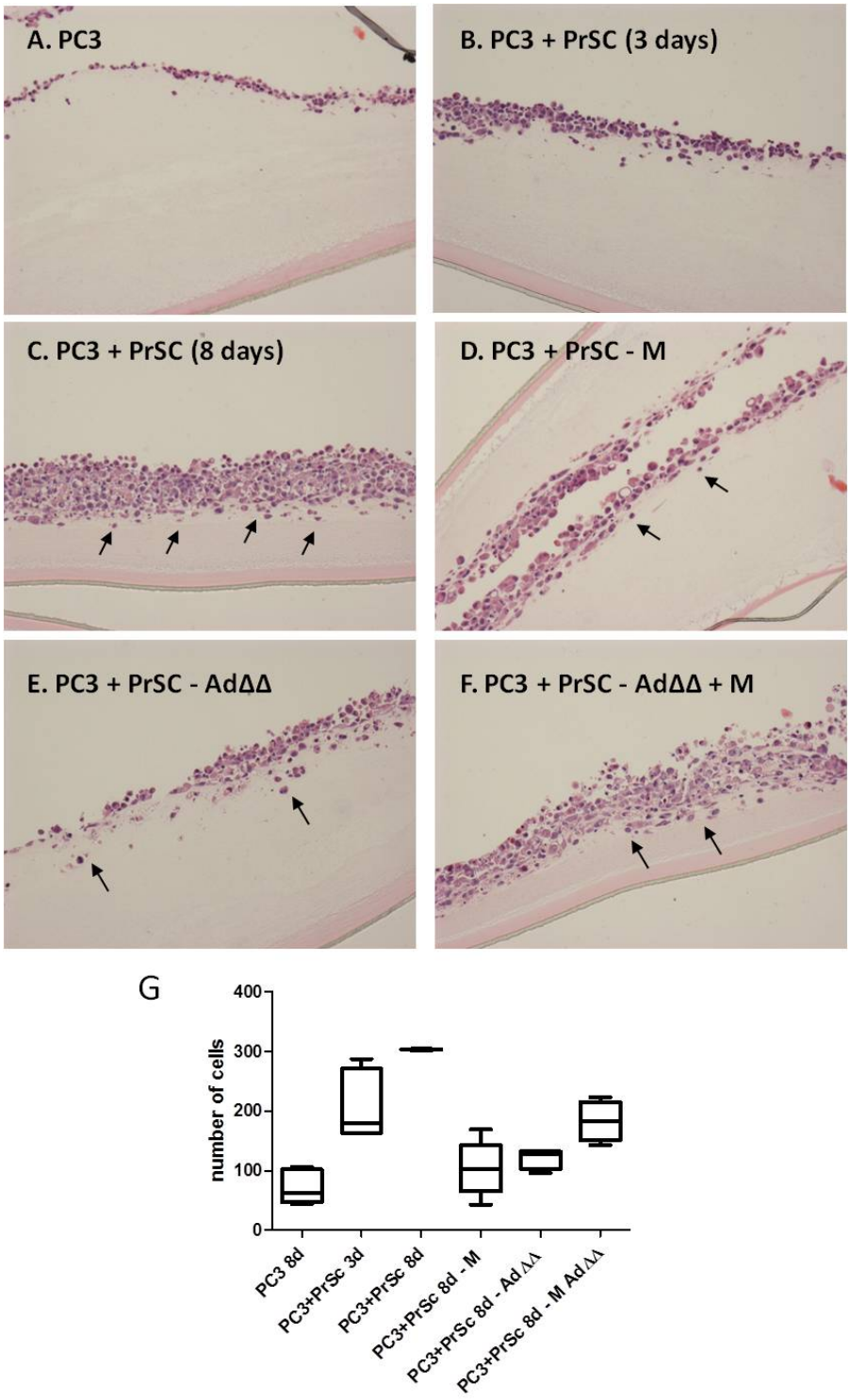

Figure 75. AdΔΔ and mitoxantrone treatments kill PC3 cells in 3-dimensional co-cultures. A. PC3 cells seeded alone on top of collagen/matrigels and collected 8 days after seeding**. B.** PC3 and PrSC cells were seeded on top of collagen/matrigels and collected 3 days after seeding. **C – D.** PC3 and PrSC cells were seeded on top of collagen/matrigels at a ratio of 2:1 (stromal/epithelial cells) and collected 8 days after seeding. Black arrows indicate invasion. **C.** Untreated**. D.** Cells were treated on day 3 and 5 after seeding with mitoxantrone at 450nM. **E.** Cells were infected on day 3 and 5 after seeding with AdΔΔ at 1000ppc. **F.** Cells were treated on day 3 and 5 after seeding with mitoxantrone at 450nM and AdΔΔ at 1000ppc. **A-F.** Samples were fixed in formalin, embedded in paraffin, sectioned (4μm) and

stained for Hematoxylin and Eosin (H/E). **G.** Quantification of the number of cells in each tissue, box and whikers graph, n=1 (3 to 6 sections per condition). Data generated with AdΔΔ batch 050314.

In order to investigate the cell killing efficacy of AdΔΔ in PrSC-22Rv1 3-dimensional cultures, cells were infected with AdΔΔ at 100ppc on day 2 and 6 after seeding. This dose was 4-fold higher than the highest 25ppc dose used in 2-dimensional mono-cultures of 22Rv1 cells. Infection with AdΔΔ efficiently killed cells in 3-dimensional cultures, seen as decreased thickness of the cell layer and decreased invasion into the matrix (indicated with black arrow), but did not result in a complete elimination of the cell layers (**Figure *76***). Therefore, a higher dose of AdΔΔ would be needed in order to completely eliminate cell growth in 3-dimensional cultures.

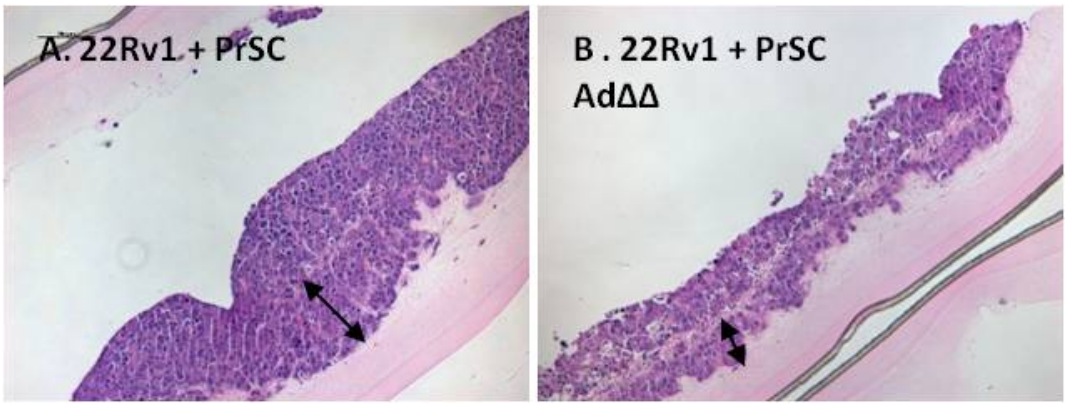

Figure 76. AdΔΔ-infection kills 22Rv1 cells in 3-dimensional co-cultures with PrSC cells. (A - B) 22Rv1 and PrSC cells were seeded on top of collagen/matrigels at a ratio of 2:1 (stromal/epithelial cells) and fixed 10 days after seeding. Black arrows indicate invasion. Samples were fixed in formalin, embedded in paraffin, sectioned (4µm) and stained for Hematoxylin and Eosin (H/E). **A.** Untreated control. **B.** Cells were infected on day 2 and 6 after seeding with AdΔΔ at 100ppc, n=1. Data generated with AdΔΔ batch 050314.

Next, the PrSC-22Rv1 co-cultures were treated with AdΔΔ at 200ppc, mitoxantrone at 25nM or the combination of both agents. Mitoxantrone treatment was added on day 2 and 6 after seeding and AdΔΔ on day 2 and 6, or on day 2, 4 and 6, and cultures were terminated, fixed and stained with H/E 10 days after seeding (**Figure *77***). Cell growth but not invasion was detected as early as 2 days after seeding (**Figure *77A***). The untreated PrSC-22Rv1 co-cultures showed a distinct morphology with the majority of cells invading into the gel. This morphology was only detected in the untreated sample and might be due either to high levels of proliferation of the PrSC-22Rv1 cells or to defects in the collagen/matrigel during preparation (**Figure *77B***). The number of cells increased around 4-fold after 10 days compared to the cells collected at 2 days (**Figure *77H***). Mitoxantrone-treatment at 25nM caused a

thinner cell layer and fewer invading cells compared to the untreated cells (**Figure *77C and H***). AdΔΔ-infection also caused reduced thickness and invasion when compared to the untreated control cells (**Figure *77D and H***). A characteristic invasion pattern in which cells formed channels to invade into the gel was observed in tissues infected at day 2 and 6 (**Figure *77D***). The combined treatment of mitoxantrone and AdΔΔ resulted in a trend towards decreased cell growth and invasion when compared to the single agent treatments (**Figure *77E, G and H***). The reduction in cell growth and invasion was higher when AdΔΔ was added three times compared to two times in combination with mitoxantrone (**Figure *77G and H*)**.

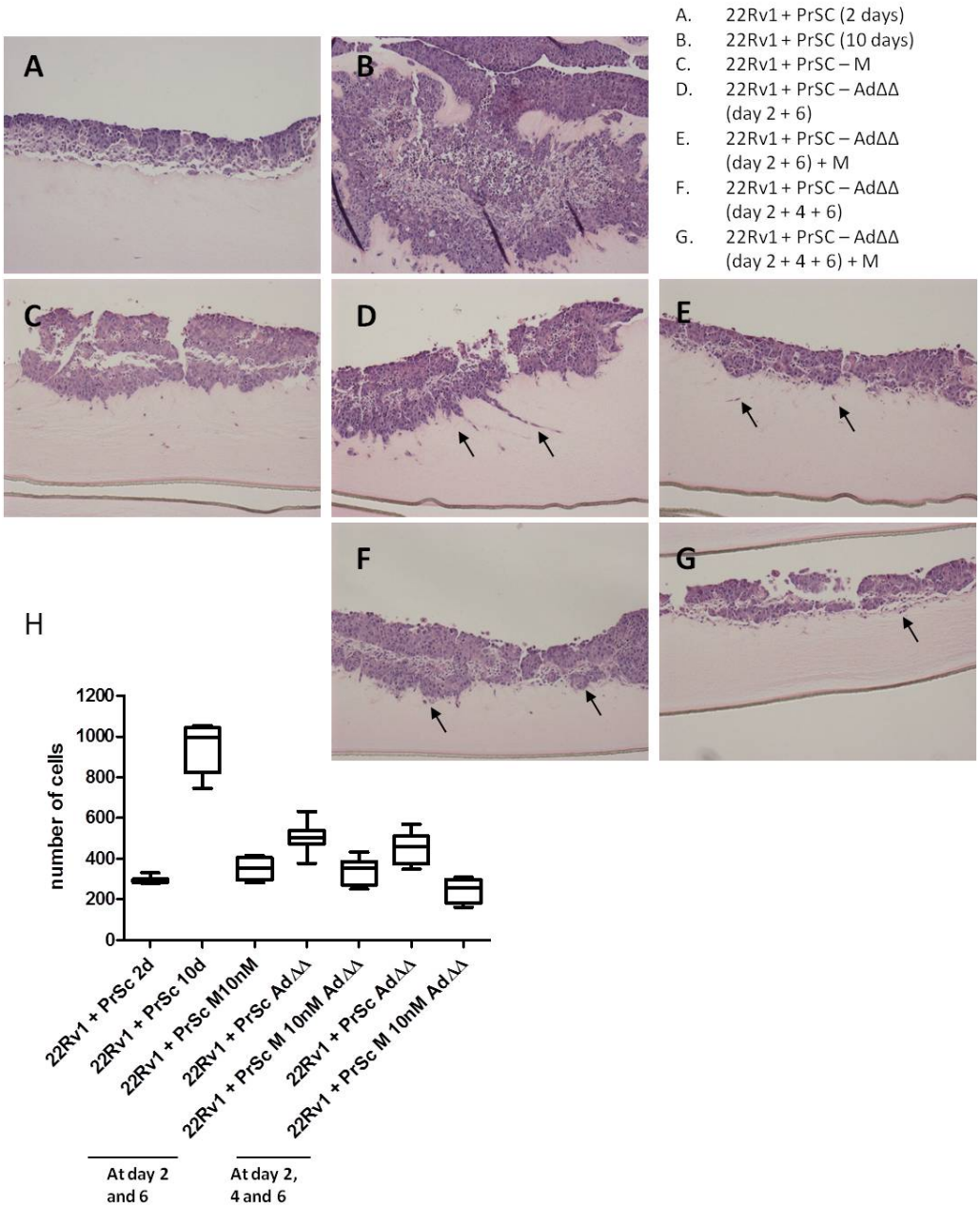

Figure 77. AdΔΔ-infection and mitoxantrone-treatment kill 22Rv1 cells in 3-dimensional co-cultures. **A.** 22Rv1 and PrSC cells were seeded on top of collagen/matrigels and fixed 2 days after seeding,

untreated. **B – G.** 22Rv1 and PrSC cells were seeded on top of collagen/matrigels at a ratio of 2:1 (stromal/epithelial cells) and fixed 10 days after seeding. Black arrows indicate invasion. **B.** Untreated control. **C.** Cells were treated on day 2 and 6 after seeding with mitoxantrone at 25nM. **D.** Cells were infected on day 2 and 6 after seeding with AdΔΔ at 200ppc. **E.** Cells were treated on day 2 and 6 after seeding with mitoxantrone at 25nM and AdΔΔ at 200ppc. **F.** Cells were infected on day 2, 4 and 6 after seeding with AdΔΔ at 200ppc. **G.** Cells were treated on day 2 and 6 after seeding with mitoxantrone at 25nM and infected with AdΔΔ at 200ppc on day 2, 4 and 6 after seeding. **A-G.** Samples were fixed in formalling, embebed in paraffin, sectioned (4µm) and stained for Hematoxylin and Eosin (H/E). **H.** Quantification of the number of cells in each tissue, box and whiskers graph, n=1 (4 to 8 sections per condition). Data generated with AdΔΔ batch 050314.

In summary, these preliminary studies in PC3 and 22Rv1 cells co-cultured with PrSC cells indicated that cell killing in response to mitoxantrone, AdΔΔ or the combination of both treatments was efficacious also in the 3-dimensional models. In PrSC-22Rv1 cultures, cell death as a result of AdΔΔ-infection did not seem to be dose-dependent since 200ppc did not cause more cell death than 100ppc when administered twice. However, the addition of AdΔΔ at 200ppc three times, resulted in increased cell killing efficacy when compared to the same dose of AdΔΔ added twice. The combined treatment of AdΔΔ and mitoxantrone caused a trend towards reduced cell growth in PrSC-22Rv1 co-cultures, when compared single agent treatments.

3.5.4 AdΔΔ infects both 22Rv1 and PrSC cells in the 3-dimensional co-culture models.

I have previously shown that PrSC cells expressed low levels of hCAR and were resistant to adenoviral infection (**Figure *73***), as it was expected for non-epithelial normal cells (Wold and Horwitz 2007, Arnberg 2012). To investigate whether AdΔΔ infected PrSC cells in the 3-dimensional co-culture models, the cultures were stained for the early viral protein E1A. The cells were also stained for smooth muscle actin (α-SMA) as a marker for stromal fibroblast cells (Gravina, Mancini et al. 2013).

The PrSC-22Rv1 co-cultures were treated with AdΔΔ at 100ppc alone or in combination with mitoxantrone at 25nM at day 2 and 6 after seeding and fixed 10 days after seeding, followed by staining for E1A and α-SMA (**Figure *78***). The α-SMA staining was detected in PrSC-22Rv1 co-cultures (**Figure *78B, C and D***) but not when 22Rv1 cells were grown alone confirming the specificity of the antibody (**Figure *78A***). The E1A staining was detected in both PrSC and 22Rv1 cells after infection with AdΔΔ both alone and in combination with mitoxantrone (**Figure *78C and D***). The majority of infected cells were not positive for α-SMA demonstrating that AdΔΔ predominantly infected the epithelial 22Rv1 cells as expected. However, cells positive for

both E1A and α-SMA (PrSC cells; indicated with white arrows) were detected although these double stained cells were fewer than cells positive only for E1A (22Rv1 cells) (**Figure *78C and D***).

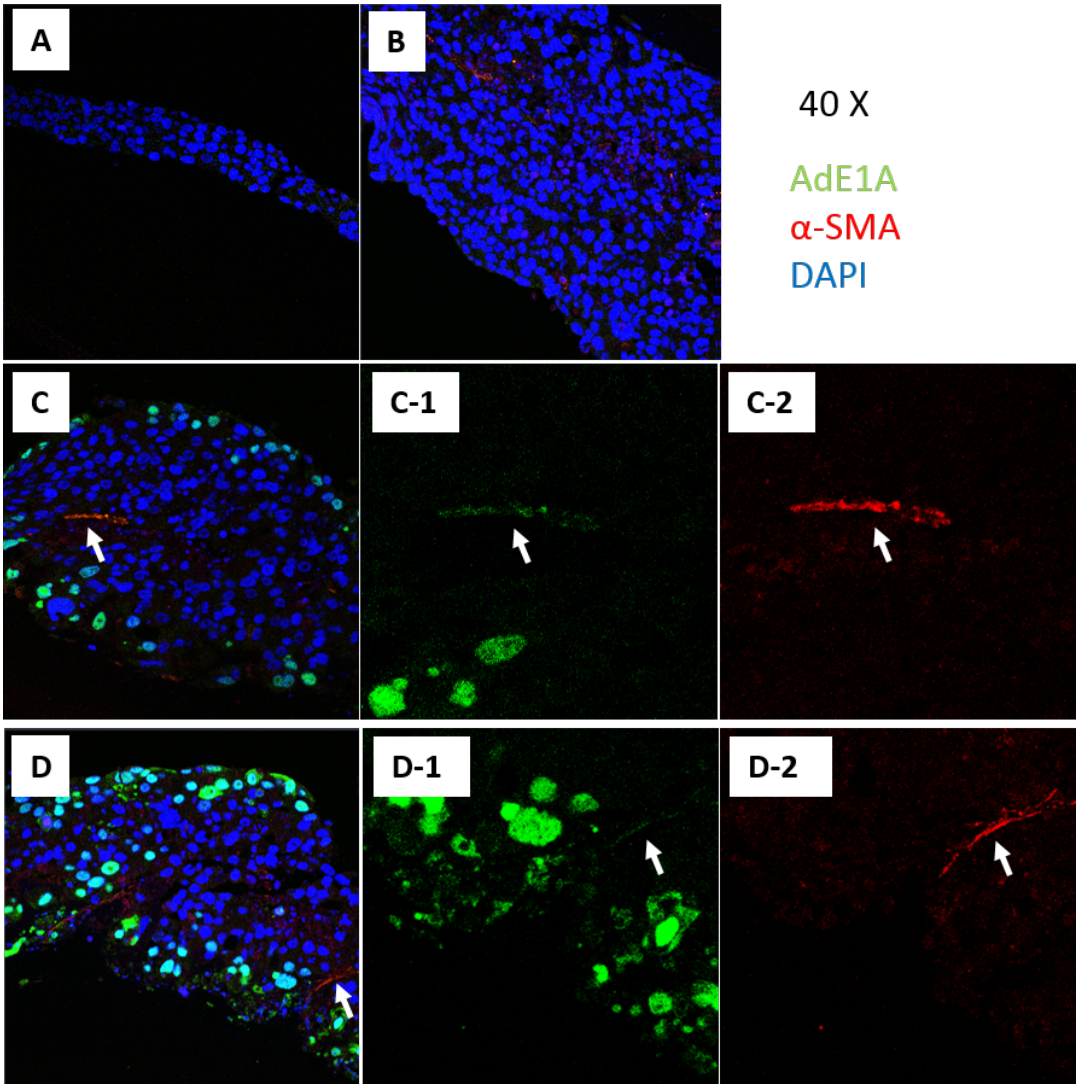

Figure 78. AdΔΔ infects both PrSC and 22Rv1 cells in 3-dimensional co-cultures. A. 22Rv1 cells were seeded on top of collagen/matrigels and fixed 10 days after seeding **B-D**. 22Rv1 and PrSC cells were seeded on top of collagen/matrigels at a ratio of 2:1 (stromal/epithelial cells) and fixed 10 days after seeding. **B.** Untreated control. **C.** Cells were infected on day 2 and 6 after seeding with AdΔΔ at 100ppc. **C-1.** Green channel. Magnification of co-stained cell (E1A positive staining). **C-2.** Red channel. Magnification of co-stained cell (α-SMA). **D.** Cells were treated on day 2 and 6 after seeding with mitoxantrone at 25nM and infected with AdΔΔ at 100ppc. **D-1.** Green channel. Magnification of co-stained cell (E1A positive staining). **D-2.** Red channel. Magnification of co-stained cell (α-SMA). All sections were stained with AdE1A (green) and α-SMA (red). Double positive cells for AdE1A and α-SMA appear as orange staining. Data generated with AdΔΔ batch 050314.

3.5.5 The early autophagy marker LC3BII does not co-stain with adenovirus E1A in 3-dimensional co-cultures of PC3 or 22Rv1 cells with PrSC cells.

In order to investigate whether the mitoxantrone-mediated initiation and the AdΔΔ-dependent attenuation of autophagy, occurred in the 3-dimensional co-culture models, the cells were co-stained for E1A and LC3II. The conversion of LC3BI to LC3BII was detected as punctate staining, which corresponded to LC3BII-positive autophagosome vesicles.

The PrSC-PC3 co-cultures treated with AdΔΔ at 1000ppc, mitoxantrone at 450nM or the combined treatment (***Figure 75***), were stained for E1A and LC3BII (**Figure *79***). E1A staining was only detected in AdΔΔ infected cultures, both in cells infected with AdΔΔ alone and in combination with mitoxantrone and showed that around 10-15% of cells were infected (**Figure *79F, G, H, I and J***). LC3BII staining was detected in cells regardless of treatment. The untreated cells showed around 10% of LC3BII positive cells (**Figure *79B, C, and J***). There were no detectable significant differences in LC3BII staining between untreated cells, mitoxantrone alone or in combination with AdΔΔ. Infection with AdΔΔ alone resulted in decreased LC3BII staining compared to untreated and mitoxantrone treated cells. Interestingly, none of the infected cells were positive for LC3BII staining neither in cells treated with AdΔΔ alone or in combination with mitoxantrone (**Figure *79F, G, H, I and J***).

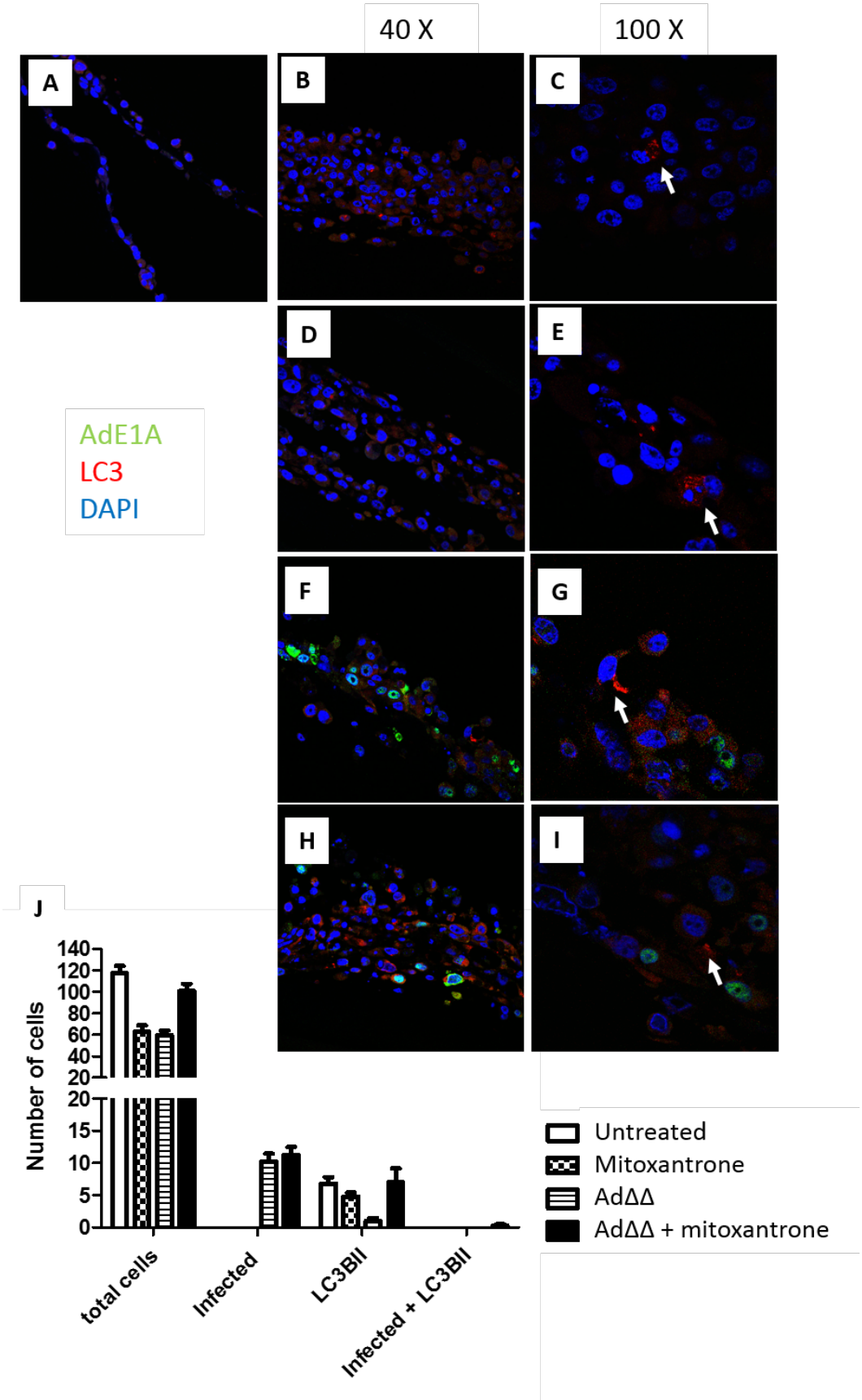

Figure 79. AdΔΔ-infected PC3 cells are not positive for LC3BII in the 3-dimensional co-cultures. A. PC3 cells were seeded on top of collagen/matrigels and fixed 8 days after seeding. **B – I.** PC3 and PrSC

cells were seeded on top of collagen/matrigels at a ratio of 2:1 (stromal/epithelial cells) and fixed 8 days after seeding. White arrows indicate LC3BII positive cells. **B – C.** Untreated control. **D – E.** Cells were treated on day 3 and 5 after seeding with mitoxantrone at 450nM. **F – G.** Cells were treated on day 3 and 5 after seeding with AdΔΔ at 1000ppc. **H – I.** Cells were treated on day 3 and 5 after seeding with mitoxantrone at 450nM and AdΔΔ at 1000ppc. All sections were stained with AdE1A (green) and LC3 (red). **J.** Quantification of the total number of cells and cells positive for E1A or LC3 staining per section at 40X, n=1 (3-4 sections per condition).

Staining for LC3BII and E1A was also explored in the PrSC-22Rv1 co-cultures treated with AdΔΔ 100ppc alone or in combination with mitoxantrone at 25nM at day 2 and 6 after seeding and collected at day 10 (**Figure *78***). E1A signals were only detected in AdΔΔ infected cells (**Figure *80***) and showed that around 10% of cells were infected cells (**Figure *80C and G***). Surprisingly, the addition of mitoxantrone increased infection to 30% of cells (**Figure *80E and G***). LC3BII staining was detected in cells treated with all conditions and was decreased as a result of AdΔΔ-infection, both alone and in combination with mitoxantrone (**Figure *80C, E and G***). In agreement with the PrSC-PC3 co-culture data, none of the infected cells were positive for LC3BII staining in PrSC-22Rv1 (**Figure *80C, E and G***).

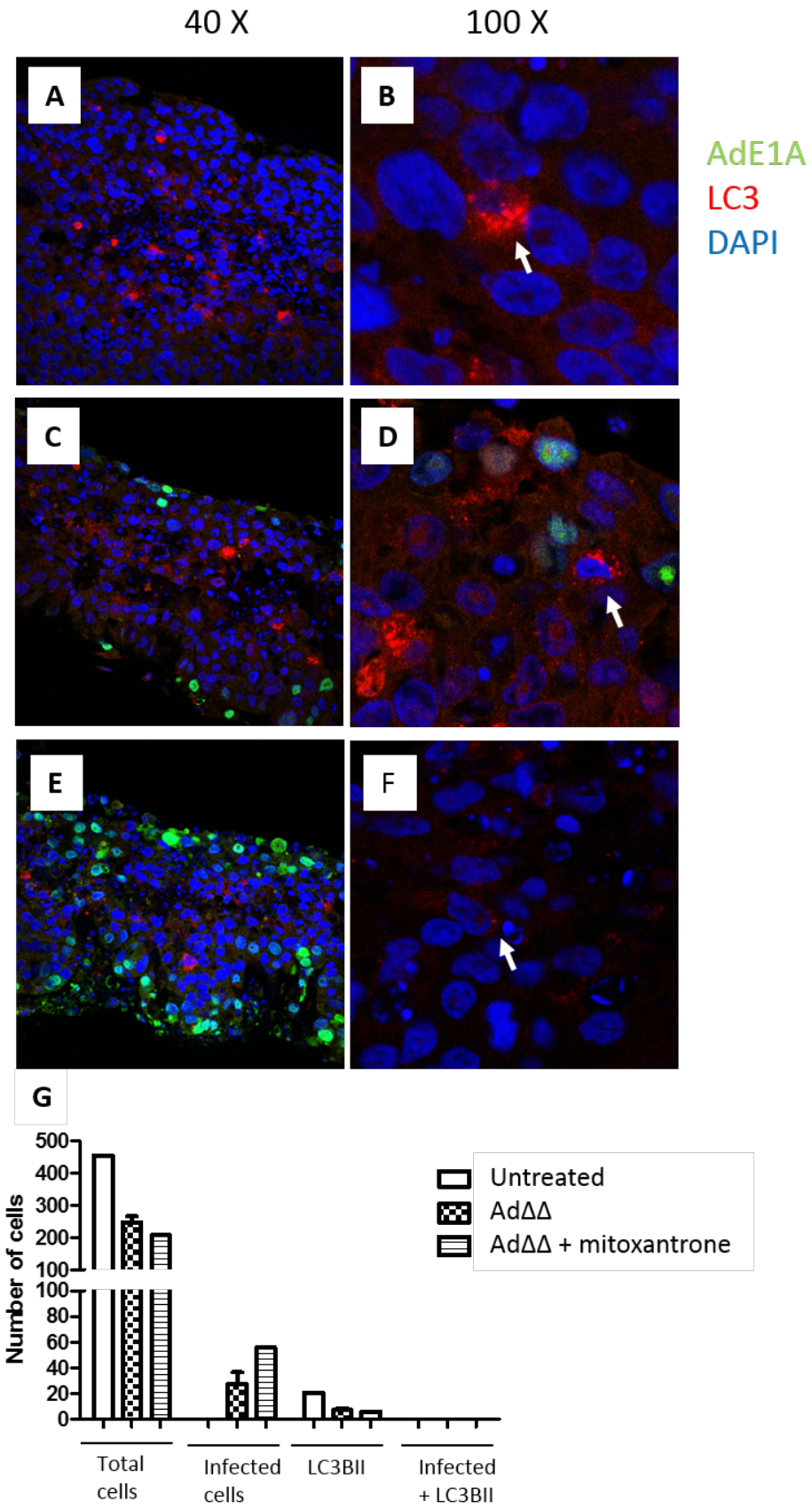

Figure 80. AdΔΔ-infected 22Rv1 cells are not positive for LC3BII in co-cultures with PrSC cells. A-F. 22Rv1 and PrSC cells were seeded on top of collagen/matrigels at a ratio of 2:1 (stromal/epithelial

cells) and fixed 10 days after seeding. White arrows indicate LC3BII positive cells. **A-B.** Untreated control. **C-D.** Cells were treated on day 2 and 6 after seeding with AdΔΔ at 100ppc. **E-F.** Cells were treated on day 2 and 6 after seeding with mitoxantrone at 25nM and AdΔΔ at 100ppc. All sections were stained with AdE1A (green) and LC3 (red). **G.** Quantification of the total number of cells and cells positive for E1A or LC3 staining per section at 40X, n=1 (1-3 sections per condition).

3.5.6 Summary of the studies on prostate cancer and stromal cells in 3-dimensional co-cultures.

These findings demonstrated that co-cultures of the epithelial prostate carcinoma PC3 or 22Rv1 cells with normal prostate stromal PrSC cells promoted cancer cell growth and invasion in 3-dimensional collagen/matrigel models. Treatment with mitoxantrone, infection with AdΔΔ or the combined treatment reduced cell growth in both co-culture models compared to untreated cells grown under the same conditions. Moreover, the combined treatment of AdΔΔ and mitoxantrone in PrSC-22Rv1 co-cultures had the greatest effects on prevention of cell growth and invasion. AdΔΔ infection was confirmed by E1A staining in both stromal and epithelial cells in the PrSC-PC3 and PrSC-22Rv1 co-culture models. Interestingly, no LC3BII staining was detected in AdΔΔ-infected E1A-expressing cells. These findings suggested that AdΔΔ-infection prevented LC3BII conversion and consequently autophagy initiation. However, these data are preliminary with limited number of experiments, and need to be repeated to finalise our conclusions. AdΔΔ-infection was demonstrated to enhance mitoxantrone-induced apoptotic cell killing and attenuate mitoxantrone-induced autophagy initiation in 2-dimensional monocultures of PC3 or 22Rv1 cells (sections 3.1.4, 3.1.5 and 3.1.6). Findings in this section indicated that our previous data could be replicated in a more physiologically relevant environment.

3.6 GOLD NANOPARTICLES ENHANCE AdΔΔ CELL KILLING EFFICACY BY INCREASING INFECTION IN PC3 AND 22Rv1 CELLS.

3.6.1 Gold nanoparticles enhance adenoviral infection in PC3 and 22Rv1 cells.

My findings demonstrated that AdΔΔ potently enhanced mitoxantrone-induced cell killing in PC3 cells (sections 3.1.2 and 3.1.3). However, due to the poor infectivity of PC3 cells, high doses of AdΔΔ had to be used. Aiming to increase infection, AdΔΔ was coated with positively charged gold nanoparticles (NP) through electrostatic interactions. The NPs had previously been synthesised by Dr. Jesus Martinez de la Fuente (Instituto de Nanociencia de Aragon; INA, Zaragoza, Spain) and are composed of a gold core and functionalised with polyethylene glycol-containing ammonium groups (PEG-$N^{+}R_4$) to generate positively charged particles (Sanz, Conde et al. 2012). The NPs had been designed to facilitate attachment of negatively charged compounds, including the adenoviral particle, to the negatively charged cell membrane. The NP studies were performed in collaboration with both Prof Pilar Martinez (Universidad Francisco de Vitoria; UFV, Madrid, Spain) and Dr de la Fuente.

In order to investigate whether incubation with NPs enhanced adenoviral infection in PC3 and 22Rv1 cells, cells were infected with the non-replicating GFP-expressing AdGFP mutant in the presence of NPs, followed by assessment of viral infection by flow cytometry. PC3 cells were infected with AdGFP alone or coated with 0.5pmoles NPs. AdGFP infection alone at 10, 100 and 500ppc resulted in low levels of viral infection while AdGFP pre-incubated with NPs resulted in potent increases in viral transduction at all tested doses (10, 100 and 500pc) (**Figure *81A***), determined as increased GFP-expression. AdGFP transduction was increased in the presence of NPs to 13.6 ± 9.8 %, 61.6 ± 16.9 % and 84.7 ± 9.4 % of cells compared to virus alone at 0.16 ± 0.12 %, 1.6 ± 0.8 % and 6.7 ± 2.6 % of cells, for infection with 10, 100 and 500ppc, respectively. The increases were significant ($p<0.01$ for 10ppc and $p<0.0001$ for 100 and 500ppc) (**Figure *81A***). In 22Rv1 cells, NP-AdGFP pre-incubation also resulted in increased viral transduction at all tested doses (10 and 50ppc) (**Figure *81B***). Viral transduction was increased in the presence of NPs to 29.0 ± 12.9 % and 63.4 ± 18.4 % of infected cells compared to infection with virus alone at 13.2 ± 6.7 % and 41.1 ± 13.4 % of cells, for infection with 10 and 50ppc, respectively (**Figure *81B***). The increases were significant ($p<0.05$). Single agent treatment with NPs in the absence of infection did not produce any detectable signal, confirming that the detected increases in NP-AdGFP cells was specific for GFP expression.

In summary, infection with NP-coated AdGFP significantly enhanced infection in PC3 and 22Rv1 cells. This increase was higher in PC3 cells. In PC3 cells, precoating of AdGFP with NPs increased viral uptake 85-fold, 38-fold and 13-fold for 10, 100 and 500ppc, respectively, compared to AdGFP alone. In 22Rv1 cells, precoating of AdGFP with NPs increased viral uptake 2.2-fold, 1.5-fold for 10 and 50ppc, respectively, when compared to infection with AdGFP alone.

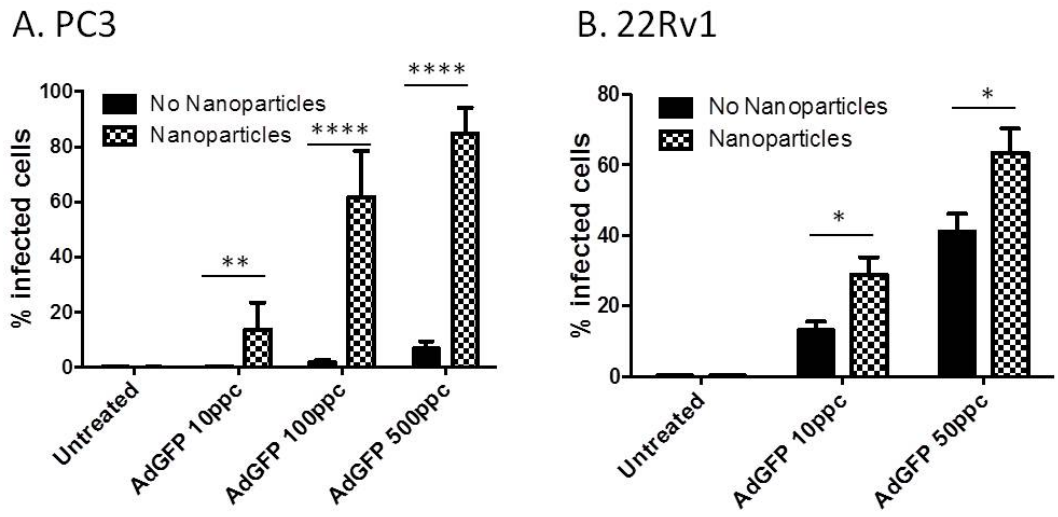

Figure 81. The nanoparticles increase adenoviral infection in PC3 and 22Rv1 cells. **A.** PC3 cells were infected with indicated doses of AdGFP at 10, 100 and 500ppc in the presence or absence of gold nanoparticles. Averages ± SD, n=3, Un-paired t-test, **p<0.01, ****p<0.0001. **B.** 22Rv1 cells were infected with indicated doses of AdGFP at 10 and 50ppc in the presence or absence of gold nanoparticles. Averages ± SD, n=3, Unpaired t-test *p<0.05. **A-B.** Samples were analysed 48 h after infection, GFP signal was measured as an indication of infection by flow cytometry.

3.6.2 The nanoparticles enhance AdΔΔ cell killing efficacy in PC3 and 22Rv1 cells both alone and in combination with mitoxantrone.

These findings (section 3.6.1) demonstrated that NP-coating of adenovirus significantly increased viral infection. In order to investigate whether the increased viral uptake correlated with enhanced cell killing, PC3 and 22Rv1 cells were infected with NP-coated AdΔΔ and assessed for cell viability.

PC3 cells were infected with increasing doses of AdΔΔ alone, or AdΔΔ pre-incubated with the NPs. The addition of NPs resulted in 5-fold decreases in AdΔΔ EC_{50}-values (***Figure 82A and B***). EC_{50}-values were 3119.3 ± 784.8ppc and 625.6 ± 510.6ppc for AdΔΔ alone or combined with NPs, respectively. The decrease was significant ($p<0.05$). In 22Rv1 cells, the pre-incubation of AdΔΔ with NPs also increased AdΔΔ cell killing efficacy. A 2.7-fold decrease in EC_{50}-value

was observed (***Figure 82C and D***). The EC_{50}-values were 125.8 ± 8.02 and 46.1 ± 19.2ppc for AdΔΔ alone or combined with NPs, respectively. This decrease was significant ($p<0.01$). In order to assess whether the NP-dependent increases in AdΔΔ cytotoxicity were maintained in the presence of mitoxantrone, PC3 cells were treated with AdΔΔ at 500ppc alone or in combination with 450nM mitoxantrone, in the presence or absence of NPs. NP-coating of AdΔΔ resulted in increased cell killing efficacy in combination with mitoxantrone compared to combination treatment in the absence of NPs (***Figure 82E***). Coating of AdΔΔ with NPs increased AdΔΔ cell killing from 16.1 ± 4.8 % to 58.2 ± 14.2 % and from 63.0 ± 7.0 % to 86.8 ± 2.6 % for AdΔΔ alone or in combination with mitoxantrone, respectively. Cell death in response to mitoxantrone alone was not modified in the presence of NPs. Moreover, single agent treatment with NP in the absence of virus or drug did not result in any cell death, confirming that NPs are not cytotoxic at the tested dose (***Figure 82E***).

In summary, the coating of AdΔΔ with positively charged gold nanoparticles enhanced AdΔΔ cell killing efficacy in PC3 and 22Rv1 cells. This increase in cell killing was maintained in the presence of mitoxantrone.

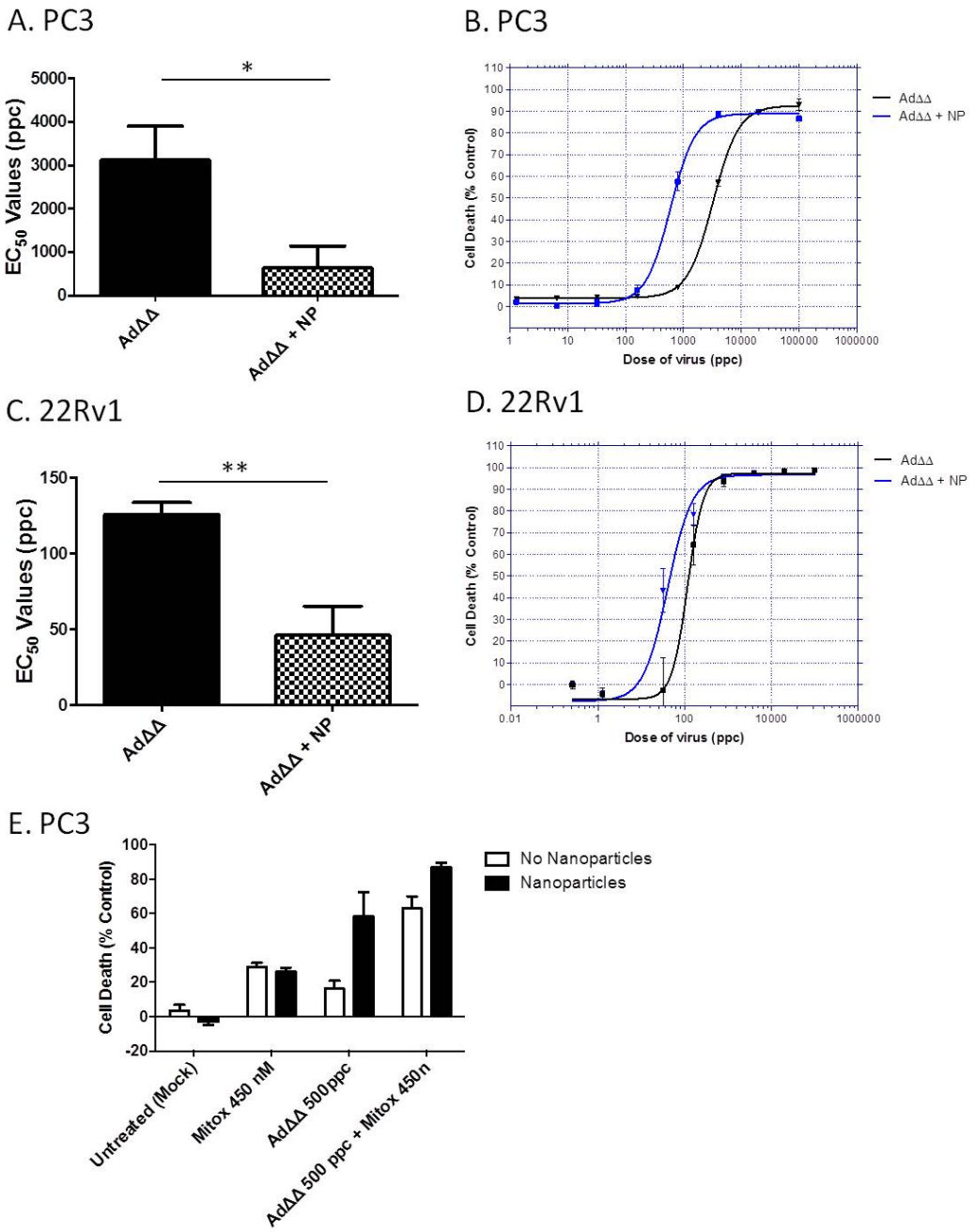

Figure 82. The nanoparticles greatly enhance AdΔΔ-induced cell death in PC3 and 22Rv1 cells. A. EC_{50}-values generated in PC3 cells treated with increasing doses of AdΔΔ alone or in combination with 0.1pmol gold nanoparticles (NP). Cell viability was measured by MTS assay 4 days after infection. Averages ± SD, n=3, Unpaired T-test *p≤0.05. **B.** Representative dose-response curves to AdΔΔ (black) and AdΔΔ+NP (blue) from A. **C.** EC_{50}-values generated in 22Rv1 cells treated with dose-response curves to AdΔΔ alone or in combination with 0.1pmol gold nanoparticles (NP). Cell viability was measured by MTS assay 3 days after infection. Averages ± SD, n=3, Unpaired T-test **p<0.01. **D.** Representative dose-response curves to AdΔΔ (black) and AdΔΔ+NP (blue) from C. **E.** PC3 cells treated with fixed doses of AdΔΔ at 500ppc and/or mitoxantrone at 450nM. Cell viability was measured by MTS assay 4 days after infection. Averages ± SD, n=2. Data generated with AdΔΔ batch 050314.

3.6.3 The nanoparticles promote AdΔΔ replication in PC3 and 22Rv1 cells.

In order to investigate whether NP-dependent enhancement of AdΔΔ cytoxicity was due to increased viral replication, PC3 and 22Rv1 cells were infected with AdΔΔ alone or pre-incubated with NPs and assessed for viral replication by the $TCID_{50}$ assay.

PC3 and 22Rv1 cells were infected with AdΔΔ at 100ppc alone or pre-incubated with 0.5pmoles NPs. In PC3 cells, infection with NP-coated AdΔΔ resulted in a trend towards increased replication at 48 and 72h post-infection, compared to infection with AdΔΔ alone (***Figure 83A***). The presence of NPs increased AdΔΔ replication to $6.52x10^8 \pm 8.03x10^8$ pfu/ml and $5.96x10^8 \pm 7.07x10^8$ pfu/ml at 48 and 72h respectively, compared to $1.36x10^7 \pm 1.97x10^7$ pfu/ml and $2.18x10^7 \pm 1.63x10^7$ pfu/ml with AdΔΔ alone. A strong trend towards increased replication in PC3 cells in the presence of NPs was seen, while the trend in 22Rv1 cells was less potent (the increases were not significant) (***Figure 83B***). AdΔΔ-replication did not appear to significantly increase from 48 to 72h in these experiments (***Figure 83***).

In summary, a non-significant increase in AdΔΔ replication in the presence of NPs was detected in PC3 and, to a lesser degree in 22Rv1. In agreement with the infectivity data (**Figure *81***), the increase in viral replication was greater in PC3 cells although the small increases in replication did not parallel the significant increases in infectivity and cell killing. In contrast to both infectivity and cell viability data, the increases in replication were not significant. This lack of significance could be due to cells having reached their maximum capacity to support viral replication. The increased replication was likely due to increased infection.

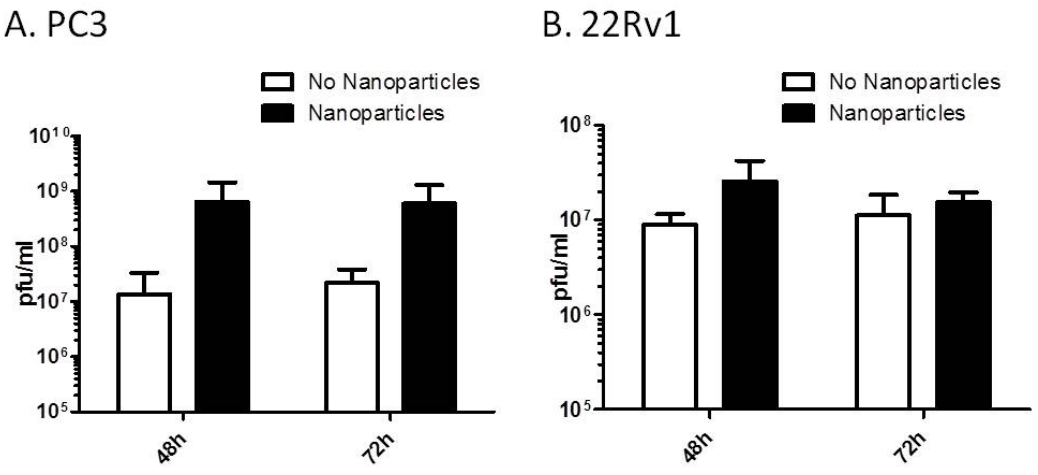

Figure 83. The addition of nanoparticles resulted in trends towards increased replication in PC3 and 22Rv1 cells. A. PC3 cells were infected with AdΔΔ at 100ppc in the presence or absence of 0.5 pmoles

gold nanoparticles, n=3. **B.** 22Rv1 cells were infected with AdΔΔ at 100ppc in the presence or absence 0.5pmoles of gold nanoparticles, n=3**. A-B.** Viral burst was measured by $TCID_{50}$ assays. Data generated with AdΔΔ batch 050314.

3.6.4 Summary of studies of pre-coating virus with nanoparticles, effects on infection, cell killing and replication in PC3 and 22Rv1 cells.

In conclusion I have shown that pre-coating of adenovirus with NPs significantly increased viral transduction in both PC3 and 22Rv1 cells. The increases were significantly higher in the infection-insensitive PC3 cells. In addition, pre-coating of AdΔΔ with the NPs significantly enhanced AdΔΔ cell killing efficacy in 22Rv1 and PC3 cells that was further enhanced or maintained in the presence of mitoxantrone in PC3 cells. Infection with NP-coated AdΔΔ resulted in an insignificant increase in viral replication in PC3. These data suggested that the NPs mainly enhanced viral transduction and consequently viral cell killing efficacy. The effects were more potent in PC3 cells, which are insensitive to virus infection and have low levels of cellular receptors such as hCAR and $\alpha_v\beta$3-integrin and $\alpha_v\beta$5-integrin (Radhakrishnan, Miranda et al. 2010).

The coating of adenoviral mutants with positively charged nanoparticles suggested a promising new strategy to enhance viral uptake and thereby increase the potency of oncolytic adenoviruses alone and in combination with cytotoxic drugs. It reminds to be determined whether the observed increase in viral transduction was receptor-specific or was due to non-specific electrostatic interactions. Further characterization of the NP-coated virus could include the study of size, zeta potential and polydispersity of the complex and might help to better understand the mechanism of enhanced infection.

4 DISCUSSION

PCa is the second most common male cancer in the western world and its incidence has been increasing in the past years (Jemal, Bray et al. 2011). Although initial treatments such as radical prostatectomy and radiotherapy are mostly curative for early stage PCa patients, the disease frequently progresses and once it becomes resistant to hormone therapy and later to chemotherapy, there are no curative treatments available (Carles, Castellano et al. 2012). The appearance of resistance to current therapies is therefore one of the mayor issues for treatment of late stage mCRPC.

In my thesis project I investigated the role of oncolytic adenoviruses in the resistance to chemotherapy treatment with mitoxantrone in 22Rv1, PC3 and PC3M PCa cells and the involvement of autophagy. 22Rv1 and PC3 cells were selected so that the treatment could be tested in both treatment-insensitive and a treatment-sensitive cell lines. 22Rv1 cells express AR and are a model for early stage PCa, while PC3 and PC3M cells are AR-negative, and are models for more aggressive, later stage PCa (Sobel and Sadar 2005, Chappell, Lehmann et al. 2012, Liu, Zhu et al. 2013). Multiple therapies for PCa, including hormone therapy with bicalutamide (Bennett, Stockley et al. 2013) or the novel enzalutamide (Nguyen, Yang et al. 2014); taxane chemotherapy (Farrow, Yang et al. 2014) and radiotherapy (Koukourakis, Kalamida et al. 2015) have been reported to upregulate autophagy resulting in lower treatment efficacy or development of treatment resistance. Previously my team developed the replication-selective AdΔΔ (E1ACR2- and E1B19K-deleted) oncolytic mutant that selectively replicates in cancer cells with deregulated cell cycle (Oberg, Yanover et al. 2010, Cherubini, Kallin et al. 2011) and synergised with the chemotherapy drugs mitoxantrone and docetaxel greatly enhancing cell killing in PC3, DU145, LNCaP, and 22Rv1 PCa cell lines. AdΔΔ also promoted tumour regression *in vivo* in DU145 and PC3 xenografts (Oberg, Yanover et al. 2010). In addition, my team reported that deletion of the anti-apoptotic Bcl-2 homolog E1B19K enhanced gemcitabine-induced apoptotic cell death in PT45 and Suit-2 pancreatic carcinoma cells (Leitner, Sweeney et al. 2009, Pantelidou, Cherubini et al. 2016).

In my project, I demonstrated that the combined treatment of mitoxantrone with the replication-selective AdΔΔ or the non-replicating Ad12S resulted in enhanced cell killing in additional PCa cell lines by promoting mitoxantrone-induced apoptosis and attenuating autophagy initiation. Modulation of the autophagic process with either the late-stage autophagy inhibitor chloroquine or siRNA-mediated knockdown of the key autophagy factor

Atg7, resulted in increased depolarization of the mitochondrial membrane, in cells treated with mitoxantrone or the combined treatment, indicating increased apoptosis. Interestingly, I demonstrated that expression of the anti-apoptotic and anti-autophagic protein Bcl-2 was required for AdΔΔ-mediated sensitization to mitoxantrone. Preliminary data showed that the combined treatment-induced enhanced cell killing could be replicated in 3-D cultures. Finally, in collaboration with Prof Pilar Martinez (Universidad Francisco de Vitoria, UFV; Madrid, Spain), we demonstrated that the incubation of AdΔΔ with positively-charged gold nanoparticles resulted in increased viral infection and cell killing in PCa cells.

4.1 AdΔΔ enhances mitoxantrone-induced cell killing in 22Rv1, PC3 and PC3M prostate cancer cells.

I demonstrated that sensitivity to AdΔΔ was higher than to Ad5wt in all tested cell lines. The AdΔΔ mutant carries a deletion in the E1B19K gene, which facilitates E1A-induced apoptotic cell death. It was previously reported that E1AΔCR2 viruses were more potent than Ad5wt in certain cell types, including PC3 cells (Oberg, Yanover et al. 2010).

I demonstrated that PC3 cells were significantly more resistant to adenovirus-induced cytotoxicity than 22Rv1. I also demonstrated that 22Rv1 cells were the most sensitive to mitoxantrone treatment resulting in the lowest EC_{50}-value to mitoxantrone. 22Rv1 and PC3 cells have several genotypic differences that may explain the observed differences in sensitivity to virus and drug-induced cell death. Increased resistance to mitoxantrone- or adenovirus-induced cytotoxicity in PC3 cells may be explained by lack of p53 and PTEN expression, which hampers apoptosis induction. In contrast, the 22Rv1 cells, which were more sensitive to both mitoxantrone and viruses, express both p53 and PTEN (Skjoth and Issinger 2006, Cunningham and You 2015). Different sensitivities to virus-induced cytotoxicity can also be explained by different degrees of infection. I demonstrated that infection with approximately 100-fold higher doses of adenovirus was required to achieve similar levels of infection in PC3 cells, when compared to the lower doses used for 22Rv1 cells. Differences in viral uptake may be explained by differential expression of the cell surface receptors hCAR and $\alpha_v\beta3$ or $\alpha_v\beta5$ integrins, which are required for viral attachment and internalization, respectively (Leopold and Crystal 2007). PC3 cells have been reported to express very low levels of hCAR and $\alpha_v\beta3$ or $\alpha_v\beta5$ integrins (Pandha, Stockwin et al. 2003, Adam, Ekblad et al. 2012). I demonstrated that 22Rv1 cells expressed higher levels of hCAR and $\alpha_v\beta5$, when compared to PC3 cells. These findings are in agreement with the studies by

Pandha *et al* (Pandha, Stockwin et al. 2003), that reported that PC3 cells were much more resistant to adenoviral infection than other tested PCa cell lines (DU145 and LNCaP). The decreased infection was correlated with lower levels of hCAR expression in PC3 cells, when compared to DU145 and LNCaP cells (Pandha, Stockwin et al. 2003). Therefore, increased sensitivity to adenovirus-induced cytotoxicity in 22Rv1 can be explained by the combination of higher susceptibility to cell killing due to p53 and PTEN expression and increased viral transduction, which may be explained by increased expression of hCAR and $\alpha_v\beta5$ integrin.

The efficacy of replication-selective oncolytic viruses was reported to increase in combination with chemotherapy in preclinical studies and clinical trials. Treatment with H101 (E1B55K- and E3B-deleted) adenoviral mutant in combination with the chemotherapeutic agents cisplatin and 5-FU resulted in increased treatment efficacy and tumour regression and successfully passed a phase III clinical trial for head and neck cancers in China, obtaining market approval in this country (Lu, Zheng et al. 2004, Xia, Chang et al. 2004, Garber 2006, Hughes, Alusi et al. 2015). Since then, numerous preclinical studies have tested various combinations of viral mutants and cytotoxic drugs. As an example, the combination of docetaxel and paclitaxel with CV787 (E1A and E1B are placed under control of hTERT and PSA promoters, respectively) resulted in synergistic cell killing and increased p53 expression in LNCaP cells (Yu, Chen et al. 2001).

Treatment with the topoisomerase II inhibitor mitoxantrone induces DNA double strand breaks that results in apoptotic cell death (Wu, Li et al. 2013). In addition, mitoxantrone-treatment was reported to promote apoptosis by enhancing NF-κB transcriptional activity (Karl, Pritschow et al. 2009) or by increasing FAS expression (Symes, Kurin et al. 2008).The anthracenedione agent mitoxantrone is currently used in the clinic for treatment of CRPC after appearance of docetaxel resistance (Tannock, de Wit et al. 2004, Pommier, Leo et al. 2010, Carles, Castellano et al. 2012).

The combination of oncolytic adenoviral mutants with topoisomerase inhibitors has been tested in various cancers, including PCa (Gomez-Manzano, Alonso et al. 2006, Ma, Kawamura et al. 2010, Oberg, Yanover et al. 2010, Radhakrishnan, Miranda et al. 2010). As an example, the combination of AdΔ24 (E1ACR-deleted) with irinotecan resulted in enhanced cell killing in U-87 MG and U-251 glioma cells and prolonged survival in *in vivo* U-87 MG xenografts (Gomez-Manzano, Alonso et al. 2006). In this report, the combined treatment of AdΔ24 and irinotecan resulted in upregulation of topoisomerase I expression and activity and promotion S-phase cell accumulation. The combination of Onyx-015 with the topoisomerase II inhibitor

Vp-16 (etoposide) resulted in enhancement of cell death *in vitro* (TE-1, TE-2, TE-10, TE-11 YES-2, YES-4, YES-5, YES-6 esophageal carcinoma cells) and in TE-11 xenografts (Ma, Kawamura et al. 2010).

Previous work in our team demonstrated that the mutants *dl*922-947 (E1ACR2- and E3B-deleted) and AdΔΔ, synergistically enhanced mitoxantrone- and docetaxel-induced cell death *in vitro* in PC3, DU145 and LNCaP cells and promoted tumour regression in PC3 and DU145 xenografts (Oberg, Yanover et al. 2010, Radhakrishnan, Miranda et al. 2010). In agreement with these findings, I demonstrated that the addition of AdΔΔ to cells treated with increasing doses of mitoxantrone resulted in potent sensitization to the drug in PC3 cells and a trend towards sensitization in 22Rv1 cells. Moreover, I found that the combined treatment of suboptimal doses of mitoxantrone with AdΔΔ or Ad12S, but not with Ad5wt, resulted in more than additive cell killing in PC3 and PC3M cells and additive cell killing in 22Rv1 cells. My results agreed with previous findings and confirmed that AdΔΔ can synergise with chemotherapy drugs such as mitoxantrone and efficiently kill PCa cells (Oberg, Yanover et al. 2010, Miranda, Maya Pineda et al. 2012). Previous work in our group demonstrated that expression of the E1A12S protein (E1ACR3-deleted) was sufficient to sensitise PC3 and DU145 cells to mitoxantrone and docetaxel. The sensitization was dependent on the p300/CBP-binding domain in E1ACR1 (Miranda, Maya Pineda et al. 2012). In agreement with Miranda *et al.* I showed that treatment with the non-replicating Ad12S mutant, which solely expresses the E1A12S protein under control of a constitutively active CMV promoter, also resulted in enhancement of mitoxantrone-induced cell killing. However, I showed that EC_{50}-values to Ad12S were higher than those for the replicating Ad5wt or AdΔΔ, these data suggested that Ad-induced cytotoxicity was, at least partially, dependent on viral replication and cell lysis, which is not possible after infection with Ad12S.

4.2 AD-MEDIATED ATTENUATION OF MITOXANTRONE-INDUCED AUTOPHAGY AND ITS ASSOCIATION WITH INCREASED APOPTOSIS.

Infection with Ad5wt or with the AdΔ24 (E1ACR2-deleted) was reported to induce autophagy, demonstrated by increased LC3BI to LC3BII conversion in A549 and U-87 MG cells (Piya, White et al. 2011, Rodriguez-Rocha, Gomez-Gutierrez et al. 2011). However, infection with different adenoviral mutants containing the E1B19K deletion or the entire E1B gene deleted failed to induce autophagy in those cells, indicating that this protein was required for autophagy induction. In addition, the E1B19K protein was reported to interact with the

cellular protein Beclin 1, disrupting the inhibitory Beclin 1-Bcl-2 complex thereby promoting autophagy initiation (Piya, White et al. 2011). More recently, adenovirus (AdΔ24) was reported to mediate phosphorylation of JNK1 and JNK2, therefore promoting Bcl-2 phosphorylation and its dissociation from the Beclin 1-Bcl-2 complex, resulting in autophagy induction (Klein, Piya et al. 2015). These reports agreed with the fact that E1B19K-deleted adenoviruses were not able to induce autophagy initiation, as I also showed in my work. However, I demonstrated that single infection with all tested adenoviral vectors Ad5wt, AdΔΔ or Ad12S did not induce autophagy in any of the tested PCa cell lines. It is possible that Ad5wt-mediated induction of autophagy initiation, that was reported by other teams in A549 and U-87 MG cells (Piya, White et al. 2011, Rodriguez-Rocha, Gomez-Gutierrez et al. 2011) was cell-line dependent.

As discussed at the beginning of this section, chemotherapy treatment can result in autophagy upregulation (Farrow, Yang et al. 2014), which may contribute to the development of treatment resistance by promoting cell survival. Preliminary findings in my team (Maya Pineda 2013) suggested that mitoxantrone-induced autophagy was attenuated by infection with AdΔΔ or Ad12S in PC3 and 22Rv1 cells. Therefore, we speculated that autophagy-inhibition may be developed as a therapeutic strategy for chemotherapy-resistant PCa. I found that treatment with mitoxantrone resulted in autophagy induction in a dose dependent manner, demonstrated by increased LC3BI to LC3BII conversion and increased number of acidic vesicles. Interestingly, I showed that co-infection with AdΔΔ attenuated mitoxantrone-induced LC3BII conversion, indicating attenuation of autophagy initiation. Infection with Ad12S resulted in similar attenuation of autophagy than AdΔΔ, indicating that expression of the E1A12S protein was sufficient for attenuation of mitoxantrone-induced LC3BI to LC3BII conversion. I also showed that infection with Ad5wt did not affect mitoxantrone-induced LC3BI to LC3BII conversion in PC3 and 22Rv1 cells, indicating that expression of E1B19K protein, which is not present in the AdΔΔ or Ad12S viruses and was reported to promote autophagy (Piya, White et al. 2011), might prevent E1A from attenuating autophagy initiation. I found that AdΔΔ-mediated attenuation of mitoxantrone-induced autophagy could also be detected at later stages in the autophagic pathway, shown by Lysotracker staining, and indicated that the fusion of the autophagosome and lysosome was decreased by co-infection with AdΔΔ. The E3-encoded protein RID-α and protein VI have been reported to disrupt the endosome membrane during viral internalization into the infected cell (Wiethoff, Wodrich et al. 2005, Cianciola and Carlin 2009). Therefore, in addition to the observed E1A-dependent attenuation of mitoxantrone-

induced LC3BI to LC3BII conversion, the viral proteins RID-α and protein VI might contribute to AdΔΔ-mediated attenuation of mitoxantrone-induced increased fusion of the autophagosome and lysosome.

The p62 protein is required for the sequestration of ubiquitinated proteins into the autophagosome and is degraded at the end of the autophagic process (Pankiv, Clausen et al. 2007). I demonstrated that mitoxantrone treatment induced completion of the autophagy process by degradation of p62 in 22Rv1 and PC3M cells. However, mitoxantrone did not cause decreases in basal levels of p62 in PC3 cells. Also in my work, AdΔΔ or Ad12S did not prevent mitoxantrone-induced p62 degradation and, under some conditions, further promoted its degradation. These data might indicate that infection with AdΔΔ or Ad12S only affected initial steps in the autophagy process. Degradation of p62 is also known to be mediated by proteasomal inhibitors, independently of the autophagic process (Klionsky, Abdelmohsen et al. 2016). Degradation of p62 was also suggested to be cell line dependent and it was observed that levels of p62 might not change despite strong levels of autophagy induction (Klionsky, Abdelmohsen et al. 2016). Therefore, although p62 is a marker for autophagy completion, it is possible that, in some cases, p62 expression levels might not correlate with autophagy activity. Accordingly, I could not conclude whether infection with AdΔΔ or Ad12S in my studies attenuated completion of autophagy or its initiation only.

Taken together, from the LC3B and Lysotracker data it can be concluded that AdΔΔ infection attenuated mitoxantrone-induced autophagy at an early stage and also decreased the fusion of the autophagosome and the lysosome. To the best of my knowledge, Ad-mediated attenuation of chemotherapy-induced autophagy has not been previously reported.

The E1A protein is well known to induce both p53-dependent and -independent apoptosis. E1A was also reported to induce apoptosis in p53-deficient cells (Putzer, Stiewe et al. 2000). Expression of E1A can promote p53 stabilization by multiple mechanisms resulting in apoptosis induction (Putzer, Stiewe et al. 2000, Chattopadhyay, Ghosh et al. 2001, Li, Day et al. 2004, White 2006). E1A-dependent release of E2F upregulates p14ARF expression resulting in inhibition of MDM2-induced p53-degradation (Putzer, Stiewe et al. 2000). E1A was also reported to facilitate p53 binding to MDM4, preventing p53 nuclear export (Li, Day et al. 2004). Finally, E1A down-regulates p21 and MDM2 resulting in p53 stabilization (Chattopadhyay, Ghosh et al. 2001, Yamasaki, Tazawa et al. 2012). E1A enhances TNFα-dependent apoptosis induction by down-regulation of the TNF-inhibitor c-FLIP and inhibition of the nuclear factor NF-κB (Deng, Kloosterbooer et al. 2002, Perez and White 2003). In

contrast, the E1B-encoded proteins can protect the cell from apoptotic cell death. E1B55K counteracts E1A-induced p53 stabilization while the Bcl-2 homolog E1B19K binds to BAX, preventing mitochondrial depolarisation (Berk 2005). Our team previously reported that infection with E1B19K-deleted mutants, including AdΔΔ, induced apoptosis in DU145 and 22Rv1 PCa cells (Oberg, Yanover et al. 2010). In addition, infection with AdΔE1B19K (E1B19K-deleted) in combination with the cytotoxic drug gemcitabine, enhanced drug-induced apoptosis in PT45 and Suit-2 pancreatic carcinoma cells (Leitner, Sweeney et al. 2009).

Mitoxantrone-treatment was shown to induce apoptosis in PCa cells lines (DU145, PC3 and LNCaP) and in patient-derived primary PCa cells (Symes, Kurin et al. 2008, Sánchez, Mendoza et al. 2009). In agreement with published reports (Symes, Kurin et al. 2008, Sánchez, Mendoza et al. 2009), I showed that mitoxantrone-treatment induced apoptosis in all tested cell lines, demonstrated by PARP cleavage, mitochondrial depolarization, and Annexin V staining.

I also demonstrated that infection with AdΔΔ further promoted apoptosis in mitoxantrone-treated PC3, 22Rv1 and PC3M cells. Infection with Ad12S mimicked the AdΔΔ effect and even increased promotion of mitoxantrone-induced PARP cleavage, indicating that the expression of the E1A12S protein might be responsible of apoptosis promotion, possibly by attenuation of mitoxantrone-induced autophagy. My data were in agreement with previous studies in my team that demonstrated that Ad12S infection enhanced mitoxantrone-induced mitochondrial depolarization in PC3 and DU145 PCa cells (Miranda, Maya Pineda et al. 2012). In contrast, I found that infection with Ad5wt decreased mitoxantrone-induced PARP-cleavage in 22Rv1 cells but promoted PARP activation in PC3 cells, although to a lesser extent than when infected with either AdΔΔ or Ad12S. Interestingly, I showed that mitoxantrone-induced depolarization of the mitochondrial membrane could only be enhanced by AdΔΔ infection at low doses of mitoxantrone but not at the higher tested dose in PC3 and 22Rv1 cells. These findings could be related to my autophagy studies, in which infection with AdΔΔ or Ad12S could only attenuate mitoxantrone-induced autophagy initiation at low doses of drug, and indicated that at the highest tested dose of mitoxantrone, autophagy induction was too potent for the virus to counteract. It is possible that high doses of mitoxantrone resulted in high induction of both autophagy and apoptotis and therefore, the viruses could not further increase apoptosis.

In conclusion, I showed that infection with AdΔΔ enhanced mitoxantrone-induced apoptosis and attenuated mitoxantrone-induced autophagy initiation in PCa cells. My data indicated

that AdΔΔ-mediated enhancement of mitoxantrone-induced cell death was due to promotion of apoptotic cell death and prevention of autophagy initiation. To the best of my knowledge, the demonstrated Ad-dependent correlation of autophagy attenuation and apoptosis induction has not been previously reported.

4.3 The effect of autophagy modulation with rapamycin or chloroquine in cell death and in the viral life cycle in combination-treated PC3 and 22Rv1 cells

Autophagy plays a dual role in PCa. During early stages, autophagy may be required to protect the cell from accumulation of free radicals. On the contrary, at later stages, active autophagy can provide the cell with new nutrients and promote cell survival (Ziparo, Petrungaro et al. 2013). Autophagy modulation by either inhibition or upregulation of the process is currently being studied to improve the efficacy of PCa therapies (Ziparo, Petrungaro et al. 2013). Here I showed that chloroquine treatment enhanced the efficacy of mitoxantrone treatment alone and in combination with AdΔΔ and Ad12S in 22Rv1 and PC3 cells by decreasing EC_{50}-values to mitoxantrone and enhancing mitoxantrone-induced apoptosis. My findings indicated that autophagy inhibition might enhance the efficacy of chemotherapeutic drugs. Chloroquine and other autophagy inhibitors such bafilomycin or 3-methylladenine are currently being tested in combination with standard therapies in several clinical trials for treatment of various solid tumours (Cheong 2015). More specifically, hydroxychloroquine (HCQ) is currently being tested in combination with docetaxel in a phase II clinical trial for PCa (Cheong 2015).

Interestingly, I demonstrated that autophagy promotion with rapamycin desensitised cells to mitoxantrone, reverted Ad-mediated sensitization to the drug and attenuated mitoxantrone-induced mitochondrial depolarization in PC3 cells but not in 22Rv1 cells. My data suggested that the effect on cell death of autophagy regulation was cell-line dependent. Autophagy regulation is dependent on the p53 cellular status and localization. Nuclear p53 was reported to induce autophagy by promoting transactivation of the mTOR negative regulator AMPK (Feng, Hu et al. 2007). AMPK promotes autophagy by phosphorylating TSC1 and TSC2, which promote deregulation of mTOR (Feng, Zhang et al. 2005). In turn, AMPK can phosphorylate p53 promoting its stabilization and inducing protective cell cycle arrest (Jones, Plas et al. 2005). In addition, in response to stress, p53 can transactivate the pro-apoptotic Bcl-2 family members Bax and PUMA, which may induce autophagy by disrupting Beclin 1-

Bcl-2- interaction (Yee, Wilkinson et al. 2009). On the other hand, cytoplasmic p53 was shown to inhibit autophagy. p53 deficiency-mediated autophagy-induction promoted cell survival in cancer cells under conditions of hypoxia and nutrient deprivation (Tasdemir, Maiuri et al. 2008). 22Rv1 cells are p53+ while PC3 cells are p53- and may therefore respond differently to autophagy modulation (Sobel and Sadar 2005, Cunningham and You 2015). p53-induced autophagy might be constitutively active up to a certain level in 22Rv1 cells, as I showed with a constitutively strong LC3BII band, when compared to PC3 cells. This might help to explain why, in my studies, rapamycin treatment, although slightly enhancing autophagy induction, did not have any additional effect in prevention of cell death or apoptosis in 22Rv1 cells.

In addition, rapamycin-dependent prevention of AdΔΔ-mediated sensitization to mitoxantrone could have been due to the fact that active autophagy protected the cell from either viral infection or mitoxantrone by directly degrading virus or drug; or by upregulating cellular mechanisms that might prevent its function. Further studies on the effect of autophagy modulation in the viral life cycle were aimed at providing more information on these issues.

Our team previously demonstrated that chemotherapy treatment with either docetaxel or mitoxantrone enhanced viral infection in DU145 and PC3 cells (Radhakrishnan, Miranda et al. 2010). In agreement with previous findings, I demonstrated that pre-treatment with mitoxantrone increased viral uptake in both PC3 and 22Rv1 cells. However, the addition of rapamycin or chloroquine to mitoxantrone-treated cells did not further affect viral uptake in my studies. Therefore, the differences in cell death and apoptosis induction that I observed as a result of chloroquine or rapamycin treatments were not due to differences in viral uptake.

It has been suggested that active autophagy facilitates adenoviral replication (Jiang, White et al. 2008, Rodriguez-Rocha, Gomez-Gutierrez et al. 2011, Cheng, Lian et al. 2013). Jiang *et al* reported that adenoviral infection upregulated autophagy in infected MDNSC11 brain tumour stem cells to facilitate release of viral progeny (Jiang, White et al. 2008). Rodriguez-Rocha and colleges reported that autophagy inhibition with 3-MA in A549 and H1299 cells attenuated viral replication, shown by decreased expression of capsid proteins while rapamycin treatment enhanced replication (Rodriguez-Rocha, Gomez-Gutierrez et al. 2011). Rapamycin-induced autophagy in A549 cells was also shown to enhance E1A expression and adenoviral replication by Cheng *et al* (Cheng, Lian et al. 2013). In agreement with published

reports, I showed that rapamycin treatment resulted in a trend towards increased viral replication. Interestingly, I also showed that the combined treatment of AdΔΔ, mitoxantrone and chloroquine that had resulted in increased apoptotic cell death, resulted in a strong attenuation of viral replication in PC3 cells with a similar trend in the 22Rv1 cells. My data suggested that chloroquine-enhancement of adenovirus-mediated cell death was not due to increased E1A expression or enhanced viral replication. However, my findings also suggested that E1A-induced cytotoxicity was effective at very low expression levels.

4.4 THE EFFECT OF ATG5 AND ATG7 KNOCK-DOWN ON CELL VIABILITY, AUTOPHAGY AND APOPTOSIS IN PC3 CELLS

It was reported that inhibition of autophagy initiation with either 3-MA or Atg5 knock-down promoted apoptosis in PC3 cells in the presence of the anti-tumour compound ursolic acid (Shin, Kim et al. 2012). In addition, the combination of Akt inhibitors with autophagy inhibitors such as chloroquine, 3-MA, bafilomycin or with Atg7 knock-down resulted in enhanced cell death and apoptosis in PC3 cells (Lamoureux, Thomas et al. 2013).

In order to confirm the pro-apoptotic effect of autophagy-inhibition by AdΔΔ, Atg5 and Atg7, which are necessary for autophagy initiation, were targeted for knock-down. I found that Atg5 or Atg7 knock-down resulted in inhibition of autophagy initiation, demonstrated by no LC3BI to LC3II conversion. Interestingly, I demonstrated that autophagy inhibition as a result of siAtg7 transfection enhanced mitoxantrone-induced apoptosis both in cells treated with drug only and in AdΔΔ co-infected cells. Atg7 knock-down resulted in promotion of apoptosis in agreement with my chloroquine data that also enhanced apoptotic death in cells treated with mitoxantrone or the combination. These findings were important for my project and confirmed that autophagy inhibition promoted mitoxantrone-induced apoptosis. Interestingly, I found that autophagy inhibition with either chloroquine or siAtg7 did not affect basal levels of apoptosis. My data indicated that promotion of apoptosis under conditions of autophagy inhibition only occurred in the presence of the cytotoxic drug mitoxantrone.

Previously published reports (Shin, Kim et al. 2012, Lamoureux, Thomas et al. 2013), together with my data strongly suggest that autophagy inhibition can be directly correlated with an increase in apoptosis in PC3 cells.

Drug-mediated upregulation of autophagy was suggested to play a cytoprotective function while pharmacological inhibition of drug-induced autophagy was demonstrated to increase cell death and tumour regression in lung cancer preclinical models (Ren, He et al. 2010, Wang, Peng et al. 2011, Pan, Zhang et al. 2013, Park, Lee et al. 2014, Wu, Wang et al. 2015). As an example, chloroquine treatment was reported to enhance cisplatin-induced apoptosis and inhibited cell growth in A549 lung carcinoma cells (Wu, Wang et al. 2015). In this study, cisplatin-induced autophagy was reported to be mediated by activation of the AMPK/mTOR signalling pathway. The regulation of the autophagic and apoptotic processes is tightly related. Autophagy inhibition frequently correlates with an increase in apoptosis as I demonstrated. However, apoptosis enhancement might not contribute to increased cell death, on the contrary, it might represent a switch between autophagy-related cytotoxic-mediated cell death and apoptotic cell death (Gewirtz 2016). I demonstrated that, despite preventing autophagy initiation, neither siAtg5 nor siAtg7 transfection sensitised PC3 cells to mitoxantrone. In addition, I found that AdΔΔ-mediated sensitization to mitoxantrone was not affected in siAtg5 or siAtg7 transfected PC3 cells, indicating that active autophagy may not be required for AdΔΔ to mediate sensitization to mitoxantrone. Eng and colleges (Eng, Wang et al. 2016) recently reported that treatment with either radiation or a panel of 30 different chemotherapeutic drugs in Atg7-deficient A549 cells resulted in no change in EC_{50}-values, when compared to Atg7-wildtype A549 cells. These findings were in agreement with the lack of effect on cell viability of siAtg7 and siAtg5 transfected mitoxantrone-treated PC3 cells that I demonstrated.

My data were surprising as I demonstrated that siAtg7 resulted in increased apoptosis but did not increase inhibition of cell proliferation neither promoted cell death and chloroquine treatment resulted in enhancement of Ad-mediated sensitization to mitoxantrone and further promoted apoptosis. Chloroquine is a late-stage autophagy inhibitor that prevents the fusion of the autophagosome with the lysosome while siAtg5 or siAtg7 inhibit autophagy initiation by preventing LC3BI to LC3BII conversion. Consequently, it is reasonable that inhibition at the two different stages of the pathway resulted in different outcomes. My data also indicated that, although it was proven that inhibition of mitoxantrone-induced autophagy correlated with apoptosis promotion, autophagy inhibition might not be the main mechanism used by AdΔΔ to sensitise PCa cells to mitoxantrone.

Treatment with chloroquine or with its derivate hydroxychloroquine is currently being tested in several clinical trials for various cancers (Sui, Chen et al. 2013). However, chloroquine-

mediated sensitization to cisplatin in 67NR and 4T1 mouse breast cancer cells was reported to be independent of the autophagic process as it was maintained after silencing of Atg12 and was not mimicked by Atg12 or Beclin 1 knock-downs (Maycotte, Aryal et al. 2012). Chloroquine treatment was reported to induce lysosome-mediated apoptosis in SH-EP, SH-N-AS and Kelly neuroblastoma cells treated with the PI3K/mTOR inhibitor BEZ235 independently of autophagy modulation (Seitz, Hugle et al. 2013). Chloroquine treatment was also reported to promote cathepsin D-dependent lysosomal malfunction and cause apoptosis in p53-negative LN308 glioma cells (Geng, Kohli et al. 2010). Lysosome-mediated apoptosis is preceded by lysosomal membrane permeabilization (LMP). LMP is a process that involves the loss of lysosomal membrane integrity and can be caused by osmotic lysis or chemical surfactants (Repnik, Hafner Česen et al. 2014). LMP results in the release in the cytosol of lysosomal hydrolases, including cysteine cathepsins, which, in the cytosol can process Bid into t-Bid promoting depolarization of the mitochondrial membrane and subsequent apoptosis (Repnik, Hafner Česen et al. 2014). In addition, cysteine cathepsins can degrade anti-apoptotic Bcl-2 family members further promoting mitochondrial depolarization (Droga-Mazovec, Bojic et al. 2008, Repnik, Hafner Česen et al. 2014). Treatment with hydroxychloroquine was reported to promote LMP and result in mitochondrial membrane depolarization in HeLa cells (Boya, Gonzalez-Polo et al. 2003). More recently, chloroquine treatment was reported to promote LMP and reduce cell viability in HCTI5 colorectal cancer cells (Park, Lee et al. 2014). It can be suggested that the chloroquine-mediated promotion of mitoxantrone-induced apoptotic cell death that I have shown in this work might be due to LMP induction rather than autophagy blockage.

Interestingly, autophagy deficiency as a result of either Atg5 or Atg7 deletion was reported to activate p53 and reduce tumour growth in mice by stabilization of p53 (Guo, Karsli-Uzunbas et al. 2013, Rao, Tortola et al. 2014). However, as previously mentioned, PC3 cells are deficient in p53, and may respond differently to cell death induction.

Autophagy inhibition has been proposed to reduce adenoviral infection or replication (Rodriguez-Rocha, Gomez-Gutierrez et al. 2011). However, siAtg5 or siAtg7 transfection resulted in no changes in the expression of the E1A and hexon proteins, when compared to the siNT control, indicating that the viral life cycle was not affected and the virus remined functional in the absence of Atg5 or Atg7 expression. Therefore, the lack of effect on cell viability of siAtg5 or siAtg7 was not due to inactivation of AdΔΔ.

4.5 The effect of Bcl-2 knock-down in autophagy modulation and AdΔΔ mediated sensitization to mitoxantrone

The Bcl-2 protein may play an important role in in the crosstalk between apoptosis and autophagy (Marquez and Xu 2012). Bcl-2 is a well-known anti-apoptotic protein that binds to Bak and prevents depolarization of the mitochondrial membrane (Shore and Nguyen 2008). Bcl-2 is also an anti-autophagic protein that binds to Beclin 1 (Pattingre, Tassa et al. 2005). The formation of the Beclin 1-Bcl-2 complex prevents the formation of the Beclin 1-Vps34-Vps35 complex, which promotes autophagy initiation (Pattingre, Tassa et al. 2005, Gordy and He 2012). I demonstrated that siRNA-mediated Bcl-2 knock-down resulted in autophagy induction, shown by increased LC3BI to LC3BII conversion, which was not prevented by AdΔΔ infection. However, I found that siBcl-2 did not affect mitochondrial depolarization in PC3 cells treated with mitoxantrone or the combined treatment, when compared to the siNT control. As Bcl-2 is an anti-apoptotic protein, it was surprising that siBcl-2 did not enhance mitochondrial depolarization. It is possible that siBcl-2-mediated promotion of autophagy may, to some extent, prevent promotion of apoptosis through other mechanisms.

Expression of pro-survival molecules, such as Bcl-2, Bcl-xL and Mcl-1, is frequently found upregulated in PCa and is associated with development of androgen independence (Sun, Tang et al. 2008, Zielinski, Eigl et al. 2013). Moreover, overexpression of Bcl-2 was reported to promote resistance to chemotherapy and disease recurrence, and was associated with poor prognosis (Yoshino, Shiina et al. 2006, Khor, Moughan et al. 2007, Zielinski, Eigl et al. 2013). As an example, treatment with the microtubule-targeting drug paclitaxel resulted in increased expression of Bcl-2 in PC3 cells, that was associated with appearance of drug resistance (Sobue, Mizutani et al. 2016). Down-regulation of Bcl-2 expression is currently being studied as a therapeutic strategy for PCa treatment. Atorvastatin, in combination with docetaxel, resulted in a strong decrease in Bcl-2 expression, inhibited cell growth and promoted apoptosis in PC3 cells (Chen, Liu et al. 2016). Down-regulation of Bcl-2 was reported to successfully sensitise LnCaP cells to androgen deprivation therapy and radiation (Shi, Gumerlock et al. 2001, Scott, Higdon et al. 2002). Therefore, the mitoxantrone-mediated down-regulation of Bcl-2 expression, that I demonstrated, would likely facilitate apoptosis induction and finally result in cell death. In contrast with these reports, I demonstrated that Bcl-2 knock-down resulted in a significant increase in EC_{50}-values to

mitoxantrone, indicating that higher doses of the drug would have to be used in siBcl-2 transfected PC3 cells to achieve similar cell killing. This increased resistance to mitoxantrone-induced cytotoxicity could possibly be explained by the strong autophagy induction that I found that resulted from Bcl-2 knock-down, which may be outperforming the antiapoptosis role of Bcl-2. Surprisingly, I found that Bcl-2 expression was required for AdΔΔ-mediated enhancement of mitoxantrone-induced cell killing. Knock-down of Bcl-2 completely prevented AdΔΔ-mediated sensitization to the drug. In agreement with my sensitization data, I showed that the combined treatment of mitoxantrone and AdΔΔ did not significantly enhance cell killing in siBcl-2 cells, while it significantly enhanced cell killing in siNT cells. This is, to the best of my knowledge, the first time that Bcl-2 is shown to be required for Ad-mediated sensitization to mitoxantrone.

The role of Bcl-2 expression in the adenoviral cell cycle and in Ad-mediated sensitization to chemotherapy is poorly understood. Bcl-2 expression was reported to both, facilitate expression of viral proteins (Bilbao, Contreras et al. 1999) and to interfere in viral production (Sandhu and Al-Rubeai 2009). I demonstrated that expression of E1A and hexon viral proteins was hampered in the absence of Bcl-2 expression in combination-treated cells. Viral protein expression was not affected in AdΔΔ single-infected PC3 cells. My data suggested that expression of early adenoviral proteins and probably AdΔΔ replication was impaired by mitoxantrone treatment in siBcl2 transfected PC3 cells. Impaired viral expression and replication could partially explain the lack of AdΔΔ-mediated sensitization to mitoxantrone. I also demonstrated that mitoxantrone treatment resulted in downregulation of Bcl-2 expression at both mRNA and protein levels. I showed that the decreased Bcl-2 mRNA expression was maintained after simultaneous infection with either Ad5wt or AdΔΔ. However, I found a trend towards attenuation of mitoxantrone-induced decreases in Bcl-2 protein levels after infection with AdΔΔ but not with Ad5wt. Infection with Ad12S strongly counteracted mitoxantrone-induced decreases in Bcl-2 protein levels, indicating that this effect is probably due to expression of the E1A12S protein. I also found that single infection with either Ad5wt, AdΔΔ or Ad12S resulted in a trend towards increased Bcl-2 protein expression when compared to basal levels. My findings indicated that E1A expression, in the absence of the E1B19K protein, increased Bcl-2 protein levels. These findings suggested that E1A expresssion stabilized Bcl-2 protein and prevented the degradation, which, to the best of my knowledge, has not been previously reported.

The role of Bcl-2 in the regulation of AdΔΔ-mediated enhancement of mitoxantrone-induced cell death is definitely intriguing but also contradictory. I demonstrated that infection with AdΔΔ enhanced mitoxantrone-induced cell death and attenuated mitoxantrone-induced decreased Bcl-2 expression. In addition, siBcl-2 prevented AdΔΔ-mediated sensitization to mitoxantrone. Further studies are needed to completely understand this interaction and may result in the identification of novel therapeutic targets for PCa treatment.

4.6 THE EFFECT OF DNA VIRUSES IN AUTOPHAGY MODULATION

In addition to adenovirus, several DNA viruses are able to modulate the autophagy processes at different stages. Autophagy plays an important role in immunity and inflammation (Levine, Mizushima et al. 2011), it contributes to the presentation of viral antigens by the MHC class I and class II. Some viruses, such as the EBV modulate autophagy to suppress host cellular immune responses (Mack and Munger 2012). Upon infection with EBV, autophagy was reported to mediate MHC class II-dependent presentation of the viral protein EBNA 1 (Paludan, Schmid et al. 2005, Chiramel, Brady et al. 2013). Interestingly, the E3gp19K adenoviral protein attenuates the host immune response by hampering antigen presentation. Expression of E3gp19K blocks the transport of MHC class I to the plasma membrane and reduces the levels of cell surface receptors for natural killer cells (Burgert, Maryanski et al. 1987, McSharry, Burgert et al. 2008). Furthermore, deletion of E3gp19K promoted activation of the host immune response by enhancing tumour antigen presentation (Halldén, Hill et al. 2003, Wang, Hallden et al. 2003, Lichtenstein, Toth et al. 2004). In addition, active autophagy was recently reported to be required for MHC class II-mediated presentation of adenoviral antigens in infected cells (Klein, Jiang et al. 2016). According to Klein *et al*., autophagy inhibition prevented detection of viral-encoded antigens (Klein, Jiang et al. 2016). Several adenoviral genes appear to prevent autophagy-mediated elimination of the virus. The adenoviral protein VI has been reported to disrupt the endosome membrane (Wiethoff, Wodrich et al. 2005, Zeng and Carlin 2013), in addition, the RIDα protein facilitates virus escape from the endosome (Cianciola and Carlin 2009).

The Bcl-2 protein interacts with Beclin 1 to form a complex that prevents autophagy initiation (Pattingre, Tassa et al. 2005, Gordy and He 2012). Beclin 1 is also a target of viral Bcl-2 homologues, which may inhibit autophagy. For example, the Bcl-2 homologue encoded by Kaposi's sarcoma associated herpesvirus (KSHV) cannot be phosphorylated by JNKs and therefore, upon binding to Beclin 1, maintains its sequestration preventing autophagy

induction (Liang, E et al. 2008, Mack and Munger 2012). In addition, the herpes simplex-encoded protein Nef has been proposed to block autophagy maturation, although the mechanism is still unknown (Orvedahl, Alexander et al. 2007). However, adenovirus was recently reported to mediate phosphorylation of JNK1 and JNK2 promoting Bcl-2 phosphorylation and its dissociation from the Beclin 1-Bcl-2 complex (Klein, Piya et al. 2015). This interaction has been shown to induce autophagy in different cell lines (UG87MG, U251MG, A549 and MEF) although those did not include prostate cancer models (Klein, Jiang et al. 2016). The exact mechanism that mediates adenovirus-induced phosphorylation of JNK1 and JNK2 has not been described yet.

The tumour suppressor p53 regulates transcription of several genes that interfere with the autophagic pathways by upregulating transcription of negative regulators of the PI3K-AKT-mTOR pathway, such as AMPK, thereby promoting autophagy initiation (Mack and Munger 2012). Multiple DNA viruses, including adenovirus, interact with p53 and therefore could indirectly modulate autophagy through this pathway (White 2006, Mack and Munger 2012). However, in most cancers, including PCa, p53 is non-functional (Lorenzo, Arnoldussen et al. 2007), therefore, this pathway is not likely to play a role for oncolytic adenoviruses. I demonstrated that AdΔΔ attenuated mitoxantrone-induced autophagy in PC3 cells, which are p53 deficient, therefore, AdΔΔ-mediated autophagy modulation was probably p53-independent. Alternatively, several DNA viruses such as the Epstein-Barr virus (EBV), human papiloma virus (HPV), hepatitis B virus (HBV) and hepatitis C virus (HCV) have also been reported to upregulate the PI3KI-AKT-mTOR pathway promoting autophagy inhibition (Longnecker and Kieff 1990, Portis and Longnecker 2004, Mannová and Beretta 2005, Zhou and Münger 2009, Spangle and Münger 2010, Mack and Munger 2012). The EBV-encoded protein LMP2A has been reported to activate this pathway (Longnecker and Kieff 1990, Portis and Longnecker 2004). In addition, the HPV-encoded proteins E6 and E7 have been reported to activate AKT although, whether this interaction results in autophagy induction has not been demonstrated yet (Zhou and Münger 2009, Spangle and Münger 2010). The expression of the AKT negative-regulator PTEN is frequently lost in PCa (Majumder and Sellers 2005), resulting in active AKT that may also hamper viral interaction through this pathway.

4.7 Exploring viral efficacy and autophagy in 3-Dimensional co-cultures

We developed 3-dimensional cultures to investigate whether the AdΔΔ-mediated increased cell killing and attenuation of autophagy initiation also occurred in PCa models that more

accurately resembled the tumour microenvironment *in situ*. The normal human prostate stromal cells (PrSC) were grown together with the epithelial prostate carcinoma PC3 and 22Rv1 cells in a matrix composed of collagen type-I and matrigel.

Adenoviruses hold natural tropism for epithelial cells (Arnberg 2012, Wold and Toth 2013), therefore I investigated sensitivity to virus-induced cytotoxicity, viral infection, replication and the expression of the cellular surface receptors in PrSC cells in 2-dimensional cultures, prior to development of 3-dimensional cultures. My group previously demonstrated that AdΔΔ selectively replicated in cancer cells (Oberg, Yanover et al. 2010). In agreement with these observations I demonstrated that AdΔΔ replicated poorly in PrSC cells. Therefore, the high EC_{50}-values for AdΔΔ in PrSC cells could be explained by low levels of infection, because of low expression levels of hCAR, and low levels of replication (100-fold lower than Ad5wt) in these cells. Interestingly, I showed that expression of $\alpha_v\beta3$ and $\alpha_v\beta5$ integrins did not significantly facilitate infection in the absence of hCAR in PrSC cells. My findings are in agreement with Pandha *et al* (Pandha, Stockwin et al. 2003) that showed that in PC3 cells the absence of hCAR hampered adenoviral infection even in the presence of $\alpha_v\beta5$ integrin. PrSC cells also showed high EC_{50}-values to mitoxantrone, similar to those in PC3 cells.

Previously, the co-culture of epithelial pancreatic cancer cells with stromal fibroblasts on top of a collagen/matrigel matrix has been extensively studied at our institute (Froeling, Mirza et al. 2009, Froeling, Marshall et al. 2010, Coleman, Watt et al. 2014). Fibroblasts were reported to promote cell growth and invasion in these pancreatic 3-dimensional models. The interaction between the epithelial and the stromal compartments in prostate cancer has been reported to modulate the prostate cancer tumour microenvironment and contribute to prostate cancer growth and progression (Krušlin, Ulamec et al. 2015). In addition, the co-culture of PC3 cells with bone stromal derived HS5 cells was reported to promote growth and invasion in 3-dimensional matrigel-embedded cultures (Windus, Glover et al. 2013) and resulted in increased aggressiveness and mimicked bone metastasis in three-dimensional hydrogel cultures (Fong, Wan et al. 2016). I have demonstrated that the co-culture of either PC3 or 22Rv1 with PrSC in 3-dimensional cultures resulted in increased cell growth and proliferation into the matrix in preliminary studies, when compared to 3-dimensional epithelial monocultures. My preliminary data agreed with published findings and indicated that the proposed 3-dimensional culture model can be adapted for the study of prostate cancer.

The use of 3-dimensional cultures for pre-clinical testing of oncolytic adenovirus has not been widely studied yet. Adenovirus has been shown to effectively deliver transgenes into organoids (Wang, Zhang et al. 2014). The 3-dimensional model that we used is a powerful strategy to allow testing of novel therapies, including oncolytic viruses, in a more relevant environment. I showed that AdΔΔ, mitoxantrone, and the combination treatment were still effective in the PC3 and 22Rv1 co-culture models resulting in reduced invasion and increased cell death, indicated by reduced thickness. Despite being preliminary studies, these results are promising, as they confirmed the efficacy of the treatment and validated the model for further testing of oncolytic viral therapies in PCa.

It was previously reported that 3-dimensional ovarian cancer spheroids were used for testing adenoviral infection (Lam, Hemminki et al. 2007). The authors reported that viral infection and replication were 4-fold lower in 3-dimensional spheroids than in monolayers one week after infection. However, replication levels were equal 2 weeks after infection, suggesting that, although encountering initial resistance due to the decreased surface/volume ratio, the virus had successfully replicated and penetrated several cell layers in the 3-dimensional spheroid culture. In addition, the stromal compartment and the extracellular matrix have been suggested to hamper viral transduction into cancer cells and the spread of viral vectors (Kuppen, van der Eb et al. 2001). In my studies, viral doses were increased around 10-fold and 2-fold for 22Rv1 and PC3 cells, respectively, compared to the 2-dimensional cultures and both virus and drug were added 2-3 times over the indicated time-periods to overcome increased resistance to infection due to decreased surface/volume ratios and increased thickness of the matrix. Treatment with AdΔΔ, or the combination treatment resulted in AdΔΔ infection in 3-dimensional cultures, that was demonstrated with positive E1A staining. Infection of AdΔΔ was detected in all cell types, including PrSC.

Autophagy induction was detected with LC3B punctate staining. Interestingly, no LC3BII staining was detected in AdΔΔ-infected cells in either PrSC-22Rv1 or PrSC-PC3 cultures. These findings were in agreement with data generated in 2-dimensional monocultures and further indicated AdΔΔ-mediated attenuation of mitoxantrone-induced autophagy.

4.8 THE EFFECT OF GOLD NANOPARTICLES IN AdΔΔ CELL KILLING EFFICACY AND INFECTION IN PC3 AND 22Rv1 CELLS

The systemic administration of oncolytic adenoviruses would be desirable to target distant metastasis but is not widely used due to the difficulties of viral vectors to reach the tumours. The main issues are expression of hCAR, which is found in numerous non-target tissues (Arnberg 2012); binding of the viral vector to erythrocytes (Carlisle, Di et al. 2009); sequestration of the vector by Kupffer cells in the liver (Tao, Gao et al. 2001, Xu, Tian et al. 2008); up take of virus by hepatocytes (Waddington, McVey et al. 2008). Finally, viral transduction can be hampered by low expression of hCAR in the target cells, as it has been demonstrated in PC3 cells (Pandha, Stockwin et al. 2003, Adam, Ekblad et al. 2012).

Numerous strategies have been developed to increase targeted viral transduction and prevent its clearance from the circulation, such as modification of the viral capsid (Fueyo, Alemany et al. 2003, Takagi-Kimura, Yamano et al. 2013, Teigler, Penaloza-MacMaster et al. 2014), coating of the viral vectors with chemical polymers, such as PEG (Mok, Palmer et al. 2005, Kim, Kim et al. 2012) or preloading mesenchymal stem cells with the oncolytic vectors (Sherman, Shaker et al. 2016).

In my project I demonstrated that the combined treatment of AdΔΔ and mitoxantrone enhanced mitoxantrone-induced cell death by further promoting apoptosis and attenuating drug-induced autophagy in 22Rv1 and treatment resistant-PC3 cells. Despite demonstrated AdΔΔ-mediated enhancement of drug efficacy, high doses of the virus had to be used in PC3 cells to achieve this effect. I also showed that resistance to infection in PC3 cells, due to lack of expression of the cell surface receptors used by adenovirus, was probably the reason behind this requirement for higher doses. We hypothesized that the coating of oncolytic adenoviruses with positively-charged gold nanoparticles could enhance viral attachment to the negatively charged plasma membrane and prevent the rapid clearance from circulation of adenoviral vectors and its binding to erythrocytes. In collaboration with Prof Pilar Martinez (Universidad Francisco de Vitoria; UFV, Madrid, Spain), AdΔΔ was incubated with positively-charged gold nanoparticles to enhance viral attachment and uptake in cancer cells.

Gold nanoparticles (NP) are easy to functionalise and are currently being studied for drug delivery. Kamei *et al*. (Kamei, Mukai et al. 2009) demonstrated that a complex formed of an adenoviral vector and gold/iron magnetic nanoparticles easily penetrated the plasma membrane following the application of a magnetic force and independently of cellular

receptors. I have demonstrated that the coating of the oncolytic adenovirus AdΔΔ with positively-charged, PEG-functionalised gold nanoparticles enhanced treatment efficacy by increasing viral uptake. This enhancement in infection was likely due to neutralization of negatively-charged adenoviral particles and consequent facilitation of non-specific viral attachment and internalitation. Consequently, NP-mediated enhancement of viral infection, which, as I demonstrated, was higher in hCAR-negative PC3 cells and was possibly receptor-independent and non-specific, as previously reported (Kamei, Mukai et al. 2009). This hypothesis could be validated by testing viral uptake in hCAR-ablated cells. The chemotherapy agent 5-FU was reported to enhance adenoviral uptake in a receptor-independent manner by promoting morphological changes in the lipid bilayer (Cabrele, Vogel et al. 2006). NP could be enhancing adenoviral infection in a similar way. In addition, I showed that NP enhanced AdΔΔ-induced cytotoxicity, likely by increasing viral uptake. I also found that NP-coating of AdΔΔ resulted in a trend towards increased replication. The lack of correlation between increased viral uptake and cytotoxicity with lesser increases in viral replication might be due to the fact that cells were overloaded with viral particles and had reached their maximum replication or gene expression capacity. It is also possible that the NP-induced increased AdΔΔ-mediated cell death eliminated infected cells before viral replication could take place.

The gold nanoparticles that I used were functionalised with PEG-NR_4^+ (3000 PEG molecules per nanoparticle) but had not been tested in combination with adenovirus *in vivo* yet. Unfortunately, the coating of either adenoviral vectors (Mok, Palmer et al. 2005, Kim, Kim et al. 2012) or gold nanoparticles (Khlebtsov and Dykman 2011) with PEG had previously been reported to result in liver accumulation. Interestingly, the functionalization of gold nanoparticles with TNF has been reported to selectively target solid tumours (Khlebtsov and Dykman 2011). Therefore, functionalization of gold nanoparticles with cancer-targeting molecules would likely improve on tumour transduction and attenuate liver accumulation.

4.9 CONCLUDING REMARKS

I have shown in my work that AdΔΔ infection or E1A12S expression alone enhanced mitoxantrone-induced apoptotic cell death and attenuated mitoxantrone-induced autophagy initiation in the PCa cell lines PC3 and 22Rv1. Treatment with the late stage autophagy-inhibitor chloroquine enhanced mitoxantrone-induced apoptotic cell death in the presence or absence of AdΔΔ while autophagy induction with rapamycin desensitised cells

to mitoxantrone, prevented drug-induced apoptosis and the enhanced cell killing with AdΔΔ and mitoxantrone. Atg7-targeted knock-down in PC3 cells prevented autophagy initiation and enhanced mitoxantrone-induced apoptosis. These findings confirmed that autophagy inhibition with either chloroquine or Atg7-targeted knock-down enhanced mitoxantrone-induced apoptosis. However, siAtg7 transfection did not result in any effect on AdΔΔ-mediated sensitization to mitoxantrone. Importantly, despite the findings indicating that AdΔΔ infection promoted apoptosis and attenuated autophagy in mitoxantrone-treated cells, autophagy inhibition may not be the mechanism behind the observed AdΔΔ-mediated sensitization to mitoxantrone. Preliminary data showed that the combined treatment-induced enhanced cell killing and AdΔΔ-mediated prevention of autophagy were replicated in 3-dimensional cultures.

I have also shown that expression of the Bcl-2 protein was required for AdΔΔ-mediated sensitization to mitoxantrone in PC3 cells possibly because of the attenuation of E1A and hexon expression in mitoxantrone-treated Bcl-2 knocked-down PC3 cells. In addition, mitoxantrone-treatment decreased Bcl-2 mRNA and protein expression while AdΔΔ infection or E1A expression alone resulted in stabilization of the Bcl-2 protein. It can be concluded that the Bcl-2 protein plays a key role in AdΔΔ-mediated sensitization to mitoxantrone (**Figure *84***).

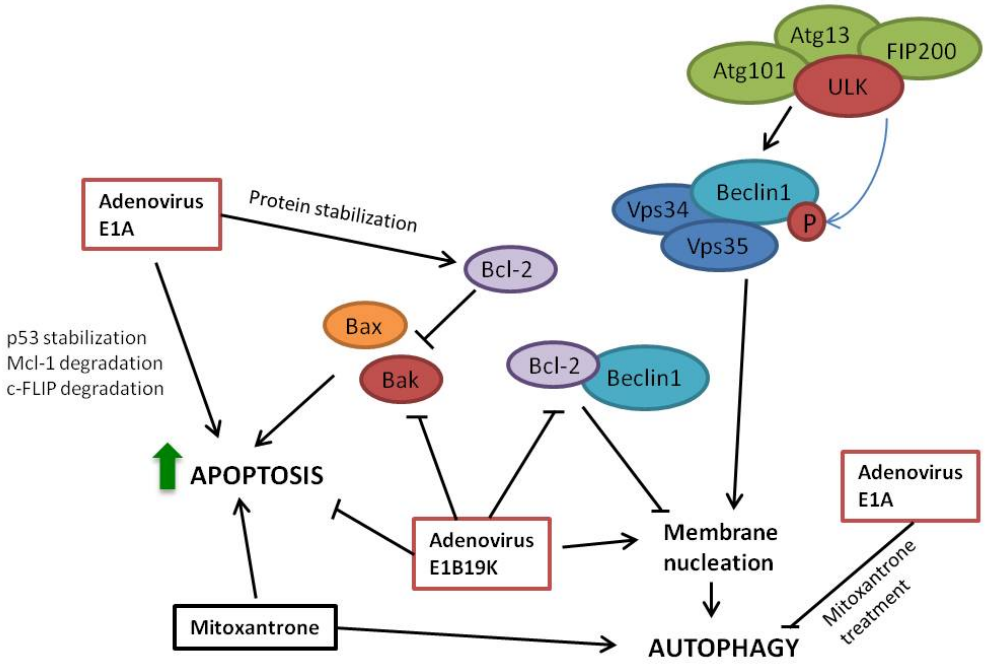

Figure 84. Schematic representation of the proposed role of E1A and E1B19K proteins and the chemotherapeutic agent mitoxantrone in the modulation of autophagic and apoptotic pathways in PC3 cells. Mitoxantrone treatment alone induced both apoptosis and autophagy. AdΔΔ infection or E1A12S expression prevented mitoxantrone-induced autophagy initiation and promoted apoptosis

and Bcl-2 stabilization. In addition, the E1A protein induces both p53-dependent and -independent apoptosis. The E1B19K protein interacts with Bax and Bad, in addition, it has been proposed to interact with Beclin 1, disrupting its interaction with Bcl-2.

4.10 FUTURE DIRECTIONS

Knock-down of Atg7 caused autophagy inhibition and promoted mitoxantrone-induced apoptosis but resulted in no additional effect in mitoxantrone-induced cell killing. Further studies are required to understand and better interpret these observations.

- Increased apoptosis in Atg7 knocked-down cells treated with mitoxantrone could be confirmed by testing additional time-points (shorter and longer) or slightly lower doses, as the tested mitoxantrone dose already promoted mitochondrial depolarization in 50-60% of cells.
- Other apoptotic markers such as detection of Annexin V staining could be used to confirm apoptosis regulation in mitoxantrone treated siAtg7 transfected PC3 cells.
- Apoptosis experiments should be correlated with cell viability detection under similar conditions to confirm if the increased mitochondrial depolarization correlates with increased cell death or decreased cell proliferation. Cell death or cell proliferation could be measured at later time points, and possibly by alternative methods such as trypan blue or crystal violet.
- To investigate whether chloroquine-mediated sensitization to mitoxantrone is independent of the effects on autophagy inhibition, it would be interesting to assess whether this sensitization to mitoxantrone is maintained in siAtg7 transfected PC3 cells.
- Findings should be validated in additional PCa cell lines (such as DU145 and LnCaP cells).

I have demonstrated that Bcl-2 expression was required for AdΔΔ-mediated sensitization to mitoxantrone. However, the exact mechanism used by the virus to interact with Bcl-2 has not been elucidated yet.

- The first step would be to perform sensitization assays to mitoxantrone with both Ad5wt and the Ad12S mutant in siBcl-2 transfected cells.
- If Ad12S fails to sensitise PC3 cells to mitoxantrone in the absence of Bcl-2 expression, as shown with AdΔΔ, it would be interesting to examine whether the E1A protein can directly interact with autophagy-related factors such as Beclin 1 or Bcl-

2. Therefore, a co-immunoprecipitation assay could be performed to confirm these interactions.

- It would also be informative to perform the same co-immunoprecipitation assays in Ad5wt-infected cells to show whether expression of the viral Bcl-2 homolog E1B19K interfered with this binding.
- Sensitization assays to mitoxantrone with either AdΔΔ or Ad12S could be performed in siBeclin 1 transfected cells to investigate the role of the autophagy modulator Beclin 1 in AdΔΔ-mediated enhancement of mitoxantrone-induced cell death.
- AdΔΔ infection and E1A12S expression were shown to attenuate mitoxantrone-induced decreases in expression of Bcl-2 at the protein level but not at the mRNA level. The effect of the combination treatment in Bcl-2 expression could be further studied with the use of proteasome inhibitors or ribosome inhibitors to further confirm if E1A expression can stabilise the Bcl-2 protein.
- Infection with AdΔ24 (E1ACR2 deleted) has been reported to promote phosphorylation of Bcl-2 therefore disrupting the Bcl-2-Beclin 1 complex (Klein, Piya et al. 2015). The study of Bcl-2 phosphorylation status as a result of the combination treatment would provide additional information on Bcl-2 and adenovirus interactions.
- I found that mitoxantrone treatment prevented the expression of E1A and hexon viral proteins in siBcl-2 transfected PC3 cells. A viral replication assay, such as the $TCID_{50}$ assay could be performed to assess whether sBcl-2 knock-down prevents AdΔΔ replication in mitoxantrone-treated PC3 cells.
- Findings should be validated in additional cancer cell lines.

5 REFERENCES

Abbink, P., A. A. Lemckert, B. A. Ewald, D. M. Lynch, M. Denholtz, S. Smits, L. Holterman, I. Damen, R. Vogels, A. R. Thorner, K. L. O'Brien, A. Carville, K. G. Mansfield, J. Goudsmit, M. J. Havenga and D. H. Barouch (2007). "Comparative seroprevalence and immunogenicity of six rare serotype recombinant adenovirus vaccine vectors from subgroups B and D." J Virol **81**(9): 4654-4663.

Adam, V., M. Ekblad, K. Sweeney, H. Müller, K. H. Busch, C. T. Johnsen, N. R. Kang, N. R. Lemoine and G. Halldén (2012). "Synergistic and Selective Cancer Cell Killing Mediated by the Oncolytic Adenoviral Mutant AdΔΔ and Dietary Phytochemicals in Prostate Cancer Models." Hum Gene Ther **23**(9): 1003-1015.

Alberti, C. (2013). "Taxane- and epothilone-based chemotherapy: from molecule cargo cytoskeletal logistics to management of castration-resistant prostate carcinoma." Eur Rev Med Pharmacol Sci **17**(12): 1658-1664.

Albertsen, P. C., L. Klotz, B. Tombal, J. Grady, T. K. Olesen and J. Nilsson (2014). "Cardiovascular morbidity associated with gonadotropin releasing hormone agonists and an antagonist." Eur Urol **65**(3): 565-573.

Alemany, R., K. Suzuki and D. T. Curiel (2000). "Blood clearance rates of adenovirus type 5 in mice." J Gen Virol **81**(Pt 11): 2605-2609.

Anderson, K. M. and S. Liao (1968). "Selective retention of dihydrotestosterone by prostatic nuclei." Nature **219**(5151): 277-279.

Anghelina, D., E. Lam and E. Falck-Pedersen (2016). "Diminished Innate Antiviral Response to Adenovirus Vectors in cGAS/STING-Deficient Mice Minimally Impacts Adaptive Immunity." J Virol **90**(13): 5915-5927.

Antonarakis, E. S., C. Lu, B. Luber, H. Wang, Y. Chen, M. Nakazawa, R. Nadal, C. J. Paller, S. R. Denmeade, M. A. Carducci, M. A. Eisenberger and J. Luo (2015). "Androgen Receptor Splice Variant 7 and Efficacy of Taxane Chemotherapy in Patients With Metastatic Castration-Resistant Prostate Cancer." JAMA Oncol **1**(5): 582-591.

Ao, M., O. E. Franco, D. Park, D. Raman, K. Williams and S. W. Hayward (2007). "Cross-talk between paracrine-acting cytokine and chemokine pathways promotes malignancy in benign human prostatic epithelium." Cancer Res **67**(9): 4244-4253.

Araujo, F. D., T. H. Stracker, C. T. Carson, D. V. Lee and M. D. Weitzman (2005). "Adenovirus type 5 E4orf3 protein targets the Mre11 complex to cytoplasmic aggresomes." J Virol **79**(17): 11382-11391.

Arnberg, N. (2012). "Adenovirus receptors: implications for targeting of viral vectors." Trends Pharmacol Sci **33**(8): 442-448.

Ashkenazi, A. (2008). "Targeting the extrinsic apoptosis pathway in cancer." Cytokine Growth Factor Rev **19**(3-4): 325-331.

Aslam, H. M., N. Shahid, N. A. Shaikh, H. A. Shaikh, S. Saleem and A. Mughal (2013). "Spectrum of prostatic lesions." Int Arch Med **6**(1): 36.

Atlas, T. H. P. (2017, 4th April 2017). "CD46." from http://www.proteinatlas.org/ENSG00000117335-CD46/tissue.

Ayala, G., T. Satoh, R. Li, M. Shalev, Y. Gdor, E. Aguilar-Cordova, A. Frolov, T. M. Wheeler, B. J. Miles, K. Rauen, B. S. Teh, E. B. Butler, T. C. Thompson and D. Kadmon (2006). "Biological response determinants in HSV-tk + ganciclovir gene therapy for prostate cancer." Mol Ther **13**(4): 716-728.

Azad, A. A., S. V. Volik, A. W. Wyatt, A. Haegert, S. Le Bihan, R. H. Bell, S. A. Anderson, B. McConeghy, R. Shukin, J. Bazov, J. Youngren, P. Paris, G. Thomas, E. J. Small, Y. Wang, M. E. Gleave, C. C. Collins and K. N. Chi (2015). "Androgen Receptor Gene Aberrations in Circulating Cell-Free DNA: Biomarkers of Therapeutic Resistance in Castration-Resistant Prostate Cancer." Clin Cancer Res **21**(10): 2315-2324.

Azzouni, F., A. Godoy, Y. Li and J. Mohler (2012). "The 5 alpha-reductase isozyme family: a review of basic biology and their role in human diseases." Adv Urol **2012**: 530121.

Bachmann, I. M., O. J. Halvorsen, K. Collett, I. M. Stefansson, O. Straume, S. A. Haukaas, H. B. Salvesen, A. P. Otte and L. A. Akslen (2006). "EZH2 expression is associated with high proliferation rate and aggressive tumor subgroups in cutaneous melanoma and cancers of the endometrium, prostate, and breast." J Clin Oncol **24**(2): 268-273.

Backström, E., K. B. Kaufmann, X. Lan and G. Akusjärvi (2010). "Adenovirus L4-22K stimulates major late transcription by a mechanism requiring the intragenic late-specific transcription factor-binding site." Virus Res **151**(2): 220-228.

Baker, A., K. J. Rohleder, L. A. Hanakahi and G. Ketner (2007). "Adenovirus E4 34k and E1b 55k oncoproteins target host DNA ligase IV for proteasomal degradation." J Virol **81**(13): 7034-7040.

Baker, S. J. and E. P. Reddy (2013). "Understanding the temporal sequence of genetic events that lead to prostate cancer progression and metastasis." Proc Natl Acad Sci U S A **110**(37): 14819-14820.

Baniecki, M. L., W. J. McGrath and W. F. Mangel (2013). "Regulation of a viral proteinase by a peptide and DNA in one-dimensional space: III. atomic resolution structure of the nascent form of the adenovirus proteinase." J Biol Chem **288**(3): 2081-2091.

Barentsz, J. O., J. Richenberg, R. Clements, P. Choyke, S. Verma, G. Villeirs, O. Rouviere, V. Logager, J. J. Futterer and R. European Society of Urogenital (2012). "ESUR prostate MR guidelines 2012." Eur Radiol **22**(4): 746-757.

Barron, D. A. and D. R. Rowley (2012). "The reactive stroma microenvironment and prostate cancer progression." Endocr Relat Cancer **19**(6): R187-204.

Barton, K. N., H. Stricker, M. A. Elshaikh, J. Pegg, J. Cheng, Y. Zhang, K. C. Karvelis, M. Lu, B. Movsas and S. O. Freytag (2011). "Feasibility of adenovirus-mediated hNIS gene transfer and

131I radioiodine therapy as a definitive treatment for localized prostate cancer." Mol Ther **19**(7): 1353-1359.

Bastos, D. A. and E. S. Antonarakis (2016). "Galeterone for the treatment of advanced prostate cancer: the evidence to date." Drug Des Devel Ther **10**: 2289-2297.

Bastus, N. C., L. K. Boyd, X. Mao, E. Stankiewicz, S. C. Kudahetti, R. T. Oliver, D. M. Berney and Y. J. Lu (2010). "Androgen-induced TMPRSS2:ERG fusion in nonmalignant prostate epithelial cells." Cancer Res **70**(23): 9544-9548.

Bates, R. C., N. S. Edwards and J. D. Yates (2000). "Spheroids and cell survival." Crit Rev Oncol Hematol **36**(2-3): 61-74.

Beahrs, O., D. Henson, R. Hutter and B. Kennedy (1992). American Joint Committee on Cancer staging manual for staging of cancer, 4th edn. Philadelphia, PA, Lippincott.

Beer, T. M., A. J. Armstrong, D. E. Rathkopf, Y. Loriot, C. N. Sternberg, C. S. Higano, P. Iversen, S. Bhattacharya, J. Carles, S. Chowdhury, I. D. Davis, J. S. de Bono, C. P. Evans, K. Fizazi, A. M. Joshua, C. S. Kim, G. Kimura, P. Mainwaring, H. Mansbach, K. Miller, S. B. Noonberg, F. Perabo, D. Phung, F. Saad, H. I. Scher, M. E. Taplin, P. M. Venner, B. Tombal and P. Investigators (2014). "Enzalutamide in metastatic prostate cancer before chemotherapy." N Engl J Med **371**(5): 424-433.

Bell, E., B. Ivarsson and C. Merrill (1979). "Production of a tissue-like structure by contraction of collagen lattices by human fibroblasts of different proliferative potential in vitro." Proc Natl Acad Sci U S A **76**(3): 1274-1278.

Benedict, C. A., P. S. Norris, T. I. Prigozy, J. L. Bodmer, J. A. Mahr, C. T. Garnett, F. Martinon, J. Tschopp, L. R. Gooding and C. F. Ware (2001). "Three adenovirus E3 proteins cooperate to evade apoptosis by tumor necrosis factor-related apoptosis-inducing ligand receptor-1 and -2." J Biol Chem **276**(5): 3270-3278.

Bennett, H. L., J. Stockley, J. T. Fleming, R. Mandal, J. O'Prey, K. M. Ryan, C. N. Robson and H. Y. Leung (2013). "Does androgen-ablation therapy (AAT) associated autophagy have a pro-survival effect in LNCaP human prostate cancer cells?" BJU Int **111**(4): 672-682.

Bergelson, J. M., J. A. Cunningham, G. Droguett, E. A. Kurt-Jones, A. Krithivas, J. S. Hong, M. S. Horwitz, R. L. Crowell and R. W. Finberg (1997). "Isolation of a common receptor for Coxsackie B viruses and adenoviruses 2 and 5." Science **275**(5304): 1320-1323.

Berk, A. J. (2005). "Recent lessons in gene expression, cell cycle control, and cell biology from adenovirus." Oncogene **24**(52): 7673-7685.

Bhatia-Gaur, R., A. A. Donjacour, P. J. Sciavolino, M. Kim, N. Desai, P. Young, C. R. Norton, T. Gridley, R. D. Cardiff, G. R. Cunha, C. Abate-Shen and M. M. Shen (1999). "Roles for Nkx3.1 in prostate development and cancer." Genes Dev **13**(8): 966-977.

Biasiotto, R. and G. Akusjärvi (2015). "Regulation of human adenovirus alternative RNA splicing by the adenoviral L4-33K and L4-22K proteins." Int J Mol Sci **16**(2): 2893-2912.

Bilbao, G., J. L. Contreras, H. G. Zhang, M. J. Pike, K. Overturf, G. Mikheeva, V. Krasnykh and D. T. Curiel (1999). "Adenovirus-mediated gene expression in vivo is enhanced by the antiapoptotic bcl-2 gene." J Virol **73**(8): 6992-7000.

Birgersdotter, A., R. Sandberg and I. Ernberg (2005). "Gene expression perturbation in vitro--a growing case for three-dimensional (3D) culture systems." Semin Cancer Biol **15**(5): 405-412.

Boehnke, K., N. Mirancea, A. Pavesio, N. E. Fusenig, P. Boukamp and H. J. Stark (2007). "Effects of fibroblasts and microenvironment on epidermal regeneration and tissue function in long-term skin equivalents." Eur J Cell Biol **86**(11-12): 731-746.

Bolla, M., G. Van Tienhoven, P. Warde, J. B. Dubois, R. O. Mirimanoff, G. Storme, J. Bernier, A. Kuten, C. Sternberg, I. Billiet, J. L. Torecilla, R. Pfeffer, C. L. Cutajar, T. Van der Kwast and L. Collette (2010). "External irradiation with or without long-term androgen suppression for prostate cancer with high metastatic risk: 10-year results of an EORTC randomised study." Lancet Oncol **11**(11): 1066-1073.

Bonkhoff, H. (2001). "Morphogenesis of prostate cancer." Eur Urol **39 Suppl 4**: 5-7.
Boulanger, P. A. and G. E. Blair (1991). "Expression and interactions of human adenovirus oncoproteins." Biochem J **275 (Pt 2)**: 281-299.

Bowen, C. and E. P. Gelmann (2010). "NKX3.1 activates cellular response to DNA damage." Cancer Res **70**(8): 3089-3097.

Boya, P., R. A. Gonzalez-Polo, D. Poncet, K. Andreau, H. L. Vieira, T. Roumier, J. L. Perfettini and G. Kroemer (2003). "Mitochondrial membrane permeabilization is a critical step of lysosome-initiated apoptosis induced by hydroxychloroquine." Oncogene **22**(25): 3927-3936.

Bressy, C. and K. Benihoud (2014). "Association of oncolytic adenoviruses with chemotherapies: an overview and future directions." Biochem Pharmacol **90**(2): 97-106.

Brockmann, D., B. Tries and H. Esche (1990). "Isolation and characterization of novel adenovirus type 12 E1A mRNAs by cDNA PCR technique." Virology **179**(2): 585-590.

Brooke, G. N. and C. L. Bevan (2009). "The role of androgen receptor mutations in prostate cancer progression." Curr Genomics **10**(1): 18-25.

Bruchovsky, N. and J. D. Wilson (1968). "The intranuclear binding of testosterone and 5-alpha-androstan-17-beta-ol-3-one by rat prostate." J Biol Chem **243**(22): 5953-5960.

Buijsen, J., J. van den Bogaard, B. Jutten, E. Belgers, M. Sosef, J. W. Leijtens, G. L. Beets, R. L. Jansen, R. G. Riedl, R. Clarijs, G. Lammering and P. Lambin (2015). "A phase I-II study on the combination of rapamycin and short course radiotherapy in rectal cancer." Radiother Oncol **116**(2): 214-220.

Burckhardt, C. J., M. Suomalainen, P. Schoenenberger, K. Boucke, S. Hemmi and U. F. Greber (2011). "Drifting motions of the adenovirus receptor CAR and immobile integrins initiate virus uncoating and membrane lytic protein exposure." Cell Host Microbe **10**(2): 105-117.

Burgert, H. G., J. L. Maryanski and S. Kvist (1987). ""E3/19K" protein of adenovirus type 2 inhibits lysis of cytolytic T lymphocytes by blocking cell-surface expression of histocompatibility class I antigens." Proc Natl Acad Sci U S A **84**(5): 1356-1360.

Burgert, H. G., Z. Ruzsics, S. Obermeier, A. Hilgendorf, M. Windheim and A. Elsing (2002). "Subversion of host defense mechanisms by adenoviruses." Curr Top Microbiol Immunol **269**: 273-318.

Bussemakers, M. J., A. van Bokhoven, G. W. Verhaegh, F. P. Smit, H. F. Karthaus, J. A. Schalken, F. M. Debruyne, N. Ru and W. B. Isaacs (1999). "DD3: a new prostate-specific gene, highly overexpressed in prostate cancer." Cancer Res **59**(23): 5975-5979.

Cabrele, C., M. Vogel, P. Piso, M. Rentsch, J. Schröder, K. W. Jauch, H. J. Schlitt and A. Beham (2006). "5-Fluorouracil-related enhancement of adenoviral infection is Coxsackievirus-adenovirus receptor independent and associated with morphological changes in lipid membranes." World J Gastroenterol **12**(32): 5168-5174.

Cao, Q., J. Yu, S. M. Dhanasekaran, J. H. Kim, R. S. Mani, S. A. Tomlins, R. Mehra, B. Laxman, X. Cao, C. G. Kleer, S. Varambally and A. M. Chinnaiyan (2008). "Repression of E-cadherin by the polycomb group protein EZH2 in cancer." Oncogene **27**(58): 7274-7284.

Carles, J., D. Castellano, M. A. Climent, P. Maroto, R. Medina and A. Alcaraz (2012). "Castration-resistant metastatic prostate cancer: current status and treatment possibilities." Clin Transl Oncol **14**(3): 169-176.

Carlisle, R. C., Y. Di, A. M. Cerny, A. F. Sonnen, R. B. Sim, N. K. Green, V. Subr, K. Ulbrich, R. J. Gilbert, K. D. Fisher, R. W. Finberg and L. W. Seymour (2009). "Human erythrocytes bind and inactivate type 5 adenovirus by presenting Coxsackie virus-adenovirus receptor and complement receptor 1." Blood **113**(9): 1909-1918.

Carter, G., K. Clover, B. Britton, A. J. Mitchell, M. White, N. McLeod, J. Denham and S. D. Lambert (2015). "Wellbeing during Active Surveillance for localised prostate cancer: a systematic review of psychological morbidity and quality of life." Cancer Treat Rev **41**(1): 46-60.

Castro, E., C. Goh, D. Olmos, E. Saunders, D. Leongamornlert, M. Tymrakiewicz, N. Mahmud, T. Dadaev, K. Govindasami, M. Guy, E. Sawyer, R. Wilkinson, A. Ardern-Jones, S. Ellis, D. Frost, S. Peock, D. G. Evans, M. Tischkowitz, T. Cole, R. Davidson, D. Eccles, C. Brewer, F. Douglas, M. E. Porteous, A. Donaldson, H. Dorkins, L. Izatt, J. Cook, S. Hodgson, M. J. Kennedy, L. E. Side, J. Eason, A. Murray, A. C. Antoniou, D. F. Easton, Z. Kote-Jarai and R. Eeles (2013). "Germline BRCA mutations are associated with higher risk of nodal involvement, distant metastasis, and poor survival outcomes in prostate cancer." J Clin Oncol **31**(14): 1748-1757.

Catalona, W. J., D. S. Smith, T. L. Ratliff, K. M. Dodds, D. E. Coplen, J. J. Yuan, J. A. Petros and G. L. Andriole (1991). "Measurement of prostate-specific antigen in serum as a screening test for prostate cancer." N Engl J Med **324**(17): 1156-1161.

Center, M. M., A. Jemal, J. Lortet-Tieulent, E. Ward, J. Ferlay, O. Brawley and F. Bray (2012). "International variation in prostate cancer incidence and mortality rates." Eur Urol **61**(6): 1079-1092.

Chang, Y. W., M. C. Hung and J. L. Su (2014). "The anti-tumor activity of E1A and its implications in cancer therapy." Arch Immunol Ther Exp (Warsz) **62**(3): 195-204.

Chappell, W. H., B. D. Lehmann, D. M. Terrian, S. L. Abrams, L. S. Steelman and J. A. McCubrey (2012). "p53 expression controls prostate cancer sensitivity to chemotherapy and the MDM2 inhibitor Nutlin-3." Cell Cycle **11**(24): 4579-4588.

Chattopadhyay, D., M. K. Ghosh, A. Mal and M. L. Harter (2001). "Inactivation of p21 by E1A leads to the induction of apoptosis in DNA-damaged cells." J Virol **75**(20): 9844-9856.

Chen, H. and M. C. Hung (1997). "Involvement of co-activator p300 in the transcriptional regulation of the HER-2/neu gene." J Biol Chem **272**(10): 6101-6104.

Chen, N. and V. Karantza (2011). "Autophagy as a therapeutic target in cancer." Cancer Biol Ther **11**(2): 157-168.

Chen, X., Y. Liu, J. Wu, H. Huang, Z. Du, K. Zhang, D. Zhou, K. Hung, S. Goodin and X. Zheng (2016). "Mechanistic Study of Inhibitory Effects of Atorvastatin and Docetaxel in Combination on Prostate Cancer." Cancer Genomics Proteomics **13**(2): 151-160.

Cheng, L., R. Montironi, D. G. Bostwick, A. Lopez-Beltran and D. M. Berney (2012). "Staging of prostate cancer." Histopathology **60**(1): 87-117.

Cheng, P. H., S. Lian, R. Zhao, X. M. Rao, K. M. McMasters and H. S. Zhou (2013). "Combination of autophagy inducer rapamycin and oncolytic adenovirus improves antitumor effect in cancer cells." Virol J **10**: 293.

Cheong, H. (2015). "Integrating autophagy and metabolism in cancer." Arch Pharm Res **38**(3): 358-371.

Cherubini, G., C. Kallin, A. Mozetic, K. Hammaren-Busch, H. Muller, N. R. Lemoine and G. Hallden (2011). "The oncolytic adenovirus AdDeltaDelta enhances selective cancer cell killing in combination with DNA-damaging drugs in pancreatic cancer models." Gene Ther **18**(12): 1157-1165.

Chikte, S., N. Panchal and G. Warnes (2014). "Use of LysoTracker dyes: a flow cytometric study of autophagy." Cytometry A **85**(2): 169-178.

Chinnadurai, G. (2009). "The transcriptional corepressor CtBP: a foe of multiple tumor suppressors." Cancer Res **69**(3): 731-734.

Chinnadurai, G. (2011). "Opposing oncogenic activities of small DNA tumor virus transforming proteins." Trends Microbiol **19**(4): 174-183.

Chipuk, J. E. and D. R. Green (2006). "Dissecting p53-dependent apoptosis." Cell Death Differ **13**(6): 994-1002.

Chiramel, A. I., N. R. Brady and R. Bartenschlager (2013). "Divergent roles of autophagy in virus infection." Cells **2**(1): 83-104.

Cho, Y. S., S. Challa, D. Moquin, R. Genga, T. D. Ray, M. Guildford and F. K. Chan (2009). "Phosphorylation-driven assembly of the RIP1-RIP3 complex regulates programmed necrosis and virus-induced inflammation." Cell **137**(6): 1112-1123.

Choi, J. W., J. Kim, Q. N. Bui, Y. Li, C. O. Yun, D. S. Lee and S. W. Kim (2015). "Tuning Surface Charge and PEGylation of Biocompatible Polymers for Efficient Delivery of Nucleic Acid or Adenoviral Vector." Bioconjug Chem **26**(8): 1818-1829.

Cianciola, N. L. and C. R. Carlin (2009). "Adenovirus RID-alpha activates an autonomous cholesterol regulatory mechanism that rescues defects linked to Niemann-Pick disease type C." J Cell Biol **187**(4): 537-552.

Cichon, G., S. Boeckh-Herwig, H. H. Schmidt, E. Wehnes, T. Müller, P. Pring-Akerblom and R. Burger (2001). "Complement activation by recombinant adenoviruses." Gene Ther **8**(23): 1794-1800.

Clifford, B., M. Beljin, G. R. Stark and W. R. Taylor (2003). "G2 arrest in response to topoisomerase II inhibitors: the role of p53." Cancer Res **63**(14): 4074-4081.

Coleman, S. J., J. Watt, P. Arumugam, L. Solaini, E. Carapuca, M. Ghallab, R. P. Grose and H. M. Kocher (2014). "Pancreatic cancer organotypics: High throughput, preclinical models for pharmacological agent evaluation." World J Gastroenterol **20**(26): 8471-8481.

Conde, J., A. Ambrosone, V. Sanz, Y. Hernandez, V. Marchesano, F. Tian, H. Child, C. Berry, M. Ibarra, P. Baptista, C. Tortiglione and J. de la Fuente (2012). "Design of Multifunctional Gold Nanoparticles for In Vitro and In Vivo Gene Silencing." Acs Nano **6**(9): 8316-8324.

Cotter, K., B. Konety and M. A. Ordonez (2016). "Contemporary Management of Prostate Cancer." F1000Res **5**.

Coughlan, L., A. C. Bradshaw, A. L. Parker, H. Robinson, K. White, J. Custers, J. Goudsmit, N. Van Roijen, D. H. Barouch, S. A. Nicklin and A. H. Baker (2012). "Ad5:Ad48 hexon hypervariable region substitutions lead to toxicity and increased inflammatory responses following intravenous delivery." Mol Ther **20**(12): 2268-2281.

Cox, J. H., J. R. Bennink and J. W. Yewdell (1991). "Retention of adenovirus E19 glycoprotein in the endoplasmic reticulum is essential to its ability to block antigen presentation." J Exp Med **174**(6): 1629-1637.

Cuconati, A., C. Mukherjee, D. Perez and E. White (2003). "DNA damage response and MCL-1 destruction initiate apoptosis in adenovirus-infected cells." Genes Dev **17**(23): 2922-2932.

Cunha, G. R., S. W. Hayward, Y. Z. Wang and W. A. Ricke (2003). "Role of the stromal microenvironment in carcinogenesis of the prostate." Int J Cancer **107**(1): 1-10.

Cunha, G. R., W. Ricke, A. Thomson, P. C. Marker, G. Risbridger, S. W. Hayward, Y. Z. Wang, A. A. Donjacour and T. Kurita (2004). "Hormonal, cellular, and molecular regulation of normal and neoplastic prostatic development." J Steroid Biochem Mol Biol **92**(4): 221-236.

Cunningham, D. and Z. You (2015). "In vitro and in vivo model systems used in prostate cancer research." J Biol Methods **2**(1).

Cuzick, J., M. A. Thorat, G. Andriole, O. W. Brawley, P. H. Brown, Z. Culig, R. A. Eeles, L. G. Ford, F. C. Hamdy, L. Holmberg, D. Ilic, T. J. Key, C. La Vecchia, H. Lilja, M. Marberger, F. L. Meyskens, L. M. Minasian, C. Parker, H. L. Parnes, S. Perner, H. Rittenhouse, J. Schalken, H. P. Schmid, B. J. Schmitz-Drager, F. H. Schroder, A. Stenzl, B. Tombal, T. J. Wilt and A. Wolk (2014). "Prevention and early detection of prostate cancer." Lancet Oncol **15**(11): e484-492.

D'Amico, A. V., R. Whittington, S. B. Malkowicz, Y. H. Wu, M. H. Chen, M. Hurwitz, P. W. Kantoff, J. E. Tomaszewski, A. A. Renshaw, A. Wein and J. P. Richie (2000). "Utilizing predictions of early prostate-specific antigen failure to optimize patient selection for adjuvant systemic therapy trials." J Clin Oncol **18**(18): 3240-3246.

Danila, D. C., M. J. Morris, J. S. de Bono, C. J. Ryan, S. R. Denmeade, M. R. Smith, M. E. Taplin, G. J. Bubley, T. Kheoh, C. Haqq, A. Molina, A. Anand, M. Koscuiszka, S. M. Larson, L. H. Schwartz, M. Fleisher and H. I. Scher (2010). "Phase II multicenter study of abiraterone acetate plus prednisone therapy in patients with docetaxel-treated castration-resistant prostate cancer." J Clin Oncol **28**(9): 1496-1501.

Davies Cde, L., D. A. Berk, A. Pluen and R. K. Jain (2002). "Comparison of IgG diffusion and extracellular matrix composition in rhabdomyosarcomas grown in mice versus in vitro as spheroids reveals the role of host stromal cells." Br J Cancer **86**(10): 1639-1644.

Dayyani, F., G. E. Gallick, C. J. Logothetis and P. G. Corn (2011). "Novel therapies for metastatic castrate-resistant prostate cancer." J Natl Cancer Inst **103**(22): 1665-1675.

De Jong, W., W. Hagens, P. Krystek, M. Burger, A. Sips and R. Geertsma (2008). "Particle size-dependent organ distribution of gold nanoparticles after intravenous administration." Biomaterials **29**(12): 1912-1919.

De Marzo, A. M., E. A. Platz, S. Sutcliffe, J. Xu, H. Gronberg, C. G. Drake, Y. Nakai, W. B. Isaacs and W. G. Nelson (2007). "Inflammation in prostate carcinogenesis." Nat Rev Cancer **7**(4): 256-269.

de Vrij, J., R. A. Willemsen, L. Lindholm, R. C. Hoeben, C. H. Bangma, C. Barber, J. P. Behr, S. Briggs, R. Carlisle, W. S. Cheng, I. J. Dautzenberg, C. de Ridder, H. Dzojic, P. Erbacher, M. Essand, K. Fisher, A. Frazier, L. J. Georgopoulos, I. Jennings, S. Kochanek, D. Koppers-Lalic, R. Kraaij, F. Kreppel, M. Magnusson, N. Maitland, P. Neuberg, R. Nugent, M. Ogris, J. S. Remy, M. Scaife, E. Schenk-Braat, E. Schooten, L. Seymour, M. Slade, P. Szyjanowicz, T. Totterman, T. G. Uil, K. Ulbrich, L. van der Weel, W. van Weerden, E. Wagner, G. Zuber and G. Consortium (2010). "Adenovirus-derived vectors for prostate cancer gene therapy." Hum Gene Ther **21**(7): 795-805.

Deng, J., F. Kloosterbooer, W. Xia and M. C. Hung (2002). "The NH(2)-terminal and conserved region 2 domains of adenovirus E1A mediate two distinct mechanisms of tumor suppression." Cancer Res **62**(2): 346-350.

Denmeade, S. R. and J. T. Isaacs (2002). "A history of prostate cancer treatment." Nat Rev Cancer **2**(5): 389-396.

DeWeese, T. L., H. van der Poel, S. Li, B. Mikhak, R. Drew, M. Goemann, U. Hamper, R. DeJong, N. Detorie, R. Rodriguez, T. Haulk, A. M. DeMarzo, S. Piantadosi, D. C. Yu, Y. Chen, D. R.

Henderson, M. A. Carducci, W. G. Nelson and J. W. Simons (2001). "A phase I trial of CV706, a replication-competent, PSA selective oncolytic adenovirus, for the treatment of locally recurrent prostate cancer following radiation therapy." Cancer Res **61**(20): 7464-7472.

Di Paolo, N. C., E. A. Miao, Y. Iwakura, K. Murali-Krishna, A. Aderem, R. A. Flavell, T. Papayannopoulou and D. M. Shayakhmetov (2009). "Virus binding to a plasma membrane receptor triggers interleukin-1 alpha-mediated proinflammatory macrophage response in vivo." Immunity **31**(1): 110-121.

Doronin, K. and D. M. Shayakhmetov (2012). "Construction of targeted and armed oncolytic adenoviruses." Methods Mol Biol **797**: 35-52.

Droga-Mazovec, G., L. Bojic, A. Petelin, S. Ivanova, R. Romih, U. Repnik, G. S. Salvesen, V. Stoka, V. Turk and B. Turk (2008). "Cysteine cathepsins trigger caspase-dependent cell death through cleavage of bid and antiapoptotic Bcl-2 homologues." J Biol Chem **283**(27): 19140-19150.

Duff, J. and I. J. McEwan (2005). "Mutation of histidine 874 in the androgen receptor ligand-binding domain leads to promiscuous ligand activation and altered p160 coactivator interactions." Mol Endocrinol **19**(12): 2943-2954.

Dunigan, D. D., S. B. Waters and T. C. Owen (1995). "Aqueous soluble tetrazolium/formazan MTS as an indicator of NADH- and NADPH-dependent dehydrogenase activity." Biotechniques **19**(4): 640-649.

Edge, S. B. and C. C. Compton (2010). "The American Joint Committee on Cancer: the 7th edition of the AJCC cancer staging manual and the future of TNM." Ann Surg Oncol **17**(6): 1471-1474.

Ehrbar, M., S. C. Rizzi, R. G. Schoenmakers, B. S. Miguel, J. A. Hubbell, F. E. Weber and M. P. Lutolf (2007). "Biomolecular hydrogels formed and degraded via site-specific enzymatic reactions." Biomacromolecules **8**(10): 3000-3007.

Eikenes, L., I. Tufto, E. A. Schnell, A. Bjorkoy and C. De Lange Davies (2010). "Effect of collagenase and hyaluronidase on free and anomalous diffusion in multicellular spheroids and xenografts." Anticancer Res **30**(2): 359-368.

Ellem, S. J., E. M. De-Juan-Pardo and G. P. Risbridger (2014). "In vitro modeling of the prostate cancer microenvironment." Adv Drug Deliv Rev **79-80**: 214-221.

Eng, C. H., Z. Wang, D. Tkach, L. Toral-Barza, S. Ugwonali, S. Liu, S. L. Fitzgerald, E. George, E. Frias, N. Cochran, R. De Jesus, G. McAllister, G. R. Hoffman, K. Bray, L. Lemon, J. Lucas, V. R. Fantin, R. T. Abraham, L. O. Murphy and B. Nyfeler (2016). "Macroautophagy is dispensable for growth of KRAS mutant tumors and chloroquine efficacy." Proc Natl Acad Sci U S A **113**(1): 182-187.

Epstein, J. I., W. C. Allsbrook, M. B. Amin, L. L. Egevad and I. G. Committee (2005). "The 2005 International Society of Urological Pathology (ISUP) Consensus Conference on Gleason Grading of Prostatic Carcinoma." Am J Surg Pathol **29**(9): 1228-1242.

Epstein, J. I., L. Egevad, M. B. Amin, B. Delahunt, J. R. Srigley, P. A. Humphrey and G. Committee (2016). "The 2014 International Society of Urological Pathology (ISUP) Consensus Conference on Gleason Grading of Prostatic Carcinoma: Definition of Grading Patterns and Proposal for a New Grading System." Am J Surg Pathol **40**(2): 244-252.

Eum, K. H. and M. Lee (2011). "Crosstalk between autophagy and apoptosis in the regulation of paclitaxel-induced cell death in v-Ha-ras-transformed fibroblasts." Mol Cell Biochem **348**(1-2): 61-68.

Everts, M., V. Saini, J. L. Leddon, R. J. Kok, M. Stoff-Khalili, M. A. Preuss, C. L. Millican, G. Perkins, J. M. Brown, H. Bagaria, D. E. Nikles, D. T. Johnson, V. P. Zharov and D. T. Curiel (2006). "Covalently linked Au nanoparticles to a viral vector: potential for combined photothermal and gene cancer therapy." Nano Lett **6**(4): 587-591.

Fallica, B., J. S. Maffei, S. Villa, G. Makin and M. Zaman (2012). "Alteration of cellular behavior and response to PI3K pathway inhibition by culture in 3D collagen gels." PLoS One **7**(10): e48024.

Fang, X., S. Sittadjody, K. Gyabaah, E. C. Opara and K. C. Balaji (2013). "Novel 3D co-culture model for epithelial-stromal cells interaction in prostate cancer." PLoS One **8**(9): e75187.

Farrow, J. M., J. C. Yang and C. P. Evans (2014). "Autophagy as a modulator and target in prostate cancer." Nat Rev Urol **11**(9): 508-516.

Favaloro, B., N. Allocati, V. Graziano, C. Di Ilio and V. De Laurenzi (2012). "Role of apoptosis in disease." Aging (Albany NY) **4**(5): 330-349.

Feng, Z., W. Hu, E. de Stanchina, A. K. Teresky, S. Jin, S. Lowe and A. J. Levine (2007). "The regulation of AMPK beta1, TSC2, and PTEN expression by p53: stress, cell and tissue specificity, and the role of these gene products in modulating the IGF-1-AKT-mTOR pathways." Cancer Res **67**(7): 3043-3053.

Feng, Z., H. Zhang, A. J. Levine and S. Jin (2005). "The coordinate regulation of the p53 and mTOR pathways in cells." Proc Natl Acad Sci U S A **102**(23): 8204-8209.

Ferreon, J. C., M. A. Martinez-Yamout, H. J. Dyson and P. E. Wright (2009). "Structural basis for subversion of cellular control mechanisms by the adenoviral E1A oncoprotein." Proc Natl Acad Sci U S A **106**(32): 13260-13265.

Festjens, N., T. Vanden Berghe, S. Cornelis and P. Vandenabeele (2007). "RIP1, a kinase on the crossroads of a cell's decision to live or die." Cell Death Differ **14**(3): 400-410.

Festjens, N., T. Vanden Berghe and P. Vandenabeele (2006). "Necrosis, a well-orchestrated form of cell demise: signalling cascades, important mediators and concomitant immune response." Biochim Biophys Acta **1757**(9-10): 1371-1387.

Fisher, K. D., Y. Stallwood, N. K. Green, K. Ulbrich, V. Mautner and L. W. Seymour (2001). "Polymer-coated adenovirus permits efficient retargeting and evades neutralising antibodies." Gene Ther **8**(5): 341-348.

Fizazi, K. (2007). "The role of Src in prostate cancer." Ann Oncol **18**(11): 1765-1773.

Fizazi, K., L. Faivre, F. Lesaunier, R. Delva, G. Gravis, F. Rolland, F. Priou, J. M. Ferrero, N. Houede, L. Mourey, C. Theodore, I. Krakowski, J. F. Berdah, M. Baciuchka, B. Laguerre, A. Fléchon, A. Ravaud, I. Cojean-Zelek, S. Oudard, J. L. Labourey, P. Chinet-Charrot, E. Legouffe, J. L. Lagrange, C. Linassier, G. Deplanque, P. Beuzeboc, J. L. Davin, A. L. Martin, M. Habibian, A. Laplanche and S. Culine (2015). "Androgen deprivation therapy plus docetaxel and estramustine versus androgen deprivation therapy alone for high-risk localised prostate cancer (GETUG 12): a phase 3 randomised controlled trial." Lancet Oncol **16**(7): 787-794.

Fong, E. L., X. Wan, J. Yang, M. Morgado, A. G. Mikos, D. A. Harrington, N. M. Navone and M. C. Farach-Carson (2016). "A 3D in vitro model of patient-derived prostate cancer xenograft for controlled interrogation of in vivo tumor-stromal interactions." Biomaterials **77**: 164-172.
Freytag, S. O., M. Khil, H. Stricker, J. Peabody, M. Menon, M. DePeralta-Venturina, D. Nafziger, J. Pegg, D. Paielli, S. Brown, K. Barton, M. Lu, E. Aguilar-Cordova and J. H. Kim (2002). "Phase I study of replication-competent adenovirus-mediated double suicide gene therapy for the treatment of locally recurrent prostate cancer." Cancer Res **62**(17): 4968-4976.

Freytag, S. O., B. Movsas, I. Aref, H. Stricker, J. Peabody, J. Pegg, Y. Zhang, K. N. Barton, S. L. Brown, M. Lu, A. Savera and J. H. Kim (2007). "Phase I trial of replication-competent adenovirus-mediated suicide gene therapy combined with IMRT for prostate cancer." Mol Ther **15**(5): 1016-1023.

Freytag, S. O., K. R. Rogulski, D. L. Paielli, J. D. Gilbert and J. H. Kim (1998). "A novel three-pronged approach to kill cancer cells selectively: concomitant viral, double suicide gene, and radiotherapy." Hum Gene Ther **9**(9): 1323-1333.

Freytag, S. O., H. Stricker, J. Peabody, J. Pegg, D. Paielli, B. Movsas, K. N. Barton, S. L. Brown, M. Lu and J. H. Kim (2007). "Five-year follow-up of trial of replication-competent adenovirus-mediated suicide gene therapy for treatment of prostate cancer." Mol Ther **15**(3): 636-642.

Freytag, S. O., H. Stricker, J. Pegg, D. Paielli, D. G. Pradhan, J. Peabody, M. DePeralta-Venturina, X. Xia, S. Brown, M. Lu and J. H. Kim (2003). "Phase I study of replication-competent adenovirus-mediated double-suicide gene therapy in combination with conventional-dose three-dimensional conformal radiation therapy for the treatment of newly diagnosed, intermediate- to high-risk prostate cancer." Cancer Res **63**(21): 7497-7506.

Freytag, S. O., Y. Zhang and F. Siddiqui (2015). "Preclinical toxicology of oncolytic adenovirus-mediated cytotoxic and interleukin-12 gene therapy for prostate cancer." Mol Ther Oncolytics **2**.

Frisch, S. M. (1994). "E1a induces the expression of epithelial characteristics." J Cell Biol **127**(4): 1085-1096.

Froeling, F. E., J. F. Marshall and H. M. Kocher (2010). "Pancreatic cancer organotypic cultures." J Biotechnol **148**(1): 16-23.

Froeling, F. E., T. A. Mirza, R. M. Feakins, A. Seedhar, G. Elia, I. R. Hart and H. M. Kocher (2009). "Organotypic culture model of pancreatic cancer demonstrates that stromal cells modulate E-cadherin, beta-catenin, and Ezrin expression in tumor cells." Am J Pathol **175**(2): 636-648.

Frolov, M. V. and N. J. Dyson (2004). "Molecular mechanisms of E2F-dependent activation and pRB-mediated repression." J Cell Sci **117**(Pt 11): 2173-2181.

Fueyo, J., R. Alemany, C. Gomez-Manzano, G. N. Fuller, A. Khan, C. A. Conrad, T. J. Liu, H. Jiang, M. G. Lemoine, K. Suzuki, R. Sawaya, D. T. Curiel, W. K. Yung and F. F. Lang (2003). "Preclinical characterization of the antiglioma activity of a tropism-enhanced adenovirus targeted to the retinoblastoma pathway." J Natl Cancer Inst **95**(9): 652-660.

Fueyo, J., C. Gomez-Manzano, R. Alemany, P. S. Lee, T. J. McDonnell, P. Mitlianga, Y. X. Shi, V. A. Levin, W. K. Yung and A. P. Kyritsis (2000). "A mutant oncolytic adenovirus targeting the Rb pathway produces anti-glioma effect in vivo." Oncogene **19**(1): 2-12.

Fulda, S. (2015). "Targeting apoptosis for anticancer therapy." Semin Cancer Biol **31C**: 84-88.
Gallagher, L. E., L. E. Williamson and E. Y. Chan (2016). "Advances in Autophagy Regulatory Mechanisms." Cells **5**(2).

Gallagher, S. R. (2001). "Quantification of DNA and RNA with absorption and fluorescence spectroscopy." Curr Protoc Cell Biol **Appendix 3**: Appendix 3D.

Gallimore, P. H. and A. S. Turnell (2001). "Adenovirus E1A: remodelling the host cell, a life or death experience." Oncogene **20**(54): 7824-7835.

Garber, K. (2006). "China approves world's first oncolytic virus therapy for cancer treatment." J Natl Cancer Inst **98**(5): 298-300.

García-Castro, J., R. Alemany, M. Cascalló, J. Martínez-Quintanilla, M. e. M. Arriero, A. Lassaletta, L. Madero and M. Ramírez (2010). "Treatment of metastatic neuroblastoma with systemic oncolytic virotherapy delivered by autologous mesenchymal stem cells: an exploratory study." Cancer Gene Ther **17**(7): 476-483.

Gardner, T. A., B. D. Elzey and N. M. Hahn (2012). "Sipuleucel-T (Provenge) autologous vaccine approved for treatment of men with asymptomatic or minimally symptomatic castrate-resistant metastatic prostate cancer." Hum Vaccin Immunother **8**(4): 534-539.

Gelmann, E. P. (2002). "Molecular biology of the androgen receptor." J Clin Oncol **20**(13): 3001-3015.

Genesys, C. (2005, June 27, 2005). "A Phase I/II Dose Finding Trial of the Intravenous Injection of CV787, a Prostate-Specific Antigen Cytolytic Adenovirus, in Patients With Hormone Refractory Metastatic Prostate Cancer." Retrieved March 25th, 2015, from https://clinicaltrials.gov/ct2/show/record/NCT00116155.

Geng, Y., L. Kohli, B. J. Klocke and K. A. Roth (2010). "Chloroquine-induced autophagic vacuole accumulation and cell death in glioma cells is p53 independent." Neuro Oncol **12**(5): 473-481.

Gewirtz, D. A. (2016). "The Challenge of Developing Autophagy Inhibition as a Therapeutic Strategy." Cancer Res **76**(19): 5610-5614.

Giberson, A. N., A. R. Davidson and R. J. Parks (2012). "Chromatin structure of adenovirus DNA throughout infection." Nucleic Acids Res **40**(6): 2369-2376.

Gleason, D. F. and G. T. Mellinger (1974). "Prediction of prognosis for prostatic adenocarcinoma by combined histological grading and clinical staging." J Urol **111**(1): 58-64.
Glick, D., S. Barth and K. F. Macleod (2010). "Autophagy: cellular and molecular mechanisms." J Pathol **221**(1): 3-12.

Goh, C. L. and R. A. Eeles (2014). "Germline genetic variants associated with prostate cancer and potential relevance to clinical practice." Recent Results Cancer Res **202**: 9-26.

Goldufsky J, S. S., Harcharik S, Pan M, Bernardo S, Stern RH, Friedlander P, Ruby CE, Saenger Y, Kaufman HL (2013). "Oncolytic virus therapy for cancer." Oncolytic Virotherapy **2**: 31-46.

Golstein, P. and G. Kroemer (2007). "Cell death by necrosis: towards a molecular definition." Trends Biochem Sci **32**(1): 37-43.

Gomez-Manzano, C., M. M. Alonso, W. K. Yung, F. McCormick, D. T. Curiel, F. F. Lang, H. Jiang, B. N. Bekele, X. Zhou, R. Alemany and J. Fueyo (2006). "Delta-24 increases the expression and activity of topoisomerase I and enhances the antiglioma effect of irinotecan." Clin Cancer Res **12**(2): 556-562.

Goodrum, F. D. and D. A. Ornelles (1998). "p53 status does not determine outcome of E1B 55-kilodalton mutant adenovirus lytic infection." J Virol **72**(12): 9479-9490.
Gordy, C. and Y. W. He (2012). "The crosstalk between autophagy and apoptosis: where does this lead?" Protein Cell **3**(1): 17-27.

Graff, J. R., B. W. Konicek, A. M. McNulty, Z. Wang, K. Houck, S. Allen, J. D. Paul, A. Hbaiu, R. G. Goode, G. E. Sandusky, R. L. Vessella and B. L. Neubauer (2000). "Increased AKT activity contributes to prostate cancer progression by dramatically accelerating prostate tumor growth and diminishing p27Kip1 expression." J Biol Chem **275**(32): 24500-24505.

Gravina, G. L., A. Mancini, G. Ranieri, B. Di Pasquale, F. Marampon, L. Di Clemente, E. Ricevuto and C. Festuccia (2013). "Phenotypic characterization of human prostatic stromal cells in primary cultures derived from human tissue samples." Int J Oncol **42**(6): 2116-2122.
Guan, H., J. Jiao and R. P. Ricciardi (2008). "Tumorigenic adenovirus type 12 E1A inhibits phosphorylation of NF-kappaB by PKAc, causing loss of DNA binding and transactivation." J Virol **82**(1): 40-48.

Gundem, G., P. Van Loo, B. Kremeyer, L. B. Alexandrov, J. M. Tubio, E. Papaemmanuil, D. S. Brewer, H. M. Kallio, G. Hognas, M. Annala, K. Kivinummi, V. Goody, C. Latimer, S. O'Meara, K. J. Dawson, W. Isaacs, M. R. Emmert-Buck, M. Nykter, C. Foster, Z. Kote-Jarai, D. Easton, H. C. Whitaker, I. P. U. Group, D. E. Neal, C. S. Cooper, R. A. Eeles, T. Visakorpi, P. J. Campbell, U. McDermott, D. C. Wedge and G. S. Bova (2015). "The evolutionary history of lethal metastatic prostate cancer." Nature **520**(7547): 353-357.

Guo, J. Y., G. Karsli-Uzunbas, R. Mathew, S. C. Aisner, J. J. Kamphorst, A. M. Strohecker, G. Chen, S. Price, W. Lu, X. Teng, E. Snyder, U. Santanam, R. S. Dipaola, T. Jacks, J. D. Rabinowitz and E. White (2013). "Autophagy suppresses progression of K-ras-induced lung tumors to oncocytomas and maintains lipid homeostasis." Genes Dev **27**(13): 1447-1461.

Gurel, B., T. Iwata, C. M. Koh, S. Yegnasubramanian, W. G. Nelson and A. M. De Marzo (2008). "Molecular alterations in prostate cancer as diagnostic, prognostic, and therapeutic targets." Adv Anat Pathol **15**(6): 319-331.

Gurski, L. A., A. K. Jha, C. Zhang, X. Jia and M. C. Farach-Carson (2009). "Hyaluronic acid-based hydrogels as 3D matrices for in vitro evaluation of chemotherapeutic drugs using poorly adherent prostate cancer cells." Biomaterials **30**(30): 6076-6085.

Gustin, K. E. and M. J. Imperiale (1998). "Encapsidation of viral DNA requires the adenovirus L1 52/55-kilodalton protein." J Virol **72**(10): 7860-7870.

Gustin, K. E., P. Lutz and M. J. Imperiale (1996). "Interaction of the adenovirus L1 52/55-kilodalton protein with the IVa2 gene product during infection." J Virol **70**(9): 6463-6467.

Hakkarainen, T., M. Särkioja, P. Lehenkari, S. Miettinen, T. Ylikomi, R. Suuronen, R. A. Desmond, A. Kanerva and A. Hemminki (2007). "Human mesenchymal stem cells lack tumor tropism but enhance the antitumor activity of oncolytic adenoviruses in orthotopic lung and breast tumors." Hum Gene Ther **18**(7): 627-641.

Hallden, G., Wang, Y., Wong, H., Lemoine, N. R. (2013). Oncolytic adenoviruses for cancer gene therapy. Advanced Textbook on Gene Transfer, Gene Therapy and Genetic Pharmacology. D. Scherman, Imperial College Press. **Part III**.

Halldén, G., R. Hill, Y. Wang, A. Anand, T. C. Liu, N. R. Lemoine, J. Francis, L. Hawkins and D. Kirn (2003). "Novel immunocompetent murine tumor models for the assessment of replication-competent oncolytic adenovirus efficacy." Mol Ther **8**(3): 412-424.

Halldén, G. and G. Portella (2012). "Oncolytic virotherapy with modified adenoviruses and novel therapeutic targets." Expert Opin Ther Targets **16**(10): 945-958.

Hanahan, D. and R. A. Weinberg (2000). "The hallmarks of cancer." Cell **100**(1): 57-70.

Harris, W. P., E. A. Mostaghel, P. S. Nelson and B. Montgomery (2009). "Androgen deprivation therapy: progress in understanding mechanisms of resistance and optimizing androgen depletion." Nat Clin Pract Urol **6**(2): 76-85.
Hart, L. S., D. Ornelles and C. Koumenis (2007). "The adenoviral E4orf6 protein induces atypical apoptosis in response to DNA damage." J Biol Chem **282**(9): 6061-6067.

Hasson, T. B., D. A. Ornelles and T. Shenk (1992). "Adenovirus L1 52- and 55-kilodalton proteins are present within assembling virions and colocalize with nuclear structures distinct from replication centers." J Virol **66**(10): 6133-6142.

Haupt, S., M. Berger, Z. Goldberg and Y. Haupt (2003). "Apoptosis - the p53 network." J Cell Sci **116**(Pt 20): 4077-4085.

Hayward, S. W. and G. R. Cunha (2000). "The prostate: development and physiology." Radiol Clin North Am **38**(1): 1-14.

Heidenreich, A., P. J. Bastian, J. Bellmunt, M. Bolla, S. Joniau, T. van der Kwast, M. Mason, V. Matveev, T. Wiegel, F. Zattoni, N. Mottet and E. A. o. Urology (2014). "EAU guidelines on

prostate cancer. part 1: screening, diagnosis, and local treatment with curative intent-update 2013." Eur Urol **65**(1): 124-137.

Heidenreich, A., P. J. Bastian, J. Bellmunt, M. Bolla, S. Joniau, T. van der Kwast, M. Mason, V. Matveev, T. Wiegel, F. Zattoni, N. Mottet and E. A. o. Urology (2014). "EAU guidelines on prostate cancer. Part II: Treatment of advanced, relapsing, and castration-resistant prostate cancer." Eur Urol **65**(2): 467-479.

Heise, C., T. Hermiston, L. Johnson, G. Brooks, A. Sampson-Johannes, A. Williams, L. Hawkins and D. Kirn (2000). "An adenovirus E1A mutant that demonstrates potent and selective systemic anti-tumoral efficacy." Nat Med **6**(10): 1134-1139.

Heise, C., A. Sampson-Johannes, A. Williams, F. McCormick, D. D. Von Hoff and D. H. Kirn (1997). "ONYX-015, an E1B gene-attenuated adenovirus, causes tumor-specific cytolysis and antitumoral efficacy that can be augmented by standard chemotherapeutic agents." Nat Med **3**(6): 639-645.

Hermiston, T. W., R. A. Tripp, T. Sparer, L. R. Gooding and W. S. Wold (1993). "Deletion mutation analysis of the adenovirus type 2 E3-gp19K protein: identification of sequences within the endoplasmic reticulum lumenal domain that are required for class I antigen binding and protection from adenovirus-specific cytotoxic T lymphocytes." J Virol **67**(9): 5289-5298.

Hoeben, R. C. and T. G. Uil (2013). "Adenovirus DNA replication." Cold Spring Harb Perspect Biol **5**(3): a013003.

Hong, S. S., E. Szolajska, G. Schoehn, L. Franqueville, S. Myhre, L. Lindholm, R. W. Ruigrok, P. Boulanger and J. Chroboczek (2005). "The 100K-chaperone protein from adenovirus serotype 2 (Subgroup C) assists in trimerization and nuclear localization of hexons from subgroups C and B adenoviruses." J Mol Biol **352**(1): 125-138.

Horning, J. L., S. K. Sahoo, S. Vijayaraghavalu, S. Dimitrijevic, J. K. Vasir, T. K. Jain, A. K. Panda and V. Labhasetwar (2008). "3-D tumor model for in vitro evaluation of anticancer drugs." Mol Pharm **5**(5): 849-862.

Horwitz, M. S. (2004). "Function of adenovirus E3 proteins and their interactions with immunoregulatory cell proteins." J Gene Med **6 Suppl 1**: S172-183.

Howard, C. M., F. Forsberg, C. Minimo, J. B. Liu, D. A. Merton and P. P. Claudio (2006). "Ultrasound guided site specific gene delivery system using adenoviral vectors and commercial ultrasound contrast agents." J Cell Physiol **209**(2): 413-421.

Huang, T. G., M. J. Savontaus, K. Shinozaki, B. V. Sauter and S. L. Woo (2003). "Telomerase-dependent oncolytic adenovirus for cancer treatment." Gene Ther **10**(15): 1241-1247.

Huard, J., H. Lochmüller, G. Acsadi, A. Jani, B. Massie and G. Karpati (1995). "The route of administration is a major determinant of the transduction efficiency of rat tissues by adenoviral recombinants." Gene Ther **2**(2): 107-115.

Huggins, C. and C. V. Hodges (2002). "Studies on prostatic cancer: I. The effect of castration, of estrogen and of androgen injection on serum phosphatases in metastatic carcinoma of the prostate. 1941." J Urol **168**(1): 9-12.

Hughes, J. P., G. Alusi and Y. Wang (2015). "Viral gene therapy for head and neck cancer." J Laryngol Otol: 1-7.

Huncharek, M., K. S. Haddock, R. Reid and B. Kupelnick (2010). "Smoking as a risk factor for prostate cancer: a meta-analysis of 24 prospective cohort studies." Am J Public Health **100**(4): 693-701.

Hörnberg, E., E. B. Ylitalo, S. Crnalic, H. Antti, P. Stattin, A. Widmark, A. Bergh and P. Wikström (2011). "Expression of androgen receptor splice variants in prostate cancer bone metastases is associated with castration-resistance and short survival." PLoS One **6**(4): e19059.

Iacobelli-Martinez, M. and G. R. Nemerow (2007). "Preferential activation of Toll-like receptor nine by CD46-utilizing adenoviruses." J Virol **81**(3): 1305-1312.

Imparato, G., F. Urciuolo and a. N. P. A. (2015). "In vitro three-dimensional models in cancer research: a review." International Materials Reviews **60**(6): 297-311.

Ip, S., I. J. Dahabreh, M. Chung, W. W. Yu, E. M. Balk, R. C. Iovin, P. Mathew, T. Luongo, T. Dvorak and J. Lau (2011). "An evidence review of active surveillance in men with localized prostate cancer." Evid Rep Technol Assess (Full Rep)(204): 1-341.

Ito, H., H. Aoki, F. Kuhnel, Y. Kondo, S. Kubicka, T. Wirth, E. Iwado, A. Iwamaru, K. Fujiwara, K. R. Hess, F. F. Lang, R. Sawaya and S. Kondo (2006). "Autophagic cell death of malignant glioma cells induced by a conditionally replicating adenovirus." J Natl Cancer Inst **98**(9): 625-636.

Jayaram, S., T. Gilson, E. S. Ehrlich, X. F. Yu, G. Ketner and L. Hanakahi (2008). "E1B 55k-independent dissociation of the DNA ligase IV/XRCC4 complex by E4 34k during adenovirus infection." Virology **382**(2): 163-170.

Jemal, A., F. Bray, M. M. Center, J. Ferlay, E. Ward and D. Forman (2011). "Global cancer statistics." CA Cancer J Clin **61**(2): 69-90.

Jemal, A., R. Siegel, E. Ward, Y. Hao, J. Xu and M. J. Thun (2009). "Cancer statistics, 2009." CA Cancer J Clin **59**(4): 225-249.

Jia, L., S. Kim and H. Yu (2013). "Tracking spindle checkpoint signals from kinetochores to APC/C." Trends Biochem Sci **38**(6): 302-311.

Jiang, H., C. Gomez-Manzano, F. F. Lang, R. Alemany and J. Fueyo (2009). "Oncolytic adenovirus: preclinical and clinical studies in patients with human malignant gliomas." Curr Gene Ther **9**(5): 422-427.

Jiang, H., Z. Wang, D. Serra, M. M. Frank and A. Amalfitano (2004). "Recombinant adenovirus vectors activate the alternative complement pathway, leading to the binding of human complement protein C3 independent of anti-ad antibodies." Mol Ther **10**(6): 1140-1142.

Jiang, H., E. J. White, C. Gomez-Manzano and J. Fueyo (2008). "Adenovirus's last trick: you say lysis, we say autophagy." Autophagy **4**(1): 118-120.

Jones, R. G., D. R. Plas, S. Kubek, M. Buzzai, J. Mu, Y. Xu, M. J. Birnbaum and C. B. Thompson (2005). "AMP-activated protein kinase induces a p53-dependent metabolic checkpoint." Mol Cell **18**(3): 283-293.

Jordan, M. A., K. Wendell, S. Gardiner, W. B. Derry, H. Copp and L. Wilson (1996). "Mitotic block induced in HeLa cells by low concentrations of paclitaxel (Taxol) results in abnormal mitotic exit and apoptotic cell death." Cancer Res **56**(4): 816-825.

Jordan, M. A. and L. Wilson (2004). "Microtubules as a target for anticancer drugs." Nat Rev Cancer **4**(4): 253-265.

Josset, E., H. Burckel, G. Noël and P. Bischoff (2013). "The mTOR inhibitor RAD001 potentiates autophagic cell death induced by temozolomide in a glioblastoma cell line." Anticancer Res **33**(5): 1845-1851.

Kaighn, M. E., K. S. Narayan, Y. Ohnuki, J. F. Lechner and L. W. Jones (1979). "Establishment and characterization of a human prostatic carcinoma cell line (PC-3)." Invest Urol **17**(1): 16-23.

Kamei, K., Y. Mukai, H. Kojima, T. Yoshikawa, M. Yoshikawa, G. Kiyohara, T. A. Yamamoto, Y. Yoshioka, N. Okada, S. Seino and S. Nakagawa (2009). "Direct cell entry of gold/iron-oxide magnetic nanoparticles in adenovirus mediated gene delivery." Biomaterials **30**(9): 1809-1814.

Kanellopoulos, P. N., H. van der Zandt, D. Tsernoglou, P. C. van der Vliet and P. A. Tucker (1995). "Crystallization and preliminary X-ray crystallographic studies on the adenovirus ssDNA binding protein in complex with ssDNA." J Struct Biol **115**(1): 113-116.

Kanerva, A., G. V. Mikheeva, V. Krasnykh, C. J. Coolidge, J. T. Lam, P. J. Mahasreshti, S. D. Barker, M. Straughn, M. N. Barnes, R. D. Alvarez, A. Hemminki and D. T. Curiel (2002). "Targeting adenovirus to the serotype 3 receptor increases gene transfer efficiency to ovarian cancer cells." Clin Cancer Res **8**(1): 275-280.

Kang, E. and C. O. Yun (2010). "Current advances in adenovirus nanocomplexes: more specificity and less immunogenicity." BMB Rep **43**(12): 781-788.

Kang, R., H. J. Zeh, M. T. Lotze and D. Tang (2011). "The Beclin 1 network regulates autophagy and apoptosis." Cell Death Differ **18**(4): 571-580.

Karantanos, T., P. G. Corn and T. C. Thompson (2013). "Prostate cancer progression after androgen deprivation therapy: mechanisms of castrate resistance and novel therapeutic approaches." Oncogene **32**(49): 5501-5511.

Karen, K. A. and P. Hearing (2011). "Adenovirus core protein VII protects the viral genome from a DNA damage response at early times after infection." J Virol **85**(9): 4135-4142.

Karl, S., Y. Pritschow, M. Volcic, S. Häcker, B. Baumann, L. Wiesmüller, K. M. Debatin and S. Fulda (2009). "Identification of a novel pro-apopotic function of NF-kappaB in the DNA damage response." J Cell Mol Med **13**(10): 4239-4256.

Karlin, S. and V. Brendel (1988). "Charge configurations in viral proteins." Proc Natl Acad Sci U S A **85**(24): 9396-9400.

Khare, R., V. S. Reddy, G. R. Nemerow and M. A. Barry (2012). "Identification of adenovirus serotype 5 hexon regions that interact with scavenger receptors." J Virol **86**(4): 2293-2301.

Khlebtsov, N. and L. Dykman (2011). "Biodistribution and toxicity of engineered gold nanoparticles: a review of in vitro and in vivo studies." Chemical Society Reviews **40**(3): 1647-1671.

Khor, L. Y., J. Moughan, T. Al-Saleem, E. H. Hammond, V. Venkatesan, S. A. Rosenthal, M. A. Ritter, H. M. Sandler, G. E. Hanks, W. U. Shipley and A. Pollack (2007). "Bcl-2 and Bax expression predict prostate cancer outcome in men treated with androgen deprivation and radiotherapy on radiation therapy oncology group protocol 92-02." Clin Cancer Res **13**(12): 3585-3590.

Kilcher, S. and J. Mercer (2015). "DNA virus uncoating." Virology **479-480**: 578-590.

Kim, J., P. Kim, S. Kim and C. Yun (2012). "Enhancing the therapeutic efficacy of adenovirus in combination with biomaterials." Biomaterials **33**(6): 1838-1850.

Kim, J. H., K. W. Kim, M. H. Kim and Y. S. Yu (2009). "Intravenously administered gold nanoparticles pass through the blood-retinal barrier depending on the particle size, and induce no retinal toxicity." Nanotechnology **20**(50): 505101.

Kim, J. S., S. D. Lee, S. J. Lee and M. K. Chung (2013). "Development of an immunotherapeutic adenovirus targeting hormone-independent prostate cancer." Onco Targets Ther **6**: 1635-1642.

Kim, K. H., I. P. Dmitriev, S. Saddekni, E. A. Kashentseva, R. D. Harris, R. Aurigemma, S. Bae, K. P. Singh, G. P. Siegal, D. T. Curiel and R. D. Alvarez (2013). "A phase I clinical trial of Ad5/3-Delta24, a novel serotype-chimeric, infectivity-enhanced, conditionally-replicative adenovirus (CRAd), in patients with recurrent ovarian cancer." Gynecol Oncol **130**(3): 518-524.

Kimball, K. J., M. A. Preuss, M. N. Barnes, M. Wang, G. P. Siegal, W. Wan, H. Kuo, S. Saddekni, C. R. Stockard, W. E. Grizzle, R. D. Harris, R. Aurigemma, D. T. Curiel and R. D. Alvarez (2010). "A phase I study of a tropism-modified conditionally replicative adenovirus for recurrent malignant gynecologic diseases." Clin Cancer Res **16**(21): 5277-5287.

King, A. J. and P. C. van der Vliet (1994). "A precursor terminal protein-trinucleotide intermediate during initiation of adenovirus DNA replication: regeneration of molecular ends in vitro by a jumping back mechanism." EMBO J **13**(23): 5786-5792.

King, J. C., J. Xu, J. Wongvipat, H. Hieronymus, B. S. Carver, D. H. Leung, B. S. Taylor, C. Sander, R. D. Cardiff, S. S. Couto, W. L. Gerald and C. L. Sawyers (2009). "Cooperativity of TMPRSS2-ERG with PI3-kinase pathway activation in prostate oncogenesis." Nat Genet **41**(5): 524-526.

Klein, S. R., H. Jiang, M. B. Hossain, X. Fan, J. Gumin, A. Dong, M. M. Alonso, C. Gomez-Manzano and J. Fueyo (2016). "Critical Role of Autophagy in the Processing of Adenovirus Capsid-Incorporated Cancer-Specific Antigens." PLoS One **11**(4): e0153814.

Klein, S. R., S. Piya, Z. Lu, Y. Xia, M. M. Alonso, E. J. White, J. Wei, C. Gomez-Manzano, H. Jiang and J. Fueyo (2015). "C-Jun N-terminal kinases are required for oncolytic adenovirus-mediated autophagy." Oncogene.

Kleinman, H. K. and G. R. Martin (2005). "Matrigel: basement membrane matrix with biological activity." Semin Cancer Biol **15**(5): 378-386.

Klionsky, D. J., K. Abdelmohsen, A. Abe, M. J. Abedin, H. Abeliovich, A. Acevedo Arozena, H. Adachi, C. M. Adams, P. D. Adams, K. Adeli, P. J. Adhihetty, S. G. Adler, G. Agam, R. Agarwal, M. K. Aghi, M. Agnello, P. Agostinis, P. V. Aguilar, J. Aguirre-Ghiso, E. M. Airoldi, S. Ait-Si-Ali, T. Akematsu, E. T. Akporiaye, M. Al-Rubeai, G. M. Albaiceta, C. Albanese, D. Albani, M. L. Albert, J. Aldudo, H. Algül, M. Alirezaei, I. Alloza, A. Almasan, M. Almonte-Beceril, E. S. Alnemri, C. Alonso, N. Altan-Bonnet, D. C. Altieri, S. Alvarez, L. Alvarez-Erviti, S. Alves, G. Amadoro, A. Amano, C. Amantini, S. Ambrosio, I. Amelio, A. O. Amer, M. Amessou, A. Amon, Z. An, F. A. Anania, S. U. Andersen, U. P. Andley, C. K. Andreadi, N. Andrieu-Abadie, A. Anel, D. K. Ann, S. Anoopkumar-Dukie, M. Antonioli, H. Aoki, N. Apostolova, S. Aquila, K. Aquilano, K. Araki, E. Arama, A. Aranda, J. Araya, A. Arcaro, E. Arias, H. Arimoto, A. R. Ariosa, J. L. Armstrong, T. Arnould, I. Arsov, K. Asanuma, V. Askanas, E. Asselin, R. Atarashi, S. S. Atherton, J. D. Atkin, L. D. Attardi, P. Auberger, G. Auburger, L. Aurelian, R. Autelli, L. Avagliano, M. L. Avantaggiati, L. Avrahami, S. Awale, N. Azad, T. Bachetti, J. M. Backer, D. H. Bae, J. S. Bae, O. N. Bae, S. H. Bae, E. H. Baehrecke, S. H. Baek, S. Baghdiguian, A. Bagniewska-Zadworna, H. Bai, J. Bai, X. Y. Bai, Y. Bailly, K. N. Balaji, W. Balduini, A. Ballabio, R. Balzan, R. Banerjee, G. Bánhegyi, H. Bao, B. Barbeau, M. D. Barrachina, E. Barreiro, B. Bartel, A. Bartolomé, D. C. Bassham, M. T. Bassi, R. C. Bast, A. Basu, M. T. Batista, H. Batoko, M. Battino, K. Bauckman, B. L. Baumgarner, K. U. Bayer, R. Beale, J. F. Beaulieu, G. R. Beck, C. Becker, J. D. Beckham, P. A. Bédard, P. J. Bednarski, T. J. Begley, C. Behl, C. Behrends, G. M. Behrens, K. E. Behrns, E. Bejarano, A. Belaid, F. Belleudi, G. Bénard, G. Berchem, D. Bergamaschi, M. Bergami, B. Berkhout, L. Berliocchi, A. Bernard, M. Bernard, F. Bernassola, A. Bertolotti, A. S. Bess, S. Besteiro, S. Bettuzzi, S. Bhalla, S. Bhattacharyya, S. K. Bhutia, C. Biagosch, M. W. Bianchi, M. Biard-Piechaczyk, V. Billes, C. Bincoletto, B. Bingol, S. W. Bird, M. Bitoun, I. Bjedov, C. Blackstone, L. Blanc, G. A. Blanco, H. K. Blomhoff, E. Boada-Romero, S. Böckler, M. Boes, K. Boesze-Battaglia, L. H. Boise, A. Bolino, A. Boman, P. Bonaldo, M. Bordi, J. Bosch, L. M. Botana, J. Botti, G. Bou, M. Bouché, M. Bouchecareilh, M. J. Boucher, M. E. Boulton, S. G. Bouret, P. Boya, M. Boyer-Guittaut, P. V. Bozhkov, N. Brady, V. M. Braga, C. Brancolini, G. H. Braus, J. M. Bravo-San Pedro, L. A. Brennan, E. H. Bresnick, P. Brest, D. Bridges, M. A. Bringer, M. Brini, G. C. Brito, B. Brodin, P. S. Brookes, E. J. Brown, K. Brown, H. E. Broxmeyer, A. Bruhat, P. C. Brum, J. H. Brumell, N. Brunetti-Pierri, R. J. Bryson-Richardson, S. Buch, A. M. Buchan, H. Budak, D. V. Bulavin, S. J. Bultman, G. Bultynck, V. Bumbasirevic, Y. Burelle, R. E. Burke, M. Burmeister, P. Bütikofer, L. Caberlotto, K. Cadwell, M. Cahova, D. Cai, J. Cai, Q. Cai, S. Calatayud, N. Camougrand, M. Campanella, G. R. Campbell, M. Campbell, S. Campello, R. Candau, I. Caniggia, L. Cantoni, L. Cao, A. B. Caplan, M. Caraglia, C. Cardinali, S. M. Cardoso, J. S. Carew, L. A. Carleton, C. R. Carlin, S. Carloni, S. R. Carlsson, D. Carmona-Gutierrez, L. A. Carneiro, O. Carnevali, S. Carra, A. Carrier, B. Carroll, C. Casas, J. Casas, G. Cassinelli, P. Castets, S. Castro-Obregon, G. Cavallini, I. Ceccherini, F. Cecconi, A. I. Cederbaum, V. Ceña, S. Cenci, C. Cerella, D. Cervia, S. Cetrullo, H. Chaachouay, H. J. Chae, A. S. Chagin, C. Y. Chai, G. Chakrabarti, G. Chamilos, E. Y. Chan, M. T. Chan, D. Chandra, P. Chandra, C. P. Chang, R.

C. Chang, T. Y. Chang, J. C. Chatham, S. Chatterjee, S. Chauhan, Y. Che, M. E. Cheetham, R. Cheluvappa, C. J. Chen, G. Chen, G. C. Chen, H. Chen, J. W. Chen, J. K. Chen, M. Chen, P. Chen, Q. Chen, S. D. Chen, S. Chen, S. S. Chen, W. Chen, W. J. Chen, W. Q. Chen, X. Chen, Y. H. Chen, Y. G. Chen, Y. Chen, Y. J. Chen, Y. Q. Chen, Z. Chen, A. Cheng, C. H. Cheng, H. Cheng, H. Cheong, S. Cherry, J. Chesney, C. H. Cheung, E. Chevet, H. C. Chi, S. G. Chi, F. Chiacchiera, H. L. Chiang, R. Chiarelli, M. Chiariello, M. Chieppa, L. S. Chin, M. Chiong, G. N. Chiu, D. H. Cho, S. G. Cho, W. C. Cho, Y. Y. Cho, Y. S. Cho, A. M. Choi, E. J. Choi, E. K. Choi, J. Choi, M. E. Choi, S. I. Choi, T. F. Chou, S. Chouaib, D. Choubey, V. Choubey, K. C. Chow, K. Chowdhury, C. T. Chu, T. H. Chuang, T. Chun, H. Chung, T. Chung, Y. L. Chung, Y. J. Chwae, V. Cianfanelli, R. Ciarcia, I. A. Ciechomska, M. R. Ciriolo, M. Cirone, S. Claerhout, M. J. Clague, J. Clària, P. G. Clarke, R. Clarke, E. Clementi, C. Cleyrat, M. Cnop, E. M. Coccia, T. Cocco, P. Codogno, J. Coers, E. E. Cohen, D. Colecchia, L. Coletto, N. S. Coll, E. Colucci-Guyon, S. Comincini, M. Condello, K. L. Cook, G. H. Coombs, C. D. Cooper, J. M. Cooper, I. Coppens, M. T. Corasaniti, M. Corazzari, R. Corbalan, E. Corcelle-Termeau, M. D. Cordero, C. Corral-Ramos, O. Corti, A. Cossarizza, P. Costelli, S. Costes, S. L. Cotman, A. Coto-Montes, S. Cottet, E. Couve, L. R. Covey, L. A. Cowart, J. S. Cox, F. P. Coxon, C. B. Coyne, M. S. Cragg, R. J. Craven, T. Crepaldi, J. L. Crespo, A. Criollo, V. Crippa, M. T. Cruz, A. M. Cuervo, J. M. Cuezva, T. Cui, P. R. Cutillas, M. J. Czaja, M. F. Czyzyk-Krzeska, R. K. Dagda, U. Dahmen, C. Dai, W. Dai, Y. Dai, K. N. Dalby, L. Dalla Valle, G. Dalmasso, M. D'Amelio, M. Damme, A. Darfeuille-Michaud, C. Dargemont, V. M. Darley-Usmar, S. Dasarathy, B. Dasgupta, S. Dash, C. R. Dass, H. M. Davey, L. M. Davids, D. Dávila, R. J. Davis, T. M. Dawson, V. L. Dawson, P. Daza, J. de Belleroche, P. de Figueiredo, R. C. de Figueiredo, J. de la Fuente, L. De Martino, A. De Matteis, G. R. De Meyer, A. De Milito, M. De Santi, W. de Souza, V. De Tata, D. De Zio, J. Debnath, R. Dechant, J. P. Decuypere, S. Deegan, B. Dehay, B. Del Bello, D. P. Del Re, R. Delage-Mourroux, L. M. Delbridge, L. Deldicque, E. Delorme-Axford, Y. Deng, J. Dengjel, M. Denizot, P. Dent, C. J. Der, V. Deretic, B. Derrien, E. Deutsch, T. P. Devarenne, R. J. Devenish, S. Di Bartolomeo, N. Di Daniele, F. Di Domenico, A. Di Nardo, S. Di Paola, A. Di Pietro, L. Di Renzo, A. DiAntonio, G. Díaz-Araya, I. Díaz-Laviada, M. T. Diaz-Meco, J. Diaz-Nido, C. A. Dickey, R. C. Dickson, M. Diederich, P. Digard, I. Dikic, S. P. Dinesh-Kumar, C. Ding, W. X. Ding, Z. Ding, L. Dini, J. H. Distler, A. Diwan, M. Djavaheri-Mergny, K. Dmytruk, R. C. Dobson, V. Doetsch, K. Dokladny, S. Dokudovskaya, M. Donadelli, X. C. Dong, X. Dong, Z. Dong, T. M. Donohue, K. S. Doran, G. D'Orazi, G. W. Dorn, V. Dosenko, S. Dridi, L. Drucker, J. Du, L. L. Du, L. Du, A. du Toit, P. Dua, L. Duan, P. Duann, V. K. Dubey, M. R. Duchen, M. A. Duchosal, H. Duez, I. Dugail, V. I. Dumit, M. C. Duncan, E. A. Dunlop, W. A. Dunn, N. Dupont, L. Dupuis, R. V. Durán, T. M. Durcan, S. Duvezin-Caubet, U. Duvvuri, V. Eapen, D. Ebrahimi-Fakhari, A. Echard, L. Eckhart, C. L. Edelstein, A. L. Edinger, L. Eichinger, T. Eisenberg, A. Eisenberg-Lerner, N. T. Eissa, W. S. El-Deiry, V. El-Khoury, Z. Elazar, H. Eldar-Finkelman, C. J. Elliott, E. Emanuele, U. Emmenegger, N. Engedal, A. M. Engelbrecht, S. Engelender, J. M. Enserink, R. Erdmann, J. Erenpreisa, R. Eri, J. L. Eriksen, A. Erman, R. Escalante, E. L. Eskelinen, L. Espert, L. Esteban-Martínez, T. J. Evans, M. Fabri, G. Fabrias, C. Fabrizi, A. Facchiano, N. J. Færgeman, A. Faggioni, W. D. Fairlie, C. Fan, D. Fan, J. Fan, S. Fang, M. Fanto, A. Fanzani, T. Farkas, M. Faure, F. B. Favier, H. Fearnhead, M. Federici, E. Fei, T. C. Felizardo, H. Feng, Y. Feng, T. A. Ferguson, Á. Fernández, M. G. Fernandez-Barrena, J. C. Fernandez-Checa, A. Fernández-López, M. E. Fernandez-Zapico, O. Feron, E. Ferraro, C. V. Ferreira-Halder, L. Fesus, R. Feuer, F. C. Fiesel, E. C. Filippi-Chiela, G. Filomeni, G. M. Fimia, J. H. Fingert, S. Finkbeiner, T. Finkel, F. Fiorito, P. B. Fisher, M. Flajolet, F. Flamigni, O. Florey, S. Florio, R. A. Floto, M. Folini, C. Follo, E. A. Fon, F. Fornai, F. Fortunato, A. Fraldi, R. Franco, A. Francois, A. François, L. B. Frankel, I. D. Fraser, N. Frey, D. G. Freyssenet, C. Frezza, S. L. Friedman, D. E. Frigo, D. Fu, J. M. Fuentes, J. Fueyo, Y. Fujitani, Y. Fujiwara, M. Fujiya, M. Fukuda, S. Fulda, C. Fusco, B. Gabryel, M. Gaestel, P. Gailly, M. Gajewska, S. Galadari, G. Galili, I. Galindo, M. F. Galindo, G. Galliciotti, L. Galluzzi, V. Galy, N. Gammoh, S. Gandy, A. K. Ganesan, S. Ganesan, I. G. Ganley, M. Gannagé, F. B. Gao, F. Gao, J.

X. Gao, L. García Nannig, E. García Véscovi, M. Garcia-Macía, C. Garcia-Ruiz, A. D. Garg, P. K. Garg, R. Gargini, N. C. Gassen, D. Gatica, E. Gatti, J. Gavard, E. Gavathiotis, L. Ge, P. Ge, S. Ge, P. W. Gean, V. Gelmetti, A. A. Genazzani, J. Geng, P. Genschik, L. Gerner, J. E. Gestwicki, D. A. Gewirtz, S. Ghavami, E. Ghigo, D. Ghosh, A. M. Giammarioli, F. Giampieri, C. Giampietri, A. Giatromanolaki, D. J. Gibbings, L. Gibellini, S. B. Gibson, V. Ginet, A. Giordano, F. Giorgini, E. Giovannetti, S. E. Girardin, S. Gispert, S. Giuliano, C. L. Gladson, A. Glavic, M. Gleave, N. Godefroy, R. M. Gogal, K. Gokulan, G. H. Goldman, D. Goletti, M. S. Goligorsky, A. V. Gomes, L. C. Gomes, H. Gomez, C. Gomez-Manzano, R. Gómez-Sánchez, D. A. Gonçalves, E. Goncu, Q. Gong, C. Gongora, C. B. Gonzalez, P. Gonzalez-Alegre, P. Gonzalez-Cabo, R. A. González-Polo, I. S. Goping, C. Gorbea, N. V. Gorbunov, D. R. Goring, A. M. Gorman, S. M. Gorski, S. Goruppi, S. Goto-Yamada, C. Gotor, R. A. Gottlieb, I. Gozes, D. Gozuacik, Y. Graba, M. Graef, G. E. Granato, G. D. Grant, S. Grant, G. L. Gravina, D. R. Green, A. Greenhough, M. T. Greenwood, B. Grimaldi, F. Gros, C. Grose, J. F. Groulx, F. Gruber, P. Grumati, T. Grune, J. L. Guan, K. L. Guan, B. Guerra, C. Guillen, K. Gulshan, J. Gunst, C. Guo, L. Guo, M. Guo, W. Guo, X. G. Guo, A. A. Gust, Å. Gustafsson, E. Gutierrez, M. G. Gutierrez, H. S. Gwak, A. Haas, J. E. Haber, S. Hadano, M. Hagedorn, D. R. Hahn, A. J. Halayko, A. Hamacher-Brady, K. Hamada, A. Hamai, A. Hamann, M. Hamasaki, I. Hamer, Q. Hamid, E. M. Hammond, F. Han, W. Han, J. T. Handa, J. A. Hanover, M. Hansen, M. Harada, L. Harhaji-Trajkovic, J. W. Harper, A. H. Harrath, A. L. Harris, J. Harris, U. Hasler, P. Hasselblatt, K. Hasui, R. G. Hawley, T. S. Hawley, C. He, C. Y. He, F. He, G. He, R. R. He, X. H. He, Y. W. He, Y. Y. He, J. K. Heath, M. J. Hébert, R. A. Heinzen, G. V. Helgason, M. Hensel, E. P. Henske, C. Her, P. K. Herman, A. Hernández, C. Hernandez, S. Hernández-Tiedra, C. Hetz, P. R. Hiesinger, K. Higaki, S. Hilfiker, B. G. Hill, J. A. Hill, W. D. Hill, K. Hino, D. Hofius, P. Hofman, G. U. Höglinger, J. Höhfeld, M. K. Holz, Y. Hong, D. A. Hood, J. J. Hoozemans, T. Hoppe, C. Hsu, C. Y. Hsu, L. C. Hsu, D. Hu, G. Hu, H. M. Hu, H. Hu, M. C. Hu, Y. C. Hu, Z. W. Hu, F. Hua, Y. Hua, C. Huang, H. L. Huang, K. H. Huang, K. Y. Huang, S. Huang, W. P. Huang, Y. R. Huang, Y. Huang, T. B. Huber, P. Huebbe, W. K. Huh, J. J. Hulmi, G. M. Hur, J. H. Hurley, Z. Husak, S. N. Hussain, S. Hussain, J. J. Hwang, S. Hwang, T. I. Hwang, A. Ichihara, Y. Imai, C. Imbriano, M. Inomata, T. Into, V. Iovane, J. L. Iovanna, R. V. Iozzo, N. Y. Ip, J. E. Irazoqui, P. Iribarren, Y. Isaka, A. J. Isakovic, H. Ischiropoulos, J. S. Isenberg, M. Ishaq, H. Ishida, I. Ishii, J. E. Ishmael, C. Isidoro, K. Isobe, E. Isono, S. Issazadeh-Navikas, K. Itahana, E. Itakura, A. I. Ivanov, A. K. Iyer, J. M. Izquierdo, Y. Izumi, V. Izzo, M. Jäättelä, N. Jaber, D. J. Jackson, W. T. Jackson, T. G. Jacob, T. S. Jacques, C. Jagannath, A. Jain, N. R. Jana, B. K. Jang, A. Jani, B. Janji, P. R. Jannig, P. J. Jansson, S. Jean, M. Jendrach, J. H. Jeon, N. Jessen, E. B. Jeung, K. Jia, L. Jia, H. Jiang, L. Jiang, T. Jiang, X. Jiang, Y. Jiang, A. Jiménez, C. Jin, H. Jin, L. Jin, M. Jin, S. Jin, U. K. Jinwal, E. K. Jo, T. Johansen, D. E. Johnson, G. V. Johnson, J. D. Johnson, E. Jonasch, C. Jones, L. A. Joosten, J. Jordan, A. M. Joseph, B. Joseph, A. M. Joubert, D. Ju, J. Ju, H. F. Juan, K. Juenemann, G. Juhász, H. S. Jung, J. U. Jung, Y. K. Jung, H. Jungbluth, M. J. Justice, B. Jutten, N. O. Kaakoush, K. Kaarniranta, A. Kaasik, T. Kabuta, B. Kaeffer, K. Kågedal, A. Kahana, S. Kajimura, O. Kakhlon, M. Kalia, D. V. Kalvakolanu, Y. Kamada, K. Kambas, V. O. Kaminskyy, H. H. Kampinga, M. Kandouz, C. Kang, R. Kang, T. C. Kang, T. Kanki, T. D. Kanneganti, H. Kanno, A. G. Kanthasamy, M. Kantorow, M. Kaparakis-Liaskos, O. Kapuy, V. Karantza, M. R. Karim, P. Karmakar, A. Kaser, S. Kaushik, T. Kawula, A. M. Kaynar, P. Y. Ke, Z. J. Ke, J. H. Kehrl, K. E. Keller, J. K. Kemper, A. K. Kenworthy, O. Kepp, A. Kern, S. Kesari, D. Kessel, R. Ketteler, I. o. C. Kettelhut, B. Khambu, M. M. Khan, V. K. Khandelwal, S. Khare, J. G. Kiang, A. A. Kiger, A. Kihara, A. L. Kim, C. H. Kim, D. R. Kim, D. H. Kim, E. K. Kim, H. Y. Kim, H. R. Kim, J. S. Kim, J. H. Kim, J. C. Kim, K. W. Kim, M. D. Kim, M. M. Kim, P. K. Kim, S. W. Kim, S. Y. Kim, Y. S. Kim, Y. Kim, A. Kimchi, A. C. Kimmelman, T. Kimura, J. S. King, K. Kirkegaard, V. Kirkin, L. A. Kirshenbaum, S. Kishi, Y. Kitajima, K. Kitamoto, Y. Kitaoka, K. Kitazato, R. A. Kley, W. T. Klimecki, M. Klinkenberg, J. Klucken, H. Knævelsrud, E. Knecht, L. Knuppertz, J. L. Ko, S. Kobayashi, J. C. Koch, C. Koechlin-Ramonatxo, U. Koenig, Y. H. Koh, K. Köhler, S. D. Kohlwein, M. Koike, M. Komatsu, E. Kominami, D. Kong, H. J. Kong, E. G. Konstantakou, B. T. Kopp, T.

Korcsmaros, L. Korhonen, V. I. Korolchuk, N. V. Koshkina, Y. Kou, M. I. Koukourakis, C. Koumenis, A. L. Kovács, T. Kovács, W. J. Kovacs, D. Koya, C. Kraft, D. Krainc, H. Kramer, T. Kravic-Stevovic, W. Krek, C. Kretz-Remy, R. Krick, M. Krishnamurthy, J. Kriston-Vizi, G. Kroemer, M. C. Kruer, R. Kruger, N. T. Ktistakis, K. Kuchitsu, C. Kuhn, A. P. Kumar, A. Kumar, D. Kumar, R. Kumar, S. Kumar, M. Kundu, H. J. Kung, A. Kuno, S. H. Kuo, J. Kuret, T. Kurz, T. Kwok, T. K. Kwon, Y. T. Kwon, I. Kyrmizi, A. R. La Spada, F. Lafont, T. Lahm, A. Lakkaraju, T. Lam, T. Lamark, S. Lancel, T. H. Landowski, D. J. Lane, J. D. Lane, C. Lanzi, P. Lapaquette, L. R. Lapierre, J. Laporte, J. Laukkarinen, G. W. Laurie, S. Lavandero, L. Lavie, M. J. LaVoie, B. Y. Law, H. K. Law, K. B. Law, R. Layfield, P. A. Lazo, L. Le Cam, K. G. Le Roch, H. Le Stunff, V. Leardkamolkarn, M. Lecuit, B. H. Lee, C. H. Lee, E. F. Lee, G. M. Lee, H. J. Lee, H. Lee, J. K. Lee, J. Lee, J. H. Lee, M. Lee, M. S. Lee, P. J. Lee, S. W. Lee, S. J. Lee, S. Y. Lee, S. H. Lee, S. S. Lee, S. Lee, Y. R. Lee, Y. J. Lee, Y. H. Lee, C. Leeuwenburgh, S. Lefort, R. Legouis, J. Lei, Q. Y. Lei, D. A. Leib, G. Leibowitz, I. Lekli, S. D. Lemaire, J. J. Lemasters, M. K. Lemberg, A. Lemoine, S. Leng, G. Lenz, P. Lenzi, L. O. Lerman, D. Lettieri Barbato, J. I. Leu, H. Y. Leung, B. Levine, P. A. Lewis, F. Lezoualc'h, C. Li, F. Li, F. J. Li, J. Li, K. Li, L. Li, M. Li, Q. Li, R. Li, S. Li, W. Li, X. Li, Y. Li, J. Lian, C. Liang, Q. Liang, Y. Liao, J. Liberal, P. P. Liberski, P. Lie, A. P. Lieberman, H. J. Lim, K. L. Lim, K. Lim, R. T. Lima, C. S. Lin, C. F. Lin, F. Lin, F. C. Lin, K. Lin, K. H. Lin, P. H. Lin, T. Lin, W. W. Lin, Y. S. Lin, Y. Lin, R. Linden, D. Lindholm, L. M. Lindqvist, P. Lingor, A. Linkermann, L. A. Liotta, M. M. Lipinski, V. A. Lira, M. P. Lisanti, P. B. Liton, B. Liu, C. Liu, C. F. Liu, F. Liu, H. J. Liu, J. Liu, J. J. Liu, J. L. Liu, K. Liu, L. Liu, Q. Liu, R. Y. Liu, S. Liu, W. Liu, X. D. Liu, X. Liu, X. H. Liu, Y. Liu, Z. Liu, J. P. Liuzzi, G. Lizard, M. Ljujic, I. J. Lodhi, S. E. Logue, B. L. Lokeshwar, Y. C. Long, S. Lonial, B. Loos, C. López-Otín, C. López-Vicario, M. Lorente, P. L. Lorenzi, P. Lõrincz, M. Los, M. T. Lotze, P. E. Lovat, B. Lu, J. Lu, Q. Lu, S. M. Lu, S. Lu, Y. Lu, F. Luciano, S. Luckhart, J. M. Lucocq, P. Ludovico, A. Lugea, N. W. Lukacs, J. J. Lum, A. H. Lund, H. Luo, J. Luo, S. Luo, C. Luparello, T. Lyons, J. Ma, Y. Ma, Z. Ma, J. Machado, G. M. Machado-Santelli, F. Macian, G. C. MacIntosh, J. P. MacKeigan, K. F. Macleod, J. D. MacMicking, L. A. MacMillan-Crow, F. Madeo, M. Madesh, J. Madrigal-Matute, A. Maeda, T. Maeda, G. Maegawa, E. Maellaro, H. Maes, M. Magariños, K. Maiese, T. K. Maiti, L. Maiuri, M. C. Maiuri, C. G. Maki, R. Malli, W. Malorni, A. Maloyan, F. Mami-Chouaib, N. Man, J. D. Mancias, E. M. Mandelkow, M. A. Mandell, A. A. Manfredi, S. N. Manié, C. Manzoni, K. Mao, Z. Mao, Z. W. Mao, P. Marambaud, A. M. Marconi, Z. Marelja, G. Marfe, M. Margeta, E. Margittai, M. Mari, F. V. Mariani, C. Marin, S. Marinelli, G. Mariño, I. Markovic, R. Marquez, A. M. Martelli, S. Martens, K. R. Martin, S. J. Martin, S. Martin, M. A. Martin-Acebes, P. Martín-Sanz, C. Martinand-Mari, W. Martinet, J. Martinez, N. Martinez-Lopez, U. Martinez-Outschoorn, M. Martínez-Velázquez, M. Martinez-Vicente, W. K. Martins, H. Mashima, J. A. Mastrianni, G. Matarese, P. Matarrese, R. Mateo, S. Matoba, N. Matsumoto, T. Matsushita, A. Matsuura, T. Matsuzawa, M. P. Mattson, S. Matus, N. Maugeri, C. Mauvezin, A. Mayer, D. Maysinger, G. D. Mazzolini, M. K. McBrayer, K. McCall, C. McCormick, G. M. McInerney, S. C. McIver, S. McKenna, J. J. McMahon, I. A. McNeish, F. Mechta-Grigoriou, J. P. Medema, D. L. Medina, K. Megyeri, M. Mehrpour, J. L. Mehta, Y. Mei, U. C. Meier, A. J. Meijer, A. Meléndez, G. Melino, S. Melino, E. J. de Melo, M. A. Mena, M. D. Meneghini, J. A. Menendez, R. Menezes, L. Meng, L. H. Meng, S. Meng, R. Menghini, A. S. Menko, R. F. Menna-Barreto, M. B. Menon, M. A. Meraz-Ríos, G. Merla, L. Merlini, A. M. Merlot, A. Meryk, S. Meschini, J. N. Meyer, M. T. Mi, C. Y. Miao, L. Micale, S. Michaeli, C. Michiels, A. R. Migliaccio, A. S. Mihailidou, D. Mijaljica, K. Mikoshiba, E. Milan, L. Miller-Fleming, G. B. Mills, I. G. Mills, G. Minakaki, B. A. Minassian, X. F. Ming, F. Minibayeva, E. A. Minina, J. D. Mintern, S. Minucci, A. Miranda-Vizuete, C. H. Mitchell, S. Miyamoto, K. Miyazawa, N. Mizushima, K. Mnich, B. Mograbi, S. Mohseni, L. F. Moita, M. Molinari, A. B. Møller, B. Mollereau, F. Mollinedo, M. Mongillo, M. M. Monick, S. Montagnaro, C. Montell, D. J. Moore, M. N. Moore, R. Mora-Rodriguez, P. I. Moreira, E. Morel, M. B. Morelli, S. Moreno, M. J. Morgan, A. Moris, Y. Moriyasu, J. L. Morrison, L. A. Morrison, E. Morselli, J. Moscat, P. L. Moseley, S. Mostowy, E. Motori, D. Mottet, J. C.

Mottram, C. E. Moussa, V. E. Mpakou, H. Mukhtar, J. M. Mulcahy Levy, S. Muller, R. Muñoz-Moreno, C. Muñoz-Pinedo, C. Münz, M. E. Murphy, J. T. Murray, A. Murthy, I. U. Mysorekar, I. R. Nabi, M. Nabissi, G. A. Nader, Y. Nagahara, Y. Nagai, K. Nagata, A. Nagelkerke, P. Nagy, S. R. Naidu, S. Nair, H. Nakano, H. Nakatogawa, M. Nanjundan, G. Napolitano, N. I. Naqvi, R. Nardacci, D. P. Narendra, M. Narita, A. C. Nascimbeni, R. Natarajan, L. C. Navegantes, S. T. Nawrocki, T. Y. Nazarko, V. Y. Nazarko, T. Neill, L. M. Neri, M. G. Netea, R. T. Netea-Maier, B. M. Neves, P. A. Ney, I. P. Nezis, H. T. Nguyen, H. P. Nguyen, A. S. Nicot, H. Nilsen, P. Nilsson, M. Nishimura, I. Nishino, M. Niso-Santano, H. Niu, R. A. Nixon, V. C. Njar, T. Noda, A. A. Noegel, E. M. Nolte, E. Norberg, K. K. Norga, S. K. Noureini, S. Notomi, L. Notterpek, K. Nowikovsky, N. Nukina, T. Nürnberger, V. B. O'Donnell, T. O'Donovan, P. J. O'Dwyer, I. Oehme, C. L. Oeste, M. Ogawa, B. Ogretmen, Y. Ogura, Y. J. Oh, M. Ohmuraya, T. Ohshima, R. Ojha, K. Okamoto, T. Okazaki, F. J. Oliver, K. Ollinger, S. Olsson, D. P. Orban, P. Ordonez, I. Orhon, L. Orosz, E. J. O'Rourke, H. Orozco, A. L. Ortega, E. Ortona, L. D. Osellame, J. Oshima, S. Oshima, H. D. Osiewacz, T. Otomo, K. Otsu, J. H. Ou, T. F. Outeiro, D. Y. Ouyang, H. Ouyang, M. Overholtzer, M. A. Ozbun, P. H. Ozdinler, B. Ozpolat, C. Pacelli, P. Paganetti, G. Page, G. Pages, U. Pagnini, B. Pajak, S. C. Pak, K. Pakos-Zebrucka, N. Pakpour, Z. Palková, F. Palladino, K. Pallauf, N. Pallet, M. Palmieri, S. R. Paludan, C. Palumbo, S. Palumbo, O. Pampliega, H. Pan, W. Pan, T. Panaretakis, A. Pandey, A. Pantazopoulou, Z. Papackova, D. L. Papademetrio, I. Papassideri, A. Papini, N. Parajuli, J. Pardo, V. V. Parekh, G. Parenti, J. I. Park, J. Park, O. K. Park, R. Parker, R. Parlato, J. B. Parys, K. R. Parzych, J. M. Pasquet, B. Pasquier, K. B. Pasumarthi, D. Patschan, C. Patterson, S. Pattingre, S. Pattison, A. Pause, H. Pavenstädt, F. Pavone, Z. Pedrozo, F. J. Peña, M. A. Peñalva, M. Pende, J. Peng, F. Penna, J. M. Penninger, A. Pensalfini, S. Pepe, G. J. Pereira, P. C. Pereira, V. Pérez-de la Cruz, M. E. Pérez-Pérez, D. Pérez-Rodríguez, D. Pérez-Sala, C. Perier, A. Perl, D. H. Perlmutter, I. Perrotta, S. Pervaiz, M. Pesonen, J. E. Pessin, G. J. Peters, M. Petersen, I. Petrache, B. J. Petrof, G. Petrovski, J. M. Phang, M. Piacentini, M. Pierdominici, P. Pierre, V. Pierrefite-Carle, F. Pietrocola, F. X. Pimentel-Muiños, M. Pinar, B. Pineda, R. Pinkas-Kramarski, M. Pinti, P. Pinton, B. Piperdi, J. M. Piret, L. C. Platanias, H. W. Platta, E. D. Plowey, S. Pöggeler, M. Poirot, P. Polčic, A. Poletti, A. H. Poon, H. Popelka, B. Popova, I. Poprawa, S. M. Poulose, J. Poulton, S. K. Powers, T. Powers, M. Pozuelo-Rubio, K. Prak, R. Prange, M. Prescott, M. Priault, S. Prince, R. L. Proia, T. Proikas-Cezanne, H. Prokisch, V. J. Promponas, K. Przyklenk, R. Puertollano, S. Pugazhenthi, L. Puglielli, A. Pujol, J. Puyal, D. Pyeon, X. Qi, W. B. Qian, Z. H. Qin, Y. Qiu, Z. Qu, J. Quadrilatero, F. Quinn, N. Raben, H. Rabinowich, F. Radogna, M. J. Ragusa, M. Rahmani, K. Raina, S. Ramanadham, R. Ramesh, A. Rami, S. Randall-Demllo, F. Randow, H. Rao, V. A. Rao, B. B. Rasmussen, T. M. Rasse, E. A. Ratovitski, P. E. Rautou, S. K. Ray, B. Razani, B. H. Reed, F. Reggiori, M. Rehm, A. S. Reichert, T. Rein, D. J. Reiner, E. Reits, J. Ren, X. Ren, M. Renna, J. E. Reusch, J. L. Revuelta, L. Reyes, A. R. Rezaie, R. I. Richards, D. R. Richardson, C. Richetta, M. A. Riehle, B. H. Rihn, Y. Rikihisa, B. E. Riley, G. Rimbach, M. R. Rippo, K. Ritis, F. Rizzi, E. Rizzo, P. J. Roach, J. Robbins, M. Roberge, G. Roca, M. C. Roccheri, S. Rocha, C. M. Rodrigues, C. I. Rodríguez, S. R. de Cordoba, N. Rodriguez-Muela, J. Roelofs, V. V. Rogov, T. T. Rohn, B. Rohrer, D. Romanelli, L. Romani, P. S. Romano, M. I. Roncero, J. L. Rosa, A. Rosello, K. V. Rosen, P. Rosenstiel, M. Rost-Roszkowska, K. A. Roth, G. Roué, M. Rouis, K. M. Rouschop, D. T. Ruan, D. Ruano, D. C. Rubinsztein, E. B. Rucker, A. Rudich, E. Rudolf, R. Rudolf, M. A. Ruegg, C. Ruiz-Roldan, A. A. Ruparelia, P. Rusmini, D. W. Russ, G. L. Russo, G. Russo, R. Russo, T. E. Rusten, V. Ryabovol, K. M. Ryan, S. W. Ryter, D. M. Sabatini, M. Sacher, C. Sachse, M. N. Sack, J. Sadoshima, P. Saftig, R. Sagi-Eisenberg, S. Sahni, P. Saikumar, T. Saito, T. Saitoh, K. Sakakura, M. Sakoh-Nakatogawa, Y. Sakuraba, M. Salazar-Roa, P. Salomoni, A. K. Saluja, P. M. Salvaterra, R. Salvioli, A. Samali, A. M. Sanchez, J. A. Sánchez-Alcázar, R. Sanchez-Prieto, M. Sandri, M. A. Sanjuan, S. Santaguida, L. Santambrogio, G. Santoni, C. N. Dos Santos, S. Saran, M. Sardiello, G. Sargent, P. Sarkar, S. Sarkar, M. R. Sarrias, M. M. Sarwal, C. Sasakawa, M. Sasaki, M. Sass, K. Sato, M. Sato, J. Satriano, N. Savaraj, S. Saveljeva, L. Schaefer, U. E.

Schaible, M. Scharl, H. M. Schatzl, R. Schekman, W. Scheper, A. Schiavi, H. M. Schipper, H. Schmeisser, J. Schmidt, I. Schmitz, B. E. Schneider, E. M. Schneider, J. L. Schneider, E. A. Schon, M. J. Schönenberger, A. H. Schönthal, D. F. Schorderet, B. Schröder, S. Schuck, R. J. Schulze, M. Schwarten, T. L. Schwarz, S. Sciarretta, K. Scotto, A. I. Scovassi, R. A. Screaton, M. Screen, H. Seca, S. Sedej, L. Segatori, N. Segev, P. O. Seglen, J. M. Seguí-Simarro, J. Segura-Aguilar, E. Seki, C. Sell, I. Seiliez, C. F. Semenkovich, G. L. Semenza, U. Sen, A. L. Serra, A. Serrano-Puebla, H. Sesaki, T. Setoguchi, C. Settembre, J. J. Shacka, A. N. Shajahan-Haq, I. M. Shapiro, S. Sharma, H. She, C. K. Shen, C. C. Shen, H. M. Shen, S. Shen, W. Shen, R. Sheng, X. Sheng, Z. H. Sheng, T. G. Shepherd, J. Shi, Q. Shi, Y. Shi, S. Shibutani, K. Shibuya, Y. Shidoji, J. J. Shieh, C. M. Shih, Y. Shimada, S. Shimizu, D. W. Shin, M. L. Shinohara, M. Shintani, T. Shintani, T. Shioi, K. Shirabe, R. Shiri-Sverdlov, O. Shirihai, G. C. Shore, C. W. Shu, D. Shukla, A. A. Sibirny, V. Sica, C. J. Sigurdson, E. M. Sigurdsson, P. S. Sijwali, B. Sikorska, W. A. Silveira, S. Silvente-Poirot, G. A. Silverman, J. Simak, T. Simmet, A. K. Simon, H. U. Simon, C. Simone, M. Simons, A. Simonsen, R. Singh, S. V. Singh, S. K. Singh, D. Sinha, S. Sinha, F. A. Sinicrope, A. Sirko, K. Sirohi, B. J. Sishi, A. Sittler, P. M. Siu, E. Sivridis, A. Skwarska, R. Slack, I. Slaninová, N. Slavov, S. S. Smaili, K. S. Smalley, D. R. Smith, S. J. Soenen, S. A. Soleimanpour, A. Solhaug, K. Somasundaram, J. H. Son, A. Sonawane, C. Song, F. Song, H. K. Song, J. X. Song, W. Song, K. Y. Soo, A. K. Sood, T. W. Soong, V. Soontornniyomkij, M. Sorice, F. Sotgia, D. R. Soto-Pantoja, A. Sotthibundhu, M. J. Sousa, H. P. Spaink, P. N. Span, A. Spang, J. D. Sparks, P. G. Speck, S. A. Spector, C. D. Spies, W. Springer, D. S. Clair, A. Stacchiotti, B. Staels, M. T. Stang, D. T. Starczynowski, P. Starokadomskyy, C. Steegborn, J. W. Steele, L. Stefanis, J. Steffan, C. M. Stellrecht, H. Stenmark, T. M. Stepkowski, S. T. Stern, C. Stevens, B. R. Stockwell, V. Stoka, Z. Storchova, B. Stork, V. Stratoulias, D. J. Stravopodis, P. Strnad, A. M. Strohecker, A. L. Ström, P. Stromhaug, J. Stulik, Y. X. Su, Z. Su, C. S. Subauste, S. Subramaniam, C. M. Sue, S. W. Suh, X. Sui, S. Sukseree, D. Sulzer, F. L. Sun, J. Sun, S. Y. Sun, Y. Sun, V. Sundaramoorthy, J. Sung, H. Suzuki, K. Suzuki, N. Suzuki, T. Suzuki, Y. J. Suzuki, M. S. Swanson, C. Swanton, K. Swärd, G. Swarup, S. T. Sweeney, P. W. Sylvester, Z. Szatmari, E. Szegezdi, P. W. Szlosarek, H. Taegtmeyer, M. Tafani, E. Taillebourg, S. W. Tait, K. Takacs-Vellai, Y. Takahashi, S. Takáts, G. Takemura, N. Takigawa, N. J. Talbot, E. Tamagno, J. Tamburini, C. P. Tan, L. Tan, M. L. Tan, M. Tan, Y. J. Tan, K. Tanaka, M. Tanaka, D. Tang, G. Tang, I. Tanida, K. Tanji, B. A. Tannous, J. A. Tapia, I. Tasset-Cuevas, M. Tatar, I. Tavassoly, N. Tavernarakis, A. Taylor, G. S. Taylor, G. A. Taylor, J. P. Taylor, M. J. Taylor, E. V. Tchetina, A. R. Tee, F. Teixeira-Clerc, S. Telang, T. Tencomnao, B. B. Teng, R. J. Teng, F. Terro, G. Tettamanti, A. L. Theiss, A. E. Theron, K. J. Thomas, M. P. Thomé, P. G. Thomes, A. Thorburn, J. Thorner, T. Thum, M. Thumm, T. L. Thurston, L. Tian, A. Till, J. P. Ting, V. I. Titorenko, L. Toker, S. Toldo, S. A. Tooze, I. Topisirovic, M. L. Torgersen, L. Torosantucci, A. Torriglia, M. R. Torrisi, C. Tournier, R. Towns, V. Trajkovic, L. H. Travassos, G. Triola, D. N. Tripathi, D. Trisciuoglio, R. Troncoso, I. P. Trougakos, A. C. Truttmann, K. J. Tsai, M. P. Tschan, Y. H. Tseng, T. Tsukuba, A. Tsung, A. S. Tsvetkov, S. Tu, H. Y. Tuan, M. Tucci, D. A. Tumbarello, B. Turk, V. Turk, R. F. Turner, A. A. Tveita, S. C. Tyagi, M. Ubukata, Y. Uchiyama, A. Udelnow, T. Ueno, M. Umekawa, R. Umemiya-Shirafuji, B. R. Underwood, C. Ungermann, R. P. Ureshino, R. Ushioda, V. N. Uversky, N. L. Uzcátegui, T. Vaccari, M. I. Vaccaro, L. Váchová, H. Vakifahmetoglu-Norberg, R. Valdor, E. M. Valente, F. Vallette, A. M. Valverde, G. Van den Berghe, L. Van Den Bosch, G. R. van den Brink, F. G. van der Goot, I. J. van der Klei, L. J. van der Laan, W. G. van Doorn, M. van Egmond, K. L. van Golen, L. Van Kaer, M. van Lookeren Campagne, P. Vandenabeele, W. Vandenberghe, I. Vanhorebeek, I. Varela-Nieto, M. H. Vasconcelos, R. Vasko, D. G. Vavvas, I. Vega-Naredo, G. Velasco, A. D. Velentzas, P. D. Velentzas, T. Vellai, E. Vellenga, M. H. Vendelbo, K. Venkatachalam, N. Ventura, S. Ventura, P. S. Veras, M. Verdier, B. G. Vertessy, A. Viale, M. Vidal, H. L. Vieira, R. D. Vierstra, N. Vigneswaran, N. Vij, M. Vila, M. Villar, V. H. Villar, J. Villarroya, C. Vindis, G. Viola, M. T. Viscomi, G. Vitale, D. T. Vogl, O. V. Voitsekhovskaja, C. von Haefen, K. von Schwarzenberg, D. E. Voth, V. Vouret-Craviari, K. Vuori, J. M. Vyas, C.

Waeber, C. L. Walker, M. J. Walker, J. Walter, L. Wan, X. Wan, B. Wang, C. Wang, C. Y. Wang, D. Wang, F. Wang, G. Wang, H. J. Wang, H. Wang, H. G. Wang, H. D. Wang, J. Wang, M. Wang, M. Q. Wang, P. Y. Wang, P. Wang, R. C. Wang, S. Wang, T. F. Wang, X. Wang, X. J. Wang, X. W. Wang, Y. Wang, Y. J. Wang, Y. T. Wang, Z. N. Wang, P. Wappner, C. Ward, D. M. Ward, G. Warnes, H. Watada, Y. Watanabe, K. Watase, T. E. Weaver, C. D. Weekes, J. Wei, T. Weide, C. C. Weihl, G. Weindl, S. N. Weis, L. Wen, X. Wen, Y. Wen, B. Westermann, C. M. Weyand, A. R. White, E. White, J. L. Whitton, A. J. Whitworth, J. Wiels, F. Wild, M. E. Wildenberg, T. Wileman, D. S. Wilkinson, S. Wilkinson, D. Willbold, C. Williams, K. Williams, P. R. Williamson, K. F. Winklhofer, S. S. Witkin, S. E. Wohlgemuth, T. Wollert, E. J. Wolvetang, E. Wong, G. W. Wong, R. W. Wong, V. K. Wong, E. A. Woodcock, K. L. Wright, C. Wu, D. Wu, G. S. Wu, J. Wu, M. Wu, S. Wu, W. K. Wu, Y. Wu, Z. Wu, C. P. Xavier, R. J. Xavier, G. X. Xia, T. Xia, W. Xia, Y. Xia, H. Xiao, J. Xiao, S. Xiao, W. Xiao, C. M. Xie, Z. Xie, M. Xilouri, Y. Xiong, C. Xu, F. Xu, H. Xu, J. Xu, L. Xu, X. Xu, Y. Xu, Z. X. Xu, Z. Xu, Y. Xue, T. Yamada, A. Yamamoto, K. Yamanaka, S. Yamashina, S. Yamashiro, B. Yan, X. Yan, Z. Yan, Y. Yanagi, D. S. Yang, J. M. Yang, L. Yang, M. Yang, P. M. Yang, P. Yang, Q. Yang, W. Yang, W. Y. Yang, X. Yang, Y. Yang, Z. Yang, M. C. Yao, P. J. Yao, X. Yao, Z. Yao, L. S. Yasui, M. Ye, B. Yedvobnick, B. Yeganeh, E. S. Yeh, P. L. Yeyati, F. Yi, L. Yi, X. M. Yin, C. K. Yip, Y. M. Yoo, Y. H. Yoo, S. Y. Yoon, K. Yoshida, T. Yoshimori, K. H. Young, H. Yu, J. J. Yu, J. T. Yu, J. Yu, L. Yu, W. H. Yu, X. F. Yu, Z. Yu, J. Yuan, Z. M. Yuan, B. Y. Yue, J. Yue, Z. Yue, D. N. Zacks, E. Zacksenhaus, N. Zaffaroni, T. Zaglia, Z. Zakeri, V. Zecchini, J. Zeng, M. Zeng, Q. Zeng, A. S. Zervos, D. D. Zhang, F. Zhang, G. Zhang, G. C. Zhang, H. Zhang, J. Zhang, J. P. Zhang, L. Zhang, M. Y. Zhang, X. Zhang, X. D. Zhang, Y. Zhang, M. Zhao, W. L. Zhao, X. Zhao, Y. G. Zhao, Y. Zhao, Y. X. Zhao, Z. Zhao, Z. J. Zhao, D. Zheng, X. L. Zheng, X. Zheng, B. Zhivotovsky, Q. Zhong, G. Z. Zhou, G. Zhou, H. Zhou, S. F. Zhou, X. J. Zhou, H. Zhu, W. G. Zhu, W. Zhu, X. F. Zhu, Y. Zhu, S. M. Zhuang, X. Zhuang, E. Ziparo, C. E. Zois, T. Zoladek, W. X. Zong, A. Zorzano and S. M. Zughaier (2016). "Guidelines for the use and interpretation of assays for monitoring autophagy (3rd edition)." Autophagy **12**(1): 1-222.

Klionsky, D. J., H. Abeliovich, P. Agostinis, D. K. Agrawal, G. Aliev, D. S. Askew, M. Baba, E. H. Baehrecke, B. A. Bahr, A. Ballabio, B. A. Bamber, D. C. Bassham, E. Bergamini, X. Bi, M. Biard-Piechaczyk, J. S. Blum, D. E. Bredesen, J. L. Brodsky, J. H. Brumell, U. T. Brunk, W. Bursch, N. Camougrand, E. Cebollero, F. Cecconi, Y. Chen, L. S. Chin, A. Choi, C. T. Chu, J. Chung, P. G. Clarke, R. S. Clark, S. G. Clarke, C. Clave, J. L. Cleveland, P. Codogno, M. I. Colombo, A. Coto-Montes, J. M. Cregg, A. M. Cuervo, J. Debnath, F. Demarchi, P. B. Dennis, P. A. Dennis, V. Deretic, R. J. Devenish, F. Di Sano, J. F. Dice, M. Difiglia, S. Dinesh-Kumar, C. W. Distelhorst, M. Djavaheri-Mergny, F. C. Dorsey, W. Droge, M. Dron, W. A. Dunn, Jr., M. Duszenko, N. T. Eissa, Z. Elazar, A. Esclatine, E. L. Eskelinen, L. Fesus, K. D. Finley, J. M. Fuentes, J. Fueyo, K. Fujisaki, B. Galliot, F. B. Gao, D. A. Gewirtz, S. B. Gibson, A. Gohla, A. L. Goldberg, R. Gonzalez, C. Gonzalez-Estevez, S. Gorski, R. A. Gottlieb, D. Haussinger, Y. W. He, K. Heidenreich, J. A. Hill, M. Hoyer-Hansen, X. Hu, W. P. Huang, A. Iwasaki, M. Jaattela, W. T. Jackson, X. Jiang, S. Jin, T. Johansen, J. U. Jung, M. Kadowaki, C. Kang, A. Kelekar, D. H. Kessel, J. A. Kiel, H. P. Kim, A. Kimchi, T. J. Kinsella, K. Kiselyov, K. Kitamoto, E. Knecht, M. Komatsu, E. Kominami, S. Kondo, A. L. Kovacs, G. Kroemer, C. Y. Kuan, R. Kumar, M. Kundu, J. Landry, M. Laporte, W. Le, H. Y. Lei, M. J. Lenardo, B. Levine, A. Lieberman, K. L. Lim, F. C. Lin, W. Liou, L. F. Liu, G. Lopez-Berestein, C. Lopez-Otin, B. Lu, K. F. Macleod, W. Malorni, W. Martinet, K. Matsuoka, J. Mautner, A. J. Meijer, A. Melendez, P. Michels, G. Miotto, W. P. Mistiaen, N. Mizushima, B. Mograbi, I. Monastyrska, M. N. Moore, P. I. Moreira, Y. Moriyasu, T. Motyl, C. Munz, L. O. Murphy, N. I. Naqvi, T. P. Neufeld, I. Nishino, R. A. Nixon, T. Noda, B. Nurnberg, M. Ogawa, N. L. Oleinick, L. J. Olsen, B. Ozpolat, S. Paglin, G. E. Palmer, I. Papassideri, M. Parkes, D. H. Perlmutter, G. Perry, M. Piacentini, R. Pinkas-Kramarski, M. Prescott, T. Proikas-Cezanne, N. Raben, A. Rami, F. Reggiori, B. Rohrer, D. C. Rubinsztein, K. M. Ryan, J. Sadoshima, H. Sakagami, Y. Sakai, M. Sandri, C. Sasakawa, M. Sass, C. Schneider, P. O. Seglen, O.

Seleverstov, J. Settleman, J. J. Shacka, I. M. Shapiro, A. Sibirny, E. C. Silva-Zacarin, H. U. Simon, C. Simone, A. Simonsen, M. A. Smith, K. Spanel-Borowski, V. Srinivas, M. Steeves, H. Stenmark, P. E. Stromhaug, C. S. Subauste, S. Sugimoto, D. Sulzer, T. Suzuki, M. S. Swanson, I. Tabas, F. Takeshita, N. J. Talbot, Z. Talloczy, K. Tanaka, I. Tanida, G. S. Taylor, J. P. Taylor, A. Terman, G. Tettamanti, C. B. Thompson, M. Thumm, A. M. Tolkovsky, S. A. Tooze, R. Truant, L. V. Tumanovska, Y. Uchiyama, T. Ueno, N. L. Uzcategui, I. van der Klei, E. C. Vaquero, T. Vellai, M. W. Vogel, H. G. Wang, P. Webster, J. W. Wiley, Z. Xi, G. Xiao, J. Yahalom, J. M. Yang, G. Yap, X. M. Yin, T. Yoshimori, L. Yu, Z. Yue, M. Yuzaki, O. Zabirnyk, X. Zheng, X. Zhu and R. L. Deter (2008). "Guidelines for the use and interpretation of assays for monitoring autophagy in higher eukaryotes." Autophagy **4**(2): 151-175.

Klotz, L., L. Boccon-Gibod, N. D. Shore, C. Andreou, B. E. Persson, P. Cantor, J. K. Jensen, T. K. Olesen and F. H. Schröder (2008). "The efficacy and safety of degarelix: a 12-month, comparative, randomized, open-label, parallel-group phase III study in patients with prostate cancer." BJU Int **102**(11): 1531-1538.

Knudsen, K. E. and T. M. Penning (2010). "Partners in crime: deregulation of AR activity and androgen synthesis in prostate cancer." Trends Endocrinol Metab **21**(5): 315-324.

Komatsu, T., H. Haruki and K. Nagata (2011). "Cellular and viral chromatin proteins are positive factors in the regulation of adenovirus gene expression." Nucleic Acids Res **39**(3): 889-901.

Komorek, J., M. Kuppuswamy, T. Subramanian, S. Vijayalingam, E. Lomonosova, L. J. Zhao, J. S. Mymryk, K. Schmitt and G. Chinnadurai (2010). "Adenovirus type 5 E1A and E6 proteins of low-risk cutaneous beta-human papillomaviruses suppress cell transformation through interaction with FOXK1/K2 transcription factors." J Virol **84**(6): 2719-2731.

Kondo, Y., T. Kanzawa, R. Sawaya and S. Kondo (2005). "The role of autophagy in cancer development and response to therapy." Nat Rev Cancer **5**(9): 726-734.

Koochekpour, S. (2010). "Androgen receptor signaling and mutations in prostate cancer." Asian J Androl **12**(5): 639-657.

Koukourakis, M. I., D. Kalamida, A. Mitrakas, S. Pouliliou, S. Kalamida, E. Sivridis and A. Giatromanolaki (2015). "Intensified autophagy compromises the efficacy of radiotherapy against prostate cancer." Biochem Biophys Res Commun **461**(2): 268-274.

Krajcsi, P., T. Dimitrov, T. W. Hermiston, A. E. Tollefson, T. S. Ranheim, S. B. Vande Pol, A. H. Stephenson and W. S. Wold (1996). "The adenovirus E3-14.7K protein and the E3-10.4K/14.5K complex of proteins, which independently inhibit tumor necrosis factor (TNF)-induced apoptosis, also independently inhibit TNF-induced release of arachidonic acid." J Virol **70**(8): 4904-4913.

Krajewska, M., S. Krajewski, J. I. Epstein, A. Shabaik, J. Sauvageot, K. Song, S. Kitada and J. C. Reed (1996). "Immunohistochemical analysis of bcl-2, bax, bcl-X, and mcl-1 expression in prostate cancers." Am J Pathol **148**(5): 1567-1576.

Kreppel, F. and S. Kochanek (2008). "Modification of adenovirus gene transfer vectors with synthetic polymers: a scientific review and technical guide." Mol Ther **16**(1): 16-29.

Kreuz, S., D. Siegmund, P. Scheurich and H. Wajant (2001). "NF-kappaB inducers upregulate cFLIP, a cycloheximide-sensitive inhibitor of death receptor signaling." Mol Cell Biol **21**(12): 3964-3973.

Kroemer, G., L. Galluzzi, P. Vandenabeele, J. Abrams, E. S. Alnemri, E. H. Baehrecke, M. V. Blagosklonny, W. S. El-Deiry, P. Golstein, D. R. Green, M. Hengartner, R. A. Knight, S. Kumar, S. A. Lipton, W. Malorni, G. Nuñez, M. E. Peter, J. Tschopp, J. Yuan, M. Piacentini, B. Zhivotovsky, G. Melino and N. C. o. C. D. 2009 (2009). "Classification of cell death: recommendations of the Nomenclature Committee on Cell Death 2009." Cell Death Differ **16**(1): 3-11.

Kruse, J. P. and W. Gu (2009). "Modes of p53 regulation." Cell **137**(4): 609-622.

Krušlin, B., M. Ulamec and D. Tomas (2015). "Prostate cancer stroma: an important factor in cancer growth and progression." Bosn J Basic Med Sci **15**(2): 1-8.

Kunderfranco, P., M. Mello-Grand, R. Cangemi, S. Pellini, A. Mensah, V. Albertini, A. Malek, G. Chiorino, C. V. Catapano and G. M. Carbone (2010). "ETS transcription factors control transcription of EZH2 and epigenetic silencing of the tumor suppressor gene Nkx3.1 in prostate cancer." PLoS One **5**(5): e10547.

Kuppen, P. J., M. M. van der Eb, L. E. Jonges, M. Hagenaars, M. E. Hokland, U. Nannmark, R. H. Goldfarb, P. H. Basse, G. J. Fleuren, R. C. Hoeben and C. J. van de Velde (2001). "Tumor structure and extracellular matrix as a possible barrier for therapeutic approaches using immune cells or adenoviruses in colorectal cancer." Histochem Cell Biol **115**(1): 67-72.

Kwilas, A. R., R. N. Donahue, M. B. Bernstein and J. W. Hodge (2012). "In the field: exploiting the untapped potential of immunogenic modulation by radiation in combination with immunotherapy for the treatment of cancer." Front Oncol **2**: 104.

Lam, J. T., A. Hemminki, A. Kanerva, K. B. Lee, J. L. Blackwell, R. Desmond, G. P. Siegal and D. T. Curiel (2007). "A three-dimensional assay for measurement of viral-induced oncolysis." Cancer Gene Ther **14**(4): 421-430.

Lamb, C. A., T. Yoshimori and S. A. Tooze (2013). "The autophagosome: origins unknown, biogenesis complex." Nat Rev Mol Cell Biol **14**(12): 759-774.

Lamoureux, F., C. Thomas, C. Crafter, M. Kumano, F. Zhang, B. R. Davies, M. E. Gleave and A. Zoubeidi (2013). "Blocked autophagy using lysosomotropic agents sensitizes resistant prostate tumor cells to the novel Akt inhibitor AZD5363." Clin Cancer Res **19**(4): 833-844.

Lee, C. H., O. Akin-Olugbade and A. Kirschenbaum (2011). "Overview of prostate anatomy, histology, and pathology." Endocrinol Metab Clin North Am **40**(3): 565-575, viii-ix.

Lee, P. and D. Meisel (1982). "Adsorption and surface-enhanced raman of dyes on silver and gold sols." Journal of Physical Chemistry **86**(17): 3391-3395.

Lee, W. P., D. I. Tai, S. L. Tsai, C. T. Yeh, Y. Chao, S. D. Lee and M. C. Hung (2003). "Adenovirus type 5 E1A sensitizes hepatocellular carcinoma cells to gemcitabine." Cancer Res **63**(19): 6229-6236.

Leite, K. R., M. F. Franco, M. Srougi, L. J. Nesrallah, A. Nesrallah, R. G. Bevilacqua, E. Darini, C. M. Carvalho, M. I. Meirelles, I. Santana and L. H. Camara-Lopes (2001). "Abnormal expression of MDM2 in prostate carcinoma." Mod Pathol **14**(5): 428-436.

Leitner, S., K. Sweeney, D. Oberg, D. Davies, E. Miranda, N. R. Lemoine and G. Hallden (2009). "Oncolytic adenoviral mutants with E1B19K gene deletions enhance gemcitabine-induced apoptosis in pancreatic carcinoma cells and anti-tumor efficacy in vivo." Clin Cancer Res **15**(5): 1730-1740.

Leonard, G. T. and G. C. Sen (1996). "Effects of adenovirus E1A protein on interferon-signaling." Virology **224**(1): 25-33.

Leonard, J. P., M. L. Sherman, G. L. Fisher, L. J. Buchanan, G. Larsen, M. B. Atkins, J. A. Sosman, J. P. Dutcher, N. J. Vogelzang and J. L. Ryan (1997). "Effects of single-dose interleukin-12 exposure on interleukin-12-associated toxicity and interferon-gamma production." Blood **90**(7): 2541-2548.

Leopold, P. L. and R. G. Crystal (2007). "Intracellular trafficking of adenovirus: many means to many ends." Adv Drug Deliv Rev **59**(8): 810-821.

Levine, B., N. Mizushima and H. W. Virgin (2011). "Autophagy in immunity and inflammation." Nature **469**(7330): 323-335.

Li, M., P. Gao and J. Zhang (2016). "Crosstalk between Autophagy and Apoptosis: Potential and Emerging Therapeutic Targets for Cardiac Diseases." Int J Mol Sci **17**(3): 332.

Li, M., X. Jiang, D. Liu, Y. Na, G. F. Gao and Z. Xi (2008). "Autophagy protects LNCaP cells under androgen deprivation conditions." Autophagy **4**(1): 54-60.

Li, Z., C. P. Day, J. Y. Yang, W. B. Tsai, G. Lozano, H. M. Shih and M. C. Hung (2004). "Adenoviral E1A targets Mdm4 to stabilize tumor suppressor p53." Cancer Res **64**(24): 9080-9085.

Liang, C., X. E and J. U. Jung (2008). "Downregulation of autophagy by herpesvirus Bcl-2 homologs." Autophagy **4**(3): 268-272.

Liao, S., D. K. Howell and T. M. Chang (1974). "Action of a nonsteroidal antiandrogen, flutamide, on the receptor binding and nuclear retention of 5 alpha-dihydrotestosterone in rat ventral prostate." Endocrinology **94**(4): 1205-1209.

Lichtenstein, D. L., K. Doronin, K. Toth, M. Kuppuswamy, W. S. Wold and A. E. Tollefson (2004). "Adenovirus E3-6.7K protein is required in conjunction with the E3-RID protein complex for the internalization and degradation of TRAIL receptor 2." J Virol **78**(22): 12297-12307.

Lichtenstein, D. L., K. Toth, K. Doronin, A. E. Tollefson and W. S. Wold (2004). "Functions and mechanisms of action of the adenovirus E3 proteins." Int Rev Immunol **23**(1-2): 75-111.

Lin, C., L. Yang, B. Tanasa, K. Hutt, B. G. Ju, K. Ohgi, J. Zhang, D. W. Rose, X. D. Fu, C. K. Glass and M. G. Rosenfeld (2009). "Nuclear receptor-induced chromosomal proximity and DNA breaks underlie specific translocations in cancer." Cell **139**(6): 1069-1083.

Lin, R. Z. and H. Y. Chang (2008). "Recent advances in three-dimensional multicellular spheroid culture for biomedical research." Biotechnol J **3**(9-10): 1172-1184.

Lindzey, J., M. V. Kumar, M. Grossman, C. Young and D. J. Tindall (1994). "Molecular mechanisms of androgen action." Vitam Horm **49**: 383-432.

Liu, C., Y. Zhu, W. Lou, N. Nadiminty, X. Chen, Q. Zhou, X. B. Shi, R. W. deVere White and A. C. Gao (2013). "Functional p53 determines docetaxel sensitivity in prostate cancer cells." Prostate **73**(4): 418-427.

Liu, D., T. Kojima, M. Ouchi, S. Kuroda, Y. Watanabe, Y. Hashimoto, H. Onimatsu, Y. Urata and T. Fujiwara (2009). "Preclinical evaluation of synergistic effect of telomerase-specific oncolytic virotherapy and gemcitabine for human lung cancer." Mol Cancer Ther **8**(4): 980-987.

Liu, Q. and D. A. Muruve (2003). "Molecular basis of the inflammatory response to adenovirus vectors." Gene Ther **10**(11): 935-940.

Liu, T. C. and D. Kirn (2007). "Systemic efficacy with oncolytic virus therapeutics: clinical proof-of-concept and future directions." Cancer Res **67**(2): 429-432.

Liu, Y., M. Shipton, J. Ryan, E. Kaufman, S. Franzen and D. Feldheim (2007). "Synthesis, stability, and cellular internalization of gold nanoparticles containing mixed peptide-poly(ethylene glycol) monolayers." Analytical Chemistry **79**(6): 2221-2229.

Livak, K. J. and T. D. Schmittgen (2001). "Analysis of relative gene expression data using real-time quantitative PCR and the 2(-Delta Delta C(T)) Method." Methods **25**(4): 402-408.

Lockley, M., M. Fernandez, Y. Wang, N. F. Li, S. Conroy, N. Lemoine and I. McNeish (2006). "Activity of the adenoviral E1A deletion mutant dl922-947 in ovarian cancer: comparison with E1A wild-type viruses, bioluminescence monitoring, and intraperitoneal delivery in icodextrin." Cancer Res **66**(2): 989-998.

Longnecker, R. and E. Kieff (1990). "A second Epstein-Barr virus membrane protein (LMP2) is expressed in latent infection and colocalizes with LMP1." J Virol **64**(5): 2319-2326.

Look, D. C., W. T. Roswit, A. G. Frick, Y. Gris-Alevy, D. M. Dickhaus, M. J. Walter and M. J. Holtzman (1998). "Direct suppression of Stat1 function during adenoviral infection." Immunity **9**(6): 871-880.

Lopez-Gordo, E., L. Denby, S. A. Nicklin and A. H. Baker (2014). "The importance of coagulation factors binding to adenovirus: historical perspectives and implications for gene delivery." Expert Opin Drug Deliv **11**(11): 1795-1813.

Loprinzi, P. D. and M. Kohli (2013). "Effect of physical activity and sedentary behavior on serum prostate-specific antigen concentrations: results from the National Health and Nutrition Examination Survey (NHANES), 2003-2006." Mayo Clin Proc **88**(1): 11-21.

Lorenzo, P. I., Y. J. Arnoldussen and F. Saatcioglu (2007). "Molecular mechanisms of apoptosis in prostate cancer." Crit Rev Oncog **13**(1): 1-38.

Lovell, J. F., L. P. Billen, S. Bindner, A. Shamas-Din, C. Fradin, B. Leber and D. W. Andrews (2008). "Membrane binding by tBid initiates an ordered series of events culminating in membrane permeabilization by Bax." Cell **135**(6): 1074-1084.

Lozy, F. and V. Karantza (2012). "Autophagy and cancer cell metabolism." Semin Cell Dev Biol **23**(4): 395-401.

Lu, J., P. E. Lonergan, L. P. Nacusi, L. Wang, L. J. Schmidt, Z. Sun, T. Van der Steen, S. A. Boorjian, F. Kosari, G. Vasmatzis, G. G. Klee, S. P. Balk, H. Huang, C. Wang and D. J. Tindall (2015). "The cistrome and gene signature of androgen receptor splice variants in castration resistant prostate cancer cells." J Urol **193**(2): 690-698.

Lu, W., S. Zheng, X. F. Li, J. J. Huang, X. Zheng and Z. Li (2004). "Intra-tumor injection of H101, a recombinant adenovirus, in combination with chemotherapy in patients with advanced cancers: a pilot phase II clinical trial." World J Gastroenterol **10**(24): 3634-3638.

Lucas, J. J. and H. S. Ginsberg (1972). "Transcription and transport of virus-specific ribonucleic acids in African green monkey kidney cells abortively infected with type 2 adenovirus." J Virol **10**(6): 1109-1117.

Luo, S. and D. C. Rubinsztein (2010). "Apoptosis blocks Beclin 1-dependent autophagosome synthesis: an effect rescued by Bcl-xL." Cell Death Differ **17**(2): 268-277.

Ma, G., K. Kawamura, Q. Li, S. Okamoto, N. Suzuki, H. Kobayashi, M. Liang, Y. Tada, K. Tatsumi, K. Hiroshima, H. Shimada and M. Tagawa (2010). "Combinatory cytotoxic effects produced by E1B-55kDa-deleted adenoviruses and chemotherapeutic agents are dependent on the agents in esophageal carcinoma." Cancer Gene Ther **17**(11): 803-813.

Ma, H. C. and P. Hearing (2011). "Adenovirus structural protein IIIa is involved in the serotype specificity of viral DNA packaging." J Virol **85**(15): 7849-7855.

Mack, H. I. and K. Munger (2012). "Modulation of autophagy-like processes by tumor viruses." Cells **1**(3): 204-247.

Mainwaring, W. I. (1969). "A soluble androgen receptor in the cytoplasm of rat prostate." J Endocrinol **45**(4): 531-541.

Majumder, P. K. and W. R. Sellers (2005). "Akt-regulated pathways in prostate cancer." Oncogene **24**(50): 7465-7474.

Mak, H. Y., S. Hoare, P. M. Henttu and M. G. Parker (1999). "Molecular determinants of the estrogen receptor-coactivator interface." Mol Cell Biol **19**(5): 3895-3903.

Malvezzi, M., P. Bertuccio, T. Rosso, M. Rota, F. Levi, C. La Vecchia and E. Negri (2015). "European cancer mortality predictions for the year 2015: does lung cancer have the highest death rate in EU women?" Ann Oncol **26**((4)): 779-786.

Mangel, W. F. and C. San Martín (2014). "Structure, function and dynamics in adenovirus maturation." Viruses **6**(11): 4536-4570.

Mannová, P. and L. Beretta (2005). "Activation of the N-Ras-PI3K-Akt-mTOR pathway by hepatitis C virus: control of cell survival and viral replication." J Virol **79**(14): 8742-8749.

Maran, A. and M. B. Mathews (1988). "Characterization of the double-stranded RNA implicated in the inhibition of protein synthesis in cells infected with a mutant adenovirus defective for VA RNA." Virology **164**(1): 106-113.

Marcelli, M., M. Ittmann, S. Mariani, R. Sutherland, R. Nigam, L. Murthy, Y. Zhao, D. DiConcini, E. Puxeddu, A. Esen, J. Eastham, N. L. Weigel and D. J. Lamb (2000). "Androgen receptor mutations in prostate cancer." Cancer Res **60**(4): 944-949.

Marquez, R. T. and L. Xu (2012). "Bcl-2:Beclin 1 complex: multiple, mechanisms regulating autophagy/apoptosis toggle switch." Am J Cancer Res **2**(2): 214-221.

Marttila, M., D. Persson, D. Gustafsson, M. K. Liszewski, J. P. Atkinson, G. Wadell and N. Arnberg (2005). "CD46 is a cellular receptor for all species B adenoviruses except types 3 and 7." J Virol **79**(22): 14429-14436.

Mathews, M. B. and T. Shenk (1991). "Adenovirus virus-associated RNA and translation control." J Virol **65**(11): 5657-5662.

Mathias, P., T. Wickham, M. Moore and G. Nemerow (1994). "Multiple adenovirus serotypes use alpha v integrins for infection." J Virol **68**(10): 6811-6814.

Matoso, A. and J. I. Epstein (2016). "Grading of Prostate Cancer: Past, Present, and Future." Curr Urol Rep **17**(3): 25.

Maya Pineda, H. (2013). "Sensitization of prostate cancer cells to cytotoxic drugs induced by the small adenoviral E1A12S protein through multiple cell death/signalling pathways." PhD. Thesis.

Maycotte, P., S. Aryal, C. T. Cummings, J. Thorburn, M. J. Morgan and A. Thorburn (2012). "Chloroquine sensitizes breast cancer cells to chemotherapy independent of autophagy." Autophagy **8**(2): 200-212.

McCrea, E., T. M. Sissung, D. K. Price, C. H. Chau and W. D. Figg (2016). "Androgen receptor variation affects prostate cancer progression and drug resistance." Pharmacol Res **114**: 152-162.

McKee, T. D., P. Grandi, W. Mok, G. Alexandrakis, N. Insin, J. P. Zimmer, M. G. Bawendi, Y. Boucher, X. O. Breakefield and R. K. Jain (2006). "Degradation of fibrillar collagen in a human melanoma xenograft improves the efficacy of an oncolytic herpes simplex virus vector." Cancer Res **66**(5): 2509-2513.

McSharry, B. P., H. G. Burgert, D. P. Owen, R. J. Stanton, V. Prod'homme, M. Sester, K. Koebernick, V. Groh, T. Spies, S. Cox, A. M. Little, E. C. Wang, P. Tomasec and G. W. Wilkinson (2008). "Adenovirus E3/19K promotes evasion of NK cell recognition by intracellular sequestration of the NKG2D ligands major histocompatibility complex class I chain-related proteins A and B." J Virol **82**(9): 4585-4594.

Meijer, A. J. and P. Codogno (2007). "AMP-activated protein kinase and autophagy." Autophagy **3**(3): 238-240.

Mellinghoff, I. K., I. Vivanco, A. Kwon, C. Tran, J. Wongvipat and C. L. Sawyers (2004). "HER2/neu kinase-dependent modulation of androgen receptor function through effects on DNA binding and stability." Cancer Cell **6**(5): 517-527.

Merle, N. S., R. Noe, L. Halbwachs-Mecarelli, V. Fremeaux-Bacchi and L. T. Roumenina (2015). "Complement System Part II: Role in Immunity." Front Immunol **6**: 257.

Merrill, R. M. and A. Sloan (2012). "Risk-adjusted incidence rates for prostate cancer in the United States." Prostate **72**(2): 181-185.

Minamitani, T., D. Iwakiri and K. Takada (2011). "Adenovirus virus-associated RNAs induce type I interferon expression through a RIG-I-mediated pathway." J Virol **85**(8): 4035-4040.

Ming, L., N. M. Byrne, S. N. Camac, C. A. Mitchell, C. Ward, D. J. Waugh, S. R. McKeown and J. Worthington (2013). "Androgen deprivation results in time-dependent hypoxia in LNCaP prostate tumours: informed scheduling of the bioreductive drug AQ4N improves treatment response." Int J Cancer **132**(6): 1323-1332.

Miranda, E. (2009). Identification of adenovirus E1A gene regions involved in chemosensitisation of prostate cancer cells. Thesis (PhD), Queen Mary, University of London, 2009.

Miranda, E., H. Maya Pineda, D. Oberg, G. Cherubini, Z. Garate, N. R. Lemoine and G. Hallden (2012). "Adenovirus-mediated sensitization to the cytotoxic drugs docetaxel and mitoxantrone is dependent on regulatory domains in the E1ACR1 gene-region." PLoS One **7**(10): e46617.

Mizushima, N. (2010). "The role of the Atg1/ULK1 complex in autophagy regulation." Curr Opin Cell Biol **22**(2): 132-139.

Mok, H., D. J. Palmer, P. Ng and M. A. Barry (2005). "Evaluation of polyethylene glycol modification of first-generation and helper-dependent adenoviral vectors to reduce innate immune responses." Mol Ther **11**(1): 66-79.

Moll, U. M. and O. Petrenko (2003). "The MDM2-p53 interaction." Mol Cancer Res **1**(14): 1001-1008.

Montgomery, B., M. A. Eisenberger, M. B. Rettig, F. Chu, R. Pili, J. J. Stephenson, N. J. Vogelzang, A. J. Koletsky, L. T. Nordquist, W. J. Edenfield, K. Mamlouk, K. J. Ferrante and M. E. Taplin (2016). "Androgen Receptor Modulation Optimized for Response (ARMOR) Phase I and II Studies: Galeterone for the Treatment of Castration-Resistant Prostate Cancer." Clin Cancer Res **22**(6): 1356-1363.

Mukhopadhaya, A., J. Mendecki, X. Dong, L. Liu, S. Kalnicki, M. Garg, A. Alfieri and C. Guha (2007). "Localized hyperthermia combined with intratumoral dendritic cells induces systemic antitumor immunity." Cancer Res **67**(16): 7798-7806.

Mulholland, D. J., N. Kobayashi, M. Ruscetti, A. Zhi, L. M. Tran, J. Huang, M. Gleave and H. Wu (2012). "Pten loss and RAS/MAPK activation cooperate to promote EMT and metastasis initiated from prostate cancer stem/progenitor cells." Cancer Res **72**(7): 1878-1889.

Murphy, D. G., T. Ahlering, W. J. Catalona, H. Crowe, J. Crowe, N. Clarke, M. Cooperberg, D. Gillatt, M. Gleave, S. Loeb, M. Roobol, O. Sartor, T. Pickles, A. Wootten, P. C. Walsh and A. J. Costello (2014). "The Melbourne Consensus Statement on the early detection of prostate cancer." BJU Int **113**(2): 186-188.

Muruve, D. A. (2004). "The innate immune response to adenovirus vectors." Hum Gene Ther **15**(12): 1157-1166.

Muthana, M., A. Giannoudis, S. D. Scott, H. Y. Fang, S. B. Coffelt, F. J. Morrow, C. Murdoch, J. Burton, N. Cross, B. Burke, R. Mistry, F. Hamdy, N. J. Brown, L. Georgopoulos, P. Hoskin, M. Essand, C. E. Lewis and N. J. Maitland (2011). "Use of macrophages to target therapeutic adenovirus to human prostate tumors." Cancer Res **71**(5): 1805-1815.

Nagabhushan, M., C. M. Miller, T. P. Pretlow, J. M. Giaconia, N. L. Edgehouse, S. Schwartz, H. J. Kung, R. W. de Vere White, P. H. Gumerlock, M. I. Resnick, S. B. Amini and T. G. Pretlow (1996). "CWR22: the first human prostate cancer xenograft with strongly androgen-dependent and relapsed strains both in vivo and in soft agar." Cancer Res **56**(13): 3042-3046.

Nakatogawa, H. (2013). "Two ubiquitin-like conjugation systems that mediate membrane formation during autophagy." Essays Biochem **55**: 39-50.

Nemerow, G. R., L. Pache, V. Reddy and P. L. Stewart (2009). "Insights into adenovirus host cell interactions from structural studies." Virology **384**(2): 380-388.

Nemunaitis, J., A. W. Tong, M. Nemunaitis, N. Senzer, A. P. Phadke, C. Bedell, N. Adams, Y. A. Zhang, P. B. Maples, S. Chen, B. Pappen, J. Burke, D. Ichimaru, Y. Urata and T. Fujiwara (2010). "A phase I study of telomerase-specific replication competent oncolytic adenovirus (telomelysin) for various solid tumors." Mol Ther **18**(2): 429-434.

Nguyen, H. G., J. C. Yang, H. J. Kung, X. B. Shi, D. Tilki, P. N. Lara, R. W. DeVere White, A. C. Gao and C. P. Evans (2014). "Targeting autophagy overcomes Enzalutamide resistance in castration-resistant prostate cancer cells and improves therapeutic response in a xenograft model." Oncogene **33**(36): 4521-4530.

Niu, Y., S. Altuwaijri, K. P. Lai, C. T. Wu, W. A. Ricke, E. M. Messing, J. Yao, S. Yeh and C. Chang (2008). "Androgen receptor is a tumor suppressor and proliferator in prostate cancer." Proc Natl Acad Sci U S A **105**(34): 12182-12187.

Notte, A., L. Leclere and C. Michiels (2011). "Autophagy as a mediator of chemotherapy-induced cell death in cancer." Biochem Pharmacol **82**(5): 427-434.

O'Reilly, D., Muller, L., and Luckow, V., Ed. (1994). Virus Methods. Oxford University Press, Oxford.

O'Shea, C., K. Klupsch, S. Choi, B. Bagus, C. Soria, J. Shen, F. McCormick and D. Stokoe (2005). "Adenoviral proteins mimic nutrient/growth signals to activate the mTOR pathway for viral replication." EMBO J **24**(6): 1211-1221.

O'Shea, C. C., L. Johnson, B. Bagus, S. Choi, C. Nicholas, A. Shen, L. Boyle, K. Pandey, C. Soria, J. Kunich, Y. Shen, G. Habets, D. Ginzinger and F. McCormick (2004). "Late viral RNA export, rather than p53 inactivation, determines ONYX-015 tumor selectivity." Cancer Cell **6**(6): 611-623.

Oberg, D., E. Yanover, V. Adam, K. Sweeney, C. Costas, N. R. Lemoine and G. Hallden (2010). "Improved potency and selectivity of an oncolytic E1ACR2 and E1B19K deleted adenoviral mutant in prostate and pancreatic cancers." Clin Cancer Res **16**(2): 541-553.

Olsson, A. Y., A. Feber, S. Edwards, R. Te Poele, I. Giddings, S. Merson and C. S. Cooper (2007). "Role of E2F3 expression in modulating cellular proliferation rate in human bladder and prostate cancer cells." Oncogene **26**(7): 1028-1037.

Oncolys BioPharma, I. (2014). Phase I/II Study to Evaluate the Safety and Efficacy of Telomelysin (OBP-301) in Patients With Hepatocellular Carcinoma.

Orvedahl, A., D. Alexander, Z. Tallóczy, Q. Sun, Y. Wei, W. Zhang, D. Burns, D. A. Leib and B. Levine (2007). "HSV-1 ICP34.5 confers neurovirulence by targeting the Beclin 1 autophagy protein." Cell Host Microbe **1**(1): 23-35.

Otomo, C., Z. Metlagel, G. Takaesu and T. Otomo (2013). "Structure of the human ATG12~ATG5 conjugate required for LC3 lipidation in autophagy." Nat Struct Mol Biol **20**(1): 59-66.

Paludan, C., D. Schmid, M. Landthaler, M. Vockerodt, D. Kube, T. Tuschl and C. Münz (2005). "Endogenous MHC class II processing of a viral nuclear antigen after autophagy." Science **307**(5709): 593-596.

Pan, X., X. Zhang, H. Sun, J. Zhang, M. Yan and H. Zhang (2013). "Autophagy inhibition promotes 5-fluorouracil-induced apoptosis by stimulating ROS formation in human non-small cell lung cancer A549 cells." PLoS One **8**(2): e56679.

Pandha, H. S., L. H. Stockwin, J. Eaton, I. A. Clarke, A. G. Dalgleish, S. M. Todryk and G. E. Blair (2003). "Coxsackie B and adenovirus receptor, integrin and major histocompatibility complex class I expression in human prostate cancer cell lines: implications for gene therapy strategies." Prostate Cancer Prostatic Dis **6**(1): 6-11.

Pankiv, S., T. H. Clausen, T. Lamark, A. Brech, J. A. Bruun, H. Outzen, A. Øvervatn, G. Bjørkøy and T. Johansen (2007). "p62/SQSTM1 binds directly to Atg8/LC3 to facilitate degradation of ubiquitinated protein aggregates by autophagy." J Biol Chem **282**(33): 24131-24145.

Pantelidou, C., G. Cherubini, N. R. Lemoine and G. Halldén (2016). "The E1B19K-deleted oncolytic adenovirus mutant AdΔ19K sensitizes pancreatic cancer cells to drug-induced DNA-damage by down-regulating Claspin and Mre11." Oncotarget **7**(13): 15703-15724.

Pardo-Mateos, A. and C. S. Young (2004). "Adenovirus IVa2 protein plays an important role in transcription from the major late promoter in vivo." Virology **327**(1): 50-59.

Pardoll, D. M. (2012). "The blockade of immune checkpoints in cancer immunotherapy." Nat Rev Cancer **12**(4): 252-264.

Park, J. H., Y. R. Lee, H. S. So, K. K. Lee, S. Y. Lee, S. R. Moon, H. J. Jo, S. Lee, K. Jeong, K. B. Kwon and S. H. Yang (2014). "The role of autophagy induced by pemetrexed in lung adenocarcinoma cells." Oncol Rep **31**(5): 2365-2370.

Park, S. Y., C. A. Haiman, I. Cheng, S. L. Park, L. R. Wilkens, L. N. Kolonel, L. Le Marchand and B. E. Henderson (2015). "Racial/ethnic differences in lifestyle-related factors and prostate cancer risk: the Multiethnic Cohort Study." Cancer Causes Control **26**(10): 1507-1515.

Pattingre, S., A. Tassa, X. Qu, R. Garuti, X. H. Liang, N. Mizushima, M. Packer, M. D. Schneider and B. Levine (2005). "Bcl-2 antiapoptotic proteins inhibit Beclin 1-dependent autophagy." Cell **122**(6): 927-939.

Pelka, P., J. N. Ablack, J. Torchia, A. S. Turnell, R. J. Grand and J. S. Mymryk (2009). "Transcriptional control by adenovirus E1A conserved region 3 via p300/CBP." Nucleic Acids Res **37**(4): 1095-1106.

Perez, D. and E. White (2003). "E1A sensitizes cells to tumor necrosis factor alpha by downregulating c-FLIP S." J Virol **77**(4): 2651-2662.

Perez-Romero, P., K. E. Gustin and M. J. Imperiale (2006). "Dependence of the encapsidation function of the adenovirus L1 52/55-kilodalton protein on its ability to bind the packaging sequence." J Virol **80**(4): 1965-1971.

Pesonen, S., I. Diaconu, L. Kangasniemi, T. Ranki, A. Kanerva, S. K. Pesonen, U. Gerdemann, A. M. Leen, K. Kairemo, M. Oksanen, E. Haavisto, S. L. Holm, A. Karioja-Kallio, S. Kauppinen, K. P. Partanen, L. Laasonen, T. Joensuu, T. Alanko, V. Cerullo and A. Hemminki (2012). "Oncolytic immunotherapy of advanced solid tumors with a CD40L-expressing replicating adenovirus: assessment of safety and immunologic responses in patients." Cancer Res **72**(7): 1621-1631.

Pesonen, S., L. Kangasniemi and A. Hemminki (2011). "Oncolytic adenoviruses for the treatment of human cancer: focus on translational and clinical data." Mol Pharm **8**(1): 12-28.
Pezaro, C., H. H. Woo and I. D. Davis (2014). "Prostate cancer: measuring PSA." Intern Med J **44**(5): 433-440.

Pham, T., M. C. Sadowski, H. Li, D. J. Richard, M. C. d'Emden and K. Richard (2015). "Advances in hormonal therapies for hormone naïve and castration-resistant prostate cancers with or without previous chemotherapy." Exp Hematol Oncol **5**: 15.

Pieczonka, C. M., D. Telonis, V. Mouraviev and D. Albala (2015). "Sipuleucel-T for the Treatment of Patients With Metastatic Castrate-resistant Prostate Cancer: Considerations for Clinical Practice." Rev Urol **17**(4): 203-210.

Piya, S., E. J. White, S. R. Klein, H. Jiang, T. J. McDonnell, C. Gomez-Manzano and J. Fueyo (2011). "The E1B19K oncoprotein complexes with Beclin 1 to regulate autophagy in adenovirus-infected cells." PLoS One **6**(12): e29467.

Pommier, Y., E. Leo, H. Zhang and C. Marchand (2010). "DNA topoisomerases and their poisoning by anticancer and antibacterial drugs." Chem Biol **17**(5): 421-433.

Portis, T. and R. Longnecker (2004). "Epstein-Barr virus (EBV) LMP2A mediates B-lymphocyte survival through constitutive activation of the Ras/PI3K/Akt pathway." Oncogene **23**(53): 8619-8628.

Powers, G. L. and P. C. Marker (2013). "Recent advances in prostate development and links to prostatic diseases." Wiley Interdiscip Rev Syst Biol Med **5**(2): 243-256.

Putzer, B. M., T. Stiewe, K. Parssanedjad, S. Rega and H. Esche (2000). "E1A is sufficient by itself to induce apoptosis independent of p53 and other adenoviral gene products." Cell Death Differ **7**(2): 177-188.

Pérez-Berná, A. J., R. Marabini, S. H. Scheres, R. Menéndez-Conejero, I. P. Dmitriev, D. T. Curiel, W. F. Mangel, S. J. Flint and C. San Martín (2009). "Structure and uncoating of immature adenovirus." J Mol Biol **392**(2): 547-557.

Radhakrishnan, S., E. Miranda, M. Ekblad, A. Holford, M. T. Pizarro, N. R. Lemoine and G. Hallden (2010). "Efficacy of oncolytic mutants targeting pRb and p53 pathways is synergistically enhanced when combined with cytotoxic drugs in prostate cancer cells and tumor xenografts." Hum Gene Ther **21**(10): 1311-1325.

Rangwala, R., Y. C. Chang, J. Hu, K. M. Algazy, T. L. Evans, L. A. Fecher, L. M. Schuchter, D. A. Torigian, J. T. Panosian, A. B. Troxel, K. S. Tan, D. F. Heitjan, A. M. DeMichele, D. J. Vaughn, M. Redlinger, A. Alavi, J. Kaiser, L. Pontiggia, L. E. Davis, P. J. O'Dwyer and R. K. Amaravadi (2014). "Combined MTOR and autophagy inhibition: phase I trial of hydroxychloroquine and temsirolimus in patients with advanced solid tumors and melanoma." Autophagy **10**(8): 1391-1402.

Rao, S., L. Tortola, T. Perlot, G. Wirnsberger, M. Novatchkova, R. Nitsch, P. Sykacek, L. Frank, D. Schramek, V. Komnenovic, V. Sigl, K. Aumayr, G. Schmauss, N. Fellner, S. Handschuh, M. Glösmann, P. Pasierbek, M. Schlederer, G. P. Resch, Y. Ma, H. Yang, H. Popper, L. Kenner, G. Kroemer and J. M. Penninger (2014). "A dual role for autophagy in a murine model of lung cancer." Nat Commun **5**: 3056.

Ravikumar, B., S. Sarkar, J. E. Davies, M. Futter, M. Garcia-Arencibia, Z. W. Green-Thompson, M. Jimenez-Sanchez, V. I. Korolchuk, M. Lichtenberg, S. Luo, D. C. Massey, F. M. Menzies, K. Moreau, U. Narayanan, M. Renna, F. H. Siddiqi, B. R. Underwood, A. R. Winslow and D. C. Rubinsztein (2010). "Regulation of mammalian autophagy in physiology and pathophysiology." Physiol Rev **90**(4): 1383-1435.

Reddy, V. S. and G. R. Nemerow (2014). "Structures and organization of adenovirus cement proteins provide insights into the role of capsid maturation in virus entry and infection." Proc Natl Acad Sci U S A **111**(32): 11715-11720.

Reid, A. H., G. Attard, D. C. Danila, N. B. Oommen, D. Olmos, P. C. Fong, L. R. Molife, J. Hunt, C. Messiou, C. Parker, D. Dearnaley, J. F. Swennenhuis, L. W. Terstappen, G. Lee, T. Kheoh, A. Molina, C. J. Ryan, E. Small, H. I. Scher and J. S. de Bono (2010). "Significant and sustained antitumor activity in post-docetaxel, castration-resistant prostate cancer with the CYP17 inhibitor abiraterone acetate." J Clin Oncol **28**(9): 1489-1495.

Ren, J. H., W. S. He, L. Nong, Q. Y. Zhu, K. Hu, R. G. Zhang, L. L. Huang, F. Zhu and G. Wu (2010). "Acquired cisplatin resistance in human lung adenocarcinoma cells is associated with enhanced autophagy." Cancer Biother Radiopharm **25**(1): 75-80.

Repnik, U., M. Hafner Česen and B. Turk (2014). "Lysosomal membrane permeabilization in cell death: concepts and challenges." Mitochondrion **19 Pt A**: 49-57.

Rittenhouse, H. G., J. A. Finlay, S. D. Mikolajczyk and A. W. Partin (1998). "Human Kallikrein 2 (hK2) and prostate-specific antigen (PSA): two closely related, but distinct, kallikreins in the prostate." Crit Rev Clin Lab Sci **35**(4): 275-368.

Rodriguez, R., E. R. Schuur, H. Y. Lim, G. A. Henderson, J. W. Simons and D. R. Henderson (1997). "Prostate attenuated replication competent adenovirus (ARCA) CN706: a selective cytotoxic for prostate-specific antigen-positive prostate cancer cells." Cancer Res **57**(13): 2559-2563.

Rodriguez-Rocha, H., J. G. Gomez-Gutierrez, A. Garcia-Garcia, X. M. Rao, L. Chen, K. M. McMasters and H. S. Zhou (2011). "Adenoviruses induce autophagy to promote virus replication and oncolysis." Virology **416**(1-2): 9-15.

Rojas, L. A., R. Moreno, H. Calderón and R. Alemany (2016). "Adenovirus coxsackie adenovirus receptor-mediated binding to human erythrocytes does not preclude systemic transduction." Cancer Gene Ther.

Rubin, M. A., N. R. Mucci, J. Figurski, A. Fecko, K. J. Pienta and M. L. Day (2001). "E-cadherin expression in prostate cancer: a broad survey using high-density tissue microarray technology." Hum Pathol **32**(7): 690-697.

Russell, W. C. (2000). "Update on adenovirus and its vectors." J Gen Virol **81**(Pt 11): 2573-2604.

Russell, W. C. (2009). "Adenoviruses: update on structure and function." J Gen Virol **90**(Pt 1): 1-20.

Saftig, P., W. Beertsen and E. L. Eskelinen (2008). "LAMP-2: a control step for phagosome and autophagosome maturation." Autophagy **4**(4): 510-512.

Salerno, J., A. Finelli, C. Morash, S. C. Morgan, N. Power, N. Schieda and M. A. Haider (2016). "Multiparametric magnetic resonance imaging for pre-treatment local staging of prostate cancer: A Cancer Care Ontario clinical practice guideline." Can Urol Assoc J **10**(9-10): E332-E339.

San Martin, C. (2012). "Latest insights on adenovirus structure and assembly." Viruses **4**(5): 847-877.

Sandhu, K. S. and M. Al-Rubeai (2009). "The effect of Bcl-2, YAMA, and XIAP over-expression on apoptosis and adenovirus production in HEK293 cell line." Biotechnol Bioeng **104**(4): 752-765.

Sandow, J., W. Von Rechenberg, G. Jerzabek and W. Stoll (1978). "Pituitary gonadotropin inhibition by a highly active analog of luteinizing hormone-releasing hormone." Fertil Steril **30**(2): 205-209.

Sanz, V., J. Conde, Y. Hernandez, P. Baptista, M. Ibarra and J. de la Fuente (2012). "Effect of PEG biofunctional spacers and TAT peptide on dsRNA loading on gold nanoparticles." Journal of Nanoparticle Research **14**(6).

Saramäki, O. R., T. L. Tammela, P. M. Martikainen, R. L. Vessella and T. Visakorpi (2006). "The gene for polycomb group protein enhancer of zeste homolog 2 (EZH2) is amplified in late-stage prostate cancer." Genes Chromosomes Cancer **45**(7): 639-645.

Sarkar, S., B. A. Quinn, X. N. Shen, R. Dash, S. K. Das, L. Emdad, A. L. Klibanov, X. Y. Wang, M. Pellecchia, D. Sarkar and P. B. Fisher (2015). "Therapy of prostate cancer using a novel cancer terminator virus and a small molecule BH-3 mimetic." Oncotarget **6**(13): 10712-10727.

Schally, A. V., A. J. Kastin and A. Arimura (1971). "Hypothalamic follicle-stimulating hormone (FSH) and luteinizing hormone (LH)-regulating hormone: structure, physiology, and clinical studies." Fertil Steril **22**(11): 703-721.

Schenk, E., M. Essand, C. H. Bangma, G. F. Consortium, C. Barber, J. P. Behr, S. Briggs, R. Carlisle, W. S. Cheng, A. Danielsson, I. J. Dautzenberg, H. Dzojic, P. Erbacher, K. Fisher, A. Frazier, L. J. Georgopoulos, R. Hoeben, S. Kochanek, D. Koppers-Lalic, R. Kraaij, F. Kreppel, L. Lindholm, M. Magnusson, N. Maitland, P. Neuberg, B. Nilsson, M. Ogris, J. S. Remy, M. Scaife, E. Schooten, L. Seymour, T. Totterman, T. G. Uil, K. Ulbrich, J. L. Veldhoven-Zweistra, J. de Vrij, W. van Weerden, E. Wagner and R. Willemsen (2010). "Clinical adenoviral gene therapy for prostate cancer." Hum Gene Ther **21**(7): 807-813.

Scott, F. L., B. Stec, C. Pop, M. K. Dobaczewska, J. J. Lee, E. Monosov, H. Robinson, G. S. Salvesen, R. Schwarzenbacher and S. J. Riedl (2009). "The Fas-FADD death domain complex structure unravels signalling by receptor clustering." Nature **457**(7232): 1019-1022.
Scott, S. L., R. Higdon, L. Beckett, X. B. Shi, R. W. deVere White, J. D. Earle and P. H. Gumerlock (2002). "BCL2 antisense reduces prostate cancer cell survival following irradiation." Cancer Biother Radiopharm **17**(6): 647-656.

Searle, P., V. Mautner and E. Porfiri (2015). "The AdUP trial: combining prodrug activation with immune stimulation in locally recurrent prostate cancer." Hum Gene Ther. **26:A32–A33.** .

Segerman, A., Y. F. Mei and G. Wadell (2000). "Adenovirus types 11p and 35p show high binding efficiencies for committed hematopoietic cell lines and are infective to these cell lines." J Virol **74**(3): 1457-1467.

Seitz, C., M. Hugle, S. Cristofanon, A. Tchoghandjian and S. Fulda (2013). "The dual PI3K/mTOR inhibitor NVP-BEZ235 and chloroquine synergize to trigger apoptosis via mitochondrial-lysosomal cross-talk." Int J Cancer **132**(11): 2682-2693.

Sester, M., Z. Ruszics, E. Mackley and H. G. Burgert (2013). "The transmembrane domain of the adenovirus E3/19K protein acts as an endoplasmic reticulum retention signal and contributes to intracellular sequestration of major histocompatibility complex class I molecules." J Virol **87**(11): 6104-6117.

Shafi, A. A., M. B. Cox and N. L. Weigel (2013). "Androgen receptor splice variants are resistant to inhibitors of Hsp90 and FKBP52, which alter androgen receptor activity and expression." Steroids **78**(6): 548-554.

Shafi, A. A., V. Putluri, J. M. Arnold, E. Tsouko, S. Maity, J. M. Roberts, C. Coarfa, D. E. Frigo, N. Putluri, A. Sreekumar and N. L. Weigel (2015). "Differential regulation of metabolic pathways by androgen receptor (AR) and its constitutively active splice variant, AR-V7, in prostate cancer cells." Oncotarget **6**(31): 31997-32012.

Sharma, S. V., D. A. Haber and J. Settleman (2010). "Cell line-based platforms to evaluate the therapeutic efficacy of candidate anticancer agents." Nat Rev Cancer **10**(4): 241-253.

Shaw, A. R. and E. B. Ziff (1980). "Transcripts from the adenovirus-2 major late promoter yield a single early family of 3' coterminal mRNAs and five late families." Cell **22**(3): 905-916.
Shay, J. W. and W. E. Wright (2011). "Role of telomeres and telomerase in cancer." Semin Cancer Biol **21**(6): 349-353.

Shayakhmetov, D. M., A. Gaggar, S. Ni, Z. Y. Li and A. Lieber (2005). "Adenovirus binding to blood factors results in liver cell infection and hepatotoxicity." J Virol **79**(12): 7478-7491.

Shen, M. M. and C. Abate-Shen (2010). "Molecular genetics of prostate cancer: new prospects for old challenges." Genes Dev **24**(18): 1967-2000.

Shenk, T. E. (2001). Adenoviridae: The viruses and Their Replication. Philadelphia, PA, USA, Fields Virology.

Sherman, L. S., M. Shaker, V. Mariotti and P. Rameshwar (2016). "Mesenchymal stromal/stem cells in drug therapy: New perspective." Cytotherapy.

Shertz, C. A. and M. E. Cardenas (2011). "Exploiting and subverting Tor signaling in the pathogenesis of fungi, parasites, and viruses." PLoS Pathog **7**(9): e1002269.

Shi, X. B., P. H. Gumerlock, J. T. Muenzer and R. W. deVere White (2001). "BCL2 antisense transcripts decrease intracellular Bcl2 expression and sensitize LNCaP prostate cancer cells to apoptosis-inducing agents." Cancer Biother Radiopharm **16**(5): 421-429.

Shin, S. W., S. Y. Kim and J. W. Park (2012). "Autophagy inhibition enhances ursolic acid-induced apoptosis in PC3 cells." Biochim Biophys Acta **1823**(2): 451-457.

Shore, G. C. and M. Nguyen (2008). "Bcl-2 proteins and apoptosis: choose your partner." Cell **135**(6): 1004-1006.

Short, J. J., A. A. Rivera, H. Wu, M. R. Walter, M. Yamamoto, J. M. Mathis and D. T. Curiel (2010). "Substitution of adenovirus serotype 3 hexon onto a serotype 5 oncolytic adenovirus reduces factor X binding, decreases liver tropism, and improves antitumor efficacy." Mol Cancer Ther **9**(9): 2536-2544.

Siegel, R., J. Ma, Z. Zou and A. Jemal (2014). "Cancer statistics, 2014." CA Cancer J Clin **64**(1): 9-29.

Silvestri, I., S. Cattarino, S. Giantulli, C. Nazzari, G. Collalti and A. Sciarra (2016). "A Perspective of Immunotherapy for Prostate Cancer." Cancers (Basel) **8**(7).

Silvestry, M., S. Lindert, J. G. Smith, O. Maier, C. M. Wiethoff, G. R. Nemerow and P. L. Stewart (2009). "Cryo-electron microscopy structure of adenovirus type 2 temperature-sensitive mutant 1 reveals insight into the cell entry defect." J Virol **83**(15): 7375-7383.

Skjoth, I. H. and O. G. Issinger (2006). "Profiling of signaling molecules in four different human prostate carcinoma cell lines before and after induction of apoptosis." Int J Oncol **28**(1): 217-229.

Small, E. J., M. A. Carducci, J. M. Burke, R. Rodriguez, L. Fong, L. van Ummersen, D. C. Yu, J. Aimi, D. Ando, P. Working, D. Kirn and G. Wilding (2006). "A phase I trial of intravenous CG7870, a replication-selective, prostate-specific antigen-targeted oncolytic adenovirus, for the treatment of hormone-refractory, metastatic prostate cancer." Mol Ther **14**(1): 107-117.

Sobel, R. E. and M. D. Sadar (2005). "Cell lines used in prostate cancer research: a compendium of old and new lines--part 1." J Urol **173**(2): 342-359.

Sobue, S., N. Mizutani, Y. Aoyama, Y. Kawamoto, M. Suzuki, Y. Nozawa, M. Ichihara and T. Murate (2016). "Mechanism of paclitaxel resistance in a human prostate cancer cell line, PC3-PR, and its sensitization by cabazitaxel." Biochem Biophys Res Commun.

Sonavane, G., K. Tomoda and K. Makino (2008). "Biodistribution of colloidal gold nanoparticles after intravenous administration: effect of particle size." Colloids Surf B Biointerfaces **66**(2): 274-280.

Song, M. S., L. Salmena and P. P. Pandolfi (2012). "The functions and regulation of the PTEN tumour suppressor." Nat Rev Mol Cell Biol **13**(5): 283-296.

Sorace, A. G., J. M. Warram, M. Mahoney, K. R. Zinn and K. Hoyt (2013). "Enhancement of adenovirus delivery after ultrasound-stimulated therapy in a cancer model." Ultrasound Med Biol **39**(12): 2374-2381.

Sorace, A. G., J. M. Warram, H. Umphrey and K. Hoyt (2012). "Microbubble-mediated ultrasonic techniques for improved chemotherapeutic delivery in cancer." J Drug Target **20**(1): 43-54.

Soria, C., F. E. Estermann, K. C. Espantman and C. C. O'Shea (2010). "Heterochromatin silencing of p53 target genes by a small viral protein." Nature **466**(7310): 1076-1081.

Spangle, J. M. and K. Münger (2010). "The human papillomavirus type 16 E6 oncoprotein activates mTORC1 signaling and increases protein synthesis." J Virol **84**(18): 9398-9407.

Sramkoski, R. M., T. G. Pretlow, 2nd, J. M. Giaconia, T. P. Pretlow, S. Schwartz, M. S. Sy, S. R. Marengo, J. S. Rhim, D. Zhang and J. W. Jacobberger (1999). "A new human prostate carcinoma cell line, 22Rv1." In Vitro Cell Dev Biol Anim **35**(7): 403-409.

Stark, H. J., M. J. Willhauck, N. Mirancea, K. Boehnke, I. Nord, D. Breitkreutz, A. Pavesio, P. Boukamp and N. E. Fusenig (2004). "Authentic fibroblast matrix in dermal equivalents

normalises epidermal histogenesis and dermoepidermal junction in organotypic co-culture." Eur J Cell Biol **83**(11-12): 631-645.

Steketee, K., L. Timmerman, A. C. Ziel-van der Made, P. Doesburg, A. O. Brinkmann and J. Trapman (2002). "Broadened ligand responsiveness of androgen receptor mutants obtained by random amino acid substitution of H874 and mutation hot spot T877 in prostate cancer." Int J Cancer **100**(3): 309-317.

Stephan, C., T. Köpke, A. Semjonow, M. Lein, S. Deger, M. Schrader, K. Miller and K. Jung (2009). "Discordant total and free prostate-specific antigen (PSA) assays: does calibration with WHO reference materials diminish the problem?" Clin Chem Lab Med **47**(11): 1325-1331.

Stephens, C. and E. Harlow (1987). "Differential splicing yields novel adenovirus 5 E1A mRNAs that encode 30 kd and 35 kd proteins." EMBO J **6**(7): 2027-2035.

Stephenson, R. A., C. P. Dinney, K. Gohji, N. G. Ordonez, J. J. Killion and I. J. Fidler (1992). "Metastatic model for human prostate cancer using orthotopic implantation in nude mice." J Natl Cancer Inst **84**(12): 951-957.

Stracker, T. H., D. V. Lee, C. T. Carson, F. D. Araujo, D. A. Ornelles and M. D. Weitzman (2005). "Serotype-specific reorganization of the Mre11 complex by adenoviral E4orf3 proteins." J Virol **79**(11): 6664-6673.

Stricker, H. (2015). Phase 1 Trial of Interleukin 12 Gene Therapy for Locally Recurrent Prostate Cancer.

Strober, W. (2001). "Trypan blue exclusion test of cell viability." Curr Protoc Immunol **Appendix 3**: Appendix 3B.

Su, J. L., P. B. Chen, Y. H. Chen, S. C. Chen, Y. W. Chang, Y. H. Jan, X. Cheng, M. Hsiao and M. C. Hung (2010). "Downregulation of microRNA miR-520h by E1A contributes to anticancer activity." Cancer Res **70**(12): 5096-5108.

Subr, V., L. Kostka, T. Selby-Milic, K. Fisher, K. Ulbrich, L. Seymour and R. Carlisle (2009). "Coating of adenovirus type 5 with polymers containing quaternary amines prevents binding to blood components." Journal of Controlled Release **135**(2): 152-158.

Sui, X., R. Chen, Z. Wang, Z. Huang, N. Kong, M. Zhang, W. Han, F. Lou, J. Yang, Q. Zhang, X. Wang, C. He and H. Pan (2013). "Autophagy and chemotherapy resistance: a promising therapeutic target for cancer treatment." Cell Death Dis **4**: e838.

Sun, A., J. Tang, Y. Hong, J. Song, P. F. Terranova, J. B. Thrasher, S. Svojanovsky, H. G. Wang and B. Li (2008). "Androgen receptor-dependent regulation of Bcl-xL expression: Implication in prostate cancer progression." Prostate **68**(4): 453-461.

Sun, S., C. C. Sprenger, R. L. Vessella, K. Haugk, K. Soriano, E. A. Mostaghel, S. T. Page, I. M. Coleman, H. M. Nguyen, H. Sun, P. S. Nelson and S. R. Plymate (2010). "Castration resistance in human prostate cancer is conferred by a frequently occurring androgen receptor splice variant." J Clin Invest **120**(8): 2715-2730.

Sutherland, R. M., J. A. McCredie and W. R. Inch (1971). "Growth of multicell spheroids in tissue culture as a model of nodular carcinomas." J Natl Cancer Inst **46**(1): 113-120.

Sweeney, K. and G. Halldén (2016). "Oncolytic adenovirus-mediated therapy for prostate cancer." Oncolytic Virother **5**: 45-57.

Symes, J. C., M. Kurin, N. E. Fleshner and J. A. Medin (2008). "Fas-mediated killing of primary prostate cancer cells is increased by mitoxantrone and docetaxel." Mol Cancer Ther **7**(9): 3018-3028.

Sánchez, C., P. Mendoza, H. R. Contreras, J. Vergara, J. A. McCubrey, C. Huidobro and E. A. Castellón (2009). "Expression of multidrug resistance proteins in prostate cancer is related with cell sensitivity to chemotherapeutic drugs." Prostate **69**(13): 1448-1459.

Takagi-Kimura, M., T. Yamano, A. Tamamoto, N. Okamura, H. Okamura, T. Hashimoto-Tamaoki, M. Tagawa, N. Kasahara and S. Kubo (2013). "Enhanced antitumor efficacy of fiber-modified, midkine promoter-regulated oncolytic adenovirus in human malignant mesothelioma." Cancer Sci **104**(11): 1433-1439.

Takakura, M., M. Nakamura, S. Kyo, M. Hashimoto, N. Mori, T. Ikoma, Y. Mizumoto, T. Fujiwara, Y. Urata and M. Inoue (2010). "Intraperitoneal administration of telomerase-specific oncolytic adenovirus sensitizes ovarian cancer cells to cisplatin and affects survival in a xenograft model with peritoneal dissemination." Cancer Gene Ther **17**(1): 11-19.

Tanida, I., M. Yamasaki, M. Komatsu and T. Ueno (2012). "The FAP motif within human ATG7, an autophagy-related E1-like enzyme, is essential for the E2-substrate reaction of LC3 lipidation." Autophagy **8**(1): 88-97.

Tannock, I. F., R. de Wit, W. R. Berry, J. Horti, A. Pluzanska, K. N. Chi, S. Oudard, C. Theodore, N. D. James, I. Turesson, M. A. Rosenthal, M. A. Eisenberger and T. A. X. Investigators (2004). "Docetaxel plus prednisone or mitoxantrone plus prednisone for advanced prostate cancer." N Engl J Med **351**(15): 1502-1512.

Tao, N., G. P. Gao, M. Parr, J. Johnston, T. Baradet, J. M. Wilson, J. Barsoum and S. E. Fawell (2001). "Sequestration of adenoviral vector by Kupffer cells leads to a nonlinear dose response of transduction in liver." Mol Ther **3**(1): 28-35.

Tasdemir, E., M. C. Maiuri, L. Galluzzi, I. Vitale, M. Djavaheri-Mergny, M. D'Amelio, A. Criollo, E. Morselli, C. Zhu, F. Harper, U. Nannmark, C. Samara, P. Pinton, J. M. Vicencio, R. Carnuccio, U. M. Moll, F. Madeo, P. Paterlini-Brechot, R. Rizzuto, G. Szabadkai, G. Pierron, K. Blomgren, N. Tavernarakis, P. Codogno, F. Cecconi and G. Kroemer (2008). "Regulation of autophagy by cytoplasmic p53." Nat Cell Biol **10**(6): 676-687.

Taylor, B. S., N. Schultz, H. Hieronymus, A. Gopalan, Y. Xiao, B. S. Carver, V. K. Arora, P. Kaushik, E. Cerami, B. Reva, Y. Antipin, N. Mitsiades, T. Landers, I. Dolgalev, J. E. Major, M. Wilson, N. D. Socci, A. E. Lash, A. Heguy, J. A. Eastham, H. I. Scher, V. E. Reuter, P. T. Scardino, C. Sander, C. L. Sawyers and W. L. Gerald (2010). "Integrative genomic profiling of human prostate cancer." Cancer Cell **18**(1): 11-22.

Tazawa, H., S. Kagawa and T. Fujiwara (2013). "Oncolytic adenovirus-induced autophagy: tumor-suppressive effect and molecular basis." Acta Med Okayama **67**(6): 333-342.

Tazawa, H., S. Yano, R. Yoshida, Y. Yamasaki, T. Sasaki, Y. Hashimoto, S. Kuroda, M. Ouchi, T. Onishi, F. Uno, S. Kagawa, Y. Urata and T. Fujiwara (2012). "Genetically engineered oncolytic adenovirus induces autophagic cell death through an E2F1-microRNA-7-epidermal growth factor receptor axis." Int J Cancer **131**(12): 2939-2950.

Teigler, J. E., P. Penaloza-MacMaster, R. Obeng, N. M. Provine, R. A. Larocca, E. N. Borducchi and D. H. Barouch (2014). "Hexon hypervariable region-modified adenovirus type 5 (Ad5) vectors display reduced hepatotoxicity but induce T lymphocyte phenotypes similar to Ad5 vectors." Clin Vaccine Immunol **21**(8): 1137-1144.

Terao, S., T. Shirakawa, B. Acharya, M. Miyata, N. Hinata, K. Tanaka, A. Takenaka, I. Hara, M. Naoe, K. Fuji, T. Okegawa, E. Higashihara, S. Kamidono, M. Fujisawa and A. Gotoh (2009). "A pilot study of quality of life of patients with hormone-refractory prostate cancer after gene therapy." Anticancer Res **29**(5): 1533-1537.

Thangavel, C., E. Boopathi, S. Ciment, Y. Liu, O. N. R, A. Sharma, S. B. McMahon, H. Mellert, S. Addya, A. Ertel, R. Birbe, P. Fortina, A. P. Dicker, K. E. Knudsen and R. B. Den (2014). "The retinoblastoma tumor suppressor modulates DNA repair and radioresponsiveness." Clin Cancer Res **20**(21): 5468-5482.

Timms, B. G. (2008). "Prostate development: a historical perspective." Differentiation **76**(6): 565-577.

Toker, A. and M. Yoeli-Lerner (2006). "Akt signaling and cancer: surviving but not moving on." Cancer Res **66**(8): 3963-3966.

Tombal, B., K. Miller, L. Boccon-Gibod, F. Schröder, N. Shore, E. D. Crawford, J. Moul, J. K. Jensen, T. Kold Olesen and B. E. Persson (2010). "Additional analysis of the secondary end point of biochemical recurrence rate in a phase 3 trial (CS21) comparing degarelix 80 mg versus leuprolide in prostate cancer patients segmented by baseline characteristics." Eur Urol **57**(5): 836-842.

Tomlins, S. A., B. Laxman, S. Varambally, X. Cao, J. Yu, B. E. Helgeson, Q. Cao, J. R. Prensner, M. A. Rubin, R. B. Shah, R. Mehra and A. M. Chinnaiyan (2008). "Role of the TMPRSS2-ERG gene fusion in prostate cancer." Neoplasia **10**(2): 177-188.

Tomlins, S. A., D. R. Rhodes, S. Perner, S. M. Dhanasekaran, R. Mehra, X. W. Sun, S. Varambally, X. Cao, J. Tchinda, R. Kuefer, C. Lee, J. E. Montie, R. B. Shah, K. J. Pienta, M. A. Rubin and A. M. Chinnaiyan (2005). "Recurrent fusion of TMPRSS2 and ETS transcription factor genes in prostate cancer." Science **310**(5748): 644-648.

Tran, C., S. Ouk, N. J. Clegg, Y. Chen, P. A. Watson, V. Arora, J. Wongvipat, P. M. Smith-Jones, D. Yoo, A. Kwon, T. Wasielewska, D. Welsbie, C. D. Chen, C. S. Higano, T. M. Beer, D. T. Hung, H. I. Scher, M. E. Jung and C. L. Sawyers (2009). "Development of a second-generation antiandrogen for treatment of advanced prostate cancer." Science **324**(5928): 787-790.

Tran, L., L. H. Ouisse, P. Richard-Fiardo, P. R. Franken, J. Darcourt, G. Cornilleau, K. Benihoud and G. Vassaux (2013). "Adrenal gland infection by serotype 5 adenovirus requires coagulation factors." PLoS One **8**(4): e62191.

Trotman, L. C., N. Mosberger, M. Fornerod, R. P. Stidwill and U. F. Greber (2001). "Import of adenovirus DNA involves the nuclear pore complex receptor CAN/Nup214 and histone H1." Nat Cell Biol **3**(12): 1092-1100.

Turnell, A. S. and R. J. Grand (2012). "DNA viruses and the cellular DNA-damage response." J Gen Virol **93**(Pt 10): 2076-2097.

Turner, R. L., J. C. Wilkinson and D. A. Ornelles (2014). "E1B and E4 oncoproteins of adenovirus antagonize the effect of apoptosis inducing factor." Virology **456-457**: 205-219.

Uchino, J., D. T. Curiel and H. Ugai (2014). "Species D human adenovirus type 9 exhibits better virus-spread ability for antitumor efficacy among alternative serotypes." PLoS One **9**(2): e87342.

Ullman, A. J., N. C. Reich and P. Hearing (2007). "Adenovirus E4 ORF3 protein inhibits the interferon-mediated antiviral response." J Virol **81**(9): 4744-4752.

Vachon, V. K. and G. L. Conn (2016). "Adenovirus VA RNA: An essential pro-viral non-coding RNA." Virus Res **212**: 39-52.

van Poppel, H. and S. Nilsson (2008). "Testosterone surge: rationale for gonadotropin-releasing hormone blockers?" Urology **71**(6): 1001-1006.

Veldscholte, J., C. A. Berrevoets, C. Ris-Stalpers, G. G. Kuiper, G. Jenster, J. Trapman, A. O. Brinkmann and E. Mulder (1992). "The androgen receptor in LNCaP cells contains a mutation in the ligand binding domain which affects steroid binding characteristics and response to antiandrogens." J Steroid Biochem Mol Biol **41**(3-8): 665-669.

Vetter, A., K. Virdi, S. Espenlaub, W. Rodl, E. Wagner, P. Holm, C. Scheu, F. Kreppel, C. Spitzweg and M. Ogris (2013). "Adenoviral Vectors Coated with PAMAM Dendrimer Conjugates Allow CAR Independent Virus Uptake and Targeting to the EGF Receptor." Molecular Pharmaceutics **10**(2): 606-618.

Voigt, J. D., S. M. Zappala, E. D. Vaughan and A. J. Wein (2014). "The Kallikrein Panel for prostate cancer screening: its economic impact." Prostate **74**(3): 250-259.

Waddington, S. N., J. H. McVey, D. Bhella, A. L. Parker, K. Barker, H. Atoda, R. Pink, S. M. Buckley, J. A. Greig, L. Denby, J. Custers, T. Morita, I. M. Francischetti, R. Q. Monteiro, D. H. Barouch, N. van Rooijen, C. Napoli, M. J. Havenga, S. A. Nicklin and A. H. Baker (2008). "Adenovirus serotype 5 hexon mediates liver gene transfer." Cell **132**(3): 397-409.

Waddington, S. N., A. L. Parker, M. Havenga, S. A. Nicklin, S. M. Buckley, J. H. McVey and A. H. Baker (2007). "Targeting of adenovirus serotype 5 (Ad5) and 5/47 pseudotyped vectors in vivo: fundamental involvement of coagulation factors and redundancy of CAR binding by Ad5." J Virol **81**(17): 9568-9571.

Wagstaff, K. M. and D. A. Jans (2009). "Importins and beyond: non-conventional nuclear transport mechanisms." Traffic **10**(9): 1188-1198.

Wang, H., Z. Y. Li, Y. Liu, J. Persson, I. Beyer, T. Möller, D. Koyuncu, M. R. Drescher, R. Strauss, X. B. Zhang, J. K. Wahl, N. Urban, C. Drescher, A. Hemminki, P. Fender and A. Lieber (2011).

"Desmoglein 2 is a receptor for adenovirus serotypes 3, 7, 11 and 14." Nat Med **17**(1): 96-104.

Wang, H., R. Yumul, H. Cao, L. Ran, X. Fan, M. Richter, F. Epstein, J. Gralow, C. Zubieta, P. Fender and A. Lieber (2013). "Structural and functional studies on the interaction of adenovirus fiber knobs and desmoglein 2." J Virol **87**(21): 11346-11362.

Wang, N., H. Zhang, B. Q. Zhang, W. Liu, Z. Zhang, M. Qiao, F. Deng, N. Wu, X. Chen, S. Wen, J. Zhang, Z. Liao, Q. Zhang, Z. Yan, L. Yin, J. Ye, Y. Deng, H. H. Luu, R. C. Haydon, H. Liang and T. C. He (2014). "Adenovirus-mediated efficient gene transfer into cultured three-dimensional organoids." PLoS One **9**(4): e93608.

Wang, Y., G. Hallden, R. Hill, A. Anand, T. C. Liu, J. Francis, G. Brooks, N. Lemoine and D. Kirn (2003). "E3 gene manipulations affect oncolytic adenovirus activity in immunocompetent tumor models." Nat Biotechnol **21**(11): 1328-1335.

Wang, Y., R. Q. Peng, D. D. Li, Y. Ding, X. Q. Wu, Y. X. Zeng, X. F. Zhu and X. S. Zhang (2011). "Chloroquine enhances the cytotoxicity of topotecan by inhibiting autophagy in lung cancer cells." Chin J Cancer **30**(10): 690-700.

Wang, Y. and N. Tjandra (2013). "Structural insights of tBid, the caspase-8-activated Bid, and its BH3 domain." J Biol Chem **288**(50): 35840-35851.

Wang, Z., B. Yu, B. Wang, J. Yan, X. Feng, L. Wang, H. Zhang, H. Wu, J. Wu, W. Kong and X. Yu (2016). "A novel capsid-modified oncolytic recombinant adenovirus type 5 for tumor-targeting gene therapy by intravenous route." Oncotarget.

Warram, J. M., A. G. Sorace, R. Saini, A. V. Borovjagin, K. Hoyt and K. R. Zinn (2012). "Systemic delivery of a breast cancer-detecting adenovirus using targeted microbubbles." Cancer Gene Ther **19**(8): 545-552.

Watson, P. A., Y. F. Chen, M. D. Balbas, J. Wongvipat, N. D. Socci, A. Viale, K. Kim and C. L. Sawyers (2010). "Constitutively active androgen receptor splice variants expressed in castration-resistant prostate cancer require full-length androgen receptor." Proc Natl Acad Sci U S A **107**(39): 16759-16765.

Weaver, V. M., O. W. Petersen, F. Wang, C. A. Larabell, P. Briand, C. Damsky and M. J. Bissell (1997). "Reversion of the malignant phenotype of human breast cells in three-dimensional culture and in vivo by integrin blocking antibodies." J Cell Biol **137**(1): 231-245.

Wei, Y., S. Pattingre, S. Sinha, M. Bassik and B. Levine (2008). "JNK1-mediated phosphorylation of Bcl-2 regulates starvation-induced autophagy." Mol Cell **30**(6): 678-688.
White, E. (2006). "Mechanisms of apoptosis regulation by viral oncogenes in infection and tumorigenesis." Cell Death Differ **13**(8): 1371-1377.

Widmark, A., O. Klepp, A. Solberg, J. E. Damber, A. Angelsen, P. Fransson, J. A. Lund, I. Tasdemir, M. Hoyer, F. Wiklund, S. D. Fosså, S. P. C. G. S. 7 and S. A. f. U. O. 3 (2009). "Endocrine treatment, with or without radiotherapy, in locally advanced prostate cancer (SPCG-7/SFUO-3): an open randomised phase III trial." Lancet **373**(9660): 301-308.

Wiethoff, C. M., H. Wodrich, L. Gerace and G. R. Nemerow (2005). "Adenovirus protein VI mediates membrane disruption following capsid disassembly." J Virol **79**(4): 1992-2000.

Williams, G. J., S. P. Lees-Miller and J. A. Tainer (2010). "Mre11-Rad50-Nbs1 conformations and the control of sensing, signaling, and effector responses at DNA double-strand breaks." DNA Repair (Amst) **9**(12): 1299-1306.

Windheim, M., A. Hilgendorf and H. G. Burgert (2004). "Immune evasion by adenovirus E3 proteins: exploitation of intracellular trafficking pathways." Curr Top Microbiol Immunol **273**: 29-85.

Windus, L. C., T. T. Glover and V. M. Avery (2013). "Bone-stromal cells up-regulate tumourigenic markers in a tumour-stromal 3D model of prostate cancer." Mol Cancer **12**(1): 112.

Wirawan, E., L. Vande Walle, K. Kersse, S. Cornelis, S. Claerhout, I. Vanoverberghe, R. Roelandt, R. De Rycke, J. Verspurten, W. Declercq, P. Agostinis, T. Vanden Berghe, S. Lippens and P. Vandenabeele (2010). "Caspase-mediated cleavage of Beclin-1 inactivates Beclin-1-induced autophagy and enhances apoptosis by promoting the release of proapoptotic factors from mitochondria." Cell Death Dis **1**: e18.

Wodrich, H., A. Cassany, M. A. D'Angelo, T. Guan, G. Nemerow and L. Gerace (2006). "Adenovirus core protein pVII is translocated into the nucleus by multiple import receptor pathways." J Virol **80**(19): 9608-9618.

Wold, W. S. and L. R. Gooding (1989). "Adenovirus region E3 proteins that prevent cytolysis by cytotoxic T cells and tumor necrosis factor." Mol Biol Med **6**(5): 433-452.

Wold, W. S. and K. Toth (2013). "Adenovirus vectors for gene therapy, vaccination and cancer gene therapy." Curr Gene Ther **13**(6): 421-433.

Wold, W. S. M. and M. S. Horwitz (2007). Adenoviruses. Fields Virology. D. M. Knipe and P. M. Howley. Philadelphia, Wolters Kluwer Health/Lippincott Williams & Wilkins.

Wong, Y. N., R. Ferraldeschi, G. Attard and J. de Bono (2014). "Evolution of androgen receptor targeted therapy for advanced prostate cancer." Nat Rev Clin Oncol **11**(6): 365-376.

Wu, C. C., Y. C. Li, Y. R. Wang, T. K. Li and N. L. Chan (2013). "On the structural basis and design guidelines for type II topoisomerase-targeting anticancer drugs." Nucleic Acids Res **41**(22): 10630-10640.

Wu, E., L. Pache, D. J. Von Seggern, T. M. Mullen, Y. Mikyas, P. L. Stewart and G. R. Nemerow (2003). "Flexibility of the adenovirus fiber is required for efficient receptor interaction." J Virol **77**(13): 7225-7235.

Wu, K., D. Guimet and P. Hearing (2013). "The adenovirus L4-33K protein regulates both late gene expression patterns and viral DNA packaging." J Virol **87**(12): 6739-6747.

Wu, K., D. Orozco and P. Hearing (2012). "The adenovirus L4-22K protein is multifunctional and is an integral component of crucial aspects of infection." J Virol **86**(19): 10474-10483.

Wu, T., M. C. Wang, L. Jing, Z. Y. Liu, H. Guo, Y. Liu, Y. Y. Bai, Y. Z. Cheng, K. J. Nan and X. Liang (2015). "Autophagy facilitates lung adenocarcinoma resistance to cisplatin treatment by activation of AMPK/mTOR signaling pathway." Drug Des Devel Ther **9**: 6421-6431.

Wu, W., P. Liu and J. Li (2012). "Necroptosis: an emerging form of programmed cell death." Crit Rev Oncol Hematol **82**(3): 249-258.

Wu, Y. T., H. L. Tan, Q. Huang, C. N. Ong and H. M. Shen (2009). "Activation of the PI3K-Akt-mTOR signaling pathway promotes necrotic cell death via suppression of autophagy." Autophagy **5**(6): 824-834.

Xia, Z. J., J. H. Chang, L. Zhang, W. Q. Jiang, Z. Z. Guan, J. W. Liu, Y. Zhang, X. H. Hu, G. H. Wu, H. Q. Wang, Z. C. Chen, J. C. Chen, Q. H. Zhou, J. W. Lu, Q. X. Fan, J. J. Huang and X. Zheng (2004). "[Phase III randomized clinical trial of intratumoral injection of E1B gene-deleted adenovirus (H101) combined with cisplatin-based chemotherapy in treating squamous cell cancer of head and neck or esophagus]." Ai Zheng **23**(12): 1666-1670.

Xu, D., Y. Zhan, Y. Qi, B. Cao, S. Bai, W. Xu, S. S. Gambhir, P. Lee, O. Sartor, E. K. Flemington, H. Zhang, C. D. Hu and Y. Dong (2015). "Androgen Receptor Splice Variants Dimerize to Transactivate Target Genes." Cancer Res **75**(17): 3663-3671.

Xu, Z., J. Tian, J. S. Smith and A. P. Byrnes (2008). "Clearance of adenovirus by Kupffer cells is mediated by scavenger receptors, natural antibodies, and complement." J Virol **82**(23): 11705-11713.

Yamamoto, M. and D. T. Curiel (2010). "Current issues and future directions of oncolytic adenoviruses." Mol Ther **18**(2): 243-250.

Yamasaki, Y., H. Tazawa, Y. Hashimoto, T. Kojima, S. Kuroda, S. Yano, R. Yoshida, F. Uno, H. Mizuguchi, A. Ohtsuru, Y. Urata, S. Kagawa and T. Fujiwara (2012). "A novel apoptotic mechanism of genetically engineered adenovirus-mediated tumour-specific p53 overexpression through E1A-dependent p21 and MDM2 suppression." Eur J Cancer **48**(14): 2282-2291.

Yang, Y. F., S. Y. Xue, Z. Z. Lu, F. J. Xiao, Y. Yin, Q. W. Zhang, C. T. Wu, H. Wang and L. S. Wang (2014). "Antitumor effects of oncolytic adenovirus armed with PSA-IZ-CD40L fusion gene against prostate cancer." Gene Ther **21**(8): 723-731.

Yang, Z. and D. J. Klionsky (2010). "Mammalian autophagy: core molecular machinery and signaling regulation." Curr Opin Cell Biol **22**(2): 124-131.

Yee, K. S., S. Wilkinson, J. James, K. M. Ryan and K. H. Vousden (2009). "PUMA- and Bax-induced autophagy contributes to apoptosis." Cell Death Differ **16**(8): 1135-1145.
Yoeli-Lerner, M. and A. Toker (2006). "Akt/PKB signaling in cancer: a function in cell motility and invasion." Cell Cycle **5**(6): 603-605.

Yoshino, T., H. Shiina, S. Urakami, N. Kikuno, T. Yoneda, K. Shigeno and M. Igawa (2006). "Bcl-2 expression as a predictive marker of hormone-refractory prostate cancer treated with taxane-based chemotherapy." Clin Cancer Res **12**(20 Pt 1): 6116-6124.

You, L., Y. Wang, Y. Jin and W. Qian (2012). "Downregulation of Mcl-1 synergizes the apoptotic response to combined treatment with cisplatin and a novel fiber chimeric oncolytic adenovirus." Oncol Rep **27**(4): 971-978.

You, L., C. T. Yang and D. M. Jablons (2000). "ONYX-015 works synergistically with chemotherapy in lung cancer cell lines and primary cultures freshly made from lung cancer patients." Cancer Res **60**(4): 1009-1013.

Yousefi, S., R. Perozzo, I. Schmid, A. Ziemiecki, T. Schaffner, L. Scapozza, T. Brunner and H. U. Simon (2006). "Calpain-mediated cleavage of Atg5 switches autophagy to apoptosis." Nat Cell Biol **8**(10): 1124-1132.

Yu, D. and M. C. Hung (1998). "The erbB2 gene as a cancer therapeutic target and the tumor- and metastasis-suppressing function of E1A." Cancer Metastasis Rev **17**(2): 195-202.

Yu, D. C., Y. Chen, J. Dilley, Y. Li, M. Embry, H. Zhang, N. Nguyen, P. Amin, J. Oh and D. R. Henderson (2001). "Antitumor synergy of CV787, a prostate cancer-specific adenovirus, and paclitaxel and docetaxel." Cancer Res **61**(2): 517-525.

Yu, D. C., Y. Chen, M. Seng, J. Dilley and D. R. Henderson (1999). "The addition of adenovirus type 5 region E3 enables calydon virus 787 to eliminate distant prostate tumor xenografts." Cancer Res **59**(17): 4200-4203.

Yu, L., F. Wan, S. Dutta, S. Welsh, Z. Liu, E. Freundt, E. H. Baehrecke and M. Lenardo (2006). "Autophagic programmed cell death by selective catalase degradation." Proc Natl Acad Sci U S A **103**(13): 4952-4957.

Yue, Q. X., X. Liu and D. A. Guo (2010). "Microtubule-binding natural products for cancer therapy." Planta Med **76**(11): 1037-1043.

Zalckvar, E., H. Berissi, L. Mizrachy, Y. Idelchuk, I. Koren, M. Eisenstein, H. Sabanay, R. Pinkas-Kramarski and A. Kimchi (2009). "DAP-kinase-mediated phosphorylation on the BH3 domain of beclin 1 promotes dissociation of beclin 1 from Bcl-XL and induction of autophagy." EMBO Rep **10**(3): 285-292.

Zeng, Q., J. Han, D. Zhao, T. Gong, Z. Zhang and X. Sun (2012). "Protection of adenovirus from neutralizing antibody by cationic PEG derivative ionically linked to adenovirus." International Journal of Nanomedicine **7**: 985-997.

Zeng, X. and C. R. Carlin (2013). "Host cell autophagy modulates early stages of adenovirus infections in airway epithelial cells." J Virol **87**(4): 2307-2319.

Zhang, J. J., U. Vinkemeier, W. Gu, D. Chakravarti, C. M. Horvath and J. E. Darnell (1996). "Two contact regions between Stat1 and CBP/p300 in interferon gamma signaling." Proc Natl Acad Sci U S A **93**(26): 15092-15096.

Zhang, M., D. E. Latham, M. A. Delaney and A. Chakravarti (2005). "Survivin mediates resistance to antiandrogen therapy in prostate cancer." Oncogene **24**(15): 2474-2482.

Zhang, W. and M. J. Imperiale (2000). "Interaction of the adenovirus IVa2 protein with viral packaging sequences." J Virol **74**(6): 2687-2693.

Zhang, X., H. Wu, D. Wu, Y. Wang, J. Chang, Z. Zhai, A. Meng, P. Liu, L. Zhang and F. Fan (2010). "Toxicologic effects of gold nanoparticles in vivo by different administration routes." International Journal of Nanomedicine **5**: 771-781.

Zhou, J., J. Ralston, R. Sedev and D. Beattie (2009). "Functionalized gold nanoparticles: Synthesis, structure and colloid stability." Journal of Colloid and Interface Science **331**(2): 251-262.

Zhou, X. and K. Münger (2009). "Expression of the human papillomavirus type 16 E7 oncoprotein induces an autophagy-related process and sensitizes normal human keratinocytes to cell death in response to growth factor deprivation." Virology **385**(1): 192-197.

Zhu, J., X. Huang and Y. Yang (2007). "Innate immune response to adenoviral vectors is mediated by both Toll-like receptor-dependent and -independent pathways." J Virol **81**(7): 3170-3180.

Zielinski, R. R., B. J. Eigl and K. N. Chi (2013). "Targeting the apoptosis pathway in prostate cancer." Cancer J **19**(1): 79-89.

Zijderveld, D. C., F. d'Adda di Fagagna, M. Giacca, H. T. Timmers and P. C. van der Vliet (1994). "Stimulation of the adenovirus major late promoter in vitro by transcription factor USF is enhanced by the adenovirus DNA binding protein." J Virol **68**(12): 8288-8295.

Ziparo, E., S. Petrungaro, E. S. Marini, D. Starace, S. Conti, A. Facchiano, A. Filippini and C. Giampietri (2013). "Autophagy in prostate cancer and androgen suppression therapy." Int J Mol Sci **14**(6): 12090-12106.

Zu, K. and E. Giovannucci (2009). "Smoking and aggressive prostate cancer: a review of the epidemiologic evidence." Cancer Causes Control **20**(10): 1799-1810.